CYTOSKELETAL REGULATION OF IMMUNE RESPONSE

EDITED BY: Sudha Kumari, Balbino Alarcon and Wolfgang W. Schamel
PUBLISHED IN: Frontiers in Cell and Developmental Biology

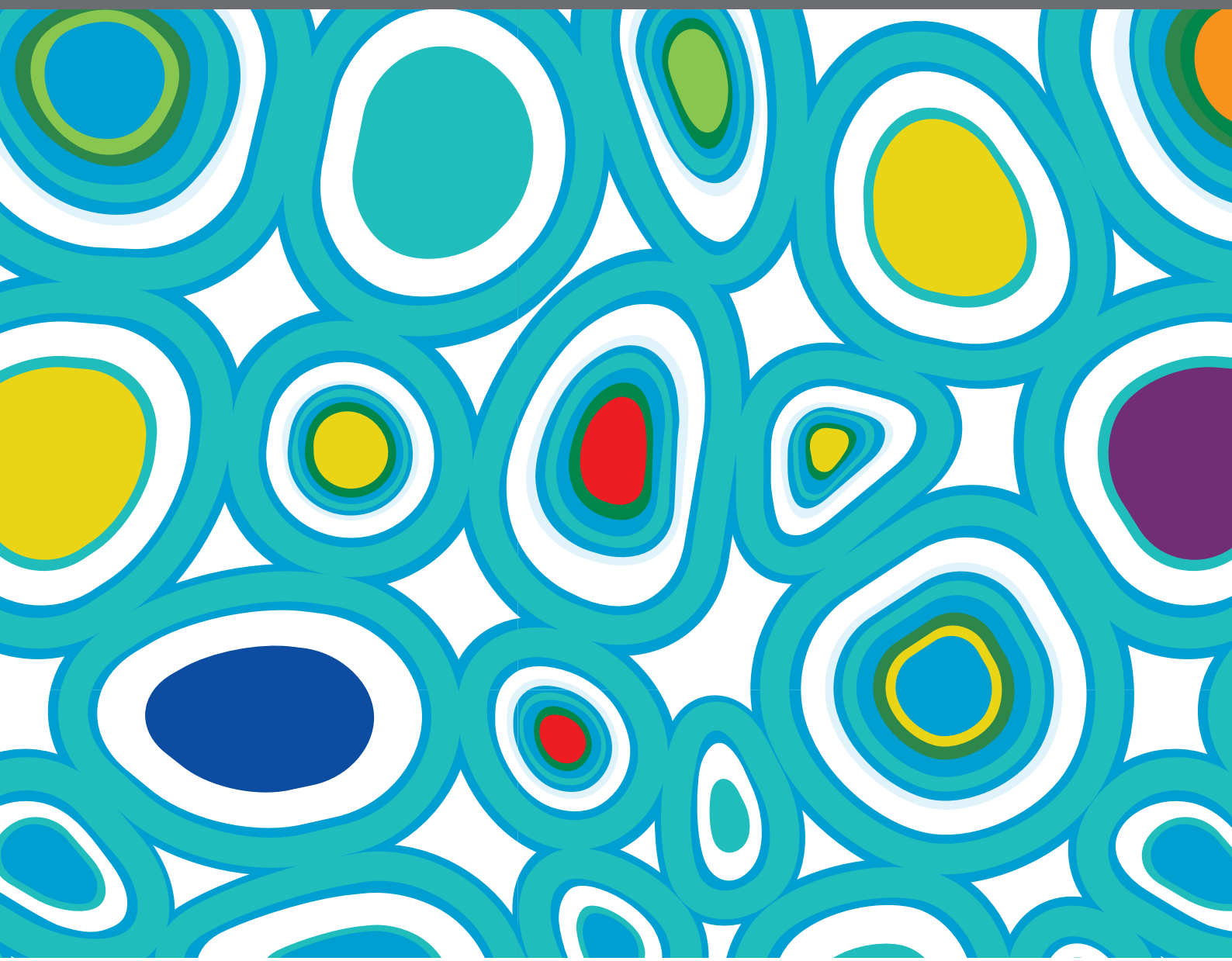

frontiers Research Topics

frontiers

ISSN 1664-8714
ISBN 978-2-88971-940-2
DOI 10.3389/978-2-88971-940-2

About Frontiers

Frontiers is more than just an open-access publisher of scholarly articles: it is a pioneering approach to the world of academia, radically improving the way scholarly research is managed. The grand vision of Frontiers is a world where all people have an equal opportunity to seek, share and generate knowledge. Frontiers provides immediate and permanent online open access to all its publications, but this alone is not enough to realize our grand goals.

Frontiers Journal Series

The Frontiers Journal Series is a multi-tier and interdisciplinary set of open-access, online journals, promising a paradigm shift from the current review, selection and dissemination processes in academic publishing. All Frontiers journals are driven by researchers for researchers; therefore, they constitute a service to the scholarly community. At the same time, the Frontiers Journal Series operates on a revolutionary invention, the tiered publishing system, initially addressing specific communities of scholars, and gradually climbing up to broader public understanding, thus serving the interests of the lay society, too.

Dedication to Quality

Each Frontiers article is a landmark of the highest quality, thanks to genuinely collaborative interactions between authors and review editors, who include some of the world's best academicians. Research must be certified by peers before entering a stream of knowledge that may eventually reach the public - and shape society; therefore, Frontiers only applies the most rigorous and unbiased reviews.
Frontiers revolutionizes research publishing by freely delivering the most outstanding research, evaluated with no bias from both the academic and social point of view. By applying the most advanced information technologies, Frontiers is catapulting scholarly publishing into a new generation.

What are Frontiers Research Topics?

Frontiers Research Topics are very popular trademarks of the Frontiers Journals Series: they are collections of at least ten articles, all centered on a particular subject. With their unique mix of varied contributions from Original Research to Review Articles, Frontiers Research Topics unify the most influential researchers, the latest key findings and historical advances in a hot research area! Find out more on how to host your own Frontiers Research Topic or contribute to one as an author by contacting the Frontiers Editorial Office: frontiersin.org/about/contact

CYTOSKELETAL REGULATION OF IMMUNE RESPONSE

Topic Editors:
Sudha Kumari, Indian Institute of Science (IISc), India
Balbino Alarcon, Spanish National Research Council (CSIC), Spain
Wolfgang W. Schamel, University of Freiburg, Germany

Citation: Kumari, S., Alarcon, B., Schamel, W. W., eds. (2021). Cytoskeletal Regulation of Immune Response. Lausanne: Frontiers Media SA.
doi: 10.3389/978-2-88971-940-2

Table of Contents

frontiers in Cell and Developmental Biology

EDITORIAL
published: 04 November 2021
doi: 10.3389/fcell.2021.791327

Editorial: Cytoskeletal Regulation of Immune Response

Sudha Kumari[1*†], *Wolfgang W. Schamel*[2,3] *and Balbino Alarcon*[4,5]

[1]*The Department of Microbiology and Cell Biology, Indian Institute of Science, Bengaluru, India,* [2]*Department of Immunology, Faculty of Biology, University of Freiburg, Freiburg, Freiburg,* [3]*Centre for Chronic Immunodeficiency (CCI), University of Freiburg, Freiburg, Germany,* [4]*Signaling Research Centers BIOSS and CIBSS, Madrid, Spain,* [5]*Centro de Biología Molecular Severo Ochoa, Consejo Superior de Investigaciones Científicas, Universidad Autónoma de Madrid, Madrid, Spain*

Keywords: immune cell cytoskeleton, actin dynamics, microtubules, immune response, immunological synapse

Editorial on the Research Topic

Cytoskeletal Regulation of Immune Response

Perhaps the most characteristic property of both the adaptive and innate arms of our immune system is the ability to patrol basically the entire organism in search for potentially dangerous intruders, and respond once they are found. This response requires the activation of a complex machinery of intracellular pathways, the release of chemicals and proteins that act as chemoattractants to activate the migration of other cells of the immune system and finally, the coordination of a multicellular response that will lead to the destruction of the intruder. Immune cell mobility, immune cell activation and destruction of the intruder requires a precise spatiotemporal dynamics of the cells' cytoskeleton. For this, the cell's cytoskeleton must rearrange in a highly regulated fashion. Thus it is not surprising that these cells have developed an intricate network of cytoskeletal regulatory proteins which sometimes are exclusively expressed by cells of the immune system.

The cytoskeleton plays a versatile role in immune cells. A testament to this multifunctionality of cytoskeleton is that immune cells harboring mutations in cytoskeletal regulatory proteins often have compromised overall immune response. These defects exist even when the cells are challenged with potent activation signals *ex vivo*, suggesting that the function of the cytoskeleton is much more than just supporting migration to reach the intruder antigen, since a number of crucial immunoreceptor signaling functions are dependent on cytoskeletal organization and dynamics. However, the precise mechanistic roles that cytoskeleton plays in immune cell signaling, especially given that it is the same unit network that would perform all of the functions, remains a mystery.

In this special issue on the cytoskeleton in immune responses we have attempted to explore the reciprocal relationship between cytoskeleton, cellular signaling, and activation. In this issue there are original, opinion, and review articles that deepen our knowledge on the molecular regulation of the cytoskeleton as well as of cellular responses regulated by the cytoskeleton, with a goal to gain insights into the cytoskeleton—intracellular signaling machinery interconnection. These articles address this topic at diverse locations (membrane, nucleus, cytosolic organelles) and scales (molecular, organelle, cellular).

Immunopathies resulting from defects in cytoskeletal regulating proteins such as ArpC, HEM, WASP, WIP, and WDR1 serve as natural perturbations to study the regulation of the cytoskeleton. The review article by Dupré et al. describes how primary immunodeficiencies lead to distinct defects in immune cell function pointing to functional specializations of the cytoskeleton. Role of the actin microfilament NPF Wasp in antigen receptor signaling has been further elaborated in a review by Ngoenkam et al.. An article by Li et al. describes the role of WASP in regulating B cell actin architecture by forming actin-rich "pods"

OPEN ACCESS

Edited and reviewed by:
Philipp Kaldis,
Lund University, Sweden

****Correspondence:***
Sudha Kumari
Kumari.Sudha@gmail.com

†Present Address:
Sudha Kumari,
Koch Institute of Integrative Cancer Research, Cambridge, MA, United States

Specialty section:
This article was submitted to Cell Growth and Division, a section of the journal Frontiers in Cell and Developmental Biology

Received: *08 October 2021*
Accepted: *19 October 2021*
Published: *04 November 2021*

Citation:
Kumari S, Schamel WW and Alarcon B (2021) Editorial: Cytoskeletal Regulation of Immune Response. Front. Cell Dev. Biol. 9:791327. doi: 10.3389/fcell.2021.791327

and cell spreading cells. Defects in WDR1, a regulator of cofilin activity, results in immunodeficiency. A report by Bolger-Munro et al. highlights the role of WDR-1 in actin remodeling and B cell responses.

This special issue covers cytoskeleton regulation and signaling in different lymphocyte types. The review by Ben-Shmuel et al. discusses NK cell cytoskeleton regulation and function, and dissects the role of individual cytoskeletal elements actin, microtubule, and NM-II in it. T cells require adhesion molecules such as integrin for activation, although their precise roles in signaling are not well understood. In a paper by Cassioli et al., the role of the integrin LFA1 at the T cell immunological synapse is explored using expression rescue experiments. The T cell line Jurkat E6.1 cells, which lack LFA1, showed restoration of architecture, signaling and activation when LFA1 was expressed at an adequate level.

Mechanical regulation of immune cell activation has gained popularity, since recent studies support the idea that the mechanical context of molecular interactions can influence the signaling output. In a report by Escolano et al., the authors find that altering the mechanical context of macrophage activation has profound effects on inflammasome signaling. Being a "novel" field the readouts (nature and magnitude of individual forces exerted at the molecular and cellular level) are still limited. A report from Wohl and Sherman uses spectral analysis to quantify ATP-dependent mechanical vibrations of plasma membranes during T cell activation. Further quantitative tools to analyze mechanics in immune cells are discussed by Fritzsche in an opinion article and by Garlick et al. focusing on cutting edge super resolution techniques and on interdisciplinary approaches to extract maximum spatiotemporal signaling information from cells. Along the same theme of using the experimental system to better extract information from cells, a paper by Lee et al. describes a method for the analysis of cell migration as a marker for T cell proliferation potential. In their review article, Record et al. discuss molecular mediators of mechanical force transduction in immune cells and emphasize a need for understanding actin dynamics in not just the cytoplasm of the cell as has been conventionally done, but also in the nucleus of the cell.

Regulation of the cytoskeleton in immune cells also involves uncharacterized and sometimes unconventional players. The precise mechanistic roles of these effectors are not completely clear. In the issue we publish articles that shed light on a few of these crucial players as regulators of subcellular localization and dynamics of filamentous actin. A review by Martín-Cófreces et al. discusses the role of the CCT chaperonin in the remodeling and positioning of the centrosome, and consequently in the dynamics of the immunological synapse. Similarly, a paper by Ibañez-Vega et al. analyses the role of the proteasome adaptor protein ECM 29 in proteosome localization and actin remodeling at the B cell immunological synapse. Another intriguing molecular player characterized here is Glial Matural Factor gamma (GMFgamma). A study by Deretic et al. uncovers a role of GMFgamma in cell spreading and actin remodeling and regtrograde flow at immunological synapse. Finally, a review by Kim et al. consolidates the knowledge about the role of transgelin in filamentous actin stabilization, and, consequently, in the stabilization of cellular microarchitectures such as microvilli.

Together, the issue covers a broad spectrum of articles on the cytoskeletal regulation in immune cells. In the future, we look forward to learn about additional players, novel mechanism on microscale architectures, emergent shape and its connection to cell functions.

AUTHOR CONTRIBUTIONS

All authors listed have made a direct and intellectual contribution to the work, and approved it for publication.

Conflict of Interest: The authors declare that the research was conducted in the absence of any commercial or financial relationships that could be construed as a potential conflict of interest.

Publisher's Note: All claims expressed in this article are solely those of the authors and do not necessarily represent those of their affiliated organizations, or those of the publisher, the editors and the reviewers. Any product that may be evaluated in this article, or claim that may be made by its manufacturer, is not guaranteed or endorsed by the publisher.

frontiers in Cell and Developmental Biology

REVIEW
published: 01 February 2021
doi: 10.3389/fcell.2021.609532

The Role of the Cytoskeleton in Regulating the Natural Killer Cell Immune Response in Health and Disease: From Signaling Dynamics to Function

*Aviad Ben-Shmuel, Batel Sabag, Guy Biber and Mira Barda-Saad**

Laboratory of Molecular and Applied Immunology, The Mina and Everard Goodman Faculty of Life Sciences, Bar-Ilan University, Ramat Gan, Israel

OPEN ACCESS

Edited by:
Sudha Kumari, Massachusetts Institute of Technology, United States

Reviewed by:
Eric O. Long, National Institutes of Health (NIH), United States
Elena Goncharova, University of California, Davis, United States

***Correspondence:**
Mira Barda-Saad
Mira.Barda-Saad@biu.ac.il

Specialty section:
This article was submitted to Cell Growth and Division, a section of the journal Frontiers in Cell and Developmental Biology

Received: *23 September 2020*
Accepted: *11 January 2021*
Published: *01 February 2021*

Citation:
Ben-Shmuel A, Sabag B, Biber G and Barda-Saad M (2021) The Role of the Cytoskeleton in Regulating the Natural Killer Cell Immune Response in Health and Disease: From Signaling Dynamics to Function. Front. Cell Dev. Biol. 9:609532. doi: 10.3389/fcell.2021.609532

Natural killer (NK) cells are innate lymphoid cells, which play key roles in elimination of virally infected and malignant cells. The balance between activating and inhibitory signals derived from NK surface receptors govern the NK cell immune response. The cytoskeleton facilitates most NK cell effector functions, such as motility, infiltration, conjugation with target cells, immunological synapse assembly, and cytotoxicity. Though many studies have characterized signaling pathways that promote actin reorganization in immune cells, it is not completely clear how particular cytoskeletal architectures at the immunological synapse promote effector functions, and how cytoskeletal dynamics impact downstream signaling pathways and activation. Moreover, pioneering studies employing advanced imaging techniques have only begun to uncover the architectural complexity dictating the NK cell activation threshold; it is becoming clear that a distinct organization of the cytoskeleton and signaling receptors at the NK immunological synapse plays a decisive role in activation and tolerance. Here, we review the roles of the actin cytoskeleton in NK cells. We focus on how actin dynamics impact cytolytic granule secretion, NK cell motility, and NK cell infiltration through tissues into inflammatory sites. We will also describe the additional cytoskeletal components, non-muscle Myosin II and microtubules that play pivotal roles in NK cell activity. Furthermore, special emphasis will be placed on the role of the cytoskeleton in assembly of immunological synapses, and how mutations or downregulation of cytoskeletal accessory proteins impact NK cell function in health and disease.

Keywords: natural killer cells, actin, signaling, cytoskeleton, immune response

INTRODUCTION

Natural killer (NK) cells are innate lymphoid cells (ILCs) that constitute a major cellular component of the immune response. They play a pivotal role in eliminating cancerous and virally transformed cells, and may also participate in auto-immune diseases (Vivier et al., 2008). NK cells carry out their effector functions by directly killing target cells and by secreting modulatory cytokines. The

cytotoxic pathway involves the release of lytic granules containing perforin and granzyme-B, or engagement of death receptors expressed on the surface of NK cells such as Fas ligand (FasL) and TNF-related apoptosis-inducing ligand (TRAIL) with cognate ligands expressed on target cells (Zamai et al., 1998; Dustin and Long, 2010). NK cells secrete IFN-γ, TNF-α, and GM-CSF to mediate their cytokine-based effector functions. Cytokines secreted by NK cells recruit and activate additional immune cells such as T-cells, B-cells, macrophages, and dendritic cells (Takeda, 1993; Martín-Fontecha et al., 2004; Walzer et al., 2005; Roetynck et al., 2006), and facilitate elimination of virally transformed target cells and cancer cells (Imai et al., 2000; Lee et al., 2007). In addition to their important roles in the innate immune response, NK cells have also been associated with adaptive immune responses, such as delivering more robust effector functions and proliferation in response to secondary Cytomegalovirus infection (Vivier et al., 2011).

The major mediator of NK cell effector activity is the cytoskeleton. Understanding the molecular regulation of the cytoskeleton in NK cells is critical, since NK cell effector functions are fundamentally linked with the cytoskeletal machinery. NK cells must circulate through blood and lymphatic vessels, traverse into tissues, recognize and eliminate relevant targets while sparing healthy cells, and recruit additional immune cells to relevant sites. Actin, which is the main component of the NK cytoskeleton, undergoes polymerization and depolymerization, from monomeric globular sub-units (G-actin) to ordered filaments (F-actin) and vice-versa during NK cell migration and conjugation with susceptible targets (Carpén et al., 1983). F-actin polymerization in NK cells is a dynamic event that is governed by activating or inhibitory signals delivered from cell surface receptors. Reorganization of the actin cytoskeleton is dependent on the activity of nucleating factors (NFs), which are responsible for direct actin nucleation. The central NFs include the Arp2/3 complex and formins. The activities of NFs are regulated by nucleation promoting factors (NPFs), such as members of the Wiskott–Aldrich Syndrome protein (WASp) family of proteins. Actin de-polymerizing factors, such as Coronin 1A, also play a direct regulatory role in NK cell cytotoxicity (Mace and Orange, 2014), as described below.

Another cytoskeletal component, non-muscle Myosin II (NM-II), the major isoform found in lymphocytes, regulates several functions of T-cells and NK cells. Myosin II utilizes ATP hydrolysis to generate contractile forces on actin filaments (Vicente-Manzanares et al., 2009). In T-cells, NM-II regulates motility (Jacobelli et al., 2004) and may regulate T-cell IS formation and stabilization (Kumari et al., 2012), however, this role remains uncertain (Jacobelli et al., 2004). While the role of Myosin in NK cell IS formation and stability remains an open question, research has revealed its importance in the cytotoxic activity of NK cells through forces exerted on lytic granules (Andzelm et al., 2007) and through regulation of cytoskeletal architecture to expedite degranulation (Carisey et al., 2018).

In addition to actin and Myosin, microtubule filaments play critical roles in NK cell and cytotoxic T cell (CTL) effector function. Microtubules are composed of alpha and beta tubulin heterodimers, and similarly to actin, undergo dynamic assembly and disassembly, which is regulated by a wide range of microtubule associated proteins (MAPS) (Akhmanova and Steinmetz, 2015). Microtubules facilitate the delivery of lytic granules to the synaptic cleft between NK cells and target cells, either directly through the centrosome or through microtubule associated motor proteins (Chen et al., 2006; Stinchcombe et al., 2006). Though studies explored microtubule-organizing center (MTOC) polarization in T-cells and possible roles the MTOC may play in maintaining IS stability (Kloc et al., 2014), it remains unclear if similar factors influence MTOC polarization in NK cells, and what other roles microtubule dynamics might serve at the NKIS aside from cargo delivery to the synaptic cleft.

It is well established that activating or inhibitory pathways differentially impact cytoskeletal rearrangement at the NKIS, yet the reciprocal role of cytoskeletal dynamics on NK signaling and maintenance of the activation threshold remains incompletely understood. Studies have, for example, suggested reciprocity in actin signaling in the context of integrin adhesion molecules. The integrin lymphocyte function-associated antigen 1 (LFA-1) induces "outside-in" signaling to promote actin polymerization during NK cell adhesion to target cells, and this actin polymerization subsequently increases LFA-1 mediated adhesion (Hoffmann et al., 2011). F-actin exerts physical forces on LFA-1 at the T-cell IS, ultimately influencing LFA-1 conformation during immunological synapse formation (Comrie et al., 2015a). F-actin dynamics may also exert forces on intracellular signaling molecules to impact NK cell output (Matalon et al., 2018). Thus, instead of merely acting as a static scaffold, the cytoskeleton may potentially possess a signaling role in NK cells via mechanotransduction. Moreover, an additional important question is how different cytoskeletal architecture at the NKIS influences signaling intensity and effector function. As we will discuss below, emerging super resolution imaging techniques are beginning to address this question, and demonstrate how distinct cytoskeletal arrangements influence receptor signaling and NK cell activation, with possible implications for NK cell priming and peripheral tolerance.

Due to the critical roles of the cytoskeleton in lymphocyte function, defects in cytoskeletal components may be detrimental to immune responses (described in detail below). Inhibition of actin polymerization has been shown to cause major defects in NK cell effector functions (Katz et al., 1982; Orange et al., 2002), and various immune deficiencies and diseases are attributed to defects of the cytoskeleton in immune cells (Matalon et al., 2013). Disorders affecting actin assembly in NK cells such as deficiencies in dedicator of cytokinesis 8 (DOCK-8), or in WASp, severely hamper NK cell responses (Orange et al., 2002; Mizesko et al., 2013). Myosin mutations have been shown to cause defects in NK cell activity in May-Hegglin anomaly patients (Sanborn et al., 2009). Furthermore, mutations that interfere with MTOC polarization to the IS also cause NK cell immunodeficiency in Hermansky–Pudlak syndrome subset 2 (HPS2) patients (Fontana et al., 2006).

In this review, we highlight the importance of the major cytoskeletal components for NK cell function. We emphasize how each cytoskeletal unit impacts different effector functions, and how together, they integrate to affect NK cell output.

Furthermore, we address how cytoskeletal dynamics impact the architecture of the NKIS, and how they might also be involved in directly regulating signaling and tuning of the NK cell activation threshold. Finally, we discuss how dysregulation of the cytoskeleton results in primary immune deficiencies.

ACTIN CYTOSKELETON – A KEY SIGNAL TRANSDUCER AND REGULATOR OF NK ACTIVATION

NK Signaling Cascades Leading to Cytoskeletal Recruitment and Reorganization

Natural killer cells express a large variety of germline-encoded receptors that regulate the immune response (Lanier, 1998). Importantly, cooperative signaling through ligation of activating receptor pairs (co-activation) appears necessary to fully stimulate NK cell activity (Bryceson et al., 2006; Kim et al., 2010). Signaling pathways in NK cells operate downstream of immunoreceptor tyrosine-based activation motifs (ITAMs) – and ITAM-independent motifs expressed on adaptor accessory molecules (Vély and Vivier, 2005). Ultimately both ITAM dependent and independent pathways initiate signaling cascades which affect actin polymerization and rearrangement, and converge into a cascade involving mitogen-activated protein kinases (MAPK), which are responsible for eliciting NK cell effector functions (Watzl and Long, 2010) (**Figure 1**).

The ITAM Pathway

The ITAM dependent pathway propagates downstream to activating receptors such as the activating killer-cell immunoglobulin-like receptor (KIR2DS), CD16, and the natural cytotoxicity receptors [NCRs- NCR1 (NKp46), NCR2 (NKp44) and NCR3 (NKp30) (Moretta et al., 2002)], which are associated with adaptor proteins such as CD3ζ, FceRIγ, and DAP12 (Lanier, 2003).

The SH2 domain containing leukocyte protein of the 76 kDa (SLP-76) adaptor protein promotes actin reorganization by facilitating interactions between VAV1, which is a guanine nucleotide exchange factor (GEF) for the Rho protein family, and the non-catalytic adaptor region of tyrosine kinase adaptor protein 1 (Nck) (Barda-saad et al., 2010; Pauker and Barda-Saad, 2011). Since VAV proteins serve as GEFs for the Rho GTPases Rac1 and Rho family GTPase Cdc42, which are critical for actin reorganization (Tapon, 1997), impairment of their activity has critical effects on NK effector function (Billadeau et al., 1998; Cella et al., 2004; Graham et al., 2006). During ITAM dependent signaling in NK cells, linker for activation of T cells (LAT) (Jevremovic et al., 1999; Matalon et al., 2016) and SLP-76 (Binstadt et al., 1998) couple upstream signaling events to downstream signaling proteins and complexes, which induce actin rearrangement. LAT was also shown to be a critical factor in NK cell activation by facilitating Phospholipase C-gamma (PLCγ) recruitment to the cell membrane (Jevremovic et al., 1999).

An additional signaling molecule that mediates actin reorganization at the NKIS is phosphatidylinositol 3-kinase (PI3K) (Cella et al., 2004). PI3K catalyzes production of phosphatidyl-inositol-3, 4,5-trisphosphate (PIP3), which is important for the recruitment of PH domain-containing proteins such as PLCγ and VAV1 (Han, 1998) to the immunological synapse. In NK cells, PI3K induces actin reorganization via STKs p21-activated kinase 1 (PAK1) (Papakonstanti and Stournaras, 2002).

ITAM Independent Pathways

In contrast to ITAM dependent cascades, NKG2D signaling is independent of LAT (Billadeau et al., 2003). The NKG2D receptor is associated with the DAP10 adaptor, which expresses a YINM motif (Upshaw et al., 2006). DAP10 can directly bind PI3K and the Grb2 adaptor. Grb2 recruits VAV1, initiating downstream actin re-organization. SLP-76 phosphorylation plays a crucial role in NK cell intracellular calcium level elevation, and activation in the context of NKG2D and 2B4 signaling. This activation causes a substantial increase in the phosphorylation of VAV1, leading to actin rearrangement (Kim and Long, 2012). Additional receptors that do not operate through ITAM motifs contain immunoreceptor tyrosine base switch motifs (ITSM) on their cytoplasmic tails, such as the receptor, 2B4 (Sidorenko and Clark, 2003). These signaling lymphocytic activation molecule (SLAM) family receptors can bind adaptors such as SLAM-associated protein (SAP) (Sayos et al., 1998) and Ewing's sarcoma-associated transcript-2 (EAT-2) (Eissmann and Watzl, 2006) (in humans). SAP can activate NK cells by recruiting the Protein Tyrosine Kinase (PTK), Fyn (Latour et al., 2003). Fyn subsequently phosphorylates and activates VAV1, or phosphorylates and inactivates the SH2 domain-containing inositol 5′ phosphatase-1 (SHIP-1) (Eissmann et al., 2005; Dong et al., 2012). EAT and SAP provide synergistic effects for 2B4 activation, as double SAP/EAT-2 deficient mice displayed greater 2B4 mediated inhibition than those deficient in one of the adaptors alone (Dong et al., 2012); these activities include phosphorylation and activation of LAT, VAV1, PLCγ1, and Grb-2 (Watzl et al., 2000; Chen et al., 2004), which are involved in actin polymerization and rearrangement.

Integrin Signaling

LFA-1 engagement with its cognate ligand, intercellular adhesion molecule 1 (ICAM-1) results in tyrosine phosphorylation of VAV1, which increases when both LFA-1 and the 2B4 are engaged with their ligands (Riteau et al., 2003). Additional cascades downstream to LFA-1 engagement in NK cells include tyrosine phosphorylation of T cell antigen receptor (TCR) ζ-chain, Syk, paxillin, and PLC-γ1/2 (March and Long, 2011), leading to the actin dependent process of granule polarization to the NKIS. Paxillin phosphorylation by proline-rich tyrosine kinase-2 (Pyk2) in NK cells was also shown downstream to β1 integrins (Gismondi et al., 1997). Furthermore, following engagement of LFA-1 with ICAM-1, the focal adhesion (FA) protein talin localizes to sites of LFA-1 engagement. Talin recruits Arp2/3, and binds phosphatidylinositol 4-phosphate 5-kinase (PIPKI). This leads to a local increase in phosphatidylinositol-4, 5-bisphosphate PIP(2), recruiting WASp, which facilitates actin

polymerization through Arp2/3 (Mace et al., 2010). Zhang et al. (2015) additionally elucidated the signaling pathways leading to actin rearrangement downstream to the DNAX accessory molecule-1 (DNAM-1) receptor, which contains a tyrosine and asparagine based ITT-like motif. In this pathway, triggering of DNAM-1 leads to phosphorylation of the ITT motif by a Src family kinase, recruitment of the adaptor Grb2, and activation of VAV1 and PLCγ-1, leading to actin rearrangement (Zhang et al., 2015).

WASp and WIP Mediated Regulation of NK Cell Cytoskeletal Dynamics and Function

Nucleating factors, such as Arp2/3 and formins, directly affect actin polymerization, and nucleation-promoting factors such as WASp and the WASp-family verprolin-homologous protein (WAVE) bind and regulate actin nucleating factors through verprolin, central, acidic (VCA) domains (Chereau et al., 2005). The central NPF families include WASp, WAVE, SCAR homolog (WASH), the WASp homolog associated with actin, membranes and microtubules (WHAMM), and the junction-mediating and -regulatory protein (JMY). The Arp2/3 complex promotes cross-linking of actin filaments, and thereby promotes formation of an actin meshwork at the leading edge of cells (Mullins et al., 1998). This activity by Arp2/3 drives cell motility and spreading at the NKIS (Butler and Cooper, 2009). Recent super resolution microscopy experiments (described in the following sections) also revealed that Arp2/3 branching activity at localized actin structures (actin puncta) at the NKIS mediated actin remodeling, which facilitates cytotoxicity (Carisey et al., 2018). Formins aid in the creation of a subset actin filaments that are not barbed and have specific functions- such as the creation of stress fibers and endosome trafficking, as well as formation of filopodia and micro-spikes at the edge of the expanding cell membrane (Gasman et al., 2003; Wallar and Alberts, 2003). Formins play various roles in T-cell synapse architecture and dynamics (Eisenmann et al., 2007; Gomez et al., 2007; Murugesan et al., 2016), however in NK cells, the function of formins has not been as extensively explored. It does appear, however, that formin family members such as hDia1 facilitate NK cell adhesion, chemotaxis, and chemokine-induced signaling (Butler and Cooper, 2009), in addition to promoting microtubule dependent movement and polarization of cytolytic granules (Butler and Cooper, 2009).

WASp

WASp contains several domains that dictate its function and regulation: WASp homolog (WH1) domain, a basic region (B), GTPase binding (GBD) domain, poly proline region, and a VCA domain (Thrasher and Burns, 2010). Under basal conditions, the WASp VCA domain lies in close proximity to the GBD domain, inhibiting binding of Arp 2/3 (Kim et al., 2000). Binding of GTP-Cdc42 to the WASp GBD domain releases WASp from auto inhibition, and enables binding of Arp2/3 to the VCA domain and initiation of actin nucleation (Abdul-Manan et al., 1999). Phosphorylation of tyrosine 291 (Tyr 291) in the GBD domain was also shown to augment WASp activity (Cory et al., 2002).

Upon NK cell activation, WASp forms a multi-protein complex with WASp-interacting protein (WIP), actin, and Myosin, and these associations are abrogated during NK cell inhibition (Krzewski et al., 2006). Moreover, NK cell stimulation (either through CD16 or through chemokine receptors and β_1 and β_2 integrin families) leads to WASp phosphorylation, strongly suggesting that these mechanisms are required for WASp dependent NK cell cytotoxicity (Orange et al., 2003; Gismondi et al., 2004; Andzelm et al., 2007; Stabile et al., 2010). In murine NK cells, engagement of LFA-1 with ICAM-1 results in WASp recruitment to the site of contact, activation of Arp2/3, and actin polymerization at the LFA-1 contact site (Mace et al., 2010).

WASp impacts multiple facets of NK cell activity which depend on cytoskeletal turnover, such as migration, IS formation, and cytotoxicity. An absence of WASp in NK cells disrupts formation of the typical cytotoxic NKIS due to a significant decrease in actin accumulation (Orange et al., 2002), and also leads to a reduction in lytic granule polarization and NK cytotoxicity (Orange et al., 2002; Huang et al., 2005). NK cells also require the function of integrins and other adhesion molecules to create conjugates with target cells and stabilize the NKIS (Davis, 2009). Studies employing NK cells with WASp mutations that lead to a low yet detectable level of WASp, and WASp mutations that completely abrogate WASp expression demonstrate a decrease in the ability of NK cells to form conjugates and hence to initiate targeted cytotoxicity; these findings suggest a possible regulatory role for WASp in cytoskeleton organization which may affect adhesion molecules on the NK cell membrane (Gismondi et al., 2004). A reciprocal regulatory mechanism may exist between WASp and actin turnover, because treatment of NK cells with cytochalasin D, an actin polymerization inhibitor, results in decreased WASp, F-actin, and perforin accumulation at the activating NKIS (Boztug et al., 2008). These results suggest a positive feedback mechanism in which WASp-dependent actin polymerization is responsible for further accumulation of WASp at the NKIS. In T cells, WASp plays a role in formation of dense actin centers, or "actin foci," which enhance downstream signaling. It would be informative to study whether WASp functions similarly in NK cells to promote formation of actin foci at the NKIS, as dense actin puncta are observed during NK cell activation and degranulation (Carisey et al., 2018), and nanoscale organization of NK cell receptors are also dependent on local cytoskeletal dynamics (Pageon et al., 2013b).

Impaired WASp activity also negatively impacts NK cell motility. NK cells from WAS and XLT patients demonstrate impaired ICAM-1, VCAM-1, and endothelial cell mediated migration (Stabile et al., 2010). The defective chemokine induced migration of these cells is correlated with reduced expression of the activated form of the β_2 integrin subunit, and the decreased adhesion to ICAM-1 and VCAM-1. Thus WASp signaling pathways are essential for NK cell LFA-1-mediated migration in response to chemokine receptor-induced inside-out signaling (Stabile et al., 2010).

Defects in cytotoxicity, cytokine secretion, and migration in WASp knockout NK cells may also be due in part to upregulation of NK cell checkpoint markers, which might down modulate the NK cell response, such as LAG-3 and KLRG1 (Kritikou et al., 2016). It appears, however, that IL-2 uptake by NK cells bypasses defects in WASp expression (Gismondi et al., 2004), suggesting alternative mechanisms which compensate for WASp function, probably through WAVE-2 actin reorganization (Orange et al., 2011). Nonetheless, WASp function is critical for NK cell effector activity, and its loss in NK cells was also recently shown to promote tumor growth *in vivo* (Catucci et al., 2014).

WIP

WIP functions as a WASp stabilizing protein, and prevents WASp degradation in immune cells (de la Fuente et al., 2007; Noy et al., 2012; Pauker et al., 2012; Reicher et al., 2012; Fried et al., 2014b). Mutations in the WASp WH1 domain, which mediates its interaction with WIP, are associated with several phenotypes in WAS patients (Imai et al., 2003). As mentioned above, NK cell activation induces formation of a multi protein complex consisting of WASp, WIP, actin, and Myosin (Krzewski et al., 2006) which facilitates actin reorganization and NK cell effector function. WIP is crucial for formation of this complex, as it recruits NM-IIA and actin to the complex, and disruption of its expression abrogates complex formation. WIP also has its own distinct role in NK cell cytotoxicity; WIP knockdown results in a significant reduction of cytotoxicity, while WIP overexpression enhances NK cell activity (Krzewski et al., 2006). The role of WIP in NK cell cytotoxicity is suggested to result from WIP colocalization with lytic granules in both resting and activated NK cells, a process that was shown to be independent of WASp (Krzewski et al., 2008; Fried et al., 2014a). WIP knockdown inhibits the observed granule polarization upon NK cell activation, suggesting that co-localized WIP and lytic granules are polarized to the NKIS in a WIP-dependent fashion. In contrast to WASp deficiency, knockdown of WIP does not disrupt NK cell conjugation to their targets, thereby indicating that WASp and WIP have distinct functions in the control of NK cell cytotoxicity.

Additional Factors Mediate Cytoskeletal Reorganization at the NKIS

Other cytoskeletal regulators have been described in the context of NK cell activity, albeit not extensively. WAVE is a WASp family protein that also regulates cytoskeletal re-arrangement (Miki et al., 1998). The WAVE2 isoform is the most abundant isoform in hematopoietic cells (Suetsugu et al., 1999). The VCA region of WAVE2 is implicated in binding Arp2/3 and actin monomers, subsequently leading to induction of actin polymerization (Takenawa and Suetsugu, 2007). Experiments in T-cells demonstrated an important role for WAVE2 in actin re-organization and adhesion; WAVE2 was shown to migrate to the IS, and WAVE2 gene silencing leads to a decrease in actin polymerization, decreased lamellopodia formation during T-cell spreading, and reduction in the ability of T-cells to form conjugates with targets (Nolz et al., 2006, 2007, 2008; Sims et al., 2007; Reicher et al., 2012; Pauker et al., 2014). In NK cells, WAVE2 activity has not been extensively studied. WAVE2 can compensate for WASp deficiency, as IL-2 administration bypasses WASp inactivity (either in WAS patients or in WASp deficient and inhibited NK cells) by activating WAVE2, thereby restoring actin polymerization at the NK cell IS and restoring NK cell cytotoxic activity (Orange et al., 2011). This suggests a bypass mechanism(s) in NK cells, operating through IL-2 to ensure actin assembly.

The DOCK GEFs, DOCK2, DOCK8, and RAS guanyl-releasing protein 1 (RASGRP1), are also cytoskeletal regulating proteins, which were shown to play roles in NK cell actin rearrangement. DOCK2 functions as a GEF for the Rho family protein Rac (Brugnera et al., 2002). DOCK2 deficient NK cells lose cytotoxic capacity against target cells due to impaired actin polymerization and subsequent lytic synapse formation (Sakai et al., 2013). DOCK8 functions as a GEF for Rac and CDC42 (Harada et al., 2012). In NK cells, DOCK8 interacts with talin and WASp, and DOCK8 deficiency also results in impaired NK cell cytolytic function and adhesion due to impaired F-actin accumulation at the NKIS (Ham et al., 2013; Mizesko et al., 2013). RASGRP1 serves as a GEF for Ras GTPase, thereby promoting lymphocyte activation and differentiation (Roose and Weiss, 2000; Stone et al., 2000). Recent studies in a young patient with RASGRP1 deficiency demonstrated impaired immune cell functions in T, B, and NK cells (Salzer et al., 2016). The patient's NK cells produced normal amounts of the effector granzyme B and perforin proteins, but demonstrated impaired cytotoxic ability due to defective IS formation. This defective IS was characterized by poor F-actin accumulation, MTOC polarization, and recruitment of lytic granules at the MTOC.

Additional cytoskeletal regulatory proteins such as WASH, hematopoietic lineage cell-specific protein 1 (HS1), and IQ domain-containing GTPase-activating protein 1 (IQGAP1) were identified to play roles in NK cell effector activity by regulating lytic granule dynamics, IS assembly, trans endothelial migration (Butler et al., 2008; Kanwar and Wilkins, 2011; Mukherjee et al., 2015; Huang et al., 2016; Abel et al., 2018). Further study is required to better understand how these proteins operate in the context of NK cell effector activity.

Coronin 1A

In addition to factors promoting actin polymerization, actin de-polymerizing proteins are also critical for actin rearrangement, as actin assembly and disassembly are the two opposing processes that drive actin dynamics at the NKIS. Moreover, since lytic granules must traverse a dense actin network at the NKIS in order to reach their destination, a regulated mechanism must exist to promote localized actin disassembly. As mentioned above, Coronin 1A, a hematopoietic regulator of actin, which promotes actin disassembly (Kueh et al., 2008), plays a critical role in NK cell cytotoxicity. Coronin 1A associates with Arp2/3 and inhibits its function, while stimulating Cofilin activity, thereby promoting actin filament de-polymerization (Humphries et al., 2002; Kueh et al., 2008). Specifically, Coronin 1A was shown to localize at the NKIS and reconstruct the actin meshwork to permit lytic granule release (Mace and Orange, 2014). Cells lacking Coronin 1A display impaired lytic granule release and

thus cytotoxic deficiencies due to their inability to induce target cell death (Mace and Orange, 2014). The presence of an actin de-polymerizing factor such as Coronin 1A at the activating NKIS, where significant actin recruitment and assembly takes place, highlights the complex and dynamic nature of actin regulation that ensures NK cell effector functions. This mechanism may also safeguard against potential bystander cell cytotoxicity by limiting the space of lytic granule delivery at the synaptic cleft. Coronin 1A and other actin de-polymerizing factors may also play an opposing role at inhibitory NK cell synapses where actin assembly and dynamics differ greatly. It is possible that the mode of regulation at the inhibitory NKIS involves not only simply blocking activating signals of actin nucleation, but also deconstructing the existing actin architecture in order to ensure target cell survival.

THE ACTIN CYTOSKELETON AND NK CELL FUNCTION

NK Cell Motility and Infiltration

Natural killer cells must retain high motility to navigate through the circulatory system and tissues and reach areas of infection (Timonen, 1997). NK cells are exceedingly motile, an important characteristic that facilitates movement through lymphoid organs and their ability to patrol peripheral tissues and organs for immuno-surveillance (Garrod et al., 2007). Migrating leukocytes change morphologically during migration as a result of actin dynamics as well as contraction of acto-Myosin-associated arcs [curved bundles of actin filaments with a periodicity of Myosin and alpha-actinin (Tojkander et al., 2012)], creating a leading edge rich in F-actin known as the lamellipodium, and a trailing edge poor in F-actin and rich in adhesion molecules known as the uropod (Vicente-Manzanares and Sánchez-Madrid, 2004). Several studies demonstrate the impaired motility of NK cells when cytoskeletal integrity is compromised. This is especially evident in NK cells deficient in WASp and other critical cytoskeletal regulators such as RASGRP1 and DOCK2 as will be described in more detail in the next sections. Artificial down modulation of actin dynamics through inhibition of Arp2/3 or hDia1, abrogates NK cell chemotaxis (Butler and Cooper, 2009) and recent studies examining pathological conditions such as aging and cancer additionally show that NK cells from aged mice contain lower levels of β-actin, reducing their migration to draining lymph nodes during viral infection (Duan et al., 2017). In a further example, down modulation of F-actin polarization in NK cells by colon tumors serves to inhibit NK cell migration (Wang et al., 2016). NK cells must also attach to blood vessels and cross endothelial barriers to reach target tissues. Attachment of the NK cells to endothelial cells occurs through NK cell adhesion molecules such as the integrins LFA-1 and very late antigen-4 (VLA-4), which bind to endothelial markers such as ICAM-1 and VCAM-1, respectively (Allavena, 1991; Fogler et al., 1996). To effectively infiltrate tissues, cellular actin reorganization must occur to generate proper forces to "squeeze" the cell through the narrow spaces of the endothelium (Worthylake and Burridge, 2001; Lämmermann et al., 2008). Blocking F-actin reorganization induced by the chemokines CX3CL1 and CCL26 prevents NK cells from undergoing the morphological changes required for proper tissue extravasation (El-Shazly et al., 2013). Accordingly, HS1 deficiency in NK cells also down regulates their capacity for trans-endothelial migration (Mukherjee et al., 2015).

Few studies examined the role of Myosin motor function in NK motility. It is possible that the balance between activating and inhibitory signaling in NK cells regulates Myosin activity to promote a stop signal, i.e., inducing NKIS formation instead of NK cell migration, as is the case for F-actin (Culley et al., 2009). Further studies could show the distribution of Myosin in NK cells and whether, in analogy to migrating T-cells, it is situated in the uropod of motile cells, and could elucidate how NK cell activation and IS formation influence Myosin placement and activity.

Organization of Signaling Receptors at the Activating NKIS

The creation of the NKIS requires intimate contact between the NK cell and its target. Large scale rearrangement of the actin cytoskeleton at the NKIS serves multiple purposes (Vyas et al., 2001) (**Figure 2**), namely (a) adhesion between the NK cell and the target cell to ensure the longevity and stability of the contact, (b) assembly of signaling complexes, and (c) controlled killing of the target cell (Vyas et al., 2002b). The NKIS shares some characteristics with the T-cell IS, though it is also characterized by its own distinct features, and performs several functions to properly integrate signals that identify transformed or virally infected cells (**Figure 3**). These include receptor-ligand recognition, creation of signaling clusters for signal enhancement, co-stimulation by co-stimulatory ligands, directed cytotoxicity, cell to cell protein transfer, signal termination, and in the case of inhibitory synapses that promote tolerance, inhibition of activation (Orange, 2008).

The T-cell IS contains areas with distinct protein compositions and actin dynamics, termed supramolecular activation clusters (SMACs). The SMACs roughly correspond to areas of distinct actin reorganization that are observed in migrating cells; the outermost peripheral "ring" known as the distal SMAC (dSMAC) and the more inner ring called the peripheral SMAC (pSMAC) may be analogous to the lamellipodium and the lamellum, respectively (Dustin et al., 2010). Thus, the dSMAC is rich in Arp2/3 and cofilin, leading to cycles of protrusion and retraction (Sims et al., 2007), and tropoMyosin localizes in the pSMAC where actoMyosin networks provide contractile forces and adhesion molecules mediate attachment to the substrate (Ponti et al., 2004; Sims et al., 2007). The central SMAC (cSMAC) can be divided into two areas: the endo-cSMAC where TCR and CD28 signaling persist, and the exo-cSMAC, which is an actin-depleted zone containing TCR-rich extracellular vesicles that bud from the plasma membrane, and where the signaling region terminates (Choudhuri et al., 2014; Dustin, 2014). Initially, the immature activating T-cell IS contains vital signaling molecules such as the TCR in the peripheral SMAC (pSMAC) and adhesion molecules in the cSMAC of the synapse; during IS maturation, the dominant signaling molecules (i.e., TCR–MHC peptide interactions) migrate toward the center of the synapse, and

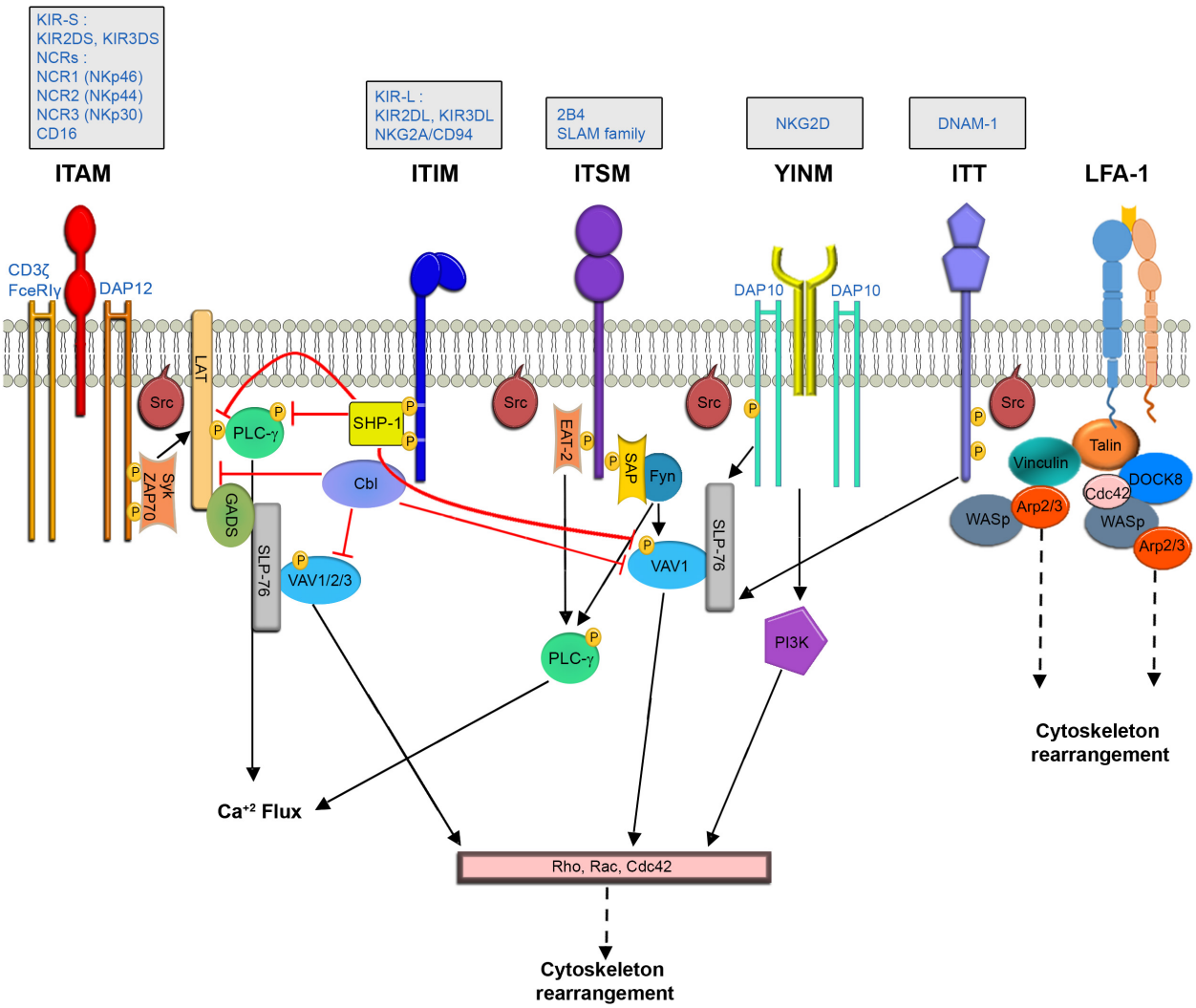

FIGURE 1 | NK Cell signaling pathways leading to cytoskeletal rearrangement.

the adhesion molecules (LFA-1-ICAM-1 interactions) localize in the pSMAC, while the CD45 membrane tyrosine phosphatase localizes in the distal SMAC (dSMAC) (Monks et al., 1998; Johnson et al., 2000). Ligation of TCR with MHC:peptide complexes induces formation of TCR micro-clusters which ultimately initiate a protein tyrosine kinase cascade resulting in T-cell activation (Dustin, 2014). Proper assembly of the IS, and subsequent signaling cascade initiation are thus highly dependent on actin reorganization (Barda-Saad et al., 2005; Yi et al., 2012; Hammer et al., 2019). The T-cell IS is characterized by rapid actin turnover at the dSMAC driven by WAVE2 and Arp2/3 activity, arcs of contracting actin filaments and Myosin at the pSMAC, which are generated by formin activity at the outer edge of the IS, and an actin poor cSMAC (Murugesan et al., 2016; Hammer et al., 2019). Additional structures at the T-cell IS include actin foci at the dSMAC and pSMAC generated via WASp and Arp2/3, which were shown to activate T-cells through the PLCγ pathway (Kumari et al., 2015).

The activating NKIS involves the accumulation of F-actin at the cell–cell junction, eliciting morphological changes in the NK cell and creating a radially symmetric and stable contact site (Orange et al., 2002; Wulfing et al., 2003; Culley et al., 2009) that is composed of the pSMAC and the cSMAC. Collectively, the formation of the activating NKIS consists of two major steps: (1) rapid accumulation of F-actin and integrins in the pSMAC, and (2) slow polarization of the cytolytic proteins, e.g., perforin and other key signaling molecules (Davis et al., 1999). The NK cell activating synapse initiates formation of a dense ring of actin, LFA-1, and talin-1 around the cSMAC (Vyas et al., 2001). This primary actin-induced spreading response is very sensitive to the balance between activating and inhibitory ligands; inhibitory ligands were shown to inhibit the spreading response even if it was already initiated under activating conditions (Culley et al., 2009; Abeyweera et al., 2011). Accumulation of signaling molecules at the NKIS was shown to enhance NK signaling (Varma et al., 2006; Giurisato et al., 2007). F-actin polymerization

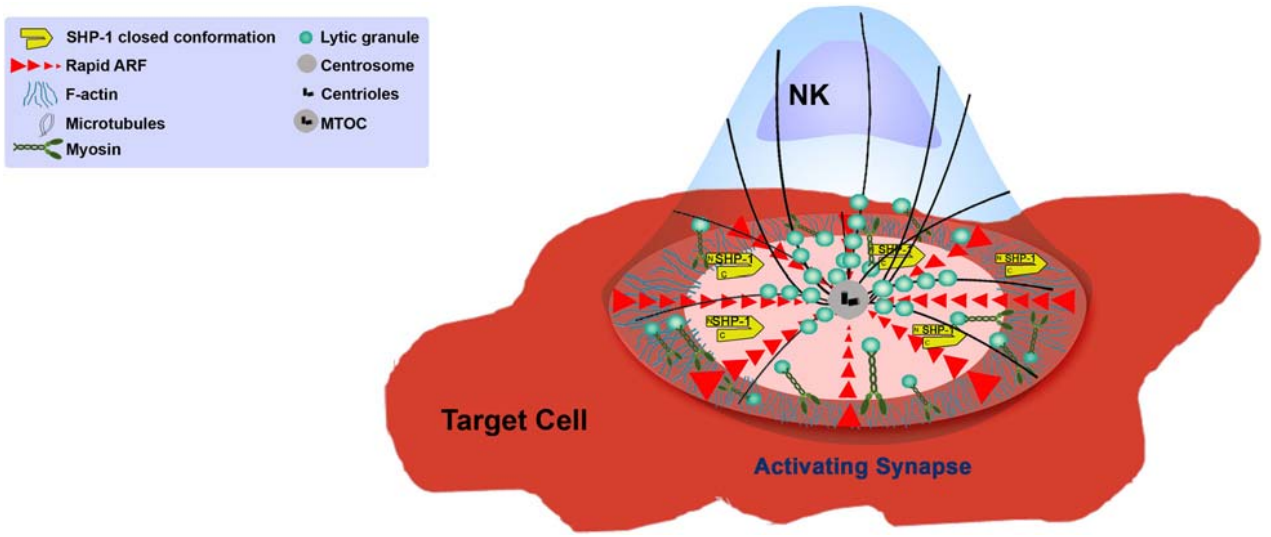

FIGURE 2 | Function of the NK cell cytoskeleton during activation.

is thought to play an important role in this signaling cluster assembly. In particular, LFA-1, MAC-1 and CD2 function as adhesion molecules in NK cells, and were shown to depend on actin polymerization for polarization and clustering at the IS (Orange et al., 2003). In addition, the 2B4 receptor is expressed on NK cells and plays a role in generating cytotoxicity and cytokine production (Nakajima et al., 1999), and it was shown that its recruitment and phosphorylation are dependent on actin dynamics (Watzl and Long, 2003). Accordingly, considering the vast and versatile function of actin in the formation and function of the IS, accumulation of F-actin at the IS decreases in the presence of actin inhibitors or in the absence of crucial actin regulators such as WASp, leading to a decrease in adhesion necessary for conjugate formation and cytotoxicity (Orange et al., 2002; Wulfing et al., 2003).

The mechanisms by which NKIS architecture influences NK cell signaling (both activation and inhibition) are complex given the large array of activating and inhibitory receptors and co-receptors. Elucidation of the organization of signaling molecules at the NKIS was facilitated through utilization of advanced and super resolution microscopy experiments. Oszmiana et al. (2016) demonstrated that the activating receptor KIR2DS1 and the DAP12 signaling adaptor associate during receptor ligation, generating large receptor clusters. These large clusters favor phosphorylation of ZAP-70 and NK cell activation (Oszmiana et al., 2016). Thus, it appears that the size of signaling clusters affects signal strength and sways NK cells toward either activation or inhibition. It is possible that these mechanisms occur to overcome large intervals between ligands on target cells, because activation of NK cells decreases with increased spacing of ligands for CD16 (Delcassian et al., 2013). NKG2D was also previously shown to organize into microclusters at the activating NKIS, and this organization depends on actin remodeling (Abeyweera et al., 2011). Furthermore, recent studies also elucidated the organization of the NKG2D receptor on the surface of NK cells following stimulation of its ligands, MHC class I polypeptide-related sequence A (MICA) or UL16 binding protein 1 (ULBP1) (Bálint et al., 2018). ULBP1, and not MICA, induces large complexes of NKG2D and the IL-2/15 receptor subunits, demonstrating the ability of different ligands to differentially activate NK cells. The different organization of NKG2D in response to its ligands could potentially be due to its different affinities for ULBP1 and MICA, however, this remains unclear. In addition, NKp46 appears to cluster during NK cell stimulation (Hadad et al., 2015), and CD16 also forms clusters upon NK cell stimulation that are eliminated during inhibition of actin cytoskeletal reorganization (Liu et al., 2012). It is still incompletely understood how distinct cytoskeletal structures mediate the different organizations of NK cell receptors in response to different ligands. As discussed in the following sections, multiple studies implemented advanced microscopic techniques that delineated novel cytoskeletal structures at the NKIS; these structures proved indispensable for proper NK cell activity. Therefore, the arrangement of receptors may be linked to the observed cytoskeletal organization at different synapses. It is possible that distinct actin architectures at the NKIS enhance or reduce signaling propagation by influencing organization of particular receptors.

Cytotoxicity

Myosin

NM-II is a motor protein, which belongs to a class of molecular motor proteins that transduce cellular free-energy into motion. There are three members of non-muscle Myosin II family: Myosin IIA, Myosin IIB, and Myosin IIC (Maravillas-Montero and Santos-Argumedo, 2012).

The dominant Myosin isoform present in hematopoietic cells is non-muscle Myosin IIA (NM-IIA) (Maravillas-Montero and Santos-Argumedo, 2012). NM-IIA is a

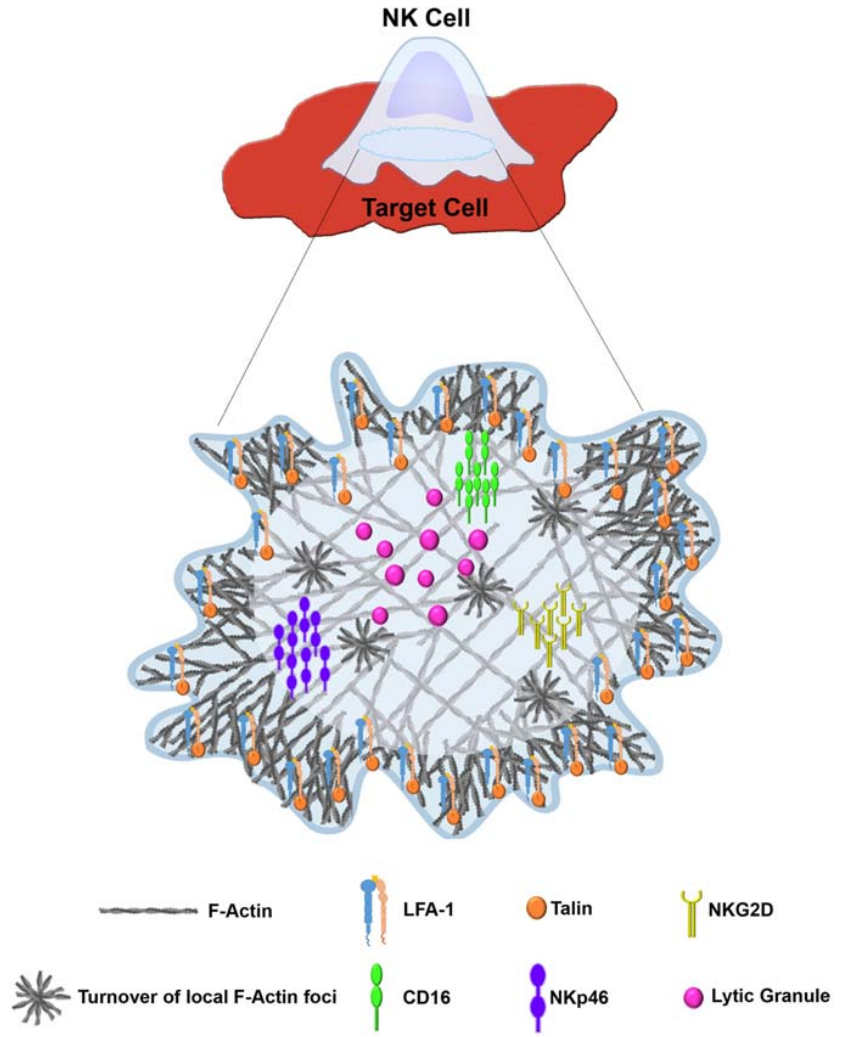

FIGURE 3 | Distinct architecture of the lytic NKIS. Figure was generated using BioRender (https://biorender.com).

hexamer that contains two heavy chains with globular "heads" in the N terminus that bind actin filaments and mediate ATPase activity, which drives contractile forces along actin filaments. The two regulatory light chains (RLC) and two essential lights chains (ELC) regulate Myosin function and structural stability, respectively (Vicente-Manzanares et al., 2009).

Several studies examined the activation induced role and regulation of Myosin at the NKIS. As mentioned above, activation of NK cells induces formation of a multiprotein complex comprised of Myosin with WIP, WASp, and actin (Krzewski et al., 2006). In the same study, inhibitory signals abrogated the recruitment of Myosin and actin to WIP/WASp. Myosin recruitment to this complex, and subsequent recruitment to the NKIS, was shown to depend on WIP. When this multiprotein complex was disrupted, NK cytotoxic potential was greatly decreased. It was suggested that Myosin motor function may aid in recruiting WASp and WIP to the NKIS, where further actin polymerization and branching occur. It is also possible that Myosin can be recruited through the WIP/WASp complex by actin to the NKIS, and associates at the interface with lytic granules for directed granule secretion. This would also explain the loss of cytotoxicity upon abrogation of the complex.

Andzelm et al. (2007) demonstrated that while Myosin is crucial for the exocytosis of lytic granules at the NKIS, it is dispensable for NK/target cell conjugation and NKIS formation. In terms of NKIS maturation in this study, only CD2, perforin, and actin accumulation were assessed. It would be interesting to examine, in a similar fashion, if important downstream signaling molecules crucial for activation are impacted as a result of NM-IIA inhibition. It is possible that though conjugation is seemingly unaffected, reduction in NK cell cytotoxicity is also a result of impaired signaling resulting from NM-IIA ATPase activity. Further studies evaluating the role of NM-IIA dynamics on NK cell signaling will need to be conducted to answer these questions. The mechanism by which NM-IIA facilitates NK cell cytotoxicity was subsequently shown by Sanborn et al. (2009),

who demonstrated that NM-IIA physically associates with lytic granules and augments granule association with actin filaments at the IS; this process ultimately expedites granule release at the synaptic cleft. Mechanistically, the Myosin IIA tailpiece is constitutively phosphorylated in NK cells on Serine 1943 (S1943); this phosphorylation is critical for Myosin association with lytic granules and NK cell cytotoxicity (Sanborn et al., 2011). The kinase that phosphorylates S1943 may be casein kinase II (Dulyaninova et al., 2005), though this is yet to be resolved in NK cells (Sanborn et al., 2011). In addition to these findings, NM-IIA was shown to recruit Ras-related protein Rab-27A and Protein unc-13 homolog D (munc13-4) to lytic granules upon NK cell stimulation (Wood et al., 2009). Rab-27A regulates vesicle trafficking, and munc13-4 regulates fusion of granules with the plasma membrane (Ménasché et al., 2000; Feldmann et al., 2003). Inhibition of NM-IIA abrogates Rab-27A and munc13-4 recruitment to lytic vesicles, down-modulating NK cell cytotoxicity (Wood et al., 2009). In agreement with the importance of NM-IIA in granule exocytosis, silencing of its co-chaperone UNC-45A in NK cells severely impairs degranulation by impacting acto-Myosin contraction (Iizuka et al., 2015). Moreover, in NK cells, contractile forces exerted by NM-IIA are critical for local nano-scale actin dynamics at the NKIS. These local events of actin reorganization define the overall synaptic architecture that is critical for NK cell cytotoxicity (Carisey et al., 2018). Nevertheless, the molecular steps that precede NM-IIA association to lytic granules and their directed delivery through the synaptic cleft are not completely understood. The overall signaling regulation of these processes have yet to be understood in context of both NK cell activation and inhibition.

NM-IIA was shown to play a critical role in T-cell motility. NM-IIA heavy chain (NMMHC-IIA) localizes in the Uropod of motile T-cells and is recruited to the interface of T-cell/APC synapses (Jacobelli et al., 2004). Inhibition of NM-IIA with blebbistatin arrests T-cell polarity and migration, and induces cell rounding. Additionally in T-cells, engagement of the TCR induces phosphorylation of NMMHC-IIA on threonine 1939, which reduces NM-IIA contractile activity, thereby potentially inducing a T-cell stop signal for locomotion (Jacobelli et al., 2004). Thus, NM-IIA may play an important role in inducing signals to transition lymphocytes from synapse formation to movement. This role of NM-IIA is perhaps mediated through LFA-1, as interactions between NMMHC-IIA and LFA-1 were shown to facilitate LFA-1 dissociation during T-cell migration (Morin et al., 2008). It would be interesting to examine whether and how NM-IIA performs similar roles in NK cells, which depend on a multitude of signaling inputs from various surface receptors. It may be possible that localized co-activating signals in NK cells are required to regulate Myosin activity in order to promote NK cell synapse formation, however, additional work is required to elucidate these mechanisms.

Microtubules

The microtubule cytoskeleton is another significant component of NK cell function. Microtubule filaments are assembled via heterodimers of αβ tubulin. Microtubule polymerization is driven by hydrolysis of GTP bound to the αβ tubulin dimer (Akhmanova and Steinmetz, 2015). The origin of microtubule polymerization is the MTOC, which consists of the centrosome and pericentriolar material (PCM) (Kloc et al., 2014). Hence, microtubule filaments can extend from the MTOC and disassemble in response to stimuli and regulatory proteins. Microtubule plus-end-tracking proteins (TIPs) can associate with growing microtubule ends and increase the polymerization rate (Schuyler and Pellman, 2001). These include microtubule polymerases such as the XMAP215 family and microtubule end binding proteins (EBs) such as EB1 (Zanic et al., 2013), as well as cytoplasmic linker protein (CLIP)-associated proteins (CLASPs) (Galjart, 2005). Furthermore, molecular motor proteins such as Dynein can associate with microtubules and stabilize them (Hendricks et al., 2012). Other proteins destabilize microtubules and enhance microtubule depolymerization by removing terminal tubulin caps. These include, for example, the microtubule depolymerases such as those of the Kinesin family (Kinesin-13, 8, and 14) (Desai et al., 1999; Sproul et al., 2005; Gardner et al., 2011).

In the context of immune cell function, there has been great interest in understanding the molecular mechanisms governing microtubule, and specifically MTOC, orientation toward the IS during T-cell/NK cell interactions with targets, and the possible function of the MTOC in IS stability. Furthermore, the process of lytic granule convergence onto the MTOC, which ensures directed cytotoxicity while preventing bystander cell killing is an ongoing field of investigation. Microtubules were shown to possess several diverse functions in T-cells. The most well-studied function of MTOC polarization in cytotoxic T-cells (CTLs) and NK cells is release of cytotoxic granules (Stinchcombe et al., 2006; Topham and Hewitt, 2009). Inhibition of MTOC polarization in NK cells disrupts cytotoxic capacity (Chen et al., 2007). Prior to MTOC polarization to the NKIS, lytic granules converge onto the MTOC via activity of Dynein motor proteins (Mentlik et al., 2010). One of the proteins that facilitates lytic granule convergence through Dynein in NK cells is the Hook-related protein 3 (HkRP3), which binds Dynein and mediates association between DOCK8 and the microtubule network (Ham et al., 2015). In addition, the small GTP binding protein, ADP-ribosylation factor-like 8b (Arl8b), binds Kinesin family member 5B (KIF5B), SifA, and Kinesin-interacting protein (SKIP), facilitating movement of the MTOC to the NKIS (Tuli et al., 2013). Another recently identified Kinesin motor protein that is important for NK cell cytotoxicity toward fungal pathogens is Eg5-Kinesin, which was shown to facilitate Dynein-mediated lytic granule convergence to the MTOC (Ogbomo et al., 2018). Recently, vasodilator-stimulated phosphoprotein (VASP), which is an actin regulatory protein belonging to the Ena/VASP family, was shown to play an important role in lytic granule convergence to the MTOC through actin filament assembly (Wilton and Billadeau, 2018). This mechanism of lytic granule convergence was recently shown to be of critical importance in NK cell biology, ensuring targeted cell lysis and preventing bystander cell death (Hsu et al., 2016). An additional member of the Ena/VASP actin regulators, EVL, was also recently shown to be recruited to the cytotoxic NKIS, where it is involved in maintaining adhesion between NK cells and targets, and in

facilitating NK cell synapse maturation (Wilton et al., 2019). Lack of EVL in NK cells resulted in decreased actin generation at the NKIS and reduced NK cell killing. EVL operates downstream to the NKG2D-Grb2-VAV1 axis, where it recruits WASp and VASP to induce F-actin accumulation at the NKIS and facilitate effector functions (Wilton et al., 2019).

Different signaling pathways lead to lytic granule convergence and microtubule reorientation to the NKIS, but not to degranulation. For example, signaling from integrin molecules, such as β2 integrins, is sufficient to promote granule polarization to the NKIS (Barber et al., 2004). Zhang et al. (2014) additionally defined this signaling pathway by decoupling additional receptors, and demonstrated that it involves activation of integrin linked kinase (ILK), Pyk2, paxillin, Rho guanine nucleotide exchange factor 7 (RhoGEF7), Cdc42, and Par6. These results extend earlier descriptions of Pyk2 in the NK cytolytic response (Sancho et al., 2000). Additional defined signaling pathways required for polarization of the MTOC were described downstream to the CD28 receptor, and include activation of PI3K which leads to phosphorylation of extracellular signal-regulated kinase 2 (ERK2) (Chen et al., 2006). It should be noted, that this CD28 dependent signaling cascade (CD28-PI3K-ERK2) was described in the YTS cell line, and not other NK cell lines or primary cells. In addition to CD28, crosslinking of the activating NK cell receptors NKG2D, NKp30, NKp46, NKG2C/CD94, or 2B4 leads to phosphorylation of either ERK2 or c-Jun N-terminal kinase 1 (JNK1), and polarization of the MTOC with cytolytic granules (Chen et al., 2007). Additional signaling molecules linked by PI3K signaling, downstream to NKG2D, include the Crk-like adaptor protein, CrkL, and Ras family GTPase Rap1, which were shown to be important for MTOC polarization and cytotoxicity (Segovis et al., 2009). In contrast to the process of MTOC reorientation, the convergence of lytic granules to the MTOC depends on early upstream Src kinase signaling (James et al., 2013).

MTOC polarization to the NKIS is thus intimately associated with and dependent on cytoskeletal reorganization (Orange et al., 2002, 2003; Graham et al., 2006; Butler and Cooper, 2009). Therefore mediatory molecules are probably involved in cytoskeletal and microtubule dynamics. One of the proteins identified, which links these two networks, is Cdc42-interacting protein-4 (CIP4), which associates with Cdc42 and WASp (Banerjee et al., 2007). CIP4 links the actin and microtubule cytoskeletons in activated NK cells, facilitating MTOC polarization and NK cell cytotoxicity. It is possible that additional mediating molecules such as CIP4 function to merge these two cytoskeletal networks, and it would be interesting to investigate how these are differentially regulated under inhibitory and activating conditions. Moreover, it is possible that decoupling of the actin and microtubule cytoskeletons promotes NK tolerance. It is interesting to speculate that abrogation of MTOC association with the actin cytoskeleton may also lead to dysfunction in primary immunodeficiency and other chronic diseases.

Interestingly, additional functions mediated by microtubule dynamics have been suggested in T-cells. For example, TCR micro clusters were shown to localize at the IS on microtubules through Myosin II and Dynein motors (Hashimoto-tane et al., 2011). Disruption of MTOC polarization to the T-cell IS through Dynein inhibition reduced phosphorylation of ZAP70, LAT, and VAV1, and caused the creation of a malformed T-cell IS characterized by low accumulation of CD3 in the center of the synapse, and low accumulation of LFA-1 at its periphery (Martín-Cófreces et al., 2008). Furthermore, inhibition of the microtubule end binding protein EB1 abrogated LAT/PLCγ-1 complex association and subsequent TCR activation signaling (Martín-Cófreces et al., 2012). This raises the question of whether the MTOC has an additional function as a scaffold to deliver further signaling molecules to the IS, thereby enabling correct signaling cascades, and whether microtubule dynamics, similar to F-actin flow, also play a role in regulating activation signaling. Just as F-actin retrograde flow was seen to impact and sustain correct PLCγ-1 activity in T-cells (Babich et al., 2012), microtubule dynamics may also play a role in influencing sustained T-cell signaling, rather than functioning solely as a signaling scaffold and delivering vesicles to the IS. The microtubule cytoskeleton is thus of great importance in controlled NK cell effector function, however, the molecular mechanisms in NK cells that induce MTOC polarity and positioning at the IS have not been extensively explored. It is possible that such signaling circuits are dysregulated during different chronic pathological conditions (i.e., chronic infection and cancer), enabling escape from NK cell immune surveillance.

NK Cell-Mediated Killing

After firm adhesion and sufficient activating signaling, the next phase of NK cell function involves reorientation of the MTOC toward the IS, and subsequent release of lytic granules for target cell killing. The actin cytoskeleton plays multiple roles in this cytotoxic phase. As described, the first step in NK cell cytotoxicity requires cytolytic granule convergence onto the MTOC before MTOC polarization to the NKIS (Mentlik et al., 2010). This process is crucial for prevention of bystander cell killing (Hsu et al., 2016). The MTOC subsequently polarizes to the NKIS, and it was shown that F-actin polymerization is vital for this process (Orange et al., 2002; Butler and Cooper, 2009). Following MTOC polarization and anchoring at the IS, lytic granules move rapidly across the dense F-actin network at the cell membrane prior to degranulation; in order to ensure persistent degranulation, the actin meshwork must remain intact (Mace et al., 2012). Lytic granules associate with Myosin IIA, and this association is believed to coordinate with the F-actin cytoskeleton for lytic granule delivery to the IS, and to provide physical forces to "squeeze" granules through the actin meshwork. Abrogation of NM-IIA activity using inhibitors or site directed mutations reduces the ability of lytic granules to bind to F-actin, and impedes granule entry into the actin meshwork at the IS (Andzelm et al., 2007; Sanborn et al., 2009). Due to the accumulation of a dense actin network at the IS prior to degranulation, the mechanism that enables escape of the lytic granule content of the NK cell is difficult to resolve. Advanced microscopic techniques from the Davis and Orange groups elucidated the mechanisms of lytic granule secretion across the actin boundary: lytic granules traverse the dense actin

network at the IS until reaching, and docking at specific areas with low actin density, from where they can be released toward the target cell (Brown et al., 2011; Rak et al., 2011). Disrupting NK cell actin dynamics immediately prior to degranulation inhibited granule release (Rak et al., 2011). In addition to lytic granule secretion, a different Myosin independent mechanism was shown to enable cytokine secretion at the NKIS, and this was similarly dependent on formation of local actin pores at the NKIS (Brown et al., 2012). As mentioned earlier, one mediator of actin clearance at the NKIS is Coronin1A, which is essential for generating precisely targeted actin clearances by promoting localized actin depolymerization (Mace and Orange, 2014). Therefore, meticulous regulation of localized actin disassembly enables precise delivery of granules across the synaptic cleft. This mechanism most probably ensures selective delivery to target cells while avoiding lytic granule spillage that can affect bystander tissue. It is not yet known how Coronin1A is regulated during stimulation of NK cells, and how its activity is coupled directly with granule exocytosis. It is possible that generation of actin clearances occur in a stochastic fashion, followed by random movement of granules across the actin network until they reach low actin areas. It would be interesting to resolve the mechanisms and mediators of Coronin1A recruitment to the IS, and how localized actin deconstruction harmonizes with the additional actin architectures present at the IS. For example, Carisey et al. (2018) recently described additional actin structures that are critical for NK cell cytotoxicity. Local actin dynamic puncta are generated via Arp2/3 and NM-IIA activity at the NKIS, and these structures are required for lytic granule exocytosis (Carisey et al., 2018). It is possible that localized actin dynamics promote additional forces for delivery of granules, or provide additional motion that resonates along the synaptic actin sheet that enhances the possibility of lytic granule arrival to areas of low actin content. Further experiments could elucidate how these structures are regulated by different early upstream signaling complexes and NPFs, and in the context of different NK cell receptor ligations.

THE CYTOSKELETON IN NK CELL-RELATED PATHOLOGIES

Due to the important and variegated roles the cytoskeleton plays in NK cell function, it is not surprising that various immune-related diseases result from cytoskeletal mis-regulation in NK cells (Lagrue et al., 2013; Ham and Billadeau, 2014) (**Table 1**). Two of the most well characterized immunodeficiencies are WAS/X-linked thrombocytopenia (XLT). WAS is an X-linked immunodeficiency characterized by mutations that have varying effects on WASp expression. Different phenotypes are caused by a complete or partial absence of WASp expression in affected patients (Derry et al., 1994). WAS patients with complete WASp depletion suffer from reduced platelet count, complications in blood clotting, eczema, recurrent infections and cancer (Sullivan et al., 1994). A less severe form of WAS known as XLT occurs due partial WASp expression resulting mainly in microthrombocytopenia (Imai et al., 2004). It was demonstrated that NK cells from healthy donors express high levels of WASp, while NK cells from WAS patients express no detectable levels (Orange et al., 2002). Given the importance of WASp in actin regulation, it is not surprising that mutations in the protein or its degradation have severe impacts. As mentioned earlier, the cytoskeleton plays a paramount role in leukocyte migration, as the actin machinery propels the cell and changes its morphology in order to navigate through blood and tissue (Vicente-Manzanares and Sánchez-Madrid, 2004). WASp deficiency in NK cells severely damages their migratory capabilities (Stabile et al., 2010). Both WAS and XLT NK cells exposed to the migration-inducing cytokines CXCL12/SDF-1 or CX3CL1/fractalkine and placed on adhesion molecule (ICAM-1/VCAM-1) coated filters show low cellular migration compared to wild-type NK cells (Stabile et al., 2010). NK cells from WASp-deficient mice exhibit defects in tumor suppression (Catucci et al., 2014), and a significantly reduced cytotoxic potential relative to healthy NK cells (Orange et al., 2002). This is predominantly due to lower actin accumulation at the NKIS that impacts synaptic clustering of activating receptors (Orange et al., 2002; Gismondi et al., 2004). As mentioned earlier, it was suggested - that bypassing WASp deficiency in NK cells might be enabled via IL-2 administration, leading to actin reorganization via WAVE2 (Orange et al., 2011).

WASp-interacting protein deficiency leads to a reduction in NK cell functional output (Noy et al., 2012). WIP helps to protect WASp from ubiquitin-mediated degradation (Fried et al., 2014b), but also has additional functions in NK cells. As described earlier, following NK activation, WIP mediates assembly of a protein complex comprising WASp, actin, and NM-IIA (Krzewski et al., 2006). In addition, WIP was also found to be essential for granule-mediated exocytosis in NK cells, since it associates with lytic granules in NK cells, and its depletion from NK cells causes a failure in lytic granule polarization (Krzewski et al., 2008). A female patient bearing a mutation containing a stop codon in the *WIPF1* gene, which encodes WIP, displayed recurrent infections, eczema, thrombocytopenia, defective T cell proliferation and chemotaxis, and impaired NK cell effector function (Lanzi et al., 2012).

Another disease impacting F-actin organization at the NKIS is DOCK8 deficiency. As described earlier, DOCK8 belongs to the superfamily of DOCK180 GEFs for the Rho protein family (such as Cdc42) (Côté and Vuori, 2002; Sinai et al., 2010; Stabile et al., 2010). NK cells from patients with DOCK8 deficiency are not able to form a mature IS due to reduced F-actin accumulation. This results in a decrease in cytotoxicity that cannot be bypassed by IL-2 administration, and could explain why patients with DOCK8 deficiency are susceptible to sino-pulmonary and cutaneous viral infections (Zhang et al., 2009; Mizesko et al., 2013). Hence, unlike WASp deficient NK cells, whose function might be recovered through IL-2 mediated activation of WAVE2, DOCK8 seems to be indispensable for proper actin accumulation at the NKIS. Additional work is expected to unravel the molecular mechanisms connecting DOCK8 to the activating or inhibiting NKIS. Similarly to DOCK8 deficiency, inherited DOCK2 mutations in five patients with recurrent bacterial and viral infections and lymphopenia were

TABLE 1 | Diseases affecting the NK cell cytoskeletal machinery.

Disease	Defect in protein	Phenotype
Wiskott–Aldrich Syndrome (WAS)/X-linked thrombocytopenia (XLT)	Partial or no expression of WASp	Patients display low blood platelet count, deficiency in blood clotting, recurrent infections and eczema. NK cells exhibit deficiency in migration, and low accumulation of F-actin at the NKIS resulting in diminished NK cell activation and cytotoxicity.
WASP-interacting protein (WIP) deficiency	No expression of WIP	Patient displayed recurrent infections, eczema, thrombocytopenia, and defective T cell proliferation and chemotaxis. NK cells demonstrated defective effector function.
Dedicator of cytokinesis 8 (DOCK8) deficiency	No expression of DOCK8	Patients display immunodeficiency characterized by sino-pulmonary and cutaneous viral infections. NK cells are impaired in IS formation due to reduction in F-actin accumulation, leading to inhibited cytolytic function.
Dedicator of cytokinesis 2 (DOCK2) deficiency	No expression of DOCK2	Patients display immunodeficiency characterized by recurrent infections, lymphopenia, and thrombocytopenia. NK cells are impaired in effector functions such as degranulation and cytokine secretion due to abrogated F-actin polymerization.
RAS guanyl-releasing protein 1 (RASGRP1) deficiency	No expression of RASGRP1	Patient displayed primary immunodeficiency disorder, characterized by recurring infections, and ultimately, development of low-grade Epstein–Barr virus (EBV)-associated B cell lymphoma. NK cells are deficient in F-actin accumulation, lytic granule convergence to the MTOC, and degranulation.
Chediak–Higashi syndrome	Mutations in the regulator of lysosomal trafficking, LYST	Patients display dysregulated immune function, albinism, predisposition to bleeding, and hyper inflammation. NK cells with LYST mutations contain enlarged lytic granules that cannot penetrate the actin mesh at the NKIS, impairing degranulation.
Coronin 1A deficiency	No expression of Coronin 1A	Patients display immunodeficiency characterized by recurrent viral infections and lymphopenia. NK cells demonstrate abrogated deconstruction of F-actin at the IS, impeding lytic granule secretion and thus, cytotoxicity.
Hermansky–Pudlak syndrome type 2	Mutations in the β3A subunit of the AP-3 adaptor protein	Patients display albinism, recurrent infections, susceptibility to bleeding, and hemophagocytic lymphohistiocytosis. NK cells are defective in degranulation due to formation of enlarged lytic granules.
Myosin IIA mutations (May-Hegglin anomaly, Sebastian syndrome, Fechtner syndrome, and Epstein syndrome)	MYH9 gene mutation	Patients present macrothrombocytopenia, leukocyte inclusion bodies, low platelet count and recurrent bleeding. Patients also display hearing loss, nephropathy, and cataracts. NK cells are characterized by impaired cytotoxicity.
Griscelli syndrome type II	Mutation in RAB27A	Patients display hypopigmentation, immunodeficiency, and hemophagocytic lymphohistiocytosis. NK cells display impaired cytotoxicity due to docking failure of granules at the plasma membrane.
Familial Hemophagocytic Lymphohistiocytosis Types 2–5	Mutations in perforin 1 (FHL type 2), Munc13-4 (FHL type 3), syntaxin 11 (FHL type 4), and Munc18-2 (FHL type 5)	Patients display immune dysregulation characterized by hyper inflammation, fever, enlarged spleen and liver, and hemophagocytosis. NK cell degranulation and/or cytotoxicity is severely impaired.

shown to impact T/B cell and NK cell responses (Dobbs et al., 2015). NK cells in these patients show reduced migration and actin polymerization, as well as impaired degranulation.

A role for RASGRP1 was also demonstrated in an NK cell immunodeficiency (Salzer et al., 2016). As mentioned earlier, RASGRP1 acts as a GEF for Ras, thereby activating the Ras pathway and the MAPK cascade (Downward et al., 1990; Roose and Weiss, 2000; Stone et al., 2000). A patient with RASGRP1 deficiency displayed a primary immunodeficiency disorder, characterized by recurring infections, and ultimately developed low-grade Epstein–Barr virus (EBV)-associated B cell lymphoma (Salzer et al., 2016). NK cells from patients with RASGRP1 deficiency do not form a mature NKIS, and their IS is characterized by decreased actin accumulation and polarization of the MTOC, and accordingly, a lower capacity for cytotoxicity toward target cells (Salzer et al., 2016). These phenotypes might arise due to the importance of the MAPK pathway in NK cell actin rearrangement (Vély and Vivier, 2005). Interestingly the same study reported association of RASGRP1 with Dynein light chain DYNLL1. Imaging NK cells from this patient revealed defective granule motility, and because Dynein is important for convergence of lytic granules onto the MTOC, this may account for an additional factor inducing lower NK cell-mediated cytotoxicity (Mentlik et al., 2010; Salzer et al., 2016).

Highlighting another aspect of cytoskeletal regulation, the inability to properly clear the actin meshwork at the NKIS for granule secretion in NK cells was recently described in Chediak–Higashi syndrome (Gil-Krzewska et al., 2017). This disease is caused by mutations in the regulator of lysosomal trafficking, LYST (Nagle et al., 1996), and is characterized by hyper inflammation and impaired functionality of CD8 T and NK cells (Introne et al., 1999; Karim et al., 2002; Lozano et al., 2014). NK cells with impaired LYST function contain enlarged granules, and thus, the NKIS effectively acts as a barrier for exocytosis. Use of the actin inhibitors latrunculin A or swinholide A increases the permeability of the actin mesh and restores secretion from these NK cells (Gil-Krzewska et al., 2017). This study further illustrates that actin disassembly is also critical in maintaining proper cytolytic function. In addition to Chediak–Higashi syndrome, Hermansky–Pudlak syndrome type 2 also causes formation of enlarged granules, induced by mutations in the β3A subunit of AP-3 (Dell'Angelica et al., 1999). AP-3 is an adaptor protein that interacts with the clathrin scaffold protein, facilitating sorting of proteins to lysosomes (Dell'Angelica et al., 1997). NK cells from patients with Hermansky–Pudlak syndrome type 2 also show disrupted effector functions (Fontana et al., 2006). It is possible that this disorder also disrupts secretion of enlarged lytic granules at the NKIS, but additional studies are required to verify this mechanism.

Mutations in the heavy chain of Myosin IIA also lead to a variety of diseases such as May-Hegglin anomaly, Sebastian syndrome, Fechtner syndrome, and Epstein syndrome, characterized by macrothrombocytopenia with leukocyte inclusions (Seri et al., 2003). As discussed, NM-IIA is important for delivery of cytolytic granules through the NKIS (Andzelm et al., 2007). Several mutations that alter normative NM-IIA conformation impact its regulation of cytotoxicity in NK cells. For example, a mutation in May-Hegglin anomaly patients with a C-terminal truncation of MYH9 at position 1933 causes a reduction in NK cell cytotoxicity (Sanborn et al., 2009). Furthermore, Sanborn et al. (2011) mapped various mutations in NM-IIA which cause similar phenotypes of reduced NK cell cytotoxicity. For example, a S96L mutation in the head region and T1155I mutation in the S2 region result in a decrease in NK cell killing. A truncation of the protein at residue 1942, which is located on the tailpiece, also causes a reduction in NK cell killing (Sanborn et al., 2011). Interestingly, the same study showed that phosphorylation of the NM-IIA tailpiece at S1943 is critical for Myosin function at the NKIS; hence, mutations in this regulatory area may account for the phenotypes observed (Sanborn et al., 2011). It is also possible that additional activity of Myosin at the NKIS influences the dysfunction of NK cell cytotoxicity. As mentioned previously, NM-IIA forms a complex with actin, WIP, and WASp during NK cell activation (Krzewski et al., 2006), and it is present in the pSMAC with actin filaments in acto-Myosin arcs. Therefore, NM-IIA may also drive IS formation and stability which are restricted in NM-IIA-related diseases (Hammer and Burkhardt, 2013).

Other diseases that impact lytic granule and cytoskeletal cross-talk in NK cells include Griscelli syndrome type II and Familial Hemophagocytic Lymphohistiocytosis (FHL) Types 2-5 (Ham and Billadeau, 2014). Griscelli syndrome type II is caused by mutation in RAB27A, a member of the small GTPase family (Ménasché et al., 2000). RAB27A was shown to play a role in cytoskeletal dependent lytic granule movement in the plasma membrane and cytosol of NK cells (Liu et al., 2010), possibly through a complex with the motor protein Kinesin-1 and synaptotagmin-like protein 3 (Kurowska et al., 2012). NK cells from Griscelli syndrome type II patients display impaired cytotoxicity due to docking failure at the plasma membrane (Wood et al., 2009). FHL Type 3 is caused by mutations in Munc13-4 (Feldmann et al., 2003), which is involved in vesicle priming. Mutations in Munc13-4 that abrogate its association to RAB27A inhibit degranulation in cytotoxic T-cells (Elstak et al., 2011), and NK cells deficient in Mucn13-4 are inhibited in granule secretion (Wood et al., 2009). Importantly, recruitment of Rab27a and Munc13-4 to lytic granules is Myosin-dependent (Wood et al., 2009), further emphasizing the role of cytoskeletal compartments in effector NK cell responses. Additional FHL diseases are caused by different mutations. FHL type 2 is caused by mutations in the perforin 1 gene (Stepp et al., 1999), abrogating the ability of NK cells to lyse target cells (Marcenaro et al., 2006). FHL type 4 is caused by mutations in syntaxin 11 (Bryceson et al., 2007), inhibiting the ability of NK cells to degranulate. Finally, FHL 5 is caused by mutations in Munc18-2, which also severely impairs NK cell exocytosis (Côte et al., 2009).

Due to the great importance of NK cells in innate immunity, it is not surprising that various conditions result from functional NK cell deficiency (FNKD) syndromes that may arise from defects in the NK cytoskeleton, such as Herpesvirus infection, multiple infections, presence of intracellular bacteria, and Human Papillomavirus (HPV) (Orange, 2013). The protective effect of NK cell immune surveillance on cancer in humans has been documented (Imai et al., 2000; Ishigami et al., 2000;

Villegas et al., 2002), and this is especially evident in the outcome of patients who were administered NK cells from donors that have the advantage of having graft versus leukemia activity in the recipient without causing graft versus host disease (Hsu et al., 2005). It is not known whether tumor growth is increased on the background of FNKD syndromes that involve the NK cytoskeleton. Future studies could reveal if functional dysregulation of NK cell cytoskeletal activity may promote other diseases or malignancies, and thus prompt development of therapies to bolster NK activity.

NK CELL INHIBITORY SIGNALING AND CYTOSKELETAL DYNAMICS AT THE NKIS

Inhibition of NK cells does not occur independently on its own, that is, without input from additional activating receptors on the NK cell surface. Co-engagement of inhibitory receptors with activation receptors prevents NK cell activation; therefore, suppression of NK cell activity by inhibitory receptors can be thought of as co-inhibition (Long et al., 2013). Photo stimulation of the inhibitory killer-cell immunoglobulin-like receptor (KIR) KIR2DL2 during ongoing NK cell activation is not sufficient to prevent calcium flux, however, it induces rapid formation of inhibitory microclusters that prevent formation of activating clusters and promote retraction of the NK cell (Abeyweera et al., 2011). Therefore, inhibitory receptor signaling prevents activation of NK cells from manifesting in the first place. Inhibitory NK cell signaling involves dephosphorylation and/or degradation of upstream signaling proteins and dismantling of activating signaling complexes (Long, 2008; Peterson and Long, 2008; Watzl and Long, 2010). Accordingly, NK cell inhibition has substantial effects on actin polymerization and rearrangement. NK cells express inhibitory receptors that contain immunoreceptor tyrosine based inhibition motifs (ITIMs) in their cytoplasmic tails that bind to several Human Leukocyte Antigen (HLA) isoforms. The best defined of these receptors in humans are KIRs and NKG2A/CD94 (Wagtmann et al., 1995; Moretta et al., 2002). Engagement of inhibitory receptors with their cognate ligands results in phosphorylation of the ITIM motifs, and it has been suggested that the phosphorylation is carried out by the Src family kinases (Long, 2008). Phosphorylation on ITIMs prompts recruitment of SHIP-1 or SH2-domain-containing protein tyrosine phosphatase (SHP-1/2) (Long, 1999; Ravetch, 2000; Purdy and Campbell, 2009), which induce de-phosphorylation of downstream signaling molecules important for NK activation (Long, 2008).

Killer-cell immunoglobulin-like receptor receptors may not require actin reorganization for their recruitment to the NKIS (Davis et al., 1999). Work by Stebbins et al. (2003) using a SHP-1 trapping mutant that is catalytically inactive but capable of binding phosphorylated substrates detected VAV1 as the first verified SHP-1 substrate in NK cells. The same study also demonstrated that the process occurs independently of actin rearrangement, as dephosphorylation of VAV1 occurred in the presence of actin inhibitors (Stebbins et al., 2003). VAV1 activity may also be regulated by the E3 ubiquitin ligase c-Cbl. Cooperative activation of the activating NKG2D and 2B4 receptors is necessary to circumvent inhibition of VAV1 by c-Cbl (Kim et al., 2010). An additional inhibitory mechanism independent of VAV1 was suggested to operate through the Crk adaptor protein, which is involved in cytoskeletal remodeling (Antoku and Mayer, 2009). Crk is phosphorylated and associates with c-Abl upon clustering of inhibitory receptors (Peterson and Long, 2008). We previously demonstrated that PLCγ-1/2 and LAT are also dephosphorylated and inactivated by SHP-1 during NK cell inhibition, and that ubiquitination of LAT by c-Cbl and Cbl-b serves as an additional mechanism to ensure tolerance, by sequestering remaining phosphorylated LAT from the NKIS (Matalon et al., 2016). Therefore, it appears that NK cell inhibition involves multiple modules. These include, on the one hand, blocking substantial F-actin reorganization at the IS through dephosphorylation of VAV1 and phosphorylation of Crk, and on the other hand, inhibiting formation of activating signaling complexes such as PLCγ and LAT to possibly prevent formation of secondary messengers (i.e., IP3 and DAG), early activation, and calcium flux.

The Inhibitory NKIS

The inhibitory NKIS is characterized by disorganized molecular segregation, instability, and short lifetime. These inhibitory characteristics prevent NK cell activation and effector outcome, serving as a key checkpoint in regulating cytotoxicity and maintaining tolerance (Davis et al., 1999).

Due to the activity of VAV1 in actin polymerization and rearrangement through the Rac pathway, it is expected that its inactivation would hamper various actin-dependent processes. F-actin accumulation and density are much greater in synapses of NK cells that are exposed to susceptible activating targets, than on targets that induce an inhibitory NKIS (Banerjee and Orange, 2010). As mentioned earlier, actin accumulation and lipid raft recruitment to the NKIS were shown to be disrupted upon NKG2A/CD94 receptor-mediated inhibition, when SHP-1 is recruited to the NKIS and VAV1 phosphorylation levels are decreased (Masilamani et al., 2006). Accumulation of 2B4 and NKG2D activating receptors is actin dependent, and this clustering is also abrogated during KIR receptor-HLA binding (Watzl and Long, 2003). Inhibition via KIR2DL2 additionally inhibits activating receptor clustering, and reduces NK cell spreading via SHP1/2 activity (Abeyweera et al., 2011). Thus, NK cells developed mechanisms to first avoid reactivity by differential regulation of cytoskeletal dynamics. Due to the dependence of NK activation on accumulated actin, which recruits signaling clusters to the NKIS, regulation of actin assembly at the NKIS ensures tolerance. It is not clear whether VAV-1 dephosphorylation through SHP-1 and phosphorylation of Crk are the sole mechanisms for regulating actin dynamics at the NKIS, and what other factors, if any, sequester F-actin mediated activation at the NKIS to prevent normal synapse formation and activation. For example, Kopcow et al. (2005) showed that decidual NK cells (dNKs) do polarize actin toward their synapse; however, the synapse remains inert as the MTOC does

not polarize (Kopcow et al., 2005). Hence, additional inhibitory mechanisms that regulate cytotoxicity through maintenance of the cytoskeleton, possibly linking cytoskeletal reorganization with MTOC polarization, should be investigated. It is tempting to speculate that molecules such as CIP4, which link the microtubule and actin cytoskeletons, may be regulated or expressed differently in decidual NK cell subtypes.

The inhibitory IS favors accumulation of inhibitory KIRs into subdomains coined supra-molecular inhibition clusters (SMICs) (Davis et al., 1999). Phosphorylated KIR receptors form microclusters with the tyrosine kinase, Lck, during NK cell inhibition (Treanor et al., 2006). The SMIC of the inhibiting NKIS contains a different composition of signaling molecules, including phosphatases such as SHP-1 (Vyas et al., 2002a) and SHP-2 (Purdy and Campbell, 2009). The accumulation of inhibiting signaling molecules in the SMIC disrupts the stability of the IS, leading to detachment from the target cell, and favoring migration (Burshtyn et al., 2000; Masilamani et al., 2006). The inhibitory NKIS differs from the activating NKIS, as it is not radially symmetrical, and not stable. A similar "make and break" synapse has been characterized in T-cells, and coined the kinapse. Similarly to the kinapse, the inhibitory NKIS is characterized by smaller size and much lower NK:target cell conjugation times (Burshtyn et al., 2000; Sims et al., 2007; Culley et al., 2009).

Unlike activating synapses, the accumulation of KIRs does not cause extensive accumulation and rearrangement of actin (McCann et al., 2003). The recruitment of KIRs to the NKIS and their phosphorylation appears to be actin independent and occurs upstream to actin rearrangement; however, this issue is not yet resolved (Faure et al., 2003). An observable mesh of cortical actin seems unchanged at inhibitory synapses relative to activating synapses, yet these synapses seem to lack a dense peripheral actin ring (Brown et al., 2011). Fassett et al. (2001) showed that actin polymerization is crucial for lipid raft polarization in inhibitory NK cell synapses. In addition, using the inhibitor of actin polymerization, cytochalasin D, Standeven et al. (2004) demonstrated that actin dynamics may be important in early KIR2DL1 recruitment to the inhibitory NKIS. In NK cells engaged with multiple targets, KIR2DL1 was also shown to relocate between different synapses (Pageon et al., 2013a), and coalescence of KIRs into micro-clusters was shown to depend on cytoskeletal dynamics (Pageon et al., 2013b). Moreover, during NK cell inhibition, large KIR2DL1 clusters seem to favor the phosphorylation and activation of SHP-1 (Oszmiana et al., 2016). In this study, the localization of the activating KIR, KIR2DS1 in signaling clusters depended on the lysine 233 residue in the transmembrane sequence; yet, it is not clear if cluster size of the inhibitory and activating KIRs was also influenced by different cytoskeletal reorganization modes. Interestingly, a recent study from the Davis group investigated how KIR variation impacts organization on the cell membrane (Kennedy et al., 2019). NK cells were divided into groups with either low or high surface expression of KIRs. Higher receptor abundance correlated with increased cluster size, yet with more receptors observed outside clusters. On the other hand, cells expressing low surface abundance of KIRs appear to dominantly coalesce into clusters and to favor increased phosphorylation of Crk. Interestingly, it appears that since SHP-1 activity is favored at large KIR clusters, its activity may promote dephosphorylation of Crk and prime NK cells that express more inhibitory receptors on the cell membrane (Kennedy et al., 2019). Thus, the organization of inhibitory signaling molecules on the NK cell surface has critical ramifications for the basal NK cell activation state. How and why different KIR genotypes are expressed at different concentrations and coalesce differently into signaling clusters remains to be determined. The role of the cytoskeleton in mediating this organization is an additional intriguing area of study. As discussed in the following sections, it is possible that cytoskeleton-mediated reorganization of receptors on the NK cell membrane during development may dictate their activation threshold.

THE EFFECT OF THE TARGET CELL CYTOSKELETON ON NK CELL FUNCTION

In addition to the vast importance of cytoskeletal rearrangement on NK cell function, it is becoming increasingly evident that the cytoskeletal architecture on target cells can greatly influence NK cell effector efficacy. T-cells and B-cells are usually activated to a greater degree when confronted with stiffer *in vitro* substrates (as shown using coated slides with varying rigidities) and target cells which display stiffer properties (stiffer cortical actin and more actin stress fiber assembly) (Huse, 2017; Saitakis et al., 2017; Shaheen et al., 2017; Ben-Shmuel et al., 2019). Moreover, it is clear that constraining target cell co-stimulating ligands (such as ICAM-1) by the target cell cytoskeleton, induces higher T-cell activation (Comrie et al., 2015b; Comrie and Burkhardt, 2016). This may be due to counter force provided by the constrained ligand to receptors on T-lymphocytes. Therefore, strategies that target immune cell cytoskeletal machinery must also take into consideration the possible effects on the integrity of the target cell cytoskeleton, which impact lymphocyte activation.

In the case of NK cells, it was previously demonstrated that similar mechanisms operate on target cells to modulate the NK cell responses. Gross et al. (2010) showed that impairing cytoskeletal integrity by treating target cells with Latrunculin A (which disrupts microfilament organization by binding to monomeric G-actin) leads to inhibition of NK cell LFA-1 mediated conjugation and polarization of lytic granules to the NKIS; these effects were caused by higher mobility of ICAM-1/2 on target cells due to compromised association with the cytoskeleton. Furthermore, actin polymerization was shown to be crucial for MHC class I recruitment in dendritic cell (DCs) targets during their interaction with NK cells, resulting in KIR engagement and inhibition of NK cells. Inhibition of actin in DCs results in increased IFNγ secretion (Barreira da Silva et al., 2011).

Recently, work by Al Absi et al. (2018) demonstrated that cytoskeletal remodeling in tumor targets can have drastic ramifications on NK cell cancer surveillance. In this work, breast adenocarcinoma cells were shown to initiate an "actin-response" to NK cell conjugation. This response is characterized

by substantial amounts of actin accumulation by the cancer cell at the NKIS. Actin accumulation significantly protected the cancer cell from NK-mediated cytotoxicity. One possible explanation for escape from cell death is generation of a physical barrier that is not permissive for lytic granules. Moreover, the actin response in this study correlated with the epithelial to mesenchymal transition of the breast cancer cells, and interestingly, it induced the coalescence of HLA ligands and PD-L1 at the NKIS, possibly shedding some light on an additional mechanism of escape from NK cell surveillance, through clustering of inhibitory checkpoint ligands.

In addition to this mechanism in cancer cells, previous work demonstrated that alterations of cytoskeletal architecture through viral infection can also down modulate NK cell effector function. Stanton et al. (2014) showed that target cells infected with the HCMV pUL135 strain have dramatically altered cytoskeletal morphology, characterized by cell rounding, loss of focal adhesions, loss of actin stress fibers, loss of cell projections, and an increase in cortical actin. These features severely inhibited NK cell killing of target cells, specifically due to impaired conjugation and IS formation. It is tempting to speculate that these changes in target cell morphology decrease the mechanical characteristics of the target cell, which were shown to significantly impact the potentiation of cytotoxic T-cells (Basu et al., 2016).

A question that can be raised is how can NK cell effector function be modulated through targeting actin dynamics? In the study by Al Absi et al. (2018), targeting actin nucleation factors such as N-WASp or Cdc42 in target cells restored NK cell mediated cytotoxicity by inhibiting the cancer cell actin response. We also previously showed that the centripetal flow of actin at the inhibitory NKIS may affect the enzymatic activity of SHP-1 (Matalon et al., 2018). Interestingly, NK cells stimulated on stiff substrates are characterized by extremely reduced centripetal flow, which may constrain SHP-1 activity, inducing chronic NK cell activation (Matalon et al., 2018). Targeting NPFs to modulate inhibitory checkpoint signaling may therefore provide an additional strategy to modify NK cell activity. Furthermore, work by the Davis group examined the effect of the drug Lenalidomide on NK cell effector function against multiple myeloma. Lenalidomide enhanced NK cell effector function by reducing the periodicity of the actin mesh at the NKIS, facilitating lytic granule and cytokine secretion (Lagrue et al., 2015). In addition to this study, Lagrue et al. (2015) showed that treating B-cells with the monoclonal antibody Rituximab, which binds CD20, results in recruitment of ICAM-1, moesin [a member of the ERM family of proteins that links the cortical cytoskeleton to the plasma membrane (Tsukita and Yonemura, 1999)], and CD45 to the CD20 cap (Rudnicka et al., 2013). Rituximab also induced MTOC polarization in B-cells. The polarization events induced by rituximab treatment significantly increased NK cell mediated ADCC. It is also possible that accumulation of adhesion molecules, ERM proteins, and cytoskeletal components at the membrane of target cells treated with rituximab provides a firm substrate that more efficiently activates cytotoxic lymphocytes. These data support findings that the cell tension of target cells significantly potentiates cytotoxic T-cell activity (Basu et al., 2016). Therefore, development of treatments that can also modulate the physical properties of target cells at the interface with cytotoxic lymphocytes may be interesting to pursue.

THE ROAD AHEAD – UNLOCKING THE RECIPROCAL ROLE OF THE ACTO-MYOSIN MACHINERY ON LYMPHOCYTE SIGNALING

There are several studies that raise the exciting possibility of acto-Myosin dynamics directly influencing signaling in lymphocytes, possibly through processes of mechanotransduction (Huse, 2017; Ben-Shmuel et al., 2019). Work from the Burkhardt lab showed correlations between centripetal actin flow and levels of tyrosine phosphorylation profiles of critical cytoplasmic signaling molecules. A study by Babich et al. (2012) demonstrated that actin retrograde flow sustains T-cell signaling through PLCγ1, leading to T-cell calcium flux and activation. Interestingly, the same study demonstrated that ZAP-70 kinase phosphorylation remained intact despite perturbations in actin retrograde flow, demonstrating a selectivity that may be orchestrated by actin remodeling. Furthermore, SLP-76 seems to be uncoupled from actin dynamics, moving centrally at a faster velocity than the observed ARF in the lamellum and cell body, raising the possibility of differential regulation of signaling molecules and clusters by the cytoskeleton. This may indicate that centralization of SLP-76 relies on additional factors, possibly other cytoskeletal components such as the microtubule network. Another work by Jankowska et al. (2018) conducted in T-cells showed that after LFA-1 and VLA-4 integrins engage with cognate ligands, there is a dampening of actin retrograde flow associated with abrogation of tyrosine phosphorylation downstream to TCR engagement. Hence it is evident that there exists a complex regulatory mechanism controlled through actin movement, in addition to the roles of the cytoskeleton in assembly of signaling complexes. An interesting possibility raised by the results of Jankowska et al. (2018) is the induction of inhibitory tyrosine phosphatase activity by cytoskeletal dynamics and substrate mechanics. For example, we previously showed that F-actin dynamics at the inhibitory NKIS may regulate the enzymatic activity of SHP-1 (Matalon et al., 2018). Reduced F-actin dynamics may promote SHP-1 binding to the cytoskeleton and release it from auto-inhibition. Thus, by controlling the phosphorylation and activation profile of key signaling molecules through phosphatase function, the cytoskeleton could potentially facilitate rapid differentiation between activating and inhibiting target cells. Local actin reorganization at an activating synapse may sequester SHP-1 pools, enabling their simultaneous assembly and activity at inhibitory synapses. Another possibility is that specific pools of SHP-1 that are recruited independently of cytoskeletal rearrangement to ITIM domains decrease cytoskeletal turnover at inhibitory synapses, subsequently promoting the association of additional SHP-1 molecules to the cytoskeleton. Such a mechanism may promote assembly of SHP-1: substrate complexes in a positive feedback process promoting inhibition.

Not much is known regarding how cytoskeletal assembly can influence NK cell signaling intermediates, beyond cytoskeletal function at the NKIS. As discussed earlier, the assortment of signaling receptors at the NKIS is instrumental in determining NK cell activity. One outcome of cytoskeletal regulation of surface receptors on NK cells may be tuning of NK cell responses in the context of education. NK cell education refers to the process wherein NK cells are quantitatively primed by MHC-I molecules during development and acquire the capacity to elicit effector function. Guia et al. (2011) demonstrated that the distribution of NK cell activating/inhibitory receptors confined by the actin meshwork controls NK cell education. NK cell education is believed to be primarily regulated by NK cell exposure to inhibiting ligands, and depends on the strength and number of NK cell inhibiting receptors and target cell ligands (Orr and Lanier, 2010). Guia et al. (2011) showed that activating and inhibitory receptors are confined together by the actin cytoskeleton in hyporesponsive NK cells. Thus, the actin cytoskeleton may abrogate activating signaling by organizing activating receptors in the vicinity of inhibitory receptors. In responsive NK cells, on the other hand, activating receptors localize in nanodomains, thereby promoting favorable signaling, whereas inhibiting receptors are confined in the actin meshwork. Interestingly, Guia et al. (2011) found no significant differences in the NK transcriptional program between educated and non-educated cells. Thus, it remains unclear how ITIM bearing receptors mediate the formation of this intricate architecture through cytoskeletal regulation. Inhibition of the cytoskeleton in this study diminished the confinement of NKp46 in hypo-responsive NK cells; therefore, actin regulatory proteins may differentially orchestrate receptor architecture, and these cues might derive from ITIM signaling intermediaries such as SHP-1/2. As mentioned earlier, higher expression and clustering of KIR molecules favor the activation of SHP-1 which may dephosphorylate and activate Crk (Kennedy et al., 2019). It is interesting to consider that SHP-1-based signaling, which was shown to regulate NK cell education (Viant et al., 2014), could therefore mediate organization of receptors on educated cells through effects on cytoskeletal regulators such as Crk.

It would also be interesting to explore whether other elements that are involved in cytoskeletal regulation differ between the subsets of educated and uneducated NK cells. For example, moesin and α-actinin-1 control ICAM mobility in dendritic cells and their expression increases in mature DCs (Comrie et al., 2015b). It is possible that changes in the expression levels of moesin and α-actinin-1 occur in NK cells throughout their development, controlling NK cell education. This is in line with studies that demonstrated effects of integrins on NK cell education (Enqvist et al., 2015). Specifically, Enqvist et al. (2015) showed that educated NK cells displayed higher concentrations of DNAM-1 and LFA-1 in its high affinity conformation. This implies that the actin network, and perhaps actin dynamics, tune NK cell education by controlling integrin activity. Furthermore, Thomas et al. (2013) showed that inside-out signaling to LFA-1 occurs only in educated NK cells, preserving their cytotoxicity, as opposed to uneducated NK cells that lack proficient inside-out signaling to LFA-1 integrin.

Additional evidence for cytoskeletal regulation of NK cell education was recently shown by Staaf et al. (2018), who demonstrated that the activating NKp46 receptor is more diffuse and the inhibitory LY49A receptor is more confined to microdomains at the surface of educated NK cells. Furthermore, disrupting actin dynamics hampers NKp46 mediated calcium flux in NK cells (Staaf et al., 2018). NKp46 dynamism, mediated by cytoskeletal reorganization, may therefore enhance the probability of engagement with ligands and increase the response of NK cells. Still, it is unclear how education through MHC-I orchestrates these processes. Once again, it is possible that ITIM-dependent signaling primes NK cells through SHP-1 activation of cytoskeletal regulators. This is also evident in studies conducted in T-cells, in which SHP-1 was shown to promote adhesion by dephosphorylation of CrkII (Azoulay-Alfaguter et al., 2017). These are all exciting concepts, as they may open a path to re-sensitization of NK cells through cytoskeletal manipulation.

CONCLUDING REMARKS AND FUTURE PERSPECTIVES

The cytoskeletal machinery has been established as an indispensable element of NK cell function. NK cells rely on efficient actin and microtubule dynamics, as well as Myosin motor activity for most effector functions. Abnormalities affecting actin turnover, Myosin motor function, and MTOC polarization cause severe impairments in NK cell cytotoxicity and migration, and thereby lead to various pathologies such as primary immune deficiencies.

Multiple ground breaking studies utilizing advanced super resolution microscopy resolved many questions regarding the spatio-temporal organization of the cytoskeleton during NK cell activation and inhibition, and how these different actin morphologies facilitate specific effector functions. These studies also emphasize the importance of receptor and accessory/adhesion molecule architecture on the surface of NK cells, and how it influences the activation threshold and possibly the education state. Furthermore, classic biochemical analyses and assays using specific cytoskeletal inhibitors, or evaluation of NK cells from patients with primary immunodeficiencies enhanced our knowledge regarding key signaling components regulating the cytoskeleton in NK cells.

Important issues still require investigation. Most of the signaling pathways leading to actin reorganization that were described for T and B cells occur downstream to a single dominant receptor. NK signaling pathways are more complex due to the different constellations of activating or inhibiting receptor co-ligation, and the interplay between surface co-receptors that dictates NK cell stimulation. Much more study is needed to understand how NK cell signaling is tuned downstream to different receptor combinations (both activating and inhibitory), and how these influence cytoskeletal reorganization and receptor organization. In addition, we still know little regarding how different cytoskeletal regulators, namely NFs and NPFs play a role in shaping the architecture of the NKIS and the nano-scale organization of surface receptors.

Genetic modulation of such factors in NK cell lines and primary NK cells may reveal their roles in coordinating the organization of receptors on the NK cell surface and influencing their activation states.

In recent years, it was shown that NK cells belong to a larger family of ILCs that have unique tissue distribution and function. NK cell heterogeneity is staggering, and it will be a future challenge to uncover how the cytoskeleton shapes the receptor organization and activity of distinct NK cell subtypes during homeostasis and pathology. Since many tissue-resident NK cells display a less cytotoxic phenotype, it is likely that their cytoskeleton is regulated differently and might arrange the architecture of surface receptors in a unique manner. Furthermore, it will be interesting to examine NK cytoskeletal dysfunction in diseases such as chronic viral infection.

Finally, most studies in immune cells have focused on how signaling proteins impact actin-based mechanisms, and the consequent effect of the actin meshwork on immune cell function. Only recently has the reciprocal integration and effect of the cytoskeletal machinery on signaling cascades begun to be investigated, specifically in the context of mechanotransduction. In NK cells, these issues remain even more enigmatic, yet it is clear that the robust and versatile nature of the actin cytoskeleton in NK cells plays additional roles beyond those described to date. Elucidating further functions of actin dynamics in NK cells may enhance our understanding of global NK cell signaling integration, and how this ultimately leads to NK cell development and function. Consequently, this raises the exciting possibility of actin modifying therapies for treating immune deficiencies and for immunotherapy.

AUTHOR CONTRIBUTIONS

AB-S, BS, and MB-S wrote the manuscript. All authors contributed to the article and approved the submitted version.

ACKNOWLEDGMENTS

This research was funded by the Israel Science Foundation grant no. 747/13 and from the Chief Scientist Office of the Ministry of Health grant no. 3-10151, and a Taubenblatt Family Foundation Bio-Medicine excellence grant.

REFERENCES

Abdul-Manan, N., Aghazadeh, B., Liu, G. A., Majumdar, A., Ouerfelli, O., Siminovitch, K. A., et al. (1999). Structure of Cdc42 in complex with the GTPase-binding domain of the 'Wiskott-Aldrich syndrome' protein. *Nature* 399, 379–383. doi: 10.1038/20726

Abel, A. M., Tiwari, A. A., Gerbec, Z. J., Siebert, J. R., Yang, C., Schloemer, N. J., et al. (2018). IQ domain-containing GTPase-activating protein 1 regulates cytoskeletal reorganization and facilitates NKG2D-mediated mechanistic target of rapamycin complex 1 activation and cytokine gene translation in natural killer cells. *Front. Immunol.* 9:1168. doi: 10.3389/fimmu.2018.01168

Abeyweera, T. P., Merino, E., and Huse, M. (2011). Inhibitory signaling blocks activating receptor clustering and induces cytoskeletal retraction in natural killer cells. *J. Cell Biol.* 192, 675–690. doi: 10.1083/jcb.201009135

Akhmanova, A., and Steinmetz, M. O. (2015). Control of microtubule organization and dynamics: two ends in the limelight. *Nat. Rev. Mol. Cell Biol.* 16, 711–726. doi: 10.1038/nrm4084

Al Absi, A., Wurzer, H., Guerin, C., Hoffmann, C., Moreau, F., Mao, X., et al. (2018). Actin cytoskeleton remodeling drives breast cancer cell escape from natural killer-mediated cytotoxicity. *Cancer Res.* 78, 5631–5643. doi: 10.1158/0008-5472.can-18-0441

Allavena, P. (1991). Molecules and structures involved in the adhesion of natural killer cells to vascular endothelium. *J. Exp. Med.* 173, 439–448. doi: 10.1084/jem.173.2.439

Andzelm, M. M., Chen, X., Krzewski, K., Orange, J. S., and Strominger, J. L. (2007). Myosin IIA is required for cytolytic granule exocytosis in human NK cells. *J. Exp. Med.* 204, 2285–2291. doi: 10.1084/jem.20071143

Antoku, S., and Mayer, B. J. (2009). Distinct roles for Crk adaptor isoforms in actin reorganization induced by extracellular signals. *J. Cell Sci.* 122, 4228–4238. doi: 10.1242/jcs.054627

Azoulay-Alfaguter, I., Strazza, M., Peled, M., Novak, H. K., Muller, J., Dustin, M. L., et al. (2017). The tyrosine phosphatase SHP-1 promotes T cell adhesion by activating the adaptor protein CrkII in the immunological synapse. *Sci. Signal.* 10:eaal2880. doi: 10.1126/scisignal.aal2880

Babich, A., Li, S., O'Connor, R. S., Milone, M. C., Freedman, B. D., and Burkhardt, J. K. (2012). F-actin polymerization and retrograde flow drive sustained PLCγ1 signaling during T cell activation. *J. Cell Biol.* 197, 775–787. doi: 10.1083/jcb.201201018

Bálint, Š, Lopes, F. B., and Davis, D. M. (2018). A nanoscale reorganization of the IL-15 receptor is triggered by NKG2D in a ligand-dependent manner. *Sci. Signal.* 11:eaal3606. doi: 10.1126/scisignal.aal3606

Banerjee, P. P., and Orange, J. S. (2010). Quantitative measurement of F-actin accumulation at the NK cell immunological synapse. *J. Immunol. Methods* 355, 1–13. doi: 10.1016/j.jim.2010.02.003

Banerjee, P. P., Pandey, R., Zheng, R., Suhoski, M. M., Monaco-Shawver, L., and Orange, J. S. (2007). Cdc42-interacting protein-4 functionally links actin and microtubule networks at the cytolytic NK cell immunological synapse. *J. Exp. Med.* 204, 2305–2320. doi: 10.1084/jem.20061893

Barber, D. F., Faure, M., and Long, E. O. (2004). LFA-1 contributes an early signal for NK cell cytotoxicity. *J. Immunol.* 173, 3653–3659. doi: 10.4049/jimmunol.173.6.3653

Barda-Saad, M., Braiman, A., Titerence, R., Bunnell, S. C., Barr, V. A., and Samelson, L. E. (2005). Dynamic molecular interactions linking the T cell antigen receptor to the actin cytoskeleton. *Nat. Immunol.* 6, 80–89. doi: 10.1038/ni1143

Barda-saad, M., Shirasu, N., Pauker, M. H., Hassan, N., Perl, O., Balbo, A., et al. (2010). Cooperative interactions at the SLP-76 complex are critical for actin polymerization. *EMBO J.* 29, 2315–2328. doi: 10.1038/emboj.2010.133

Barreira da Silva, R., Graf, C., and Münz, C. (2011). Cytoskeletal stabilization of inhibitory interactions in immunologic synapses of mature human dendritic cells with natural killer cells. *Blood* 118, 6487–6498. doi: 10.1182/blood-2011-07-366328

Basu, R., Whitlock, B. M., Husson, J., Le Floc'h, A., Jin, W., Oyler-Yaniv, A., et al. (2016). Cytotoxic T cells use mechanical force to potentiate target cell killing. *Cell* 165, 100–110. doi: 10.1016/j.cell.2016.01.021

Ben-Shmuel, A., Joseph, N., Sabag, B., and Barda-Saad, M. (2019). Lymphocyte mechanotransduction: the regulatory role of cytoskeletal dynamics in signaling cascades and effector functions. *J. Leukoc. Biol.* 105, 1261–1273. doi: 10.1002/JLB.MR0718-267R

Billadeau, D. D., Brumbaugh, K. M., Dick, C. J., Schoon, R. A., Bustelo, X. R., and Leibson, P. J. (1998). The Vav-Rac1 pathway in cytotoxic lymphocytes regulates the generation of cell-mediated killing. *J. Exp. Med.* 188, 549–559. doi: 10.1084/jem.188.3.549

Billadeau, D. D., Upshaw, J. L., Schoon, R. A., Dick, C. J., and Leibson, P. J. (2003). NKG2D-DAP10 triggers human NK cell-mediated killing via a Syk-independent regulatory pathway. *Nat. Immunol.* 4, 557–564. doi: 10.1038/ni929

Binstadt, B. A., Billadeau, D. D., Jevremovic, D., Williams, B. L., Fang, N., Yi, T., et al. (1998). SLP-76 is a direct substrate of SHP-1 recruited to killer cell inhibitory receptors. *J. Biol. Chem.* 273, 27518–27523. doi: 10.1074/jbc.273.42.27518

Boztug, K., Germeshausen, M., Avedillo Díez, I., Gulacsy, V., Diestelhorst, J., Ballmaier, M., et al. (2008). Multiple independent second-site mutations in two siblings with somatic mosaicism for Wiskott-Aldrich syndrome. *Clin. Genet.* 74, 68–74. doi: 10.1111/j.1399-0004.2008.01019.x

Brown, A. C. N., Dobbie, I. M., Alakoskela, J.-M., Davis, I., and Davis, D. M. (2012). Super-resolution imaging of remodeled synaptic actin reveals different synergies between NK cell receptors and integrins. *Blood* 120, 3729–3740. doi: 10.1182/blood-2012-05-429977

Brown, A. C. N., Oddos, S., Dobbie, I. M., Alakoskela, J.-M., Parton, R. M., Eissmann, P., et al. (2011). Remodelling of cortical actin where lytic granules dock at natural killer cell immune synapses revealed by super-resolution microscopy. *PLoS Biol.* 9:e1001152. doi: 10.1371/journal.pbio.1001152

Brugnera, E., Haney, L., Grimsley, C., Lu, M., Walk, S. F., Tosello-Trampont, A.-C., et al. (2002). Unconventional Rac-GEF activity is mediated through the Dock180-ELMO complex. *Nat. Cell Biol.* 4, 574–582. doi: 10.1038/ncb824

Bryceson, Y. T., March, M. E., Ljunggren, H.-G., and Long, E. O. (2006). Synergy among receptors on resting NK cells for the activation of natural cytotoxicity and cytokine secretion. *Blood* 107, 159–166. doi: 10.1182/blood-2005-04-1351

Bryceson, Y. T., Rudd, E., Zheng, C., Edner, J., Ma, D., Wood, S. M., et al. (2007). Defective cytotoxic lymphocyte degranulation in syntaxin-11-deficient familial hemophagocytic lymphohistiocytosis 4 (FHL4) patients. *Blood* 110, 1906–1915. doi: 10.1182/blood-2007-02-074468

Burshtyn, D. N., Shin, J., Stebbins, C., and Long, E. O. (2000). Adhesion to target cells is disrupted by the killer cell inhibitory receptor. *Curr. Biol.* 10, 777–780. doi: 10.1016/s0960-9822(00)00568-6

Butler, B., and Cooper, J. A. (2009). Distinct roles for the actin nucleators Arp2/3 and hDia1 during NK-mediated cytotoxicity. *Curr. Biol.* 19, 1886–1896. doi: 10.1016/j.cub.2009.10.029

Butler, B., Kastendieck, D. H., and Cooper, J. A. (2008). Differently phosphorylated forms of the cortactin homolog HS1 mediate distinct functions in natural killer cells. *Nat. Immunol.* 9, 887–897. doi: 10.1038/ni.1630

Carisey, A. F., Mace, E. M., Saeed, M. B., Davis, D. M., and Orange, J. S. (2018). Nanoscale dynamism of actin enables secretory function in cytolytic cells. *Curr. Biol.* 28, 489–502.e9.

Carpén, O., Virtanen, I., Lehto, V. P., and Saksela, E. (1983). Polarization of NK cell cytoskeleton upon conjugation with sensitive target cells. *J. Immunol.* 131, 2695–2698.

Catucci, M., Zanoni, I., Draghici, E., Bosticardo, M., Castiello, M. C., Venturini, M., et al. (2014). Wiskott-Aldrich syndrome protein deficiency in natural killer and dendritic cells affects antitumor immunity. *Eur. J. Immunol.* 44, 1039–1045. doi: 10.1002/eji.201343935

Cella, M., Fujikawa, K., Tassi, I., Kim, S., Latinis, K., Nishi, S., et al. (2004). Differential requirements for Vav proteins in DAP10- and ITAM-mediated NK cell cytotoxicity. *J. Exp. Med.* 200, 817–823. doi: 10.1084/jem.20031847

Chen, R., Relouzat, F., Roncagalli, R., Aoukaty, A., Tan, R., Latour, S., et al. (2004). Molecular dissection of 2B4 signaling: implications for signal transduction by SLAM-related receptors. *Mol. Cell. Biol.* 24, 5144–5156. doi: 10.1128/mcb.24.12.5144-5156.2004

Chen, X., Allan, D. S. J., Krzewski, K., Ge, B., Kopcow, H., and Strominger, J. L. (2006). CD28-stimulated ERK2 phosphorylation is required for polarization of the microtubule organizing center and granules in YTS NK cells. *Proc. Natl. Acad. Sci. U.S.A.* 103, 10346–10351. doi: 10.1073/pnas.0604236103

Chen, X., Trivedi, P. P., Ge, B., Krzewski, K., and Strominger, J. L. (2007). Many NK cell receptors activate ERK2 and JNK1 to trigger microtubule organizing center and granule polarization and cytotoxicity. *Proc. Natl. Acad. Sci. U.S.A.* 104, 6329–6334. doi: 10.1073/pnas.0611655104

Chereau, D., Kerff, F., Graceffa, P., Grabarek, Z., Langsetmo, K., and Dominguez, R. (2005). Actin-bound structures of Wiskott-Aldrich syndrome protein (WASP)-homology domain 2 and the implications for filament assembly. *Proc. Natl. Acad. Sci. U.S.A.* 102, 16644–16649. doi: 10.1073/pnas.0507021102

Choudhuri, K., Llodrá, J., Roth, E. W., Tsai, J., Gordo, S., Wucherpfennig, K. W., et al. (2014). Polarized release of T-cell-receptor-enriched microvesicles at the immunological synapse. *Nature* 507, 118–123. doi: 10.1038/nature12951

Comrie, W. A., Babich, A., and Burkhardt, J. K. (2015a). F-actin flow drives affinity maturation and spatial organization of LFA-1 at the immunological synapse. *J. Cell Biol.* 208, 475–491. doi: 10.1083/jcb.201406121

Comrie, W. A., Li, S., Boyle, S., and Burkhardt, J. K. (2015b). The dendritic cell cytoskeleton promotes T cell adhesion and activation by constraining ICAM-1 mobility. *J. Cell Biol.* 208, 457–473. doi: 10.1083/jcb.201406120

Comrie, W. A., and Burkhardt, J. K. (2016). Action and traction: cytoskeletal control of receptor triggering at the immunological synapse. *Front. Immunol.* 7:68. doi: 10.3389/fimmu.2016.00068

Cory, G. O. C., Garg, R., Cramer, R., and Ridley, A. J. (2002). Phosphorylation of tyrosine 291 enhances the ability of WASp to stimulate actin polymerization and filopodium formation. Wiskott-aldrich syndrome protein. *J. Biol. Chem.* 277, 45115–45121. doi: 10.1074/jbc.m203346200

Côté, J.-F., and Vuori, K. (2002). Identification of an evolutionarily conserved superfamily of DOCK180-related proteins with guanine nucleotide exchange activity. *J. Cell Sci.* 115(Pt 24), 4901–4913. doi: 10.1242/jcs.00219

Côte, M., Ménager, M. M., Burgess, A., Mahlaoui, N., Picard, C., Schaffner, C., et al. (2009). Munc18-2 deficiency causes familial hemophagocytic lymphohistiocytosis type 5 and impairs cytotoxic granule exocytosis in patient NK cells. *J. Clin. Invest.* 119, 3765–3773. doi: 10.1172/jci40732

Culley, F. J., Johnson, M., Evans, J. H., Kumar, S., Crilly, R., Casasbuenas, J., et al. (2009). Natural killer cell signal integration balances synapse symmetry and migration. *PLoS Biol.* 7:e1000159. doi: 10.1371/journal.pbio.1000159

Davis, D. M. (2009). Mechanisms and functions for the duration of intercellular contacts made by lymphocytes. *Nat. Rev. Immunol.* 9, 543–555. doi: 10.1038/nri2602

Davis, D. M., Chiu, I., Fassett, M., Cohen, G. B., Mandelboim, O., and Strominger, J. L. (1999). The human natural killer cell immune synapse. *Proc. Natl. Acad. Sci. U.S.A.* 96, 15062–15067.

de la Fuente, M. A., Sasahara, Y., Calamito, M., Antón, I. M., Elkhal, A., Gallego, M. D., et al. (2007). WIP is a chaperone for Wiskott-Aldrich syndrome protein (WASP). *Proc. Natl. Acad. Sci. U.S.A.* 104, 926–931.

Delcassian, D., Depoil, D., Rudnicka, D., Liu, M., Davis, D. M., Dustin, M. L., et al. (2013). Nanoscale ligand spacing influences receptor triggering in T cells and NK cells. *Nano Lett.* 13, 5608–5614. doi: 10.1021/nl403252x

Dell'Angelica, E. C., Ohno, H., Ooi, C. E., Rabinovich, E., Roche, K. W., and Bonifacino, J. S. (1997). AP-3: an adaptor-like protein complex with ubiquitous expression. *EMBO J.* 16, 917–928. doi: 10.1093/emboj/16.5.917

Dell'Angelica, E. C., Shotelersuk, V., Aguilar, R. C., Gahl, W. A., and Bonifacino, J. S. (1999). Altered trafficking of lysosomal proteins in hermansky-pudlak syndrome due to mutations in the β3A subunit of the AP-3 adaptor. *Mol. Cell* 3, 11–21. doi: 10.1016/s1097-2765(00)80170-7

Derry, J. M. J., Ochs, H. D., and Francke, U. (1994). Isolation of a novel gene mutated in Wiskott-Aldrich syndrome. *Cell* 78, 635–644. doi: 10.1016/0092-8674(94)90528-2

Desai, A., Verma, S., Mitchison, T. J., and Walczak, C. E. (1999). Kin I kinesins are microtubule-destabilizing enzymes. *Cell* 96, 69–78. doi: 10.1016/s0092-8674(00)80960-5

Dobbs, K., Domínguez Conde, C., Zhang, S.-Y., Parolini, S., Audry, M., Chou, J., et al. (2015). Inherited DOCK2 deficiency in patients with early-onset invasive infections. *N. Engl. J. Med.* 372, 2409–2422.

Dong, Z., Davidson, D., Pérez-Quintero, L. A., Kurosaki, T., Swat, W., and Veillette, A. (2012). The adaptor SAP controls NK cell activation by regulating the enzymes Vav-1 and SHIP-1 and by enhancing conjugates with target cells. *Immunity* 36, 974–985. doi: 10.1016/j.immuni.2012.03.023

Downward, J., Graves, J. D., Warne, P. H., Rayter, S., and Cantrell, D. A. (1990). Stimulation of p21ras upon T-cell activation. *Nature* 346, 719–723. doi: 10.1038/346719a0

Duan, X., Lu, J., Wang, H., Liu, X., Wang, J., Zhou, K., et al. (2017). Bidirectional factors impact the migration of NK cells to draining lymph node in aged mice during influenza virus infection. *Exp. Gerontol.* 96, 127–137. doi: 10.1016/j.exger.2017.06.021

Dulyaninova, N. G., Malashkevich, V. N., Almo, S. C., and Bresnick, A. R. (2005). Regulation of Myosin-IIA assembly and Mts1 binding by heavy chain phosphorylation †. *Biochemistry* 44, 6867–6876. doi: 10.1021/bi0500776

Dustin, M. L. (2014). The immunological synapse. *Cancer Immunol. Res.* 2, 1023–1033.

Dustin, M. L., Chakraborty, A. K., and Shaw, A. S. (2010). Understanding the structure and function of the immunological synapse. *Cold Spring Harb. Perspect. Biol.* 2:a002311. doi: 10.1101/cshperspect.a002311

Dustin, M. L., and Long, E. O. (2010). Cytotoxic immunological synapses. *Immunol. Rev.* 235, 24–34. doi: 10.1111/j.0105-2896.2010.00904.x

Eisenmann, K. M., West, R. A., Hildebrand, D., Kitchen, S. M., Peng, J., Sigler, R., et al. (2007). T cell responses in mammalian diaphanous-related formin mDia1 knock-out mice. *J. Biol. Chem.* 282, 25152–25158. doi: 10.1074/jbc.m703243200

Eissmann, P., Beauchamp, L., Wooters, J., Tilton, J. C., Long, E. O., and Watzl, C. (2005). Molecular basis for positive and negative signaling by the natural killer cell receptor 2B4 (CD244). *Blood* 105, 4722–4729. doi: 10.1182/blood-2004-09-3796

Eissmann, P., and Watzl, C. (2006). Molecular analysis of NTB-A signaling: a role for EAT-2 in NTB-A-mediated activation of human NK cells. *J. Immunol.* 177, 3170–3177. doi: 10.4049/jimmunol.177.5.3170

El-Shazly, A. E., Doloriert, H. C., Bisig, B., Lefebvre, P. P., Delvenne, P., and Jacobs, N. (2013). Novel cooperation between CX3CL1 and CCL26 inducing NK cell chemotaxis via CX3CR1: a possible mechanism for NK cell infiltration of the allergic nasal tissue. *Clin. Exp. Allergy* 43, 322–331. doi: 10.1111/cea.12022

Elstak, E. D., Neeft, M., Nehme, N. T., Voortman, J., Cheung, M., Goodarzifard, M., et al. (2011). The munc13-4-rab27 complex is specifically required for tethering secretory lysosomes at the plasma membrane. *Blood* 118, 1570–1578. doi: 10.1182/blood-2011-02-339523

Enqvist, M., Ask, E. H., Forslund, E., Carlsten, M., Abrahamsen, G., Beziat, V., et al. (2015). Coordinated expression of DNAM-1 and LFA-1 in educated NK cells. *J. Immunol.* 194, 4518–4527. doi: 10.4049/jimmunol.1401972

Fassett, M. S., Davis, D. M., Valter, M. M., Cohen, G. B., and Strominger, J. L. (2001). Signaling at the inhibitory natural killer cell immune synapse regulates lipid raft polarization but not class I MHC clustering. *Proc. Natl. Acad. Sci. U.S.A.* 98, 14547–14552. doi: 10.1073/pnas.211563598

Faure, M., Barber, D. F., Takahashi, S. M., Jin, T., and Long, E. O. (2003). Spontaneous clustering and tyrosine phosphorylation of NK cell inhibitory receptor induced by ligand binding. *J. Immunol.* 170, 6107–6114. doi: 10.4049/jimmunol.170.12.6107

Feldmann, J., Callebaut, I., Raposo, G., Certain, S., Bacq, D., Dumont, C., et al. (2003). Munc13-4 is essential for cytolytic granules fusion and is mutated in a form of familial hemophagocytic lymphohistiocytosis (FHL3). *Cell* 115, 461–473. doi: 10.1016/s0092-8674(03)00855-9

Fogler, W. E., Volker, K., McCormick, K. L., Watanabe, M., Ortaldo, J. R., and Wiltrout, R. H. (1996). NK cell infiltration into lung, liver, and subcutaneous B16 melanoma is mediated by VCAM-1/VLA-4 interaction. *J. Immunol.* 156, 4707–4714.

Fontana, S., Parolini, S., Vermi, W., Booth, S., Gallo, F., Donini, M., et al. (2006). Innate immunity defects in hermansky-pudlak type 2 syndrome. *Blood* 107, 4857–4864. doi: 10.1182/blood-2005-11-4398

Fried, S., Matalon, O., Noy, E., and Barda-Saad, M. (2014a). WIP: more than a WASp-interacting protein. *J. Leukoc. Biol.* 96, 713–727. doi: 10.1189/jlb.2ru0314-162r

Fried, S., Reicher, B., Pauker, M. H., Eliyahu, S., Matalon, O., Noy, E., et al. (2014b). Triple-color FRET analysis reveals conformational changes in the WIP-WASp actin-regulating complex. *Sci. Signal.* 7:ra60. doi: 10.1126/scisignal.2005198

Galjart, N. (2005). CLIPs and CLASPs and cellular dynamics. *Nat. Rev. Mol. Cell Biol.* 6, 487–498. doi: 10.1038/nrm1664

Gardner, M. K., Zanic, M., Gell, C., Bormuth, V., and Howard, J. (2011). Depolymerizing kinesins Kip3 and MCAK shape cellular microtubule architecture by differential control of catastrophe. *Cell* 147, 1092–1103. doi: 10.1016/j.cell.2011.10.037

Garrod, K. R., Wei, S. H., Parker, I., and Cahalan, M. D. (2007). Natural killer cells actively patrol peripheral lymph nodes forming stable conjugates to eliminate MHC-mismatched targets. *Proc. Natl. Acad. Sci. U.S.A.* 104, 12081–12086. doi: 10.1073/pnas.0702867104

Gasman, S., Kalaidzidis, Y., and Zerial, M. (2003). RhoD regulates endosome dynamics through Diaphanous-related Formin and Src tyrosine kinase. *Nat. Cell Biol.* 5, 195–204. doi: 10.1038/ncb935

Gil-Krzewska, A., Saeed, M. B., Oszmiana, A., Fischer, E. R., Lagrue, K., Gahl, W. A., et al. (2017). An actin cytoskeletal barrier inhibits lytic granule release from natural killer cells in patients with Chediak-Higashi syndrome. *J. Allergy Clin. Immunol.* 142, 914–927.e6. doi: 10.1016/j.jaci.2017.10.040

Gismondi, A., Bisogno, L., Mainiero, F., Palmieri, G., Piccoli, M., Frati, L., et al. (1997). Proline-rich tyrosine kinase-2 activation by beta 1 integrin fibronectin receptor cross-linking and association with paxillin in human natural killer cells. *J. Immunol.* 159, 4729–4736.

Gismondi, A., Cifaldi, L., Mazza, C., Giliani, S., Parolini, S., Morrone, S., et al. (2004). Impaired natural and CD16-mediated NK cell cytotoxicity in patients with WAS and XLT: ability of IL-2 to correct NK cell functional defect. *Blood* 104, 436–443. doi: 10.1182/blood-2003-07-2621

Giurisato, E., Cella, M., Takai, T., Kurosaki, T., Feng, Y., Longmore, G. D., et al. (2007). Phosphatidylinositol 3-kinase activation is required to form the NKG2D immunological synapse. *Mol. Cell. Biol.* 27, 8583–8599. doi: 10.1128/mcb.01477-07

Gomez, T. S., Kumar, K., Medeiros, R. B., Shimizu, Y., Leibson, P. J., and Billadeau, D. D. (2007). Formins regulate the actin-related protein 2/3 complex-independent polarization of the centrosome to the immunological synapse. *Immunity* 26, 177–190. doi: 10.1016/j.immuni.2007.01.008

Graham, D. B., Cella, M., Giurisato, E., Fujikawa, K., Miletic, A. V., Kloeppel, T., et al. (2006). Vav1 Controls DAP10-mediated natural cytotoxicity by regulating actin and microtubule dynamics. *J. Immunol.* 177, 2349–2355. doi: 10.4049/jimmunol.177.4.2349

Gross, C. C., Brzostowski, J. A., Liu, D., and Long, E. O. (2010). Tethering of intercellular adhesion molecule on target cells is required for LFA-1-dependent NK cell adhesion and granule polarization. *J. Immunol.* 185, 2918–2926. doi: 10.4049/jimmunol.1000761

Guia, S., Jaeger, B. N., Piatek, S., Mailfert, S., Trombik, T., Fenis, A., et al. (2011). Confinement of activating receptors at the plasma membrane controls natural killer cell tolerance. *Sci. Signal.* 4:ra21. doi: 10.1126/scisignal.2001608

Hadad, U., Thauland, T. J., Martinez, O. M., Butte, M. J., Porgador, A., and Krams, S. M. (2015). NKp46 clusters at the immune synapse and regulates NK cell polarization. *Front. Immunol.* 6:495. doi: 10.3389/fimmu.2015.00495

Ham, H., and Billadeau, D. D. (2014). Human immunodeficiency syndromes affecting human natural killer cell cytolytic activity. *Front. Immunol.* 5:2. doi: 10.3389/fimmu.2014.00002

Ham, H., Guerrier, S., Kim, J., Schoon, R. A., Anderson, E. L., Hamann, M. J., et al. (2013). Dedicator of cytokinesis 8 interacts with talin and Wiskott-Aldrich syndrome protein to regulate NK cell cytotoxicity. *J. Immunol.* 190, 3661–3669. doi: 10.4049/jimmunol.1202792

Ham, H., Huynh, W., Schoon, R. A., Vale, R. D., and Billadeau, D. D. (2015). HkRP3 is a microtubule-binding protein regulating lytic granule clustering and NK cell killing. *J. Immunol.* 194, 3984–3996. doi: 10.4049/jimmunol.1402897

Hammer, J. A., Wang, J., Saeed, M., and Pedrosa, A. (2019). Origin, organization, dynamics, and function of Actin and Actomyosin networks at the T cell immunological synapse. *Annu. Rev. Immunol.* 37, 201–224. doi: 10.1146/annurev-immunol-042718-041341

Han, J. (1998). Role of substrates and products of PI 3-kinase in regulating activation of rac-related guanosine Triphosphatases by Vav. *Science* 279, 558–560. doi: 10.1126/science.279.5350.558

Harada, Y., Tanaka, Y., Terasawa, M., Pieczyk, M., Habiro, K., Katakai, T., et al. (2012). DOCK8 is a Cdc42 activator critical for interstitial dendritic cell migration during immune responses. *Blood* 119, 4451–4461. doi: 10.1182/blood-2012-01-407098

Hashimoto-tane, A., Yokosuka, T., Sakata-sogawa, K., Sakuma, M., and Ishihara, C. (2011). Article dynein-driven transport of T cell receptor microclusters regulates immune synapse formation and T cell activation. *Immunity* 34, 919–931. doi: 10.1016/j.immuni.2011.05.012

Hendricks, A. G., Lazarus, J. E., Perlson, E., Gardner, M. K., Odde, D. J., Goldman, Y. E., et al. (2012). Dynein tethers and stabilizes dynamic microtubule plus ends. *Curr. Biol.* 22, 632–637. doi: 10.1016/j.cub.2012.02.023

Hoffmann, S. C., Cohnen, A., Ludwig, T., and Watzl, C. (2011). 2B4 engagement mediates rapid LFA-1 and actin-dependent NK cell adhesion to tumor cells as measured by single cell force spectroscopy. *J. Immunol.* 186, 2757–2764. doi: 10.4049/jimmunol.1002867

Hsu, H.-T., Mace, E. M., Carisey, A. F., Viswanath, D. I., Christakou, A. E., Wiklund, M., et al. (2016). NK cells converge lytic granules to promote cytotoxicity and prevent bystander killing. *J. Cell Biol.* 215, 875–889. doi: 10.1083/jcb.201604136

Hsu, K. C., Keever-Taylor, C. A., Wilton, A., Pinto, C., Heller, G., Arkun, K., et al. (2005). Improved outcome in HLA-identical sibling hematopoietic stem-cell

transplantation for acute myelogenous leukemia predicted by KIR and HLA genotypes. *Blood* 105, 4878–4884. doi: 10.1182/blood-2004-12-4825

Huang, L., Zhu, P., Xia, P., and Fan, Z. (2016). WASH has a critical role in NK cell cytotoxicity through Lck-mediated phosphorylation. *Cell Death Dis.* 7:e2301. doi: 10.1038/cddis.2016.212

Huang, W., Ochs, H. D., Dupont, B., and Vyas, Y. M. (2005). The Wiskott-Aldrich syndrome protein regulates nuclear translocation of NFAT2 and NF-kappa B (RelA) independently of its role in filamentous actin polymerization and actin cytoskeletal rearrangement. *J. Immunol.* 174, 2602–2611. doi: 10.4049/jimmunol.174.5.2602

Humphries, C. L., Balcer, H. I., D'Agostino, J. L., Winsor, B., Drubin, D. G., Barnes, G., et al. (2002). Direct regulation of Arp2/3 complex activity and function by the actin binding protein coronin. *J. Cell Biol.* 159, 993–1004. doi: 10.1083/jcb.200206113

Huse, M. (2017). Mechanical forces in the immune system. *Nat. Rev. Immunol.* 17, 679–690. doi: 10.1038/nri.2017.74

Hammer, J. A., and Burkhardt, J. K. (2013). Controversy and consensus regarding myosin II function at the immunological synapse. *Curr. Opin. Immunol.* 25, 300–306. doi: 10.1016/j.coi.2013.03.010

Iizuka, Y., Cichocki, F., Sieben, A., Sforza, F., Karim, R., Coughlin, K., et al. (2015). UNC-45A Is a nonmuscle myosin IIA chaperone required for NK Cell cytotoxicity via control of lytic granule secretion. *J. Immunol.* 195, 4760–4770. doi: 10.4049/jimmunol.1500979

Imai, K., Matsuyama, S., Miyake, S., Suga, K., and Nakachi, K. (2000). Natural cytotoxic activity of peripheral-blood lymphocytes and cancer incidence: an 11-year follow-up study of a general population. *Lancet* 356, 1795–1799. doi: 10.1016/s0140-6736(00)03231-1

Imai, K., Morio, T., Zhu, Y., Jin, Y., Itoh, S., Kajiwara, M., et al. (2004). Clinical course of patients with WASP gene mutations. *Blood* 103, 456–464. doi: 10.1182/blood-2003-05-1480

Imai, K., Nonoyama, S., and Ochs, H. D. (2003). WASP (Wiskott-Aldrich syndrome protein) gene mutations and phenotype. *Curr. Opin. Allergy Clin. Immunol.* 3, 427–436. doi: 10.1097/00130832-200312000-00003

Introne, W., Boissy, R. E., and Gahl, W. A. (1999). Clinical, molecular, and cell biological aspects of chediak-higashi syndrome. *Mol. Genet. Metab.* 68, 283–303. doi: 10.1006/mgme.1999.2927

Ishigami, S., Natsugoe, S., Tokuda, K., Nakajo, A., Che, X., Iwashige, H., et al. (2000). Prognostic value of intratumoral natural killer cells in gastric carcinoma. *Cancer* 88, 577–583. doi: 10.1002/(sici)1097-0142(20000201)88:3<577::aid-cncr13>3.0.co;2-v

Jacobelli, J., Chmura, S. A., Buxton, D. B., Davis, M. M., and Krummel, M. F. (2004). A single class II myosin modulates T cell motility and stopping, but not synapse formation. *Nat. Immunol.* 5, 531–538. doi: 10.1038/ni1065

James, A. M., Hsu, H.-T., Dongre, P., Uzel, G., Mace, E. M., Banerjee, P. P., et al. (2013). Rapid activation receptor- or IL-2-induced lytic granule convergence in human natural killer cells requires Src, but not downstream signaling. *Blood* 121, 2627–2637. doi: 10.1182/blood-2012-06-437012

Jankowska, K. I., Williamson, E. K., Roy, N. H., Blumenthal, D., Chandra, V., Baumgart, T., et al. (2018). Integrins modulate T cell receptor signaling by constraining actin flow at the immunological synapse. *Front. Immunol.* 9:25. doi: 10.3389/fimmu.2018.00025

Jevremovic, D., Billadeau, D. D., Schoon, R. A., Dick, C. J., Irvin, B. J., Zhang, W., et al. (1999). Cutting edge: a role for the adaptor protein LAT in human NK Cell-mediated cytotoxicity. *J. Immunol.* 162, 2453–2456.

Johnson, K. G., Bromley, S. K., Dustin, M. L., and Thomas, M. L. (2000). A supramolecular basis for CD45 tyrosine phosphatase regulation in sustained T cell activation. *Proc. Natl. Acad. Sci. U.S.A.* 97, 10138–10143. doi: 10.1073/pnas.97.18.10138

Kanwar, N., and Wilkins, J. A. (2011). IQGAP1 involvement in MTOC and granule polarization in NK-cell cytotoxicity. *Eur. J. Immunol.* 41, 2763–2773. doi: 10.1002/eji.201040444

Karim, M. A., Suzuki, K., Fukai, K., Oh, J., Nagle, D. L., Moore, K. J., et al. (2002). Apparent genotype-phenotype correlation in childhood, adolescent, and adult Chediak-Higashi syndrome. *Am. J. Med. Genet.* 108, 16–22. doi: 10.1002/ajmg.10184

Katz, P., Zaytoun, A. M., and Lee, J. H. (1982). Mechanisms of human cell-mediated cytotoxicity. III. Dependence of natural killing on microtubule and microfilament integrity. *J. Immunol.* 129, 2816–2825.

Kennedy, P. R., Barthen, C., Williamson, D. J., Pitkeathly, W. T. E., Hazime, K. S., Cumming, J., et al. (2019). Genetic diversity affects the nanoscale membrane organization and signaling of natural killer cell receptors. *Sci. Signal.* 12:eaaw9252. doi: 10.1126/scisignal.aaw9252

Kim, A. S., Kakalis, L. T., Abdul-Manan, N., Liu, G. A., and Rosen, M. K. (2000). Autoinhibition and activation mechanisms of the Wiskott-Aldrich syndrome protein. *Nature* 404, 151–158. doi: 10.1038/35004513

Kim, H. S., Das, A., Gross, C. C., Bryceson, Y. T., and Long, E. O. (2010). Synergistic signals for natural cytotoxicity are required to overcome inhibition by c-Cbl ubiquitin ligase. *Immunity* 32, 175–186. doi: 10.1016/j.immuni.2010.02.004

Kim, H. S., and Long, E. O. (2012). Complementary phosphorylation sites in the adaptor protein SLP-76 promote synergistic activation of natural killer cells. *Sci. Signal.* 5:ra49. doi: 10.1126/scisignal.2002754

Kloc, M., Kubiak, J. Z., Li, X. C., and Ghobrial, R. M. (2014). The newly found functions of MTOC in immunological response. *J. Leukoc. Biol.* 95, 417–430. doi: 10.1189/jlb.0813468

Kopcow, H. D., Allan, D. S. J., Chen, X., Rybalov, B., Andzelm, M. M., Ge, B., et al. (2005). Human decidual NK cells form immature activating synapses and are not cytotoxic. *Proc. Natl. Acad. Sci. U.S.A.* 102, 15563–15568. doi: 10.1073/pnas.0507835102

Kritikou, J. S., Dahlberg, C. I. M., Baptista, M. A. P., Wagner, A. K., Banerjee, P. P., Gwalani, L. A., et al. (2016). IL-2 in the tumor microenvironment is necessary for Wiskott-Aldrich syndrome protein deficient NK cells to respond to tumors in vivo. *Sci. Rep.* 6:30636.

Krzewski, K., Chen, X., Orange, J. S., and Strominger, J. L. (2006). Formation of a WIP-, WASp-, actin-, and myosin IIA-containing multiprotein complex in activated NK cells and its alteration by KIR inhibitory signaling. *J. Cell Biol.* 173, 121–132. doi: 10.1083/jcb.200509076

Krzewski, K., Chen, X., and Strominger, J. L. (2008). WIP is essential for lytic granule polarization and NK cell cytotoxicity. *Proc. Natl. Acad. Sci. U.S.A.* 105, 2568–2573. doi: 10.1073/pnas.0711593105

Kueh, H. Y., Charras, G. T., Mitchison, T. J., and Brieher, W. M. (2008). Actin disassembly by cofilin, coronin, and Aip1 occurs in bursts and is inhibited by barbed-end cappers. *J. Cell Biol.* 182, 341–353. doi: 10.1083/jcb.200801027

Kumari, S., Depoil, D., Martinelli, R., Judokusumo, E., Carmona, G., Gertler, F. B., et al. (2015). Actin foci facilitate activation of the phospholipase C-γ in primary T lymphocytes via the WASP pathway. *eLife* 4:e04953.

Kumari, S., Vardhana, S., Cammer, M., Curado, S., Santos, L., Sheetz, M. P., et al. (2012). T Lymphocyte Myosin IIA is required for maturation of the immunological synapse. *Front. Immunol.* 3:230. doi: 10.3389/fimmu.2012.00230

Kurowska, M., Goudin, N., Nehme, N. T., Court, M., Garin, J., Fischer, A., et al. (2012). Terminal transport of lytic granules to the immune synapse is mediated by the kinesin-1/Slp3/Rab27a complex. *Blood* 119, 3879–3889. doi: 10.1182/blood-2011-09-382556

Lagrue, K., Carisey, A., Morgan, D. J., Chopra, R., and Davis, D. M. (2015). Lenalidomide augments actin remodeling and lowers NK-cell activation thresholds. *Blood* 126, 50–60. doi: 10.1182/blood-2015-01-625004

Lagrue, K., Carisey, A., Oszmiana, A., Kennedy, P. R., Williamson, D. J., Cartwright, A., et al. (2013). The central role of the cytoskeleton in mechanisms and functions of the NK cell immune synapse. *Immunol. Rev.* 256, 203–221. doi: 10.1111/imr.12107

Lämmermann, T., Bader, B. L., Monkley, S. J., Worbs, T., Wedlich-Söldner, R., Hirsch, K., et al. (2008). Rapid leukocyte migration by integrin-independent flowing and squeezing. *Nature* 453, 51–55. doi: 10.1038/nature06887

Lanier, L. L. (1998). NK cell receptors. *Annu. Rev. Immunol.* 16, 359–393.

Lanier, L. L. (2003). Natural killer cell receptor signaling. *Curr. Opin. Immunol.* 15, 308–314. doi: 10.1016/s0952-7915(03)00039-6

Lanzi, G., Moratto, D., Vairo, D., Masneri, S., Delmonte, O., Paganini, T., et al. (2012). A novel primary human immunodeficiency due to deficiency in the WASP-interacting protein WIP. *J. Exp. Med.* 209, 29–34. doi: 10.1084/jem.20110896

Latour, S., Roncagalli, R., Chen, R., Bakinowski, M., Shi, X., Schwartzberg, P. L., et al. (2003). Binding of SAP SH2 domain to FynT SH3 domain reveals a novel mechanism of receptor signalling in immune regulation. *Nat. Cell Biol.* 5, 149–154. doi: 10.1038/ncb919

Lee, S.-H., Miyagi, T., and Biron, C. A. (2007). Keeping NK cells in highly regulated antiviral warfare. *Trends Immunol.* 28, 252–259. doi: 10.1016/j.it.2007.04.001

Liu, D., Meckel, T., and Long, E. O. (2010). Distinct role of Rab27a in granule movement at the plasma membrane and in the cytosol of NK cells. *PLoS One* 5:e12870. doi: 10.1371/journal.pbio.10012870

Liu, D., Peterson, M. E., and Long, E. O. (2012). The adaptor protein Crk controls activation and inhibition of natural killer cells. *Immunity* 36, 600–611. doi: 10.1016/j.immuni.2012.03.007

Long, E. O. (1999). Regulation of immune responses through inhibitory receptors. *Annu. Rev. Immunol.* 17, 875–904. doi: 10.1146/annurev.immunol.17.1.875

Long, E. O. (2008). Negative signaling by inhibitory receptors: the NK cell paradigm. *Immunol. Rev.* 224, 70–84. doi: 10.1111/j.1600-065x.2008.00660.x

Long, E. O., Kim, H. S., Liu, D., Peterson, M. E., and Rajagopalan, S. (2013). Controlling natural killer cell responses: integration of signals for activation and inhibition. *Annu. Rev. Immunol.* 31, 227–258. doi: 10.1146/annurev-immunol-020711-075005

Lozano, M. L., Rivera, J., Sánchez-Guiu, I., and Vicente, V. (2014). Towards the targeted management of chediak-higashi syndrome. *Orphanet J. Rare Dis.* 9:132.

Mace, E. M., and Orange, J. S. (2014). Lytic immune synapse function requires filamentous actin deconstruction by Coronin 1A. *Proc. Natl. Acad. Sci. U.S.A.* 111, 6708–6713. doi: 10.1073/pnas.1314975111

Mace, E. M., Wu, W. W., Ho, T., Mann, S. S., Hsu, H.-T., and Orange, J. S. (2012). NK cell lytic granules are highly motile at the immunological synapse and require F-actin for post-degranulation persistence. *J. Immunol.* 189, 4870–4880. doi: 10.4049/jimmunol.1201296

Mace, E. M., Zhang, J., Siminovitch, K. A., and Takei, F. (2010). Elucidation of the integrin LFA-1-mediated signaling pathway of actin polarization in natural killer cells. *Blood* 116, 1272–1279. doi: 10.1182/blood-2009-12-261487

Maravillas-Montero, J. L., and Santos-Argumedo, L. (2012). The myosin family: unconventional roles of actin-dependent molecular motors in immune cells. *J. Leukoc. Biol.* 91, 35–46. doi: 10.1189/jlb.0711335

Marcenaro, S., Gallo, F., Martini, S., Santoro, A., Griffiths, G. M., Aricó, M., et al. (2006). Analysis of natural killer-cell function in familial hemophagocytic lymphohistiocytosis (FHL): defective CD107a surface expression heralds Munc13-4 defect and discriminates between genetic subtypes of the disease. *Blood* 108, 2316–2323. doi: 10.1182/blood-2006-04-015693

March, M. E., and Long, E. O. (2011). 2 Integrin induces TCR -Syk-Phospholipase C- phosphorylation and paxillin-dependent granule polarization in human NK cells. *J. Immunol.* 186, 2998–3005. doi: 10.4049/jimmunol.1002438

Martín-Cófreces, N. B., Baixauli, F., López, M. J., Gil, D., Monjas, A., Alarcón, B., et al. (2012). End-binding protein 1 controls signal propagation from the T cell receptor. *EMBO J.* 31, 4140–4152. doi: 10.1038/emboj.2012.242

Martín-Cófreces, N. B., Robles-Valero, J., Cabrero, J. R., Mittelbrunn, M., Gordón-Alonso, M., Sung, C.-H., et al. (2008). MTOC translocation modulates IS formation and controls sustained T cell signaling. *J. Cell Biol.* 182, 951–962. doi: 10.1083/jcb.200801014

Martín-Fontecha, A., Thomsen, L. L., Brett, S., Gerard, C., Lipp, M., Lanzavecchia, A., et al. (2004). Induced recruitment of NK cells to lymph nodes provides IFN-gamma for T(H)1 priming. *Nat. Immunol.* 5, 1260–1265. doi: 10.1038/ni1138

Masilamani, M., Nguyen, C., Kabat, J., Borrego, F., and Coligan, J. E. (2006). CD94/NKG2A inhibits NK cell activation by disrupting the actin network at the immunological synapse. *J. Immunol.* 177, 3590–3596. doi: 10.4049/jimmunol.177.6.3590

Matalon, O., Ben-Shmuel, A., Kivelevitz, J., Sabag, B., Fried, S., Joseph, N., et al. (2018). Actin retrograde flow controls natural killer cell response by regulating the conformation state of SHP-1. *EMBO J.* 37:e96264.

Matalon, O., Fried, S., Ben-Shmuel, A., Pauker, M. H., Joseph, N., Keizer, D., et al. (2016). Dephosphorylation of the adaptor LAT and phospholipase C-γ by SHP-1 inhibits natural killer cell cytotoxicity. *Sci. Signal.* 9:ra54. doi: 10.1126/scisignal.aad6182

Matalon, O., Reicher, B., and Barda-Saad, M. (2013). Wiskott-Aldrich syndrome protein–dynamic regulation of actin homeostasis: from activation through function and signal termination in T lymphocytes. *Immunol. Rev.* 256, 10–29. doi: 10.1111/imr.12112

McCann, F. E., Vanherberghen, B., Eleme, K., Carlin, L. M., Newsam, R. J., Goulding, D., et al. (2003). The size of the synaptic cleft and distinct distributions of filamentous actin, ezrin, CD43, and CD45 at activating and inhibitory human NK cell immune synapses. *J. Immunol.* 170, 2862–2870. doi: 10.4049/jimmunol.170.6.2862

Ménasché, G., Pastural, E., Feldmann, J., Certain, S., Ersoy, F., Dupuis, S., et al. (2000). Mutations in RAB27A cause Griscelli syndrome associated with haemophagocytic syndrome. *Nat. Genet.* 25, 173–176. doi: 10.1038/76024

Mentlik, A. N., Sanborn, K. B., Holzbaur, E. L., and Orange, J. S. (2010). Rapid lytic granule convergence to the MTOC in natural killer cells is dependent on dynein but not cytolytic commitment. *Mol. Biol. Cell* 21, 2241–2256. doi: 10.1091/mbc.e09-11-0930

Miki, H., Suetsugu, S., and Takenawa, T. (1998). WAVE, a novel WASP-family protein involved in actin reorganization induced by Rac. *EMBO J.* 17, 6932–6941. doi: 10.1093/emboj/17.23.6932

Mizesko, M. C., Banerjee, P. P., Monaco-Shawver, L., Mace, E. M., Bernal, W. E., Sawalle-Belohradsky, J., et al. (2013). Defective actin accumulation impairs human natural killer cell function in patients with dedicator of cytokinesis 8 deficiency. *J. Allergy Clin. Immunol.* 131, 840–848. doi: 10.1016/j.jaci.2012.12.1568

Monks, C. R., Freiberg, B. A., Kupfer, H., Sciaky, N., and Kupfer, A. (1998). Three-dimensional segregation of supramolecular activation clusters in T cells. *Nature* 395, 82–86. doi: 10.1038/25764

Moretta, L., Bottino, C., Pende, D., Mingari, M. C., Biassoni, R., and Moretta, A. (2002). Human natural killer cells: their origin, receptors and function. *Eur. J. Immunol.* 32:1205. doi: 10.1002/1521-4141(200205)32:5<1205::aid-immu1205>3.0.co;2-y

Morin, N. A., Oakes, P. W., Hyun, Y.-M., Lee, D., Chin, Y. E., King, M. R., et al. (2008). Nonmuscle myosin heavy chain IIA mediates integrin LFA-1 de-adhesion during T lymphocyte migration. *J. Exp. Med.* 205, 195–205. doi: 10.1084/jem.20071543

Mukherjee, S., Kim, J., Mooren, O. L., Shahan, S. T., Cohan, M., and Cooper, J. A. (2015). Role of cortactin homolog HS1 in transendothelial migration of natural killer cells. *PLoS One* 10:e0118153. doi: 10.1371/journal.pone.0118153

Mullins, R. D., Heuser, J. A., and Pollard, T. D. (1998). The interaction of Arp2/3 complex with actin: nucleation, high affinity pointed end capping, and formation of branching networks of filaments. *Proc. Natl. Acad. Sci. U.S.A.* 95, 6181–6186. doi: 10.1073/pnas.95.11.6181

Murugesan, S., Hong, J., Yi, J., Li, D., Beach, J. R., Shao, L., et al. (2016). Formin-generated actomyosin arcs propel T cell receptor microcluster movement at the immune synapse. *J. Cell Biol.* 215, 383–399. doi: 10.1083/jcb.201603080

Nagle, D. L., Karim, M. A., Woolf, E. A., Holmgren, L., Bork, P., Misumi, D. J., et al. (1996). Identification and mutation analysis of the complete gene for chediak-higashi syndrome. *Nat. Genet.* 14, 307–311. doi: 10.1038/ng1196-307

Nakajima, H., Cella, M., Langen, H., Friedlein, A., and Colonna, M. (1999). Activating interactions in human NK cell recognition: the role of 2B4-CD48. *Eur. J. Immunol.* 29, 1676–1683. doi: 10.1002/(sici)1521-4141(199905)29:05<1676::aid-immu1676>3.0.co;2-y

Nolz, J. C., Gomez, T. S., Zhu, P., Li, S., Medeiros, R. B., Shimizu, Y., et al. (2006). The WAVE2 complex regulates actin cytoskeletal reorganization and CRAC-mediated calcium entry during T cell activation. *Curr. Biol.* 16, 24–34. doi: 10.1016/j.cub.2005.11.036

Nolz, J. C., Medeiros, R. B., Mitchell, J. S., Zhu, P., Freedman, B. D., Shimizu, Y., et al. (2007). WAVE2 regulates high-affinity integrin binding by recruiting vinculin and talin to the immunological synapse. *Mol. Cell. Biol.* 27, 5986–6000. doi: 10.1128/mcb.00136-07

Nolz, J. C., Nacusi, L. P., Segovis, C. M., Medeiros, R. B., Mitchell, J. S., Shimizu, Y., et al. (2008). The WAVE2 complex regulates T cell receptor signaling to integrins via Abl- and CrkL-C3G-mediated activation of Rap1. *J. Cell Biol.* 182, 1231–1244. doi: 10.1083/jcb.200801121

Noy, E., Fried, S., Matalon, O., and Barda-Saad, M. W. I. P. (2012). Remodeling actin behind the scenes: how WIP reshapes immune and other functions. *Int. J. Mol. Sci.* 13, 7629–7647. doi: 10.3390/ijms13067629

Ogbomo, H., Timm-McCann, M., Barnes, T., Xiang, R. F., Jamil, K., Ganguly, A., et al. (2018). Granule-dependent NK cell killing of cryptococcus requires kinesin to reposition the cytolytic machinery for directed cytotoxicity. *Cell Rep.* 24, 3017–3032. doi: 10.1016/j.celrep.2018.08.027

Orange, J. S. (2008). Formation and function of the lytic NK-cell immunological synapse. *Nat. Rev. Immunol.* 8, 713–725. doi: 10.1038/nri2381

Orange, J. S. (2013). Natural killer cell deficiency. *J. Allergy Clin. Immunol.* 132, 515–525.

Orange, J. S., Harris, K. E., Andzelm, M. M., Valter, M. M., Geha, R. S., and Strominger, J. L. (2003). The mature activating natural killer cell immunologic synapse is formed in distinct stages. *Proc. Natl. Acad. Sci. U.S.A.* 100, 14151–14156. doi: 10.1073/pnas.1835830100

Orange, J. S., Ramesh, N., Remold-O'Donnell, E., Sasahara, Y., Koopman, L., Byrne, M., et al. (2002). Wiskott-Aldrich syndrome protein is required for NK cell cytotoxicity and colocalizes with actin to NK cell-activating immunologic synapses. *Proc. Natl. Acad. Sci. U.S.A.* 99, 11351–11356. doi: 10.1073/pnas.162376099

Orange, J. S., Roy-Ghanta, S., Mace, E. M., Maru, S., Rak, G. D., Sanborn, K. B., et al. (2011). IL-2 induces a WAVE2-dependent pathway for actin reorganization that enables WASp-independent human NK cell function. *J. Clin. Invest.* 121, 1535–1548. doi: 10.1172/jci44862

Orr, M. T., and Lanier, L. L. (2010). Natural killer cell education and tolerance. *Cell* 142, 847–856. doi: 10.1016/j.cell.2010.08.031

Oszmiana, A., Williamson, D. J., Cordoba, S.-P., Morgan, D. J., Kennedy, P. R., Stacey, K., et al. (2016). The size of activating and inhibitory killer Ig-like receptor nanoclusters is controlled by the transmembrane sequence and affects signaling. *Cell Rep.* 15, 1957–1972. doi: 10.1016/j.celrep.2016.04.075

Pageon, S. V., Aquino, G., Lagrue, K., Köhler, K., Endres, R. G., and Davis, D. M. (2013a). Dynamics of natural killer cell receptor revealed by quantitative analysis of photoswitchable protein. *Biophys. J.* 105, 1987–1996. doi: 10.1016/j.bpj.2013.09.025

Pageon, S. V., Cordoba, S.-P., Owen, D. M., Rothery, S. M., Oszmiana, A., and Davis, D. M. (2013b). Superresolution microscopy reveals nanometer-scale reorganization of inhibitory natural killer cell receptors upon activation of NKG2D. *Sci. Signal.* 6:ra62. doi: 10.1126/scisignal.2003947

Papakonstanti, E. A., and Stournaras, C. (2002). Association of PI-3 kinase with PAK1 leads to actin phosphorylation and cytoskeletal reorganization. *Mol. Biol. Cell* 13, 2946–2962. doi: 10.1091/mbc.02-01-0599

Pauker, M. H., and Barda-Saad, M. (2011). Studies of novel interactions between Nck and VAV SH3 domains. *Commun. Integr. Biol.* 4, 175–177. doi: 10.4161/cib.4.2.14235

Pauker, M. H., Hassan, N., Noy, E., Reicher, B., and Barda-Saad, M. (2012). Studying the dynamics of SLP-76, Nck, and Vav1 multimolecular complex formation in live human cells with triple-color FRET. *Sci. Signal.* 5:rs3. doi: 10.1126/scisignal.2002423

Pauker, M. H., Reicher, B., Joseph, N., Wortzel, I., Jakubowicz, S., Noy, E., et al. (2014). WASp family verprolin-homologous protein-2 (WAVE2) and Wiskott-Aldrich syndrome protein (WASp) engage in distinct downstream signaling interactions at the T cell antigen receptor site. *J. Biol. Chem.* 289, 34503–34519. doi: 10.1074/jbc.m114.591685

Peterson, M. E., and Long, E. O. (2008). Inhibitory receptor signaling via tyrosine phosphorylation of the adaptor Crk. *Immunity* 29, 578–588. doi: 10.1016/j.immuni.2008.07.014

Ponti, A., Machacek, M., Gupton, S. L., Waterman-Storer, C. M., and Danuser, G. (2004). Two distinct actin networks drive the protrusion of migrating cells. *Science* 305, 1782–1786. doi: 10.1126/science.1100533

Purdy, A. K., and Campbell, K. S. (2009). SHP-2 expression negatively regulates NK cell function. *J. Immunol.* 183, 7234–7243. doi: 10.4049/jimmunol.0900088

Rak, G. D., Mace, E. M., Banerjee, P. P., Svitkina, T., and Orange, J. S. (2011). Natural killer cell lytic granule secretion occurs through a pervasive actin network at the immune synapse. *PLoS Biol.* 9:e1001151. doi: 10.1371/journal.pbio.1001151

Ravetch, J. V. (2000). Immune inhibitory receptors. *Science* 290, 84–89. doi: 10.1126/science.290.5489.84

Reicher, B., Joseph, N., David, A., Pauker, M. H., Perl, O., and Barda-Saad, M. (2012). Ubiquitylation-dependent negative regulation of WASp is essential for actin cytoskeleton dynamics. *Mol. Cell. Biol.* 32, 3153–3163. doi: 10.1128/mcb.00161-12

Riteau, B., Barber, D. F., and Long, E. O. (2003). Vav1 phosphorylation is induced by beta2 integrin engagement on natural killer cells upstream of actin cytoskeleton and lipid raft reorganization. *J. Exp. Med.* 198, 469–474. doi: 10.1084/jem.20021995

Roetynck, S., Baratin, M., Johansson, S., Lemmers, C., Vivier, E., and Ugolini, S. (2006). Natural killer cells and malaria. *Immunol. Rev.* 214, 251–263.

Roose, J., and Weiss, A. (2000). T cells: getting a GRP on Ras. *Nat. Immunol.* 1, 275–276. doi: 10.1038/79713

Rudnicka, D., Oszmiana, A., Finch, D. K., Strickland, I., Schofield, D. J., Lowe, D. C., et al. (2013). Rituximab causes a polarization of B cells that augments its therapeutic function in NK-cell-mediated antibody-dependent cellular cytotoxicity. *Blood* 121, 4694–4702. doi: 10.1182/blood-2013-02-482570

Saitakis, M., Dogniaux, S., Goudot, C., Bufi, N., Asnacios, S., Maurin, M., et al. (2017). Different TCR-induced T lymphocyte responses are potentiated by stiffness with variable sensitivity. *Elife* 6:e23190.

Sakai, Y., Tanaka, Y., Yanagihara, T., Watanabe, M., Duan, X., Terasawa, M., et al. (2013). The Rac activator DOCK2 regulates natural killer cell-mediated cytotoxicity in mice through the lytic synapse formation. *Blood* 122, 386–393. doi: 10.1182/blood-2012-12-475897

Salzer, E., Cagdas, D., Hons, M., Mace, E. M., Garncarz, W., Petronczki, ÖY., et al. (2016). RASGRP1 deficiency causes immunodeficiency with impaired cytoskeletal dynamics. *Nat. Immunol.* 17, 1352–1360. doi: 10.1038/ni.3575

Sanborn, K. B., Mace, E. M., Rak, G. D., Difeo, A., Martignetti, J. A., Pecci, A., et al. (2011). Phosphorylation of the myosin IIA tailpiece regulates single myosin IIA molecule association with lytic granules to promote NK-cell cytotoxicity. *Blood* 118, 5862–5871. doi: 10.1182/blood-2011-03-344846

Sanborn, K. B., Rak, G. D., Maru, S. Y., Demers, K., Difeo, A., Martignetti, J. A., et al. (2009). Myosin IIA associates with NK cell lytic granules to enable their interaction with F-actin and function at the immunological synapse. *J. Immunol.* 182, 6969–6984. doi: 10.4049/jimmunol.0804337

Sancho, D., Nieto, M., Llano, M., Rodríguez-Fernández, J. L., Tejedor, R., Avraham, S., et al. (2000). The tyrosine kinase PYK-2/RAFTK regulates natural killer (NK) cell cytotoxic response, and is translocated and activated upon specific target cell recognition and killing. *J. Cell Biol.* 149, 1249–1262. doi: 10.1083/jcb.149.6.1249

Sayos, J., Wu, C., Morra, M., Wang, N., Zhang, X., Allen, D., et al. (1998). The X-linked lymphoproliferative-disease gene product SAP regulates signals induced through the co-receptor SLAM. *Nature* 395, 462–469. doi: 10.1038/26683

Schuyler, S. C., and Pellman, D. (2001). Microtubule "Plus-End-Tracking Proteins": the end is just the beginning. *Cell* 105, 421–424. doi: 10.1016/s0092-8674(01)00364-6

Segovis, C. M., Schoon, R. A., Dick, C. J., Nacusi, L. P., Leibson, P. J., and Billadeau, D. D. (2009). PI3K links NKG2D signaling to a CrkL pathway involved in natural killer cell adhesion, polarity, and granule secretion. *J. Immunol.* 182, 6933–6942. doi: 10.4049/jimmunol.0803840

Seri, M., Pecci, A., Di Bari, F., Cusano, R., Savino, M., Panza, E., et al. (2003). MYH9-Related Disease. *Medicine* 82, 203–215.

Shaheen, S., Wan, Z., Li, Z., Chau, A., Li, X., Zhang, S., et al. (2017). Substrate stiffness governs the initiation of B cell activation by the concerted signaling of PKCβ and focal adhesion kinase. *eLife* 6:e23060.

Sidorenko, S. P., and Clark, E. A. (2003). The dual-function CD150 receptor subfamily: the viral attraction. *Nat. Immunol.* 4, 19–24. doi: 10.1038/ni0103-19

Sims, T. N., Soos, T. J., Xenias, H. S., Dubin-Thaler, B., Hofman, J. M., Waite, J. C., et al. (2007). Opposing effects of PKCtheta and WASp on symmetry breaking and relocation of the immunological synapse. *Cell* 129, 773–785. doi: 10.1016/j.cell.2007.03.037

Sinai, P., Nguyen, C., Schatzle, J. D., and Wülfing, C. (2010). Transience in polarization of cytolytic effectors is required for efficient killing and controlled by Cdc42. *Proc. Natl. Acad. Sci. U.S.A.* 107, 11912–11917. doi: 10.1073/pnas.0913422107

Sproul, L. R., Anderson, D. J., Mackey, A. T., Saunders, W. S., and Gilbert, S. P. (2005). Cik1 targets the minus-end kinesin depolymerase kar3 to microtubule plus ends. *Curr. Biol.* 15, 1420–1427. doi: 10.1016/j.cub.2005.06.066

Staaf, E., Hedde, P. N., Bagawath Singh, S., Piguet, J., Gratton, E., and Johansson, S. (2018). Educated natural killer cells show dynamic movement of the activating receptor NKp46 and confinement of the inhibitory receptor Ly49A. *Sci. Signal.* 11:eaai9200. doi: 10.1126/scisignal.aai9200

Stabile, H., Carlino, C., Mazza, C., Giliani, S., Morrone, S., Notarangelo, L. D., et al. (2010). Impaired NK-cell migration in WAS/XLT patients: role of Cdc42/WASp pathway in the control of chemokine-induced β2 integrin high-affinity state. *Blood* 115, 2818–2826. doi: 10.1182/blood-2009-07-235804

Standeven, L. J., Carlin, L. M., Borszcz, P., Davis, D. M., and Burshtyn, D. N. (2004). The Actin cytoskeleton controls the efficiency of killer Ig-Like receptor accumulation at inhibitory NK Cell immune synapses. *J. Immunol.* 173, 5617–5625. doi: 10.4049/jimmunol.173.9.5617

Stanton, R. J., Prod'homme, V., Purbhoo, M. A., Moore, M., Aicheler, R. J., Heinzmann, M., et al. (2014). HCMV pUL135 remodels the actin cytoskeleton to impair immune recognition of infected cells. *Cell Host Microbe* 16, 201–214. doi: 10.1016/j.chom.2014.07.005

Stebbins, C. C., Watzl, C., Billadeau, D. D., Leibson, P. J., Burshtyn, D. N., and Long, E. O. (2003). Vav1 dephosphorylation by the tyrosine phosphatase SHP-1 as a mechanism for inhibition of cellular cytotoxicity. *Mol. Cell. Biol.* 23, 6291–6299. doi: 10.1128/mcb.23.17.6291-6299.2003

Stepp, S. E., Dufourcq-Lagelouse, R., Le Deist, F., Bhawan, S., Certain, S., Mathew, P. A., et al. (1999). Perforin gene defects in familial hemophagocytic lymphohistiocytosis. *Science* 286, 1957–1959. doi: 10.1126/science.286.5446.1957

Stinchcombe, J. C., Majorovits, E., Bossi, G., Fuller, S., and Griffiths, G. M. (2006). Centrosome polarization delivers secretory granules to the immunological synapse. *Nature* 443, 462–465. doi: 10.1038/nature05071

Stone, J. C., Dower, N. A., Stang, S. L., Bottorff, D. A., Ebinu, J. O., Dickie, P., et al. (2000). RasGRP is essential for mouse thymocyte differentiation and TCR signaling. *Nat. Immunol.* 1, 317–321. doi: 10.1038/79766

Suetsugu, S., Miki, H., and Takenawa, T. (1999). Identification of two human WAVE/SCAR homologues as general actin regulatory molecules which associate with the Arp2/3 complex. *Biochem. Biophys. Res. Commun.* 260, 296–302. doi: 10.1006/bbrc.1999.0894

Sullivan, K. E., Mullen, C. A., Blaese, R. M., and Winkelstein, J. A. (1994). A multiinstitutional survey of the Wiskott-Aldrich syndrome. *J. Pediatr.* 125, 876–885. doi: 10.1016/s0022-3476(05)82002-5

Takeda, K. (1993). The development of autoimmunity in C57BL/6 lpr mice correlates with the disappearance of natural killer type 1-positive cells: evidence for their suppressive action on bone marrow stem cell proliferation, B cell immunoglobulin secretion, and autoimmune sy. *J. Exp. Med.* 177, 155–164. doi: 10.1084/jem.177.1.155

Takenawa, T., and Suetsugu, S. (2007). The WASP-WAVE protein network: connecting the membrane to the cytoskeleton. *Nat. Rev. Mol. Cell Biol.* 8, 37–48. doi: 10.1038/nrm2069

Tapon, N. (1997). Rho, Rac and Cdc42 GTPases regulate the organization of the Actin cytoskeleton. *Curr. Opin. Cell Biol.* 9, 86–92. doi: 10.1016/s0955-0674(97)80156-1

Thomas, L. M., Peterson, M. E., and Long, E. O. (2013). Cutting edge: NK cell licensing modulates adhesion to target cells. *J. Immunol.* 191, 3981–3985. doi: 10.4049/jimmunol.1301159

Thrasher, A. J., and Burns, S. O. (2010). WASP: a key immunological multitasker. *Nat. Rev. Immunol.* 10, 182–192. doi: 10.1038/nri2724

Timonen, T. (1997). Natural killer cells: endothelial interactions, migration, and target cell recognition. *J. Leukoc. Biol.* 62, 693–701. doi: 10.1002/jlb.62.6.693

Tojkander, S., Gateva, G., and Lappalainen, P. (2012). Actin stress fibers - Assembly, dynamics and biological roles. *J. Cell Sci.* 125, 1855–1864. doi: 10.1242/jcs.098087

Topham, N. J., and Hewitt, E. W. (2009). Natural killer cell cytotoxicity: how do they pull the trigger? *Immunology* 128, 7–15. doi: 10.1111/j.1365-2567.2009.03123.x

Treanor, B., Lanigan, P. M. P., Kumar, S., Dunsby, C., Munro, I., Auksorius, E., et al. (2006). Microclusters of inhibitory killer immunoglobulin-like receptor signaling at natural killer cell immunological synapses. *J. Cell Biol.* 174, 153–161. doi: 10.1083/jcb.200601108

Tsukita, S., and Yonemura, S. (1999). Cortical actin organization: lessons from ERM (ezrin/radixin/moesin) proteins. *J. Biol. Chem.* 274, 34507–34510. doi: 10.1074/jbc.274.49.34507

Tuli, A., Thiery, J., James, A. M., Michelet, X., Sharma, M., Garg, S., et al. (2013). Arf-like GTPase Arl8b regulates lytic granule polarization and natural killer cell-mediated cytotoxicity. *Mol. Biol. Cell* 24, 3721–3735. doi: 10.1091/mbc.e13-05-0259

Upshaw, J. L., Arneson, L. N., Schoon, R. A., Dick, C. J., Billadeau, D. D., and Leibson, P. J. (2006). NKG2D-mediated signaling requires a DAP10-bound Grb2-Vav1 intermediate and phosphatidylinositol-3-kinase in human natural killer cells. *Nat. Immunol.* 7, 524–532. doi: 10.1038/ni1325

Varma, R., Campi, G., Yokosuka, T., Saito, T., and Dustin, M. L. (2006). T cell receptor-proximal signals are sustained in peripheral microclusters and terminated in the central supramolecular activation cluster. *Immunity* 25, 117–127. doi: 10.1016/j.immuni.2006.04.010

Vély, F., and Vivier, E. (2005). Natural killer cell receptor signaling pathway. *Sci. Signal.* 2005:cm6. doi: 10.1126/stke.2922005cm6

Viant, C., Fenis, A., Chicanne, G., Payrastre, B., Ugolini, S., and Vivier, E. (2014). SHP-1-mediated inhibitory signals promote responsiveness and anti-tumour functions of natural killer cells. *Nat. Commun.* 5:5108.

Vicente-Manzanares, M., Ma, X., Adelstein, R. S., and Horwitz, A. R. (2009). Non-muscle myosin II takes centre stage in cell adhesion and migration. *Nat. Rev. Mol. Cell Biol.* 10, 778–790. doi: 10.1038/nrm2786

Vicente-Manzanares, M., and Sánchez-Madrid, F. (2004). Role of the cytoskeleton during leukocyte responses. *Nat. Rev. Immunol.* 4, 110–122. doi: 10.1038/nri1268

Villegas, F. R., Coca, S., Villarrubia, V. G., Jiménez, R., Chillón, M. J., Jareño, J., et al. (2002). Prognostic significance of tumor infiltrating natural killer cells subset CD57 in patients with squamous cell lung cancer. *Lung Cancer* 35, 23–28. doi: 10.1016/s0169-5002(01)00292-6

Vivier, E., Raulet, D. H., Moretta, A., Caligiuri, M. A., Zitvogel, L., Lanier, L. L., et al. (2011). Innate or adaptive immunity? The example of natural killer cells. *Science* 331, 44–49.

Vivier, E., Tomasello, E., Baratin, M., Walzer, T., and Ugolini, S. (2008). Functions of natural killer cells. *Nat. Immunol.* 9, 503–510.

Vyas, Y. M., Maniar, H., and Dupont, B. (2002a). Cutting edge: differential segregation of the SRC homology 2-containing protein tyrosine phosphatase-1 within the early NK cell immune synapse distinguishes noncytolytic from cytolytic interactions. *J. Immunol.* 168, 3150–3154. doi: 10.4049/jimmunol.168.7.3150

Vyas, Y. M., Maniar, H., and Dupont, B. (2002b). Visualization of signaling pathways and cortical cytoskeleton in cytolytic and noncytolytic natural killer cell immune synapses. *Immunol. Rev.* 189, 161–178. doi: 10.1034/j.1600-065x.2002.18914.x

Vyas, Y. M., Mehta, K. M., Morgan, M., Maniar, H., Butros, L., Jung, S., et al. (2001). Spatial organization of signal transduction molecules in the NK cell immune synapses during MHC class I-regulated noncytolytic and cytolytic interactions. *J. Immunol.* 167, 4358–4367. doi: 10.4049/jimmunol.167.8.4358

Wagtmann, N., Rajagopalan, S., Winter, C. C., Peruui, M., and Long, E. O. (1995). Killer cell inhibitory receptors specific for HLA-C and HLA-B identified by direct binding and by functional transfer. *Immunity* 3, 801–809. doi: 10.1016/1074-7613(95)90069-1

Wallar, B. J., and Alberts, A. S. (2003). The formins: active scaffolds that remodel the cytoskeleton. *Trends Cell Biol.* 13, 435–446. doi: 10.1016/s0962-8924(03)00153-3

Walzer, T., Dalod, M., Robbins, S. H., Zitvogel, L., and Vivier, E. (2005). Natural-killer cells and dendritic cells: 'l'union fait la force'. *Blood* 106, 2252–2258. doi: 10.1182/blood-2005-03-1154

Wang, Y., Sun, J., Ma, C., Gao, W., Song, B., Xue, H., et al. (2016). Reduced expression of Galectin-9 contributes to a poor outcome in colon cancer by inhibiting NK cell chemotaxis partially through the Rho/ROCK1 signaling pathway. *PLoS One* 11:e0152599. doi: 10.1371/journal.pone.0152599

Watzl, C., and Long, E. O. (2003). Natural killer cell inhibitory receptors block actin cytoskeleton-dependent recruitment of 2B4 (CD244) to lipid rafts. *J. Exp. Med.* 197, 77–85. doi: 10.1084/jem.20020427

Watzl, C., and Long, E. O. (2010). Signal transduction during activation and inhibition of natural killer cells. *Curr. Protoc. Immunol.* 11:Unit11.9B.

Watzl, C., Stebbins, C. C., and Long, E. O. (2000). Cutting edge: NK cell inhibitory receptors prevent tyrosine phosphorylation of the activation receptor 2B4 (CD244). *J. Immunol.* 165, 3545–3548. doi: 10.4049/jimmunol.165.7.3545

Wilton, K. M., and Billadeau, D. D. V. A. S. P. (2018). Regulates NK cell lytic granule convergence. *J. Immunol.* 201, 2899–2909. doi: 10.4049/jimmunol.1800254

Wilton, K. M., Overlee, B. L., and Billadeau, D. D. (2019). NKG2D-DAP10 signaling recruits EVL to the cytotoxic synapse to generate F-actin and promote NK cell cytotoxicity. *J. Cell Sci.* 133:jcs230508. doi: 10.1242/jcs.230508

Wood, S. M., Meeths, M., Chiang, S. C. C., Bechensteen, A. G., Boelens, J. J., Heilmann, C., et al. (2009). Different NK cell-activating receptors preferentially recruit Rab27a or Munc13-4 to perforin-containing granules for cytotoxicity. *Blood* 114, 4117–4127. doi: 10.1182/blood-2009-06-225359

Worthylake, R. A., and Burridge, K. (2001). Leukocyte transendothelial migration: Orchestrating the underlying molecular machinery. *Curr. Opin. Cell Biol.* 13, 569–577. doi: 10.1016/s0955-0674(00)00253-2

Wulfing, C., Purtic, B., Klem, J., and Schatzle, J. D. (2003). Stepwise cytoskeletal polarization as a series of checkpoints in innate but not adaptive cytolytic killing. *Proc. Natl. Acad. Sci. U.S.A.* 100, 7767–7772. doi: 10.1073/pnas.1336920100

Yi, J., Wu, X. S., Crites, T., and Hammer, J. A. (2012). Actin retrograde flow and actomyosin II arc contraction drive receptor cluster dynamics at the immunological synapse in Jurkat T cells. *Mol. Biol. Cell* 23, 834–852. doi: 10.1091/mbc.e11-08-0731

Zamai, L., Ahmad, M., Bennett, I. M., Azzoni, L., Alnemri, E. S., and Perussia, B. (1998). Natural Killer (NK) cell-mediated cytotoxicity: differential use of ?TRAIL and Fas ligand by immature and mature primary human NK cells. *J. Exp. Med.* 188:2375. doi: 10.1084/jem.188.12.2375

Zanic, M., Widlund, P. O., Hyman, A. A., and Howard, J. (2013). Synergy between XMAP215 and EB1 increases microtubule growth rates to physiological levels. *Nat. Cell Biol.* 15, 688–693. doi: 10.1038/ncb2744

Zhang, M., March, M. E., Lane, W. S., and Long, E. O. (2014). A signaling network stimulated by 2 integrin promotes the polarization of lytic granules in cytotoxic cells. *Sci. Signal.* 7:ra96. doi: 10.1126/scisignal.2005629

Zhang, Q., Davis, J. C., Lamborn, I. T., Freeman, A. F., Jing, H., Favreau, A. J., et al. (2009). Combined immunodeficiency associated with DOCK8 mutations. *N. Engl. J. Med.* 361, 2046–2055.

Zhang, Z., Wu, N., Lu, Y., Davidson, D., Colonna, M., and Veillette, A. (2015). DNAM-1 controls NK cell activation via an ITT-like motif. *J. Exp. Med.* 212, 2165–2182. doi: 10.1084/jem.20150792

Conflict of Interest: The authors declare that the research was conducted in the absence of any commercial or financial relationships that could be construed as a potential conflict of interest.

frontiers in Cell and Developmental Biology

OPINION
published: 25 February 2021
doi: 10.3389/fcell.2021.612539

What Is the Right Mechanical Readout for Understanding the Mechanobiology of the Immune Response?

Marco Fritzsche [1,2]*

[1] Rosalind Franklin Institute, Didcot, United Kingdom, [2] Kennedy Institute for Rheumatology, University of Oxford, Oxford, United Kingdom

Keywords: mechanics, biophysics, mechanical force, mechanical properties, feedback, dynamics, stiffness, tension

Mechanobiology is a critical frontier in the biomedical sciences. Across many of its fields a new perspective is emerging to perceive the immune response as a single multi-scale super-organism continuously interacting and interpreting the biochemical and biomechanical micro-environment. Large numbers of immune cells communicate through a combination of chemical and mechanical signals to organise and orchestrate their behaviour and function against an immunological threat. However, disease often circumvents and even exploits mechanobiological features of this defence machinery, highlighting the need to better understand the intimate coupling between biology and mechanics.

OPEN ACCESS

Edited by:
Sudha Kumari, Massachusetts Institute of Technology, United States

Reviewed by:
Brian Gabrielli, The University of Queensland, Australia

***Correspondence:**
Marco Fritzsche
marco.fritzsche@kennedy.ox.ac.uk

Specialty section:
This article was submitted to Cell Growth and Division, a section of the journal Frontiers in Cell and Developmental Biology

Received: *30 September 2020*
Accepted: *02 February 2021*
Published: *25 February 2021*

Citation:
Fritzsche M (2021) What Is the Right Mechanical Readout for Understanding the Mechanobiology of the Immune Response? Front. Cell Dev. Biol. 9:612539. doi: 10.3389/fcell.2021.612539

Mechanical force underpins the immune response at the multi-scale (Fritzsche, 2020). While almost all physical forces relevant to immune cell biology are practically restricted to the sub-cellular level such as electrostatics (e.g., receptor ligand binding) and thermodynamics (e.g., molecule diffusion), biomechanics takes on a special importance as mechanical force influences many functional features and behavior of immune cells over multiple scales in space and time (Dumont and Prakash, 2014; Egan et al., 2015). Mechanics contributes to the dynamics of single molecules, cells, tissues, and entire organisms (Blanchard and Adams, 2011; Chen and Zhu, 2013). The effects on the biology result from contributions of mechanics that are combination of those generated locally and those that influence from a distance. Importantly, both mechanical force and mechanical properties differ at distinct spatio-temporal frequencies such as constant and oscillatory forces, tension, or elasticity and viscosity (see **Figure 1**), respectively. For example, living cells can be elastic, viscous, or visco-elastic depending on the spatial and temporal measurement frequency (see **Figure 1A**). Adequate quantification promises thus a deeper understanding of the multi-scale spatio-temporal coupling of biology and mechanics and its control over the immune response (Fritzsche, 2020).

Central to the immune defense against an invading threat is a well-orchestrated sequence of events carried out by specialized cells of the multi-scale super-organism of the immune system (Chaplin, 2010). The Success of the process relies on the quality of the spatiotemporal organization of the cellular responses in the tissue micro-environment of the host organism for instance against cancer or an invading pathogenic threat (Swartz and Lund, 2012). Cytotoxic immune cells circulate through tissue, track soluble cytokines and chemokines, respond to antigens, and kill diverse immuno-targets (Andersen et al., 2006; Grivennikov et al., 2010). Among many of these events, they involve a combination of biological and mechanical spheres of influence, as immune cells continuously interact and interpret the physical surroundings (Colin-York et al., 2016; Schwarz, 2017). This environment is also mechanically diverse over scales of space and time. It is comprised of different types of molecules, cells, and tissues (Needleman and Dogic, 2017). Mechanical aspects of the tissue environment are known to influence both the function and behavior of cells (Schwarz, 2017; Colin-York and Fritzsche, 2018). The complex multi-scale nature of mechanical force may have evolutionary been the reason for immune cells to develop the ability to adjust their

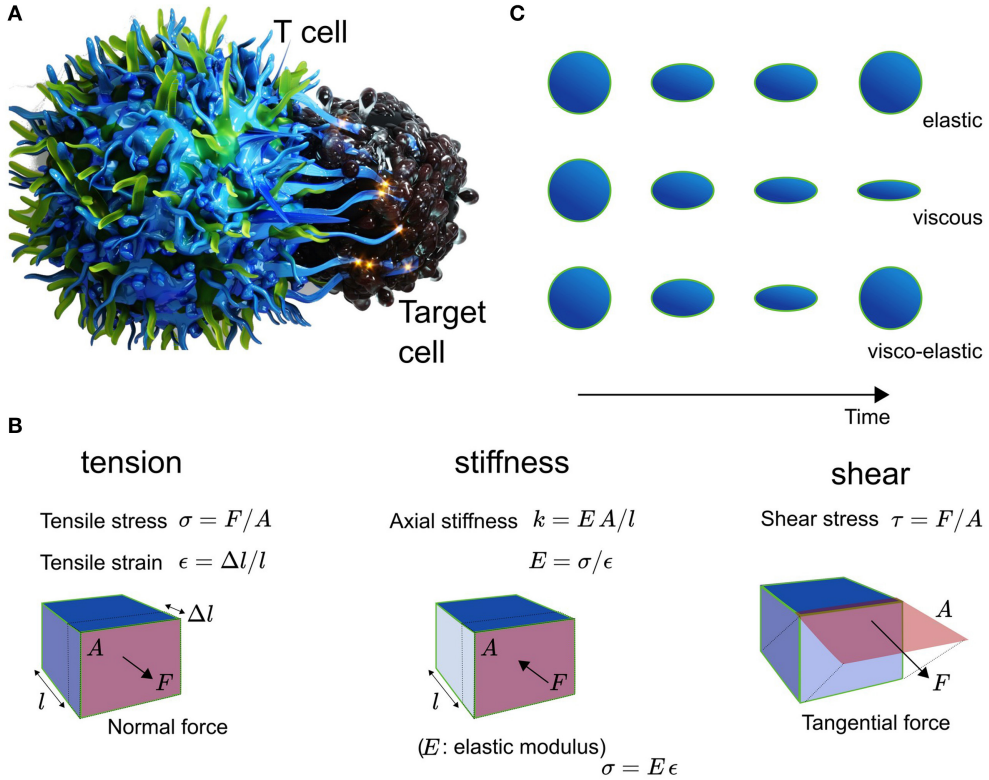

FIGURE 1 | (A) Schematic of the T cell (left) and Target cell (right) interplay. **(B)** Explanation of the mechanical metric tension with tensile stress σ in units of N/m^2 and tensile strain ε being dimenionless, and shear with shear stress τ in N/m^2, as well as the elasticity with Youngst modulus E, which equals the ratio of stress over strain. The stiffness of a material is given by EA/l. **(C)** Cells are elastic, viscous, or visco-elastic.

own biomechanics to their physiological needs in response to the ever-changing physical world. Strikingly, when cells loose mechanosensation, the immune response is hampered to robustly and/or reliably achieve its protective function, which has been demonstrated for example during cell-cell interactions such as activation and cytotoxicity (Huse, 2017; Kumari et al., 2019), as well as during cellular interactions with the tumor micro-environment (Mohammadi and Sahai, 2018; Majedi et al., 2020). Consequently, this gives a special significance to mechanobiology of being important for the understanding of the functioning of the immune response as a whole in health and disease.

One of the most illustrative and visually impressive examples for the impact of mechanobiology is the activation of T cells and antigen presenting cells (APCs) (Chen and Zhu, 2013; Harrison et al., 2019). Micron-scale ruffles protruding from the T cell initiate contact and binding between T cell receptors (TCRs) and the APC's peptide-loaded major hist-compatibility complexes (pMHCs) (Fritz-Laylin et al., 2017; Fritzsche et al., 2017). In the event of recognition and binding of pMHCs by a TCR, the T cell rearranges, assisted by its cytoskeleton, the totality of its metabolism, inner organelles, membrane, and its surface receptors and ligands (English and Voeltz, 2013; Maciver et al., 2013; Carlton et al., 2020). Strikingly, physical symmetry plays a major factor in these re-arrangements, possibly because of the need to balance and direct mechanical force between the T cell and the APC (Sims et al., 2007; Dustin, 2009; Arsenio et al., 2015). Calcium release in response to TCR-pMHC binding leads to the depolymerisation of microtubules, which in turn facilitates the rearrangement of organelles such as the nucleus and endoplasmic reticulum to the center of the T-cell body volume (Joseph et al., 2014; Ilan-Ber and Ilan, 2019). Cytoskeletal ruffles depolymerise and actin-rich lamellum and lamellipodium polymerise at the contact between both cells. The lamellipodium constantly propels freshly forming TCR clusters to the center of the contact (Fritzsche et al., 2017), whose function is thought to amplify the pMHC binding and recognition (Harrison et al., 2019). At the interface between the T cell and the APC, the immunological synapse (IS) takes shape involving a complex spatio-temporal orchestration of receptors, positive and negative co-stimulatory co-receptors, and integrins (Dustin, 2009). They contribute in concert to the force balance between the T cell and the APC. As antigens are processed at the IS, the T cell ensures a mechanically stable and flat contact interface in the form of a ramified actin network (Fritzsche et al., 2017). Visual inspection suggested, that this network is shaped under mechanical tension and held stable over time through the actively polymerising actin-rich lamellipodium and its shear force producing actin retrograde flow (Colin-York et al., 2019b). These interfacial processes are further supported by mechanically active protrusions (Tamzalit et al., 2019). On one side of IS, the T cell constantly assembles and disassembles short-lived actin foci facilitating and perhaps ensuring localized contact between both cells (Kumari et al.,

2019, 2020). On the other side of the interaction, the APC forms mechano-transducing podosomes in the outer periphery of the IS (Malinova et al., 2016), which may serve to monitor the mechanical stiffness at the contact interface. The mechanical properties of the cytoskeletal actin architectures and protrusions are also time-dependent with distinct viscosities depending on the observation frequency, because they and their crosslinkers are constantly turning over (Fritzsche et al., 2016; Gat et al., 2020). Loss of symmetry at the IS, and thus loss of mechanical force balance at the contact, has been demonstrated to influence instability and success of immune cell activation (Sims et al., 2007; Lee et al., 2017). These outlined processes are further underpinned by dynamic molecular changes in the nanoscale organization and turnover of actin filaments in the actin cortex and lamellipodium as a function of the antigen affinity (Billadeau et al., 2007; Colin-York et al., 2019b; Wahl et al., 2019), suggesting mechanical feedback on multiple length- and time-scales. Over the years, a multitude of measurements in the study of immune cell activation reported the importance of different mechanical metrics such as stiffness, tension, shear, and structural integrity, highlighting the diversity of current mechanical quantifications (**Figure 1B**) (Egan et al., 2015).

Together, having uncovered the presence of a variety of length- and time-scale dependent mechanical force regimes and properties during immune cell activation (Pageon et al., 2018), and moreover, knowing that T cells and APCs integrate a variety of mechanical readouts (Jain et al., 2019), leads to the question what mechanical measurements are necessary and sufficient to understand the mechanobiology of the immune response? More specifically, how do these mechanical signatures couple and feed into biology over space and time, and are thus integrated into cellular function and behavior (Harris et al., 2018)? To add further complexity to this picture, the T cell-APC interplay is usually not insulated but maintains processes of continuous communication and interpretation of the surrounding biochemical and biomechanical micro-environment. Consequently, without understanding comprehensively the dynamic relationship of these processes, it is challenging to determine the biological significance of mechanobiology in health and disease.

Hence, a grand challenge for the understanding of mechanbiology is the determination of the right mechanical readout. Ideally, from the theoretical physics point of view, one aims for a full quantitative parametrisation of the desired biological phenomena, which ultimately comes down to identification and determination of a well-defined control parameter (Bechhoefer, 2005). The determinant at which biomechanics regulates behavior and/or function of the immunological process of interest. The prospect of knowing the one (or the many) mechanical control parameter(s) against all other system parameters is of particular importance in the context of stability of the biological function (Bechhoefer, 2005; McEvoy, 2018). For example the stability of IS formation could be regulated through changes in mechanical feedback between the T cell and the APC (Harrison et al., 2019). Stability of such a biological feature is mathematically determined by the so-called eigenmodes of its stability matrix, which grow or shrink when the control parameter for example mechanical feedback changes (Bechhoefer, 2005). Crucially, while experimentally, changes in different mechanical parameters could be observed throughout a biological process (Dumont and Prakash, 2014; Egan et al., 2015), only the determination of the biological control parameter aids to the understanding of the biological mechanisms and concepts being at play (McEvoy, 2018). In other words, one may observe quantitative changes in mechanical metrics such as stiffness and/or tension but in practice misinterpret the observed phenomena, let it be for example mechanical feedback during IS formation, if the control parameter *feedback* has not been correctly identified and parameterized.

FUTURE PERSPECTIVE

How to then find the right mechanical readout? The answer to this question is not trivial and practically challenging for many biological systems due to the numerous molecular players involved, the number and complexity of their interactions, but probably mostly due to a broad lack of quantitative technology with the right sensitivity (Polacheck and Chen, 2016; Roca-Cusachs et al., 2017).

Over the last 10 years, recent advances in quantitative technology have enabled the spatio-temporal sensitivity demanded by the immune response drawing a promising perspective for the future. These new methodologies will enable a complete quantitative characterization of biological processes to the best of the experimentalist's abilities allowing the full parameterization of theoretical physics descriptions (McEvoy, 2018). For this, a variety of different technologies are needed to quantify correlatively or co-incidentally the mechanical setting with the sensitivity demanded by the biology of interest. We and others have spent significant efforts in evolving the sensitivity of traction force microscopy, probably the most widely applied force quantification methodology, which offers the simultaneous quantification of mechanical force production and the dynamics of cells (Colin-York and Fritzsche, 2018; Colin-York et al., 2019a; Stubb et al., 2020; Vorselen et al., 2020). More recent efforts of combining different types of quantitative simultaneous measurements hold the promise to achieve a more complete understanding of how biomechanics feeds into immune cell physiology of the immune response (Skamrahl et al., 2019; Hobson et al., 2020; Moreno-Flores, 2020; Nelsen et al., 2020). Quantifying the mechanical settings of the immune response in full utilizing methodologies with the right sensitivity may thus be the route to enable broad recognition of mechanobiology in health and disease.

AUTHOR CONTRIBUTIONS

MF designed and wrote the perspective article.

ACKNOWLEDGMENTS

MF would like to acknowledge generous funding from the Rosalind Franklin Institute and the Kennedy Trust for Rheumatology Research. MF also thanks the Wellcome Trust (212343/Z/18/Z) and EPSRC (EP/S004459/1).

REFERENCES

Andersen, M. H., Schrama, D., Thor Straten, P., and Becker, J. C. (2006). Cytotoxic T cells. *J. Invest. Dermatol.* 126, 32–41. doi: 10.1038/sj.jid.5700001

Arsenio, J., Metz, P. J., and Chang, J. T. (2015). Asymmetric cell division in T lymphocyte fate diversification. *Trends Immunol.* 36, 670–683. doi: 10.1016/j.it.2015.09.004

Bechhoefer, J. (2005). Feedback for physicists: a tutorial essay on contro. *Rev. Mod. Phys.* 77, 783–836. doi: 10.1103/RevModPhys.77.783

Billadeau, D. D., Nolz, J. C., and Gomez, T. S. (2007). Regulation of T-cell activation by the cytoskeleton. *Nat. Rev. Immunol.* 7, 131–143. doi: 10.1038/nri2021

Blanchard, G. B., and Adams, R. J. (2011). Measuring the multi-scale integration of mechanical forces during morphogenesis. *Curr. Opin. Genet. Dev.* 21, 653–663. doi: 10.1016/j.gde.2011.08.008

Carlton, J. G., Jones, H., and Eggert, U. S. (2020). Membrane and organelle dynamics during cell division. *Nat. Rev. Mol. Cell Biol.* 21, 151–166. doi: 10.1038/s41580-019-0208-1

Chaplin, D. D. (2010). Overview of the immune response. *J. Allergy Clin. Immunol.* 125:S3. doi: 10.1016/j.jaci.2009.12.980

Chen, W., and Zhu, C. (2013). Mechanical regulation of T-cell functions. *Immunol. Rev.* 256, 160–176. doi: 10.1111/imr.12122

Colin-York, H., and Fritzsche, M. (2018). The future of traction force microscopy. *Curr. Opin. Biomed. Eng.* 5, 1–5. doi: 10.1016/J.COBME.2017.10.002

Colin-York, H., Javanmardi, Y., Barbieri, L., Li, D., Korobchevskaya, K., Guo, Y., et al. (2019a). Spatiotemporally super-resolved volumetric traction force microscopy. *Nano Lett.* 19, 4427–4434. doi: 10.1021/acs.nanolett.9b01196

Colin-York, H., Javanmardi, Y., Skamrahl, M., Cerundolo, V., Eggeling, C., and Correspondence, M. F. (2019b). Cytoskeletal control of antigen-dependent T cell activation. *CellRep.* 26, 3369–3379.e5. doi: 10.1016/j.celrep.2019.02.074

Colin-York, H., Shrestha, D., Felce, J. H., Waithe, D., Moeendarbary, E., Davis, S. J., et al. (2016). Super-resolved traction force microscopy (STFM). *Nano Lett.* 16, 2633–2638. doi: 10.1021/acs.nanolett.6b00273

Dumont, S., and Prakash, M. (2014). Emergent mechanics of biological structures. *Mol. Biol. Cell* 25, 3461–3465. doi: 10.1091/mbc.E14-03-0784

Dustin, M. L. (2009). The cellular context of T cell signaling. *Immunity* 30, 482–492. doi: 10.1016/j.immuni.2009.03.010

Egan, P., Sinko, R., Leduc, P. R., and Keten, S. (2015). The role of mechanics in biological and bio-inspired systems. *Nat. Commun.* 6, 1–12. doi: 10.1038/ncomms8418

English, A. R., and Voeltz, G. K. (2013). Endoplasmic reticulum structure and interconnections with other organelles. *Cold Spring Harb. Perspect. Biol.* 5, 1–16. doi: 10.1101/cshperspect.a013227

Fritz-Laylin, L. K., Riel-Mehan, M., Chen, B. C., Lord, S. J., Goddard, T. D., Ferrin, T. E., et al. (2017). Actin-based protrusions of migrating neutrophils are intrinsically lamellar and facilitate direction changes. *Elife* 6:e26990. doi: 10.7554/eLife.26990

Fritzsche, M. (2020). Thinking multi-scale to advance mechanobiology. *Commun. Biol.* 3, 1–2. doi: 10.1038/s42003-020-01197-5

Fritzsche, M., Erlenkämper, C., Moeendarbary, E., Charras, G., and Kruse, K. (2016). Actin kinetics shapes cortical network structure and mechanics. *Sci. Adv.* 2:e1501337. doi: 10.1126/sciadv.1501337

Fritzsche, M., Fernandes, R. A., Chang, V. T., Colin-York, H., Clausen, M. P., Felce, J. H., et al. (2017). Cytoskeletal actin dynamics shape a ramifying actin network underpinning immunological synapse formation. *Sci. Adv.* 3:e1603032. doi: 10.1126/sciadv.1603032

Gat, S., Simon, C., Campillo, C., Bernheim-Groswasser, A., and Sykes, C. (2020). Finger-like membrane protrusions are favored by heterogeneities in the actin network. *Soft Matter* 16, 7222–7230. doi: 10.1039/c9sm02444a

Grivennikov, S. I., Greten, F. R., and Karin, M. (2010). Immunity, inflammation, and cancer. *Cell* 140, 883–899. doi: 10.1016/j.cell.2010.01.025

Harris, M. J., Wirtz, D., and Wu, P.-H. (2018). Dissecting cellular mechanics: implications for aging, cancer, and immunity. *Semin. Cell Dev. Biol.* 93, 16–25. doi: 10.1016/j.semcdb.2018.10.008

Harrison, D. L., Fang, Y., and Huang, J. (2019). T-cell mechanobiology: force sensation, potentiation, and translation. *Front. Phys.* 7:45. doi: 10.3389/fphy.2019.00045

Hobson, C. M., Kern, M., O'Brien, E. T., Stephens, A. D., Falvo, M. R., and Superfine, R. (2020). Correlating nuclear morphology and external force with combined atomic force microscopy and light sheet imaging separates roles of chromatin and lamin A/C in nuclear mechanics. *Mol. Biol. Cell* 31, 1788–1801. doi: 10.1091/mbc.E20-01-0073

Huse, M. (2017). Mechanical forces in the immune system. *Nat. Rev. Immunol.* 17, 679–690. doi: 10.1038/nri.2017.74

Ilan-Ber, T., and Ilan, Y. (2019). The role of microtubules in the immune system and as potential targets for gut-based immunotherapy. *Mol. Immunol.* 111, 73–82. doi: 10.1016/j.molimm.2019.04.014

Jain, N., Moeller, J., and Vogel, V. (2019). Mechanobiology of macrophages: how physical factors coregulate macrophage plasticity and phagocytosis. *Annu. Rev. Biomed. Eng.* 21, 267–297. doi: 10.1146/annurev-bioeng-062117-121224

Joseph, N., Reicher, B., and Barda-Saad, M. (2014). The calcium feedback loop and T cell activation: how cytoskeleton networks control intracellular calcium flux. *Biochim. Biophys. Acta - Biomembr.* 1838, 557–568. doi: 10.1016/j.bbamem.2013.07.009

Kumari, S., Colin-York, H., Irvine, D. J., and Fritzsche, M. (2019). Not all T cell synapses are built the same way. *Trends Immunol.* 40, 977–980. doi: 10.1016/j.it.2019.09.009

Kumari, S., Mak, M., Poh, Y., Tohme, M., Watson, N., Melo, M., et al. (2020). Cytoskeletal tension actively sustains the migratory T-cell synaptic contact. *EMBO J.* 39:e102783. doi: 10.15252/embj.2019102783

Lee, A. M., Colin-York, H., and Fritzsche, M. (2017). CalQuo 2 : Automated Fourier-space, population-level quantification of global intracellular calcium responses. *Sci. Rep.* 7:5416. doi: 10.1038/s41598-017-05322-z

Maciver, N. J., Michalek, R. D., and Rathmell, J. C. (2013). Metabolic regulation of T lymphocytes. *Annu. Rev. Immunol.* 31, 259–283. doi: 10.1146/annurev-immunol-032712-095956

Majedi, F. S., Hasani-Sadrabadi, M. M., Thauland, T. J., Li, S., Bouchard, L. S., and Butte, M. J. (2020). T-cell activation is modulated by the 3D mechanical microenvironment. *Biomaterials* 252:120058. doi: 10.1016/j.biomaterials.2020.120058

Malinova, D., Fritzsche, M., Nowosad, C. R., Armer, H., Munro, P. M. G., Blundell, M. P., et al. (2016). WASp-dependent actin cytoskeleton stability at the dendritic cell immunological synapse is required for extensive, functional T cell contacts. *J. Leukoc. Biol.* 99, 699–710. doi: 10.1189/jlb.2a0215-050rr

McEvoy, P. B. (2018). Theoretical contributions to biological control success. *BioControl* 63, 87–103. doi: 10.1007/s10526-017-9852-6

Mohammadi, H., and Sahai, E. (2018). Mechanisms and impact of altered tumour mechanics. *Nat. Cell Biol.* 20, 766–774. doi: 10.1038/s41556-018-0131-2

Moreno-Flores, S. (2020). Hallmarks of life in single cell contact mechanics: outstanding challenges and perspectives. *Front. Mech. Eng.* 6:58. doi: 10.3389/fmech.2020.00058

Needleman, D., and Dogic, Z. (2017). Active matter at the interface between materials science and cell biology. *Nat. Rev. Mater.* 2, 1–14. doi: 10.1038/natrevmats.2017.48

Nelsen, E., Hobson, C. M., Kern, M. E., Hsiao, J. P., O'Brien, E. T., Watanabe, T., et al. (2020). Combined atomic force microscope and volumetric light sheet system for correlative force and fluorescence mechanobiology studies. *Sci. Rep.* 10, 1–12. doi: 10.1038/s41598-020-65205-8

Pageon, S. V., Govendir, M. A., Kempe, D., and Biro, M. (2018). Mechanoimmunology: molecular-scale forces govern immune cell functions. *Mol. Biol. Cell* 29, 1919–1926. doi: 10.1091/mbc.E18-02-0120

Polacheck, W. J., and Chen, C. S. (2016). Measuring cell-generated forces: a guide to the available tools. *Nat. Methods* 13, 415–423. doi: 10.1038/nmeth.3834

Roca-Cusachs, P., Conte, V., and Trepat, X. (2017). Quantifying forces in cell biology. *Nat. Cell Biol.* 19, 742–751 doi: 10.1038/ncb3564

Schwarz, U. S. (2017). Mechanobiology by the numbers: a close relationship between biology and physics. *Nat. Rev. Mol. Cell Biol.* 18, 711–712. doi: 10.1038/nrm.2017.109

Sims, T. N., Soos, T. J., Xenias, H. S., Dubin-Thaler, B., Hofman, J. M., Waite, J. C., et al. (2007). Opposing effects of PKCθ and WASp on symmetry breaking and relocation of the immunological synapse. *Cell* 129, 773–785. doi: 10.1016/j.cell.2007.03.037

Skamrahl, M., Colin-York, H., Barbieri, L., and Fritzsche, M. (2019). Simultaneous quantification of the interplay between molecular turnover and cell

mechanics by AFM–FRAP. *Small* 15:1902202. doi: 10.1002/smll.201902202

Stubb, A., Laine, R. F., Miihkinen, M., Hamidi, H., Guzmán, C., Henriques, R., et al. (2020). Fluctuation-based super-resolution traction force microscopy. *Nano Lett.* 20, 2230–2245. doi: 10.1021/acs.nanolett.9b04083

Swartz, M. A., and Lund, A. W. (2012). Lymphatic and interstitial flow in the tumour microenvironment: linking mechanobiology with immunity. *Nat. Rev. Cancer* 12, 210–219. doi: 10.1038/nrc3186

Tamzalit, F., Wang, M. S., Jin, W., Tello-Lafoz, M., Boyko, V., Heddleston, J. M., et al. (2019). Interfacial actin protrusions mechanically enhance killing by cytotoxic T cells. *Sci. Immunol.* 4:eaav5445. doi: 10.1126/sciimmunol.aav5445

Vorselen, D., Wang, Y., de Jesus, M. M., Shah, P. K., Footer, M. J., Huse, M., et al. (2020). Microparticle traction force microscopy reveals subcellular force exertion patterns in immune cell–target interactions. *Nat. Commun.* 11, 1–14. doi: 10.1038/s41467-019-13804-z

Wahl, A., Dinet, C., Dillard, P., Nassereddine, A., Puech, P.-H., Limozin, L., et al. (2019). Biphasic mechanosensitivity of T cell receptor-mediated spreading of lymphocytes. *Proc. Natl. Acad. Sci. U.S.A.* 116, 5908–5913. doi: 10.1073/pnas.1811516116

Conflict of Interest: The author declares that the research was conducted in the absence of any commercial or financial relationships that could be construed as a potential conflict of interest.

The handling editor declared a past co-authorship with one of the authors MF.

frontiers in Cell and Developmental Biology

ORIGINAL RESEARCH
published: 29 March 2021
doi: 10.3389/fcell.2021.639815

Compliant Substrates Enhance Macrophage Cytokine Release and NLRP3 Inflammasome Formation During Their Pro-Inflammatory Response

*Joan-Carles Escolano[1,2], Anna V. Taubenberger[1], Shada Abuhattum[1,2], Christine Schweitzer[2], Aleeza Farrukh[3], Aránzazu del Campo[3], Clare E. Bryant[4] and Jochen Guck[1,2]**

[1] Biotechnology Center, Center for Molecular and Cellular Bioengineering, Technische Universität Dresden, Dresden, Germany, [2] Max Planck Institute for the Science of Light & Max-Planck-Zentrum für Physik und Medizin, Erlangen, Germany, [3] INM – Leibniz-Institut für Neue Materialien, Saarbrücken, Germany, [4] Department of Veterinary Medicine, University of Cambridge, Cambridge, United Kingdom

OPEN ACCESS

Edited by:
Sudha Kumari,
Massachusetts Institute of Technology, United States

Reviewed by:
Arpita Upadhyaya,
University of Maryland, College Park, United States
Lance Kam,
Columbia University, United States

***Correspondence:**
Jochen Guck
jochen.guck@mpl.mpg.de

Specialty section:
This article was submitted to Cell Growth and Division, a section of the journal Frontiers in Cell and Developmental Biology

Received: 09 December 2020
Accepted: 08 March 2021
Published: 29 March 2021

Citation:
Escolano JC, Taubenberger AV, Abuhattum S, Schweitzer C, Farrukh A, del Campo A, Bryant CE and Guck J (2021) Compliant Substrates Enhance Macrophage Cytokine Release and NLRP3 Inflammasome Formation During Their Pro-Inflammatory Response. Front. Cell Dev. Biol. 9:639815. doi: 10.3389/fcell.2021.639815

Immune cells process a myriad of biochemical signals but their function and behavior are also determined by mechanical cues. Macrophages are no exception to this. Being present in all types of tissues, macrophages are exposed to environments of varying stiffness, which can be further altered under pathological conditions. While it is becoming increasingly clear that macrophages are mechanosensitive, it remains poorly understood how mechanical cues modulate their inflammatory response. Here we report that substrate stiffness influences the expression of pro-inflammatory genes and the formation of the NLRP3 inflammasome, leading to changes in the secreted protein levels of the cytokines IL-1β and IL-6. Using polyacrylamide hydrogels of tunable elastic moduli between 0.2 and 33.1 kPa, we found that bone marrow-derived macrophages adopted a less spread and rounder morphology on compliant compared to stiff substrates. Upon LPS priming, the expression levels of the gene encoding for TNF-α were higher on more compliant hydrogels. When additionally stimulating macrophages with the ionophore nigericin, we observed an enhanced formation of the NLRP3 inflammasome, increased levels of cell death, and higher secreted protein levels of IL-1β and IL-6 on compliant substrates. The upregulation of inflammasome formation on compliant substrates was not primarily attributed to the decreased cell spreading, since spatially confining cells on micropatterns led to a reduction of inflammasome-positive cells compared to well-spread cells. Finally, interfering with actomyosin contractility diminished the differences in inflammasome formation between compliant and stiff substrates. In summary, we show that substrate stiffness modulates the pro-inflammatory response of macrophages, that the NLRP3 inflammasome is one

of the components affected by macrophage mechanosensing, and a role for actomyosin contractility in this mechanosensory response. Thus, our results contribute to a better understanding of how microenvironment stiffness affects macrophage behavior, which might be relevant in diseases where tissue stiffness is altered and might potentially provide a basis for new strategies to modulate inflammatory responses.

Keywords: innate immunity, macrophages, mechanosensing, substrate stiffness, NLRP3 inflammasome, ASC, actomyosin contractility

INTRODUCTION

Macrophages are innate immune cells responsible for engulfing microbes and cell debris and orchestrating inflammatory responses to maintain tissue homeostasis. While patrolling within different organs and tissues, macrophages are exposed not only to multiple biochemical signals but also to mechanical cues, including tissue stiffness. For instance, microglia residing in the human brain are exposed to shear moduli of a few hundred Pa (Sack et al., 2008; Christ et al., 2010; Elkin et al., 2010), alveolar macrophages in the lung to a Young's modulus of 2 kPa (Booth et al., 2012), macrophages within dermal tissue to shear moduli of 7–100 kPa (Wang et al., 2017) and bone osteoclasts face a Young's moduli in the GPa range (Mirzaali et al., 2016). Moreover, pathological disorders such as tumors (Emon et al., 2018) or tissue fibrosis (Wells, 2013) can also promote changes in the stiffness range these and other immune cells encounter.

It is becoming increasingly clear that macrophages respond to mechanical cues (McWhorter et al., 2013; Moshayedi et al., 2014; Ip and Medzhitov, 2015; Jain and Vogel, 2018; Li et al., 2018), but although considerable efforts have been made to understand how microenvironment stiffness influences macrophage phenotype and function, the data are inconclusive. Some studies suggest that stiffer substrates upregulate macrophage pro-inflammatory responses and polarize them towards an M1 phenotype (Blakney et al., 2012; Previtera and Sengupta, 2015; Okamoto et al., 2018; Hsieh et al., 2019; Sridharan et al., 2019), while others show that more compliant materials enhance their pro-inflammatory behavior (Adlerz et al., 2015; Scheraga et al., 2016; Gruber et al., 2018). Parameters such as the stiffness range, the adhesive ligand, the activation stimulus and the specific cell type used vary across the different studies and all these factors could influence the results. It is clear that further research is required to dissect how substrate stiffness modulates the behavior of macrophages and how this impacts on their ability to induce inflammatory responses.

Inflammasomes are one of the key elements required for the processing and release of the major pro-inflammatory cytokines IL-1β and IL-18 (Martinon et al., 2002; Dinarello, 2011; Kaplanski, 2018). They are multimeric complexes comprised by a characteristic pattern-recognition receptor (PRR) that acts as sensor protein, the adaptor protein apoptotic speck-like protein containing a caspase recruitment domain (ASC) and the effector pro-caspase-1. Different PRRs can assemble different inflammasomes in response to a variety of exogenous and endogenous danger signals (Malik and Kanneganti, 2017). Among them, the nucleotide oligomerization domain (NOD)-like receptor (NLR) family member NLRP3 reacts to several substances such as the K^+ ionophore nigericin, extracellular adenosine triphosphate (ATP) or monosodium urate crystals (MSU) (Mariathasan et al., 2006; Martinon et al., 2006). For the NLRP3 inflammasome to become canonically active, two steps are required. First, a priming signal is necessary to activate the transcription factor NFκB. Several danger molecules containing pathogen-associated molecular patterns (PAMPs) and endogenous damage-associated molecular patterns (DAMPs) engage with specific PRRs (Takeuchi and Akira, 2010). These respond by activating downstream signaling pathways that trigger the activation of NFκB and its translocation into the nucleus, where it promotes the transcription and translation of cytokines such as TNF-α, IL-6, pro-IL-1β and pro-IL-18 (Dorrington and Fraser, 2019), and the synthesis of other inflammation-related proteins, including NLRP3 (Bauernfeind et al., 2009). After priming, a second danger stimulus triggers the oligomerization of NLRP3 and the recruitment of ASC and pro-caspase-1 to form an inflammasome (Agostini et al., 2004). Finally, this causes the activation of caspase-1, enzyme that cleaves pro-IL-1β and pro-IL-18 into their biologically active forms (Agostini et al., 2004) and simultaneously promotes pyroptotic cell death via cleavage and maturation of the pore-forming protein gasdermin D (GSDMD) (Liu et al., 2016). The induced pyroptosis enhances the secretion of cytokines and facilitates the release of intracellular danger molecules to potentiate the response of neighboring cells (Evavold et al., 2018).

Although extensive research has been done to understand which biochemical signals modulate inflammasome activation (Swanson et al., 2019), little is known about how mechanical cues could influence its formation. Recent work indicates that biophysical signals could also modulate inflammasomes (Ip and Medzhitov, 2015; Maruyama et al., 2018) and, importantly, it has been shown that mechanotransducers such as the cytoskeleton components F-actin and microtubules may play an important role as regulators of inflammasome assembly (Man et al., 2014; Burger et al., 2016; Magupalli et al., 2020). Despite that, whether substrate stiffness has an impact on macrophage inflammasome formation remains unknown.

Here, we use polyacrylamide hydrogels of varying elastic moduli to investigate how substrate stiffness modulates the pro-inflammatory response of macrophages and influences the activation of the NLRP3 inflammasome. Bone marrow-derived macrophages cultured on substrates with a Young's modulus of 0.2 kPa adopted a radically different morphology from macrophages grown on 33.1 kPa polyacrylamide gels, exhibiting lower spreading area and higher circularity, with less

extended processes but numerous ruffles and folds displayed on the cell surface. Despite not notably affecting most of their pro-inflammatory gene expression patterns, upon LPS priming and nigericin stimulation the more compliant hydrogels enhanced NLRP3 inflammasome assembly, pyroptosis onset and secretion of the cytokines IL-1β and IL-6. Limiting cell spreading through a micropatterning approach revealed that reduced cell area alone could not explain the enhanced inflammasome activation observed on lower substrate stiffness. In contrast, inhibiting myosin activity diminished the differences in inflammasome formation induced by varying substrate compliance. Together, these findings reveal the influence of substrate stiffness on the formation of the NLRP3 inflammasome and on its downstream effects and suggest a role of actomyosin contractility in mediating the integration of mechanical cues into the macrophage inflammatory machinery.

RESULTS

Substrate Stiffness Modifies Macrophage Morphology

To investigate the effect of substrate stiffness on macrophages, we cultured murine bone marrow-derived macrophages (BMDMs) on flat polyacrylamide hydrogels of different rigidity but comparable adhesive RGD coating. We started testing three different stiffnesses with a mean Young's moduli of 0.2, 14.3, and 33.1 kPa (**Figure 1A**). These stiffnesses encompass the different elastic moduli values found in the bone marrow, from 0.1 kPa in the central part and more vascularized areas to a range of 30–100 kPa near the bone surface (Ivanovska et al., 2017). After culturing BMDMs on the gels for 14–18 h, they were well adhered to the material in all conditions and their viability was above 85% (**Figures 1B**, **3E**). In line with previously reported observations (Blakney et al., 2012; Patel et al., 2012; Adlerz et al., 2015; Hsieh et al., 2019; Sridharan et al., 2019; Xing et al., 2020), imaging F-actin revealed that while macrophages on more compliant polyacrylamide remained rounder and less spread, cells on stiffer substrates displayed a significantly larger area, longer processes and higher actin density in some clusters (**Figures 1D–F**). When quantifying their morphological features, we also determined that, compared to the most compliant gel (0.2 kPa), macrophages on the stiffest substrate (33.1 kPa) had a 229% higher mean spreading area, a 202% bigger mean perimeter and 57% lower mean circularity (**Figures 1D–F**). Therefore, the stiffer the substrate, the higher the spreading area and perimeter, and the lower the cell circularity. Out of the different hydrogel stiffnesses, for the remainder of the study we decided to use the most compliant (0.2 kPa) and the stiffest (33.1 kPa) materials because they were the most distant from each other and they consistently and substantially influenced macrophage morphology. To better observe whether the cells adopted different morphological features, we also acquired images of the macrophages on the hydrogels using scanning electron microscopy. Cells on 0.2 kPa gels had considerably more membrane ruffles and folds than cells on 33.1 kPa substrates, where the increased spreading was associated with a smoother plasma membrane (**Figure 1C**).

Substrate Stiffness Influences Pro-Inflammatory Behavior of Macrophages

To study their pro-inflammatory response, we primed the BMDMs with lipopolysaccharide (LPS), a molecule present in the wall of gram-negative bacteria. LPS activates toll-like receptors (TLRs) present in the macrophage cell membrane and triggers downstream signaling cascades that promote the transcription of pro-inflammatory genes. We first assessed whether the morphological differences caused by varying substrate stiffness persisted after macrophage priming. After treatment with LPS for 4.5 h, we observed similar relative differences between the compliant and stiff conditions as in the non-primed macrophages (**Figures 2A–D**). Nevertheless, when compared to unstimulated, LPS-primed cells became larger on both substrates. On 0.2 kPa gels, LPS-treated macrophages had an 83% larger area, an 85% longer perimeter and a 40% lower circularity compared to untreated controls. On 33.1 kPa stiff substrates, they were only 38% more spread, had an 8% longer perimeter but similar circularity. The LPS-induced increase in spreading area and perimeter and the decrease in circularity were more notable in the cells cultured on the compliant than on the stiffer substrate. As previously reported (Jain and Vogel, 2018), LPS tends to promote cell spreading and, since macrophages were already well spread on the stiff gels before their priming, it seems logical that we detected more pronounced changes in the 0.2 kPa gels.

Next, we investigated whether substrate stiffness influences the expression levels of several pro-inflammatory genes after LPS priming via quantitative RT-PCR. In absence of LPS, the expression of the analyzed pro-inflammatory genes (*Tnf*-α, *Il6, Il1b, Nos2, Tlr2, Tlr4, Cxcl2,* and *Cxcl9*) was minimal except for *Tlr4* and there were no differences between macrophages cultured on 0.2 kPa and 33.1 kPa hydrogels (**Figure 2E** and **Supplementary Figure S1**). As expected, after LPS priming most of the gene expression levels were significantly increased and, interestingly, when comparing the two stiffnesses we detected a significantly higher expression higher expression of *Tnf*-α on the more compliant gels. Despite not being statistically significant, also the genes encoding for the cytokines *Il6* and *Il1b* were following a similar trend, and the receptor *Tlr2* and the chemokine *Cxcl2* were also upregulated on more compliant substrates. No differences in the expression of *Nos2*, *Tlr4,* and *Cxcl9* were detected.

While substrate stiffness did not strongly alter pro-inflammatory gene expression, we decided to assess whether it influenced the synthesis and release of the cytokines IL-6 and IL-1β. Priming with LPS alone is sufficient to induce the production and secretion of IL-6, so we quantified its concentration after 4.5 h of treatment. When macrophages were cultured on compliant gels, we detected on average an 11% higher concentration of secreted IL-6 in the supernatant (**Figures 3A,C,D**). To secrete IL-1β, macrophages need to be not only primed with LPS but also provided with a second stimulus

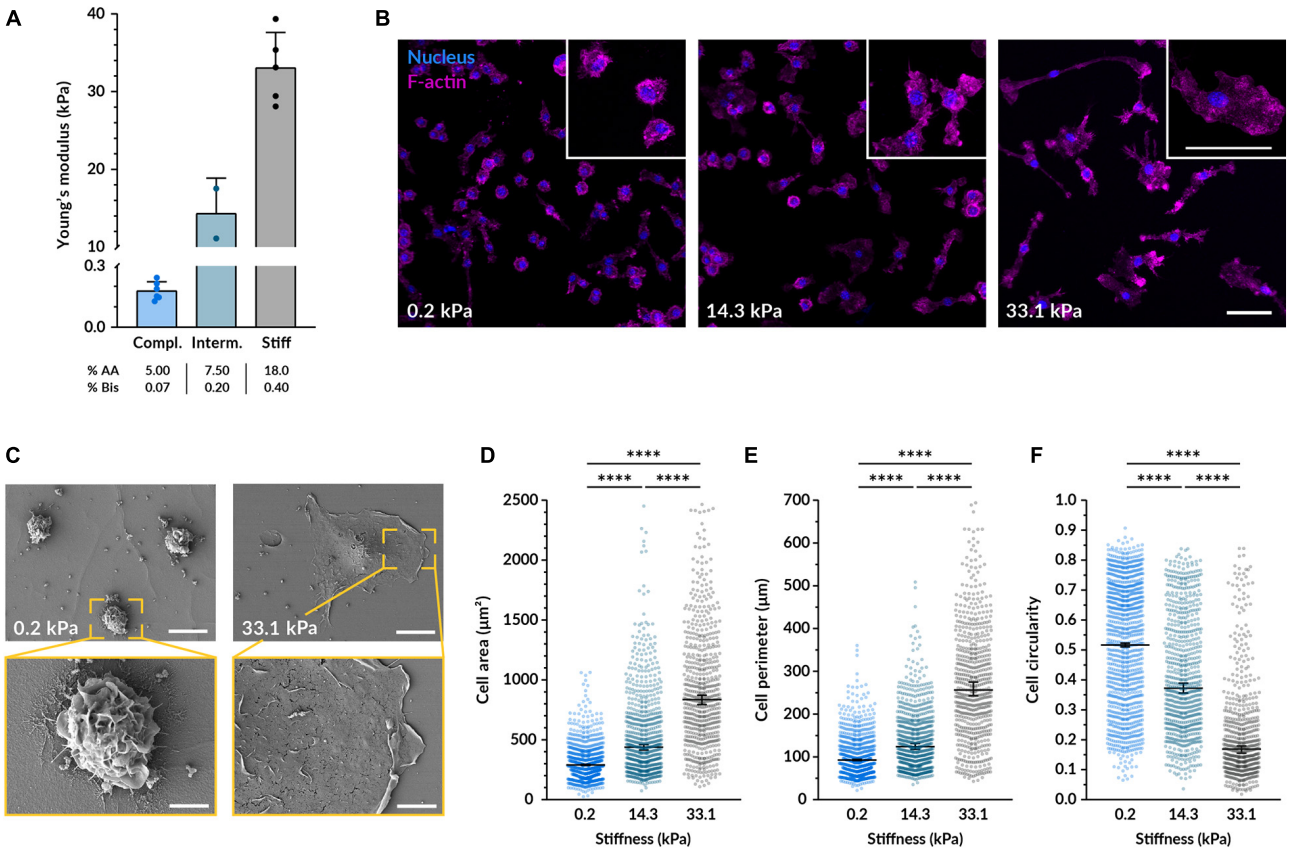

FIGURE 1 | Substrate stiffness affects the morphology of macrophages. **(A)** Young's moduli of the three different polyacrylamide 2D hydrogels used as cell substrate obtained by AFM. The mean ± SD was 0.18 ± 0.04 kPa for the compliant, 14.32 ± 4.54 kPa for the intermediate, and 33.07 ± 4.55 kPa for the stiff gel. **(B)** Representative confocal microscopy images of fluorescent BMDMs cultured on the different gels for 14–18 h. Nuclei shown in blue (DAPI) and F-actin in magenta (phalloidin-TRITC). Enlarged examples of cells of each condition are displayed in the insets. Scale bars, 50 µm. **(C)** Scanning electron micrographs of BMDMs on the compliant and stiff gels cultured as in **(B)**. Scale bars on top, 50 µm, and bottom, 20 µm. **(D–F)** Quantification of the cell area **(D)**, perimeter **(E)**, and circularity **(F)** from images taken under the same conditions as **(B)**. In all plots, each dot represents a cell and the black bars indicate mean ± SEM. The number of analyzed cells was 1117 for compliant, 771 for intermediate and 629 for stiff; data were obtained from 3 independent experiments done with cells from three different mice. Statistical analysis was performed using a Kruskal–Wallis ANOVA followed by Dunn's *post hoc* analysis to obtain the multiple comparison *p*-values. ****$p < 0.0001$.

that triggers the final maturation and release of the cytokine. In this study, we employed nigericin: a potent K^+ efflux inducer that triggers the formation of the NLRP3 inflammasome. This large multiprotein complex mediates the final processing of IL-1β, which is then secreted outside the cell (Martinon et al., 2002; Agostini et al., 2004). Following the same trend as with IL-6, we found that after 1.5 h nigericin stimulation macrophages on 0.2 kPa hydrogels consistently secreted higher amounts of IL-1β, representing a mean 44% increase over macrophages on 33.1 kPa hydrogels (**Figures 3B–D**).

Since nigericin treatment also triggered the onset of pyroptotic cell death, we expected that the higher IL-1β release would be associated with increased cell death. For this reason, we also assessed cell viability by measuring LDH release (**Figures 3C,E** and **Supplementary Figure S2**). Before macrophage priming and activation, we did not find a significant difference between both stiffnesses. After 90 min of incubation with nigericin, however, we detected that macrophage viability was significantly lower when stimulated while being cultured on the 0.2 kPa polyacrylamide, indicating that pyroptosis was increased on the compliant gels (**Figures 3C,E**). While this difference was also detectable after 60 min and 6 h of initiating the nigericin treatment (**Supplementary Figure S2**), we kept using the 90 min timepoint for the rest of the study because at this point the macrophage pyroptotic response was robust enough but still submaximal. Collectively, these data show that substrate stiffness influences pro-inflammatory cytokine secretion and suggest that the upstream signaling events leading to cytokine maturation and release may become enhanced when macrophages are cultured on a more compliant substrate.

According to this hypothesis, we tested whether substrate stiffness influenced the formation of the NLRP3 inflammasome, which is the corresponding inflammasome activated by the nigericin-induced K^+ efflux. We imaged macrophage inflammasomes by immunostaining for the linker protein ASC after the same stimulation treatment. ASC is the protein linking NLRP3 and pro-caspase1, three proteins that, upon K^+ efflux, cluster together forming a 1-µm structure that can be

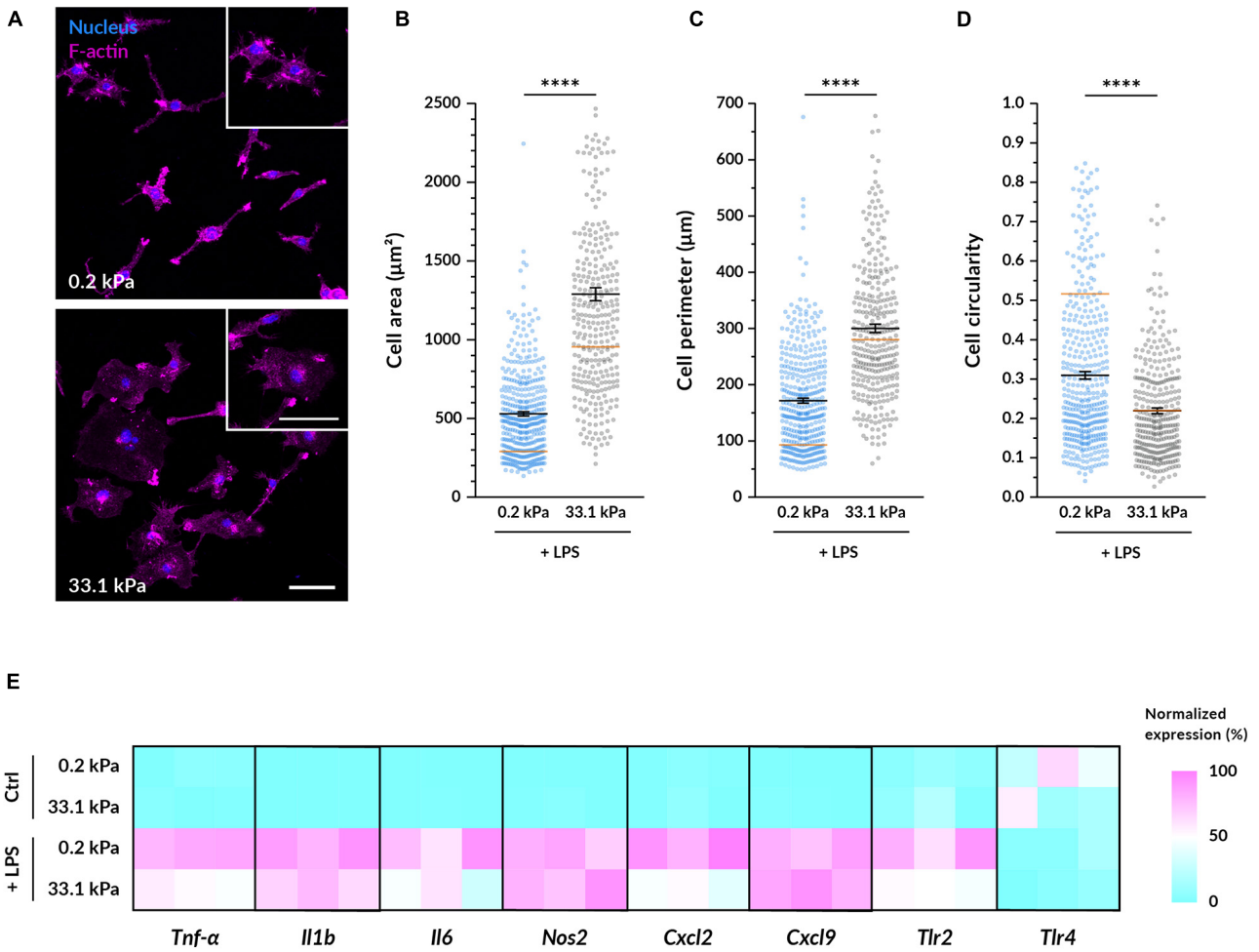

FIGURE 2 | Substrate stiffness influences LPS-primed macrophages. **(A)** Representative fluorescence microscopy images of BMDMs cultured on the different gels for 14–18 h and then primed with 100 ng/ml LPS for 4.5 h. Nuclei are shown in blue and F-actin in magenta. Enlarged examples of cells of each condition are displayed in the insets. Scale bars, 50 µm. **(B–D)** Quantification of the cell area **(B)**, perimeter **(C)**, and circularity **(D)** from images taken under the same conditions as **(A)**. In all plots, each dot represents a cell, the black bars indicate mean ± SEM, and the reference orange bar indicates the mean of the non-primed macrophages in **Figures 1D–F**. The number of analyzed cells was 390 for compliant and 322 for stiff; and data were obtained from three independent experiments done with different animals. Statistical analysis was performed using a Mann–Whitney test. ****$p < 0.0001$. **(E)** Relative gene expression levels of pro-inflammatory genes in non-treated macrophages and in cells primed with 100 ng/ml of LPS for 6 h. Normalized data are presented as heatmaps (see **Supplementary Figure S1** for absolute fold changes).

easily identified in fluorescence images (**Figure 3F**). Cells that have an assembled inflammasome and triggered the onset of pyroptosis tend to progressively reduce their cell area, which we could especially distinguish on the better spread cells on stiff gels (**Supplementary Figure S3**). Besides ASC-positive specks, we also observed some decreased levels of F-actin, indicating the impairment of the actin cytoskeleton caused by the activation of the pyroptotic machinery. By determining the ratio of ASC-positive specks to cell number after 90 min of nigericin stimulation, we found that macrophages on 0.2 kPa gels displayed 4 times more ASC specks than macrophages on 33.1 kPa (**Figure 3G**). This strongly indicates that the assembly of the NLRP3 inflammasome is upregulated in cells on more compliant substrates. Altogether, our data show that more compliant substrates enhance the assembly of macrophage NLRP3 inflammasomes, the secretion of the pro-inflammatory cytokines IL-1β and IL-6 and the release of the pyroptotic marker LDH, suggesting that substrate stiffness may modulate the formation of the inflammasome and the downstream activation of the pyroptotic machinery.

Inhibiting Myosin but Not Limiting Cell Spreading Suppresses Stiffness-Induced Differences in Inflammasome Formation

We first hypothesized that the distinct cell spreading we had observed on compliant and stiff gels could serve as a mechanosensory element directly involved in modulating the inflammatory response of macrophages. To test if spreading alone affects inflammasome formation, we analyzed as above

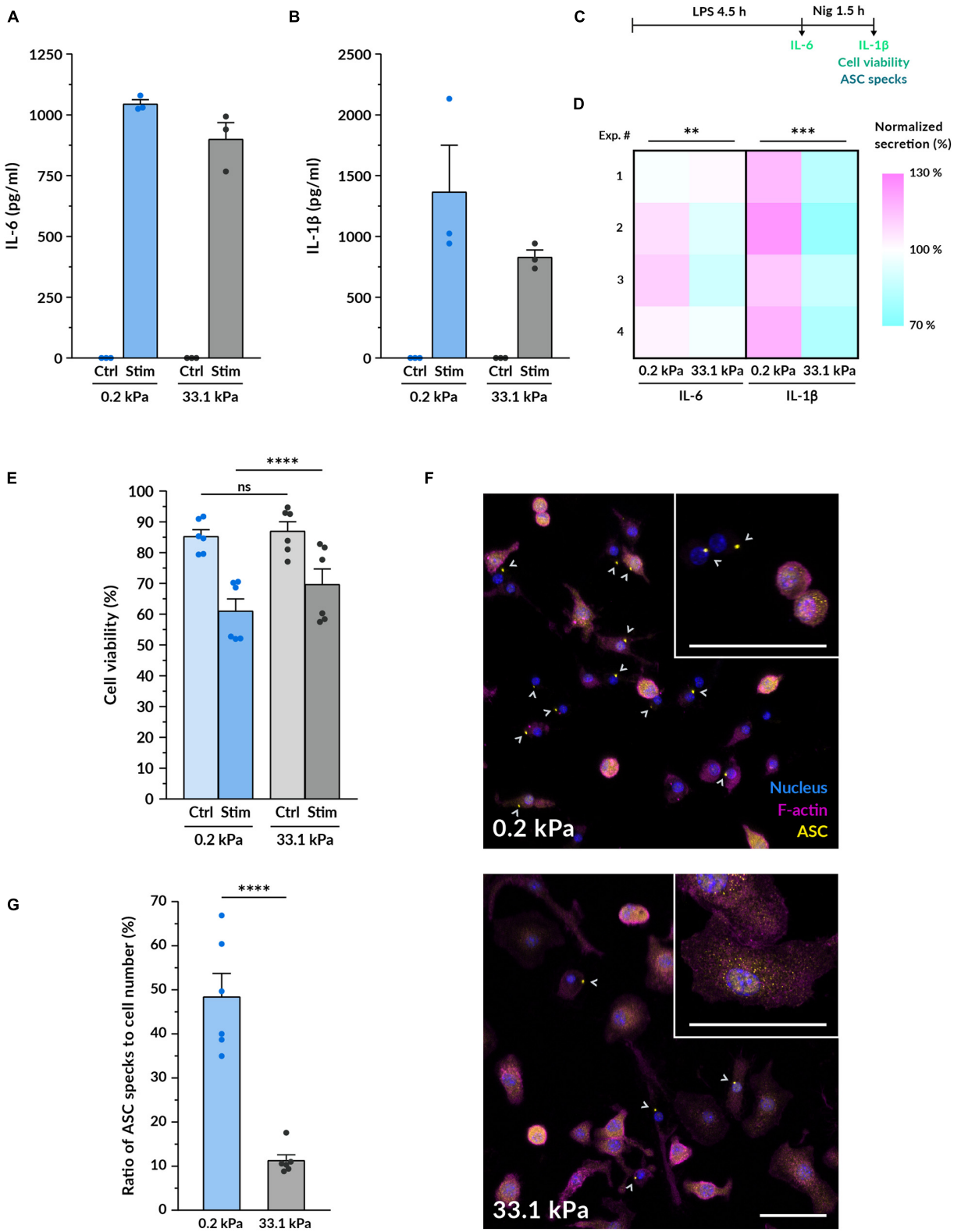

FIGURE 3 | Macrophage pro-inflammatory response is upregulated by more compliant substrates. **(A,B)** Quantification of the protein levels of the cytokines IL-6 **(A)** and IL-1β **(B)** secreted by macrophages on compliant and stiff polyacrylamide hydrogels via ELISA. BMDMs were cultured for 14–18 h on the hydrogels, primed with 100 ng/ml LPS for 4.5 h and stimulated with 10 μM nigericin for 1.5 h. IL-6 supernatants were collected after LPS priming, for IL-1β after nigericin treatment. Results

(Continued)

FIGURE 3 | Continued
of one representative experiment are shown (mean ± SEM), each dot represents one replicate. All experiments were independently repeated three times using cells from three different mice and with similar results. **(C)** Scheme of the experimental treatment applied in **(A–G)**. **(D)** Heatmap of the IL-6 and IL-1β cytokine quantification performed as described in **(A,B)**. Each square represents an independent experiment. Statistical analysis was performed using a 1D linear mixed model and *p*-values were determined by a likelihood ratio test. ***$p < 0.001$. **(E)** Assessment of cell viability after macrophage priming and stimulation. Cell viability was determined by LDH assay for untreated control BMDMs cultured on gels and for macrophages treated as described in **(A,B)**. Mean ± SEM are shown and each dot represents a replicate obtained from three independent experiments. Statistical analysis was performed using a 1D linear mixed model and *p*-values were determined by a likelihood ratio test. ***$p < 0.001$. **(F)** Representative confocal microscopy images of fluorescent ASC specks as a measure of inflammasome formation. BMDMs cultured on the different gels for 14–18 h, primed and stimulated as in **(A,B)**. Nuclei shown in blue, F-actin in magenta and the inflammasome linker protein ASC in yellow. Gray arrowheads indicate ASC specks, markers of inflammasome assembly. Insets display higher magnification examples of cells on each stiffness. Scale bars, 50 μm. **(G)** Quantification of the ratio of ASC specks to cell number. Mean ± SEM are shown and each dot indicates one of the different replicates obtained from three independent experiments. The total number of cells analyzed was 4327 (compliant hydrogels) and 5030 (stiff hydrogels). Statistical analysis was performed using a 1D linear mixed model and *p*-values were determined by a likelihood ratio test. ns, not significant, **$p < 0.01$, ***$p < 0.001$, ****$p < 0.0001$.

ASC specks, this time limiting the macrophage spreading area. Therefore, we cultured BMDMs on fibronectin-coated round islands with a diameter of 20 μm micropatterned on a glass substrate (**Figure 4A**). The adhesion area of each island was 314 μm^2, resembling the mean spreading area of macrophages on compliant hydrogels (**Figure 1D**). Confined macrophages were compared to unconfined cells cultured on the same glass substrate functionalized with non-micropatterned fibronectin (**Figure 4A**). Surprisingly, after nigericin stimulation confined macrophages had on average significantly less ASC specks than macrophages grown in an unconfined area (**Figure 4B**). Limiting cell spreading under these conditions did not recapitulate what we had observed on the compliant hydrogels since it did not enhance inflammasome formation but actually reduced it. Therefore, cell spreading alone does not seem to be the element positively modulating the increased response of macrophages on softer substrates.

Given that the conformation of the F-actin cytoskeleton in BMDMs is also altered by substrate stiffness and actomyosin is involved in mechanosensing (Elosegui-Artola et al., 2018), we decided to investigate whether actomyosin contractility could play a role as a mechanotransducer in the context of macrophage pro-inflammatory activation. To this end, we primed and stimulated macrophages under the effect of blebbistatin, a non-muscle myosin II inhibitor, and Y-27632, which blocks the activity of ROCK1 and ROCK2 (**Figures 4C,D**). Compared to the DMSO control, cells incubated with 10 μM blebbistatin did not show notable changes in their morphology (**Figure 4C** and **Supplementary Figure S4**), as also noted in Jain and Vogel (2018). Nevertheless, when using 10 μM Y-27632, macrophages qualitatively appeared thinner and formed some elongated processes, a change that could be especially perceived when imaging the cells treated with nigericin on stiff substrates. After quantifying inflammasome formation we first observed that when growing macrophages on 0.2 kPa gels, both blebbistatin and Y-27632 reduced the ratio of ASC specks (**Figure 4E**). On the other side, when cultured on 33.1 kPa substrates there were no differences to the DMSO control. When comparing the data of the two substrate stiffnesses under the effect of the each inhibitor, it was particularly interesting to note that blebbistatin greatly diminished the differences between the compliant and stiff gels. In contrast, inhibiting ROCK did not seem to balance out the differences induced by culturing macrophages on substrates of different stiffness. These data indicate that inhibiting actomyosin contractility with blebbistatin had a significant impact on the enhanced ability of macrophages to assemble the NLRP3 inflammasome on more compliant substrates, decreasing the inflammasome formation rate and equalizing it to the one on stiffer gels. Altogether, these results suggest that actomyosin contractility may be an element involved in the integration of substrate stiffness as a modulatory parameter of macrophage inflammasome formation.

DISCUSSION

It is becoming increasingly clear that macrophages respond to mechanical cues and that biophysical stimuli such as interstitial fluid flow (Li et al., 2018), hyperosmotic shocks (Ip and Medzhitov, 2015) or the modification of cell shape (McWhorter et al., 2013) can have an impact on their phenotype and function. In the present study, we explored the mechanosensitive response of macrophages by exposing BMDMs to substrate stiffness in the range of 0.2 to 33.1 kPa. Our results indicate that more compliant substrates increase the sensitivity of BMDMs to pro-inflammatory stimuli, enhancing inflammasome formation, pyroptosis onset and cytokine release, and that this might be mediated through actomyosin contractility.

The culture of macrophages on substrates of varying stiffness affected several morphological parameters including spreading area, circularity and membrane topography. This is in line with what most previous studies have shown in several stiffness ranges and different macrophage cell types, including murine BMDMs (Hsieh et al., 2019), RAW 264.7 murine cells (Blakney et al., 2012; Patel et al., 2012), THP-1-differentiated macrophages (Sridharan et al., 2019; Xing et al., 2020) and human monocyte-derived macrophages (Adlerz et al., 2015). We report that BMDMs on 0.2 kPa polyacrylamide substrates upregulated their pro-inflammatory response when compared to the 33.1 kPa hydrogels. Despite not observing major changes in the expression of pro-inflammatory genes, upon LPS priming and nigericin stimulation we detected higher secretion levels of IL-6 and IL-1β on the most compliant hydrogels. Several studies using polyacrylamide gels within a similar stiffness range also reported an enhanced secretion of pro-inflammatory cytokines on more compliant substrates. For instance, Scheraga et al. (2016) cultured BMDMs on fibronectin-coated polyacrylamide gels with a Young's modulus between 1 and 25 kPa. Upon LPS

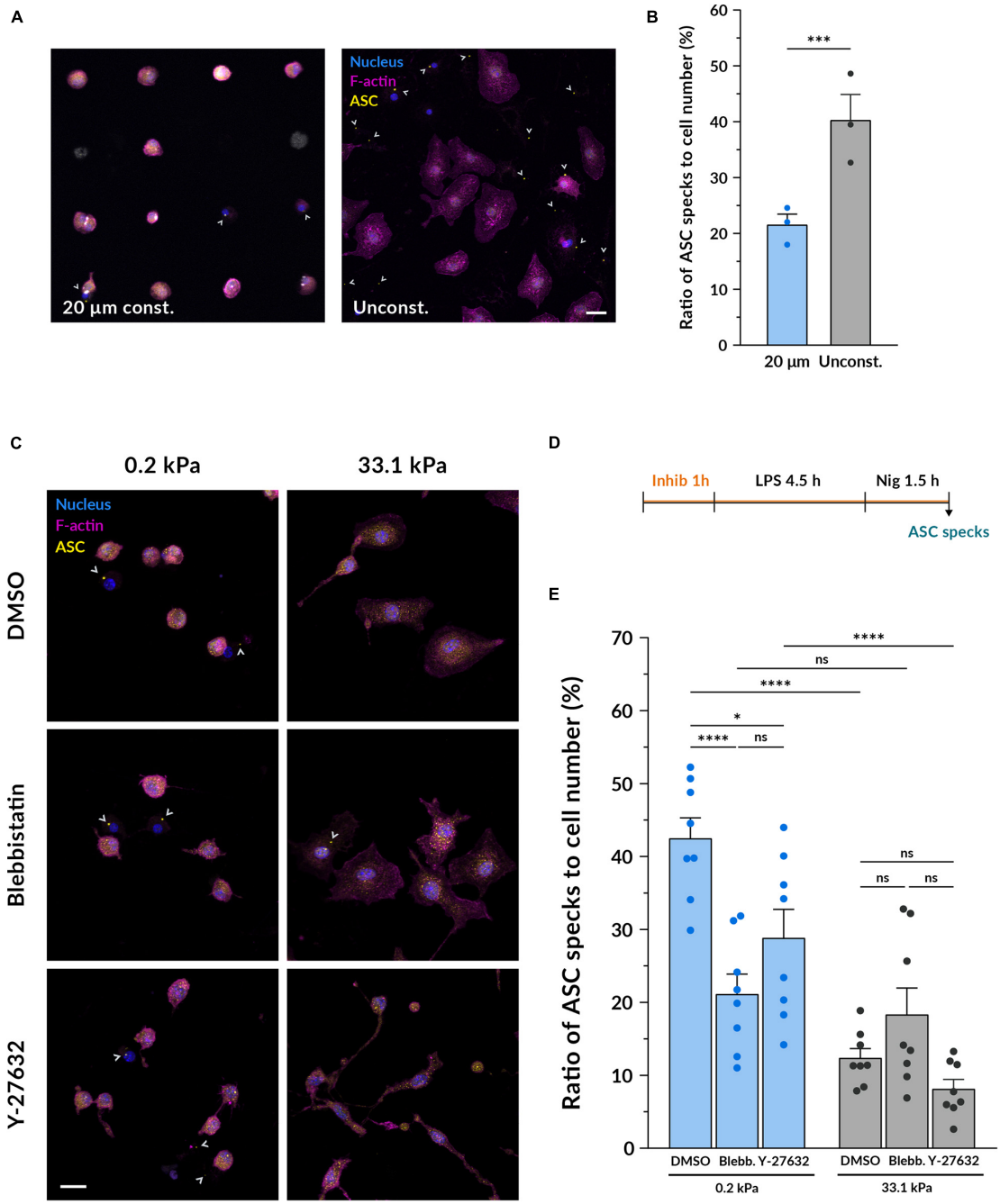

FIGURE 4 | Inhibiting myosin but not limiting cell spreading diminishes the differences induced by stiffness on inflammasome formation. **(A)** Representative confocal microscopy images of inflammasome formation under cell confinement. BMDMs were cultured on fibronectin-coated circular islands micropatterned on a glass substrate with a diameter of 20 µm. Unconfined cells were grown on fibronectin-coated glass coverslips growing in an unconfined manner. After 14–18 h of culture, they were primed with 100 ng/ml LPS for 4.5 h and stimulated with 10 µM nigericin for 1.5 h. Nuclei shown in blue, F-actin in magenta and ASC in yellow. Scale bar, 20 µm. **(B)** Quantification of the ratio of ASC specks to cell number. Mean ± SEM are shown and each dot indicates an independent experiment done with BMDMs from different mice. The total number of cells analyzed was 1560 for the 20 µm confined and 1524 for the unconfined adhesion area. Statistical analysis was performed using a 1D linear mixed model and *p*-values were determined by a likelihood ratio test. ****$p < 0.0001$. **(C)** Representative confocal microscopy images of inflammasome formation under actomyosin inhibition. BMDMs cultured on hydrogels for 14–18 h were pretreated with either 1:1700 DMSO as a control, 10 µM blebbistatin or 10 µM Y-27632 for 1 h. Keeping the respective inhibitor molecules, cells were then primed with 100 ng/ml LPS for 4.5 h and stimulated with 10 µM nigericin for 1.5 h. Nuclei shown in blue, F-actin in magenta and ASC in yellow. Scale bar, 20 µm. **(D)** Scheme of the experimental treatment applied in **(C,E). (E)** Quantification of the ratio of ASC specks to cell number. Mean ± SEM are shown and each dot indicates one of the different replicates obtained from three independent experiments. The total number of cells analyzed was, for compliant gels, 4673 (DMSO), 3528 (blebbistatin) and 5182 (Y-27632); and for stiff gels, 4859 (DMSO), 5447 (blebbistatin), and 5214 (Y-27632). Statistical analysis was performed using a one-way ANOVA followed by Bonferroni's *post hoc* analysis to obtain the multiple comparison *p*-values. ns, not significant, *$p < 0.05$, ***$p < 0.001$, ****$p < 0.0001$.

priming, they detected higher concentrations of IL-1β on their most compliant gels and, interestingly, they detected higher levels of the anti-inflammatory cytokine IL-10 on the stiffer material. Using the same type of gels, cells, and stimulus, Gruber et al. (2018) reported that BMDMs released higher amounts of the pro-inflammatory cytokine TNF-α on 1 kPa substrates than on 20 and 150 kPa hydrogels. In this case, though, the concentration of IL-10 was higher on the compliant substrates. In line with that, Patel et al. (2012) cultured RAW 264.7 macrophages on poly-D-lysine (PDL)-coated polyacrylamide gels between 1 and 150 kPa and quantified that the lower the stiffness, the higher the secretion of the TNF-α upon LPS challenge. Additionally, some recent reports point out that higher stiffness could promote a shift from M1 to M2-like phenotype. Carnicer-Lombarte et al. (2019) tested the influence of different PDL-coated polyacrylamide gels in the phenotype of BMDMs, detecting higher levels of M1-like genes on 1 kPa gels and higher levels of M2-like genes on 50 kPa materials. And recently, Xing et al. (2020) described that when THP-1 macrophages were cultured on collagen-coated PAA hydrogels between 6 and 16 kPa, the stiffer substrates promote higher expression of M2 markers.

In contrast, there are other reports stating that stiffer microenvironments are the ones upregulating macrophage pro-inflammatory behavior (Blakney et al., 2012; Previtera and Sengupta, 2015; Okamoto et al., 2018; Hsieh et al., 2019; Sridharan et al., 2019). For example, Previtera and Sengupta (2015) exposed BMDMs to polyacrylamide gels ranging from 0.3 to 230 kPa and after LPS treatment they detected higher concentrations of secreted IL-1β, TNF-α and NO on stiffer substrates. This discrepancy in the response of macrophages across different studies might be caused by the choice of different cell lines, adhesion protein, its coating density or the type of stimulatory challenge. In the present study we should note that we collected the samples to quantify IL-6 only after 4.5 h of LPS priming and, unlike all the mentioned studies, we induced the release of IL-1β with the ionophore nigericin. Moreover, it is important to consider the possibility that macrophages might not react to substrates of varying stiffness in a monotonous manner. Sridharan et al. (2019) observed that in THP-1-derived macrophages the influence of material stiffness on phagocytosis and several M1 genes and cytokines followed a biphasic response. The data obtained by Gruber et al. (2018) in RAW 264.7 cells reported a similar behavior in LPS-induced TNF-α secretion. The biphasic response to substrate mechanics has already been described in other cell types such as fibroblasts (Wang et al., 2019) and, therefore, the existence of a non-linear relationship between substrate stiffness and macrophage behavior should not be discarded until more data is collected.

The inflammasome represents one of the main signaling hubs activated in macrophages upon inflammatory stimuli. Despite the fact that most of the described inflammasome regulators consist of biochemical signals (Swanson et al., 2019), recent studies suggest that mechanical cues could also be modulating its formation. For example, cycling stretch has been shown to downregulate the release of IL-1β by inhibiting NLRP3 inflammasome formation (Maruyama et al., 2018) and hyperosmotic shocks have been described to trigger the reverse effect (Ip and Medzhitov, 2015). Here, we provide evidence for the first time that microenvironment stiffness can also influence the activation of the NLRP3 inflammasome. In order to test whether the higher IL-1β secretion we observed on more compliant gels was accompanied by an upregulation of inflammasome assembly, we quantified the presence of ASC specks as a proxy of inflammasome activation. Our results showed that, upon LPS priming and nigericin stimulation, the most compliant substrates led to increased inflammasome formation. This suggests that substrate stiffness plays a role in regulating the assembly of the NLRP3 inflammasome and indirectly influences the activity of pyroptotic effectors such as caspase-1 and gasdermin D, which would explain the higher amounts of released LDH we also detected in the supernatant. All these effects could be caused by a decrease in the inflammasome activation threshold or by higher formation rates, but more detailed time-dependent data is necessary to understand the specific dynamics behind this process.

Based on the severe differences in cell shape and membrane topography induced by the compliant and stiff gels, we first tried to assess whether there was a relationship between macrophage spreading and inflammasome assembly. Larger cell spreading could indirectly cause an increase in membrane curvature and tension which mechanosensory elements like caveolae and mechanically gated ion channels could detect (Le Roux et al., 2019). Here, we firstly hypothesized that the lower spreading BMDMs adopted on more compliant substrates might have enhanced the formation of the NLRP3 inflammasome. We found that, however, limiting cell spreading on a stiff substrate did not enhance inflammasome formation but rather reduced it. Despite the difference that this experiment was not directly performed using stiff polyacrylamide gels but stiff glass substrates, these imply that reducing cell spreading alone may not recapitulate the downstream inflammatory effects we observed on gels of different stiffness. Previous research done by Jain and Vogel (2018) showed that spatial confinement of BMDMs on a glass surface downregulated the expression of pro-inflammatory genes *Il6*, *Cxcl9*, *Il1b* and *Nos2* and the subsequent secretion of TNF-α, IL-6 and IL-12 via the indirect modulation of chromatin compaction. Our data support the idea that cell confinement reduces the response of macrophages to pro-inflammatory stimuli and suggests that the NLRP3 inflammasome could be an additional signaling component affected by it.

Actomyosin contractility has been described as one of the key elements of the stiffness mechanotransduction machinery (Elosegui-Artola et al., 2018) and as necessary for macrophages to exert traction forces on their substrates (Hind et al., 2015). Here we tested whether interfering with it would have any effect on the activation of the NLRP3 inflammasome in BMDMs exposed to different material stiffness. The inhibition of myosin II's motor activity with blebbistatin during macrophage priming and stimulation strongly decreased the amount of inflammasome-activated cells on the compliant hydrogels and slightly increased it on the stiff ones, reducing the original differences between both stiffnesses. Inhibiting ROCK1 and ROCK2 with Y-27632 also downregulated the formation of inflammasomes on compliant gels but in a less substantial

manner than blocking myosin II activity alone. We should note that while blebbistatin specifically inhibits the motor activity of myosin II, pharmacologically blocking ROCK1/2 with Y-27632 not only inhibits the phosphorylation of myosin but also promotes F-actin destabilization (Maekawa et al., 1999; Horváth et al., 2020), possibly contributing to the different results obtained with these two molecules. Moreover, as shown in Hind et al. (2016), the generation of traction forces in M1 macrophages depends on myosin II activity but not on upstream ROCK activation. As they propose, perhaps other myosin II regulatory proteins such as MLCK contribute to promote actin contractility, explaining why we did not observe an effect of the same magnitude as when directly inhibiting myosin II. We speculate that there might be an optimal level of actomyosin contractility at which inflammasome formation is promoted and that macrophages on more compliant substrates might be closer to it, leading to an increase in inflammasome assembly. Overall, our results suggest that actomyosin contractility may play an important role in the integration of mechanical signals into the NLRP3 inflammasome regulatory pathways, but further studies are required to determine the exact sequence of events needed to couple them.

Recent papers also propose the idea that the actin cytoskeleton may be involved directly in the control of inflammasome activation. Man et al. (2014) showed that, upon exposing macrophages to *Salmonella*, actin polymerization is necessary for NLRC4 inflammasome formation, pyroptosis onset and IL-1β release, and Burger et al. (2016) determined that F-actin interacts with NLRP3 and ASC and negatively regulates the activity of the NLRP3 inflammasome. Moreover, other cytoskeletal components have also been described as regulators of inflammasome activation. dos Santos et al. (2015) detected that the intermediate filament vimentin interacts with NLRP3 and regulates inflammasome formation and Magupalli et al. (2020) showed that NLRP3 and pyrin inflammasomes are assembled at the centrosomes with the requirement of HDAC6-dependent microtubule transport. Since it has been reported that the actin cytoskeleton can cross-talk with microtubules to guide and redirect their growth (López et al., 2014), we could speculate that perhaps certain levels of actomyosin contractility could be required to enable a correct organization of microtubules, which would then facilitate inflammasome formation. The importance the cytoskeleton may have as an additional inflammasome regulator has just begun to be uncovered and what the exact link between mechanical cues, cytoskeleton activity and inflammasome formation is remains an open question to be addressed in the future.

The study of immune mechanosensing offers the possibility to provide a better insight of pathologies that trigger changes in the mechanical properties of affected tissues. For instance, the downregulation of the pro-inflammatory response of macrophages on substrates with higher stiffness could be relevant in the context of cancer. Tumor-associated macrophages (TAMs) are one of the key immune cell types present in the tumor microenvironment. TAMs with an M2-like phenotype infiltrated within cancerous tissues secrete cytokines that downregulate the immune response against neoplastic cells and they tend to favor tumor growth (Zhou, 2020). Compared to their healthy tissue counterparts, primary tumors are often associated with higher tissue stiffness (Nia et al., 2020). For example, in murine breast cancer the elastic modulus increases from an average of 0.17 kPa in a normal mammary gland to 4 kPa in mammary tumors (Paszek et al., 2005). And in human brain tumors the elastic modulus can increase from a few hundred Pa in non-cancerous tissue up to 13.5 kPa in advanced glioblastomas (Miroshnikova et al., 2016). Thus, in synergy with biochemical signals, the increased stiffness of malignant tissues may promote downregulation of an M1-like pro-inflammatory response of TAMs and induce the polarization towards an M2-like phenotype, promoting cancer progression. Additional knowledge on how microenvironment stiffness governs macrophage phenotype and function could, thus, help identifying novel therapeutic targets. Moreover, a deeper understanding of macrophage mechanobiology would also be beneficial for the development of better immunomodulatory treatments and the design of superior biomaterials to be used in implantable medical devices (Lacour et al., 2016).

MATERIALS AND METHODS

Preparation of Polyacrylamide Hydrogels (PAA Gels)

Gels were produced on aminosilanized glass coverslips. Briefly, 13 mm round glass coverslips were washed with 0.1 M NaOH for 15 min, washed with ethanol and water and dried. They were incubated for 20 min in a solution of 0.1% (v/v) allyltrichlorosilane and 0.1% (v/v) triethylamine diluted in chloroform, washed and dried. Finally, they were covered with 0.5% glutaraldehyde for 30 min, washed and dried. To obtain hydrogels with a range of different stiffness, acrylamide (AA) and N,N′-methylenebisacrylamide (BisA) were pre-mixed in different proportions. For compliant gels we used 5% AA and 0.07% BisA; for intermediate 12% AA and 0.2% BisA; and for stiff 18% AA and 0.4% BisA (all v/v and dissolved in PBS). Tetramethylethylenediamine (TEMED) was added to the pre-mixes to a final concentration of 0.3% (v/v). The mixture was degassed for 10 min. We used custom-made methylsulfone acrylate (MS) monomers as a thiol-reactive compound for functionalization with adhesion molecules, as recently described in Farrukh et al., 2016. The MS monomers are incorporated to the AA/BisA mix and after the gels are polymerized they can react with the thiol group present at the Cys residue of the employed adhesion peptide. This strategy enables the uncoupling of polyacrylamide stiffness from adhesion ligand density, ensuring a comparable density of peptides between different hydrogels. MS monomers were dissolved at 32 mg/ml in dimethylformamide (DMF). To initiate the polymerization, a final mixture 1:8 (v/v) of MS monomers and the AA/BisA pre-mixes was prepared and ammonium persulfate (APS) was added to a final concentration of 0.1% (w/v). 9.3 μl of the solution were placed between a glass coverslip and a flexible hydrophobic polyester sheet to gel for 30 min. Polymerized hydrogels were peeled off, immersed in water in a 24-well plate

to swell for a minimum of 1 h, washed, UV-sterilized for 30 min and washed again. Hydrogels were functionalized with 0.5 mg/ml of cRGD-Phe-Cys (Pepnet #PCI-3686-PI) diluted in ddH_2O at room temperature overnight. They were finally washed and then stored in water at 4°C for a maximum of 14 days until they were used for either mechanical characterization or cell culture. All chemicals mentioned were from Sigma-Aldrich unless specified.

Mechanical Characterization of PAA Hydrogels by Atomic Force Microscopy (AFM)

Hydrogels bound to the glass coverslips were mounted on a 35 mm dish using vacuum grease and covered with PBS at room temperature. The characterization was performed with a Nanowizard 4 (JPK Instruments) using cantilevers (arrow T1, Nanoworld) equipped with 5 μm diameter polystyrene beads (microParticles GmbH) and calibrated with the thermal noise method. Gels were probed in liquid with an indentation speed of 5 μm/s and a relative force setpoint ranging from 0.6 to 8 nN to achieve comparable indentation depths of approximately 2 μm. The obtained force-distance curves were analyzed using the JPK data processing software. Parts of the curves corresponding to the first 2 μm of indentation depth were fitted using the Hertz/Sneddon model for a spherical indenter and Poisson ratio of 0.5 was assumed (Hertz, 1881; Sneddon, 1965).

Macrophage Cell Culture, Stimulation, and Inhibitors

Primary bone marrow-derived macrophages (BMDMs) were produced by cultivating bone marrow harvested from C57BL/6J young mice (Janvier Labs; ethics approval number DD24.1-5131/396/9, Landesdirektion Sachsen) in BMDM medium consisting of high glucose DMEM + GlutaMAX (Thermo Fisher Scientific), 10% heat-inactivated FBS (v/v; Thermo Fisher Scientific), 1% penicillin-streptomycin (v/v; Thermo Fisher Scientific) and 20% L929 conditioned media (v/v) on Corning™ not TC-treated petri dishes (Sigma-Aldrich) for 6 days. Differentiated BMDMs were detached, seeded on hydrogels within a 24-well plate format at the concentration specified for each experimental approach and cultured for 14–18 h. For LPS priming, cells were challenged with 100 ng/ml ultrapure LPS from *Escherichia coli* (InvivoGen) for 4.5 h for most of the experiments and for 6 h for the gene expression experiments. For nigericin stimulation, BMDMs were treated with 10 μM nigericin (InvivoGen) for 1.5 h. For inhibitor experiments, 0.06% DMSO (v/v; Sigma-Aldrich), 10 μM blebbistatin (Sigma-Adlrich #B0560) or 10 μM Y-27632 (Sigma-Aldrich #Y0503) were used. BMDMs were pre-treated with the inhibitors for 1 h, and the inhibitors were kept in the medium during the subsequent priming with LPS priming and stimulation with nigericin.

Fluorescence Confocal Microscopy and Image Analysis

Cells were cultured at a density of approximately 50000 cells/cm^2 (10^5 in a 24-well plate). They were fixed with 4% paraformaldehyde (v/v; Thermo Fisher Scientific) for 12 min and permeabilized with 0.2% Triton™ X-100 (v/v; Sigma-Aldrich) for 10 min. Blocking was done with 10% goat serum (v/v; Jackson ImmunoResearch), 0.1% bovine serum albumin (w/v; Sigma-Aldrich) for 1 h. To visualize ASC specks, samples were incubated with anti-ASC antibody (1:400; pAb AL177, AdipoGen #AG-25B-0006) overnight at 4°C and Alexa Fluor 488 anti-rabbit (1:400; Thermo Fisher Scientific #A-11034) for 1 h at room temperature. Nuclei and F-actin were stained with DAPI (1:2000; Sigma-Aldrich #32670) and phalloidin-TRITC (1:800; Sigma-Aldrich #P1951), respectively, for 1 h. All washes were done with PBS. Samples were mounted by inverting them over a #1.5 glass coverslip with a PBS drop to avoid excessive drying.

Cells were imaged using an LSM700 inverted confocal microscope and a 20x/0.8 objective (Zeiss), acquiring z-stacks with 0.89 μm steps in each position of interest. Image analysis was done using the software Image J/Fiji (Schindelin et al., 2012; Schneider et al., 2012) and Ilastik (Berg et al., 2019). Cell nuclei and cell body were automatically segmented based on the intensity signal of the DNA and the F-actin labeling, respectively, and morphological parameters were extracted. Circularity was calculated as $4\pi\frac{Area}{Perimeter^2}$. The ratio of specks to cell number was determined semi-automatically. Briefly, ASC specks were quantified manually, considering only mature, clearly formed single specks, with an approx. diameter of 1 μm. Since pyroptosis causes the release of cytoplasmic material out of the cell, both intra- and extracellular specks were included in the analysis. Macrophages with more than one mature speck were highly rare, counted as single-specked and included into the analysis. The number of cells per image was obtained by automatically segmenting their nuclei.

Scanning Electron Microscopy (SEM)

Samples were fixed in 1 % glutaraldehyde in 100 mM phosphate buffer for at least 2 hours at room temperature and then washed in buffer (2x) and in water (4x). Samples were postfixed in 1% osmium tetroxide in water, washed several times in water, dehydrated in ascending ethanol concentrations (30, 50, 70, 90, 96% ethanol, 3x 100% ethanol on molecular sieve), and critical-point-dried using the Leica CPD300 drier (Leica Microsystems). Samples were mounted on 12 mm aluminum stubs, sputtered with gold (60 mA, 60 sec), and analyzed with a Jeol JSM 7500F cold field emission scanning electron microscope (Jeol Germany GmbH; acceleration voltage: 5 kV, emission: 10 μA, working distance: 8 mm, detector: lower secondary electron detector).

Gene Expression Analysis Using Quantitative Real-Time PCR (qRT-PCR)

Total RNA was extracted from 1.2×10^6 BMDMs grown on compliant/stiff gels using the RNeasy Mini Kit (Qiagen #74104). For this, 6 wells with 2×10^5 cells each were pooled for every experimental condition. For each stiffness, 6 wells were primed with lipopolysaccharide, while 6 wells received no treatment. Reverse transcription of 1 μg RNA was performed with iScript™ Advanced cDNA Synthesis Kit

(Bio-Rad #1725037), using a combination of oligo(dT) and random hexamer primers. qRT-PCR was performed at 56°C using GoTaq qPCR Mastermix (Promega #6002) on a Stratagene cycler Mx3005P system. Several primers of pro-inflammatory genes were used (**Supplementary Table S1**). Samples were run in duplicates and expression levels were normalized to the geometric mean of β-*actin*, *Gapdh,* and *18S* rRNA controls. Relative expression values were calculated as $2^{(-\Delta\Delta CT)}$ (relative to geometric mean of housekeeping genes and plastic controls). Fold-changes can be found in **Supplementary Figure S1**. For heatmaps, relative expression values were normalized to values between 0 and 100% for each gene. Heatmaps were generated in R (R Core Team, 2020).

Cytokine Quantification Assays

Bone marrow-derived macrophages were cultured at a density of approximately 100000 cells/cm^2 ($2{\cdot}10^5$ in a 24-well plate). Supernatants from cell cultures were collected and dead cells removed by centrifugation. The amounts of IL-6 and IL-1β were determined using the IL-6 Mouse Uncoated ELISA Kit (Thermo Fisher Scientific #88-7064-88) and the IL-1β Mouse Uncoated ELISA Kit (Thermo Fisher Scientific #88-7013-88), respectively, according to the manufacturer's instructions. Final absorbance was measured with a TECAN Infinite Pro plate reader, subtracting the 570 nm values from the 450 nm.

Cell Viability Assay

Bone marrow-derived macrophages were also seeded at density of approximately 100000 cells/cm^2 ($2{\cdot}10^5$ in a 24-well plate). Lactate dehydrogenase (LDH) activity in supernatants was measured using the LDH-Glo^{TM} Cytotoxicity assay (Promega #J2380) according to the manufacturer's instructions. Luminescence was recorded with a GloMax^{TM} 96 microplate luminometer (Promega). Total amount of cells was inferred by lysing cells with Triton^{TM} X-100 at the end of the experiments and comparing the values to the ones of an included standard curve.

Cell Micropatterning

Micropatterned glass slides were purchased from 4Dcell. The glass slides consisted of different areas with adhesion disks of a specific diameter ranging from 10 to 100 μm and non-adherent surface was passivated with PEG. The micropatterned surface was functionalized using 0.1 mg/ml fibronectin and cells were seeded at a density of approximately 10400 cells/cm^2 (10^5 in a 6-well plate). Cells were incubated overnight and the next day unattached cells were washed out before the start of the experiment.

Statistical Analysis

Statistical tests are indicated in each plot. Linear mixed model analysis was performed using R (R Core Team, 2020) and the rest of statistical analysis was performed using GraphPad Prism 6 (GraphPad Software). All data are presented as mean ± SEM unless specified. In all cases, p values < 0.05 were considered statistically significant (ns, not significant; $^*p < 0.05$; $^{**}p < 0.01$; $^{***}p < 0.001$; $^{****}p < 0.0001$).

DATA AVAILABILITY STATEMENT

The raw data supporting the conclusions of this article will be made available by the authors, without undue reservation.

ETHICS STATEMENT

The animal study was reviewed and approved by DD24.1-5131/396/9.

AUTHOR CONTRIBUTIONS

JG, CB, AT, and JCE conceived the project and designed the experiments. JCE carried out bulk of the experiments. AF and AC synthetized and provided MS monomers for the polyacrylamide gels. SA and AT optimized the hydrogel preparation. CS performed qRT-PCR experiments. JCE, CS, SA, and AT analyzed the data and performed its evaluation. JCE, AT, JG, and CB wrote the manuscript. All authors contributed to the article and approved the submitted version.

FUNDING

The work done by JCE, SA, and JG was supported by the EU's Horizon 2020 Research and Innovation Program under the Marie Skłodowska-Curie Grant Agreement No. 641639 (ITN Biopol). CB was supported by a Wellcome Trust Investigator Award 108045/Z/15/Z, and AT is fellow of the Mildred Scheel Early Career Center Dresden P2 funded by the German Cancer Aid (Deutsche Krebshilfe).

ACKNOWLEDGMENTS

We thank the animal, light, and electron microscopy facilities at the CMCB, TU Dresden (partly funded by the State of Saxony and the European Fund for Regional Development – EFRE). We are grateful to Thomas Kurth (CMCB, TU Dresden) for providing assistance with the SEM experiments, Benoit Lombardot (MPI-CBG, Dresden) for helping with image analysis, and Sam Pearson and Adrián de Miguel (INM, Saarbrücken) for helping with hydrogel preparation. We appreciate JPK Instruments, Elke Ulbricht, Maria Winzi, and Maik Herbig (CMCB, TU Dresden) for providing technical support and Helena Jambor (Medical Faculty, TU Dresden) for figure proofreading. We would also like to thank Christophe Lamaze (Institut Curie, Paris), the research groups of Miguel Ángel del Pozo (CNIC, Madrid) and Michael Sieweke (CMCB, TU Dresden), and all the members of the Guck team (MPL, Erlangen) for fruitful discussions.

SUPPLEMENTARY MATERIAL

The Supplementary Material for this article can be found online at: https://www.frontiersin.org/articles/10.3389/fcell.2021.639815/full#supplementary-material

REFERENCES

Adlerz, K. M., Aranda-Espinoza, H., and Hayenga, H. N. (2015). Substrate elasticity regulates the behavior of human monocyte-derived macrophages. *Eur. Biophys. J.* 45, 301–309.

Agostini, L., Martinon, F., Burns, K., McDermott, M. F., Hawkins, P. N., and Tschopp, J. (2004). NALP3 forms an IL-1β-processing inflammasome with increased activity in muckle-wells autoinflammatory disorder. *Immunity* 20, 319–325. doi: 10.1016/S1074-7613(04)00046-9

Bauernfeind, F. G., Horvath, G., Stutz, A., Alnemri, E. S., MacDonald, K., Speert, D., et al. (2009). Cutting edge: NF-κB activating pattern recognition and cytokine receptors license NLRP3 inflammasome activation by regulating NLRP3 expression. *J. Immunol.* 183, 787–791. doi: 10.4049/jimmunol.0901363

Berg, S., Kutra, D., Kroeger, T., Straehle, C. N., Kausler, B. X., Haubold, C., et al. (2019). ilastik: interactive machine learning for (bio)image analysis. *Nat. Methods* 16, 1226–1232. doi: 10.1038/s41592-019-0582-9

Blakney, A. K., Swartzlander, M. D., and Bryant, S. G. (2012). The effects of substrate stiffness on the in vitro activation of macrophages and in vivo host response to poly(ethylene glycol)-based hydrogels. *J. Biomed. Mater. Res. A* 100:12.

Booth, A. J., Hadley, R., Cornett, A. M., Dreffs, A. A., Matthes, S. A., Tsui, J. L., et al. (2012). Acellular normal and fibrotic human lung matrices as a culture system for in vitro investigation. *Am. J. Respir. Crit. Care Med.* 186, 866–876. doi: 10.1164/rccm.201204-0754OC

Burger, D., Fickentscher, C., de Moerloose, P., and Brandt, K. J. (2016). F-actin dampens NLRP3 inflammasome activity via Flightless-I and LRRFIP2. *Sci. Rep.* 6:29834. doi: 10.1038/srep29834

Carnicer-Lombarte, A., Barone, D. G., Dimov, I. B., Hamilton, R. S., Prater, M., Zhao, X., et al. (2019). Mechanical matching of implant to host minimises foreign body reaction. *bioRxiv* [Preprint] doi: 10.1101/829648

Christ, A. F., Franze, K., Gautier, H., Moshayedi, P., Fawcett, J., Franklin, R. J. M., et al. (2010). Mechanical difference between white and gray matter in the rat cerebellum measured by scanning force microscopy. *J. Biomech.* 43, 2986–2992. doi: 10.1016/j.jbiomech.2010.07.002

Dinarello, C. A. (2011). A clinical perspective of IL-1β as the gatekeeper of inflammation. *Eur. J. Immunol.* 41, 1203–1217. doi: 10.1002/eji.201141550

Dorrington, M. G., and Fraser, I. D. C. (2019). NF-κB signaling in macrophages: dynamics, crosstalk, and signal integration. *Front. Immunol.* 10:705. doi: 10.3389/fimmu.2019.00705

dos Santos, G., Rogel, M. R., Baker, M. A., Troken, J. R., Urich, D., Morales-Nebreda, L., et al. (2015). Vimentin regulates activation of the NLRP3 inflammasome. *Nat. Commun.* 6:6574. doi: 10.1038/ncomms7574

Elkin, B. S., Ilankovan, A., and Morrison, B. (2010). Age-dependent regional mechanical properties of the rat hippocampus and cortex. *J. Biomech. Eng.* 132:011010. doi: 10.1115/1.4000164

Elosegui-Artola, A., Trepat, X., and Roca-Cusachs, P. (2018). Control of mechanotransduction by molecular clutch dynamics. *Trends Cell Biol.* 28, 356–367. doi: 10.1016/j.tcb.2018.01.008

Emon, B., Bauer, J., Jain, Y., Jung, B., and Saif, T. (2018). Biophysics of tumor microenvironment and cancer metastasis – a mini review. *Comput. Struct. Biotechnol. J.* 16, 279–287. doi: 10.1016/j.csbj.2018.07.003

Evavold, C. L., Ruan, J., Tan, Y., Xia, S., Wu, H., and Kagan, J. C. (2018). The pore-forming protein Gasdermin D regulates Interleukin-1 secretion from living macrophages. *Immunity* 48, 35–44.e6. doi: 10.1016/j.immuni.2017.11.013

Farrukh, A., Paez, J. I., Salierno, M., and del Campo, A. (2016). Bioconjugating thiols to poly(acrylamide) gels for cell culture using Methylsulfonyl co-monomers. *Angew. Chem. Int. Ed.* 55, 2092–2096. doi: 10.1002/anie.201509986

Gruber, E., Heyward, C., Cameron, J., and Leifer, C. (2018). Toll-like receptor signaling in macrophages is regulated by extracellular substrate stiffness and Rho-associated coiled-coil kinase (ROCK1/2). *Int. Immunol.* 30, 267–278. doi: 10.1093/intimm/dxy027

Hertz, H. (1881). Über die berührung fester elastischer körper. *J. Für Reine Angew. Math.* 92, 156–171.

Hind, L. E., Dembo, M., and Hammer, D. A. (2015). Macrophage motility is driven by frontal-towing with a force magnitude dependent on substrate stiffness. *Integr. Biol.* 7, 447–453. doi: 10.1039/c4ib00260a

Hind, L. E., Lurier, E. B., Dembo, M., Spiller, K. L., and Hammer, D. A. (2016). Effect of M1–M2 polarization on the motility and traction stresses of primary human macrophages. *Cell Mol. Bioeng.* 9, 455–465. doi: 10.1007/s12195-016-0435-x

Horváth, ÁI., Gyimesi, M., Várkuti, B. H., Képiró, M., Szegvári, G., Lőrincz, I., et al. (2020). Effect of allosteric inhibition of non-muscle myosin 2 on its intracellular diffusion. *Sci. Rep.* 10:13341. doi: 10.1038/s41598-020-69853-8

Hsieh, J. Y., Keating, M. T., Smith, T. D., Meli, V. S., Botvinick, E. L., and Liu, W. F. (2019). Matrix crosslinking enhances macrophage adhesion, migration, and inflammatory activation. *APL Bioeng.* 3:016103. doi: 10.1063/1.5067301

Ip, W. K. E., and Medzhitov, R. (2015). Macrophages monitor tissue osmolarity and induce inflammatory response through NLRP3 and NLRC4 inflammasome activation. *Nat. Commun.* 6:6931. doi: 10.1038/ncomms7931

Ivanovska, I. L., Swift, J., Spinler, K., Dingal, D., Cho, S., and Discher, D. E. (2017). Cross-linked matrix rigidity and soluble retinoids synergize in nuclear lamina regulation of stem cell differentiation. *Mol. Biol. Cell* 28, 2010–2022. doi: 10.1091/mbc.e17-01-0010

Jain, N., and Vogel, V. (2018). Spatial confinement downsizes the inflammatory response of macrophages. *Nat. Mater.* 17, 1134–1144. doi: 10.1038/s41563-018-0190-6

Kaplanski, G. (2018). Interleukin-18: biological properties and role in disease pathogenesis. *Immunol. Rev.* 281, 138–153. doi: 10.1111/imr.12616

Lacour, S. P., Courtine, G., and Guck, J. (2016). Materials and technologies for soft implantable neuroprostheses. *Nat. Rev. Mater.* 1, 1–14. doi: 10.1038/natrevmats.2016.63

Le Roux, A.-L., Quiroga, X., Walani, N., Arroyo, M., and Roca-Cusachs, P. (2019). The plasma membrane as a mechanochemical transducer. *Philos. Trans. R. Soc. B Biol. Sci.* 374:20180221. doi: 10.1098/rstb.2018.0221

Li, R., Serrano, J. C., Xing, H., Lee, T. A., Azizgolshani, H., Zaman, M., et al. (2018). Interstitial flow promotes macrophage polarization toward an M2 phenotype. *Mol. Biol. Cell* 29, 1927–1940. doi: 10.1091/mbc.E18-03-0164

Liu, X., Zhang, Z., Ruan, J., Pan, Y., Magupalli, V. G., Wu, H., et al. (2016). Inflammasome-activated gasdermin D causes pyroptosis by forming membrane pores. *Nature* 535, 153–158. doi: 10.1038/nature18629

López, M. P., Huber, F., Grigoriev, I., Steinmetz, M. O., Akhmanova, A., Koenderink, G. H., et al. (2014). Actin–microtubule coordination at growing microtubule ends. *Nat. Commun.* 5:4778. doi: 10.1038/ncomms5778

Maekawa, M., Ishizaki, T., Boku, S., Watanabe, N., Fujita, A., Iwamatsu, A., et al. (1999). Signaling from Rho to the actin cytoskeleton through protein kinases ROCK and LIM-kinase. *Science* 285, 895–898. doi: 10.1126/science.285.5429.895

Magupalli, V. G., Negro, R., Tian, Y., Hauenstein, A. V., Caprio, G. D., Skillern, W., et al. (2020). HDAC6 mediates an aggresome-like mechanism for NLRP3 and pyrin inflammasome activation. *Science* 369:eaas8995. doi: 10.1126/science.aas8995

Malik, A., and Kanneganti, T.-D. (2017). Inflammasome activation and assembly at a glance. *J. Cell Sci.* 130, 3955–3963. doi: 10.1242/jcs.207365

Man, S. M., Ekpenyong, A., Tourlomousis, P., Achouri, S., Cammarota, E., Hughes, K., et al. (2014). Actin polymerization as a key innate immune effector mechanism to control *Salmonella* infection. *Proc. Natl. Acad. Sci. U.S.A.* 111, 17588–17593. doi: 10.1073/pnas.1419925111

Mariathasan, S., Weiss, D. S., Newton, K., McBride, J., O'Rourke, K., Roose-Girma, M., et al. (2006). Cryopyrin activates the inflammasome in response to toxins and ATP. *Nature* 440, 228–232. doi: 10.1038/nature04515

Martinon, F., Burns, K., and Tschopp, J. (2002). The inflammasome: a molecular platform triggering activation of inflammatory caspases and processing of proIL-β. *Mol. Cell* 10, 417–426. doi: 10.1016/S1097-2765(02)00599-3

Martinon, F., Pétrilli, V., Mayor, A., Tardivel, A., and Tschopp, J. (2006). Gout-associated uric acid crystals activate the NALP3 inflammasome. *Nature* 440, 237–241. doi: 10.1038/nature04516

Maruyama, K., Sakisaka, Y., Suto, M., Tada, H., Nakamura, T., Yamada, S., et al. (2018). Cyclic stretch negatively regulates IL-1β secretion through the inhibition of NLRP3 inflammasome activation by attenuating the AMP kinase pathway. *Front. Physiol.* 9:802. doi: 10.3389/fphys.2018.00802

McWhorter, F. Y., Wang, T., Nguyen, P., Chung, T., and Liu, W. F. (2013). Modulation of macrophage phenotype by cell shape. *Proc. Natl. Acad. Sci. U.S.A.* 110, 17253–17258. doi: 10.1073/pnas.1308887110

Miroshnikova, Y. A., Mouw, J. K., Barnes, J. M., Pickup, M. W., Lakins, J. N., Kim, Y., et al. (2016). Tissue mechanics promote IDH1-dependent HIF1α–tenascin C feedback to regulate glioblastoma aggression. *Nat. Cell Biol.* 18, 1336–1345. doi: 10.1038/ncb3429

Mirzaali, M. J., Schwiedrzik, J. J., Thaiwichai, S., Best, J. P., Michler, J., Zysset, P. K., et al. (2016). Mechanical properties of cortical bone and their relationships with age, gender, composition and microindentation properties in the elderly. *Bone* 93, 196–211. doi: 10.1016/j.bone.2015.11.018

Moshayedi, P., Ng, G., Kwok, J. C. F., Yeo, G. S. H., Bryant, C. E., Fawcett, J. W., et al. (2014). The relationship between glial cell mechanosensitivity and foreign body reactions in the central nervous system. *Biomaterials* 35, 3919–3925. doi: 10.1016/j.biomaterials.2014.01.038

Nia, H. T., Munn, L. L., and Jain, R. K. (2020). Physical traits of cancer. *Science* 370:eaaz0868. doi: 10.1126/science.aaz0868

Okamoto, T., Takagi, Y., Kawamoto, E., Park, E. J., Usuda, H., Wada, K., et al. (2018). Reduced substrate stiffness promotes M2-like macrophage activation and enhances peroxisome proliferator-activated receptor γ expression. *Exp. Cell Res.* 367, 264–273. doi: 10.1016/j.yexcr.2018.04.005

Paszek, M. J., Zahir, N., Johnson, K. R., Lakins, J. N., Rozenberg, G. I., Gefen, A., et al. (2005). Tensional homeostasis and the malignant phenotype. *Cancer Cell* 8, 241–254.

Patel, N. R., Bole, M., Chen, C., Hardin, C. C., Kho, A. T., Mih, J., et al. (2012). Cell elasticity determines macrophage function. *PLoS One* 7:e41024. doi: 10.1371/journal.pone.0041024

Previtera, M. L., and Sengupta, A. (2015). Substrate stiffness regulates proinflammatory mediator production through TLR4 activity in macrophages. *PLoS One* 10:e0145813. doi: 10.1371/journal.pone.0145813

R Core Team (2020). *R: A Language and Environment for Statistical Computing*. Vienna: R Foundation for Statistical Computing.

Sack, I., Beierbach, B., Hamhaber, U., Klatt, D., and Braun, J. (2008). Non-invasive measurement of brain viscoelasticity using magnetic resonance elastography. *NMR Biomed.* 21, 265–271. doi: 10.1002/nbm.1189

Scheraga, R. G., Abraham, S., Niese, K. A., Southern, B. D., Grove, L. M., Hite, R. D., et al. (2016). TRPV4 mechanosensitive ion channel regulates lipopolysaccharide-stimulated macrophage phagocytosis. *J. Immunol.* 196, 428–436. doi: 10.4049/jimmunol.1501688

Schindelin, J., Arganda-Carreras, I., Frise, E., Kaynig, V., Longair, M., Pietzsch, T., et al. (2012). Fiji: an open-source platform for biological-image analysis. *Nat. Methods* 9, 676–682. doi: 10.1038/nmeth.2019

Schneider, C. A., Rasband, W. S., and Eliceiri, K. W. (2012). NIH Image to ImageJ: 25 years of image analysis. *Nat. Methods* 9, 671–675. doi: 10.1038/nmeth.2089

Sneddon, I. N. (1965). The relation between load and penetration in the axisymmetric boussinesq problem for a punch of arbitrary profile. *Int. J. Eng. Sci.* 3, 47–57. doi: 10.1016/0020-7225(65)90019-4

Sridharan, R., Cavanagh, B., Cameron, A. R., Kelly, D. J., and O'Brien, F. J. (2019). Material stiffness influences the polarization state, function and migration mode of macrophages. *Acta Biomater.* 89, 47–59. doi: 10.1016/j.actbio.2019.02.048

Swanson, K. V., Deng, M., and Ting, J. P.-Y. (2019). The NLRP3 inflammasome: molecular activation and regulation to therapeutics. *Nat. Rev. Immunol.* 19, 477–489. doi: 10.1038/s41577-019-0165-0

Takeuchi, O., and Akira, S. (2010). Pattern recognition receptors and inflammation. *Cell* 140, 805–820. doi: 10.1016/j.cell.2010.01.022

Wang, L., Yan, F., Yang, Y., Xiang, X., and Qiu, L. (2017). Quantitative assessment of skin stiffness in localized scleroderma using ultrasound shear-wave elastography. *Ultrasound Med. Biol.* 43, 1339–1347. doi: 10.1016/j.ultrasmedbio.2017.02.009

Wang, W. Y., Davidson, C. D., Lin, D., and Baker, B. M. (2019). Actomyosin contractility-dependent matrix stretch and recoil induces rapid cell migration. *Nat. Commun.* 10:1186. doi: 10.1038/s41467-019-09121-0

Wells, R. G. (2013). Tissue mechanics and fibrosis. *Biochim. Biophys. Acta Mol. Basis Dis.* 1832, 884–890. doi: 10.1016/j.bbadis.2013.02.007

Xing, X., Wang, Y., Zhang, X., Gao, X., Li, M., Wu, S., et al. (2020). Matrix stiffness-mediated effects on macrophages polarization and their LOXL2 expression. *FEBS J.* doi: 10.1111/febs.15566 [Epub ahead of print].

Zhou, X. (2020). Tumor-associated macrophages: recent insights and therapies. *Front. Oncol.* 10:13. doi: 10.3389/fonc.2020.00188

Conflict of Interest: The authors declare that the research was conducted in the absence of any commercial or financial relationships that could be construed as a potential conflict of interest.

frontiers in Cell and Developmental Biology

REVIEW
published: 08 April 2021
doi: 10.3389/fcell.2021.606149

Transgelin-2: A Double-Edged Sword in Immunity and Cancer Metastasis

*Hye-Ran Kim[1,2], Jeong-Su Park[1,2], Hatice Karabulut[1,2], Fatima Yasmin[1,2] and Chang-Duk Jun[1,2]**

[1] School of Life Sciences, Gwangju Institute of Science and Technology (GIST), Gwangju, South Korea, [2] Immune Synapse and Cell Therapy Research Center, Gwangju Institute of Science and Technology (GIST), Gwangju, South Korea

Transgelin-2, a small actin-binding protein, is the only transgelin family member expressed in immune cells. In T and B lymphocytes, transgelin-2 is constitutively expressed, but in antigen-presenting cells, it is significantly upregulated upon lipopolysaccharide stimulation. Transgelin-2 acts as a molecular staple to stabilize the actin cytoskeleton, and it competes with cofilin to bind filamentous (F)-actin. This action may enable immune synapse stabilization during T-cell interaction with cognate antigen-presenting cells. Furthermore, transgelin-2 blocks Arp2/3 complex-nucleated actin branching, which is presumably related to small filopodia formation, enhanced phagocytic function, and antigen presentation. Overall, transgelin-2 is an essential part of the molecular armament required for host defense against neoplasms and infectious diseases. However, transgelin-2 acts as a double-edged sword, as its expression is also essential for a wide range of tumor development, including drug resistance and metastasis. Thus, targeting transgelin-2 can also have a therapeutic advantage for cancer treatment; selectively suppressing transgelin-2 expression may prevent multidrug resistance in cancer chemotherapy. Here, we review newly discovered molecular characteristics of transgelin-2 and discuss clinical applications for cancer and immunotherapy.

Keywords: immune synapse, dendritic cell therapy, T cell immunotherapy, cancer treatment, actin regulation

OPEN ACCESS

Edited by:
Balbino Alarcon, Consejo Superior de Investigaciones Científicas (CSIC), Spain

Reviewed by:
Elena Goncharova, University of California, Davis, United States
Noa B. Martin-Cofreces, Hospital Universitario Princess, Spain
Michael R. Gold, University of British Columbia, Canada

***Correspondence:**
Chang-Duk Jun
cdjun@gist.ac.kr

Specialty section:
This article was submitted to Cell Growth and Division, a section of the journal Frontiers in Cell and Developmental Biology

Received: *14 September 2020*
Accepted: *17 March 2021*
Published: *08 April 2021*

Citation:
Kim H-R, Park J-S, Karabulut H, Yasmin F and Jun C-D (2021) Transgelin-2: A Double-Edged Sword in Immunity and Cancer Metastasis. Front. Cell Dev. Biol. 9:606149. doi: 10.3389/fcell.2021.606149

INTRODUCTION

Transgelin-2 is an actin-binding protein that is encoded by the *TAGLN2* gene in humans and the *Tagln2* gene in mice. It is one of the three transgelin isoforms with transgelin-1 (also known as SM22α) and transgelin-3 (NP25) (Camoretti-Mercado et al., 1998). These proteins were first named "transgelins" because of their transformation-sensitive and shape-sensitive properties (Shapland et al., 1993). However, the functional and physiologic significance of these proteins has not yet been fully elucidated. Transgelin-2 is the only transgelin family member expressed in immune cells (Na et al., 2015). It plays pivotal roles in mediating various immune responses, including stabilizing the immune synapse between T cells and antigen-presenting cells (APCs) and potentiating phagocytosis in activated macrophages (Na and Jun, 2015; Na et al., 2015; Kim et al., 2017). These roles are afforded by the distinct biochemical properties of transgelin-2 (Shapland et al., 1993; Fu et al., 2000; Li et al., 2008; Na and Jun, 2015; Na et al., 2015; Kim et al., 2017, Kim H.-R. et al., 2018). Immune cells expressing high levels of transgelin-2 have dynamic membrane structures that facilitate the immune surveillance of the entire body for sensing pathologic insults. Conversely,

these molecular characteristics of transgelin-2 in cancer cells may aid tumor metastasis or tissue invasion. In agreement with this, transgelin-2 is considered a potential oncogenic factor in various cancer types (Meng et al., 2017). Therefore, transgelin-2 can be an excellent molecular target in both immune cells and cancer cells. Upregulation of transgelin-2 by cell-permeable recombinant protein in immune cells, downregulation by microRNA approaches in cancer cells may simultaneously improve immunity and defeat cancer cells.

Transgelin-2 and Transgelin Family Members

Transgelins are members of the calponin family of proteins comprising an N-terminal single calponin homology (CH) domain and a C-terminal short calponin repeated (CR) region (Pearlstone et al., 1987; Kranewitter et al., 2001; Gimona et al., 2002). All family members contain an actin-binding motif (ABM) and have an actin-bundling function under certain circumstances (**Figure 1**; Jo et al., 2018). The ABM includes two positively charged amino acid residues, KK (153/154) and KR (159/160), that are involved in actin binding. Mutation or deletion of these amino acids significantly reduces actin binding (Fu et al., 2000; Na et al., 2015; Kim H.-R. et al., 2018). The CH domain has been identified in a variety of proteins, ranging from actin-binding proteins to signaling molecules, and is predicted to function as an autonomous actin-binding region (Castresana and Saraste, 1995). Transgelin interacts with actin stress fibers and podosomes in smooth muscle cells via the CH domain (Gimona et al., 2003; Matsui et al., 2018). However, *in vitro*, the single CH domain is not sufficient for actin binding (Gimona and Mital, 1998; Fu et al., 2000), suggesting that both the CH domain and ABM or CR region together are necessary for the control of actin dynamics in cells. Proteins containing a single CH domain include calponin, IQGAP, Vav, and transgelin, and they display a high degree of sequence similarity with each other (**Figure 1**; Gimona and Mital, 1998). Interestingly, both Vav1 and IQGAP1 are key cytoskeletal-regulatory proteins in T-cell immunity (Ritter et al., 2013). The three transgelin isoforms preserve approximately 60% homology in the CH domain (Li et al., 2008).

Biochemical Properties of Transgelin-2

Transgelin was first characterized as a transformation- and shape-sensitive actin gelling protein. Electron microscopic (EM) analysis revealed that the addition of transgelin to filamentous (F)-actin converts the formation from a loose, random distribution into a tangled, cross-linked meshwork (**Figure 2A**; Shapland et al., 1993). Transgelin also has a modest effect on actin bundling and localizes at stress fiber bundles and podosomes in various cell types, including smooth muscle cells and neuronal cells (Mori et al., 2004; Thompson et al., 2012; Matsui et al., 2018). Since its identification, however, the biochemical characteristics of transgelin in regulating the actin cytoskeleton have not been fully elucidated. Additionally, whether transgelin directly binds actin has remained controversial (Morgan and Gangopadhyay, 2001). It was reported that transgelin causes actin to precipitate at low-ionic states and that it co-localizes with F-actin in cultured smooth muscle cells (Fu et al., 2000). However, another group documented that transgelin fails to bind F-actin in co-sedimentation assays and does not co-localize with actin in transfected fibroblasts (Gimona and Mital, 1998).

Recently, we corroborated that recombinant transgelin-2 binds to F-actin and weakly cross-links F-actin in bundles (Na et al., 2015). The binding of transgelin-2 to actin monomers in F-actin was saturated at a 1:1 ratio ($B_{max} = 0.915 \pm 0.102$ mol/mol), with a K_d of 7.39 μM (Na et al., 2015). Although it has been generally accepted that transgelin is a cross-linking protein, its bundling activity was observed only at higher concentrations (16–24 μM) than the well-known actin-bundling protein α-actinin (∼1 μM). The optimal ratio of actin to general actin-bundling proteins, such as fimbrin, fascin, filamin, and α-actinin, ranges from 1:0.05 to 1:0.5 (Glenney et al., 1981; Stokes and DeRosier, 1991; Van der Flier and Sonnenberg, 2001; Gordón-Alonso et al., 2012). However, the exceptionally higher concentrations of transgelin-2 needed to cross-link F-actin imply that this protein may have more functions in addition to F-actin cross-linking (Na et al., 2015).

For instance, transgelin-2 can instead regulate actin turnover dynamics. Interestingly, we found that transgelin-2 blocks spontaneous actin depolymerization and cofilin-mediated depolymerization (Na et al., 2015). This suggested that transgelin-2 binds to the sides of actin filaments and may act as an "insulator" that blocks the binding of other side-binding proteins, in particular the actin-disassembly protein cofilin (**Figure 2A**). Indeed, we found that transgelin-2 competes with cofilin for binding to F-actin (Na et al., 2015). The inability of a mutant with no ABM to block F-actin depolymerization suggests that transgelin-2 function is associated with its actin binding (Na et al., 2015). Based on the three-dimensional structure determined by single-particle image analysis (Egelman, 2000), we found that reconstructed F-actin combined with trangelin-2 revealed a higher density of transgelin-2 on actin subdomain (SD)1 and SD3 (Kim H.-R. et al., 2018), demonstrating its binding on SD1 and SD3 in actin. Interestingly, negatively charged aspartate or glutamate in the C-terminal's protrusion of transgelin-2 and the positively charged lysine in the N-terminal showed the possibility of ionic interaction between two transgelin-2 molecules in close distance (**Figure 2A**; Kim H.-R. et al., 2018), suggesting that transgelin-2 acts as a molecular "stapler" and mediates F-actin stabilization. This property of transgelin-2 contrasts with cofilin, which induces bending and twisting of actin filaments, leading to severing (McCullough et al., 2011). Interestingly, however, we observed that these two actin-binding proteins localize to different places during immune synapse formation (Na et al., 2015). Transgelin-2 is mainly localized at the bottom region of the distal-supramolecular activation cluster (d-SMAC) of the immune synapse where T cells directly contact APCs. By contrast, cofilin is enriched in the upper region of d-SMAC during immune synapse formation (**Figure 2B**; Na et al., 2015). Because these two molecules have opposite functions *in vitro*, these findings suggest that transgelin-2 may not compete with cofilin *in vivo*, but instead these proteins cooperate to maintain a stable centripetal actin flow in the immune synapse.

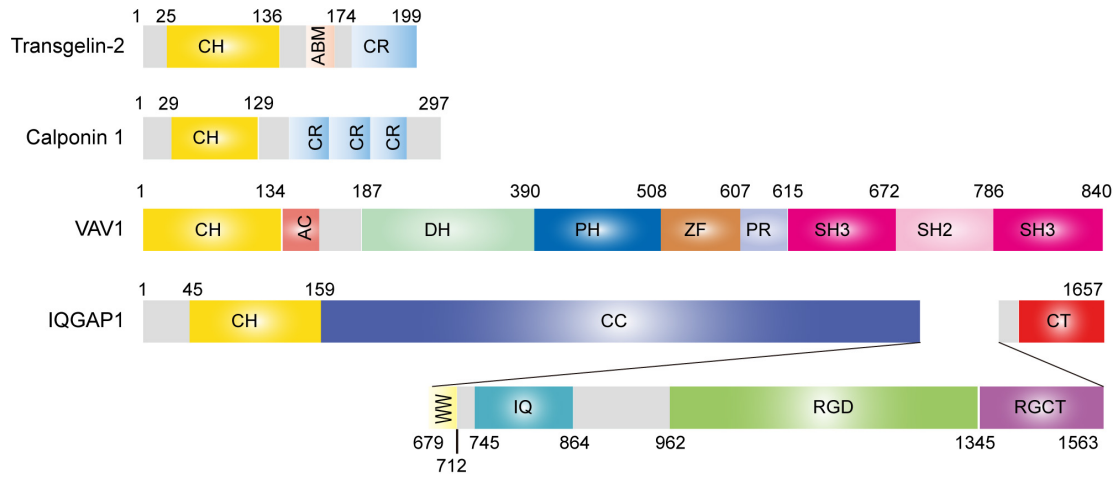

FIGURE 1 | Structure of transgelin-2 and comparison with other single calponin homology domain proteins.

Under physiologic concentrations of salt, transgelin-2 prevents secondary nucleation mediated by the Arp2/3 complex (Kim H.-R. et al., 2018). The binding sites (SD1 and SD3) of transgelin-2 in actin also overlaps with the Arp2/3 actin-binding site (Ge et al., 2014), thereby generating fewer actin-branched junctions in the presence of transgelin-2 (**Figure 2A**; Kim H.-R. et al., 2018). Further, it is also possible that transgelin-2 can cross-bridge actin filaments by binding SD1 and 3 on neighboring actin molecules. This action of transgelin-2 is similar to the epithelial protein lost in neoplasm (EPLIN), which inhibits F-actin depolymerization and cross-links filaments in bundles (Maul et al., 2003). Neither transgelin-2 nor EPLIN affects actin polymerization or elongation at the barbed end, but they block branched actin nucleation via the Arp2/3 complex (Maul et al., 2003; Kim H.-R. et al., 2018). Why do cells require transgelin-2 or EPLIN in addition to general Arp2/3 inhibitors? Although no enough data are accumulated, proteins that both inhibit Arp2/3 complex binding and crosslink actin may provide a coordinated mechanism for constructing bundled linear actin filaments. The molecular characteristics of transgelin-2 imply that this protein is essential to induce small filopodia formation and membrane ruffling (**Figure 2B**). In support of this idea, we found that overexpression of transgelin-2 generated spike-like filopodia at the leading edge of the lamellipodia in COS-7 cells (Kim H.-R. et al., 2018).

Fu et al. (2000) reported that transgelin co-precipitates actin under low-ionic conditions. Surprisingly, we observed that all three transgelin isoforms directly nucleate G-actin polymerization in low-ionic conditions, where actin polymerization usually is suppressed (**Figure 2A**; Kim H.-R. et al., 2018). Although a previous report demonstrated that the CH domain is unnecessary for F-actin binding (Gimona and Mital, 1998), we observed that this domain, together with the actin-binding loop, is required to mechanically link two adjacent G-actins, thereby mediating multimeric interactions (Kim H.-R. et al., 2018). The binding of transgelin-2 to G-actin was saturated at a 2.5:1 ratio under low-salt conditions (B_{max} = 2.8817 ± 0.072028 mol/mol) with a K_d of 0.921 μM (Kim H.-R. et al., 2018). This ratio is much higher than the 1:1 ratio of transgelin-2 binding to F-actin (Na et al., 2015). In this context, we hypothesized that the transgelin-2-mediated actin polymers (F-T/actin) might act as actin seeds to generate multiple actin filaments at the site where dynamic spatiotemporal actin rearrangement is required (**Figure 2A**).

Notably, only a few proteins can polymerize G-actin under low-salt conditions. These proteins contain nebulin fragments, myosin S-1, or a vinculin tail region (Chaussepied and Kasprzak, 1989; Valentin-Ranc et al., 1991; Shih, 1993; Wen et al., 2009). However, there is no evidence that these fragments are directly involved in actin polymerization in living cells. Therefore, it is unlikely that the fragments of some large proteins are physiologically functional *in vivo*. However, some proteins have actions *in vitro*. For instance, LL-37, which is an antimicrobial peptide secreted from macrophages and neutrophils, induces G-actin polymerization *in vitro* (Sol et al., 2012) and enhances macrophage phagocytosis (Wan et al., 2014). Moreover, like transgelin-2, this peptide induces actin bundling and affects actin structure (Sol et al., 2012). We identified that transgelin-2 is significantly upregulated in macrophages upon stimulation with lipopolysaccharide (LPS) and potentiates the phagocytic function (**Figure 2B**; Kim et al., 2017). *Salmonella* invasion protein A (SipA) is another example of *in vitro* evidence of G-actin polymerization under low-salt conditions (Zhou, 1999; Galkin et al., 2002; Higashide et al., 2002; Lilic et al., 2003). Interestingly, this protein triggers large-scale membrane protrusions and ruffles at the site of *Salmonella* entry (McGhie et al., 2001; Le Clainche and Drubin, 2004). Because G-actin polymerization does not naturally occur under low-salt conditions, it is hard to predict the *in vivo* physiology. However, these results suggest that proteins that drive G-actin polymerization in low-salt conditions may induce membrane ruffling as well as small filopodia formation (McGhie et al., 2001; Le Clainche and Drubin, 2004; Kim H.-R. et al., 2018). The biochemical properties of transgelin-2 and its subcellular localization in various biological situations are

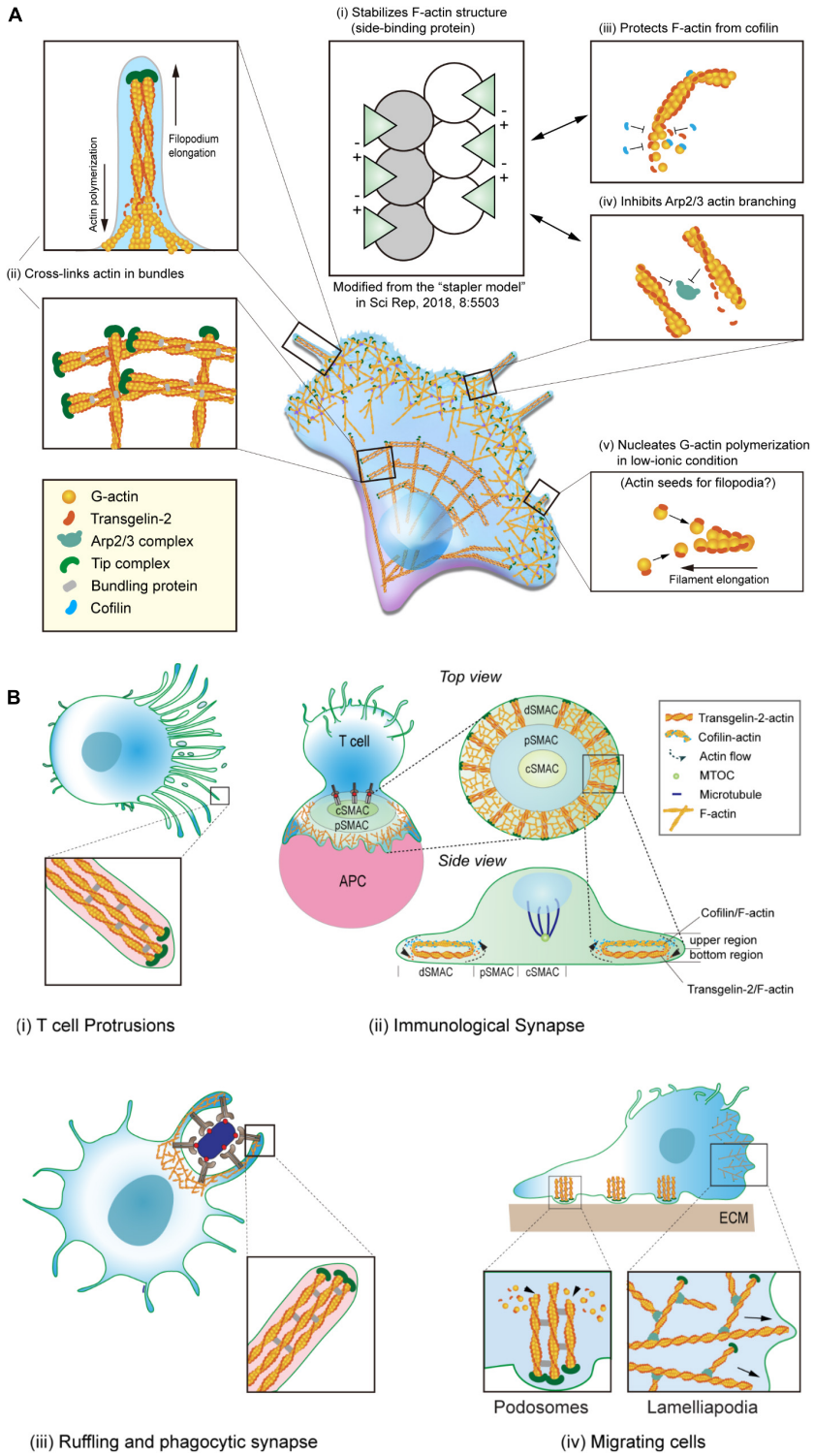

FIGURE 2 | Biochemical properties cellular localization of transgelin-2. **(A)** Biochemical properties of transgelin-2. Transgelin-2 directly binds to F-actin and stabilizes its structure (i) (Kim H.-R. et al., 2018). Transgelin-2 cross-links actin in bundles (ii) (Na et al., 2015; Kim H.-R. et al., 2018). It also acts as a side-binding protein and stabilizes F-actin (ii). This property is important to protect F-actin from cofilin-mediated depolymerization (iii) and to compete with Arp2/3 complex-mediated actin branching (iv) (Kim H.-R. et al., 2018). Transgelin-2 also can polymerize G-actin in low-ionic conditions, in which actin polymerization is prohibited (Kim H.-R. et al., 2018). **(B)** Localization of transgelin-2 in immune cells. Transgelin-2 is localized at the membrane-protrusive regions of T cells during antigen-recognition on antigen-presenting cells (APCs) (i). It also is located at the distal-supramolecular activation cluster (d-SMAC) area in mature immune synapse (ii). In professional phagocytes, this protein is enriched at the phagocytic cup or phagocytic synapse (iii). In dynamically moving cells, transgelin-2 localizes at the filopodial tips and podosomes (iv).

summarized in **Figure 2** (Shapland et al., 1993; Fu et al., 2000; Li et al., 2008; Na and Jun, 2015; Na et al., 2015; Kim et al., 2017, Kim H.-R. et al., 2018).

Transgelin-2 Is Essential for Immune Functions

In contrast to transgelin-1 and transgelin-3, which are mainly expressed in smooth muscle cells and the brain, respectively (Camoretti-Mercado et al., 1998; Mori et al., 2004; Depaz and Wilce, 2006), transgelin-2 is the only transgelin member expressed in immune cells, including T and B cells and macrophages (Na et al., 2015, 2016; Kim et al., 2017). In T and B cells, basal expression of transgelin-2 is constitutively high, but its expression is significantly altered in B cells by external stimuli such as anti-Ig and LPS (Francés et al., 2006; Na et al., 2015, 2016). In both bone marrow-derived and peritoneal macrophages, transgelin-2 is generally very low but significantly upregulated upon stimulation with the bacterial endotoxin LPS, suggesting that transgelin-2 expression is triggered by external inflammatory signals and plays a role in activated macrophages, involving in the actions of these cells to protect against infectious and neoplastic diseases. Transgelin-2 expression is controlled by the NF-κB pathway via toll-like receptor-4 (TLR4) in macrophages (Kim et al., 2017). Interestingly, transgelin-2 is the only transgelin member that contains an NF-κB consensus motif, which is located at the −174 to −179 region of the coding sequence.

After the initial recognition of antigen/MHC on APCs, T cells polarize many elongated microvilli or filopodia toward APCs to scan their surface antigen ligands. Transgelin-2 is localized in the protrusive region of polarized T cells and builds many small protrusions in this region (**Figure 2B**; Kim H.-R. et al., 2018). This phenotype was also achieved by the transfection of wild-type *Tagln2* cDNA in COS-7 cells (Kim H.-R. et al., 2018). However, knockout of *Tagln2* reduces protrusive structures on the surface of T cells (Kim H.-R. et al., 2018), suggesting that transgelin-2 is important for the formation of filopodia-like small membrane protrusions.

Immune synapse formation requires the tight regulation of actin rearrangement by many actin-polymerizing/depolymerizing proteins (Dustin and Cooper, 2000; Dustin, 2008a; Piragyte and Jun, 2012; Fritzsche et al., 2017). Interestingly, after the maturation of the immune synapse, transgelin-2 predominantly localizes to the d-SMAC and increases the duration of the immune synapse formation by maintaining F-actin contents and activating lymphocyte function-associated antigen (LFA)-1 after T-cell receptor stimulation (Na et al., 2015). *Tagln2*$^{-/-}$ T cells display attenuated cytokine production and cytotoxic effector function to kill antigen-bearing target cells (Na et al., 2015). In addition to its direct interaction with F-actin, transgelin-2 is physically connected with LFA-1, a β2-integrin expressed in lymphocytes, by which transgelin-2 regulates LFA-1 avidity. This achieves via activation of Rap1, a key regulator of LFA-1-dependent adhesion and migration of T cells, therefore increasing T-cell adhesion to cognate target cells (Na et al., 2015; Jeon et al., 2018). Interestingly, transgelin-2 also contributes to boosting APC functions for T-cell expansion (Na et al., 2016). Although *Tagln2*$^{-/-}$ B cells show normal development and activation, they are defective in supporting T-cell activation in terms of cytokine expression and proliferation (Na et al., 2016). In B cells, the activity of transgelin-2 is correlated with increased B-to-T-cell conjugation, suggesting that transgelin-2 in B cells enhances the adhesion of B cells to cognate T cells. These results strongly suggest that transgelin-2 is an essential actin regulator that facilitates the proper function of both T and B cells.

Although transgelin-2 is constitutively expressed in B cells, it is upregulated in B-2 cells by mitogenic stimuli such as IgM or bacterial endotoxin LPS (Francés et al., 2006), suggesting that transgelin-2 expression is regulated under inflammatory conditions. Accordingly, a clinical report demonstrated that transgelin-2 is upregulated in B cells in the lymph nodes and kidneys of patients with systemic lupus erythematosus (Kiso et al., 2017), a prototypical autoimmune disease associated with polyclonal B-cell hyper reactivity (Mok and Lau, 2003; Dörner et al., 2011). The presence of an NF-κB consensus motif at the 5′-promoter region of the *Tagln2* gene further corroborates that inflammatory signals control transgelin-2 expression. In this context, the action of transgelin-2 may be more important in professional APCs, such as macrophages and DCs (Kim et al., 2017), than in T cells. Because phagocytosis requires dramatic actin rearrangement at the phagocytic synapse, cells that professionally phagocytose pathogens or cell debris may have a demand for proteins such as transgelin-2 (Na et al., 2016; Kim et al., 2017) and fascin (Yoshihiko et al., 2011; Van Audenhove et al., 2015). Indeed, transgelin-2 knockout in macrophages remarkably reduces the phagocytic activity of IgM- and IgG-coated sheep red blood cells and bacteria (Kim et al., 2017). Furthermore, *Tagln2*$^{-/-}$ mice show higher mortality after bacterial infection than their wild-type littermates, revealing that transgelin-2 is essentially required for host defense. Bacterial infection is a leading cause of sepsis, which raises morbidity and mortality (Cohen, 2002). Thus, optimized control of phagocytosis is one of the most critical initial steps that can block the early dissemination of pathogenic bacteria (Andrews and Sullivan, 2003). Thus, the development of cell-permeable peptides with transgelin-2 functions have potential clinical value to treat sepsis induced by bacterial infection. Verified functions of transgelin-2 in immune cells are summarized in **Table 1**.

Transgelin-2 (*Tagln2*$^{-/-}$)-knockout in T cells or macrophages reduces the motility of these cells (Na et al., 2015; Kim et al., 2017). The function of transgelin-2 is presumably due to its biochemical properties to induce small filopodia-like membrane protrusions at the leading edge of migrating cells and to increase dynamic actin-rich membrane ruffles in phagocytic cells (Kim et al., 2017, Kim H.-R. et al., 2018). Moreover, both *Tagln2*$^{-/-}$ T cells and macrophages showed a remarkable decrease in F-actin content (Na et al., 2015; Kim et al., 2017, Kim H.-R. et al., 2018), indicating that although transgelin-2 is not directly involved in spontaneous actin polymerization *in vitro*, it is indirectly involved in actin polymerization *in vivo* (Na et al., 2015). The increased F-actin content can be caused by inhibiting the decomposition of polymerized F-actin, rather than increasing actin polymerization directly by transgelin-2

TABLE 1 | Known and putative functions of transgelin-2 in immune and cancer cells.

System	Cell types	Expression	Functions or results	References
Immune system	Helper T cells	Constitutive	Immunological synapse; T-cell activation	Na et al., 2015
	Cytotoxic T cells	Constitutive	Adhesion to target cells; Increased tumor cell killing	Na and Jun, 2015; Jeon et al., 2018
	B cells	Constitutive/Inducible*	Immunological synapse; T-cell activation	Francés et al., 2006; Na et al., 2015, 2016
	Macrophages	Inducible*	Increased phagocytic function; Reduced mortality against bacterial infection	Kim et al., 2017
Cancer	Colorectal cancer	Upregulated**	Tumorigenesis	Ali et al., 2010; Zhang et al., 2010; Yoshino et al., 2011
	Cervical cancer	Upregulated	Tumorigenesis	Yakabe et al., 2016
	Lung cancer	Upregulated	Tumorigenesis	Moriya et al., 2012
	Gastric cancer	Upregulated	Tumorigenesis	Xu et al., 2014
	Hepatic cancer	Upregulated	Tumorigenesis	Huang et al., 2006
	Renal cancer	Upregulated	Tumorigenesis	Kawakami et al., 2012
	Pancreatic cancer	Upregulated	Tumorigenesis	Lin et al., 2013
	Bladder cancer	Upregulated	Tumorigenesis	Yoshino et al., 2011
	Prostate cancer	Upregulated	Tumorigenesis	Jie et al., 2009
	Esophageal cancer	Upregulated	Tumorigenesis	Du et al., 2016
	Oral cancer	Upregulated	Tumorigenesis	Kawahara et al., 2016
	Head and neck SCC	Upregulated	Tumorigenesis	Nohata et al., 2011a,b
	Meningiomas	Upregulated	Tumorigenesis	Sharma et al., 2015
	Lymphoma and leukemia	Upregulated	Tumorigenesis	Gez et al., 2007
	Breast cancer	Upregulated	Paclitaxel resistant MCF-7/PTX cells	Zheng et al., 2015
	Choriocarcinoma	Upregulated	Methotrexate-resistant JAR/MTX cells	Chen et al., 2004
	Breast cancer	Downregulated	Highly metastatic MDA-MB-231HM cells	Xu et al., 2010
	Cervical cancer	Downregulated	Metastatic tissues	Yoshida et al., 2013
	Endometrial cancer	Downregulated	Metastatic tissues	Yoshida et al., 2013
	Hepatic cancer	Phosphorylation	Tumorigenesis	Leung et al., 2011

**Induced by LPS via NF-κB pathway.*
***Upregulated by TGF-β-Smad4-dependent pathway.*

(Na and Jun, 2015; Na et al., 2015; Kim H.-R. et al., 2018). Interestingly, some leukemia and lymphoid tumor cells, such as MEC1 (B-cell chronic lymphocytic leukemia) and Raji (B-cell Burkitt's lymphoma), express high levels of transgelin-2 (Gez et al., 2007). Unlike metastatic spread of other cancers, because lymphoma dissemination generally conserved physiological behavior reflecting basic rules of lymphocyte homing, it will be worth investigating whether lymphomas with high transgelin-2 has increased tissue-specific dissemination.

DCs also undergo remarkable cytoskeletal rearrangement during antigen presentation to their cognate T cells via immune synapse formation (Dustin, 2008b, 2014; Fisher et al., 2008). Following antigen capture, DCs mature and present antigens to the surface of T cells, triggering T-cell expansion. This step generates large T-cell pools, which aid in antibody generation from B cells, traffic to sites of infection to release cytokines, or directly kill infected or neoplastic cells. In this regard, the action of transgelin-2 in DCs may critically affect immune responses. In contrast to inflammatory conditions, because the tumor microenvironment provides an immunosuppressive condition, the expression of transgelin-2 in DCs in a tumor area or tumor draining lymph nodes may be reduced. Therefore, although careful approach is certainly needed, the application of cell-permeable transgelin-2 peptide in DCs obtained from cancer patients may be an alternative method to boost DC function to enhance T cells and humoral immunity.

Transgelin-2 Is an Oncogenic Factor in Cancer Cells

Previously, transgelin (transgelin-1 or SM22α) was considered to act as a tumor suppressor (Assinder et al., 2009). Because its expression is lost in breast, colon, and prostate cancers (Shields et al., 2002; Wulfkuhle et al., 2002; Yang et al., 2007), it was suggested that the loss of transgelin accounts in part for the development of cancer (Assinder et al., 2009). Interestingly, the downregulation of transgelin-1 disrupted the normal actin organization that leads to changes in the motile behavior of REF52 fibroblasts (Thompson et al., 2012). Additionally, transgelin-1 depletion led to the spontaneous formation of podosomes in cells with a concomitant increase in invasive cellular activity (Thompson et al., 2012).

In contrast to the transgelin-1, in many studies, transgelin-2 expression was proposed as a potential cancer biomarker (Zhang et al., 2010; Dvorakova et al., 2014; Meng et al., 2017; Yin et al., 2019). Transcriptional and translational upregulation of transgelin-2 has been described for many cancers, including colorectal, gastric, pancreatic, esophageal, prostate, lung, hepatic,

renal, bladder, and oral cancers (Yang et al., 2007; Huang et al., 2008; Rho et al., 2009; Zhang et al., 2010; Leung et al., 2011; Yoshino et al., 2011; Kawakami et al., 2012; Lin et al., 2013; Kawahara et al., 2016), in addition to meningiomas, head and neck squamous cell carcinoma (SCC), lymphoma, and leukemia (Gez et al., 2007; Nohata et al., 2011b; Sharma et al., 2015). Together, these data suggest that the upregulation of transgelin-2 is associated with tumorigenesis and cancer development. Transgelin-2 upregulation in tumor tissue is correlated with clinical stage, tumor size, and neural invasion (Jin et al., 2016). Putative roles of transgelin-2 in various cancers are summarized in **Table 1**.

Several studies have demonstrated that transgelin-2 expression in cancer cells is also associated with increased drug resistance (Yoshida et al., 2013; Cai et al., 2014b; Zheng et al., 2015). Multidrug resistance is one of the primary causes for failure in cancer therapy, but the mechanism is not yet clearly verified. Therefore, transgelin-2 is also a primary therapeutic target for which inhibition may restore the sensitivity of drug-resistant cancers (Nohata et al., 2011a,b; Kawakami et al., 2012; Moriya et al., 2012; Yoshida et al., 2013; Cai et al., 2014a,b; Xiao et al., 2014; Du et al., 2016). However, the precise mechanisms for the involvement of transgelin-2 in cancer development largely remain to be elucidated.

Upregulation of transgelin-2 expression is associated with metastasis and invasion of various cancer cells, including lung, bladder, colorectal, esophageal, and gastric cancers (Huang et al., 2008; Zhang et al., 2010; Chen et al., 2015; Du et al., 2016; Jin et al., 2016). However, a few reports demonstrated that transgelin-2 instead inhibits the motility of cancer cells, such as hepatocarcinoma cells, by suppressing actin polymerization (Leung et al., 2011; Yoshida et al., 2013; Yang et al., 2019). Indeed, transgelin-2 is downregulated in metastatic tumors compared with primary cancers (Yoshida et al., 2013), suggesting that transgelin-2 is a suppressor of metastasis. Consistently, the downregulation of transgelin-2 promoted the metastasis of breast cancer cells by activating reactive oxygen species and the NF-κB signaling pathway (Yang et al., 2019). Although more research should be done, these contradictory results suggest that different cancer cells may express distinct molecules that can be connected to trangelin-2, which is a possible reason for apparently opposed roles for the protein in the particular context of each tumor. For instance, it will be important to consider the levels of other actin-binding or -regulatory proteins, such as cofilin, plastin family of actin-bundling proteins, and ERM (ezrin/radixin/moesin) proteins (Wang et al., 2007; Shinomiya, 2012; Stevenson et al., 2012; Clucas and Valderrama, 2014). In fact, many cancer cells express distinct proteins related with actin cytoskeletons (Olson and Sahai, 2009). From a similar point of view, several reports demonstrated that, in contrast to the known action as a tumor suppressor, transgelin-1 promotes motility in normal cells, and stable overexpression of transgelin-1 leads to increased invasiveness and lung metastasis in a mouse model (Wu et al., 2014; Zhou et al., 2016).

The expression of transgelin-2 in cancer cells is different from that of immune cells, in which NF-κB pathway is dominant (Kim et al., 2017). Instead, its expression is regulated by transforming growth factor (TGF)-β in A549 cancer cells and by epidermal growth factor receptor/KRAS-ERK signaling pathways in pancreatic ductal adenocarcinoma (PDAC) (Keshamouni et al., 2006; Yu et al., 2008; Dhiraj and Lowenfels, 2013; Sun et al., 2018). Because transgelin-2 is necessary for both immune cells and cancer cells to exert their optimal functions, the different expression mechanisms of transgelin-2 in immune cells and cancer cells suggest that these cells express transgelin-2 as a strategy for their survival, migration, and invasion. However, it also suggests that this small actin-binding protein may be a molecular target for cancer treatment by boosting the immune response via overexpression of transgelin-2 and suppressing tumor growth or metastasis through its inhibition.

Although it has not yet been importantly recognized, transgelin-2 is expressed not only in the cytoplasm but also in the nucleus (Na et al., 2015). However, little is known about the function of transgelin-2 in the nucleus. The emerging roles of actin and actin-binding proteins in the nucleus have become a new frontier in cell biology (Percipalle and Vartiainen, 2019). Actin-based functions may contribute to genome stability and integrity through the interactions of actin cytoskeletons with various nuclear components (Visa and Percipalle, 2010; Weston et al., 2012; Falahzadeh et al., 2015). Thus, an exciting future challenge is to understand whether this transgelin-2-mediated actin regulation in the nucleus controls cancer development and metastasis. One example is investigating how the transgelin-2-actin network regulates nuclear architecture for the expression and silencing of genes required for cancer cell growth.

Transgelin-2, a Double-Edged Sword: Application for Cancer Treatment

Transgelin-2 is an essential actin-binding protein for both immune function and cancer cell malignancy (Jo et al., 2018; Yin et al., 2019). In immune cells, transgelin-2 stabilizes actin structure and also is physically associated with LFA-1. This interaction enhances the inside-out signaling of LFA-1, thereby improving the adhesion of T cells and stabilizing the immune synapse (Na et al., 2015). Overexpression of transgelin-2 in cytotoxic $CD8^+$ T cells increases adhesion to ICAM-1-positive E0771 breast cancer cells, but not ICAM-1-negative B16/F10 melanoma cells, suggesting the therapeutic potential of transgelin-2 in T-cell immunotherapy (Jeon et al., 2018).

A recent study reported a new function of transgelin-2 in the pathogenesis of asthma, revealing transgelin-2 as a therapeutic target for asthmatic pulmonary resistance (Yin et al., 2018). Transgelin-2 is involved in the relaxation of the myosin cytoskeleton of the airway smooth muscle cells (ASMCs). Authors demonstrated that transgelin-2 can trigger an intracellular signaling pathway leading to the dephosphorylation of myosin light chain and relaxation of the myosin cytoskeleton (Yin et al., 2018). Interestingly, TSG12, a specific agonist of trasngelin-2, could reduce pulmonary resistance in asthma (Yin et al., 2018). Their works are particularly interesting because the TSG12 can be applied to the activation of transgelin-2 function in immune cells, as it may also control the adhesion of T cells to the target cancer cells, thereby potentiating antitumor activity.

However, since the signaling pathways triggered by transgelin-2 in T cells are likely to be different from ASMCs (Na et al., 2015; Yin et al., 2018), further careful approach will be needed.

Because the expression of transgelin-2 is significantly upregulated in macrophages (Kim et al., 2017), we speculate that transgelin-2 function may be more important for professional APC-based cancer immunotherapy. Although the upregulation of transgelin-2 in cytotoxic T cells potentiates their cytotoxic activity, it does not increase the number of T-cell pools that selectively recognize cancer antigens. However, the potentiation of APC function can trigger the clonal expansion of T cells. Therefore, it will be interesting to develop strategies to increase the expression of transgelin-2 in professional APCs. In our previous work, we found that, in macrophages, transgelin-2 is only minimally expressed by stimulation with interferon (IFN)-γ, but it is dramatically induced by LPS (Kim et al., 2017). Although LPS is a potent adjuvant, it is too toxic to be safely applied in human vaccines. However, an exogenously transduced transgelin-2 peptide may enhance APC functions to increase cognate T-cell adhesion, followed by T-cell activation and clonal expansion. It will be interesting to test whether previously developed protein transduction domain (PTD)-tagged transgelin-2 protein (TG2P), which is easier and faster to transduce into primary cells (Jeon et al., 2018), may potentiate cancer immunotherapy based on DCs. It also will be of interest to investigate whether any substances can selectively induce transgelin-2 similarly to LPS-treated macrophages. Taken together, current results strongly suggest that transgelin-2 is an interesting and promising target molecule by which immunity can be upregulated in response to infectious and neoplastic diseases.

Because transgelin-2 expression contributes to cancer development, resistance, and metastasis (Yin et al., 2019), transgelin-2 is a potential target protein for anticancer therapy. Along this line, there are reports that salvianolic acid A (SAA), a natural compound extracted from *Salvia miltiorrhiza*, reverses the paclitaxel resistance and migration and invasion abilities of MCF-7 breast cancer cells by inactivating transgelin-2 (Cai et al., 2014b; Zheng et al., 2015). Additionally, transgelin-2 (*Tagln2*) is a direct molecular target of the potential tumor suppressor microRNAs miR-1 and miR-133a/b (Nohata et al., 2011a,b; Yoshino et al., 2011; Kawakami et al., 2012; Moriya et al., 2012; Du et al., 2016). Although it is still unclear, phosphorylation of transgelin-2 is also related to the cellular motility and oncogenic transformation of cells (Leung et al., 2011; Sun et al., 2018). Transgelin-2 has potential phosphorylation sites at Serine (S)11, S83, S94, S145, S155, S163, and S185 (Leung et al., 2011). It has been shown that KRAS mutation in pancreatic ductal adenocarcinoma (PDAC) induces transgelin-2 expression via ERK activation (Sun et al., 2018). Interestingly, ERK2 interacts with transgelin-2 and subsequently phosphorylates the S145 residue of transgelin-2, which plays important roles in cell proliferation and tumorigenesis of PDAC (Sun et al., 2018). Transgelin-2 is also known to be phosphorylated at S83 and S163 residues via PFTK1, a cdc2-related serine/threonine protein kinase that has been shown to confer cell migratory properties in hepatocellular carcinoma (HCC) (Leung et al., 2011). Interestingly, phosphorylation at S83 and S163 by PFTK1 inhibits physical interaction of transgelin-2 to actin, which results in enhanced HCC cell motility (Leung et al., 2011). Thus, inhibition of transgelin-2 phosphorylation could be a potentially effective strategy for cancer treatment. Although more aggressive studies are needed, if transgelin-2 in the nucleus controls cancer cell growth, exogenous treatment of cancer cells with cell-permeable transgelin-2, instead of reducing its expression by miRNAs, may help treat some cancers.

CONCLUDING REMARKS

Although transgelin-2 is constitutively expressed in lymphocytes (Na et al., 2015), its expression is significantly upregulated under inflammatory conditions such as bacterial infection (Na et al., 2016; Kim et al., 2017). This upregulation suggests that the activity of transgelin-2 in immune cells is essential during host defense against infectious agents or neoplastic disease. However, because tumor microenvironments are typically immunosuppressive due to the dominant populations of malignant cells, stroma, and regulatory T cells, immunologically suppressed effector cells in the tumor microenvironment may express low levels of transgelin-2. Thus, an exogenous supplement of cell-permeable transgelin-2 in immune effector cells such as cytotoxic T cells and DCs may enhance their anticancer activities. Interestingly, however, transgelin-2 is also crucial for the induction of malignancy, metastasis, and invasion of cancer cells (Meng et al., 2017). In contrast to transgelin-2 expression in immune cells, its expression in cancer cells is upregulated by hypoxia (Kim I.G. et al., 2018) or TGF-β (Yu et al., 2008), i.e., conditions that suppress immune activity. Thus, to some extent, shifting the tumor microenvironment from immunosuppressive to inflammatory may provide a therapeutic advantage for transgelin-2-associated cancer treatment (Qu et al., 2018). Compared with transgelin-1, however, because transgelin-2 is dominantly restricted to cancer cells (Dvorakova et al., 2014), the strategy that selectively targets transgelin-2, instead of targeting the cytoskeleton itself, may diminish the potentially toxic side effects of cytoskeletal-directed cancer therapeutics (Trendowski, 2014). In the future, new strategies or methods that selectively control the expression or suppression of transgelin-2 in immune cells and cancer cells may help treat transgelin-2-associated cancers.

AUTHOR CONTRIBUTIONS

H-RK and J-SP wrote and created the figures. HK and FY supported the data. C-DJ wrote and finalized the review. All authors contributed to the article and approved the submitted version.

FUNDING

This work was supported by the Creative Research Initiative Program (2015R1A3A2066253) and the Bio and Medical Technology Development Program (2020M3A9G3080281)

through National Research Foundation (NRF) grants funded by the Ministry of Science and ICT (MSIT), the Basic Science Program (2019R1C1C1009570) through National Research Foundation (NRF) grants funded by the Ministry of Education, the National R&D Program for Cancer Control, Ministry for Health and Welfare (1911264), and supported by GIST Research Institute (GRI) IBBR grant funded by the GIST in 2020, South Korea.

REFERENCES

Ali, N. A., McKay, M. J., and Molloy, M. P. (2010). Proteomics of Smad4 regulated transforming growth factor-beta signalling in colon cancer cells. *Mol. Biosyst.* 6, 2332–2338. doi: 10.1039/c0mb00016g

Andrews, T., and Sullivan, K. E. (2003). Infections in patients with inherited defects in phagocytic function. *Clin. Microbiol. Rev.* 16, 597–621. doi: 10.1128/CMR.16.4.597-621.2003

Assinder, S. J., Stanton, J.-A. L. A., and Prasad, P. D. (2009). Transgelin: an actin-binding protein and tumour suppressor. *Int. J. Biochem. Cell Biol.* 41, 482–486. doi: 10.1016/j.biocel.2008.02.011

Cai, J., Chen, S., Zhang, W., Hu, S., Lu, J., Xing, J., et al. (2014a). Paeonol reverses paclitaxel resistance in human breast cancer cells by regulating the expression of transgelin 2. *Phytomedicine* 21, 984–991. doi: 10.1016/j.phymed.2014.02.012

Cai, J., Chen, S., Zhang, W., Zheng, X., Hu, S., Pang, C., et al. (2014b). Salvianolic acid a reverses paclitaxel resistance in human breast cancer MCF-7 cells via targeting the expression of transgelin 2 and attenuating PI3 K/Akt pathway. *Phytomedicine* 21, 1725–1732. doi: 10.1016/j.phymed.2014.08.007

Camoretti-Mercado, B., Forsythe, S. M., LeBeau, M. M., Espinosa, R., Vieira, J. E., Halayko, A. J., et al. (1998). Expression and cytogenetic localization of the human SM22 gene (TAGLN). *Genomics* 49, 452–457. doi: 10.1006/geno.1998.5267

Castresana, J., and Saraste, M. (1995). Does Vav bind to F-actin through a CH domain? *FEBS Lett.* 374, 149–151. doi: 10.1016/0014-5793(95)01098-Y

Chaussepied, P., and Kasprzak, A. A. (1989). Change in the actin-myosin subfragment 1 interaction during actin polymerization. *J. Biol. Chem.* 264, 20752–20759.

Chen, C. L., Chung, T., Wu, C. C., Ng, K. F., Yu, J. S., Tsai, C. H., et al. (2015). Comparative tissue proteomics of microdissected specimens reveals novel candidate biomarkers of bladder cancer. *Mol. Cell. Proteom.* 14, 2466–2478. doi: 10.1074/mcp.M115.051524

Chen, Y., Xie, X., and Cheng, Q. (2004). cDNA microarray analysis of gene expression in acquired methotrexate-resistant of human choriocarcinoma. *Zhonghua Fu Chan Ke Za Zhi* 39, 396–399.

Clucas, J., and Valderrama, F. (2014). ERM proteins in cancer progression. *J. Cell Sci.* 127, 267–275. doi: 10.1242/jcs.170027

Cohen, J. (2002). The immunopathogenesis of sepsis. *Nature* 420, 885–891. doi: 10.1038/nature01326

Depaz, I. M., and Wilce, P. A. (2006). The novel cytoskeleton-associated protein neuronal protein 22: elevated expression in the developing rat brain. *Brain Res.* 1081, 59–64. doi: 10.1016/j.brainres.2006.01.126

Dhiraj, Y., and Lowenfels, A. B. (2013). The epidemiology of pancreatitis and pancreatic Cancer. *Gastroenterology* 144, 1252–1261.

Dörner, T., Jacobi, A. M., Lee, J., and Lipsky, P. E. (2011). Abnormalities of B cell subsets in patients with systemic lupus erythematosus. *J. Immunol. Methods* 363, 187–197. doi: 10.1016/j.jim.2010.06.009

Du, Y. Y., Zhao, L. M., Chen, L., Sang, M. X., Li, J., Ma, M., et al. (2016). The tumor-suppressive function of miR-1 by targeting LASP1 and TAGLN2 in esophageal squamous cell carcinoma. *J. Gastroenterol. Hepatol.* 31, 384–393. doi: 10.1111/jgh.13180

Dustin, M. L. (2008a). Hunter to gatherer and back: immunological synapses and kinapses as variations on the theme of amoeboid locomotion. *Annu. Rev. Cell Dev. Biol.* 24, 577–596. doi: 10.1146/annurev.cellbio.24.110707.175226

Dustin, M. L. (2008b). T-cell activation through immunological synapses and kinapses. *Immunol. Rev.* 221, 77–89. doi: 10.1111/j.1600-065X.2008.00589.x

Dustin, M. L. (2014). The immunological synapse. *Cancer Immunol. Res.* 2, 1023–1034. doi: 10.1158/2326-6066.CIR-14-0161

Dustin, M. L., and Cooper, J. A. (2000). The immunological synapse and the actin cytoskeleton: molecular hardware for T cell signaling. *Nat. Immunol.* 1, 23–29. doi: 10.1038/76877

Dvorakova, M., Nenutil, R., and Bouchal, P. (2014). Transgelins, cytoskeletal proteins implicated in different aspects of cancer development. *Expert Rev. Proteomics* 11, 149–165. doi: 10.1586/14789450.2014.860358

Egelman, E. H. (2000). A robust algorithm for the reconstruction of helical filaments using single-particle methods. *Ultramicroscopy* 85, 225–234. doi: 10.1016/S0304-3991(00)00062-60

Falahzadeh, K., Banaei-Esfahani, A., and Shahhoseini, M. (2015). The potential roles of actin in the nucleus. *Cell J.* 17, 7–14. doi: 10.22074/cellj.2015.507

Fisher, P. J., Bulur, P. A., Vuk-Pavlovic, S., Prendergast, F. G., Dietz, A. B., Doc, S. V. C., et al. (2008). Dendritic cell microvilli — a novel membrane structure associated with the multifocal synapse and T cell clustering. *Blood* 112, 5037–5046. doi: 10.1182/blood-2008-04-149526

Francés, R., Tumang, J. R., Kaku, H., Gurdak, S. M., and Rothstein, T. L. (2006). B-1 cells express transgelin 2: unexpected lymphocyte expression of a smooth muscle protein identified by proteomic analysis of peritoneal B-1 cells. *Mol. Immunol.* 43, 2124–2129. doi: 10.1016/j.molimm.2005.12.011

Fritzsche, M., Fernandes, R. A., Chang, V. T., Colin-York, H., Clausen, M. P., Felce, J. H., et al. (2017). Cytoskeletal actin dynamics shape a ramifying actin network underpinning immunological synapse formation. *Sci. Adv.* 3, e1603032. doi: 10.1126/sciadv.1603032

Fu, Y., Liu, H. W., Forsythe, S. M., Kogut, P., McConville, J. F., Halayko, A. J., et al. (2000). Mutagenesis analysis of human SM22: characterization of actin binding. *J. Appl. Physiol.* 89, 1985–1990. doi: 10.1152/jappl.2000.89.5.1985

Galkin, V. E., Orlova, A., VanLoock, M. S., Zhou, D., Galán, J. E., and Egelman, E. H. (2002). The bacterial protein SipA polymerizes G-actin and mimics muscle nebulin. *Nat. Struct. Biol.* 9, 518–521. doi: 10.1038/nsb811

Ge, P., Durer, Z. A. O., Kudryashov, D., Zhou, Z. H., and Reisler, E. (2014). Cryo-EM reveals different coronin binding modes for ADP- and ADP-BeFx actin filaments. *Nat. Struct. Mol. Biol.* 21, 1075–1081. doi: 10.1038/nsmb.2907

Gez, S., Crossett, B., and Christopherson, R. I. (2007). Differentially expressed cytosolic proteins in human leukemia and lymphoma cell lines correlate with lineages and functions. *Biochim. Biophys. Acta - Proteins Proteomics* 1774, 1173–1183. doi: 10.1016/j.bbapap.2007.06.011

Gimona, M., Djinovic-Carugo, K., Kranewitter, W. J., and Winder, S. J. (2002). Functional plasticity of CH domains. *FEBS Lett.* 513, 98–106. doi: 10.1016/S0014-5793(01)03240-3249

Gimona, M., Kaverina, I., Resch, G. P., Vignal, E., and Burgstaller, G. (2003). Calponin repeats regulate actin filament stability and formation of podosomes in smooth muscle cells. *Mol. Biol. Cell* 14, 2482–2491. doi: 10.1091/mbc.E02

Gimona, M., and Mital, R. (1998). The single CH domain of calponin is neither sufficient nor necessary for F-actin binding. *J. Cell Sci.* 111, 1813–1821.

Glenney, J. R., Kaulfus, P., and Weber, K. (1981). F-actin binding and bundling properties of fimbrin, a major cytoskeletal protein of microvillus core filaments. *J Biol Chem* 256, 9283–9288.

Gordón-Alonso, M., Sala-Valdés, M., Rocha-Perugini, V., Pérez-Hernández, D., López-Martín, S., Ursa, A., et al. (2012). EWI-2 association with α-Actinin regulates T cell immune synapses and HIV viral infection. *J. Immunol.* 189, 689–700. doi: 10.4049/jimmunol.1103708

Higashide, W., Dai, S., Hombs, V. P., and Zhou, D. (2002). Involvement of SipA in modulating actin dynamics during *Salmonella* invasion into cultured epithelial cells. *Cell. Microbiol.* 4, 357–365. doi: 10.1046/j.1462-5822.2002.00196.x

Huang, J., Sheng, H. H., Shen, T., Hu, Y. J., Xiao, H. S., Zhang, Q., et al. (2006). Correlation between genomic DNA copy number alterations and transcriptional expression in hepatitis B virus-associated hepatocellular carcinoma. *FEBS Lett.* 580, 3571–3581. doi: 10.1016/j.febslet.2006.05.032

Huang, Q., Huang, Q., Chen, W., Wang, L., Lin, W., Lin, J., et al. (2008). Identification of transgelin as a potential novel biomarker for gastric adenocarcinoma based on proteomics technology. *J. Cancer Res. Clin. Oncol.* 134, 1219–1227. doi: 10.1007/s00432-008-0398-y

Jeon, B.-N., Kim, H.-R., Chung, Y. S., Na, B.-R., Park, H., Hong, C., et al. (2018). Actin stabilizer TAGLN2 potentiates adoptive T cell therapy by boosting

the inside-out costimulation via lymphocyte function-associated antigen-1. *Oncoimmunology* 7:e1500674. doi: 10.1080/2162402X.2018.1500674

Jie, C., Watanabe, M., Huang, P., Sakguch, M., Ochia, K., Nasu, Y., et al. (2009). REIC/Dkk-3 stable transfection reduces the malignant phenotype of mouse prostate cancer RM9 cells. *Int. J. Mol. Med.* 24, 789–794. doi: 10.3892/ijmm

Jin, H., Cheng, X., Pei, Y., Fu, J., Lyu, Z., Peng, H., et al. (2016). Identification and verification of transgelin-2 as a potential biomarker of tumor-derived lung-cancer endothelial cells by comparative proteomics. *J. Proteomics* 136, 77–88. doi: 10.1016/j.jprot.2015.12.012

Jo, S., Kim, H. R., Mun, Y. V., and Jun, C. D. (2018). Transgelin-2 in immunity: its implication in cell therapy. *J. Leukoc. Biol.* 104, 903–910. doi: 10.1002/JLB.MR1117-470R

Kawahara, R., Bollinger, J. G., Rivera, C., Ribeiro, A. C. P., Brandão, T. B., Leme, A. F. P., et al. (2016). A targeted proteomic strategy for the measurement of oral cancer candidate biomarkers in human saliva. *Proteomics* 16, 159–173. doi: 10.1002/pmic.201500224

Kawakami, K., Enokida, H., Chiyomaru, T., Tatarano, S., Yoshino, H., Kagara, I., et al. (2012). The functional significance of miR-1 and miR-133a in renal cell carcinoma. *Eur. J. Cancer* 48, 827–836. doi: 10.1016/j.ejca.2011.06.030

Keshamouni, V. G., Michailidis, G., Grasso, C. S., Anthwal, S., Strahler, J. R., Walker, A., et al. (2006). Differential protein expression profiling by iTRAQ-2DLC-MS/MS of lung cancer cells undergoing epithelial-mesenchymal transition reveals a migratory/invasive phenotype. *J. Proteome Res.* 5, 1143–1154. doi: 10.1021/pr050455t

Kim, H.-R., Kwon, M.-S., Lee, S., Mun, Y., Lee, K.-S., Kim, C.-H., et al. (2018). TAGLN2 polymerizes G-actin in a low-ionic state but blocks Arp2/3-nucleated actin branching in a physiologic condition. *Sci. Rep.* 8, 5503–5518. doi: 10.1038/s41598-018-23816-23812

Kim, I. G., Lee, J. H., Kim, S. Y., Hwang, H. M., Kim, T. R., and Cho, E. W. (2018). Hypoxia-inducible transgelin 2 selects epithelial-to-mesenchymal transition and γ-radiation-resistant subtypes by focal adhesion kinase-associated insulin-like growth factor 1 receptor activation in non-small-cell lung cancer cells. *Cancer Sci.* 109, 3519–3531. doi: 10.1111/cas.13791

Kim, H.-R., Lee, H.-S., Lee, K.-S., Jung, I. D., Kwon, M.-S., Kim, C.-H., et al. (2017). An essential role for TAGLN2 in phagocytosis of lipopolysaccharide-activated macrophages. *Sci. Rep.* 7, 8731–8744. doi: 10.1038/s41598-017-09144-x

Kiso, K., Yoshifuji, H., Oku, T., Hikida, M., Kitagori, K., Hirayama, Y., et al. (2017). Transgelin-2 is upregulated on activated B-cells and expressed in hyperplastic follicles in lupus erythematosus patients. *PLoS One* 12:e0184738. doi: 10.1371/journal.pone.0184738

Kranewitter, W. J., Ylanne, J., and Gimona, M. (2001). UNC-87 Is an Actin-bundling Protein. *J. Biol. Chem.* 276, 6306–6312. doi: 10.1074/jbc.M009561200

Le Clainche, C., and Drubin, D. G. (2004). Actin lessons from pathogens. *Mol. Cell* 13, 453–454. doi: 10.1016/S1097-2765(04)00088-87

Leung, W. K. C., Ching, A. K. K., Chan, A. W. H., Poon, T. C. W., Mian, H., Wong, A. S. T., et al. (2011). A novel interplay between oncogenic PFTK1 protein kinase and tumor suppressor TAGLN2 in the control of liver cancer cell motility. *Oncogene* 30, 4464–4475. doi: 10.1038/onc.2011.161

Li, M., Li, S., Lou, Z., Liao, X., Zhao, X., Meng, Z., et al. (2008). Crystal structure of human transgelin. *J. Struct. Biol.* 162, 229–236. doi: 10.1016/j.jsb.2008.01.005

Lilic, M., Galkin, V. E., Orlova, A., VanLoock, M. S., Egelman, E. H., and Stebbins, C. E. (2003). *Salmonella* SipA polymerizes actin by stapling filaments with nonglobular protein arms. *Science* 301, 1918–1921. doi: 10.1126/science.1088433

Lin, H., Chen, Q. L., Wang, X. Y., Han, W., He, T. Y., Yan, D., et al. (2013). Clinical significance of pituitary tumor transforming gene 1 and transgelin-2 in pancreatic cancer. *Int. J. Immunopathol. Pharmacol.* 26, 147–156. doi: 10.1177/039463201302600114

Matsui, T. S., Ishikawa, A., and Deguchi, S. (2018). Transgelin-1 (SM22α) interacts with actin stress fibers and podosomes in smooth muscle cells without using its actin binding site. *Biochem. Biophys. Res. Commun.* 505, 879–884. doi: 10.1016/j.bbrc.2018.09.176

Maul, R. S., Song, Y., Amann, K. J., Gerbin, S. C., Pollard, T. D., and Chang, D. D. (2003). EPLIN regulates actin dynamics by cross-linking and stabilizing filaments. *J. Cell Biol.* 160, 399–407. doi: 10.1083/jcb.200212057

McCullough, B. R., Grintsevich, E. E., Chen, C. K., Kang, H., Hutchison, A. L., Henn, A., et al. (2011). Cofilin-linked changes in actin filament flexibility promote severing. *Biophys. J.* 101, 151–159. doi: 10.1016/j.bpj.2011.05.049

McGhie, E. J., Hayward, R. D., and Koronakis, V. (2001). Cooperation between actin-binding proteins of invasive *Salmonella*: SipA potentiates SipC nucleation and bundling of actin. *EMBO J.* 20, 2131–2139. doi: 10.1093/emboj/20.9.2131

Meng, T., Liu, L., Hao, R., Chen, S., and Dong, Y. (2017). Transgelin-2: a potential oncogenic factor. *Tumor Biol.* 39:101042831770265. doi: 10.1177/1010428317702650

Mok, C. C., and Lau, C. S. (2003). Pathogenesis of systemic lupus erythematosus. *J. Clin. Pathol.* 56, 481–490. doi: 10.1136/jcp.56.7.481

Morgan, K. G., and Gangopadhyay, S. S. (2001). Cross-bridge regulation by thin filament-associated proteins. *J. Appl. Physiol.* 91, 953–961. doi: 10.1152/jappl.2001.91.3.1438

Mori, K., Muto, Y., Kokuzawa, J., Yoshioka, T., Yoshimura, S., Iwama, T., et al. (2004). Neuronal protein NP25 interacts with F-actin. *Neurosci. Res.* 48, 439–446. doi: 10.1016/j.neures.2003.12.012

Moriya, Y., Nohata, N., Kinoshita, T., Mutallip, M., Okamoto, T., Yoshida, S., et al. (2012). Tumor suppressive microRNA-133a regulates novel molecular networks in lung squamous cell carcinoma. *J. Hum. Genet.* 57, 38–45. doi: 10.1038/jhg.2011.126

Na, B. R., and Jun, C. D. (2015). TAGLN2-mediated actin stabilization at the immunological synapse: implication for cytotoxic T cell control of target cells. *BMB Rep.* 48, 369–370. doi: 10.5483/BMBRep.2015.48.7.132

Na, B.-R., Kim, H.-R., Piragyte, I., Oh, H.-M., Kwon, M.-S., Akber, U., et al. (2015). TAGLN2 regulates T cell activation by stabilizing the actin cytoskeleton at the immunological synapse. *J. Cell Biol.* 209, 143–162. doi: 10.1083/jcb.201407130

Na, B.-R., Kwon, M.-S., Chae, M.-W., Kim, H.-R., Kim, C.-H., Jun, C.-D., et al. (2016). Transgelin-2 in B cells controls T-cell activation by stabilizing T cell - B cell conjugates. *PLoS One* 11:e0156429. doi: 10.1371/journal.pone.0156429

Nohata, N., Hanazawa, T., Kikkawa, N., Sakurai, D., Sasaki, K., Chiyomaru, T., et al. (2011a). Identification of novel molecular targets regulated by tumor suppressive miR-1/miR-133a in maxillary sinus squamous cell carcinoma. *Int. J. Oncol.* 39, 1099–1107. doi: 10.3892/ijo.2011.1096

Nohata, N., Sone, Y., Hanazawa, T., Fuse, M., Kikkawa, N., Yoshino, H., et al. (2011b). miR-1 as a tumor suppressive microRNA targeting TAGLN2 in head and neck squamous cell carcinoma. *Oncotarget* 2, 29–42. doi: 10.18632/oncotarget.213

Olson, M. F., and Sahai, E. (2009). The actin cytoskeleton in cancer cell motility. *Clin. Exp. Metastasis* 26, 273–287. doi: 10.1007/s10585-008-9174-9172

Pearlstone, J. R., Weber, M., Lees-Miller, J. P., Carpenter, M. R., and Smillie, L. B. (1987). Amino acid sequence of chicken gizzard smooth muscle SM22 alpha. *J. Biol. Chem.* 262, 5985–5991.

Percipalle, P., and Vartiainen, M. (2019). Cytoskeletal proteins in the cell nucleus: a special nuclear actin perspective. *Mol. Biol. Cell* 30, 1781–1785. doi: 10.1091/mbc.E18-10-0645

Piragyte, I., and Jun, C.-D. (2012). Actin engine in immunological synapse. *Immune Netw.* 12, 71–83. doi: 10.4110/in.2012.12.3.71

Qu, X., Tang, Y., and Hua, S. (2018). Immunological approaches towards cancer and inflammation: a cross talk. *Front. Immunol.* 9:563. doi: 10.3389/fimmu.2018.00563

Rho, J. H., Roehrl, M. H. A., and Wang, J. Y. (2009). Tissue proteomics reveals differential and compartment-specific expression of the homologs transgelin and transgelin-2 in lung adenocarcinoma and its stroma. *J. Proteome Res.* 8, 5610–5618. doi: 10.1021/pr900705r

Ritter, A. T., Angus, K. L., and Griffiths, G. M. (2013). The role of the cytoskeleton at the immunological synapse. *Immunol. Rev.* 256, 107–117. doi: 10.1111/imr.12117

Shapland, C., Hsuan, J. J., Totty, N. F., and Lawson, D. (1993). Purification and properties of transgelin: a transformation and shape change sensitive actin-gelling protein. *J. Cell Biol.* 121, 1065–1073. doi: 10.1083/jcb.121.5.1065

Sharma, S., Ray, S., Mukherjee, S., Moiyadi, A., Sridhar, E., and Srivastava, S. (2015). Multipronged quantitative proteomic analyses indicate modulation of various signal transduction pathways in human meningiomas. *Proteomics* 15, 394–407. doi: 10.1002/pmic.201400328

Shields, J. M., Rogers-Graham, K., and Der, C. J. (2002). Loss of transgelin in breast and colon tumors and in RIE-1 cells by Ras deregulation of gene expression through Raf-independent pathways. *J. Biol. Chem.* 277, 9790–9799. doi: 10.1074/jbc.M110086200

Shih, C. (1993). Nebulin as an actin zipper: a two-module nebulin fragment promotes actin nucleation and stabilizes actin filaments. *J. Biol. Chem.* 268, 20327–20334.

Shinomiya, H. (2012). Plastin family of actin-bundling proteins: its functions in leukocytes, neurons, intestines, and cancer. *Int. J. Cell Biol.* 2012:213492. doi: 10.1155/2012/213492

Sol, A., Blotnick, E., Bachrach, G., and Muhlrad, A. (2012). LL-37 induces polymerization and bundling of actin and affects actin structure. *PLoS One* 7:e50078. doi: 10.1371/journal.pone.0050078

Stevenson, R. P., Veltman, D., and Machesky, L. M. (2012). Actin-bundling proteins in cancer progression at a glance. *J. Cell Sci.* 125, 1073–1079. doi: 10.1242/jcs.093799

Stokes, D. L., and DeRosier, D. J. (1991). Growth conditions control the size and order of actin bundles in vitro. *Biophys. J.* 59, 456–465. doi: 10.1016/S0006-3495(91)82239-82231

Sun, Y., Peng, W., He, W., Luo, M., Chang, G., Shen, J., et al. (2018). Transgelin-2 is a novel target of KRAS-ERK signaling involved in the development of pancreatic cancer. *J. Exp. Clin. Cancer Res.* 37:166. doi: 10.1186/s13046-018-0818-z

Thompson, O., Moghraby, J. S., Ayscough, K. R., and Winder, S. J. (2012). Depletion of the actin bundling protein SM22/transgelin increases actin dynamics and enhances the tumourigenic phenotypes of cells. *BMC Cell Biol.* 13:1. doi: 10.1186/1471-2121-13-11

Trendowski, M. (2014). Exploiting the cytoskeletal filaments of neoplastic cells to potentiate a novel therapeutic approach. *Biochim. Biophys. Acta - Rev. Cancer* 1846, 599–616. doi: 10.1016/j.bbcan.2014.09.007

Valentin-Ranc, C., Combeau, C., Carlier, M. F., and Pantaloni, D. (1991). Myosin subfragment-1 interacts with two G-actin molecules in the absence of ATP. *J. Biol. Chem.* 266, 17872–17879.

Van Audenhove, I., Debeuf, N., Boucherie, C., and Gettemans, J. (2015). Fascin actin bundling controls podosome turnover and disassembly while cortactin is involved in podosome assembly by its SH3 domain in THP-1 macrophages and dendritic cells. *Biochim. Biophys. Acta - Mol. Cell Res.* 1853, 940–952. doi: 10.1016/j.bbamcr.2015.01.003

Van der Flier, A., and Sonnenberg, A. (2001). Structural and functional aspects of filamins. *Biochim. Biophys. Acta - Mol. Cell Res.* 1538, 99–117. doi: 10.1016/S0167-4889(01)00072-76

Visa, N., and Percipalle, P. (2010). Nuclear functions of actin. *Cold Spring Harb. Perspect. Biol.* 2:a000620. doi: 10.1101/cshperspect.a000620

Wan, M., van der Does, A. M., Tang, X., Lindbom, L., Agerberth, B., and Haeggstrom, J. Z. (2014). Antimicrobial peptide LL-37 promotes bacterial phagocytosis by human macrophages. *J. Leukoc. Biol.* 95, 971–981. doi: 10.1189/jlb.0513304

Wang, W., Eddy, R., and Condeelis, J. (2007). The cofilin pathway in breast cancer invasion and metastasis. *Nat. Rev. Cancer* 7, 429–440. doi: 10.1038/nrc2148

Wen, K.-K., Rubenstein, P. A., and DeMali, K. A. (2009). Vinculin nucleates actin polymerization and modifies actin filament structure. *J. Biol. Chem.* 284, 30463–30473. doi: 10.1074/jbc.M109.021295

Weston, L., Coutts, A. S., and La Thangue, N. B. (2012). Actin nucleators in the nucleus: an emerging theme. *J. Cell Sci.* 125, 3519–3527. doi: 10.1242/jcs.099523

Wu, X., Dong, L., Zhang, R., Ying, K., and Shen, H. (2014). Transgelin overexpression in lung adenocarcinoma is associated with tumor progression. *Int. J. Mol. Med.* 34, 585–591. doi: 10.3892/ijmm.2014.1805

Wulfkuhle, J. D., Sgroi, D. C., Krutzsch, H., McLean, K., McGarvey, K., Knowlton, M., et al. (2002). Proteomics of human breast ductal carcinoma in Situ. *Cancer Res.* 62, 6740–6749.

Xiao, G., Xia, C., Yang, J., Liu, J., Du, H., Kang, X., et al. (2014). MiR-133b regulates the expression of the actin protein TAGLN2 during oocyte growth and maturation: a potential target for infertility therapy. *PLoS One* 9:e100751. doi: 10.1371/journal.pone.0100751

Xu, S. G., Yan, P. J., and Shao, Z. M. (2010). Differential proteomic analysis of a highly metastatic variant of human breast cancer cells using two-dimensional differential gel electrophoresis. *J. Cancer Res. Clin. Oncol.* 136, 1545–1556. doi: 10.1007/s00432-010-0812-810

Xu, X. C., Zhang, Y. H., Zhang, W. B., Li, T., Gao, H., and Wang, Y. H. (2014). MicroRNA-133a functions as a tumor suppressor in gastric cancer. *J. Biol. Regul. Homeost. Agents* 28, 615–624.

Yakabe, K., Murakami, A., Kajimura, T., Nishimoto, Y., Sueoka, K., Sato, S., et al. (2016). Functional significance of transgelin-2 in uterine cervical squamous cell carcinoma. *J. Obstet. Gynaecol. Res.* 42, 566–572. doi: 10.1111/jog.12935

Yang, L., Hong, Q., Xu, S. G., Kuang, X. Y., Du, G. H., Luu, G. Y., et al. (2019). Downregulation of transgelin 2 promotes breast cancer metastasis by activating the reactive oxygen species/nuclear factor-κB signaling pathway. *Mol. Med. Rep.* 20, 4045–4058. doi: 10.3892/mmr.2019.10643

Yang, Z., Chang, Y. J., Miyamoto, H., Ni, J., Niu, Y., Chen, Z., et al. (2007). Transgelin functions as a suppressor via inhibition of ARA54-enhanced androgen receptor transactivation and prostate cancer cell growth. *Mol. Endocrinol.* 21, 343–358. doi: 10.1210/me.2006-2104

Yin, L. M., Ulloa, L., and Yang, Y. Q. (2019). Transgelin-2: biochemical and clinical implications in Cancer and Asthma. *Trends Biochem. Sci.* 44, 885–896. doi: 10.1016/j.tibs.2019.05.004

Yin, L. M., Xu, Y. D., Peng, L. L., Duan, T. T., Liu, J. Y., Xu, Z., et al. (2018). Transgelin-2 as a therapeutic target for asthmatic pulmonary resistance. *Sci. Transl. Med.* 10:eaam8604. doi: 10.1126/scitranslmed.aam8604

Yoshida, A., Okamoto, N., Tozawa-Ono, A., Koizumi, H., Kiguchi, K., Ishizuka, B., et al. (2013). Proteomic analysis of differential protein expression by brain metastases of gynecological malignancies. *Hum. Cell* 26, 56–66. doi: 10.1007/s13577-012-0053-54

Yoshihiko, Y., Matsumura, F., Lipscomb, M. W., Chou, P., Werlen, G., Burkhardt, J. K., et al. (2011). Fascin1 promotes cell migration of mature dendritic cells. *J. Immunol.* 186, 2850–2859.

Yoshino, H., Chiyomaru, T., Enokida, H., Kawakami, K., Tatarano, S., Nishiyama, K., et al. (2011). The tumour-suppressive function of miR-1 and miR-133a targeting TAGLN2 in bladder cancer. *Br. J. Cancer* 104, 808–818. doi: 10.1038/bjc.2011.23

Yu, H., Königshoff, M., Jayachandran, A., Handley, D., Seeger, W., Kaminski, N., et al. (2008). Transgelin is a direct target of TGF-β/Smad3-dependent epithelial cell migration in lung fibrosis. *FASEB J.* 22, 1778–1789. doi: 10.1096/fj.07-083857

Zhang, Y., Ye, Y., Shen, D., Jiang, K., Zhang, H., Sun, W., et al. (2010). Identification of transgelin-2 as a biomarker of colorectal cancer by laser capture microdissection and quantitative proteome analysis. *Cancer Sci.* 101, 523–529. doi: 10.1111/j.1349-7006.2009.01424.x

Zheng, X., Chen, S., Yang, Q., Cai, J., Zhang, W., You, H., et al. (2015). Salvianolic acid a reverses the paclitaxel resistance and inhibits the migration and invasion abilities of human breast cancer cells by inactivating transgelin 2. *Cancer Biol. Ther.* 16, 1407–1414. doi: 10.1080/15384047.2015.1070990

Zhou, D. (1999). Role of the *S. typhimurium* actin-binding protein siPA in bacterial internalization. *Science* 283, 2092–2095. doi: 10.1126/science.283.5410.2092

Zhou, H. M., Fang, Y. Y., Weinberger, P. M., Ding, L. L., Cowell, J. K., Hudson, F. Z., et al. (2016). Transgelin increases metastatic potential of colorectal cancer cells in vivo and alters expression of genes involved in cell motility. *BMC Cancer* 16:55. doi: 10.1186/s12885-016-2105-2108

Conflict of Interest: The authors declare that the research was conducted in the absence of any commercial or financial relationships that could be construed as a potential conflict of interest.

frontiers in Cell and Developmental Biology

BRIEF RESEARCH REPORT
published: 09 April 2021
doi: 10.3389/fcell.2021.648925

Multi-Factor Clustering Incorporating Cell Motility Predicts T Cell Expansion Potential

*Joanne H. Lee[1], Shuai Shao[1], Michelle Kim[1], Stacey M. Fernandes[2], Jennifer R. Brown[2] and Lance C. Kam[1]**

[1] Department of Biomedical Engineering, Columbia University, New York, NY, United States, [2] Department of Medical Oncology, Harvard Medical School, Dana-Farber Cancer Institute, Boston, MA, United States

Expansion of an initial population of T cells is essential for cellular immunotherapy. In Chronic Lymphocytic Leukemia (CLL), expansion is often complicated by lack of T cell proliferation, as these cells frequently show signs of exhaustion. This report seeks to identify specific biomarkers or measures of cell function that capture the proliferative potential of a starting population of cells. Mixed CD4+/CD8+ T cells from healthy donors and individuals previously treated for CLL were characterized on the basis of proliferative potential and *in vitro* cellular functions. Single-factor analysis found little correlation between the number of populations doublings reached during expansion and either Rai stage (a clinical measure of CLL spread) or PD-1 expression. However, inclusion of *in vitro* IL-2 secretion and the propensity of cells to align onto micropatterned features of activating proteins as factors identified three distinct groups of donors. Notably, these group assignments provided an elegant separation of donors with regards to proliferative potential. Furthermore, these groups exhibited different motility characteristics, suggesting a mechanism that underlies changes in proliferative potential. This study describes a new set of functional readouts that augment surface marker panels to better predict expansion outcomes and clinical prognosis.

Keywords: T cell, Leukemia, machine learning, immunotherapy, cell migration

OPEN ACCESS

Edited by:
Sudha Kumari, Massachusetts Institute of Technology, United States

Reviewed by:
Siddharth Jhunjhunwala, Indian Institute of Science (IISc), India
Enrico Klotzsch, Humboldt University of Berlin, Germany

****Correspondence:***
Lance C. Kam
lance.kam@columbia.edu; lk2141@columbia.edu

Specialty section:
This article was submitted to Cell Growth and Division, a section of the journal Frontiers in Cell and Developmental Biology

Received: *02 January 2021*
Accepted: *18 March 2021*
Published: *09 April 2021*

Citation:
Lee JH, Shao S, Kim M, Fernandes SM, Brown JR and Kam LC (2021) Multi-Factor Clustering Incorporating Cell Motility Predicts T Cell Expansion Potential. Front. Cell Dev. Biol. 9:648925. doi: 10.3389/fcell.2021.648925

INTRODUCTION

T cells have emerged as a compelling agent in the treatment of diseases ranging from cancer to autoimmunity. However, clinical use of T cells as a therapy relies on the production of cells of sufficient quantity and quality from a small starting population; the inability of an individual's cells to carry out this expansion would make a cellular approach inappropriate for both therapy and participation in clinical trials (Frey, 2015). This poses a particular challenge as disease state often dampens immune function and response including expansion. As a key example, T cells from individuals with Chronic Lymphocytic Leukemia (CLL) show defects in expansion and subsequent function (Wherry, 2011; Tonino et al., 2012; Riches et al., 2013; Palma et al., 2017; McLane et al., 2019), which resembles exhaustion and is associated with lower remission of CLL than Acute Lymphoblastic Leukemia through autologous CAR-T cell therapy (Maude et al., 2014; Porter et al., 2015). CLL is also associated with higher levels of key exhaustion markers such as PD-1, TIM-3, LAG-3, CTLA-4, TIGIT, and CD160 (Wherry, 2011; Long et al., 2015; McClanahan et al., 2015;

Wherry and Kurachi, 2015), as well as deficits in cell function such as migration and formation of immune synapse structures (Ramsay et al., 2008, 2012, 2013). However, a clear understanding of how biomarkers are associated with cellular function, disease progression, and potential treatment remains elusive. Using a machine learning approach, this report seeks to develop a framework for combining molecular biomarkers, measures of cell function, and other inputs to characterize T cells from individuals with CLL, ultimately in an effort to improve production of cells for cellular immunotherapy.

MATERIALS AND METHODS

Cell Culture

Mixed $CD4^+/CD8^+$ populations of primary human T cells were isolated from peripheral blood lymphocyte fractions (Leukopaks, New York Blood Center) by negative selection (Rosette-Sep kit, Stem Cell Technology) and density centrifugation (Ficoll-Paque PLUS, GE). Mixed $CD4^+/CD8^+$ T cells from individuals who were previously treated for CLL were purified using identical selection techniques. Clinical biomarkers were collected over the course of treatment. In particular, Rai stage, a standardized measure of CLL spread, was determined during patient care from blood tests (cell counts) and physical exams (tissue enlargement). For all experiments, cells were cultured in RPMI 1640 supplemented with 10% fetal bovine serum, 10 mM HEPES, 2 mM L-glutamine, 50 U/mL penicillin, 50 μg/mL streptomycin, and 50 μM β-mercaptoethanol (Sigma or Life Technologies, unless otherwise noted). T cell populations were analyzed for PD-1 expression by flow cytometry using α-PD-1 (PE-Cy7, clone EH12.2H7, Biolegend).

Design and Fabrication of Microscopy Chambers

Conical-well, open-bottom wells were used to improve the efficiency of microscopy-based cell function analysis. Individual wells had a cylindrical well geometry of 5 mm in internal diameter and 4.5 mm depth, but with a 45° conical bottom ending with a 1-mm diameter opening at the bottom of the structure. Multiple wells in a 2 × 4 rectangular array were arranged into chambers following the layout and center-to-center distance of standard 96-well plates. Chambers were fabricated out of polypropylene by injection molding (Protolabs). For use in microscopy, chambers were affixed onto test surfaces using transfer tape (3 M) that was laser cut to provide correct overall dimensions and provide holes for the 1-mm openings.

Surface Micropatterning

Micropatterned surfaces were created by microcontact printing (20, 21). Briefly, glass coverslips were patterned with 2-μm diameter circular features of activating proteins, spaced in square arrays at a center-to-center distance of 15 μm. Microcontact printing was carried out by coating topographically defined, polydimethylsiloxane stamps with a mixture of α-CD3 (clone OKT3, Bio X Cell) and α-CD28 (clone 9.3, Bio X Cell) antibodies. The strength of TCR/CD3 activating signal was modulated by changing the amount of α-CD3 in the stamping solutions, which contained α-CD28 at 15 μg/ml, α-CD3 at a specified concentration (5, 3, 1.5, or 1 μg/ml), and an inert antibody (chicken α-goat IgG, Life Technologies) for a total concentration to 20 μg/ml. The strength of α-CD3 signal was expressed as percent of antibody solution associated with OKT3 (e.g., 15 μg/ml α-CD28 + 3 μg/ml α-CD3 + 2 μg/ml α-gt was denoted as 15% OKT3). A microscopy chamber was then adhered onto the coverslips, aligning the wells with the patterned regions. Finally, open areas of the coverslip were coated with 2 μg/ml of ICAM-1 (ICAM-1/Fc chimera protein, R&D Systems).

Expansion

Assays of cell expansion were carried out as previously described (O'Connor et al., 2012; Dang et al., 2018). Briefly, mixed $CD4^+/CD8^+$ populations of 1×10^6 T cells were stimulated with Human T-Activator CD3/CD28 Dynabeads (ThermoFisher) at a bead to cell ratio of 3:1 on day 0 of an expansion process. On day 3 and every second day after that, the number of T cells was counted, and additional media added to reduce cell concentration to 5×10^5 cells/ml. Proliferative capacity was quantified as the maximum number of doublings achieved over the expansion, after which cell number decreased; the expansion process was terminated at that point.

Microscopy-Based Assays of Cell Function

Cell alignment, motility, and IL-2 secretion assays were carried out by seeding 1×10^4 T cells in a 50 μl volume into prepared microscopy chambers attached to micropatterned coverslips or other experimental surface. Cell culture was carried out under standard conditions (37°C, humidified environment, 5% CO_2 environment).

Cell alignment and IL-2 secretion were measured 6 h after seeding. IL-2 secretion was measured using a surface capture method (Shen et al., 2008; Bashour et al., 2014). Briefly, cells were incubated with a bi-reactive antibody, which binds to the T cell surface and presents a site for IL-2 capture. Secreted IL-2 is captured over the course of the 6 h incubation, and then detected using an APC-labeled α-IL2 antibody. Cells were fixed with 4% paraformaldehyde. Amplification of the IL-2 signal was provided by incubation with a tertiary, biotinylated α-APC antibody followed by streptavidin-AF647. Interference reflection microscopy provided an outline of each cell, which was used to determine the fraction of cells that had aligned with an activating pattern. Fluorescence imaging allowed cell-by-cell measurement of surface-captured IL-2, which was collected for cells aligned to the patterns.

Cell motion was recorded by live-cell microscopy in the first hour after seeding using a stage top incubator (Tokai). Images were collected at 30 s intervals over the 60 min observation period. Only T cells with fully formed lamellipodia were considered for motility analysis. Velocity was defined as average velocity before cells stopped on an activation feature. A stop was defined as a cessation of overall motion for longer

than 3 min, thus not including encounters where cells crossed a feature without halting. For a subset of experiments, T cells were stained with α-PD1 BB515 (clone EH12.1, Becton Dickinson) prior to seeding.

Statistics and Analysis

Analysis of donor cells was carried out in the R and MATLAB software environments. To identify the smallest set of factors that can account for the majority of variance in the donor data set (**Supplementary Table 1**), Factor Analysis of Mixed Data (FAMD) was carried out using the "FactoMineR" and "factoextra" libraries in R. Sex and IgVH were treated as categorical factors. Rai stage, represented by the integer associated with the analysis (0–4) was rank transformed and then treated as a numerical factor, noting that increasing Rai stage corresponds to greater CLL spread. Missing data was imputed by Multiple Imputation by Chained Equations (MICE) using the "mice" library in R. Numerical data was normalized (mean = 0, standard deviation = 1) prior to analysis by FAMD. Once variables to be included for clustering were identified, data was analyzed by k-medoids using the "cluster" library in R. Resampling analysis was carried out using the R "boot" library. MATLAB was used to reconcile cluster assignments between runs.

Quantitative comparisons between multiple conditions were carried out using two-tailed ANOVA methods. When validated by ANOVA ($\alpha = 0.05$), comparison of data between multiple conditions was carried out using Tukey's honest significance test methods. As specified in the figure captions, data were alternatively analyzed using Kruskal-Wallis test by ranks ($\alpha = 0.05$). These tests, including permutation analysis when specified, were carried out using the MATLAB software environment.

Study Approval

All experiments were performed in accordance with protocols approved by either the Dana-Farber Cancer Institute or Columbia University. Clinical information was provided from patient records from the Dana-Farber Cancer Institute. Informed consent was obtained for each patient on an ongoing research protocol approved by the Dana-Farber Cancer Institute Institutional Review Board (no. 99-224).

RESULTS

CLL T Cells Show Reduced Proliferative Capacity

As a measure of cell suitability for production, we compared *ex vivo* expansion of T cells from individuals being treated for CLL to those from healthy counterparts. Mixed $CD4^+/CD8^+$ populations of T cells were activated using Dynabeads (α-CD3 + α-CD28) then expanded in media supplemented with serum but without additional cytokines. Cells from healthy donors entered a phase of rapid growth, after which expansion decreased and cells came to rest (**Figure 1A**). Cells from CLL patients was often less robust, manifested as a shorter period of rapid growth and/or slower rate of doubling; three examples illustrating strong (similar to healthy donors), moderate, and minimal growth are shown in **Figure 1A**. Toward a systematic understanding of this variability, we examined a larger set of donors (**Supplementary Table 1**) seeking to identify parameters that can be associated with different degrees of expansion. This report uses the maximum number of doublings reached during growth, illustrated in each profile of **Figure 1A** by an open symbol, as an indicative measure of proliferative potential during expansion. We first examined Rai stage, a clinical designation based on disease progression (Apelgren et al., 2006). Cells from healthy donors exhibited 5.5 ± 0.4 (mean ± SD, $n = 5$) doublings. Cells from CLL patients showed a wider range, with no dependence on Rai stage ($P < 0.72$, permutation on Kruskal-Wallis test). We next considered the percentage of cells in the starting population expressing the checkpoint inhibitor PD-1 (Arasanz et al., 2017). An overall negative correlation was observed between maximum doublings and PD-1 expression (**Figure 1C**), but with a dip in doublings for intermediate values of PD-1 expression. Analysis of maximum doublings as a function of sex and IgVH mutation status showed no significant effect of the individual parameters ($P < 0.43$ and $P < 0.29$, respectively, two-tailed t-test). Recognizing that cellular functions are central to disease progression, we next turned to more complex measures of cell state.

Cell Sensitivity to Micropatterned, Activating Signals Is Dependent on PD-1 Expression

CLL impacts cellular-level functions of T cells, including motility, migration, and activation (Ramsay et al., 2013; Dupre et al., 2015). In this section, we seek to characterize such functions under well-defined conditions, potentially leading to a new quantifier that can be used to determine cell state. These assays typically require observation of live cells, and have been complicated by both the limited number of cells available from diagnostic samples and large, unobservable dead volumes associated with microscopy systems. To address the microscopy-associated limitation, we introduced the use of conical wells to collect cells into a small region of observation. The chambers are based on 96-well plates, with each well concentrating cells that would settle onto the 5-mm diameter bottom surface to a 1-mm diameter observation area (**Figure 2A**). By concentrating cells onto the observation area, the number of cells needed for an experiment was reduced by a factor of 20, facilitating experiments with smaller diagnostic samples and/or testing of more parameters from a single sample. Here, these chambers were used in conjunction with a second experimental system, protein-micropatterned surfaces for measuring response of living cells (**Figure 2A**). Microcontact printing (Mayya et al., 1950, 2018; Chen et al., 1997; Shen et al., 2008; Bashour et al., 2014; Kumari et al., 2015) was used to create arrays of 2-μm diameter, circular features containing antibodies to CD3 and CD28 which provide activation and costimulatory signals, respectively. The intervening regions were coated with ICAM-1. This approach was used previously (Shen et al., 2008) to investigate sensitivity

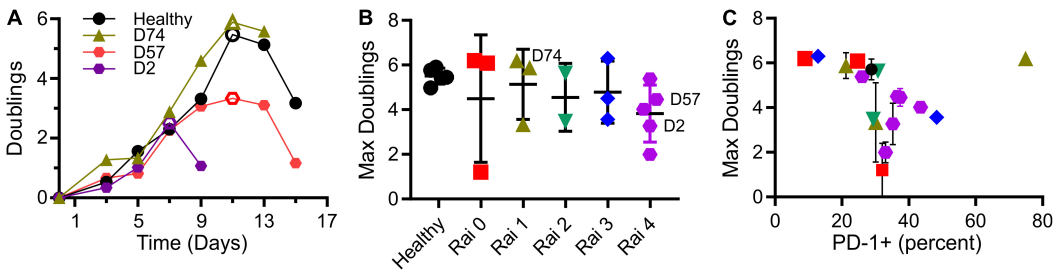

FIGURE 1 | T cells from CLL patients show deficits in expansion. **(A)** Timecourse of expansion for cells from three individuals, including a control condition of cells from a healthy donor, a CLL patient with cells showing moderate deficit in expansion (D57), and one with minimal proliferative potential (D2). The maximum number of doublings reached over an experiment (indicated by the open symbols) was used as a single, characteristic measure of expansion. **(B)** Maximum doublings for cells as a function of Rai stage (not including healthy donors) were compared by permutation analysis applied to Kruskal Wallis test, indicating no significant difference ($P < 0.72$; 1×10^6 permutation samples). Data are mean ± SD The donors included in **(A)** are indicated in this figure. **(C)** Maximum doublings as a function of percentage of cells that were PD-1+. Data are presented as means, and when included, error bars indicate standard deviations over technical replicates for that donor. The symbols in **(C)** correspond to Rai stage indicated in **(B)**.

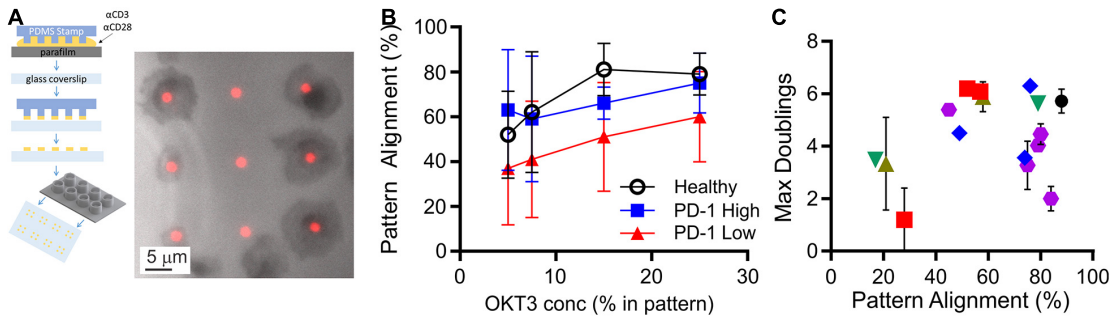

FIGURE 2 | Measurement of cell function from limited samples. **(A)** Microcontact printing was used to pattern isolated features containing activating antibodies to CD3 and CD28, allowing microscopy-based analysis of cell function. These micropatterned surfaces were attached under custom-made, open-bottomed conical chambers, which provide a 20-fold improvement in cell utilization. Cell-substrate contact areas were determined by interference reflection microscopy (gray), which allowed determination of alignment with activating features of α-CD3 + α-CD28 (red). **(B)** Alignment of T cells to the activating features was dependent on both the concentration of α-CD3 antibody (OKT3) and PD-1 expression. Data are mean ± SD from 3 to 14 donors for each condition. An OKT3 concentration of 15% was selected as a standard condition for subsequent experiments. **(C)** Maximum doublings as a function of Pattern Alignment. Data are means, and when included error bars indicate standard deviations over technical replicates for that donor. The symbols in **(C)** correspond to Rai stage as indicated in **Figure 1B**.

of T cells to localized CD3 activation, assayed by measuring the percentage of cells that stopped on and aligned with the features as a function of α-CD3 concentration. Repeating that approach here, primary human T cells from healthy donors aligned with micropatterned features of OKT3 (α-CD3) and 9.3 (α-CD28) as shown in **Figure 2A**. The amount of CD3 activating signal was controlled by specifying the concentration of OKT3 in the printing solution, as detailed in section "Materials and Methods." The percentage of cells that aligned with the patterns increased as OKT3 concentration increased. Cells from CLL donors similarly showed increasing alignment with higher concentrations of α-CD3, but also exhibited a dependency on PD-1 expression (**Figure 2B**). For this analysis, cells with PD-1 expression levels within the 95% confidence interval of healthy donors were designated as "PD-1 low," while those above this confidence interval were notated as "PD-1 high." At each OKT3 concentration, cells from the "low" group showed lower alignment with features than the corresponding cells from healthy donors. Surprisingly, this deficit in cell response was lost for cells from the "high" PD-1 group, illustrating the complex relationship between maximum doublings and PD-1 expression suggested in **Figure 1C**. Notably, these experiments were made practical by the improvement in cell utilization provided by the conical chamber system. Subsequent experiments, facing similar limitations in cell availability, were carried out at an OKT3 concentration of 15% (see section "Materials and Methods"), corresponding to the greatest difference between cells of the healthy and PD-1 low donors. Cell proliferative potential is plotted as a function of pattern alignment at this standardized concentration of 15% OKT3 in **Figure 2C**. While lower levels of alignment were associated with decreased proliferative potential, the number of doublings reached by cells exhibiting higher alignment varied across the range of observed values; the distribution of maximum doublings for alignment above 60% was not statistically different than those below this cutoff ($P < 0.61$, permutation of Kruskal-Wallis test, 1×10^6 random permutations). Finally, IL-2 secretion by cells adherent to these micropatterned surfaces was measured using a previously described surface capture method (Shen et al., 2008; Bashour et al., 2014). Like pattern alignment and other

biomarkers, no clear correlation between maximum doublings and IL-2 secretion alone was observed. Given these results, we next pursued a multi-factor approach toward characterizing cell proliferative potential.

Clustering Analysis Reveals Three Groups of Donors

In this section, an unsupervised clustering approach was used to identify patterns in biomarker expression within the populations of T cells isolated from CLL donors. Factors for this analysis included pattern alignment, IL-2 secretion, Rai stage, PD-1 expression, age at time of diagnosis, sex, and IgVH mutation status. Before clustering, Factor Analysis of Mixed Data (FAMD, **Figure 3A**) was used to identify which factors have the largest impact of explaining data variance. Dimensions 1 and 2 together comprised over 50% of data variability (37.3 and 19.4%, respectively, **Figure 3A**). As such, we examined the contributions of the seven input factors to combined Dim1 + Dim2. Pattern alignment, IL-2 secretion, and PD-1 expression each contributed over 14.3%, a cutoff representing equal contributions from all factors (**Figure 3B**), and were thus identified as the factors to be used in k-medoids clustering analysis. A cluster number of three was selected using the elbow method (**Supplementary Figure 1**), leading to group assignments shown in **Figure 3C**. Most strikingly, the groups stratify maximum doublings (**Figure 3D**): Group 2 is significantly lower than Group 1 ($P < 0.05$), while Group 3 is lower than both Healthy and Group 1 cells ($P < 0.05$ and $P < 0.005$, respectively). These assignments thus provide a single parameter that describes cell expansion potential without the complex relationships observed for individual factors (**Figures 1B,C**, **2C**). These group assignments also provided insight into the three factors that were used in clustering—PD-1, pattern alignment, and IL-2 secretion (**Figure 3E**). Intriguingly, clustering provided more distinct stratification of pattern alignment than max doublings (four comparisons that were significant at $\alpha = 0.05$, compared to three), but alignment showed a different order of response with Group 2 being higher than the others. A similarly altered order was observed for PD-1 expression. Finally, IL-2 secretion showed an ordering that was similar to max doublings, suggesting a connection between doublings and cytokine secretion, but fewer comparisons were significant at $\alpha = 0.05$.

It is noted that the clustering and data imputation algorithms used here incorporate randomization. Consequently, the stability

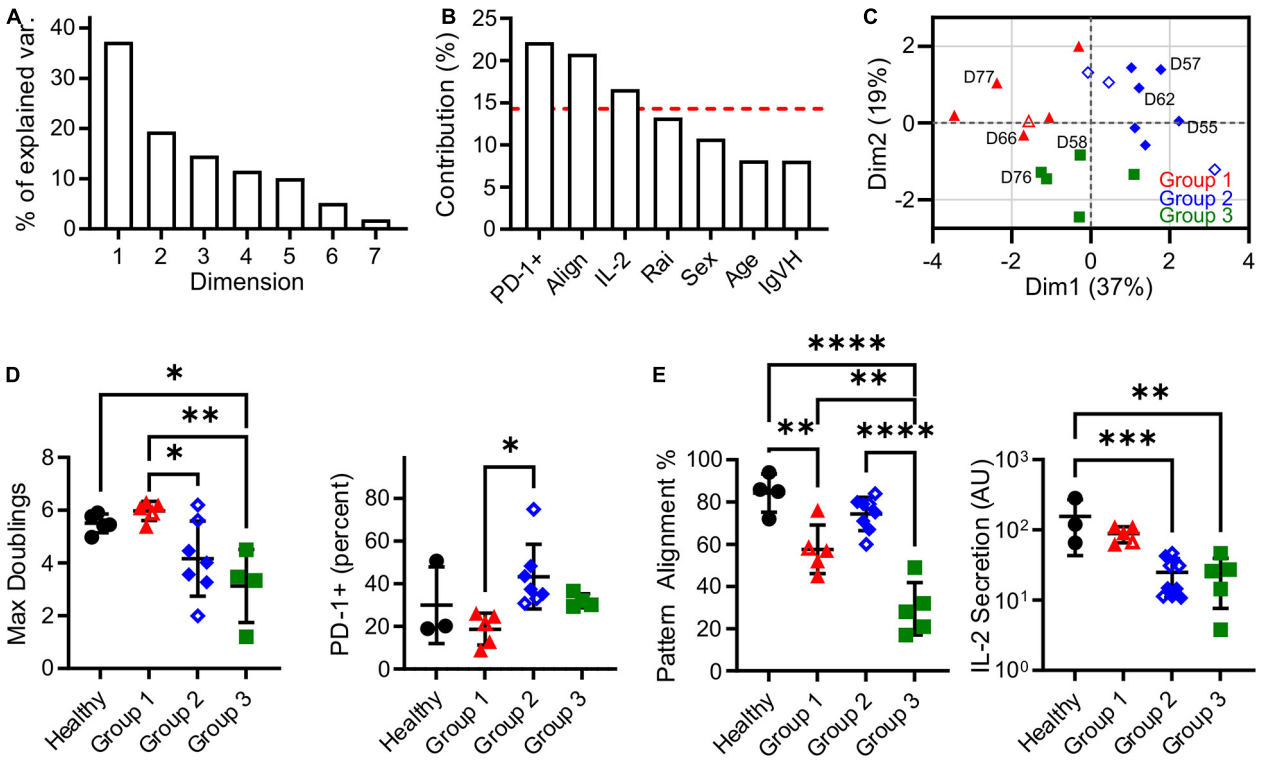

FIGURE 3 | Clustering analysis of cells from CLL patients revealed three Groups that describe proliferative potential. **(A)** Scree plot indicating the percentage of explained variance associated with each Dimension of a seven-factor FAMD analysis. Subsequent analysis focused on Dim1 + Dim2, which explains over 50% of variance. **(B)** Contribution of each factor to Dim1 + Dim2. The red line indicates 14.3%, a threshold representing equal contribution by each factor. **(C)** Analysis by k-medoids clustering using factors with contributions above the threshold indicated in **(B)** produced three Groups, which are coded in this FAMD plot showing Dim1 and Dim2. The labeled donors are examined in more detail in **Figure 4**. **(D)** Maximum doublings varied as a function of Group assignment. **(E)** PD-1, Alignment, and IL-2 secretion as a function of Group assignment. In all panels, data are mean ± SD $^{*}P < 0.05$, $^{**}P < 0.005$, $^{***}P < 0.0005$, $^{****}P < 0.0001$, using ANOVA and Tukey tests. All comparisons that were significant at $\alpha = 0.05$ are indicated in this figure. Open symbols represent conditions for which missing data was imputed.

of these analyses was tested through two types of resampling. The first is bootstrapping, in which 500 data sets were generated by random selection with replacement and then analyzed using the methods applied to the original data set. The frequency at which each donor was assigned to a given Group is listed in **Supplementary Table 2**, showing that the groups reported in our full data set (**Supplementary Table 1**) are stable; only one donor (D59) was assigned to a group different from the bootstrapped data. Data were then analyzed by subsampling, in which 500 data sets representing 90% of the original were generated by random sampling without replacement. As shown in **Supplementary Table 1**, these assignments followed the original analysis, indicating that those conclusions are not sensitive to the number of individual donors. Finally, bootstrapping was conducted on percentage of variance explained by Dim1 + Dim2 in the FAMD analysis. Analysis of 500 bootstrap sets determined a 95% confidence interval of 53.3–71.0%, placing it above the 50% criteria.

Cell Motility Varies Between Groups and PD-1 Expression

A notable result presented above is that pattern alignment is a major contributor to Dim1 + Dim2 (**Figure 3B**), and is also stratified by the cluster assignments (**Figure 3E**). To understand the cellular processes underlying pattern alignment, we examined the motion of cells following contact with a micropatterned surface (**Supplementary Movie 1**), collecting three complementary measures of cell motion from these trajectories. The first was motility speed, which reflects exploration of the ICAM-1-presenting surfaces. No significant variation in speed was observed across CLL and healthy donors (**Figure 4A**). The next two measures focused on cells as they encountered and came to a stop (defined as a halt in long-range movement for at least 3 min) on activating features of α-CD3 + α-CD28; these cells represent the ones that aligned with the pattern. The number of features a cell encountered before stopping provides insight into the sensitivity of cells to activation. Cells from Group 1 moved over more features than cells from Group 2, Group 3, and also healthy donors (**Figure 4B**) suggesting lower sensitivity to activation. As a complementary readout, the time from the beginning of the trajectory to stopping on an α-CD3 + α-CD28 feature was also measured. Cells in Group 3 showed the longest trajectory duration (**Figure 4C**). These results collectively suggest that proliferative potential is associated with different patterns of cell motility and sensitivity to activation. Specifically, longer periods of motion before coming to a stop are associated with lower maximum doublings, as illustrated for D76. However, this relationship is complex, since Group 1 showed lower sensitivity

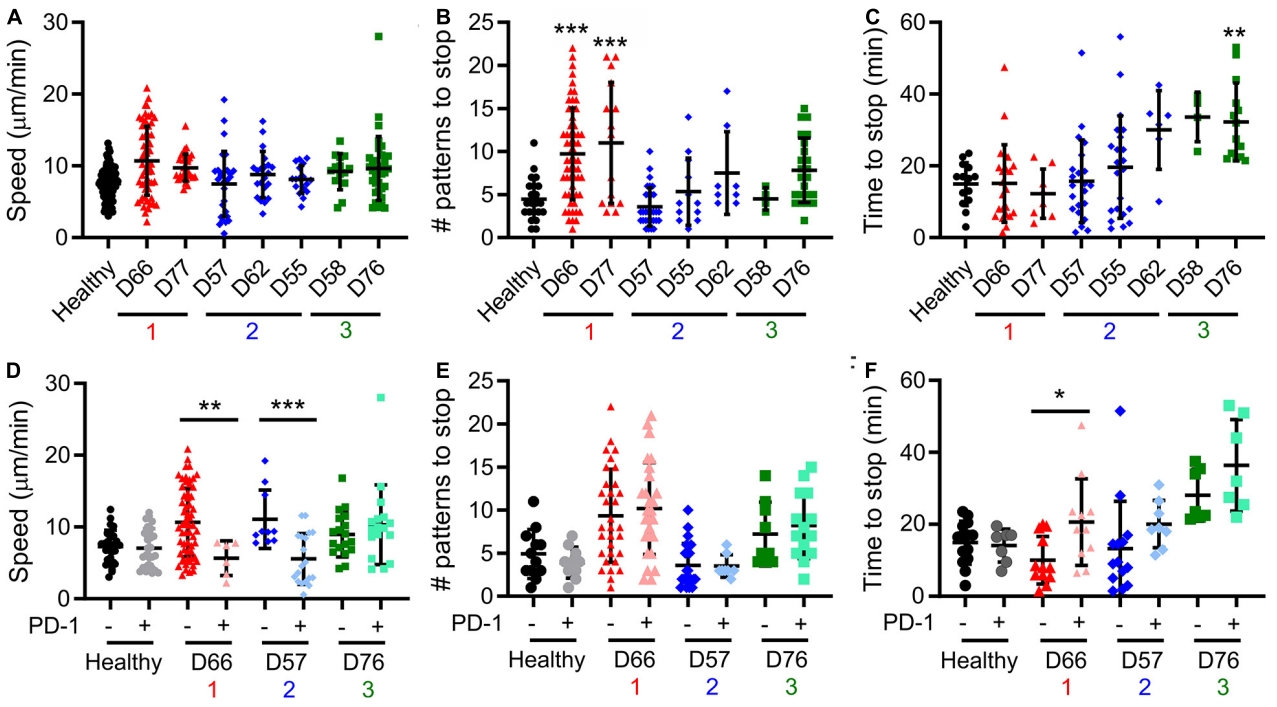

FIGURE 4 | Cell motility varies between Groups. **(A–C)** Live-cell microscopy over the first 60 min of cell-substrate interaction reveal different behaviors in motility. Cell centroid position was tracked and analyzed for average speed **(A)**, the number of patterns that a cell crossed before coming to a halt **(B)**, and time until such a halt **(C)**. Donors included in this analysis are labeled in the FAMD plots of **Figure 3**. **(D–F)** Prelabeling of cells with an α-PD-1 antibody allowed separate analysis of PD-1+ and PD-1− cells in the same experiment. In all panels, each symbol indicates an individual trajectory. The red, blue, and green numbers below the x axes indicate the Group assignments established in **Figure 3**. Data are mean ± SD of all cells tracked in 1–2 independent experiments. *$P < 0.05$, **$P < 0.005$, ***$P < 0.0005$ compared in **(A–C)** to healthy donors and in **(D–F)** between PD-1 positive and negative cells for that donor. Additional comparisons are detailed in the main text.

to activation with regards to the number of features crossed before stopping. Finally, cell motility was compared as a function of PD-1 expression by labeling cells for PD-1 prior to use in migration assays. Separating cells in this manner revealed that PD-1− cells from D66 (Group 1) moved faster than their PD-1 + counterparts (**Figure 4E**), and also cells from healthy donors, regardless of PD-1 expression ($P < 0.005$). The number of features experienced before stopping for cells from D66 was greater than for healthy donors, regardless of PD-1 expression ($P < 0.05$), in keeping with **Figure 4B**. These differences are further reflected in a longer time to stop for PD-1+ cells from D66 compared to their PD-1− counterparts (**Figure 4F**). A similar increase in migration speed for PD-1− cells vs. PD-1+ counterparts was observed for D57 (Group 2), but these differences were not significant compared to healthy donors. No effect of PD-1 expression on migration was observed for D76 (Group 3).

DISCUSSION

Cancer, like many afflictions, is multifaceted and diverse requiring specification of treatment course around the disease state and individual. This extends into surprising facets of the tools used for therapy. For example, we recently demonstrated that replacing the mechanically stiff plastic beads that are routinely used to activate T cells with a softer material can enhance subsequent expansion, providing more cells from an initial starting population and rescuing production of cells from individuals with CLL (Dang et al., 2018). Intriguingly, the stiffness of the material that produced optimal growth of cells varied between CLL donors. Through this study, we seek a framework for describing and understanding the differences in proliferative potential observed between CLL patients.

Initial attempts to use single factors such as Rai stage (as T cell expansion capabilities decrease with disease progression; Bonyhadi et al., 2005) and PD-1 expression (which is elevated in exhausted T cells; McLane et al., 2019) to capture variability in cell proliferation had modest success (**Figures 1B,C**). As such, we expanded the set of parameters to include measures of cell function, specifically cytokine secretion and the ability to align with micropatterned features on an activated surface. Individually, these measures provided limited new insight. We subsequently turned to multi-factor machine learning approaches, which have had success in classification of various tumor models (Gorris et al., 1950; Zucchetto et al., 2011; Chen and Mellman, 2017; Gonnord et al., 2019). Unsupervised clustering based on PD-1, alignment, and IL-2 provided a compelling approach for categorizing cells from CLL patients into three groups, which differed with respect to proliferative potential, an independent factor that was not included in the analysis but is important to cell production. Designing future studies around this clustering approach may provide a streamlined method for understanding cell exhaustion and developing tools for improving cell expansion.

Pattern alignment emerged as a key factor describing T cell response. In FAMD analysis, alignment contributed to Dim1 + Dim2 to an extent almost equal to PD-1 expression (**Figure 3B**). Moreover, of the six potential pairwise comparisons possible between Groups and Healthy donors, four of these were statistically significant for pattern alignment. By comparison, PD-1 and IL-2 secretion showed fewer significant comparisons, suggesting that alignment provides the greatest stratification between groups. However, pattern alignment is a complex process, involving adhesion to a micropatterned surface, motion across that surface, interaction with multiple activating features, and finally (in the window of our assay) cessation of motility. Most prominently, cells from Group 1 passed over more features before stopping than the other groups and healthy donors (**Figure 4B**). Compared to uniformly coated surfaces, these micropatterned features more accurately capture the physiological process of T cells encountering and even competing for a limited number of conjugate cells (Mayya et al., 1950, 2018). As described in the Results section, a simple interpretation of this is that passing over multiple patterns reflects the sensitivity of cells to activation, or the need to integrate multiple encounters before cessation of motion, which is associated with TCR-induced actin polymerization, through proteins such as Wiskott-Aldrich syndrome protein (WASP), overcoming polarization of cytoskeletal dynamics and tension (Kumari et al., 2020). However, another interpretation is that moving over multiple features can reflect persistence of cell motion, with a stop being more likely to happen at the same phase of motion as a change of direction. Maiuri et al. (2012) elegantly demonstrated that persistence and cell speed are correlated, developing a model in which actin flow maintains polarization (Maiuri et al., 2015). Correspondingly, the increase in features passed over by cells in Group 1 is associated with faster motion, but only for PD-1− cells (D66, **Figure 4D**). PD-1 expression, even in the absence of ligand on the underlying surface, reduced cell speed while not affecting the number of features passed over, suggesting a further complexity in how processes are balanced in cell migration. Intriguingly, Group 1 showed lower pattern alignment than healthy donors (potentially reflecting increased motion persistence) but strong proliferative potential. Perhaps counterintuitively, it is possible that modulating cell alignment by increasing migration speed could lead to improved cell activation and production for immunotherapy. A clearer understanding of how cytoskeletal polarization and dynamics interact is needed to more fully realize this potential.

DATA AVAILABILITY STATEMENT

The original contributions presented in the study are included in the article/**Supplementary Material**, further inquiries can be directed to the corresponding author/s.

ETHICS STATEMENT

The studies involving human participants were reviewed and approved by the Dana-Farber Cancer Institute Columbia

University. The patients/participants provided their written informed consent to participate in this study.

AUTHOR CONTRIBUTIONS

JL and LK designed the study. JL, SS, MK, and LK performed data collection and analysis. SF and JB provided expertise on CLL and management of donor samples. All authors contributed to the article and approved the submitted version.

FUNDING

This work was supported in part by the National Institutes of Health (U24AI118669 and R01AI110593 to LK, and Cancer Center Support Grant P30CA013696) and the National Science Foundation (CBET 1743420 to LK). JB has been supported by the National Cancer Institute (R01CA213442 and PO1CA206978), and the DFCI CLL Biorepository has been particularly supported by the Melton Family Fund for CLL Research, the Susan and Gary Rosenbach Fund for Lymphoma Research, and the Okonow Lipton Family Lymphoma Research Fund.

ACKNOWLEDGMENTS

We thank Michael Dustin (University of Oxford) for discussions surrounding the microscopy well system and Elham Azizi (Columbia University) for guidance on machine learning algorithms.

SUPPLEMENTARY MATERIAL

The Supplementary Material for this article can be found online at: https://www.frontiersin.org/articles/10.3389/fcell.2021.648925/full#supplementary-material

Supplementary Figure 1 | Determination of cluster number.

Supplementary Table 1 | Cells from healthy (H3–H9) and CLL (D2–D78) donors.

Supplementary Table 2 | Analysis of clustering stability.

Supplementary Movie 1 | Motility of T cells on micropatterned surfaces.

REFERENCES

Apelgren, P., Hasselblom, S., Werlenius, O., Nilsson-Ehle, H., Andersson, P.-O., and On Behalf, G. (2006). Of The Western Sweden Lymphoma, Evaluation of clinical staging in chronic lymphocytic leukemia- population-based study. *Leukemia Lymphoma* 47, 2505–2516. doi: 10.1080/10428190600881322

Arasanz, H., Gato-Cañas, M., Zuazo, M., Ibañez-Vea, M., Breckpot, K., Kochan, G., et al. (2017). PD1 signal transduction pathways in T cells. *Oncotarget* 8:51936. doi: 10.18632/oncotarget.17232

Bashour, K. T., Tsai, J., Shen, K., Lee, J.-H., Sun, E., Milone, M. C., et al. (2014). Cross Talk between CD3 and CD28 Is Spatially Modulated by Protein Lateral Mobility. *Mole. Cell. Biol.* 34, 955–964. doi: 10.1128/mcb.00842-13

Bonyhadi, M., Frohlich, M., Rasmussen, A., Ferrand, C., Grosmaire, L., Robinet, E., et al. (2005). In Vitro Engagement of CD3 and CD28 Corrects T Cell Defects in Chronic Lymphocytic Leukemia. *J. Immunol.* 174, 2366–2375. doi: 10.4049/jimmunol.174.4.2366

Chen, C. S., Mrksich, M., Huang, S., Whitesides, G. M., and Ingber, D. E. (1997). Geometric control of cell life and death. *Science* 276, 1425–1428. doi: 10.1126/science.276.5317.1425

Chen, D. S., and Mellman, I. (2017). Elements of cancer immunity and the cancer–immune set point. *Nature* 541, 321–330. doi: 10.1038/nature21349

Dang, A. P., De Leo, S., Bogdanowicz, D. R., Yuan, D. J., Fernandes, S. M., Brown, J. R., et al. (2018). Enhanced Activation and Expansion of T Cells Using Mechanically Soft Elastomer Fibers. *Adv. Biosyst.* 2018:1700167–n/a.

Dupre, L., Houmadi, R., Tang, C., and Rey-Barroso, J. (2015). T Lymphocyte Migration: An Action Movie Starring the Actin and Associated Actors. *Front. Immunol.* 6:586.

Frey, N. (2015). *Dose Optimization Trial of CD19 Redirected Autologous T Cells, ClinicalTrials.gov*. Bethesda, MD: National Library of Medicine.

Gonnord, P., Costa, M., Abreu, A., Peres, M., Ysebaert, L., Gadat, S., et al. (2019). Multiparametric analysis of CD8+ T cell compartment phenotype in chronic lymphocytic leukemia reveals a signature associated with progression toward therapy. *OncoImmunology* 8:e1570774. doi: 10.1080/2162402x.2019.1570774

Gorris, M. A. J., Halilovic, A., Rabold, K., van Duffelen, A., Wickramasinghe, I. N., Verweij, D., et al. (1950). Eight-Color Multiplex Immunohistochemistry for Simultaneous Detection of Multiple Immune Checkpoint Molecules within the Tumor Microenvironment. *J. Immunol.* 200, 347–354. doi: 10.4049/jimmunol.1701262

Kumari, S., Depoil, D., Martinelli, R., Judokusumo, E., Carmona, G., Gertler, F. B., et al. (2015). Actin foci facilitate activation of the phospholipase C-gamma in primary T lymphocytes via the WASP pathway. *Elife* 2015:4.

Kumari, S., Mak, M., Poh, Y. C., Tohme, M., Watson, N., Melo, M., et al. (2020). Cytoskeletal tension actively sustains the migratory T-cell synaptic contact. *EMBO J.* 39:e102783.

Long, A. H., Haso, W. M., Shern, J. F., Wanhainen, K. M., Murgai, M., Ingaramo, M., et al. (2015). 4-1BB costimulation ameliorates T cell exhaustion induced by tonic signaling of chimeric antigen receptors. *Nat. Med.* 21:581. doi: 10.1038/nm.3838

Maiuri, P., Rupprecht, J. F., Wieser, S., Ruprecht, V., Benichou, O., Carpi, N., et al. (2015). Actin flows mediate a universal coupling between cell speed and cell persistence. *Cell* 161, 374–386. doi: 10.1016/j.cell.2015.01.056

Maiuri, P., Terriac, E., Paul-Gilloteaux, P., Vignaud, T., McNally, K., Onuffer, J., et al. (2012). The first World Cell Race. *Curr. Biol.* 22, R673–R675.

Maude, S. L., Frey, N., Shaw, P. A., Aplenc, R., Barrett, D. M., Bunin, N. J., et al. (2014). Chimeric Antigen Receptor T Cells for Sustained Remissions in Leukemia. *N. Engl. J. Med.* 371, 1507–1517.

Mayya, V., Judokusumo, E., Abu Shah, E., Peel, C. G., Neiswanger, W., Depoil, D., et al. (2018). Durable Interactions of T Cells with T Cell Receptor Stimuli in the Absence of a Stable Immunological Synapse. *Cell Rep.* 22, 340–349. doi: 10.1016/j.celrep.2017.12.052

Mayya, V., Judokusumo, E., Abu-Shah, E., Neiswanger, W., Sachar, C., Depoil, D., et al. (1950). Cutting Edge: Synapse Propensity of Human Memory CD8 T Cells Confers Competitive Advantage over Naive Counterparts. *J. Immunol.* 203, 601–606. doi: 10.4049/jimmunol.1801687

McClanahan, F., Hanna, B., Miller, S., Clear, A. J., Lichter, P., Gribben, J. G., et al. (2015). PD-L1 checkpoint blockade prevents immune dysfunction and leukemia development in a mouse model of chronic lymphocytic leukemia. *Blood* 126, 203–211. doi: 10.1182/blood-2015-01-622936

McLane, L. M., Abdel-Hakeem, M. S., and Wherry, E. J. (2019). CD8 T Cell Exhaustion During Chronic Viral Infection and Cancer. *Ann. Rev. Immunol.* 37, 457–495. doi: 10.1146/annurev-immunol-041015-055318

O'Connor, R. S., Hao, X., Shen, K., Bashour, K., Akimova, T., Hancock, W. W., et al. (2012). Substrate Rigidity Regulates Human T Cell Activation and Proliferation. *J. Immunol.* 189, 1330–1339. doi: 10.4049/jimmunol.1102757

Palma, M., Gentilcore, G., Heimersson, K., Mozaffari, F., Nasman-Glaser, B., Young, E., et al. (2017). T cells in chronic lymphocytic leukemia display dysregulated expression of immune checkpoints and activation markers. *Haematologica* 102, 562–572. doi: 10.3324/haematol.2016.151100

Porter, D. L., Hwang, W.-T., Frey, N. V., Lacey, S. F., Shaw, P. A., Loren, A. W., et al. (2015). Chimeric antigen receptor T cells persist and induce sustained remissions in relapsed refractory chronic lymphocytic leukemia. *Sci. Translat. Med.* 7, ra139–ra303.

Ramsay, A. G., Clear, A. J., Fatah, R., and Gribben, J. G. (2012). Multiple inhibitory ligands induce impaired T-cell immunologic synapse function in chronic lymphocytic leukemia that can be blocked with lenalidomide: establishing a reversible immune evasion mechanism in human cancer. *Blood* 120, 1412–1421. doi: 10.1182/blood-2012-02-411678

Ramsay, A. G., Evans, R., Kiaii, S., Svensson, L., Hogg, N., and Gribben, J. G. (2013). Chronic lymphocytic leukemia cells induce defective LFA-1-directed T-cell motility by altering Rho GTPase signaling that is reversible with lenalidomide. *Blood* 121, 2704–2714. doi: 10.1182/blood-2012-08-448332

Ramsay, A. G., Johnson, A. J., Lee, A. M., Gorgün, G., Le Dieu, R., Blum, W., et al. (2008). Chronic lymphocytic leukemia T cells show impaired immunological synapse formation that can be reversed with an immunomodulating drug. *J. Clin. Investig.* 118, 2427–2437.

Riches, J. C., Davies, J. K., McClanahan, F., Fatah, R., Iqbal, S., Agrawal, S., et al. (2013). T cells from CLL patients exhibit features of T-cell exhaustion but retain capacity for cytokine production. *Blood* 121, 1612–1621. doi: 10.1182/blood-2012-09-457531

Shen, K., Thomas, V. K., Dustin, M. L., and Kam, L. C. (2008). Micropatterning of costimulatory ligands enhances $CD4^+$ T cell function. *Proc. Natl. Acad. Sci.* 105, 7791–7796. doi: 10.1073/pnas.0710295105

Tonino, S. H., van de Berg, P. J., Yong, S. L., Berge, I.J. Ten, Kersten, M. J., van Lier, R. A. W., et al. (2012). Expansion of effector T cells associated with decreased PD-1 expression in patients with indolent B cell lymphomas and chronic lymphocytic leukemia. *Leukemia Lymphoma* 53, 1785–1794. doi: 10.3109/10428194.2012.673224

Wherry, E. J. (2011). T cell exhaustion. *Nat. Immunol.* 12, 492–499.

Wherry, E. J., and Kurachi, M. (2015). Molecular and cellular insights into T cell exhaustion. *Nat. Rev. Immunol.* 15, 486–499. doi: 10.1038/nri3862

Zucchetto, A., Cattarossi, I., Nanni, P., Zaina, E., Prato, G., Gilestro, M., et al. (2011). Cluster analysis of immunophenotypic data: The example of chronic lymphocytic leukemia. *Immunol. Lett.* 134, 137–144. doi: 10.1016/j.imlet.2010.09.017

Conflict of Interest: The authors declare that the research was conducted in the absence of any commercial or financial relationships that could be construed as a potential conflict of interest.

frontiers in Cell and Developmental Biology

MINI REVIEW
published: 12 April 2021
doi: 10.3389/fcell.2021.658460

Folding for the Immune Synapse: CCT Chaperonin and the Cytoskeleton

Noa Beatriz Martín-Cófreces[1,2,3], José María Valpuesta[4] and Francisco Sánchez-Madrid[1,2,3]**

[1] Immunology Service, Hospital Universitario de la Princesa, Universidad Autonoma Madrid (UAM), Instituto Investigacion Sanitaria-Instituto Princesa (IIS-IP), Madrid, Spain, [2] Area of Vascular Pathophysiology, Laboratory of Intercellular Communication, Fundación Centro Nacional de Investigaciones Cardiovasculares-Carlos III, Madrid, Spain, [3] Centro de Investigación Biomédica en Red de Enfermedades Cardiovasculares (CIBERCV), Madrid, Spain, [4] Centro Nacional de Biotecnología (CNB-CSIC), Madrid, Spain

Lymphocytes rearrange their shape, membrane receptors and organelles during cognate contacts with antigen-presenting cells (APCs). Activation of T cells by APCs through pMHC-TCR/CD3 interaction (peptide-major histocompatibility complex-T cell receptor/CD3 complexes) involves different steps that lead to the reorganization of the cytoskeleton and organelles and, eventually, activation of nuclear factors allowing transcription and ultimately, replication and cell division. Both the positioning of the lymphocyte centrosome in close proximity to the APC and the nucleation of a dense microtubule network beneath the plasma membrane from the centrosome support the T cell's intracellular polarity. Signaling from the TCR is facilitated by this traffic, which constitutes an important pathway for regulation of T cell activation. The coordinated enrichment upon T cell stimulation of the chaperonin CCT (chaperonin-containing tailless complex polypeptide 1; also termed TRiC) and tubulins at the centrosome area support polarized tubulin polymerization and T cell activation. The proteasome is also enriched in the centrosome of activated T cells, providing a mechanism to balance local protein synthesis and degradation. CCT assists the folding of proteins coming from *de novo* synthesis, therefore favoring mRNA translation. The functional role of this chaperonin in regulating cytoskeletal composition and dynamics at the immune synapse is discussed.

Keywords: CCT, chaperonin, immune synapse, tubulin, actin, cryocorrelative microscopy, microtubule

OPEN ACCESS

Edited by:
Sudha Kumari, Massachusetts Institute of Technology, United States

Reviewed by:
Michael Loran Dustin, University of Oxford, United Kingdom
Pablo José Sáez, University Medical Center Hamburg-Eppendorf, Germany

****Correspondence:***
José María Valpuesta
jmv@cnb.csic.es
Francisco Sánchez-Madrid
fsmadrid@salud.madrid.org

Specialty section:
This article was submitted to Cell Growth and Division, a section of the journal Frontiers in Cell and Developmental Biology

Received: *25 January 2021*
Accepted: *23 March 2021*
Published: *12 April 2021*

Citation:
Martín-Cófreces NB, Valpuesta JM and Sánchez-Madrid F (2021) Folding for the Immune Synapse: CCT Chaperonin and the Cytoskeleton. Front. Cell Dev. Biol. 9:658460. doi: 10.3389/fcell.2021.658460

INTRODUCTION

Synaptic contacts involve cell-cell communication structures determined by the polarization of organelles and specific cell components allowing the interchange of information, such as neurotransmitters, cytokines and genetic information, based on cytoskeleton rails (Martin-Cofreces et al., 2014). The immune synapse (IS) is a transient, dynamic cell-to-cell communication structure that forms at the interface of T cells and antigen-presenting cells (APCs). It represents a signaling hub, facilitating the sensing of extracellular cues to enable both T cell activation and differentiation and APC reprogramming/reorganization (Martin-Cofreces et al., 2014; Mastrogiovanni et al., 2020). On the T cell side, the changes to the cytoskeleton in response to T cell receptor

(TCR) activation have been studied in the context of intracellular reorganization and, more recently, propagation of intracellular signals. An unresolved question is how the actin and tubulin cytoskeletons coordinate to rearrange both spatially and temporally. These two cytoskeletons are inter-connected through proteins that are able to physically link them, as well as by signaling proteins that control their dynamics, such as members of the protein kinase C (PKC) family, phospholipase C and formins such as INF2 (Quann et al., 2011; Andres-Delgado et al., 2012; Kumari et al., 2015; Murugesan et al., 2016). The interdependence of tubulin and actin dynamics and the occupancy of specific regions in the cell have been described in diverse contexts, mainly in highly differentiated cells such as neurons and immune cells that form synapses (Martin-Cofreces et al., 2014; Coles and Bradke, 2015).

The actin-tubulin interconnection seems to be prior to the formation of their respective filaments, initiating at their folding upon *de novo* synthesis. Present in all eukaryotes, the cytosolic group II chaperonin CCT is an oligomer of about 1 MDa composed of eight different subunits (CCT1-8) that organize into a barrel-like structure formed by two back-to-back rings (Skjærven et al., 2015), with an already defined arrangement (CCT1-4-2-5-7-8-6-3, with CCT2 and CCT6 establishing homotypic, inter-ring interactions; **Figure 1**; Leitner et al., 2012; Kalisman et al., 2013; Chagoyen et al., 2014). However, during the oligomerization process, CCT microcomplexes can be observed (Sergeeva et al., 2019). The rings operate sequentially to assist in the folding of different clients (e.g., tubulin and actin monomers) upon their synthesis at the ribosome (Willison, 2018). CCT accumulates at the centrosomes of activated T cells (Martin-Cofreces et al., 2020), together with other complex oligomers such as the proteasome (Martin-Cofreces et al., 2020), also found in B cells (Ibañez-Vega et al., 2019). The proteasome is involved in degradation of ubiquitinated and unfolded proteins at the centrosomes of different cell types, which has been linked to the control of centrosome function (Freed et al., 1999; Vora and Phillips, 2016).

CHAPERONE ACTIVITIES OF CCT: FOLDING AND OTHERS

Actin and tubulin are major clients of CCT, which is considered to have co-evolved with these two components of the cytoskeleton, facilitating their current structural and molecular mechanisms. Native actin and tubulin are absolutely essential for cells, which makes the CCT oligomer an indispensable complex for cell viability (Liu et al., 2005). Many studies performed in yeast involving genetic deletion of individual subunits have shown growth defects and a loss of viability. Cells presented aberrant morphology and abnormally large sizes (Willison, 2018). The different CCT subunits can exert independent functions in cells (Vallin and Grantham, 2019); thus, the effects observed after simultaneous knockdown of several subunits probably correspond to the holoenzyme activity, whereas differences detected upon silencing of single subunits may be attributed to that particular component.

Studies on the CCT interactome are allowing the discovery of not only potential clients for CCT (either for complete or intermediate folding), but also regulatory proteins or proteins that are controlled by CCT (Dekker et al., 2008; Yam et al., 2008). The functions of obligate clients are linked to CCT folding activity: if the chaperonin fails to properly assist the folding of these substrates, loss of function effects could occur. Consequently, an excess of substrate may provoke an excess of unfolded forms of other substrates, (i.e., competition with other substrates), leading to toxicity through protein aggregation. Actin and tubulin connect CCT to any process that depends on the function of microtubules and actin filaments (Sternlicht et al., 1993). Since actin and tubulin are major clients for CCT, probably due to their abundance and affinity (Willison, 2018), their expression likely regulates the quantity of CCT available for other substrates, thus linking this process to normal cell metabolism and cell cycle progression. Other CCT client proteins include members of the WD40 family, which contain tandem copies of a 40-amino acid repeat (WD40 motif), several of which form a β-propeller structural domain. The cell cycle regulators Cdh1 and Cdc20 belong to this family of proteins and are also folded by CCT (Camasses et al., 2003). The two proteins play critical roles as adaptors for the anaphase promoting complex/cyclosome (APC/C), a ubiquitin ligase regulating cell cycle progression (Camasses et al., 2003). CCT may also impact cell biology through the folding of another WD40 protein, mLST8 (a subunit of mTOR complexes 1 and 2; Cuellar et al., 2019), which in turn regulates protein synthesis through the ribosomes and therefore, the flux of CCT clients. mTOR is activated by TCR stimulation and CD28 co-stimulation, increasing the eukaryotic translation initiation factor 4E (eIF4E) binding proteins (4E-BP1, 2, and 3) and the p70 ribosomal S6 kinase (S6K) activity. S6K phosphorylates the S6 ribosomal subunit to initiate protein synthesis (Myers et al., 2019). S6K also phosphorylates CCT2 subunit, providing a link between mRNA translation and folding (Abe et al., 2009). Another WD40 protein is Gβ, a component of the Gβ-Gγ signaling heterodimer complex. Here, CCT not only plays a role in the folding of Gβ, but also in the stabilization of the Gβ-Gγ complex (Plimpton et al., 2015).

REGULATION OF THE ACTIN CYTOSKELETON BY CCT

Despite our understanding of how a multitude of extracellular stimuli trigger pathways that lead to actin polymerization/depolymerization, and the detailed molecular mechanism of local actin nucleation (Pollard, 2019), some challenges remain to be addressed. There is a need to learn about the mechanisms that control newly assembled F-actin into higher order structures such as stress fibers, filopodia, and other bundles including short filaments near membrane-resident receptors. Indeed, additional work on the regulatory and functional mechanisms of F-actin disassembly is required to explain its rapid pace in cells.

A pending question about actin dynamics regards the maintenance of monomer availability in cells. Newly synthesized

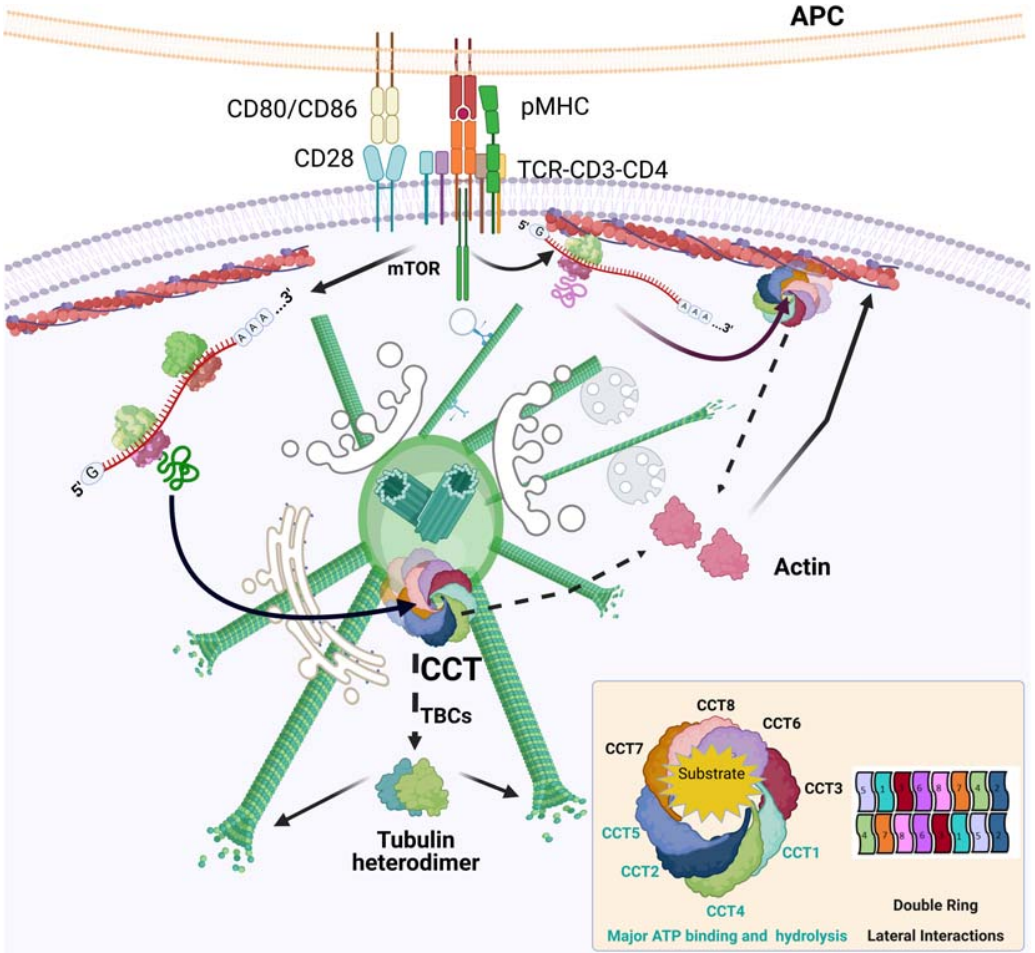

FIGURE 1 | CCT in the reorganization of actin and tubulin at the immune synapse. TCR activation promotes protein synthesis. The chaperone CCT accumulates in activated centrosomes, which then can act as folding centers for newly synthesized proteins. The new polypeptides are assisted in their folding by CCT, whose major obligate substrates are actin and tubulin. Actin is directly sorted into its native form, whereas tubulin needs the assistance of different tubulin-binding co-factors (TBCs) to form stable αβ-heterodimers. The newly formed building blocks are then ready to be incorporated into their respective filaments, F-actin and microtubules. CCT may localize to pre-existing actin filaments, where it can help in the folding of mRNAs that would then be bound to these filaments, creating local gradients of protein concentration. Organelles and cell components are not depicted to scale. Inset, CCT organization and ATP consumption.

actin requires CCT to adopt its native structure; a transient 90% silencing of CCT by siRNA only slightly affected actin synthesis, but reduced the amount of native actin and therefore cellular motility (Grantham et al., 2006). There is limited evidence of the regulation of actin filament homeostasis by synthesis and degradation of monomers, although such a process (involving specific degradation and isoform replacement of conventional actin through the proteasome) has been described in *Chlamydomonas* during stress adaptation (Onishi et al., 2018). The degradation of γ-actin by N-terminal arginylation upon removal of the N-terminal methionine depends on its ubiquitination and proteasome processing, and relies on slow translation and exposure of a Lys residue. Arginylated β-actin is more stable than the unmodified protein (Zhang et al., 2010). These modifications may heavily impact the ability of cells to expand their lamella at the front edge and migrate (Kashina, 2006). The majority of actin in lymphocytes corresponds to the β isoform (about 80%), whereas the remaining 20% is γ-actin, providing a mechanism to regulate actin availability through the proteasome. The role of the proteasome has been tested in T and B cells using different inhibitors during the establishment of synaptic contacts. The use of both MG132 and epoxomycin in activated B cells has shown effects on actin remodeling around the centrosome, which would prevent centrosome detachment from the nucleus and translocation to the synapse (Ibañez-Vega et al., 2019). All these inhibitors also showed effects on the tubulin cytoskeleton (Didier et al., 2008; Poruchynsky et al., 2008; Meregalli et al., 2014). In T cells, the highly selective proteasome inhibitor bortezomib increased tubulin dynamics at the centrosome area near the IS (Martin-Cofreces et al., 2020), while its effect on the actin cytoskeleton is not yet reported. Additional studies are needed in order to understand whether these outcomes are a direct consequence of the lack of proteasome activity on specific substrates, or rather the result of a

broad inhibition of other cell components with similar selectivity, such as calpains and cathepsin B. On the other hand, β-actin synthesis increased in centrosomes upon TCR activation, but a 40% reduction of CCT levels did not impact the total β-actin levels in T cells (as observed in other cell systems with increased reduction of the oligomer; Grantham et al., 2006). CCT reduction neither prevents the extension of the actin lamella nor adhesion to the APC, and phosphorylation of the myosin light chain is conserved (Martin-Cofreces et al., 2020).

The CCT complex co-sediments with F-actin in *in vitro* assays, where the initial rate of actin polymerization at the plus-ends is reduced, although F-actin formation is not prevented (Grantham et al., 2002). Indeed, although CCT does not assist gelsolin folding, it binds to its Ca^{2+}-activated form (Svanstrom and Grantham, 2016), which may control F-actin elongation through its severing and capping activity. The *in vivo* consequences of these interactions are under study. With regard to individual subunits, a reduced level of the CCT5 subunit narrows the cell shape and reduces the area of adhesion to substrate (Brackley and Grantham, 2010). Isolated CCT subunits are found near F-actin bundles (Brackley and Grantham, 2010), and over-expression of CCT4 induces cellular protrusions and filopodia (Spiess et al., 2015), which may reflect the individual roles of these proteins in the cell. Whether these individual CCT subunits or the oligomer play such a role in the IS deserves future experimentation.

An interesting feature of actin mRNA translation is that the zip code region at the 3′UTR of β-actin mRNA regulates its localization at the leading edge in migrating cells, in a serum-dependent manner (Kislauskis et al., 1997). Research performed on the contribution of newly synthesized β-actin to actin dynamics has suggested that it is unlikely that the calculated 6.5% of this *de novo* actin will significantly contribute to the rate of global actin polymerization at the cell front edge (Shestakova et al., 2001). However, this process performed in a restricted volume would increase the limiting monomer concentration, establishing a major location for actin polymerization. The delocalization of β-actin mRNA alters the sites and rate of cell protrusion (Shestakova et al., 2001). In this regard, the requirement of F-actin to localize its own mRNA to the front edge may also be considered a local mechanism of control by *de novo* synthesis (Sundell and Singer, 1991) in which CCT would take part. The cytoskeletal organization at the IS can be compared to that of the front-edge during migration (**Figure 1**). The interaction of tubulin and vimentin mRNAs with F-actin has also been described (Singer et al., 1989). Conceivably, this mechanism regulating the half-life of these messengers and the timing of their translation would constitute another regulatory step between the cytoskeletons.

The above model would be further supported if *de novo*-synthesized G-actin had a different effect on the polymerization rate of F-actin compared to the G-actin already present, either by its own molecular structure or by its affinity for nucleation complexes. G-actin may be subjected to post-translational modifications (PTMs) such as S-nitrosylation of β-actin on Cys374, which may change actin's molecular structure and properties (Garcia-Ortiz et al., 2017). This oxidation is relevant to regulate the ability of actin to polymerize and depolymerize at the IS, based on its interaction with profilin (Garcia-Ortiz et al., 2017). Although actin modifications have not been extensively studied in the context of synapses, more than 140 PTMs have been described in eukaryotic actin sequences. Some of them are quantitative and reversible, whereas others are infrequent and affect a minority of the actin pool. Specifically, N-terminal acetylation, arginylation and novel oxidation, phosphorylation, ubiquitination, and SUMOylation sites have been identified in recent years, some of them by global proteomics analyses (Varland et al., 2019). All these modifications may impact the native structure and stability of the protein, and constitute a growing field of research to be developed in the future.

TUBULIN REGULATION BY CCT

Tubulin molecules are the building blocks of the structure that controls cell shape and dynamics, and can originate from a large number of genes and isotypes. These diverse gene products organize into heterodimers such as αβ-tubulin (which forms microtubules) and γ-tubulin, which is found in specific structures such as the centrioles within centrosomes and in γ-TURC complexes, used as seeds to initiate microtubule polymerization at the pericentrosomal matrix and Golgi apparatus (Bettencourt-Dias and Glover, 2007; Martin-Cofreces and Sanchez-Madrid, 2018). There are other tubulins including ε-, ζ- and δ-tubulin, which are less studied and present only in some eukaryotes. Mutations in tubulin genes cause multiple human cortical malformations (tubulinopathies) that include microcephaly, lissencephaly, dysmorphic basal ganglia and polymicrogyria (Bahi-Buisson et al., 2014). Synthesis and folding of the heterodimers is a precise and complex process that requires the action of the prefoldin complex, a cochaperone that binds to the nascent polypeptide and transfers it to CCT to be folded (Llorca et al., 2000). The folded protein later depends on cooperation of different tubulin binding co-factors (TBCs) that specifically bind to α- or β-tubulin, helping in the formation of αβ-heterodimers and their incorporation into microtubules (Lopez-Fanarraga et al., 2001).

Tubulin synthesis is regulated by the cell cycle, increasing during the S phase to facilitate organization of the mitotic spindle. It is also self-regulated by its own quantity in the cells, thereby maintaining a constant pool of available heterodimers for microtubule dynamics (Baker, 1993; Brackley and Grantham, 2009; Willison, 2018). The effects of different inhibitors of protein synthesis and the proteasome have been studied in diverse cell systems. During IS formation, active tubulin synthesis is driven by TCR activation, providing increased availability of soluble heterodimers for polymerization at the centrosome. This local increase in tubulin concentration would burst microtubule polymerization from the centrosome, facilitating the radial array formed at the immune synapse (**Figure 1**). The inhibition of protein synthesis in T cells through the chemical inhibitor cycloheximide prevented tubulin dynamics during T cell activation, as did a 40% reduction in CCT levels by siRNA (Martin-Cofreces et al., 2020). At this level of expression, total cellular quantities of actin and tubulin were unaffected, whereas

a 90% reduction in CCT showed diminished levels of tubulin (Grantham et al., 2006). Despite the great increase in soluble heterodimers, polymerization from the centrosome was strongly decreased, both in terms of the number of new microtubules and the rate of incorporation. In contrast, treatment with the highly selective proteasome inhibitor bortezomib increased the rate of polymerization from the translocated centrosome, reducing soluble cytosolic heterodimers. The use of other proteasome inhibitors, such as MG132 and epoxomycin during IS formation has focused on the study of F-actin at the centrosome area, showing an inhibition of the centrosome's translocation to the IS in B cells (Ibañez-Vega et al., 2019). MG115, PS-341 and epoxomycin treatments in HeLa cells increased the amount of proteins such as γ-tubulin, dynactin, ninein and PCM-1 at the centrosomes, generating an enlargement of this organelle. Epoxomycin prevented the radial array of microtubules in interphase U2OS cells after nocodazole treatment without preventing centriole conformation, as observed through electron microscopy (Didier et al., 2008). In contrast, bortezomib treatment increases microtubule dynamics (Poruchynsky et al., 2008; Meregalli et al., 2014). These apparently contradictory results warrant further research to understand the role of the proteasome on cytoskeleton dynamics at the centrosome.

An intriguing fact is that the centrosome of T cells with reduced levels of CCT was not as distant from the IS as should be expected, as observed by soft-X-ray cryocorrelative microscopy, with a spatial resolution of about 50 nm (Martin-Cofreces et al., 2020). A recent report describes that kinesin-4 KIF21B limited the growth of microtubules shortly after TCR activation, allowing translocation of the centrosome (Hooikaas et al., 2020), which may correlate to no specific defects in centrosome translocation to the IS in T cells with diminished microtubule growth due to cycloheximide treatment or reduced CCT levels. Instead, it might be the result of different doses and timing of the different treatments, leading to diverse responses or a lack of effect. In this regard, the internal ultrastructure of the centrosome at the IS is affected by a reduction in CCT levels. The centrioles show a different orientation inside the centrosome with respect to the IS plane once the TCR is activated, which is prevented by CCT knockdown (Martin-Cofreces et al., 2020). The orientation of the centrioles seems to allow the oriented polymerization of microtubules toward the IS, even if the centrosome is not close to it. This piece of evidence may imply further biological consequences than the actual position of the centrosome in the cell, and warrants future research on how this orientation is regulated, and whether the centrioles can act as a sensor for "up and down" positioning in cells.

Additionally, a specific equilibrium between tubulin synthesis and degradation may also be required to allow correct microtubule dynamics, which might be dependent on the incorporation of building blocks into the polymer and the PTMs observed in tubulin (**Figure 2**). The de-tyrosination of tubulin at its C-terminus (Δ1-tubulin) has been observed during IS formation, with increased localization at the centrosome (Andres-Delgado et al., 2010). This PTM is also observed in soluble heterodimers upon TCR activation, concomitant with increases in Δ2-tubulin (a variant that lacks the C-terminal tyrosine and glutamic residues; Martin-Cofreces et al., 2020), which has been proposed to be a form of tubulin targeted for degradation (Paturle-Lafanechere et al., 1994). Reduced protein synthesis either by cycloheximide treatment or CCT knockdown prevents not only the incorporation of heterodimers into microtubules, but also the aforementioned PTMs, accompanied by increasing microtubule acetylation (Martin-Cofreces et al., 2020). Deacetylation of microtubules driven by HDAC6 is observed shortly after TCR activation, indicating a transient increase in dynamic microtubules during T cell reorganization (Serrador et al., 2004). Over-expression of HDAC6 prevents centrosome translocation (Serrador et al., 2004), and its knockdown decreases the distance of the centrosome to the IS (Nunez-Andrade et al., 2016), which would correspond to a sustained increased acetylation, as observed in T cells with reduced CCT levels (Martin-Cofreces et al., 2020). Indeed, knock-down of Aurora A, a Serine/threonine kinase that promotes microtubule growing from the polarized centrosome in synaptic T cells, does not affect centrosome polarization, but alters microtubule growing at the IS (Blas-Rus et al., 2017). Aurora A promotes microtubule polymerization from the centrosome (Terada et al., 2003). CCT depletion or CEP55 knock-down decrease Aurora A at the protein level and prevents ciliary disassembly; in absence of Aurora A, cilia are longer with increased acetylated microtubules (Zhang et al., 2021). Also, Aurora A phosphorylates and activates HDAC6 to allow ciliary dissasembly (Pugacheva et al., 2007). A similar mechanism can be acting at the IS as the cilia and the IS share components and features (Cassioli and Baldari, 2019). Deacetylation of microtubules may be required to disassemble the initial microtubular network and to allow the microtubule-organizing activity of the centrosome. Those results support that defects in microtubule growth show a lesser effect on centrosome translocation than an excess of polymerization during IS formation (Hooikaas et al., 2020). The lack of microtubule polymerization in T cells with reduced CCT levels might prevent tubulin clearance by the proteasome, which would be mainly loaded with Δ2-tubulin (**Figure 2**). The decrease in Δ1-tubulin allows rapid depolymerization at plus ends of microtubules by action of kinesin 13, which binds preferentially to tyrosinated tubulin (Peris et al., 2009). This would be observed as a reduced polymerization rate in TIRFm assays in terms of the number of microtubules and polymerization speed at the IS. Together, these events may result in an accumulation of unmodified tubulin heterodimers, as indeed has been observed (Martin-Cofreces et al., 2020). The lack of tubulin dynamics induces defects in the structure of the IS, including mitochondrial disorganization and failures in cell respiration. These effects may also be supported by decreased mTOR activity (Cuellar et al., 2019).

IS THERE ANY CCT CONNECTION DRIVING THE SYNCHRONIZATION OF CYTOSKELETON DYNAMICS?

It is remarkable to notice that actin dynamics, which are more readily observed upon TCR activation (from ms to s) than tubulin

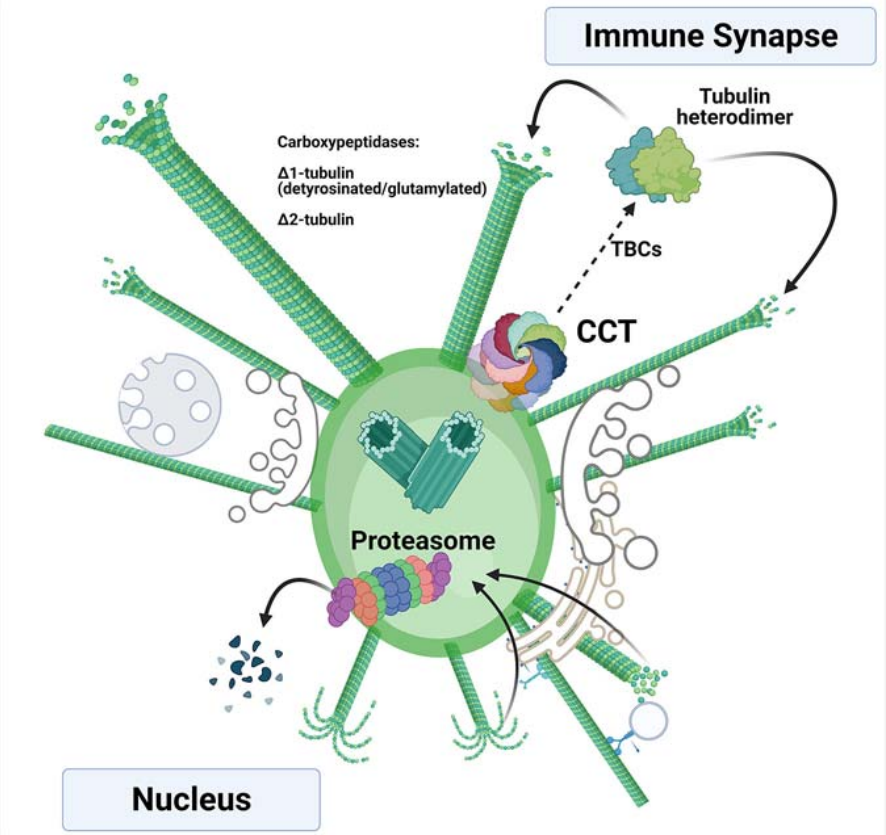

FIGURE 2 | Tubulin synthesis and degradation at the centrosome of activated T cells. Newly synthesized α- and β-tubulin are assisted in their folding by the chaperone CCT, forming heterodimers that can be incorporated into nascent microtubules with the assistance of different tubulin-binding co-factors (TBCs). The incorporated heterodimers can then be post-translationally modified by carboxypeptidases that delete the C-terminal tyrosine (Δ1-tubulin) and the glutamic acid (Δ2-tubulin). These modifications take place in the microtubules. The depolymerized, post-translationally modified heterodimers can be then proteolyzed by the proteasome upon depolymerization. The rapid synthesis and degradation of tubulins enable availability of fresh heterodimers for polymerization. If the CCT chaperonin and proteasome localize asymmetrically inside the centrosome, they can act in different orientations (i.e., the nuclear and immune synapse sides), allowing directionality of the polymerization.

dynamics (from s to min), are less dependent on the *de novo* synthesis of its constituent G-actin. This effect has been observed in different cell types (Grantham et al., 2006; Willison, 2018; Martin-Cofreces et al., 2020) and is dependent on the amount of functional CCT available. During *in vitro* translation assays with rabbit reticulocyte lysates, CCT was required for folding of actin into its native form (Garcia-Ortiz et al., 2017; Willison, 2018). However, once folded, actin seems to be more stable than tubulin, which requires a much more complex folding process and cooperation between multiple co-factors to polymerize and depolymerize (Lopez-Fanarraga et al., 2001; Kortazar et al., 2007). Even if small changes in CCT do not result in changes in the amount of actin or tubulin in resting cells, CCT's boost of tubulin polymerization may be extremely important for the cytoskeletal reorganization needed during the dramatic structural changes that occur in processes such as mitosis, leading edge extension in migrating cells, or IS formation. The differing requirements for tubulin and actin synthesis to increase the critical or limiting concentration may determine in these scenarios the timing of local polymerization for each filament type.

CONCLUDING REMARKS

An attractive hypothesis is that during T cell activation the centrosome may arrange the CCT chaperonin and the proteasome *asymmetrically*, in coordination with the change in reciprocal orientation of the centrioles, thereby allowing major depolymerization and degradation of tubulin on the "nucleus side" and synthesis and polymerization on the "IS side" (**Figure 2**). Such a hypothesis would explain how the proteasome is unequally distributed/divided between the mother and daughter cells during asymmetric division of CD8 + T cells to generate memory T cells; the correct localization of the centrosome seems to be required for this process (Chang et al., 2011; Martin-Cofreces et al., 2014). The use of inhibitors in these experiments is challenging, since their effect is global and they would be expected to act firstly at sites where the actin or tubulin cytoskeletons respond rapidly to TCR activation, such as the microvilli or the lamella at contact sites with the APC (**Figure 1**), acting only secondarily at the centrosome. Imaging methods allowing single-particle localization combined

with CRISP/Cas technology to substitute CCT subunits in cells may help to study these events. The increase in spatial resolution provided by emergent microscopy technologies, such as cryocorrelative microscopy and subsequent cryoelectron tomography and subtomogram averaging will allow localizing this kind of complexes, thus helping to better understand the biological processes described above.

AUTHOR CONTRIBUTIONS

NM-C: conceptualization, funding acquisition, image composition (**Figures 1**, **2**), and writing (original draft, review and editing). FS-M and JMV: conceptualization, resources, funding acquisition, and writing (original draft, review, and editing). All authors contributed to the article and approved the submitted version.

FUNDING

This work was supported bun the ALBA Synchrotron standard proposals 2015021148 and 2016021638 to NM-C and JMV. This study was supported by grants SAF2017-82886-R (to FS-M) and PID2019-105872GB-I00/AEI/10.13039/501100011033 (AEI/FEDER, UE) (to JMV) from the Spanish Ministry of Economy and Competitiveness (MINECO), grants INFLAMUNE-S2017/BMD-23671 (to FS-M) and P2018/NMT-4389 (to JMV) from the Comunidad de Madrid, ERC-2011-AdG 294340-GENTRIS (to FS-M), a 2019 grant from the Ramón Areces Foundation "Ciencias de la Vida y la Salud" and a 2018 grant from Ayudas Fundación BBVA a Equipos de Investigación Científica (to FS-M) and grants PRB3 (IPT17/0019—ISCIII-SGEFI/ERDF), and "La Caixa" Banking Foundation (HR17-00016 to FS-M). CIBER Cardiovascular (Fondo de Investigación Sanitaria del Instituto de Salud Carlos III and co-funding by Fondo Europeo de Desarrollo Regional FEDER). The Centro Nacional de Investigaciones Cardiovasculares (CNIC) is supported by the Spanish Ministry of Economy and Competitiveness (MINECO) and the Pro-CNIC Foundation. The Centro Nacional de Biotecnología (CNB) was a Severo Ochoa Center of Excellence (MINECO award SEV 2017-0712). Funding agencies have not intervened in the design of the studies, with no copyright over the study.

ACKNOWLEDGMENTS

The professional editing service NB Revisions was used for technical preparation of the text prior to submission. We thank M. Gómez for reading and editing the manuscript. We are grateful to Ms. M. Ángeles Vallejo for helpful assistance and management. Figures created with BioRender.com Beta version.

REFERENCES

Abe, Y., Yoon, S. O., Kubota, K., Mendoza, M. C., Gygi, S. P., and Blenis, J. (2009). p90 ribosomal S6 kinase and p70 ribosomal S6 kinase link phosphorylation of the eukaryotic chaperonin containing TCP-1 to growth factor, insulin, and nutrient signaling. *J. Biol. Chem.* 284, 14939–14948. doi: 10.1074/jbc.m900097200

Andres-Delgado, L., Anton, O. M., Bartolini, F., Ruiz-Saenz, A., Correas, I., Gundersen, G. G., et al. (2012). INF2 promotes the formation of detyrosinated microtubules necessary for centrosome reorientation in T cells. *J. Cell. Biol.* 198, 1025–1037. doi: 10.1083/jcb.201202137

Andres-Delgado, L., Anton, O. M., Madrid, R., Byrne, J. A., and Alonso, M. A. (2010). Formin INF2 regulates MAL-mediated transport of Lck to the plasma membrane of human T lymphocytes. *Blood* 116, 5919–5929. doi: 10.1182/blood-2010-08-300665

Bahi-Buisson, N., Poirier, K., Fourniol, F., Saillour, Y., Valence, S., Lebrun, N., et al. (2014). The wide spectrum of tubulinopathies: what are the key features for the diagnosis? *Brain* 137, 1676–1700. doi: 10.1093/brain/awu082

Baker, E. J. (1993). Tubulin mRNA instability and stabilization by protein synthesis inhibitors are reproducible in nontranslating extracts from Chlamydomonas. *Dev. Genet.* 14, 460–470. doi: 10.1002/dvg.1020140607

Bettencourt-Dias, M., and Glover, D. M. (2007). Centrosome biogenesis and function: centrosomics brings new understanding. *Nat. Rev. Mol. Cell Biol.* 8, 451–463. doi: 10.1038/nrm2180

Blas-Rus, N., Bustos-Moran, E., Sanchez-Madrid, F., and Martin-Cofreces, N. B. (2017). Analysis of Microtubules and Microtubule-Organizing Center at the Immune Synapse. *Methods Mol. Biol.* 1584, 31–49. doi: 10.1007/978-1-4939-6881-7_3

Brackley, K. I., and Grantham, J. (2009). Activities of the chaperonin containing TCP-1 (CCT): implications for cell cycle progression and cytoskeletal organisation. *Cell Stress Chaperones* 14, 23–31. doi: 10.1007/s12192-008-0057-x

Brackley, K. I., and Grantham, J. (2010). Subunits of the chaperonin CCT interact with F-actin and influence cell shape and cytoskeletal assembly. *Exp. Cell. Res.* 316, 543–553. doi: 10.1016/j.yexcr.2009.11.003

Camasses, A., Bogdanova, A., Shevchenko, A., and Zachariae, W. (2003). The CCT chaperonin promotes activation of the anaphase-promoting complex through the generation of functional Cdc20. *Mol. Cell* 12, 87–100. doi: 10.1016/s1097-2765(03)00244-2

Cassioli, C., and Baldari, C. T. (2019). , A Ciliary View of the Immunological Synapse. *Cells* 8:789. doi: 10.3390/cells8080789

Chagoyen, M., Carrascosa, J. L., Pazos, F., and Valpuesta, J. M. (2014). Molecular determinants of the ATP hydrolysis asymmetry of the CCT chaperonin complex. *Proteins* 82, 703–707. doi: 10.1002/prot.24510

Chang, J. T., Ciocca, M. L., Kinjyo, I., Palanivel, V. R., McClurkin, C. E., Dejong, C. S., et al. (2011). Asymmetric proteasome segregation as a mechanism for unequal partitioning of the transcription factor T-bet during T lymphocyte division. *Immunity* 34, 492–504. doi: 10.1016/j.immuni.2011.03.017

Coles, C. H., and Bradke, F. (2015). Coordinating neuronal actin-microtubule dynamics. *Curr. Biol.* 25, R677–R691.

Cuellar, J., Ludlam, W. G., Tensmeyer, N. C., Aoba, T., Dhavale, M., Santiago, C., et al. (2019). Structural and functional analysis of the role of the chaperonin CCT in mTOR complex assembly. *Nat. Commun.* 10:2865.

Dekker, C., Stirling, P. C., McCormack, E. A., Filmore, H., Paul, A., Brost, R. L., et al. (2008). The interaction network of the chaperonin CCT. *EMBO J.* 27, 1827–1839.

Didier, C., Merdes, A., Gairin, J. E., and Jabrane-Ferrat, N. (2008). Inhibition of proteasome activity impairs centrosome-dependent microtubule nucleation and organization. *Mol. Biol. Cell* 19, 1220–1229. doi: 10.1091/mbc.e06-12-1140

Freed, E., Lacey, K. R., Huie, P., Lyapina, S. A., Deshaies, R. J., Stearns, T., et al. (1999). Components of an SCF ubiquitin ligase localize to the centrosome and regulate the centrosome duplication cycle. *Genes. Dev.* 13, 2242–2257. doi: 10.1101/gad.13.17.2242

Garcia-Ortiz, A., Martin-Cofreces, N. B., Ibiza, S., Ortega, A., Izquierdo-Alvarez, A., Trullo, A., et al. (2017). eNOS S-nitrosylates beta-actin on Cys374 and regulates PKC-theta at the immune synapse by impairing actin binding to profilin-1. *PLoS Biol.* 15:e2000653. doi: 10.1371/journal.pbio.2000653

Grantham, J., Brackley, K. I., and Willison, K. R. (2006). Substantial CCT activity is required for cell cycle progression and cytoskeletal organization in mammalian cells. *Exp. Cell Res.* 312, 2309–2324. doi: 10.1016/j.yexcr.2006.03.028

Grantham, J., Ruddock, L. W., Roobol, A., and Carden, M. J. (2002). Eukaryotic chaperonin containing T-complex polypeptide 1 interacts with filamentous actin and reduces the initial rate of actin polymerization in vitro. *Cell Stress Chaperones* 7, 235–242. doi: 10.1379/1466-1268(2002)007<0235:ecctcp>2.0.co;2

Hooikaas, P. J., Damstra, H. G., Gros, O. J., van Riel, W. E., Martin, M., Smits, Y. T., et al. (2020). Kinesin-4 KIF21B limits microtubule growth to allow rapid centrosome polarization in T cells. *Elife* 9:e62876.

Ibañez-Vega, J., Del Valle Batalla, F., Saez, J. J., Soza, A., and Yuseff, M. I. (2019). Proteasome Dependent Actin Remodeling Facilitates Antigen Extraction at the Immune Synapse of B Cells. *Front. Immunol.* 10:225. doi: 10.3389/fimmu.2019.00225

Kalisman, N., Schroder, G. F., and Levitt, M. (2013). The crystal structures of the eukaryotic chaperonin CCT reveal its functional partitioning. *Structure* 21, 540–549. doi: 10.1016/j.str.2013.01.017

Kashina, A. S. (2006). Differential arginylation of actin isoforms: the mystery of the actin N-terminus. *Trends Cell Biol.* 16, 610–615. doi: 10.1016/j.tcb.2006.10.001

Kislauskis, E. H., Zhu, X., and Singer, R. H. (1997). beta-Actin messenger RNA localization and protein synthesis augment cell motility. *J. Cell Biol.* 136, 1263–1270. doi: 10.1083/jcb.136.6.1263

Kortazar, D., Fanarraga, M. L., Carranza, G., Bellido, J., Villegas, J. C., Avila, J., et al. (2007). Role of cofactors B (TBCB) and E (TBCE) in tubulin heterodimer dissociation. *Exp. Cell Res.* 313, 425–436. doi: 10.1016/j.yexcr.2006.09.002

Kumari, S., Depoil, D., Martinelli, R., Judokusumo, E., Carmona, G., Gertler, F. B., et al. (2015). Actin foci facilitate activation of the phospholipase C-gamma in primary T lymphocytes via the WASP pathway. *Elife* 4:e04953.

Leitner, A., Joachimiak, L. A., Bracher, A., Monkemeyer, L., Walzthoeni, T., Chen, B., et al. (2012). The molecular architecture of the eukaryotic chaperonin TRiC/CCT. *Structure* 20, 814–825. doi: 10.1016/j.str.2012.03.007

Liu, X., Lin, C. Y., Lei, M., Yan, S., Zhou, T., and Erikson, R. L. (2005). CCT chaperonin complex is required for the biogenesis of functional Plk1. *Mol. Cell Biol.* 25, 4993–5010. doi: 10.1128/mcb.25.12.4993-5010.2005

Llorca, O., Martin-Benito, J., Ritco-Vonsovici, M., Grantham, J., Hynes, G. M., Willison, K. R., et al. (2000). Eukaryotic chaperonin CCT stabilizes actin and tubulin folding intermediates in open quasi-native conformations. *EMBO J.* 19, 5971–5979. doi: 10.1093/emboj/19.22.5971

Lopez-Fanarraga, M., Avila, J., Guasch, A., Coll, M., and Zabala, J. C. (2001). Review: postchaperonin tubulin folding cofactors and their role in microtubule dynamics. *J. Struct. Biol.* 135, 219–229. doi: 10.1006/jsbi.2001.4386

Martin-Cofreces, N. B., Baixauli, F., and Sanchez-Madrid, F. (2014). Immune synapse: conductor of orchestrated organelle movement. *Trends Cell Biol.* 24, 61–72. doi: 10.1016/j.tcb.2013.09.005

Martin-Cofreces, N. B., Chichon, F. J., Calvo, E., Torralba, D., Bustos-Moran, E., Dosil, S. G., et al. (2020). The chaperonin CCT controls T cell receptor-driven 3D configuration of centrioles. *Sci. Adv.* 6:eabb7242. doi: 10.1126/sciadv.abb7242

Martin-Cofreces, N. B., and Sanchez-Madrid, F. (2018). Sailing to and Docking at the Immune Synapse: role of Tubulin Dynamics and Molecular Motors. *Front. Immunol.* 9:1174. doi: 10.3389/fimmu.2018.01174

Mastrogiovanni, M., Juzans, M., Alcover, A., and Di Bartolo, V. (2020). Coordinating Cytoskeleton and Molecular Traffic in T Cell Migration, Activation, and Effector Functions. *Front. Cell Dev. Biol.* 8:591348. doi: 10.3389/fcell.2020.591348

Meregalli, C., Chiorazzi, A., Carozzi, V. A., Canta, A., Sala, B., Colombo, M., et al. (2014). Evaluation of tubulin polymerization and chronic inhibition of proteasome as citotoxicity mechanisms in bortezomib-induced peripheral neuropathy. *Cell Cycle* 13, 612–621. doi: 10.4161/cc.27476

Murugesan, S., Hong, J., Yi, J., Li, D., Beach, J. R., Shao, L., et al. (2016). Formin-generated actomyosin arcs propel T cell receptor microcluster movement at the immune synapse. *J. Cell Biol.* 215, 383–399. doi: 10.1083/jcb.201603080

Myers, D. R., Wheeler, B., and Roose, J. P. (2019). mTOR and other effector kinase signals that impact T cell function and activity. *Immunol. Rev.* 291, 134–153. doi: 10.1111/imr.12796

Nunez-Andrade, N., Iborra, S., Trullo, A., Moreno-Gonzalo, O., Calvo, E., Catalan, E., et al. (2016). HDAC6 regulates the dynamics of lytic granules in cytotoxic T lymphocytes. *J. Cell Sci.* 129, 1305–1311. doi: 10.1242/jcs.180885

Onishi, M., Pecani, K., Jones, T. IV., Pringle, J. R., and Cross, F. R. (2018). F-actin homeostasis through transcriptional regulation and proteasome-mediated proteolysis. *Proc. Natl. Acad. Sci. U. S. A.* 115:E6487–E6496.

Paturle-Lafanechere, L., Manier, M., Trigault, N., Pirollet, F., Mazarguil, H., and Job, D. (1994). Accumulation of delta 2-tubulin, a major tubulin variant that cannot be tyrosinated, in neuronal tissues and in stable microtubule assemblies. *J. Cell Sci.* 107, 1529–1543.

Peris, L., Wagenbach, M., Lafanechere, L., Brocard, J., Moore, A. T., Kozielski, F., et al. (2009). Motor-dependent microtubule disassembly driven by tubulin tyrosination. *J. Cell Biol.* 185, 1159–1166. doi: 10.1083/jcb.200902142

Plimpton, R. L., Cuellar, J., Lai, C. W., Aoba, T., Makaju, A., Franklin, S., et al. (2015). Structures of the Gbeta-CCT and PhLP1-Gbeta-CCT complexes reveal a mechanism for G-protein beta-subunit folding and Gbetagamma dimer assembly. *Proc. Natl. Acad. Sci. U. S. A.* 112, 2413–2418. doi: 10.1073/pnas.1419595112

Pollard, T. D. (2019). Cell Motility and Cytokinesis: from Mysteries to Molecular Mechanisms in Five Decades. *Annu. Rev. Cell Dev. Biol.* 35, 1–28. doi: 10.1146/annurev-cellbio-100818-125427

Poruchynsky, M. S., Sackett, D. L., Robey, R. W., Ward, Y., Annunziata, C., and Fojo, T. (2008). Proteasome inhibitors increase tubulin polymerization and stabilization in tissue culture cells: a possible mechanism contributing to peripheral neuropathy and cellular toxicity following proteasome inhibition. *Cell Cycle* 7, 940–949. doi: 10.4161/cc.7.7.5625

Pugacheva, E. N., Jablonski, S. A., Hartman, T. R., Henske, E. P., and Golemis, E. A. (2007). HEF1-dependent Aurora A activation induces disassembly of the primary cilium. *Cell* 129, 1351–1363. doi: 10.1016/j.cell.2007.04.035

Quann, E. J., Liu, X., Altan-Bonnet, G., and Huse, M. (2011). A cascade of protein kinase C isozymes promotes cytoskeletal polarization in T cells. *Nat. Immunol.* 12, 647–654. doi: 10.1038/ni.2033

Sergeeva, O. A., Haase-Pettingell, C., and King, J. A. (2019). Co-expression of CCT subunits hints at TRiC assembly. *Cell Stress Chaperones* 24, 1055–1065. doi: 10.1007/s12192-019-01028-5

Serrador, J. M., Cabrero, J. R., Sancho, D., Mittelbrunn, M., Urzainqui, A., and Sanchez-Madrid, F. (2004). HDAC6 deacetylase activity links the tubulin cytoskeleton with immune synapse organization. *Immunity* 20, 417–428. doi: 10.1016/s1074-7613(04)00078-0

Shestakova, E. A., Singer, R. H., and Condeelis, J. (2001). The physiological significance of beta -actin mRNA localization in determining cell polarity and directional motility. *Proc. Natl. Acad. Sci. U. S. A.* 98, 7045–7050. doi: 10.1073/pnas.121146098

Singer, R. H., Langevin, G. L., and Lawrence, J. B. (1989). Ultrastructural visualization of cytoskeletal mRNAs and their associated proteins using double-label in situ hybridization. *J. Cell Biol.* 108, 2343–2353. doi: 10.1083/jcb.108.6.2343

Skjærven, L., Cuéllar, J., Martínez, A., and Valpuesta, J. M. (2015). Dynamics, flexibility, and allostery in molecular chaperonins. *FEBS Lett.* 589, 2522–2532. doi: 10.1016/j.febslet.2015.06.019

Spiess, M., Echbarthi, M., Svanstrom, A., Karlsson, R., and Grantham, J. (2015). Over-Expression Analysis of All Eight Subunits of the Molecular Chaperone CCT in Mammalian Cells Reveals a Novel Function for CCTdelta. *J. Mol. Biol.* 427, 2757–2764. doi: 10.1016/j.jmb.2015.06.007

Sternlicht, H., Farr, G. W., Sternlicht, M. L., Driscoll, J. K., Willison, K., and Yaffe, M. B. (1993). The t-complex polypeptide 1 complex is a chaperonin for tubulin and actin in vivo. *Proc. Natl. Acad. Sci. U. S. A.* 90, 9422–9426. doi: 10.1073/pnas.90.20.9422

Sundell, C. L., and Singer, R. H. (1991). Requirement of microfilaments in sorting of actin messenger RNA. *Science* 253, 1275–1277. doi: 10.1126/science.1891715

Svanstrom, A., and Grantham, J. (2016). The molecular chaperone CCT modulates the activity of the actin filament severing and capping protein gelsolin in vitro. *Cell Stress Chaperones* 21, 55–62. doi: 10.1007/s12192-015-0637-5

Terada, Y., Uetake, Y., and Kuriyama, R. (2003). Interaction of Aurora-A and centrosomin at the microtubule-nucleating site in Drosophila and mammalian cells. *J. Cell Biol.* 162, 757–763. doi: 10.1083/jcb.200305048

Vallin, J., and Grantham, J. (2019). The role of the molecular chaperone CCT in protein folding and mediation of cytoskeleton-associated processes: implications for cancer cell biology. *Cell Stress Chaperones* 24, 17–27. doi: 10.1007/s12192-018-0949-3

Varland, S., Vandekerckhove, J., and Drazic, A. (2019). Actin Post-translational Modifications: the Cinderella of Cytoskeletal Control. *Trends Biochem. Sci.* 44, 502–516. doi: 10.1016/j.tibs.2018.11.010

Vora, S. M., and Phillips, B. T. (2016). The benefits of local depletion: the centrosome as a scaffold for ubiquitin-proteasome-mediated degradation. *Cell Cycle* 15, 2124–2134. doi: 10.1080/15384101.2016.1196306

Willison, K. R. (2018). The substrate specificity of eukaryotic cytosolic chaperonin CCT. *Philos. Trans. R. Soc. Lond. B. Biol. Sci.* 373:20170192. doi: 10.1098/rstb.2017.0192

Yam, A. Y., Xia, Y., Lin, H. T., Burlingame, A., Gerstein, M., and Frydman, J. (2008). Defining the TRiC/CCT interactome links chaperonin function to stabilization of newly made proteins with complex topologies. *Nat. Struct. Mol. Biol.* 15, 1255–1262. doi: 10.1038/nsmb.1515

Zhang, F., Saha, S., Shabalina, S. A., and Kashina, A. (2010). Differential arginylation of actin isoforms is regulated by coding sequence-dependent degradation. *Science* 329, 1534–1537. doi: 10.1126/science.1191701

Zhang, Y. C., Bai, Y. F., Yuan, J. F., Shen, X. L., Xu, Y. L., Jian, X. X., et al. (2021). CEP55 promotes cilia disassembly through stabilizing Aurora A kinase. *J. Cell Biol.* 220:e202003149.

Conflict of Interest: The authors declare that the research was conducted in the absence of any commercial or financial relationships that could be construed as a potential conflict of interest.

frontiers in Cell and Developmental Biology

ORIGINAL RESEARCH
published: 13 April 2021
doi: 10.3389/fcell.2021.649433

The Wdr1-LIMK-Cofilin Axis Controls B Cell Antigen Receptor-Induced Actin Remodeling and Signaling at the Immune Synapse

Madison Bolger-Munro†, Kate Choi, Faith Cheung, Yi Tian Liu, May Dang-Lawson, Nikola Deretic, Connor Keane and Michael R. Gold**

Department of Microbiology & Immunology and Life Sciences Institute, University of British Columbia, Vancouver, BC, Canada

OPEN ACCESS

Edited by:
Sudha Kumari, Massachusetts Institute of Technology, United States

Reviewed by:
Wenxia Song, University of Maryland, United States
Manas Ray, National Institute of Environmental Health Sciences (NIEHS), United States

***Correspondence:**
Michael R. Gold
mgold@mail.ubc.ca
orcid.org/0000-0003-1222-3191
Madison Bolger-Munro
madison.bolger-munro@ist.ac.at
orcid.org/0000-0002-8176-4824

†Present address:
Madison Bolger-Munro, Institute of Science and Technology of Austria, Klosterneuburg, Austria

Specialty section:
This article was submitted to Cell Growth and Division, a section of the journal Frontiers in Cell and Developmental Biology

Received: *04 January 2021*
Accepted: *12 March 2021*
Published: *13 April 2021*

Citation:
Bolger-Munro M, Choi K, Cheung F, Liu YT, Dang-Lawson M, Deretic N, Keane C and Gold MR (2021) The Wdr1-LIMK-Cofilin Axis Controls B Cell Antigen Receptor-Induced Actin Remodeling and Signaling at the Immune Synapse. Front. Cell Dev. Biol. 9:649433. doi: 10.3389/fcell.2021.649433

When B cells encounter membrane-bound antigens, the formation and coalescence of B cell antigen receptor (BCR) microclusters amplifies BCR signaling. The ability of B cells to probe the surface of antigen-presenting cells (APCs) and respond to APC-bound antigens requires remodeling of the actin cytoskeleton. Initial BCR signaling stimulates actin-related protein (Arp) 2/3 complex-dependent actin polymerization, which drives B cell spreading as well as the centripetal movement and coalescence of BCR microclusters at the B cell-APC synapse. Sustained actin polymerization depends on concomitant actin filament depolymerization, which enables the recycling of actin monomers and Arp2/3 complexes. Cofilin-mediated severing of actin filaments is a rate-limiting step in the morphological changes that occur during immune synapse formation. Hence, regulators of cofilin activity such as WD repeat-containing protein 1 (Wdr1), LIM domain kinase (LIMK), and coactosin-like 1 (Cotl1) may also be essential for actin-dependent processes in B cells. Wdr1 enhances cofilin-mediated actin disassembly. Conversely, Cotl1 competes with cofilin for binding to actin and LIMK phosphorylates cofilin and prevents it from binding to actin filaments. We now show that Wdr1 and LIMK have distinct roles in BCR-induced assembly of the peripheral actin structures that drive B cell spreading, and that cofilin, Wdr1, and LIMK all contribute to the actin-dependent amplification of BCR signaling at the immune synapse. Depleting Cotl1 had no effect on these processes. Thus, the Wdr1-LIMK-cofilin axis is critical for BCR-induced actin remodeling and for B cell responses to APC-bound antigens.

Keywords: B cell, actin, immune synapse, cell spreading, cofilin, WDR1 (AIP1), LIM domain kinase, B cell receptor (BCR)

INTRODUCTION

Signaling by the B cell antigen receptor (BCR) initiates the B cell activation process. Activated B cells provide protective immunity by producing antibodies, secreting cytokines, and presenting antigens (Ags) to T cells, but can also contribute to autoimmunity (Conley et al., 2009; Shen and Fillatreau, 2015; Cashman et al., 2019; Cyster and Allen, 2019; Meffre and O'Connor, 2019). Within lymphoid organs, Ag-presenting cells (APCs) such as follicular dendritic cells, dendritic cells, and subcapsular sinus macrophages increase the efficiency of B cell activation by capturing

Ags and concentrating them on their surface (Batista and Harwood, 2009; Cyster, 2010; Heesters et al., 2016). The interaction of B cells with Ags that are mobile within a membrane initiates the reorganization of B-cell membrane proteins into an immune synapse, thereby enhancing both the signal transduction and Ag internalization functions of the BCR (Harwood and Batista, 2011; Song et al., 2014; Kuokkanen et al., 2015). Ag-bound BCRs rapidly form microclusters, which nucleate protein complexes that activate the signaling pathways controlled by phospholipase C, phosphoinositide 3-kinase, and the Ras, Rac, Cdc42, and Rap1 GTPases (Treanor et al., 2009; Packard and Cambier, 2013; Abraham et al., 2016). The centripetal movement and coalescence of BCR microclusters further amplifies microcluster-based BCR signaling, increasing the probability that the magnitude of BCR signaling exceeds the threshold for B cell activation (Bolger-Munro et al., 2019). Ultimately, BCR-Ag microclusters coalesce into a central supramolecular activation cluster (cSMAC) (Fleire et al., 2006). cSMAC formation may enhance BCR-mediated Ag internalization, which is required for B cells to present Ags to T cells and elicit second signals for B cell activation (Yuseff et al., 2013; Nowosad et al., 2016). Hence, elucidating the mechanisms that drive immune synapse formation is critical for understanding how APC-bound Ags activate B cells.

Dynamic remodeling of the actin cytoskeleton is required for immune synapse formation (Harwood and Batista, 2011; Song et al., 2014). We identified a critical role for actin-related protein 2/3 (Arp2/3) complex-nucleated actin polymerization in multiple aspects of this process (Bolger-Munro et al., 2019). The Arp2/3 complex binds to existing actin filaments and nucleates the formation of new filaments that grow at a 70° angle to the mother filament (Goley and Welch, 2006). This branched actin assembly creates a dendritic actin network that can exert outward force on the plasma membrane and drive the formation of broad lamellipodial protrusions (Mogilner and Oster, 1996). When B cells contact Ag-bearing surfaces, BCR-induced actin polymerization at the cell periphery allows B cells to extend membrane protrusions in order to scan more of the surface and encounter more Ag (Bolger-Munro et al., 2019). When Ags are mobile within a membrane, the B cell then retracts these membrane protrusions (Fleire et al., 2006), with BCR microclusters undergoing centripetal movement and coalescing into a cSMAC. We showed that these processes are driven by Arp2/3 complex-dependent actin retrograde flow (i.e., away from the cell periphery and toward the center of the cell-cell contact site) within the peripheral actin network (Bolger-Munro et al., 2019). Actin retrograde flow is a consequence of the elastic resistance of the cell membrane exerting an opposing inward force when actin polymerization at the cell membrane exerts outwards forces (Ponti et al., 2004). When the Arp2/3 complex is inhibited or depleted, the retraction of membrane protrusions is impaired, the centripetal movement of BCR microclusters is greatly reduced, and cSMAC formation is inhibited (Bolger-Munro et al., 2019). Importantly, this results in decreased microcluster-based BCR signaling and impaired B cell activation in response to APC-bound Ags (Bolger-Munro et al., 2019). Consistent with these findings, human mutations in the Arpc1B component of the Arp2/3 complex, or in activators of the Arp2/3 complex such as Wiskott-Aldrich Syndrome protein (WASp) and the Hem1 component of the WAVE regulatory complex, result in B cell dysfunction (Kahr et al., 2017; Kuijpers et al., 2017; Brigida et al., 2018; Candotti, 2018; Volpi et al., 2019; Cook et al., 2020; Sprenkeler et al., 2020).

Actin network assembly that is nucleated by the Arp2/3 complex occurs concurrently with the actions of actin disassembly factors such as cofilin, destrin (also known as actin-depolymerizing factor [ADF]), and gelsolin, which bind to and sever actin filaments (Ono, 2003; Bernstein and Bamburg, 2010; Shishkin et al., 2016). Released filament segments undergo depolymerization and the resulting actin monomers can be loaded with ATP and used for new actin polymerization (Kadzik et al., 2020). Actin network disassembly also releases Arp2/3 complexes from branch points, allowing them to be recycled and initiate the formation of new branches. In lamellipodia, the actions of the Arp2/3 complex and cofilin are tightly coupled but spatially separated (Carlier et al., 1997; Svitkina and Borisy, 1999). Cofilin severs older portions of actin filaments, which are further from the cell membrane, and in which the ATP bound to constituent actin monomers has been hydrolyzed to ADP (Pollard and Borisy, 2003; Bernstein and Bamburg, 2010). At the same time, Arp2/3 complex-dependent actin polymerization occurs primarily at the plasma membrane where membrane-bound activators of the Arp2/3 complex, such as WASp and WAVE, bind ATP-loaded actin monomers and deliver them directly to the Arp2/3 complex (Bieling et al., 2018; Mullins et al., 2018). This balanced actin polymerization and depolymerization is termed treadmilling (Carlier and Shekhar, 2017).

In addition to fueling actin polymerization, actin severing is essential for the remodeling of actin networks. Cofilin is a major actin-severing protein in murine splenic B cells (Freeman et al., 2011). We have previously shown that cofilin-mediated actin severing is required for B cell spreading as well as APC-induced microcluster formation and BCR signaling (Freeman et al., 2011). This suggests that proteins that regulate cofilin-mediated actin severing may also be important regulators of actin dynamics and immune synapse formation in B cells.

Cofilin activity is regulated by phosphorylation on serine 3 (S3), which prevents cofilin from binding to actin filaments (Bravo-Cordero et al., 2013). Dephosphorylation of cofilin on S3 causes a conformational change that allows cofilin to bind actin filaments and carry out its severing activity. The major phosphatases that dephosphorylate cofilin belong to the Slingshot (SSH) family (Niwa et al., 2002; Kanellos and Frame, 2016), although other widely expressed phosphatases such as PP1 and

Abbreviations: ADF, actin-depolymerizing factor; Ag, antigen; APC, antigen-presenting cell; Arp2/3, actin-related protein 2/3; BCR, B cell antigen receptor; BSA, bovine serum albumin; cSMAC, central supramolecular activation cluster; Cotl1, coactosin-like 1; F-actin, filamentous actin; FCS, fetal calf serum; HEL, hen egg lysozyme; Ig, immunoglobulin; ITAM, immunoreceptor tyrosine-based activation motif; LIMK, LIM domain kinase; LIMKi3, LIMK inhibitor 3; mHBS, modified HEPES-buffered saline; pCD79, phosphorylated CD79; PFA, paraformaldehyde; ROCK, Rho-associated protein kinase; STED, stimulated emission depletion; TIRF, total internal reflection fluorescence; TLR, Toll-like receptor; Wdr1, WD repeat-containing protein 1.

PP2A may also perform this function (Ambach et al., 2000; Ohashi, 2015). LIM domain kinase (LIMK) 1 and 2 are widely-expressed kinases that phosphorylate cofilin on S3 (Ohashi, 2015). The LIMKs are activated via phosphorylation by Rho-associated protein kinase (ROCK), a downstream target of the Rho GTPase, or by p21-activated kinase (PAK), an effector of the Rac and Cdc42 GTPases (Scott and Olson, 2007; Prunier et al., 2017). The Rho-ROCK-LIMK pathway modulates immune synapse formation and function in T cells (Thauland et al., 2017). Inhibiting cofilin activity by expressing constitutively active ROCK, or by depleting cofilin with siRNA, results in smaller immune synapses (i.e., less spreading on the APC surface) and decreased TCR-induced Ca^{2+} flux. Conversely, inhibiting the activity of ROCK or LIMK, which increases the amount of active cofilin, results in larger immune synapses, and increased Ca^{2+} flux. The role of LIMK in BCR-induced actin remodeling and B cell responses to APCs has not been investigated.

In addition to proteins that regulate the phosphorylation of cofilin on S3, a number of other proteins modulate cofilin-mediated actin severing. In this study we examined the role of WD repeat-containing protein 1 (Wdr1; also known as actin-interacting protein 1 [Aip1]) and coactosin-like protein 1 (Cotl1) in B cell spreading and responses to APCs. Wdr1 binds to cofilin-decorated actin filaments and increases the rate of cofilin-mediated actin severing (Rodal et al., 1999; Nadkarni and Brieher, 2014; Chen et al., 2015; Nomura et al., 2016; Ono, 2018). *In vitro*, actin filaments are stabilized when they are saturated with cofilin. However, Wdr1 optimizes the spacing of cofilin on actin filaments so that it is favorable for severing, which occurs when strain builds up at the boundaries between cofilin-decorated and bare regions (Elam et al., 2013; Gressin et al., 2015; Tanaka et al., 2018). Wdr1 creates cofilin-bare regions of actin filaments by competing with cofilin for binding to polymerized actin (Nadkarni and Brieher, 2014; Chen et al., 2015) or by inducing a conformational change in the actin binding site of cofilin that reduces its affinity for actin filaments (Aggeli et al., 2014). In addition, Wdr1-cofilin interactions at the boundary between cofilin-decorated and cofilin-bare regions of the filament promote severing at that site (Hayakawa et al., 2019). In yeast and in mammalian cell extracts the absence of Wdr1 results in reduced actin filament turnover, accumulation of actin filaments, and depletion of the actin monomer pool (Okreglak and Drubin, 2010; Nadkarni and Brieher, 2014). Importantly, loss-of-function mutations in human *Wdr1* are associated with an immunodeficiency syndrome characterized by defective motility of myeloid cells, aberrant T cell activation, and impaired B cell development (Pfajfer et al., 2018).

Cotl1 is a member of the cofilin/ADF superfamily (Shishkin et al., 2016) that is structurally homologous to cofilin and binds actin filaments with high affinity (Provost et al., 2001). *In vitro*, Cotl1 competes with cofilin for binding to actin filaments. However, in contrast to Wdr1 it stabilizes actin filaments and attenuates cofilin-mediated severing (Provost et al., 2001; Kim et al., 2014). In T cells, Cotl1 is recruited to the immune synapse where it promotes the formation of lamellipodial protrusions (Kim et al., 2014) but its function in B cells has not been studied.

Because cofilin initiates actin remodeling and fuels Arp2/3 complex-nucleated actin polymerization, we tested the hypothesis that the Wdr1-LIMK-cofilin axis and Cotl1 regulate B cell spreading, APC-induced BCR signaling, and cSMAC formation at the immune synapse.

MATERIALS AND METHODS

B Cells

The A20 murine IgG^+ B cell line was obtained from ATCC (#TIB-208). A20 D1.3 B cells, which express a transfected hen egg lysozyme (HEL)-specific BCR, were from F. Batista (Ragon Institute, Cambridge, MA) (Batista and Neuberger, 1998). Both cell lines were confirmed to be mycoplasma-negative and were cultured in RPMI-1640 supplemented with 5% heat-inactivated fetal calf serum (FCS), 2 mM glutamine, 1 mM pyruvate, 50 μM 2-mercaptoethanol, 50 U/mL penicillin, and 50 μg/mL streptomycin. A20 and A20 D1.3 B cells (2×10^6) were transiently transfected with 2 μg siRNA using AMAXA Cell Line Nucleofector Kit V (Lonza, #VCA-1003) or the Ingenio Electroporation Kit (Mirus, #MIR 50118). The siRNAs used were control non-targeting siRNA (ON-TARGETplus Non-Targeting Pool, Dharmacon, #D-00810-01-05), cofilin-1 siRNA (Dharmacon, #L-058638-01-0005), Wdr1 siRNA (SMARTpool ON-TARGETplus, Dharmacon, #L-047667-01-005), and Cotl1 siRNA (ON-TARGETplus, Dharmacon, #L-042151-01-005). Transfected A20 and A20 D1.3 B cells were cultured for 48 h before being used for experiments. siRNA-mediated decreases in protein levels were assessed by immunoblotting (see below). Murine primary B cells were isolated from the spleens of 8-−12-week old C57BL/6J mice (Jackson Laboratories, #000664) or MD4 mice (Jackson Laboratories, #002595) of either sex using a negative selection B cell isolation kit (Stemcell Technologies, #19854A). Animal protocols were approved by the University of British Columbia Animal Care Committee. Where indicated, *ex vivo* primary B cells, A20 B cells, or A20 D1.3 B cells were pre-treated for 1 h with the LIMK inhibitor, LIMKi3 (Tocris, #4745) (Ross-Macdonald et al., 2008; Scott et al., 2010), or with an equal volume of DMSO.

Analysis of Cell Surface BCR Levels and Filamentous Actin Content by Flow Cytometry

A20 or A20 D1.3 B cells that had been transfected with siRNA, or treated with either DMSO or LIMKi3, were fixed with 4% paraformaldehyde (PFA) in PBS for 10 min at room temperature and then resuspended in ice-cold FACS buffer (PBS, 2% FCS, 0.02% NaN_3). Fc receptors were blocked by adding 25 μg/mL of the 2.4G2 anti-mouse CD16/CD32 monoclonal antibody for 5 min on ice. To assess cell surface BCR levels, the cells were stained on ice for 30 min with goat anti-mouse IgG-Alexa Fluor 647 (Invitrogen, #A21236, 1:200) or with rat anti-mouse IgM-FITC (eBiosciences, #11-5890-85, 1:200) to detect the D1.3 BCR. Intracellular filamentous actin (F-actin) was detected by permeabilizing the PFA-fixed cells with 0.2% Triton X-100 for 5 min on ice and then staining with rhodamine-phalloidin

(Invitrogen, #R415, 1:100) for 30 min on ice. Flow cytometry was performed using an LSRII-561 cytometer (Becton Dickinson Biosciences) and data were analyzed using FlowJo software (Treestar Inc.), gating on single intact cells using forward and side scatter.

BCR Signaling in Response to Soluble Anti-Ig

B cells were resuspended to 2×10^7 cells/mL in modified HEPES-suffered saline (mHBS; 25 mM HEPES, pH 7.2, 125 mM NaCl, 5 mM KCl, 1 mM $CaCl_2$, 1 mM Na_2HPO_4, 1 mg/mL glucose, 2 mM glutamine, 1 mM pyruvate, 50 μM 2-mercaptoethanol). The cells (3×10^6 in 150 μL) were then stimulated with 20 μg/mL goat anti-mouse IgG (Jackson ImmunoResearch, #115-005-008) or goat anti-mouse IgM (Jackson ImmunoResearch, ##115-005-020) for the indicated times at 37°C. Reactions were stopped by adding cold PBS with 1 mM Na_3VO_4. The cells were then pelleted for 5 min at 640 RCF at 4°C and lysed in RIPA buffer (30 mM Tris-HCl, pH 7.4, 150 mM NaCl, 1% Igepal (Sigma-Aldrich), 0.5% sodium deoxycholate, 0.1% SDS, 2 mM EDTA) with protease and phosphatase inhibitors (1 mM phenylmethylsulfonyl fluoride, 10 μg/mL leupeptin, 1 μg/mL aprotinin, 1 μg/mL pepstatin A, 10 μg/mL soybean trypsin inhibitor, 25 mM β-glycerophosphate, 1 mM Na_3MoO_4, 1 mM Na_3VO_4). Protein concentrations were determined using the bicinchoninic acid assay (Thermo Fisher, #23225). Cell extracts were analyzed by immunoblotting.

Immunoblotting

Cell extracts were separated on 12% SDS-PAGE gels and transferred to nitrocellulose membranes, which were blocked with 5% milk powder in Tris-buffered saline (10 mM Tris-HCl, pH 8, 150 mM NaCl). The membranes were incubated overnight at 4°C with mouse anti-Wdr1 (Santa Cruz, #sc-393159; 1:500), sheep anti-Cotl1 (R&D Systems, #AF7865; 1:500), rabbit anti-CD79a (1:5,000) (Gold et al., 1991), or the following rabbit antibodies from Cell Signaling Technologies: phosphorylated CD79a (pCD79a; #5173; 1:1,000), phosphorylated Erk (pERK; #9101; 1:1,000), Erk (#9102, 1:1,000), phosphorylated cofilin (p-cofilin; #3313; 1:1,000), or cofilin (#3318; 1:1,000). Immunoreactive bands were visualized using horseradish peroxidase-conjugated goat anti-rabbit IgG (Bio-Rad, #170-6515; 1:3,000), mouse Igκ-binding protein (Santa Cruz, #sc-516102, 1:2,000), or donkey anti-sheep IgG (R&D Systems, #HAF016, 1:1,000), followed by ECL detection (Azure Biosystems, #AC2010). All antibodies were diluted in Tris-buffered saline. Blots were quantified and imaged using a Li-Cor C-DiGit imaging system.

Ca^{2+} Flux Assays

A20 or A20 D1.3 B cells that had been transfected with siRNA, or treated with DMSO or LIMKi3, were washed twice with Hanks' Balanced Salt Solution (HBSS) containing 10 mM HEPES and resuspended to 10^7 per mL before adding 2 μM Fura Red (Invitrogen, #F3021), 1 μM Fluo-4 (Invitrogen, #F14201), and 0.02% Pluronic F-127 (Invitrogen, #P3000MP). The cells were then incubated for 30 min at room temperature protected from light, washed with HBSS/10 mM HEPES/2% FCS, resuspended to 10^7/mL, and incubated for an additional 20 min protected from light. Flow cytometry was performed using an LSRII-561 cytometer (Becton Dickinson Biosciences). For each sample, 1–3×10^6 cells were pelleted and resuspended in 0.5 mL mHBS, with paired samples having similar number of cells. Samples were analyzed for 1 min to establish baseline values before adding either goat anti-mouse IgG (Jackson ImmunoResearch, #115-005-008, 20 μg/mL) for A20 B cells or goat anti-mouse IgM (Jackson ImmunoResearch, #115-005-020, 20 μg/mL) for A20 D1.3 B cells, and then analyzing the cells for an additional 5 min. Ionomycin (1 μM; Invitrogen, # I24222) was added to saturate the Ca^{2+}-sensing dyes and the cells were analyzed for an additional 1 min. Data were analyzed using FlowJo software (Treestar Inc.), gating on single intact cells using forward and side scatter.

Cell Area, Actin Organization, and Actin Dynamics in B Cells Spreading on Immobilized Anti-Ig

Glass coverslips were coated with 2.5 μg/cm^2 goat anti-mouse IgG (Jackson ImmunoResearch, #115-005-008) and then blocked with 2% bovine serum albumin (BSA) in PBS, as described previously (Lin et al., 2008). A20 B cells were resuspended in mHBS, or in mHBS + 2% FCS (imaging medium) before adding 7.5×10^4 cells (in 100 μL) to each coverslip. At the indicated times, the cells were fixed with 4% PFA for 10 min and then permeabilized with 0.2% Triton X-100 in PBS for 5 min at room temperature. F-actin was visualized by staining with rhodamine-conjugated phalloidin (Thermo Fisher, #R415, 1:400 in PBS + 2% BSA) for 30 min at room temperature. Coverslips were mounted onto slides using ProLong Diamond anti-fade reagent (Thermo Fisher, #P36965). Images of the B cell-coverslip interface were captured using a laser scanning confocal microscope (Leica Microsystems TCS SP5) with a 60X NA 1.4 oil objective lens. The cell area, as well as the percent of the cell area that was depleted of F-actin, was quantified from thresholded binary images using Fiji software (Schindelin et al., 2012). The outer face of the peripheral actin ring was used to define the cell edge and compute the total cell area. The inner face of the peripheral actin ring was used to delimit the central actin-depleted region of the cell and calculate its area.

For live-cell imaging at 37°C, A20 B cells were transfected with a plasmid encoding F-tractin-GFP (Johnson and Schell, 2009), or co-transfected with F-tractin-GFP and siRNAs, 48 h before being used for experiments. Cells (5×10^4 in 100 μL imaging medium) were added to anti-IgG-coated coverslips and the cell-coverslip contact site was imaged by total internal reflection fluorescence (TIRF) microscopy. Images were acquired every 1 s for 10 min using an Olympus IX81 inverted microscope equipped with a 150X NA 1.45 TIRF objective, a high performance electron multiplier charge-coupled device camera (Photometrics Evolve), and real-time data acquisition software (Metamorph). Fiji software was used to quantify cell area and generate kymographs.

Stimulated emission depletion (STED) microscopy was performed as described previously (Wang et al., 2018). A20

B cells (5×10^4 in 100 μL imaging medium) were allowed to spread on anti-IgG-coated coverslips before being fixed and permeabilized, as above, and then stained with Alexa Fluor 532-conjugated-phalloidin (Thermo Fisher, #A22282). STED images were acquired using a Leica TCS SP8 laser scanning STED system with a 592 nm depletion laser, a CX PL APO 100X NA 1.40 oil objective, and a Leica HyD high sensitivity detector. Huygens software (Scientific Volume Imaging, Hilversum, Netherlands) was used for image deconvolution.

APC-Induced cSMAC Formation and BCR Signaling

B cell-APC interactions were analyzed as described previously (Wang et al., 2018; Bolger-Munro et al., 2019). Ag-bearing APCs were generated by transiently transfecting COS-7 cells (ATCC, #CRL-1651) with a plasmid encoding the mHEL-HaloTag Ag. The mHEL-HaloTag protein contains the complete HEL protein in its extracellular domain, the transmembrane and cytosolic domains of the H-$2K^b$ protein, and the HaloTag protein fused to the C-terminus of the H-$2K^b$ cytosolic domain (Wang et al., 2018). mHEL-HaloTag-transfected COS-7 cells (2.2×10^4 cells per coverslip) were plated on glass coverslips (Thermo Fisher #12-545-100) that had been coated with 5 μg/mL fibronectin (Sigma-Aldrich, #F4759). After culturing the cells overnight, the coverslips were washed with PBS and the mHEL-HaloTag protein was labeled with the Janelia Fluor 549 HaloTag ligand (Promega, #GA1110, 1:20,000 dilution in 0.2 mL imaging medium) for 15 min at 37°C. After washing the coverslips, siRNA-transfected or inhibitor-treated B cells (5×10^5 in 100 μL imaging medium) were added to the COS-7 APCs for 3–30 min at 37°C. The cells were then fixed with 4% PFA for 10 min, permeabilized with 0.1% Triton X-100 in PBS for 3 min, and blocked with 2% BSA in PBS for 30 min, all at room temperature. The cells were stained for 1 h at room temperature with an antibody that recognizes pCD79 (Cell Signaling Technologies, #5173, 1:200 in PBS + 2% FCS), washed, and then incubated for 30 min at room temperature with Alexa Fluor 647-conjugated goat anti-rabbit IgG secondary antibody (Thermo Fisher, #A21244, 1:400 in PBS + 2% FCS) plus Alexa Fluor 488-conjugated phalloidin (Thermo Fisher, #A12379, 1:400). Coverslips were mounted onto slides and the B cell-APC interface was imaged by spinning disk confocal microscopy. For each B cell, custom Fiji macros[1] were used to quantify the total amount of pCD79 fluorescence and mHEL-HaloTag fluorescence present in clusters at the B cell-APC interface, as well as the Ag fluorescence intensity for each microcluster on an individual B cell. A cell was deemed to have formed a cSMAC when >90% of the clustered Ag fluorescence had been gathered into one or two large clusters at the center of the synapse, as defined previously (Bolger-Munro et al., 2019).

Statistical Analysis

Two-tailed paired *t*-tests were used to compare mean values for matched sets of samples. The Mann-Whitney *U* test was used to compare ranked values in samples with many cells and high variability (e.g., dot plots for immunofluorescence signaling data). Robust Regression and Outlier Removal (ROUT) was implemented in GraphPad Prism, with Q set to 1%, in order to remove outliers (Motulsky and Brown, 2006).

[1]https://github.com/mbolgermunro/FIJImacros/blob/master/APC_analyser_MBM.ijm

RESULTS

Targeting Cofilin and Its Regulators

To investigate the role of the Wdr1-LIMK-cofilin axis in BCR-induced actin reorganization, we used four different approaches to modulate either the actin-binding capability of cofilin or the ability of cofilin to promote filament severing (**Figure 1A**). We used siRNA to deplete either cofilin-1, the non-muscle isoform of cofilin, or its positive co-factor Wdr1. Cotl1, which may limit cofilin-mediated severing, was also depleted using siRNA. Immunoblotting showed that transfecting A20 B-lymphoma cells with these siRNAs routinely resulted in >90% reduction in the levels of the corresponding proteins, compared to cells transfected with a control non-targeting siRNA (**Figure 1B**). To increase the amount of "active" cofilin that is capable of binding to actin filaments, we used LIMKi3, a pharmacological inhibitor of LIMK, the kinase that phosphorylates cofilin on S3. Treating either A20 B cells or murine splenic B cells with LIMKi3 resulted in decreased phosphorylation of cofilin on S3 (**Figures 1C,D**). In control B cells, the inactive S3-phosphorylated form of cofilin (p-cofilin) was present at high levels in resting cells but decreased transiently after stimulation with soluble anti-Ig antibodies that cluster the BCR, as reported previously (Freeman et al., 2011, 2015). In LIMKi3-treated B cells, p-cofilin levels were lower than in control cells both before and after anti-Ig stimulation. Thus, inhibition of LIMK by LIMKi3 increased the amount of dephosphorylated active cofilin in the cells.

Surprisingly, depleting Wdr1 in A20 B cells also resulted in cofilin activation, as indicated by a substantial reduction in the amount of inactive S3-phosphorylated cofilin (**Figure 1E**). Similar observations have been reported in developing zebrafish neutrophils, where Wdr1 depletion results in constitutive activation of cofilin but an accumulation of actin filaments that is likely due to reduced actin severing by cofilin when Wdr1 is absent (Bowes et al., 2019). Indeed, we show below that depleting Wdr1 largely phenocopied the effects of depleting cofilin, presumably because Wdr1 optimizes cofilin-mediated filament severing.

Finally, consistent with cofilin having a major role in severing actin filaments in B cells, flow cytometry analysis showed that the amount of F-actin per cell in cofilin siRNA-transfected A20 B cells was 121.5 ± 4.8% of that in control siRNA-transfected cells ($N = 3$ independent experiments, $p = 0.046$), even though the cells were the same size (**Supplementary Table 1**). Similar results were obtained using A20 D1.3 B cells, which express a HEL-specific transgenic BCR. Targeting the cofilin regulators Wdr1 and LIMK did not have statistically significant effects on total F-actin levels (**Supplementary Table 1**).

The Wdr1-LIMK-Cofilin Axis Controls B Cell Spreading on Immobilized Anti-Ig

When B cells are added to anti-Ig-coated coverslips, BCR signaling initiates remodeling of the actin cytoskeleton. Arp2/3 complex-nucleated actin polymerization at the periphery exerts

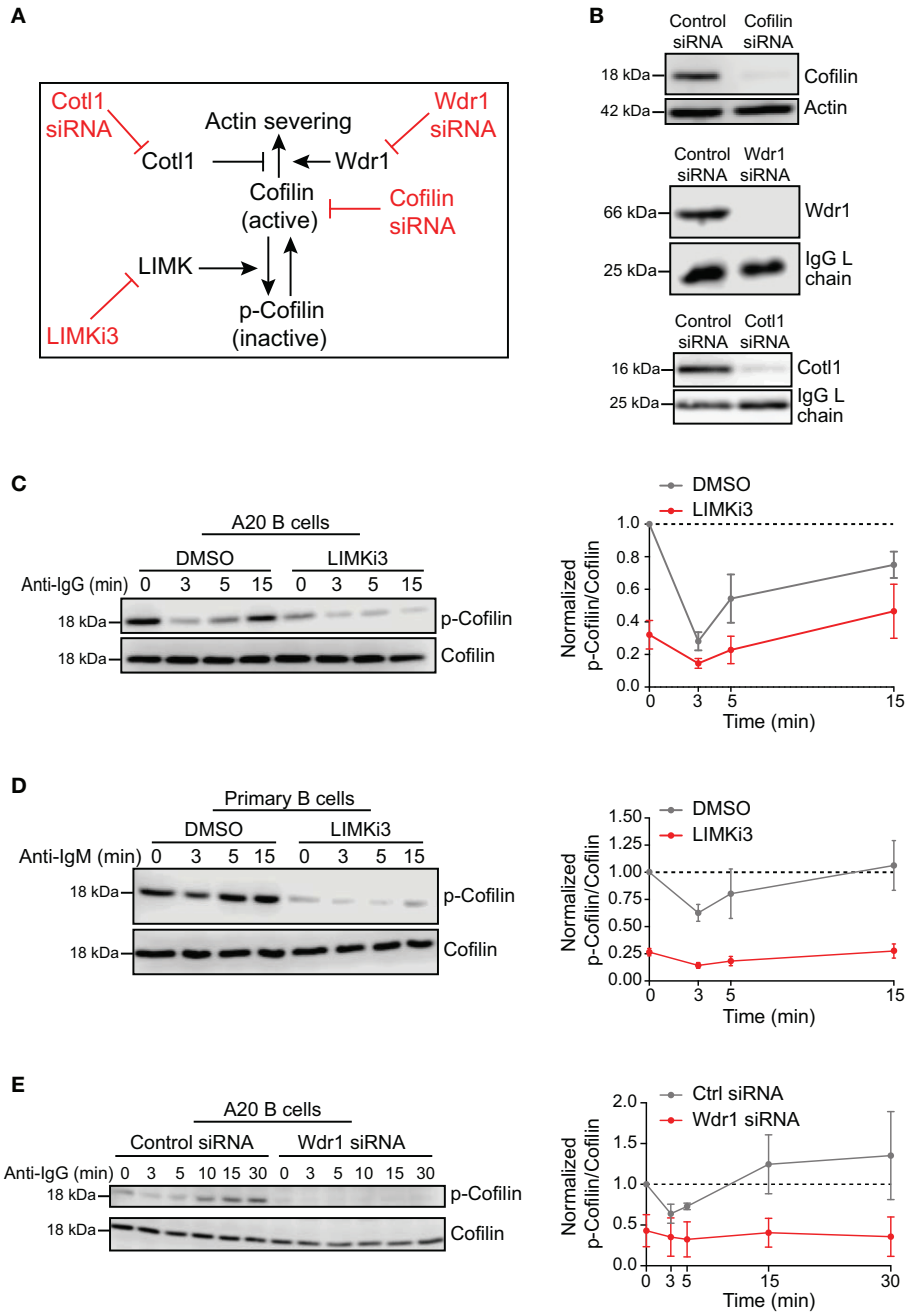

FIGURE 1 | Loss-of-function approaches for modulating cofilin activation and cofilin-mediated actin severing. **(A)** To complement siRNA-mediated depletion of cofilin, cofilin activation was enhanced by inhibiting LIMK, which phosphorylates cofilin on S3. The ability of cofilin to sever actin filaments was modulated by depleting either Wdr1 or Cotl1. **(B)** A20 B cells were transfected with control non-targeting siRNA, cofilin siRNA, Wdr1 siRNA, or Cotl1 siRNA. Cell extracts were analyzed by immunoblotting. Loading controls were actin or the endogenous Ig light (L) chain of the A20 B cells. Representative blots are shown. **(C–E)** In C, A20 B cells were pre-treated with DMSO or 50 μM LIMKi3 for 1 h before being stimulated with 20 μg/mL anti-IgG for the indicated times. In **(D)**, primary murine B cells were pre-treated with DMSO or 1 μM LIMKi3 for 1 h before being stimulated with 20 μg/mL anti-IgM. In **(E)**, A20 B cells that had been transfected with control siRNA or Wdr1 siRNA were stimulated with 20 μg/mL anti-IgG. Representative p-cofilin and total cofilin immunoblots are shown (left panels). The p-cofilin/total cofilin ratios were normalized to the ratio in unstimulated (0 min) control cells (=1.0). The means ± SEM from three independent experiments are graphed for each time point (right panels).

outward force on the cell membrane that drives the formation of broad lamellipodia-like protrusions. At the same time, F-actin is depleted from the center of the cell-substrate contract site, resulting in a distinct peripheral ring of branched F-actin. In addition to mimicking the initial stages of B cell-APC interactions, this system provides a robust discovery

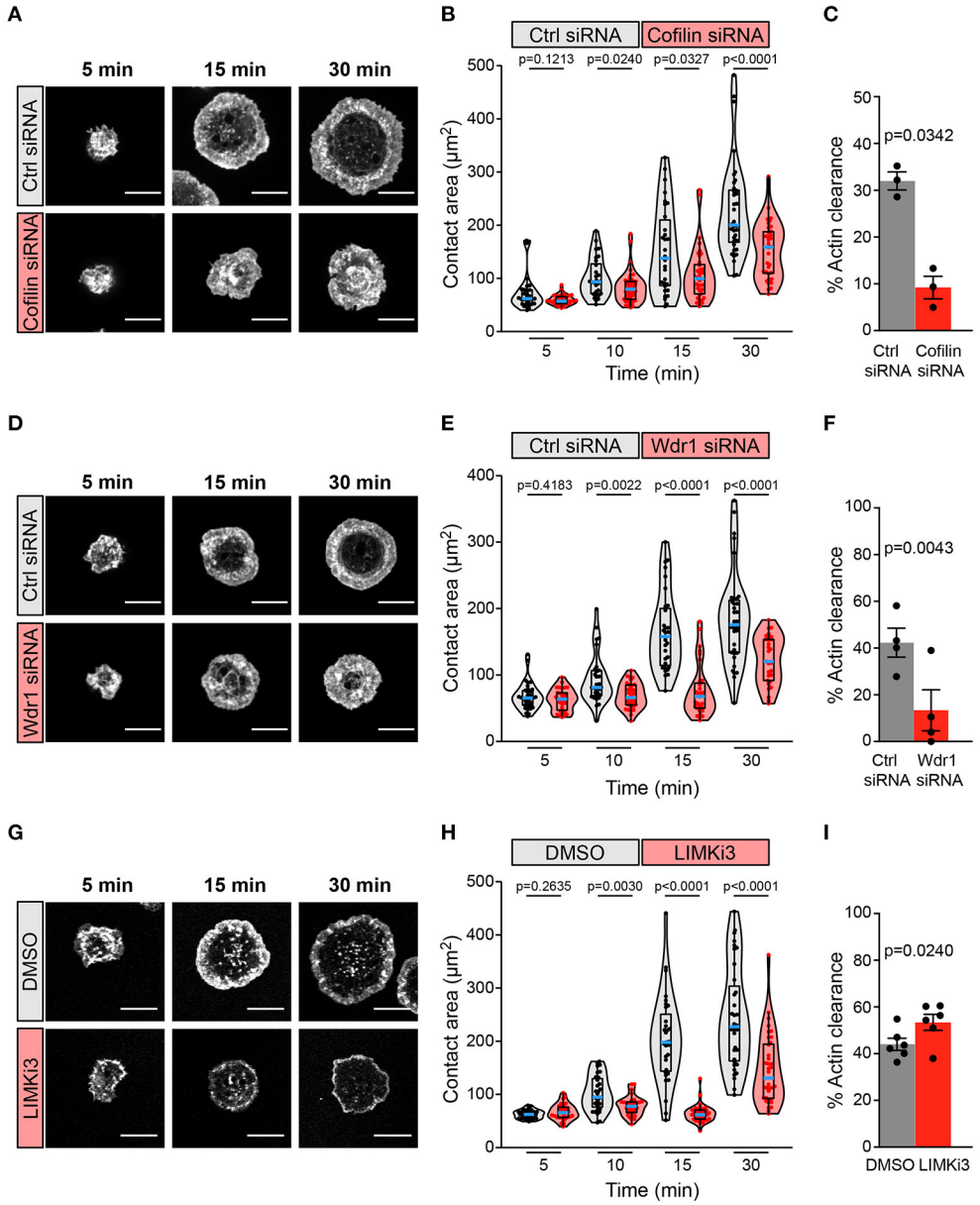

FIGURE 2 | The Wdr1-cofilin-LIMK axis regulates B-cell spreading on immobilized anti-Ig. A20 B cells were transfected with control (Ctrl) siRNA or cofilin siRNA **(A–C)**, transfected with control (Ctrl) siRNA or Wdr1 siRNA **(D–F)**, or pre-treated with DMSO or 50 μM LIMKi3 for 1 h **(G–I)**. The cells were then allowed to spread on anti-IgG-coated coverslips for the indicated times before being stained with rhodamine-phalloidin and imaged by confocal microscopy. Representative images are shown **(A,D,G)**. Scale bars: 10 μm. In **(B,E,H)** the cell area was quantified using the actin staining to define the cell edge. Each dot in the beeswarm plots represents one cell and the median (blue line) and interquartile ranges (black box) for >30 cells are shown for each time point. Representative data from one of three **(B)**, four **(E)**, or six **(H)** independent experiments are shown. p-values were determined using the Mann-Whitney *U* test. In **(C,F,I)** the percent of the total cell area at the substrate contact site that was cleared of F-actin after 30 min was quantified by using the actin staining to define both the outer cell edge and the inner face of the peripheral actin ring that surrounds the central actin-depleted region of the cell (see **Supplementary Figure 1** for examples). For each experiment, the median percent actin clearance was determined for each treatment group. Representative experiments are shown in **Supplementary Figure 1**. The bar graphs show the means ± SEM for these median values from three **(C)**, four **(F)**, or six **(I)** independent experiments, each of which is represented by a dot. p-values were determined using a two-tailed paired *t*-test.

platform for identifying proteins that regulate BCR-induced actin remodeling.

We found that siRNA-mediated depletion of cofilin greatly impaired BCR-induced cell spreading and actin remodeling when A20 B cells were added to anti-IgG-coated coverslips (**Figures 2A–C**). The cofilin siRNA-transfected cells had significantly smaller substrate contact areas at the 10, 15, and 30 min time points than cells that were transfected with a

control non-targeting siRNA (**Figures 2A,B**). BCR-induced actin reorganization was also dramatically altered. After 15 and 30 min of contact with the anti-IgG-coated coverslips, control A20 B cells developed a dense F-actin ring at the periphery of the substrate contact site while the central region of the contact site was relatively devoid of F-actin structures (**Figure 2A**; see also **Figure 3A**). Many of the cofilin siRNA-transfected A20 B cells did not effectively clear F-actin from the central region of the contact site. To quantify this, we calculated the percent of the total cell area that was depleted of actin filaments after 30 min of spreading. Single-cell analysis from one representative experiment showed that virtually all control siRNA-transfected A20 B cells cleared actin from at least 20% of the total cell-substrate contact area (median = 32%; **Supplementary Figures 1A,B**). In contrast, the cofilin siRNA-transfected cells from the same experiment had a bimodal distribution in which some cells cleared actin from >20% of the contact area but the majority of the cells exhibited reduced actin clearance and a substantial fraction did not clear actin from the center of the contact site (median = 9% of contact area cleared of actin; **Supplementary Figures 1A,B**). It is possible that the siRNA-mediated depletion of cofilin may have been incomplete in some of the cells that exhibited normal actin clearance. Nevertheless, comparing the median percent actin clearance from three experiments showed that transfection with cofilin siRNA resulted in a highly reproducible reduction in actin clearance (**Figure 2C**).

A20 B cells that had been transfected with Wdr1 siRNA also exhibited a significantly impaired spreading response at 10, 15, and 30 min after addition to anti-IgG-coated coverslips, and this was associated with reduced actin clearance at the center of the contact site (**Figures 2D–F**; see also **Figure 3B**). Single-cell analysis from one representative experiment showed that almost all control siRNA-transfected A20 B cells cleared actin from more than 20% of the total contact area (median = 43%; **Supplementary Figures 1C,D**) whereas Wdr1 siRNA-transfected cells exhibited a bimodal distribution with a substantially lower median percent actin clearance (median = 10%; **Supplementary Figures 1C,D**), similar to cofilin siRNA-transfected cells. Nevertheless, the median percent actin clearance was consistently and significantly reduced in four experiments comparing control siRNA- and Wdr1 siRNA-transfected A20 B cells (**Figure 2F**). Because siRNA transfection does not result in complete protein depletion in all cells, we could be underestimating the effect of complete loss of Wdr1. Thus, depleting either cofilin or Wdr1 results in decreased cell spreading, reduced actin clearance, and increased thickness of the peripheral actin ring. These findings are consistent with the idea that cofilin-mediated actin severing is essential for the BCR-induced actin reorganization that drives cell spreading and that Wdr1 is required for the cofilin-mediated severing of actin filaments.

Based on these findings we hypothesized that enhancing cofilin activity by inhibiting its negative regulator, LIMK, would increase B cell spreading. Surprisingly, pre-treating A20 B cells with LIMKi3 significantly reduced B cell spreading on anti-IgG-coated coverslips (**Figures 2G,H**). However, in striking contrast to depleting either cofilin or Wdr1 depletion, LIMKi3-treated B cells exhibited a thinner peripheral actin ring (**Figure 2G;** see also **Figure 3C**), which corresponded with a greater percent of the cell area being cleared of actin (**Figures 2G,I** and **Supplementary Figures 1E,F**). This could be a consequence of increased cofilin-mediated actin severing at the inner face of the peripheral actin ring. These results indicate that LIMK activity regulates BCR-induced actin remodeling and that cofilin activity must be precisely regulated in order to maximize the branched actin polymerization that drives B cell spreading.

Because Cotl1 competes with cofilin for binding to F-actin, we hypothesized that depleting Cotl1 would result in increased cofilin-mediated actin severing and reproduce the effect of inhibiting LIMK. However, we found that substantial depletion of Cotl1 (**Figure 1B**) had no effect on the ability of A20 B cells to spread on immobilized anti-IgG (**Supplementary Figure 2**). Thus, Cotl1 is not an essential, non-redundant regulator of BCR-induced actin remodeling, at least in A20 B cells.

To gain further insights into how targeting the Wdr1-LIMK-cofilin axis impairs BCR-induced cell spreading we used STED super-resolution microscopy to visualize changes in actin network architecture. When control A20 B cells were added to anti-IgG-coated coverslips, protrusions containing branched actin networks was first observed at 5 min, concomitant with the appearance of a central actin-depleted region (**Figures 3A–C**). By 10 min, the cells had assembled a thick peripheral ring of branched actin. As well, linear actin filaments formed into arc-like structures that were parallel to the inner face of peripheral actin ring and surrounded the actin-depleted region at the center of the contact site. Actin arcs, which are often associated with myosin, have been observed at T- and B-cell immune synapses (Murugesan et al., 2016; Bolger-Munro et al., 2019). When cofilin was depleted, the A20 B cells were unable to clear actin from the center of the contact site. Instead, many of these cells accumulated concentric actin arc-like structures and rings at the center of the contact site (**Figure 3A**). Wdr1-depleted A20 B cells also exhibited defective actin clearance at the center of the contact site, although some of these cells did not organize actin into concentric arc-like structures at the center of the contact site as extensively as the cofilin-depleted A20 B cells (**Figure 3B**). Conversely, A20 B cells treated with the LIMK inhibitor exhibited larger actin-depleted central regions and much thinner peripheral rings of branched actin than control cells (**Figure 3C**). Interestingly, depleting cofilin or Wdr1, as well as increasing cofilin activity by inhibiting LIMK, delayed the ability of A20 B cells to initiate actin reorganization and form a peripheral ring of branched actin (**Figures 3A–C**). Control cells formed a distinct peripheral actin ring surrounding an actin-depleted central region within 5–10 min of being added to anti-IgG-coated coverslips. In contrast, when the Wdr1-LIMK-cofilin axis was perturbed, the peripheral actin structures were disorganized at the earlier time points and a distinct peripheral ring of branched actin did not develop until the 15 or 30 min time points. This altered peripheral actin architecture was associated with decreased cell spreading. Thus,

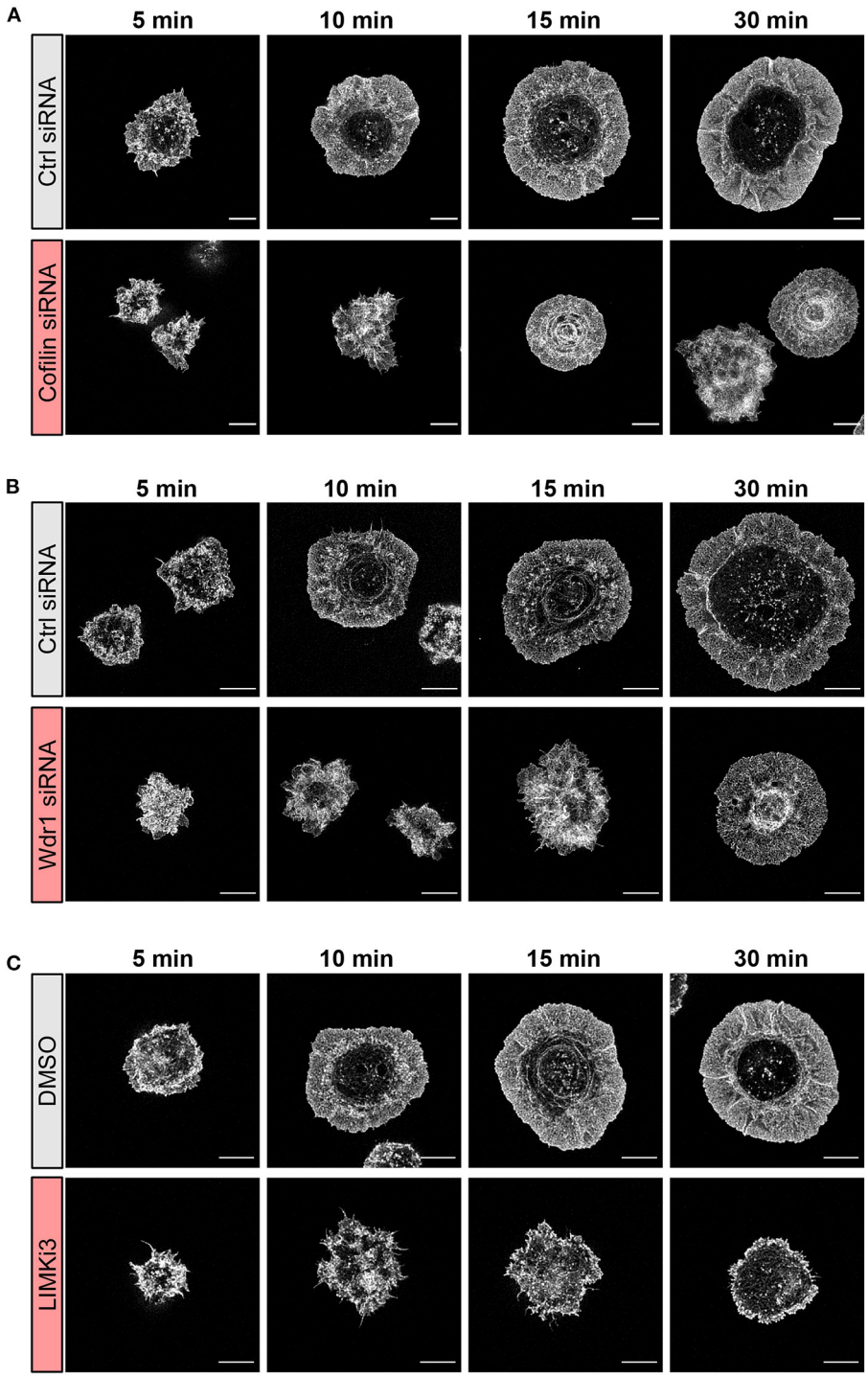

FIGURE 3 | The Wdr1-LIMK-cofilin network shapes actin network architecture in B cells spreading on immobilized anti-IgG. A20 B cells were **(A)** transfected with control (Ctrl) siRNA or cofilin siRNA, **(B)** transfected with control (Ctrl) siRNA or Wdr1 siRNA, or **(C)** pre-treated with DMSO or 50 μM LIMKi3 for 1 h. The cells were then allowed to spread on anti-IgG-coated coverslips for the indicated times before being fixed, stained for F-actin, and imaged by STED microscopy. Representative images are shown. Scale bars: 5 μm.

properly regulated cofilin activity is important for establishing the peripheral branched actin structures that drive B cell spreading on rigid substrates.

Finally, we ruled out the possibility that the impaired anti-IgG-induced spreading caused by targeting Wdr1, cofilin, or LIMK was due to reductions in BCR cell surface levels or BCR

signaling, as opposed to specific effects on actin remodeling. Flow cytometry showed that targeting Wdr1, cofilin, or LIMK did not have a significant effect on the amount of IgG-BCRs on the surface of A20 B cells and did not alter the size of the cells (**Supplementary Table 1**). We also analyzed BCR signaling in response to soluble anti-Ig antibodies, which is much less dependent on actin dynamics and organization than BCR signaling in response to APC-bound Ags that induce immune synapse formation (Bolger-Munro et al., 2019). An essential initial event in BCR signaling is phosphorylation of the immunoreceptor tyrosine-based activation motifs (ITAMs) in the CD79a/CD79b subunit of the BCR by the Lyn and Syk tyrosine kinases (Packard and Cambier, 2013). This enables the formation of signaling complexes that lead to downstream signaling reactions including ERK activation and increases in cytoplasmic Ca^{2+}. In A20 B cells, we found that depleting cofilin, depleting Wdr1, or treating the cells with LIMKi3 had no effect on the ability of soluble anti-Ig antibodies to stimulate the phosphorylation of CD79a/CD79b or ERK (**Supplementary Figure 3**). Similarly, depleting either cofilin or Wdr1 in A20 B cells or in the HEL-specific A20 D1.3 B cells did not alter Ca^{2+} responses to soluble anti-Ig antibodies (**Supplementary Figure 4**).

The Wdr1-LIMK-Cofilin Axis Regulates Actin Dynamics in B Cells

To visualize how cofilin, Wdr1, and LIMK modulate BCR-induced actin remodeling in real time, A20 B cells were transfected with F-tractin-GFP, a fluorescent fusion protein that binds dynamically to F-actin. The cells were either co-transfected with cofilin or Wdr1 siRNAs, or treated with LIMKi3, prior to being added to anti-IgG-coated coverslips and imaged by TIRF microscopy. We found that cofilin depletion, Wdr1 depletion, and LIMK inhibition all resulted in reduced spreading, as shown in **Figure 2**, and that this was accompanied by impaired peripheral actin dynamics (**Figure 4**). Arp2/3 complex-nucleated branch actin polymerization at the plasma membrane exerts outward forces that are opposed by the elastic resistance of the plasma membrane. This results in actin retrograde flow toward the center of the cell, which can be visualized by kymograph analysis. This actin retrograde flow was evident in control A20 B cells spreading on anti-IgG-coated coverslips (**Figures 4A,B** and **Supplementary Movies 1, 4**), as we have shown previously (Bolger-Munro et al., 2019). However, when cofilin or Wdr1 were depleted (**Figure 4A** and **Supplementary Movies 2, 3**), and when LIMK was inhibited (**Figure 4B** and **Supplementary Movie 5**), the peripheral actin network was relatively static and the retrograde actin flow was substantially reduced compared to control cells. To quantify this, we used the kymographs to calculate the centripetal velocity ($\Delta x/\Delta t$) for multiple actin tracks. This analysis showed that targeting cofilin, Wdr1, or LIMK reduced the median velocity of the actin retrograde flow by 50, 67, and 89%, respectively (**Figures 4C,D**). Thus, interfering with the Wdr1-LIMK-cofilin regulatory network inhibits the peripheral actin dynamics that occur when B cells spread on anti-Ig-coated coverslips.

APC-Induced cSMAC Formation and CD79 Phosphorylation Is Regulated by the Wdr1-LIMK-Cofilin Axis

When B cells interact with Ag-bearing APCs, Arp2/3 complex-dependent actin dynamics drives the centripetal movement and coalescence of BCR-Ag microclusters, which amplifies microcluster-based BCR signaling and leads to cSMAC formation (Bolger-Munro et al., 2019). This Arp2/3 complex-dependent amplification of microcluster-associated CD79 phosphorylation is most evident during the first 10 min after adding B cells to APCs. Importantly, a combination of wash-in and wash-out experiments with the Arp2/3 complex inhibitor CK-666 showed that ablating this BCR signal amplification during the initial stages of B cell-APC interaction impaired subsequent B cell activation responses. Because cofilin-mediated actin disassembly may support Arp2/3 complex-nucleated actin polymerization by recycling actin monomers and Arp2/3 complexes, we asked whether the Wdr1-LIMK-cofilin axis regulates B cell responses to APC-bound Ags.

To study Ag-specific B cell-APC interactions, A20 D1.3 B cells with a HEL-specific BCR were added to COS-7 APCs expressing the fluorescently-labeled mHEL-HaloTag Ag on their surface. The mHEL-HaloTag Ag is a transmembrane protein that contains the complete HEL protein in its extracellular domain. After 3–30 min of B cell-APC interaction, the cells were fixed and stained with an antibody that recognizes the phosphorylated CD79a/CD79b ITAMs in the cytoplasmic domains of the BCR signaling subunit. Ag-induced phosphorylation of the CD79a/CD79b ITAMs is an essential early event in BCR signaling. Imaging the B cell-APC interface allowed us to visualize BCR-Ag microclusters, monitor their coalescence into a cSMAC, and quantify the amount of pCD79 and mHEL-HaloTag Ag fluorescence that was present in microclusters.

We focused first on Wdr1 because its role in B-cell immune synapse formation and APC-induced BCR signaling has not been investigated. When control siRNA-expressing A20 D1.3 B cells were added to mHEL-HaloTag-expressing APCs, BCR-Ag microclusters formed rapidly at the B cell-APC contact site and co-localized with pCD79 clusters (**Figure 5A**). By 30 min, nearly all of the cells had coalesced BCR-Ag microclusters into a cSMAC (**Figure 5B**), which we define as >90% of the Ag fluorescence being contained in 1-2 large clusters at the center of the synapse. For this analysis, we quantified the Ag fluorescence intensity that was associated with each discrete cluster on an individual B cell and then expressed it as a percent of the total Ag fluorescence intensity for all clusters on that cell. The distribution of total Ag fluorescence intensity into individual clusters is shown for multiple cells in **Supplementary Figure 5**. When Wdr1 was depleted using siRNA, BCR-Ag microclusters formed at the B cell-APC contact site (**Figure 5A**). However, the percent of cells that formed a cSMAC was consistently lower than in control cells (**Figure 5B** and **Supplementary Figure 5A**), even though the Wdr1-depleted cells gathered more Ag into clusters at some time points (**Figure 5C**). In **Figure 5A**, the Wdr1 siRNA-transfected cell shown for the 15 min time point exemplifies a cell that did not form a cSMAC. The Ag

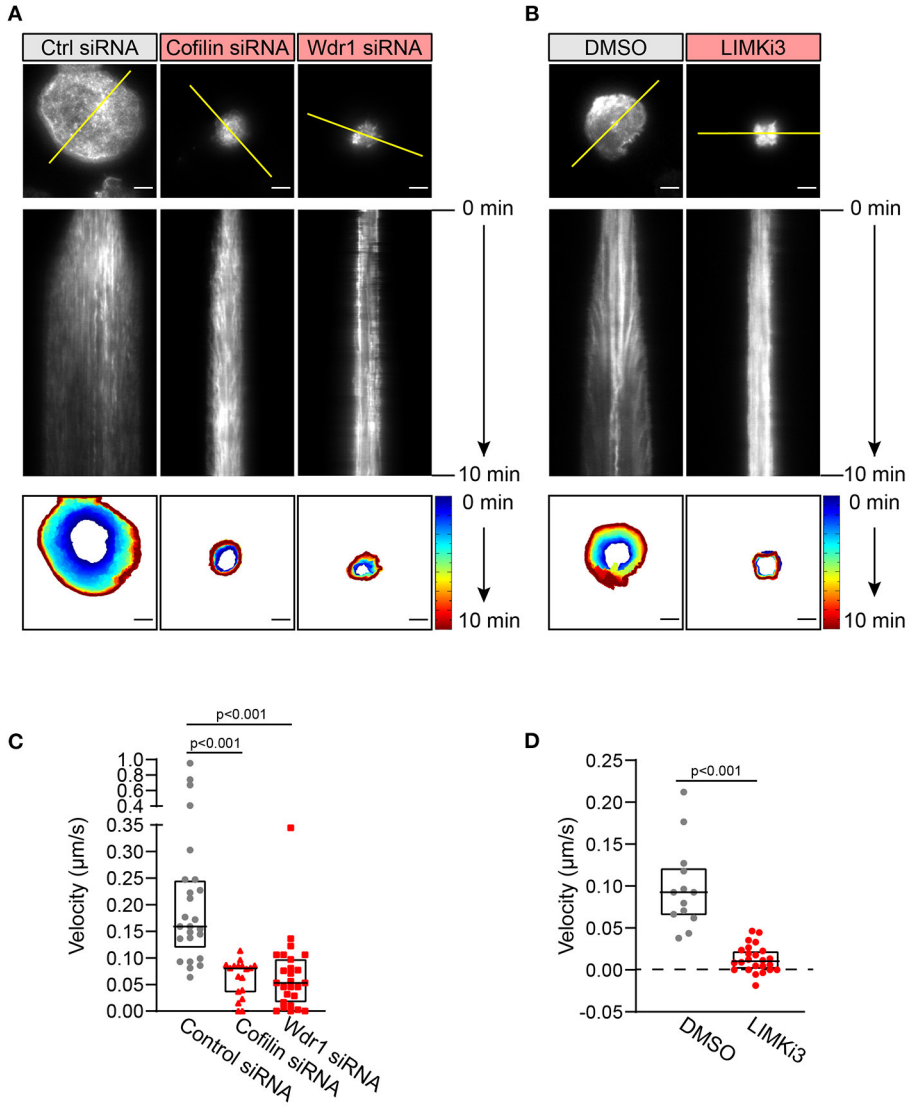

FIGURE 4 | The Wdr1-LIMK-cofilin network is important for BCR-induced actin dynamics. A20 B cells were co-transfected with F-tractin-GFP cDNA and either control (Ctrl) siRNA, cofilin siRNA, or Wdr1 siRNA **(A)**, or transfected with F-tractin-GFP cDNA and then pre-treated with DMSO or 50 μM LIMKi3 for 1 h **(B)**. The cells were then added to anti-IgG-coated coverslips and imaged by TIRF microscopy at 1 s intervals for 10 min. The top panels are the final frames, i.e., 10 min time point, from Movie 1 (control siRNA), Movie 2 (cofilin siRNA), Movie 3 (Wdr1 siRNA), Movie 4 (DMSO-treated), and Movie 5 (LIMKi3-treated). The middle panels are kymographs along the yellow lines in the top panels. Static F-actin structures appear as vertical lines. In the bottom panels, the cell edge in each frame, as defined by F-actin staining, was overlaid as a temporally-coded time series. Scale bars: 5 μm. **(C,D)** The centripetal velocity ($\Delta x/\Delta t$) was calculated for individual actin tracks on kymographs. Each dot on the graphs is an individual actin track. For each condition the velocity was determined for 13-26 actin tracks from 5 to 10 cells. The median and interquartile ranges are shown. The Mann-Whitney *U* test was used to calculate p-values.

fluorescence associated with this cell is distributed among multiple discrete clusters.

Importantly, the initial microcluster-based BCR signaling at the immune synapse was significantly reduced when Wdr1 was depleted. The amount of clustered pCD79 at the contact site with the APC was significantly lower in the Wdr1 siRNA-transfected A20 D1.3 B cells than in the control siRNA-transfected cells at the 3, 5, and 10 min time points (**Figure 5D**). Because Wdr1 depletion did not decrease the total amount of Ag that was gathered into clusters (**Figure 5C**), the decreased levels of pCD79 at the B cell-APC interface were not due to impaired formation of BCR-Ag microclusters. Indeed, calculating the ratio of clustered pCD79 divided by clustered Ag for each B cell revealed that the BCR signaling output per unit of Ag that was gathered into clusters (i.e., signal amplification) was significantly reduced at the 3, 5, and 10 min time points when Wdr1 was depleted (**Figure 5E**). Thus, for membrane-bound Ags, Wdr1 contributes to mechanisms that amplify CD79

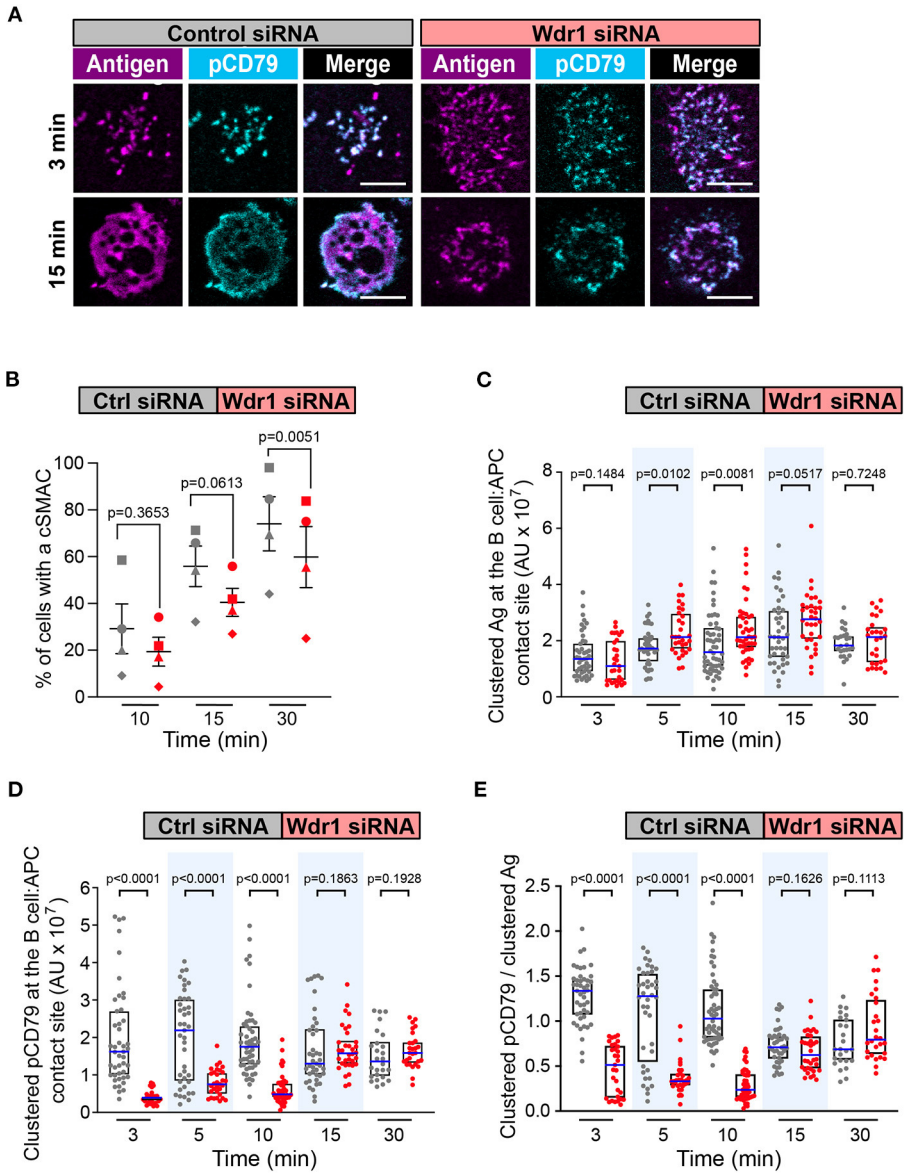

FIGURE 5 | Wdr1 is important for cSMAC formation and BCR signaling at the immune synapse. A20 D1.3 B cells that had been transfected with control (Ctrl) siRNA or Wdr1 siRNA were added to mHEL-HaloTag-expressing COS-7 APCs. The cells were then fixed at the indicated times and the B cell-APC interface was imaged by spinning disk microscopy. **(A)** Representative images. Scale bars: 5 μm. **(B)** For each time point, the percent of cells that had formed a cSMAC, defined as >90% of the total Ag fluorescence intensity being contained in 1-2 clusters, is graphed. Each symbol on the graph represents an independent experiment. Paired *t*-tests were used to calculate p-values. **(C,D)** The total fluorescence intensity of the mHEL-HaloTag Ag **(C)** or pCD79 **(D)** that was present in clusters at the B cell-APC contact site was quantified for each cell. Each dot is one cell. n >25 cells per condition. The median (blue line) and interquartile ranges (black box) are shown. **(E)** For each B cell represented in **(C,D)**, the total fluorescence intensity of clustered pCD79 was divided by the total fluorescence intensity of clustered Ag. The ratio is graphed. The median (blue line) and interquartile ranges (black box) are shown. The data in **(C–E)** are from the same experiment, which is representative of four independent experiments. The Mann-Whitney *U* test was used to calculate p-values for **(C–E)**.

phosphorylation. This is in contrast to B cell responses to soluble BCR ligands, where depleting Wdr1 had no effect on anti-Ig-induced CD79 phosphorylation, Erk phosphorylation, or Ca^{2+} flux (**Supplementary Figures 3, 4**).

Because Wdr1 optimizes the actin-severing capabilities of cofilin, we then asked whether depleting cofilin also impaired cSMAC formation and APC-induced BCR signaling. Cofilin-depleted cells rapidly formed BCR-Ag microclusters (**Figure 6A**) but the percent of cells that formed a cSMAC after 30 min was reduced compared to control cells (**Figure 6B** and **Supplementary Figure 5B**), as was the case when Wdr1 was depleted. Depleting cofilin appeared to alter the kinetics

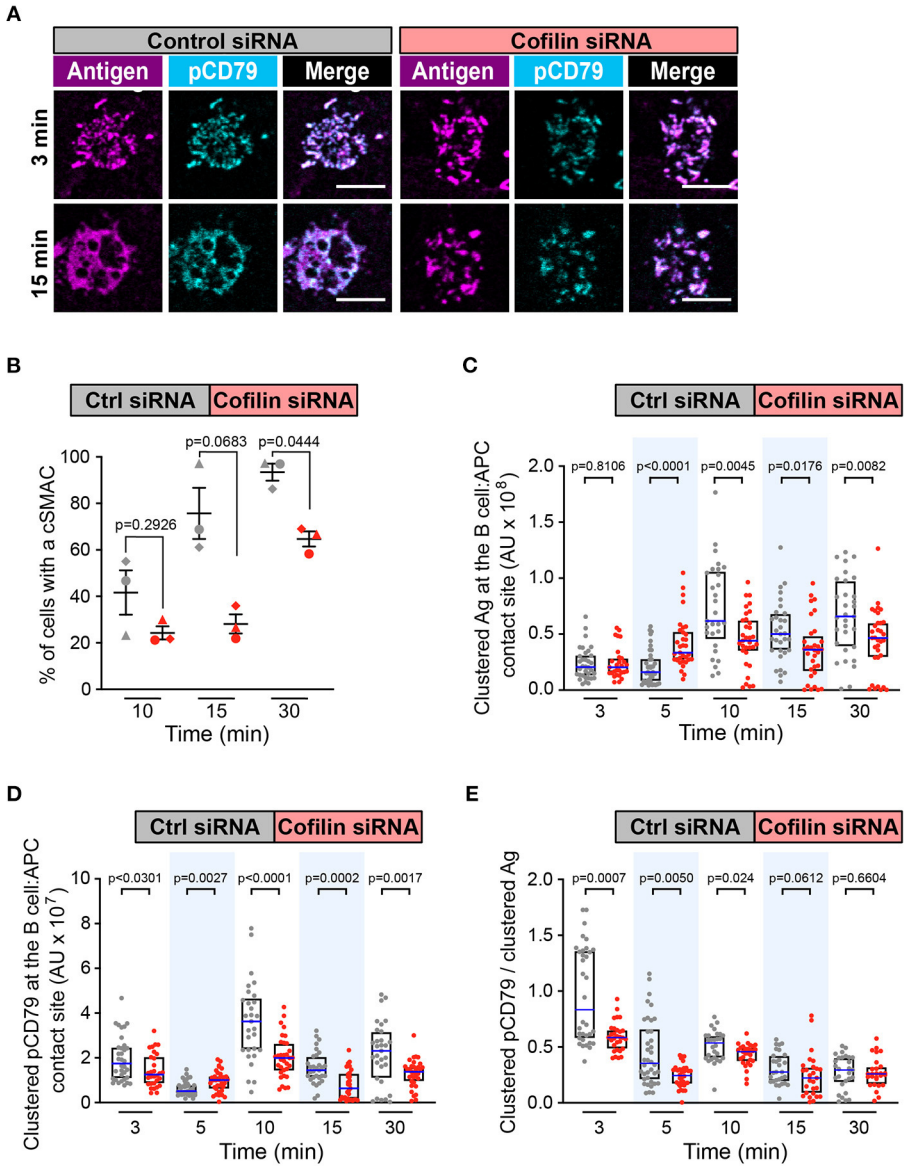

FIGURE 6 | Cofilin is important for cSMAC formation and BCR signaling at the immune synapse. A20 D1.3 B cells that had been transfected with control (Ctrl) siRNA or cofilin siRNA were added to mHEL-HaloTag-expressing COS-7 APCs. The cells were then fixed at the indicated times and the B cell-APC interface was imaged by spinning disk microscopy. **(A)** Representative images. Scale bars: 5 μm. **(B)** For each time point, the percent of cells that had formed a cSMAC is graphed. Each symbol represents an independent experiment. Paired *t*-tests were used to calculate p-values. **(C,D)** The total fluorescence intensity of the mHEL-HaloTag Ag **(C)** or pCD79 **(D)** that was present in clusters at the B cell-APC contact site was quantified for each cell. Each dot is one cell. n >30 cells per condition. The median (blue line) and interquartile ranges (black box) are shown. **(E)** For each B cell represented in **(C,D)**, the total fluorescence intensity of clustered pCD79 was divided by the total fluorescence intensity of clustered Ag. The median (blue line) and interquartile ranges (black box) are shown. The data in **(C–E)** are from the same experiment, which is representative of three independent experiments. The Mann-Whitney *U* test was used to calculate p-values for **(C–E)**.

of BCR-induced Ag clustering. Compared to control siRNA-transfected cells, the amount of Ag that was gathered into clusters was higher in the cofilin-depleted cells after 5 min but significantly lower at 10, 15, and 30 min (**Figure 6C**). Importantly, the cofilin-depleted cells had decreased amounts of clustered pCD79 at the B cell-APC interface at the 3, 10, 15, and 30 min time points (**Figure 6D**). The amount of clustered pCD79 at the 5 min time point was greater in the cofilin-depleted cells than in the control cells, which may reflect the increased amount of Ag that was gathered into BCR-Ag microclusters at that time point. Nevertheless, BCR signal amplification, the amount of clustered pCD79 per unit of Ag that was gathered into BCR-Ag microclusters per cell was significantly reduced at the 3, 5, and 10 min time points in the cofilin-depleted

cells and trended lower at the 15 and 30 min time points (**Figure 6E**). Thus, at early time points (3 min and 5 min), the loss of cofilin strongly decreases BCR signaling amplification without decreasing Ag gathering. At the later time points (10, 15, and 30 min), both reduced Ag gathering and reduced BCR signal amplification appear to contribute to the decreased pCD79 levels at the B cell-APC interface in the cofilin siRNA-transfected cells. In contrast, depleting cofilin had no effect on the ability of soluble anti-Ig to stimulate CD79 phosphorylation, Erk phosphorylation, or Ca^{2+} flux (**Supplementary Figures 3, 4**). Thus, cofilin and Wdr1 enhance BCR signaling in response to membrane-bound Ags but are not essential for BCR signaling in response to soluble ligands that are uniformly distributed in the surrounding medium.

In T cells, Cotl1 is recruited to the immune synapse where it enhances the formation of lamellipodia that spread across the surface of the APC (Kim et al., 2014). However, we found that depleting Cotl1 did not affect APC-induced cSMAC formation or BCR signal amplification at the immune synapse (data not shown).

As a gain-of-function approach for enhancing the actions of cofilin, we treated B cells with LIMKi3 in order to reduce the ability of LIMK to phosphorylate and inactivate cofilin. When A20 D1.3 B cells were treated with LIMKi3, BCR-Ag microclusters formed throughout the contact site but cSMAC formation was slightly reduced compared to control cells (**Figures 7A,B** and **Supplementary Figure 5C**). Moreover, the gathering of Ag into clusters was significantly reduced at the 5, 10, and 15 min time points in the LIMKi3-treated cells (**Figure 7C**). Importantly, the amount of clustered pCD79 present at the B cell-APC interface was significantly lower at all time points when LIMK was inhibited (**Figure 7D**). This reflects a combination of reduced BCR signal amplification at the 3, 5, and 30 min time points (**Figure 7E**) and the reduced Ag gathering that occurs at 5, 10, and 15 min (**Figure 7C**). Similar trends were observed in primary B cells from MD4 mice, which express a transgenic HEL-specific BCR (**Supplementary Figure 6**). LIMKi3 treatment of *ex vivo* MD4 B cells resulted in reduced Ag gathering at the 10, 15, and 30 min time points, substantially reduced pCD79 levels at 3 and 30 min, and reduced BCR signaling per unit of gathered Ag at the 3, 15, and 30 min time points. Thus, LIMKi3 treatment modulates both Ag gathering and BCR signaling amplification, resulting in decreased BCR signaling at the immune synapse at several time points. As for cofilin and Wdr1, targeting LIMK did not impair BCR signaling in response to soluble anti-Ig antibodies (**Supplementary Figure 3**). Overall, we found that targeting cofilin, Wdr1, or LIMK all resulted in decreased BCR signaling in response to APC-bound Ags. Although the exact time course of the APC-induced CD79 phosphorylation varied from experiment-to-experiment, both total pCD79 levels and the signal amplification parameter (clustered pCD79/clustered Ag) were routinely decreased at multiple time points over the first 30 min of B cell-APC encounter. We have previously shown that the magnitude of BCR signaling during the first 30 min of B cell-APC interaction determines whether the B cell activation program is initiated (Bolger-Munro et al., 2019).

DISCUSSION

Cellular processes that depend on actin remodeling require cofilin to disassemble existing actin networks and to support new actin polymerization. Actin filament severing by cofilin generates new barbed ends at which filament elongation can occur. Moreover, the disassembly of severed filament segments releases actin monomers, Arp2/3 complexes, and other actin-binding proteins, which can then be used for new actin assembly. The ability of cofilin to bind and sever actin filaments is controlled by a network of proteins that includes Wdr1, LIMK, and Cotl1. This regulatory network can presumably integrate input from multiple signaling pathways, enabling dynamic spatiotemporal regulation of cofilin activity. We have shown that cofilin, Wdr1, and LIMK are all essential for BCR-induced actin remodeling and cell spreading, as well as immune synapse formation and APC-induced BCR signaling. Because actin dynamics are strongly influenced by mechanical forces, it is important to point out that we analyzed actin-dependent B cell processes on both a rigid substrate coated with immobilized anti-Ig antibodies and on APCs expressing Ags that are mobile within the plasma membrane. However, B cells extend lamellipodial protrusions on both these surfaces (Bolger-Munro et al., 2019), and a common feature of lamellipodia is actin treadmilling and retrograde flow that is dependent on the concerted actions of the Arp2/3 complex and cofilin.

The Wdr1-LIMK-Cofilin Axis Regulates BCR-Induced Actin Remodeling and Spreading

The radial spreading of B cells on immobilized anti-Ig antibodies is driven by Arp2/3 complex-nucleated actin polymerization and the resulting assembly of dendritic actin networks at the cell periphery (Bolger-Munro et al., 2019). We had previously shown that the ability of B cells to spread on immobilized anti-Ig is severely impaired when cofilin is depleted in the A20 B cell line (Wang et al., 2017). Using STED super-resolution microscopy, we have extended these findings to show that cofilin-depleted B cells form a much thicker peripheral ring of branched actin than control cells and are unable to clear actin from the center of the contact site. A similar disruption of actin organization is observed when cofilin is depleted in developing neurons (Flynn et al., 2012). Developing neurons adopt a similar morphology as a spreading B cell, with a dense actin network at the periphery and an actin-depleted region at the center of the substrate contact site. Cofilin deficiency in these cells leads to "congestion of the intracellular space" as well as impaired neurite outgrowth. Similarly, localized inactivation of cofilin in the lamellipodia of neuronal cells results in expansion of the peripheral actin ring, which results from decreased filament disassembly (Vitriol et al., 2013). Thus, cofilin-mediated actin disassembly appears to be an essential prerequisite for the actin remodeling that drives membrane protrusion and cell spreading. Consistent with this idea, using jasplakinolide to stabilize actin filaments prevents B cell spreading (Freeman et al., 2011).

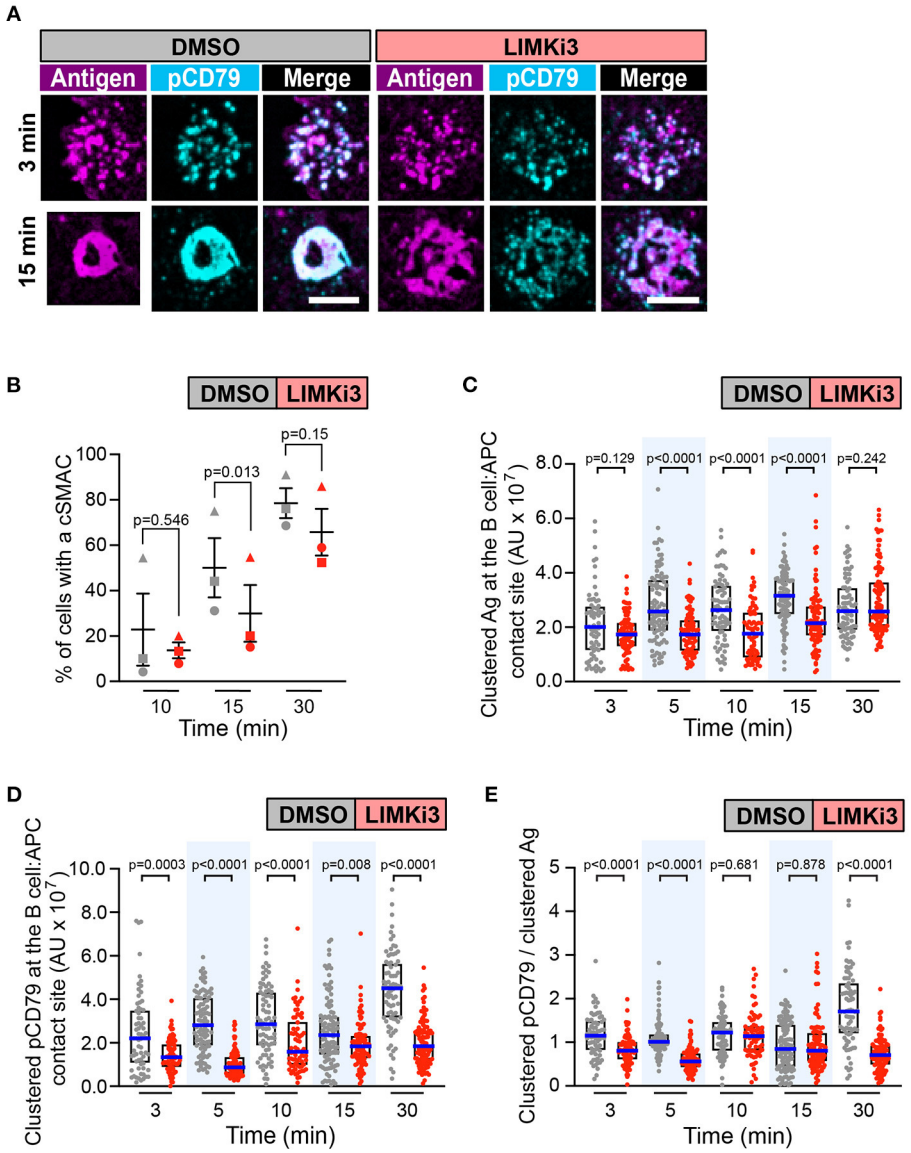

FIGURE 7 | Inhibiting LIMK in A20 D1.3 B cells impairs cSMAC formation and BCR signaling at the immune synapse. A20 D1.3 B cells were pre-treated for 1 h with DMSO or 50 μM LIMKi3 before being added to mHEL-HaloTag-expressing COS-7 APCs. The cells were then fixed at the indicated times and the B cell-APC interface was imaged by spinning disk microscopy. **(A)** Representative images. Scale bars: 5 μm. **(B)** For each time point, the percent of cells that had formed a cSMAC is graphed. Each symbol represents an independent experiment. Paired *t*-tests were used to calculate p-values. **(C,D)** The total fluorescence intensity of the mHEL-HaloTag Ag **(C)** or pCD79 **(D)** that was present in clusters at the B cell-APC contact site was quantified for each cell. Each dot is one cell. n > 67 cells per condition. The median (blue line) and interquartile ranges (black box) are shown. **(E)** For each B cell represented in **(C,D)**, the total fluorescence intensity of clustered pCD79 was divided by the total fluorescence intensity of clustered Ag. The median (blue line) and interquartile ranges (black box) are shown. The data in **(C–E)** are from the same experiment, which is representative of three independent experiments. The Mann-Whitney *U* test was used to calculate p-values for **(C–E)**.

Wdr1 optimizes the spacing of cofilin molecules on actin filaments such that filament severing is favored (Elam et al., 2013; Gressin et al., 2015; Tanaka et al., 2018). Hence, depleting Wdr1 reduces cofilin-mediated actin severing and often phenocopies cofilin depletion. In *Drosophila*, depleting either the Wdr1 homolog *flare* or the cofilin homolog *twinstar* results in similar phenotypes (Ren et al., 2007; Chu et al., 2012). Both *flare* mutants and *twinstar* mutants exhibit an accumulation of actin filaments and an increase in actin network stability. Consistent with this, we found that Wdr1-depleted B cells exhibited a similarly impaired spreading phenotype as cofilin-depleted B cells, with an expanded peripheral ring of branched actin, reduced actin clearance at the center of the substrate contact site, and impaired peripheral actin dynamics. Wdr1 depletion

in B cells also resulted in an increase in the amount of non-phosphorylated (activated) cofilin that is capable of binding actin filaments. In the absence of Wdr1, the saturation of actin filaments with cofilin would stabilize the filaments and prevent actin network remodeling. Indeed, depleting Wdr1 in the neutrophils of developing zebrafish, which also causes cofilin dephosphorylation, results in an accumulation of actin filaments (Bowes et al., 2019). A reduction in cofilin-mediated actin network disassembly may also limit the recycling of Arp2/3 complexes and actin monomers that supports new actin polymerization. In yeast, disrupting the gene encoding the Wdr1 homolog Aip1 reduces the concentration of actin monomers in cells (Okreglak and Drubin, 2010). Moreover, biochemical studies revealed a role for Wdr1/Aip1 in converting cofilin-generated actin oligomers into monomers (Okreglak and Drubin, 2010). Thus, Wdr1 may enhance the actions of cofilin in multiple ways to support actin treadmilling.

In contrast to the impaired spreading of Wdr1-depleted A20 B cells that we observed, peripheral blood B cells from patients with mutations that ablate Wdr1 expression exhibit enhanced spreading on immobilized anti-Ig (Pfajfer et al., 2018). However, this experiment was done in conjunction with CpG DNA stimulation of the B cells. CpG DNA is a ligand for Toll-like receptor (TLR) 9 and we have previously shown that TLR9 signaling increases actin turnover dynamics in B cells and impacts the activity of multiple actin-regulatory proteins, including cofilin (Freeman et al., 2015). Whether TLR-induced "dynamization" of the actin cytoskeleton requires Wdr1 is not known.

We found that B cell spreading was also impaired when we used the LIMK inhibitor to increase the amount of activated cofilin. In contrast to cofilin depletion and Wdr1 depletion, the reduced spreading in LIMKi3-treated cells was associated with a thinner peripheral actin ring. This may reflect an increased rate of cofilin- and Wdr1-dependent actin filament severing at the inner face of the actin ring, which exceeds the rate of actin polymerization at the plasma membrane. A peripheral branched actin network with reduced thickness may generate less outward force to drive membrane protrusion. Alternatively, dynamic spatiotemporal regulation of cofilin activity by LIMK may be essential for sustaining membrane protrusion. In Jurkat T cells, depleting either LIMK or cofilin inhibits SDF-1-induced chemotaxis, suggesting that rapidly turning cofilin on and off is important for directional cell movement (Nishita et al., 2004). LIMK-deficient Jurkat cells exhibit "immature protrusion events," suggesting that transient suppression of cofilin activity by LIMK enables sustained assembly of actin-based membrane protrusions. This may also be critical for B cell spreading.

B cell spreading may require complex spatial and temporal control of LIMK-mediated inhibition of cofilin. Upon contacting anti-Ig- or Ag-coated surfaces, BCR-induced activation of cofilin initiates remodeling of the submembrane actin cytoskeleton. Although the mechanism by which BCR signaling increases the amount of active, non-phosphorylated cofilin is not fully understood, it could include transient inhibition of LIMK. As the B cell spreads, localized activation of LIMK could suppress cofilin activity in nascent lamellipodia so that peripheral actin polymerization can generate stable membrane protrusions. Subsequently, LIMK could tune the level of cofilin activity in order to balance actin network disassembly at the inner face of the peripheral actin ring with actin polymerization at the cell membrane. This actin treadmilling would allow the B cell to continually extend membrane protrusions across the Ag-coated surface. The ability to image the subcellular localization of activated LIMK in real time could provide important insights into the regulation of peripheral actin dynamics. LIMK activity is controlled by the RhoA GTPase and its downstream effector ROCK (Prunier et al., 2017). The BCR activates RhoA (Saci and Carpenter, 2005) but the role of RhoA and ROCK in regulating B cell actin dynamics is not fully understood.

The Wdr1-LIMK-Cofilin Axis Regulates cSMAC Formation and BCR Signaling at the Immune Synapse

When B cells encounter Ags that are mobile within a membrane, Arp2/3 complex-dependent actin retrograde flow drives the centripetal movement of BCR-Ag microclusters that form at the periphery of B cell-APC contact site (Bolger-Munro et al., 2019). This, together with the progressive coalescence of BCR microclusters, amplifies microcluster-based BCR signaling and promotes cSMAC formation. Arp2/3 complex-dependent peripheral actin dynamics is strongly dependent on concomitant actin disassembly (Carlier et al., 1997; Svitkina and Borisy, 1999). Actin retrograde flow requires the disassembly of aged actin filaments by actin disassembly factors such as cofilin and destrin/ADF (Hotulainen et al., 2005; Delorme et al., 2007; Flynn et al., 2012). Moreover, the inactivation of cofilin decreases the speed of actin retrograde flow (Ohashi et al., 2011; Flynn et al., 2012; Vitriol et al., 2013). We found that depleting cofilin or Wdr1 in B cells substantially reduced the velocity of actin retrograde flow and that this was associated with reduced or delayed cSMAC formation as well as decreased BCR signaling and signal amplification in response to APC-bound Ags. Although LIMK inhibition results in increased cofilin activity, we showed that this also blocked actin retrograde flow, reduced cSMAC formation, and decreased BCR signal amplification. Hence, B cell responses to APC-bound Ags require an optimal level of cofilin activity and are impaired by both deficient and excessive cofilin activity.

This is the first report, to our knowledge, that Wdr1 is important for B cell responses to APC- or membrane-bound Ags. We had previously shown that cofilin-mediated actin severing is important for APC-induced microcluster formation and BCR signaling (Freeman et al., 2011). In that study, we used the phosphomimetic S3D mutant form of cofilin, as well as cell-permeable peptides containing the actin-binding domains of cofilin, both of which competitively inhibit the binding of cofilin to actin filaments and prevent severing (Eibert et al., 2004; Elam et al., 2017; Tanaka et al., 2018). However, these approaches may also interfere with the actin-binding and severing activities of destrin/ADF, which is highly related to cofilin in both

its actin-binding domain structure and actin-severing function (Lappalainen et al., 1998; Hotulainen et al., 2005). Both the non-muscle cofilin-1 isoform and destrin are co-expressed in most cell types (Lappalainen et al., 1998). We have shown here that selectively depleting cofilin-1 impairs B cell responses to APC-bound Ags. The contribution of destrin/ADF, and other actin-severing proteins such as gelsolin, to these responses remains to be determined.

Consistent with their cooperative mode of action, depleting either cofilin or Wdr1 had similar effects on B cell responses to APCs. An unexpected finding was that both cofilin depletion and Wdr1 depletion resulted in increased gathering of Ag into clusters at 5 min after the initiation of B cell-APC contact. Actin structures help maintain the integrity of BCR microclusters (Treanor et al., 2011). A reduction in cofilin-mediated disassembly of these actin structures may increase the stability of nascent microclusters and thereby increase the amount of Ag that is gathered into small microclusters during the first 5 min of B cell-APC interactions. Despite the increased Ag clustering, cSMAC formation was delayed in cofilin-depleted B cells and the percent of cells that formed a cSMAC after 15–30 min was consistently lower when cofilin or Wdr1 was depleted. This could be due in part to reduced actin retrograde flow, which would decrease the centripetal movement of BCR-Ag microclusters that form at periphery of the B cell-APC contact site. As well, cortical actin structures that act as diffusion barriers for membrane proteins would be turned over (i.e., disassembled) at a reduced rate in cells that have been depleted of cofilin or Wdr1. The increased lifetime of these actin-based diffusion barriers would limit BCR microcluster mobility within the membrane, resulting in decreased microcluster coalescence and cSMAC formation.

Although the mechanisms are not fully understood, actin retrograde flow amplifies Ag receptor signaling at the T- and B-cell immune synapses (Basu and Huse, 2017; Bolger-Munro et al., 2019). The actin-driven centripetal movement of BCR-Ag microclusters promotes their coalescence into larger clusters (Bolger-Munro et al., 2019) where BCR signaling is enhanced (Liu et al., 2010, 2011; Ketchum et al., 2014). BCR clustering is an essential early amplification event in BCR signaling that is directly related to BCR signaling output (Liu et al., 2010). Recruitment of the Syk tyrosine kinase to Ag-bound BCRs enables Syk-dependent phosphorylation of the CD79 ITAMs via BCR-BCR collisions, allowing those BCRs to recruit Syk and further activate downstream BCR signaling pathways. Microcluster growth leads to further increases in BCR signaling (Liu et al., 2010, 2011; Ketchum et al., 2014). As the microclusters grow in area, a greater number of BCRs in the interior of the cluster may be shielded from inhibitory CD22-SHP1 complexes (Gasparrini et al., 2016). CD22 is a transmembrane protein that limits BCR signaling by recruiting the SHP1, a phosphatase that can terminate BCR signaling by dephosphorylating the CD79 ITAMs. Actin retrograde flow may also amplify BCR signaling by exerting force on the cytoplasmic domains of BCRs that are bound to APC-associated Ags. The BCR is a mechanosensitive receptor and increased mechanical tension on the BCR results in enhanced recruitment of Syk and other signaling components to the BCR (Wan et al., 2013, 2015; Liu et al., 2014; Shaheen et al., 2019).

We showed that depleting either cofilin or Wdr1 significantly reduced the velocity of the actin retrograde flow and that this correlated with a reduction in BCR signal amplification. When either cofilin or Wdr1 was depleted the amount of signaling generated per unit of Ag gathered into BCR-Ag microclusters was significantly reduced during the first 10 min of B cell-APC interaction. A similar decrease in BCR signal amplification is observed when Arp2/3 complex activity is inhibited (Bolger-Munro et al., 2019). This suggests that cofilin and the Arp2/3 complex work in concert to support actin-dependent processes that amplify microcluster-based BCR signaling. The reduced signal amplification in Wdr1- and cofilin-depleted cells contributed to significant decreases in the total amount of pCD79 present in BCR microclusters during the first 10–30 min of B cell-APC interaction. We have previously shown that such decreases in initial APC-induced BCR signaling are associated with impaired B cell activation (Bolger-Munro et al., 2019).

LIMK is a key negative regulator of cofilin that phosphorylates cofilin on S3 and prevents cofilin from binding to actin filaments. LIMK inhibitors have been widely used to investigate the effects of increased cofilin activity. In T cells, inhibiting or depleting LIMK, or its upstream activator ROCK, results in a larger immune synapse area and increased APC-induced Ca^{2+} signaling (Thauland et al., 2017). Thus, in T cells, LIMK normally limits T cell spreading on the APC surface. This suggests that increased cofilin activity enhances T cell immune synapse formation and APC-induced TCR signaling. In contrast, we found that inhibiting LIMK activated cofilin in B cells but reduced B cell spreading and impaired B cell responses to APC-bound Ags. When LIMK was inhibited, the ability of A20 B cells to gather Ags into clusters at the B cell-APC interface was reduced, as was cSMAC formation. Importantly, at early time points after adding B cells to APCs, both pCD79 levels and BCR signal amplification were significantly lower in LIMKi3-treated A20 B cells and primary B cells than in control cells. The reduced cSMAC formation and BCR signal amplification in LIMKi3-treated B cells may be due to the substantially impaired actin retrograde flow in these cells, which could be a consequence of the thinner peripheral actin network that results from excessive cofilin activity. Although LIMK has multiple substrates (Prunier et al., 2017), the similar alterations in actin-dependent B cell responses caused by inhibiting LIMK, depleting cofilin, and depleting Wdr1 suggest that LIMK-mediated regulation of cofilin is essential for the dynamic actin remodeling that optimizes B cell responses to APCs. Importantly, these data show that both reduced and excessive cofilin activity inhibit actin retrograde flow and impair BCR microcluster centralization and signaling at the immune synapse.

Perspectives

Immune synapse formation allows lymphocytes to establish a polarized contact site with an APC. At this synapse, the actin-dependent centripetal movement and progressive clustering of antigen receptors amplifies their signaling and allows small amounts of APC-bound Ag to trigger lymphocyte activation.

In contrast, B cell activation by soluble Ags that are uniformly distributed in the surrounding medium does not involve the formation of polarized structures and is much less dependent on actin reorganization. Consistent with this idea, we found that actin remodeling driven by the Wdr1-cofilin-LIMK axis amplifies BCR signaling in response to membrane-bound Ags but that it is not essential for responses to soluble BCR ligands. Similarly, the Arp2/3 complex (Bolger-Munro et al., 2019) and the Rac/Cdc42 activator DOCK8 (Randall et al., 2009; Sun et al., 2018), both of which are essential for immune synapse formation, are important for B cells to respond to membrane-bound Ags but dispensable for responses to soluble Ags. Together, these findings support the idea that the actin-dependent movement and spatial reorganization of BCRs at the immune synapse has a unique and critical role in APC-induced B cell activation.

Ag presentation by APCs is an important mode of B cell activation *in vivo*, especially for large Ags that cannot freely diffuse into the B-cell follicles within lymphoid organs (Batista and Harwood, 2009; Cyster, 2010; Heesters et al., 2016). In particular, the ability of subcapsular macrophages to capture bacteria and viruses, and then present them to follicular B cells, is important for the generation of protective antibodies that prevent recurring infections (Junt et al., 2007; Gaya et al., 2015; Moran et al., 2019). The actin-dependent amplification of BCR signaling in response to APC-bound Ags may reduce the amount of Ag required to exceed the threshold for triggering B cell activation. Indeed, the increased actin dynamics in B cells that have been exposed to TLR ligands renders B cells more sensitive to small amounts of Ag (Freeman et al., 2015). Conversely, mutations that result in impaired or aberrant actin dynamics may ablate the actin-dependent amplification of BCR signaling at the immune synapse and render B cells unable to respond to low-affinity Ags or Ags that are present at low density on the APC surface. The *in vitro* activation of naïve murine B cells by APC-bound Ags is reduced when the Arp2/3 complex is inhibited, and this is associated with reduced BCR signaling during the first 5 min of B cell-APC interaction (Bolger-Munro et al., 2019). *In vivo*, B cell-specific deletion of WASp in mice impairs antibody responses to low amounts of Ag (Westerberg et al., 2005). Patients with loss-of-function mutations in WASp or DOCK8 exhibit poor vaccine responses although this may be due in large part to the impaired B cell development and maturation (Biggs et al., 2017; Candotti, 2018). Nevertheless, immune disorders linked to mutations in actin-regulatory proteins are commonly associated with recurring infections (Tur-Gracia and Martinez-Quiles, 2021). Because the actions of the Arp2/3 complex and cofilin are intertwined, cofilin and its network of regulators may also control the threshold for APC-dependent B cell activation *in vivo*, impacting the ability to mount antibody responses to pathogens and vaccines. Testing this hypothesis may require the generation of mice with hypomorphic alleles of these actin regulators such that B cell development and maturation are not impaired. Both mice and humans with hypomorphic alleles of the *Wdr1* gene have been described but their B cell responses to immunization or vaccine challenge have not been investigated (Kile et al., 2007; Seppanen, 2018). LIMK inhibitors have been used in mouse models of disease (Prunier et al., 2017). This approach could be used to test the idea that LIMK tunes the threshold for B cell activation *in vivo*.

The magnitude of BCR signaling determines whether Ag encounter results in B cell activation or immunological tolerance (Cashman et al., 2019; Meffre and O'Connor, 2019; Tan et al., 2019). Autoimmunity can result from excessive BCR signaling or from impaired BCR signaling that fails to eliminate self-reactive B cells. During B cell development, immature B cells are exposed to many self-Ags in the bone marrow. If the binding of the self-Ag to the BCR elicits strong signaling, these self-reactive B cells undergo apoptosis and are deleted. Reduced BCR signaling could impair the ability to delete self-reactive B cells. These B cells could then enter the circulation, and under certain conditions, become activated by self-Ags in peripheral tissues, leading to autoimmunity. Although it is not known whether immune synapse formation plays a role in the deletion of B cells that bind cell-associated Ags in the bone marrow, plasma membrane proteins are strong inducers of B cell clonal deletion (Hartley et al., 1991; Ait-Azzouzene et al., 2005; Nemazee, 2017). Mutations that ablate the actin-dependent amplification of APC-induced BCR signaling could lead to a failure of this central tolerance mechanism. Patients with Wdr1 loss-of-function mutations have increased numbers of immature transitional B cells in the periphery, which could be self-reactive B cells that escaped negative selection in the bone marrow (Pfajfer et al., 2018). Indeed, many of the immunodeficiency syndromes that are due to mutations in actin-regulatory proteins are accompanied by autoimmunity and the production of self-reactive antibodies (Sprenkeler et al., 2020). These immune dysregulation syndromes have been termed actinopathies (Sprenkeler et al., 2020). Further work is needed to test the hypothesis that actin-dependent amplification of BCR signaling at the immune synapse tunes the threshold for the deletion of self-reactive B cells in the bone marrow.

DATA AVAILABILITY STATEMENT

The raw data supporting the conclusions of this article will be made available by the authors, without undue reservation.

ETHICS STATEMENT

The animal study was reviewed and approved by University of British Columbia Animal Care Committee.

AUTHOR CONTRIBUTIONS

MB-M, KC, FC, and YL conceived and designed the experiments. MB-M, KC, FC, YL, MD-L, ND, and CK performed the experiments. MB-M, KC, FC, YL, and MG analyzed the results. MB-M, FC, YL, and MG wrote the manuscript with input from KC. MG was the principal investigator of the

study. All authors contributed to the article and approved the submitted version.

FUNDING

This work was supported by grants PJT-152946 and PJT-166196 (to MG) from the Canadian Institutes of Health Research. MB-M was supported by a 4-year fellowship and a Friedman Award for Scholars in Health from the University of British Columbia. FC and CK were supported by Undergraduate Summer Research Awards from the Natural Sciences and Engineering Research Council (NSERC) of Canada. YL was supported by a Science Undergraduate Research Experience Award from the University of British Columbia. An earlier version of this work was presented in MB-M's Ph.D. thesis.

ACKNOWLEDGMENTS

We thank the UBC Life Sciences Institute Imaging Facility and the UBC Flow Cytometry Facility.

SUPPLEMENTARY MATERIAL

The Supplementary Material for this article can be found online at: https://www.frontiersin.org/articles/10.3389/fcell.2021.649433/full#supplementary-material

REFERENCES

Abraham, L., Wang, J. C., Bolger-Munro, M., and Gold, M. R. (2016). Structure, function, and spatial organization of the B cell receptor (BCR). *Encycloped. Immunobiol.* 2, 40–54. doi: 10.1016/B978-0-12-374279-7.05005-0

Aggeli, D., Kish-Trier, E., Lin, M. C., Haarer, B., Cingolani, G., Cooper, J. A., et al. (2014). Coordination of the filament stabilizing versus destabilizing activities of cofilin through its secondary binding site on actin. *Cytoskeleton* 71, 361–379. doi: 10.1002/cm.21178

Ait-Azzouzene, D., Verkoczy, L., Peters, J., Gavin, A., Skog, P., Vela, J. L., et al. (2005). An immunoglobulin C kappa-reactive single chain antibody fusion protein induces tolerance through receptor editing in a normal polyclonal immune system. *J. Exp. Med.* 201, 817–828. doi: 10.1084/jem.20041854

Ambach, A., Saunus, J., Konstandin, M., Wesselborg, S., Meuer, S. C., and Samstag, Y. (2000). The serine phosphatases PP1 and PP2A associate with and activate the actin-binding protein cofilin in human T lymphocytes. *Eur. J. Immunol.* 30, 3422–3431. doi: 10.1002/1521-4141(2000012)30:12<3422::AID-IMMU3422>3.0.CO;2-J

Basu, R., and Huse, M. (2017). Mechanical communication at the immunological synapse. *Trends Cell Biol.* 27, 241–254. doi: 10.1016/j.tcb.2016.10.005

Batista, F. D., and Harwood, N. E. (2009). The who, how and where of antigen presentation to B cells. *Nat. Rev. Immunol.* 9, 15–27. doi: 10.1038/nri2454

Batista, F. D., and Neuberger, M. S. (1998). Affinity dependence of the B cell response to antigen: a threshold, a ceiling, and the importance of off-rate. *Immunity* 8, 751–759. doi: 10.1016/S1074-7613(00)80580-4

Bernstein, B. W., and Bamburg, J. R. (2010). ADF/cofilin: a functional node in cell biology. *Trends Cell Biol.* 20, 187–195. doi: 10.1016/j.tcb.2010.01.001

Bieling, P., Hansen, S. D., Akin, O., Li, T. D., Hayden, C. C., Fletcher, D. A., et al. (2018). WH2 and proline-rich domains of WASP-family proteins collaborate to accelerate actin filament elongation. *EMBO J.* 37, 102–121. doi: 10.15252/embj.201797039

Biggs, C. M., Keles, S., and Chatila, T. A. (2017). DOCK8 deficiency: Insights into pathophysiology, clinical features and management. *Clin. Immunol.* 181, 75–82. doi: 10.1016/j.clim.2017.06.003

Bolger-Munro, M., Choi, K., Scurll, J., Abraham, L., Chappell, R. S., Sheen, D., et al. (2019). Arp2/3 complex-driven spatial patterning of the BCR enhances immune synapse formation, BCR signaling and B cell activation. *eLife* 8:e44574. doi: 10.7554/eLife.44574.045

Bowes, C., Redd, M., Yousfi, M., Tauzin, M., Murayama, E., and Herbomel, P. (2019). Coronin 1A depletion restores the nuclear stability and viability of Aip1/Wdr1-deficient neutrophils. *J. Cell Biol.* 218, 3258–3271. doi: 10.1083/jcb.201901024

Bravo-Cordero, J. J., Magalhaes, M. A. O., Eddy, R. J., Hodgson, L., and Condeelis, J. (2013). Functions of cofilin in cell locomotion and invasion. *Nat. Rev. Mol. Cell Biol.* 14, 405–415. doi: 10.1038/nrm3609

Brigida, I., Zoccolillo, M., Cicalese, M. P., Pfajfer, L., Barzaghi, F., Scala, S., et al. (2018). T-cell defects in patients with ARPC1B germline mutations account for combined immunodeficiency. *Blood* 132, 2362–2374. doi: 10.1182/blood-2018-07-863431

Candotti, F. (2018). Clinical manifestations and pathophysiological mechanisms of the Wiskott-Aldrich Syndrome. *J. Clin. Immunol.* 38, 13–27. doi: 10.1007/s10875-017-0453-z

Carlier, M.-F., Laurent, V., Santolini, J., Melki, R., Didry, D., Xia, G.-X., et al. (1997). Actin depolymerizing factor (ADF/Cofilin) enhances the rate of filament turnover: implication in actin-based motility. *J. Cell Biol.* 136, 1307–1322. doi: 10.1083/jcb.136.6.1307

Carlier, M.-F., and Shekhar, S. (2017). Global treadmilling coordinates actin turnover and controls the size of actin networks. *Nat. Rev. Mol. Cell Biol.* 18, 389–401. doi: 10.1038/nrm.2016.172

Cashman, K. S., Jenks, S. A., Woodruff, M. C., Tomar, D., Tipton, C. M., Scharer, C. D., et al. (2019). Understanding and measuring human B-cell tolerance and its breakdown in autoimmune disease. *Immunol. Rev.* 292, 76–89. doi: 10.1111/imr.12820

Chen, Q., Courtemanche, N., and Pollard, T. D. (2015). Aip1 promotes actin filament severing by cofilin and regulates constriction of the cytokinetic contractile ring. *J. Biol. Chem.* 290, 2289–2300. doi: 10.1074/jbc.M114.612978

Chu, D., Pan, H., Wan, P., Wu, J., Luo, J., Zhu, H., et al. (2012). AIP1 acts with cofilin to control actin dynamics during epithelial morphogenesis. *Development* 139, 3561–3571. doi: 10.1242/dev.079491

Conley, M. E., Dobbs, A. K., Farmer, D. M., Kilic, S., Paris, K., Grigoriadou, S., et al. (2009). Primary B cell immunodeficiencies: comparisons and contrasts. *Annu. Rev. Immunol.* 27, 199–227. doi: 10.1146/annurev.immunol.021908.132649

Cook, S. A., Comrie, W. A., Poli, M. C., Similuk, M., Oler, A. J., Faruqi, A. J., et al. (2020). HEM1 deficiency disrupts mTORC2 and F-actin control in inherited immunodysregulatory disease. *Science* 369, 202–207. doi: 10.1126/science.aay5663

Cyster, J. G. (2010). B cell follicles and antigen encounters of the third kind. *Nat. Immunol.* 11, 989–996. doi: 10.1038/ni.1946

Cyster, J. G., and Allen, C. D. C. (2019). B cell responses: Cell interaction dynamics and decisions. *Cell* 177, 524–540. doi: 10.1016/j.cell.2019.03.016

Delorme, V., Machacek, M., DerMardirossian, C., Anderson, K. L., Wittmann, T., Hanein, D., et al. (2007). Cofilin activity downstream of Pak1 regulates cell protrusion efficiency by organizing lamellipodium and lamella actin networks. *Dev. Cell* 13, 646–662. doi: 10.1016/j.devcel.2007.08.011

Eibert, S. M., Lee, K. H., Pipkorn, R., Sester, U., Wabnitz, G. H., Giese, T., et al. (2004). Cofilin peptide homologs interfere with immunological synapse formation and T cell activation. *Proc. Natl. Acad. Sci. U.S.A.* 101, 1957–1962. doi: 10.1073/pnas.0308282100

Elam, W. A., Cao, W., Kang, H., Huehn, A., Hocky, G. M., Prochniewicz, E., et al. (2017). Phosphomimetic S3D cofilin binds but only weakly severs actin filaments. *J. Biol. Chem.* 292, 19565–19579. doi: 10.1074/jbc.M117.808378

Elam, W. A., Kang, H., and De La Cruz, E. M. (2013). Biophysics of actin filament severing by cofilin. *FEBS Lett.* 587, 1215–1219. doi: 10.1016/j.febslet.2013.01.062

Fleire, S. J., Goldman, J. P., Carrasco, Y. R., Weber, M., Bray, D., and Batista, F. D. (2006). B cell ligand discrimination through a spreading and contraction response. *Science* 312, 738–741. doi: 10.1126/science.1123940

Flynn, K. C., Hellal, F., Neukirchen, D., Jacob, S., Tahirovic, S., Dupraz, S., et al. (2012). ADF/cofilin-mediated actin retrograde flow directs neurite formation in the developing brain. *Neuron* 76, 1091–1107. doi: 10.1016/j.neuron.2012.09.038

Freeman, S. A., Jaumouillé, V., Choi, K., Hsu, B. E., Wong, H. S., Abraham, L., et al. (2015). Toll-like receptor ligands sensitize B-cell receptor signalling by reducing actin-dependent spatial confinement of the receptor. *Nat. Commun.* 6:6168. doi: 10.1038/ncomms7168

Freeman, S. A., Lei, V., Dang-Lawson, M., Mizuno, K., Roskelley, C. D., and Gold, M. R. (2011). Cofilin-mediated F-actin severing Is regulated by the Rap GTPase and controls the cytoskeletal dynamics that drive lymphocyte spreading and BCR microcluster formation. *J. Immunol.* 187, 5887–5900. doi: 10.4049/jimmunol.1102233

Gasparrini, F., Feest, C., Bruckbauer, A., Mattila, P. K., Muller, J., Nitschke, L., et al. (2016). Nanoscale organization and dynamics of the siglec CD22 cooperate with the cytoskeleton in restraining BCR signalling. *EMBO J.* 35, 258–280. doi: 10.15252/embj.201593027

Gaya, M., Castello, A., Montaner, B., Rogers, N., Reis e Sousa, C., Bruckbauer, A., et al. (2015). Host response. Inflammation-induced disruption of SCS macrophages impairs B cell responses to secondary infection. *Science* 347, 667–672. doi: 10.1126/science.aaa1300

Gold, M. R., Matsuuchi, L., Kelly, R. B., and DeFranco, A. L. (1991). Tyrosine phosphorylation of components of the B-cell antigen receptors following receptor crosslinking. *Proc. Natl. Acad. Sci. U.S.A.* 88, 3436–3440. doi: 10.1073/pnas.88.8.3436

Goley, E. D., and Welch, M. D. (2006). The ARP2/3 complex: an actin nucleator comes of age. *Nat. Rev. Mol. Cell Biol.* 7, 713–726. doi: 10.1038/nrm2026

Gressin, L., Guillotin, A., Guérin, C., Blanchoin, L., and Michelot, A. (2015). Architecture dependence of actin filament network disassembly. *Curr. Biol.* 25, 1437–1447. doi: 10.1016/j.cub.2015.04.011

Hartley, S. B., Crosbie, J., Brink, R., Kantor, A. B., Basten, A., and Goodnow, C. C. (1991). Elimination from peripheral lymphoid tissues of self-reactive B lymphocytes recognizing membrane-bound antigens. *Nature* 353, 765–769. doi: 10.1038/353765a0

Harwood, N. E., and Batista, F. D. (2011). The cytoskeleton coordinates the early events of B-cell activation. *Cold Spring Harb. Perspect. Biol.* 3:a002360. doi: 10.1101/cshperspect.a002360

Hayakawa, K., Sekiguchi, C., Sokabe, M., Ono, S., and Tatsumi, H. (2019). Real-time single-molecule kinetic analyses of AIP1-enhanced actin filament severing in the presence of cofilin. *J. Mol. Biol.* 431, 308–322. doi: 10.1016/j.jmb.2018.11.010

Heesters, B. A., van der Poel, C. E., Das, A., and Carroll, M. C. (2016). Antigen presentation to B cells. *Trends Immunol.* 37, 844–854. doi: 10.1016/j.it.2016.10.003

Hotulainen, P., Paunola, E., Vartiainen, M. K., and Lappalainen, P. (2005). Actin-depolymerizing factor and cofilin-1 play overlapping roles in promoting rapid F-actin depolymerization in mammalian nonmuscle cells. *Mol. Biol. Cell* 16, 649–664. doi: 10.1091/mbc.e04-07-0555

Johnson, H. W., and Schell, M. J. (2009). Neuronal IP3 3-kinase is an F-actin-bundling protein: Role in dendritic targeting and regulation of spine morphology. *Mol. Biol. Cell* 20, 5166–5180. doi: 10.1091/mbc.e09-01-0083

Junt, T., Moseman, E. A., Iannacone, M., Massberg, S., Lang, P. A., Boes, M., et al. (2007). Subcapsular sinus macrophages in lymph nodes clear lymph-borne viruses and present them to antiviral B cells. *Nature* 450, 110–114. doi: 10.1038/nature06287

Kadzik, R. S., Homa, K. E., and Kovar, D. R. (2020). F-actin cytoskeleton network self-organization through competition and cooperation. *Annu. Rev. Cell Dev. Biol.* 36, 35–60. doi: 10.1146/annurev-cellbio-032320-094706

Kahr, W. H., Pluthero, F. G., Elkadri, A., Warner, N., Drobac, M., Chen, C. H., et al. (2017). Loss of the Arp2/3 complex component ARPC1B causes platelet abnormalities and predisposes to inflammatory disease. *Nat. Commun.* 8:14816. doi: 10.1038/ncomms14816

Kanellos, G., and Frame, M. C. (2016). Cellular functions of the ADF/cofilin family at a glance. *J. Cell Sci.* 129, 3211–3218. doi: 10.1242/jcs.187849

Ketchum, C., Miller, H., Song, W., and Upadhyaya, A. (2014). Ligand mobility regulates B cell receptor clustering and signaling activation. *Biophys. J.* 106, 26–36. doi: 10.1016/j.bpj.2013.10.043

Kile, B. T., Panopoulos, A. D., Stirzaker, R. A., Hacking, D. F., Tahtamouni, L. H., Willson, T. A., et al. (2007). Mutations in the cofilin partner Aip1/Wdr1 cause autoinflammatory disease and macrothrombocytopenia. *Blood* 110, 2371–2380. doi: 10.1182/blood-2006-10-055087

Kim, J., Shapiro, M. J., Bamidele, A. O., Gurel, P., Thapa, P., Higgs, H. N., et al. (2014). Coactosin-like 1 antagonizes cofilin to promote lamellipodial protrusion at the immune synapse. *PLoS ONE* 9:e85090. doi: 10.1371/journal.pone.0085090

Kuijpers, T. W., Tool, A. T. J., van der Bijl, I., de Boer, M., van Houdt, M., de Cuyper, I. M., et al. (2017). Combined immunodeficiency with severe inflammation and allergy caused by ARPC1B deficiency. *J. Allergy Clin. Immunol.* 140:e210. doi: 10.1016/j.jaci.2016.09.061

Kuokkanen, E., Sustar, V., and Mattila, P. K. (2015). Molecular control of B cell activation and immunological synapse formation. *Traffic* 16, 311–326. doi: 10.1111/tra.12257

Lappalainen, P., Kessels, M. M., Cope, M. J., and Drubin, D. G. (1998). The ADF homology (ADF-H) domain: a highly exploited actin-binding module. *Mol. Biol. Cell* 9, 1951–1959. doi: 10.1091/mbc.9.8.1951

Lin, K. B., Freeman, S. A., Zabetian, S., Brugger, H., Weber, M., Lei, V., et al. (2008). The Rap GTPases regulate B cell morphology, immune-synapse formation, and signaling by particulate B cell receptor ligands. *Immunity* 28, 75–87. doi: 10.1016/j.immuni.2007.11.019

Liu, B., Chen, W., Evavold, B. D., and Zhu, C. (2014). Accumulation of dynamic catch bonds between TCR and agonist peptide-MHC triggers T cell signaling. *Cell* 157, 357–368. doi: 10.1016/j.cell.2014.02.053

Liu, C., Miller, H., Hui, K. L., Grooman, B., Bolland, S., Upadhyaya, A., et al. (2011). A balance of Bruton's tyrosine kinase and SHIP activation regulates B cell receptor cluster formation by controlling actin remodeling. *J. Immunol.* 187, 230–239. doi: 10.4049/jimmunol.1100157

Liu, W., Meckel, T., Tolar, P., Sohn, H. W., and Pierce, S. K. (2010). Intrinsic properties of immunoglobulin IgG1 isotype-switched B cell receptors promote microclustering and the initiation of signaling. *Immunity* 32, 778–789. doi: 10.1016/j.immuni.2010.06.006

Meffre, E., and O'Connor, K. C. (2019). Impaired B-cell tolerance checkpoints promote the development of autoimmune diseases and pathogenic autoantibodies. *Immunol. Rev.* 292, 90–101. doi: 10.1111/imr.12821

Mogilner, A., and Oster, G. (1996). Cell motility driven by actin polymerization. *Biophys. J.* 71, 3030–3045. doi: 10.1016/S0006-3495(96)79496-1

Moran, I., Grootveld, A. K., Nguyen, A., and Phan, T. G. (2019). Subcapsular sinus macrophages: the seat of innate and adaptive memory in murine lymph nodes. *Trends Immunol.* 40, 35–48. doi: 10.1016/j.it.2018.11.004

Motulsky, H. J., and Brown, R. E. (2006). Detecting outliers when fitting data with nonlinear regression - a new method based on robust nonlinear regression and the false discovery rate. *BMC Bioinformat.* 7:123. doi: 10.1186/1471-2105-7-123

Mullins, R. D., Bieling, P., and Fletcher, D. A. (2018). From solution to surface to filament: actin flux into branched networks. *Biophys. Rev.* 10, 1537–1551. doi: 10.1007/s12551-018-0469-5

Murugesan, S., Hong, J., Yi, J., Li, D., Beach, J. R., Shao, L., et al. (2016). Formin-generated actomyosin arcs propel T cell receptor microcluster movement at the immune synapse. *J. Cell Biol.* 215, 383–399. doi: 10.1083/jcb.201603080

Nadkarni, A. V., and Brieher, W. M. (2014). Aip1 destabilizes cofilin-saturated actin filaments by severing and accelerating monomer dissociation from ends. *Curr. Biol.* 24, 2749–2757. doi: 10.1016/j.cub.2014.09.048

Nemazee, D. (2017). Mechanisms of central tolerance for B cells. *Nat. Rev. Immunol.* 17, 281–294. doi: 10.1038/nri.2017.19

Nishita, M., Wang, Y., Tomizawa, C., Suzuki, A., Niwa, R., Uemura, T., et al. (2004). Phosphoinositide 3-kinase-mediated activation of cofilin phosphatase Slingshot and its role for insulin-induced membrane protrusion. *J. Biol. Chem.* 279, 7193–7198. doi: 10.1074/jbc.M312591200

Niwa, R., Nagata-Ohashi, K., Takeichi, M., Mizuno, K., and Uemura, T. (2002). Control of actin reorganization by Slingshot, a family of phosphatases that dephosphorylate ADF/cofilin. *Cell* 108, 233–246. doi: 10.1016/S0092-8674(01)00638-9

Nomura, K., Hayakawa, K., Tatsumi, H., and Ono, S. (2016). Actin-interacting protein 1 promotes disassembly of actin-depolymerizing factor/cofilin-bound actin filaments in a pH-dependent manner. *J. Biol. Chem.* 291, 5146–5156. doi: 10.1074/jbc.M115.713495

Nowosad, C. R., Spillane, K. M., and Tolar, P. (2016). Germinal center B cells recognize antigen through a specialized immune synapse architecture. *Nat. Immunol.* 17, 870–877. doi: 10.1038/ni.3458

Ohashi, K. (2015). Roles of cofilin in development and its mechanisms of regulation. *Dev. Growth Diff.* 57, 275–290. doi: 10.1111/dgd.12213

Ohashi, K., Fujiwara, S., Watanabe, T., Kondo, H., Kiuchi, T., Sato, M., et al. (2011). LIM kinase has a dual role in regulating lamellipodium extension by decelerating the rate of actin retrograde flow and the rate of actin polymerization. *J. Biol. Chem.* 286, 36340–36351. doi: 10.1074/jbc.M111.259135

Okreglak, V., and Drubin, D. G. (2010). Loss of Aip1 reveals a role in maintaining the actin monomer pool and an *in vivo* oligomer assembly pathway. *J. Cell Biol.* 188, 769–777. doi: 10.1083/jcb.200909176

Ono, S. (2003). Regulation of actin filament dynamics by actin depolymerizing factor/cofilin and actin-interacting protein 1: new blades for twisted filaments. *Biochem.* 42, 13363–13370. doi: 10.1021/bi034600x

Ono, S. (2018). Functions of actin-interacting protein 1 (AIP1)/WD repeat protein 1 (WDR1) in actin filament dynamics and cytoskeletal regulation. *Biochem. Biophys. Res. Commun.* 506, 315–322. doi: 10.1016/j.bbrc.2017.10.096

Packard, T. A., and Cambier, J. C. (2013). B lymphocyte antigen receptor signaling: initiation, amplification, and regulation. *F1000Prime Rep* 5:40. doi: 10.12703/P5-40

Pfajfer, L., Mair, M. N. K., Jiménez-Heredia, R. G. F., Gulez, N., Ardeniz, Ö., Hoeger, B., et al. (2018). Mutations affecting the actin regulator WDR1 lead to aberrant lymphoid immunity. *J. Allergy and Clin. Immunol.* 142, 1589–1604.e11. doi: 10.1016/j.jaci.2018.04.023

Pollard, T. D., and Borisy, G. G. (2003). Cellular motility driven by assembly and disassembly of actin filaments. *Cell* 112, 453–465. doi: 10.1016/S0092-8674(03)00120-X

Ponti, A., Machacek, M., Gupton, S. L., Waterman-Storer, C. M., and Danuser, G. (2004). Two distinct actin networks drive the protrusion of migrating cells. *Science* 305, 1782–1786. doi: 10.1126/science.1100533

Provost, P., Doucet, J., Stock, A., Gerisch, G., Samuelsson, B., and Radmark, O. (2001). Coactosin-like protein, a human F-actin-binding protein: critical role of lysine-75. *Biochem. J.* 359(Pt 2), 255–263. doi: 10.1042/bj3590255

Prunier, C., Prudent, R., Kapur, R., Sadoul, K., and Lafanechere, L. (2017). LIM kinases: cofilin and beyond. *Oncotarget* 8, 41749–41763. doi: 10.18632/oncotarget.16978

Randall, K. L., Lambe, T., Johnson, A. L., Treanor, B., Kucharska, E., Domaschenz, H., et al. (2009). Dock8 mutations cripple B cell immunological synapses, germinal centers and long-lived antibody production. *Nat. Immunol.* 10, 1283–1291. doi: 10.1038/ni.1820

Ren, N., Charlton, J., and Adler, P. N. (2007). The flare gene, which encodes the AIP1 protein of Drosophila, functions to regulate F-actin disassembly in pupal epidermal cells. *Genetics* 176, 2223–2234. doi: 10.1534/genetics.107.072959

Rodal, A. A., Tetreault, J. W., Lappalainen, P., Drubin, D. G., and Amberg, D. C. (1999). Aip1p interacts with cofilin to disassemble actin filaments. *J. Cell Biol.* 145, 1251–1264. doi: 10.1083/jcb.145.6.1251

Ross-Macdonald, P., de Silva, H., Guo, Q., Xiao, H., Hung, C. Y., Penhallow, B., et al. (2008). Identification of a nonkinase target mediating cytotoxicity of novel kinase inhibitors. *Mol. Cancer Ther.* 7, 3490–3498. doi: 10.1158/1535-7163.MCT-08-0826

Saci, A., and Carpenter, C. L. (2005). RhoA GTPase regulates B cell receptor signaling. *Mol. Cell* 17, 205–214. doi: 10.1016/j.molcel.2004.12.012

Schindelin, J., Arganda-Carreras, I., Frise, E., Kaynig, V., Longair, M., Pietzsch, T., et al. (2012). Fiji: an open-source platform for biological-image analysis. *Nat. Methods* 9, 676–682. doi: 10.1038/nmeth.2019

Scott, R. W., Hooper, S., Crighton, D., Li, A., Konig, I., Munro, J., et al. (2010). LIM kinases are required for invasive path generation by tumor and tumor-associated stromal cells. *J. Cell Biol.* 191, 169–185. doi: 10.1083/jcb.201002041

Scott, R. W., and Olson, M. F. (2007). LIM kinases: Function, regulation and association with human disease. *J. Mol. Med.* 85, 555–568. doi: 10.1007/s00109-007-0165-6

Seppanen, M. R. J. (2018). Novel cytoskeletal mutations with immunodeficiency: why is the raven like a writing desk? *J. Allergy Clin. Immunol.* 142, 1444–1446. doi: 10.1016/j.jaci.2018.08.020

Shaheen, S., Wan, Z., Haneef, K., Zeng, Y., Jing, W., and Liu, W. (2019). B cell mechanosensing: a mechanistic overview. *Adv. Immunol.* 144, 23–63. doi: 10.1016/bs.ai.2019.08.003

Shen, P., and Fillatreau, S. (2015). Antibody-independent functions of B cells: a focus on cytokines. *Nat. Rev. Immunol.* 15, 441–451. doi: 10.1038/nri3857

Shishkin, S., Eremina, L., Pashintseva, N., Kovalev, L., and Kovaleva, M. (2016). Cofilin-1 and other ADF/cofilin superfamily members in human malignant cells. *Int. J. Mol. Sci.* 18:E10. doi: 10.3390/ijms18010010

Song, W., Liu, C., and Upadhyaya, A. (2014). The pivotal position of the actin cytoskeleton in the initiation and regulation of B cell receptor activation. *Biochim. Biophys. Acta* 1838, 569–578. doi: 10.1016/j.bbamem.2013.07.016

Sprenkeler, E. G. G., Webbers, S. D. S., and Kuijpers, T. W. (2020). When actin is not actin' like it should: a new category of distinct primary immunodeficiency disorders. *J. Innate Immun.* 13, 3–25. doi: 10.1159/000509717

Sun, X., Wang, J., Qin, T., Zhang, Y., Huang, L., Niu, L., et al. (2018). Dock8 regulates BCR signaling and activation of memory B cells via WASP and CD19. *Blood Adv.* 2, 401–413. doi: 10.1182/bloodadvances.2017007880

Svitkina, T. M., and Borisy, G. G. (1999). Arp2/3 complex and actin depolymerizing factor/cofilin in dendritic organization and treadmilling of actin filament array in lamellipodia. *J. Cell Biol.* 145, 1009–1026. doi: 10.1083/jcb.145.5.1009

Tan, C., Noviski, M., Huizar, J., and Zikherman, J. (2019). Self-reactivity on a spectrum: a sliding scale of peripheral B cell tolerance. *Immunol. Rev.* 292, 37–60. doi: 10.1111/imr.12818

Tanaka, K., Takeda, S., Mitsuoka, K., Oda, T., Kimura-Sakiyama, C., Maeda, Y., et al. (2018). Structural basis for cofilin binding and actin filament disassembly. *Nat. Commun.* 9:1860. doi: 10.1038/s41467-018-04290-w

Thauland, T. J., Hu, K. H., Bruce, M. A., and Butte, M. J. (2017). Cytoskeletal adaptivity regulates T cell receptor signaling. *Sci. Signal.* 10:eaah3737. doi: 10.1126/scisignal.aah3737

Treanor, B., Depoil, D., Bruckbauer, A., and Batista, F. D. (2011). Dynamic cortical actin remodeling by ERM proteins controls BCR microcluster organization and integrity. *J. Exp. Med.* 208, 1055–1068. doi: 10.1084/jem.20101125

Treanor, B., Harwood, N. E., and Batista, F. D. (2009). Microsignalosomes: spatially resolved receptor signalling. *Biochem. Soc. Trans.* 37(Pt 5), 1014–1018. doi: 10.1042/BST0371014

Tur-Gracia, S., and Martinez-Quiles, N. (2021). Emerging functions of cytoskeletal proteins in immune diseases. *J. Cell Sci.* 134:jcs253534. doi: 10.1242/jcs.253534

Vitriol, E. A., Wise, A. L., Berginski, M. E., Bamburg, J. R., and Zheng, J. Q. (2013). Instantaneous inactivation of cofilin reveals its function of F-actin disassembly in lamellipodia. *Mol. Biol. Cell* 24, 2238–2247. doi: 10.1091/mbc.e13-03-0156

Volpi, S., Cicalese, M. P., Tuijnenburg, P., Tool, A. T. J., Cuadrado, E., Ahanchian, H., et al. (2019). A combined immunodeficiency with severe infections, inflammation and allergy caused by ARPC1B deficiency. *J. Allergy Clin. Immunol.* 86:177–179. doi: 10.1016/j.jaci.2019.02.003

Wan, Z., Chen, X., Chen, H., Ji, Q., Chen, Y., Wang, J., et al. (2015). The activation of IgM- or isotype-switched IgG- and IgE-BCR exhibits distinct mechanical force sensitivity and threshold. *eLife* 4:e06925. doi: 10.7554/eLife.06925.020

Wan, Z., Zhang, S., Fan, Y., Liu, K., Du, F., Davey, A. M., et al. (2013). B cell activation is regulated by the stiffness properties of the substrate presenting the antigens. *J. Immunol.* 190, 4661–4675. doi: 10.4049/jimmunol.1202976

Wang, J. C., Bolger-Munro, M., and Gold, M. R. (2018). Imaging the interactions between B cells and antigen-presenting cells. *Meth. Mol. Biol.* 1707, 131–161. doi: 10.1007/978-1-4939-7474-0_10

Wang, J. C., Lee, J. Y., Christian, S., Dang-Lawson, M., Pritchard, C., Freeman, S. A., et al. (2017). The Rap1-cofilin-1 pathway coordinates actin reorganization

and MTOC polarization at the B cell immune synapse. *J. Cell Sci.* 130, 1094–1109. doi: 10.1242/jcs.191858

Westerberg, L., Larsson, M., Hardy, S. J., Fernandez, C., Thrasher, A. J., and Severinson, E. (2005). Wiskott-Aldrich syndrome protein deficiency leads to reduced B-cell adhesion, migration, and homing, and a delayed humoral immune response. *Blood* 105, 1144–1152. doi: 10.1182/blood-2004-03-1003

Yuseff, M. I., Pierobon, P., Reversat, A., and Lennon-Dumenil, A. M. (2013). How B cells capture, process and present antigens: a crucial role for cell polarity. *Nat. Rev. Immunol.* 13, 475–486. doi: 10.1038/nri3469

Conflict of Interest: The authors declare that the research was conducted in the absence of any commercial or financial relationships that could be construed as a potential conflict of interest.

frontiers in Cell and Developmental Biology

ORIGINAL RESEARCH
published: 13 May 2021
doi: 10.3389/fcell.2021.650817

Ecm29-Dependent Proteasome Localization Regulates Cytoskeleton Remodeling at the Immune Synapse

Jorge Ibañez-Vega[1†], Felipe Del Valle[1†], Juan José Sáez[1], Fanny Guzman[2], Jheimmy Diaz[1], Andrea Soza[3,4] and María Isabel Yuseff[1]**

[1] Departamento de Biología Celular y Molecular, Facultad de Ciencias Biológicas, Pontificia Universidad Católica de Chile, Santiago, Chile, [2] Núcleo Biotecnología Curauma, Pontificia Universidad Católica de Valparaíso, Valparaíso, Chile, [3] Centro de Biología Celular y Biomedicina, Facultad de Medicina y Ciencia, Universidad San Sebastián, Santiago, Chile, [4] Centro de Envejecimiento y Regeneración (CARE), Facultad de Ciencias Biológicas, Pontificia Universidad Católica de Chile, Santiago, Chile*

OPEN ACCESS

Edited by:
Balbino Alarcon, Consejo Superior de Investigaciones Científicas (CSIC), Spain

Reviewed by:
Francisco Sanchez-Madrid, Autonomous University of Madrid, Spain
Dorothy Lerit, Emory University, United States

***Correspondence:**
Andrea Soza
andrea.soza@uss.cl
María Isabel Yuseff
myuseff@bio.puc.cl

† These authors have contributed equally to this work

Specialty section:
This article was submitted to Cell Growth and Division, a section of the journal Frontiers in Cell and Developmental Biology

Received: *08 January 2021*
Accepted: *14 April 2021*
Published: *13 May 2021*

Citation:
Ibañez-Vega J, Del Valle F, Sáez JJ, Guzman F, Diaz J, Soza A and Yuseff MI (2021) Ecm29-Dependent Proteasome Localization Regulates Cytoskeleton Remodeling at the Immune Synapse. Front. Cell Dev. Biol. 9:650817. doi: 10.3389/fcell.2021.650817

The formation of an immune synapse (IS) enables B cells to capture membrane-tethered antigens, where cortical actin cytoskeleton remodeling regulates cell spreading and depletion of F-actin at the centrosome promotes the recruitment of lysosomes to facilitate antigen extraction. How B cells regulate both pools of actin, remains poorly understood. We report here that decreased F-actin at the centrosome and IS relies on the distribution of the proteasome, regulated by Ecm29. Silencing Ecm29 decreases the proteasome pool associated to the centrosome of B cells and shifts its accumulation to the cell cortex and IS. Accordingly, Ecm29-silenced B cells display increased F-actin at the centrosome, impaired centrosome and lysosome repositioning to the IS and defective antigen extraction and presentation. Ecm29-silenced B cells, which accumulate higher levels of proteasome at the cell cortex, display decreased actin retrograde flow in lamellipodia and enhanced spreading responses. Our findings support a model where B the asymmetric distribution of the proteasome, mediated by Ecm29, coordinates actin dynamics at the centrosome and the IS, promoting lysosome recruitment and cell spreading.

Keywords: proteasome, actin cytoskeleton, Ecm29, immune synapse, lysosomes, microtubules, B cell

INTRODUCTION

The interaction of the B cell receptor (BCR) with membrane-tethered antigens (mAg) initiates the formation of an immune synapse (IS), characterized by rapid cortical actin cytoskeleton rearrangements and the formation of BCR-microclusters containing signaling molecules that elicit B cell activation (Yuseff et al., 2013; Kwak et al., 2019). In resting conditions, the lateral diffusion of the BCR is restricted by the cortical actin network, which becomes disassembled upon antigen engagement, enabling BCR lateral diffusion and subsequent clustering to promote downstream signaling (Mattila et al., 2016; Tolar, 2017; Freeman et al., 2018). During this phase, B cells exert a rapid spreading response by forming lamellipodia to expand the contact area with the antigen-presenting surface, thereby increasing the number of BCRs coupled to mAg (Fleire et al., 2006). Cell expansion is followed by a contraction phase, which serves to gather BCR microclusters at the center of the B cell synapse, which also relies on dynein-microtubule mediated transport

(Harwood and Batista, 2010; Wang and Hammer, 2020). Actin retrograde flow at the synaptic interface can also promote the gathering of signaling molecules to the center of the synapse, as observed in T lymphocytes where coalescence of PLCγ1 molecules, which enables sustained T cell signaling, relies on the inward flow of actin (Babich et al., 2012). Whether a similar mechanism contributes to the coalescence of signaling microclusters at the IS of B cells, remained to be proven (Wang and Hammer, 2020). In addition to dynamic changes exerted at the cell cortex, IS formation also involves the mobilization of the centrosome together with lysosomes toward the Ag-contact site, where secretion of their content into the synaptic space facilitates antigen extraction from stiffer surfaces (Bellaiche et al., 2011; Ritter et al., 2015; del Valle Batalla et al., 2018). Exocytic events that occur at the synaptic membrane also rely on cortical actin cytoskeleton remodeling, where local actin depletion at the synaptic membrane is required for secretion of lytic granules in NK and cytotoxic T cells (Ritter et al., 2015; Gil-Krzewska et al., 2017).

Mobilization of the centrosome to the IS of T lymphocytes relies on dynein (Martín-Cófreces et al., 2008) where microtubule shrinkage, at the synaptic region, has been proposed to act as the pulling force needed for centrosome repositioning (Yi et al., 2013). In addition to the role of microtubules, studies in B cells, revealed that translocation of the centrosome from the perinuclear region to the IS requires the depletion of the actin pool surrounding the centrosome. This step is critical to allow its uncoupling from the nucleus, thereby promoting the establishment of a polarized phenotype (Obino et al., 2016). Thus, the capacity of B cells to organize an IS and execute their antigen-presenting function is strongly dependent on actin remodeling both at the cortical and perinuclear regions. How B cells orchestrate actin dynamics at both these levels remains to be resolved.

The ubiquitin-proteasome system (UPS) has emerged as a critical regulator of cell signaling, polarization, cell division, and migration by selective proteolysis of ubiquitin-tagged proteins (Coux, 2002; Schaefer et al., 2012; Collins and Goldberg, 2017). This system comprises ubiquitin ligases that targets proteins for degradation by covalently conjugating them with ubiquitin, enabling recognition by the proteasome to drive their proteolysis (Collins and Goldberg, 2017). The proteasome is responsible for the degradation of most cytosolic proteins in mammalian cells. This protein complex is formed by the 20S core particle (CP) and the 19S regulatory particle (RP), that caps the 20S CP on one (26S proteasome) or both ends (30S proteasome) in an ATP-dependent manner and can dissociate reversibly (Collins and Goldberg, 2017). Proteasome assembly, activity, localization, and half-life is regulated by transcriptional and post-translational modifications of proteasomal subunits (Dahlmann, 2016; Collins and Goldberg, 2017; Dikic, 2017).

Among proteasome regulators, a 200 kDa protein, termed Ecm29, first characterized in yeast, binds the proteasome to motor proteins and vesicles, suggesting that it could play a role in the intracellular localization of the proteasome. Ecm29 has been shown to couple the proteasome to the Endoplasmic Reticulum (ER), microtubules, and centrosome (Gorbea et al., 2010), however, the mechanisms by which Ecm29 recruits the proteasome to specific cellular compartments are not fully understood. In neurons, Ecm29 controls proteasome localization and mobilization across the axon by modulating its association with microtubules, where its activity and localization influences neuronal development and synaptic signaling (Otero et al., 2014; Hsu et al., 2015; Pinto et al., 2016; Lee et al., 2020).

In lymphocytes, proteasome activity and localization also play a crucial role in their function. Indeed, the inhibition of proteasome activity leads to defective actin remodeling and reduced ERK signaling, impairing efficient B and T lymphocyte activation (Schmidt et al., 2018; Ibañez-Vega et al., 2019a). Moreover, during asymmetric T cell division, the unequal segregation of the proteasome between the two daughter cells enables the selective degradation of the transcriptional factor Tbet, which ultimately leads to the acquisition of different phenotypes (Dennis et al., 2012). Thus, the localization of the proteasome is regulated in lymphocytes during asymmetric cell division, where control of cell polarity is critical. Analogously, in neurons, where cell polarity is also crucial, the localization of the proteasome targets the degradation of ubiquitylated proteins, required for axon development (Otero et al., 2014; Hsu et al., 2015) and presynaptic differentiation (Pinto et al., 2016; Liu et al., 2019). Here, a polarized phenotype is achieved by the selective degradation of polarity proteins, such as PAR-2, PAR-3, PAR-6 (Laumonnerie and Solecki, 2018), and actin polymerizing factors, such as VASP by the UPS (Boyer et al., 2020).

Interestingly, upon activation, B cells upregulate the ubiquitylation of proteins, including BCR downstream signaling molecules, polarity proteins, and actin polymerizing factors (Satpathy et al., 2015), highlighting a role for the UPS in regulating actin dynamics and B cell activation. We have previously shown that B cells contain an active proteasome pool at the centrosome, which is required for efficient actin clearance at this level, which enables centrosome repositioning to the immune synapse (Ibañez-Vega et al., 2019a). However, the underlying mechanisms of proteasome localization remain to be addressed in lymphocytes.

In this study, we explored whether Ecm29 controls the localization of the proteasome in B cells during the formation of an immune synapse and how this specific localization coordinates actin remodeling responses between the synaptic interface and the centrosome. Our results show that Ecm29 mediates the association of the proteasome with the microtubule network and regulates the distribution of proteasome pools at the centrosome and the immune synapse of B cells. As a consequence of Ecm29 silencing, B cells redistribute the proteasome to the synaptic membrane, which results in defective actin dynamics at this level, evidenced by slower actin retrograde flow at lamellipodia formed at the synaptic membrane and increased spreading responses. Ecm29-silenced B cells also displayed deficient actin depolymerization at the centrosome, which impair centrosome and lysosome repositioning at the immune synapse, resulting in reduced antigen extraction and presentation. Overall, our results contribute to the understanding of how B lymphocytes efficiently coordinate actin dynamics at the centrosome and the synaptic interface by controlling the

localization of the proteasome. We propose that the distribution of the proteasome depends on Ecm29, which enables: (1) the accumulation of the proteasome at the centrosome, used to promote actin depolymerization required for centrosome re-positioning and lysosome recruitment at the IS and (2) the recruitment of proteasome to the synaptic membrane, promoting actin depolymerization at this level to enhance cell spreading and signaling.

Thus, Ecm29 emerges as a key regulator of proteasome distribution used to orchestrate key synaptic functions to facilitate antigen extraction and activation of B cells.

RESULTS

Ecm29 Regulates the Localization of the Proteasome in B Cells

Intracellular compartmentalization of proteasome activity controls actin cytoskeleton remodeling in B cells during immune synapse formation (Ibañez-Vega et al., 2019a). We sought for potential regulators involved in proteasome distribution and focused on the molecule Ecm29, a proteasome adaptor, and scaffold protein, which binds to the 26S proteasome and links it to motor proteins, vesicles, centrosome, and microtubules (Gorbea et al., 2010). To this end, we first analyzed the localization of Ecm29 in B cells activated with antigens immobilized on 3 μM beads, which triggers the formation of an IS and compared them with non-activated B cells (Yuseff et al., 2013; Ibañez-Vega et al., 2019a). We found that upon activation with antigen-coated beads, Ecm29 progressively accumulated at the synaptic interface, which was quantified as the fluorescence ratio between the bead and the whole cell (**Figures 1A,B**), similarly to the proteasome (Ibañez-Vega et al., 2019a). To further characterize the distribution of Ecm29 at the synaptic membrane, we activated B cells on antigen-coated coverslips and labeled Ecm29 together with microtubules (α-tubulin) and the centrosome, labeled with centrin-GFP, which was validated as a centrosome marker (**Supplementary Figure 1B**). We found that Ecm29 was distributed in a central and peripheral pool, associated with the centrosome and cortical microtubules, respectively (**Figure 1C**). The accumulation of Ecm29 at the centrosome of B cells was verified by immunoblot of centrosome-rich fractions, where we found that Ecm29 cofractionated with γ-tubulin, a centrosome marker (**Supplementary Figure 1A**). Imaging analysis also revealed that Ecm29 colocalized with microtubules, displaying a Pearson's mean coefficient over 0.67 in resting and activating conditions (**Figures 1C,D**). Importantly, colocalization was significatively higher compared to measurements performed after rotating a channel in 90°, used as a negative control (Pearson's mean coefficient values of 0.27 and 0.18 for resting and activating conditions, respectively). Also, we found a minor colocalization with the Golgi apparatus (**Supplementary Figure 1C**). Association of Ecm29 with the microtubule network is supported by our observations showing that treatment with Nocodazole, a microtubule destabilizing drug, changed the distribution of Ecm29 and proteasome (19S), which both displayed a more cortical localization and loss their pericentral localization under these conditions (**Supplementary Figures 1D,E**). Indeed, the association of Ecm29 with microtubules was previously described in neurons, where it was shown to mediate proteasome retrograde transport and axon development (Otero et al., 2014; Hsu et al., 2015). Interestingly, we found that upon activation, Ecm29 slightly reduced its colocalization with microtubules and accumulated at the cell periphery (**Figures 1C–E**), suggesting that Ecm29 also changes its distribution in response to BCR stimulation.

Next, we evaluated whether Ecm29 regulates the localization of the proteasome in B lymphocytes. For this purpose, we reduced the expression of Ecm29 in B cells by siRNA (**Supplementary Figures 2A,B**) and evaluated the distribution of the 26S proteasome in resting and activated B cells by immunofluorescence staining using an antibody that recognizes the 19S regulatory particle (RP). Upon Ecm29 silencing, we observed a reduction in the amount of proteasome at the centrosome of B cells under resting conditions, but not in activating conditions (**Figures 2A,C**). Moreover, upon activation both control and Ecm29-silenced B cells mobilized their proteasome away from the centrosome, suggesting that this event does not rely on Ecm29. Thus, Ecm29 is responsible for retaining the proteasome at the perinuclear region but is not required for its mobilization toward the cortex. Indeed, proteasome depletion from the centrosome of Ecm29-silenced B cells was confirmed by the detection of 19S RP by immunoblot in centrosome-rich fractions obtained from control and Ecm29-silenced cells. Quantification of the 19S RP, normalized by γ-tubulin levels, indicated there was a reduction in the amount of the proteasome at the centrosome of Ecm29-silenced B cells (**Supplementary Figures 2E,F**). Furthermore, quantification of proteasome activity in centrosome-rich fractions by using a fluorescent peptide as a substrate revealed a reduction in 50% of proteasome activity (**Supplementary Figure 2G**), which correlated with the decreased proteasome mass. When Ecm29-silenced cells were activated with antigen-coated beads, we observed enhanced accumulation of the proteasome at the antigen-bead contact site compare to control cells (blue area in line-scan) (**Figures 2A,B**). This result prompted us to further explore the distribution of the proteasome at the synaptic membrane of Ecm29-silenced B cells. To this end, we activated B cells by seeding them onto antigen-coated coverslips and labeled the 19S RP to visualize the proteasome as well as microtubules (α-tubulin), and the centrosome (Centrin-GFP). We found that the 19S RP significantly changed its distribution at the IS of Ecm29-silenced cells, exhibiting a more dispersed pattern, instead of colocalizing with microtubules (**Figures 2D,E**), suggesting that Ecm29 mediates the association of the proteasome with microtubules, analogously to what has been described in neurons (Hsu et al., 2015). Despite being more dispersed, the proteasome displayed slightly higher levels at the center of IS in Ecm29-silenced B cells (**Figures 2D,F**), suggesting that Ecm29 could be controlling proteasome distribution to the IS center, and potentially have an impact on the local degradation of protein targets within this region.

To characterize the dynamic recruitment of the proteasome at the IS in control versus Ecm29-silenced cells, we labeled

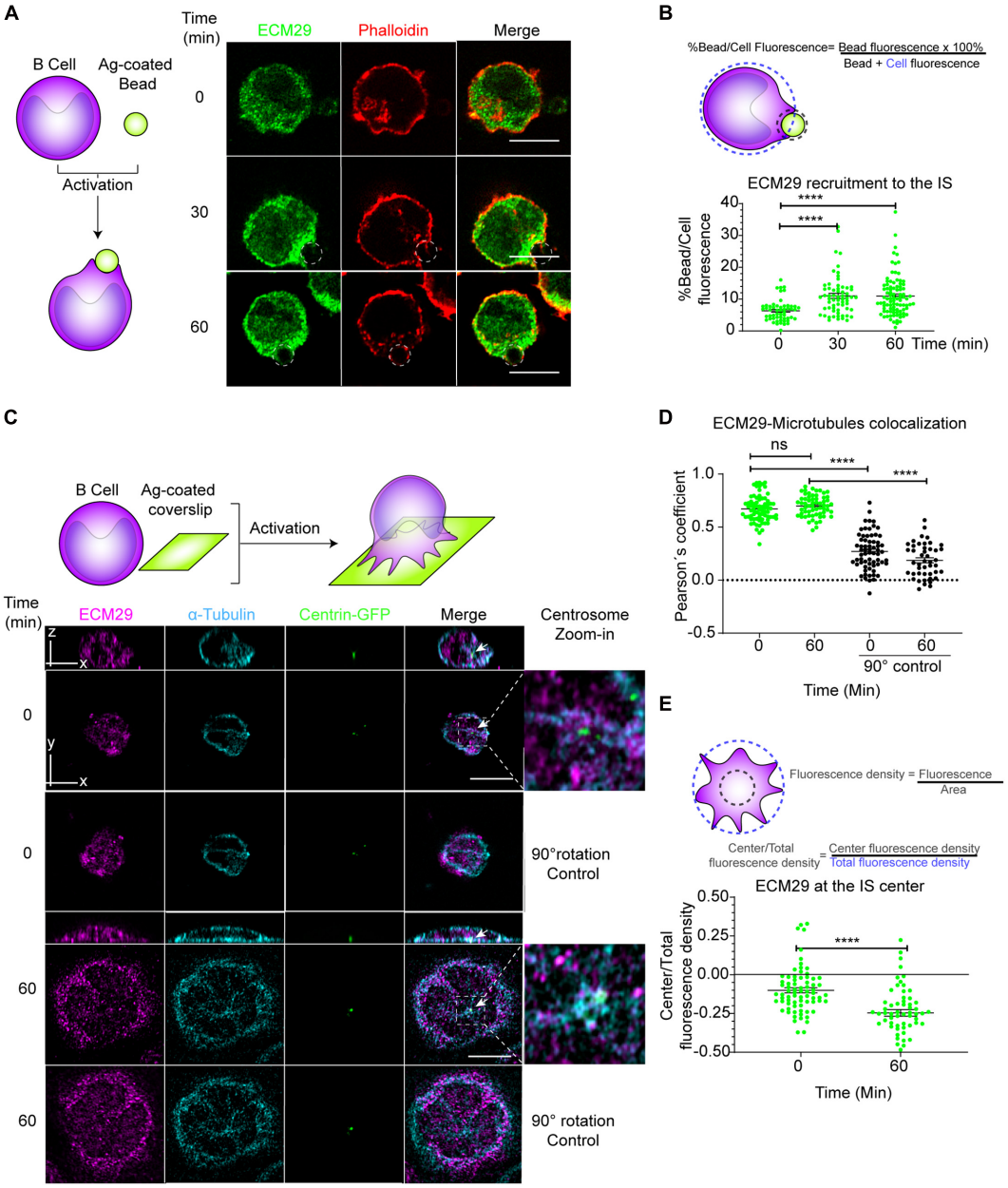

FIGURE 1 | Ecm29 co-localizes with microtubules and the centrosome and is recruited to the IS of B cells: **(A)** Scheme depicting activation of B cells with antigen-coated beads and representative Airyscan images of B cells activated for different time points (0, 30, and 60 min), labeled for actin (phalloidin) and Ecm29. Dashed white circles represent the bead. **(B)** Quantification scheme and quantification of Ecm29 recruitment at the immune synapse (Bead) after different time points of activation. $N = 4$. Cells > 54. **(C)** Scheme depicting activation of B cells onto antigen-coated coverslips. Representative Airyscan images of centrin-GFP expressing B cells in resting (0 min) and activating (60 min) conditions, labeled for Ecm29 (magenta), microtubules (α-tubulin, cyan). White arrows indicate the centrosome. Magnifications of centrosome areas (9 μm^2) are shown. 90°channel rotation control is shown for both time points (Means: 0,27 and 0,18 for 0 and 60 min of activation, respectively). **(D,E)** Quantification of the colocalization of Ecm29 with microtubules and its accumulation at the IS center (see scheme) from experiment shown in C. $N = 2$. Cells > 61. ****$p < 0.0001$. Kruskal–Wallis test with Dunn's test, and Mann–Whitney test was performed for all statistical analyses. Mean with SEM bars are shown. Scale bar = 10 μm. ns, non-significant.

the proteasome in live cells by using a specific fluorescent probe that binds to the catalytic β5 subunit (Bsc2118-FL-Bodipy). We used this probe at 5 nM in our assays, previously described not to significantly inhibit proteasome activity (Mlynarczuk-Bialy et al., 2014). Additionally, we verified that this dose did not generate an accumulation of ubiquitylated proteins (**Supplementary Figure 3A**), suggesting no significant effects over proteasome activity. Using this approach, we confirmed that the proteasome co-distributed with microtubules, displaying a central and peripheral localization at the synaptic

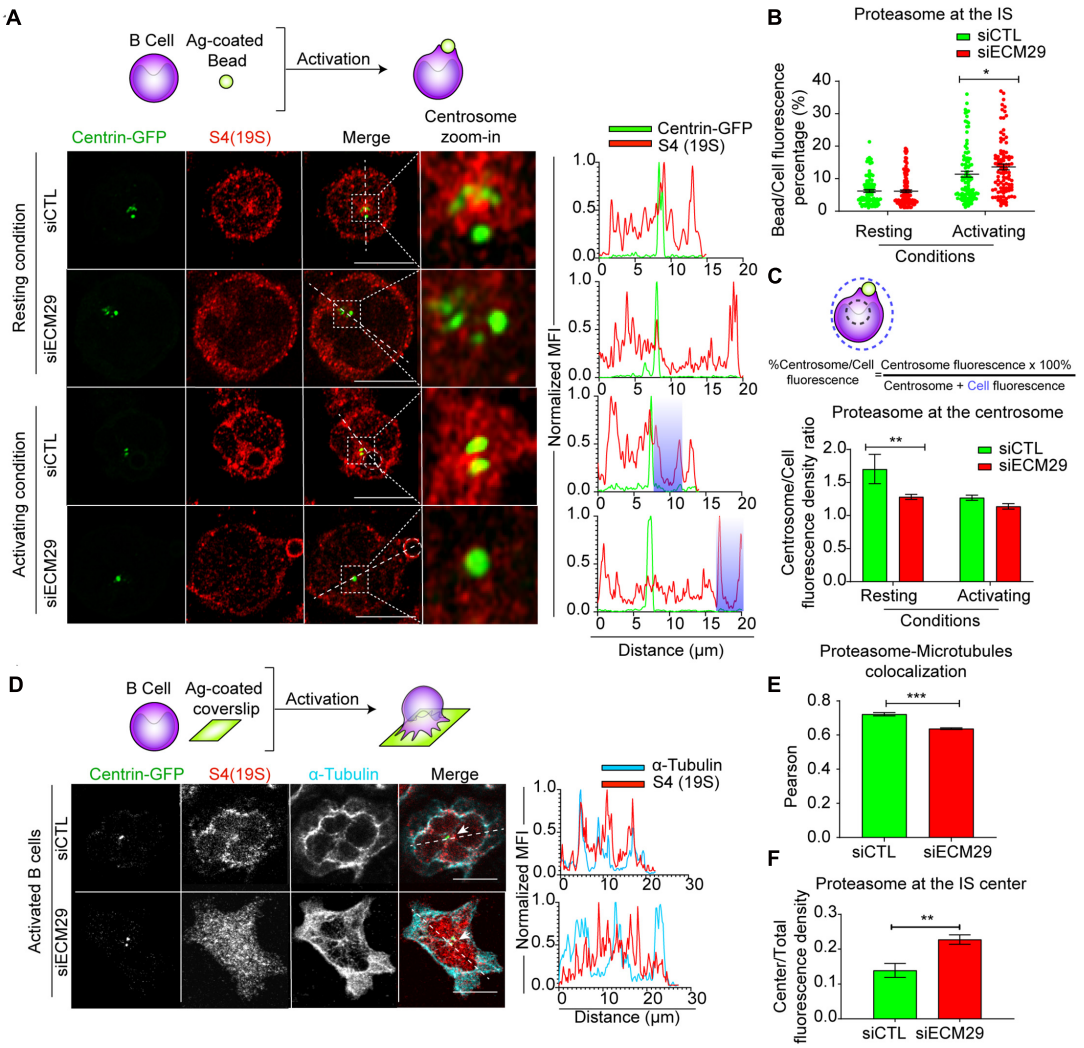

FIGURE 2 | Ecm29 regulates proteasome localization at the centrosome and microtubules: **(A)** Top: Schematic representation of B cells activated with antigen-coated beads. Representative confocal images of centrin-GFP expressing control (siCTL) and Ecm29-silenced (siECM29) B cells in resting (0 min) or activating (60 min) conditions, labeled for 19S[S4] (red). Magnifications of the centrosome area (3 μm^2) are shown. Fluorescence intensity distributions of centrin-GFP (green) and S4(19S) (red) across the cell (dashed white lines) are shown on the right. White dashed circles and shaded areas represent the bead and the centrosome area, respectively. **(B,C)** Scheme and quantification of proteasome enrichment at the centrosome and the bead in **(A)**, respectively. $N = 4$. Cells > 97. **(D)** Schematic representation of B cells activated onto antigen-coated coverslips. Representative confocal images of centrin-GFP expressing control and Ecm29-silenced B cells after 60 min of activation, labeled for 19S[S4] and α-tubulin. The fluorescence intensity distributions of α-tubulin (blue) and S4(19S) (red) across the cell (dashed white lines) are shown. White arrows indicate the centrosome. **(E,F)** Quantification of proteasome colocalization with microtubules and proteasome recruitment at the IS center, respectively. $N = 2$. Cells > 53 and >48, respectively. $^*p < 0.05$. $^{**}p < 0.01$. $^{***}p < 0.001$. Kruskal–Wallis test with Dunn's test, and Mann–Whitney test was performed for all statistical analyses. Mean with SEM bars are shown. Scale bar = 10 μm.

membrane (**Supplementary Figure 3B**), with limited diffusion rates (median: 0.074 $\mu m^2/s$) (**Supplementary Figures 3C,D**), comparable to those described in neurons (Otero et al., 2014). Using live cell imaging and Bsc2118-FL-Bodipy labeling, we also verified that in Ecm29-silenced cells, the 20S proteasome became more enriched at the IS than control counterparts, which was evidenced by a higher number and duration of proteasome tracks (**Supplementary Figures 4A,C,E**). When measuring proteasome diffusion rates, we observed that these were slightly higher in Ecm29-silenced cells without affecting their overall displacement at the IS (**Supplementary Figures 4A,B,D**). Altogether, these results suggest that Ecm29 regulates the recruitment of the 20S proteasome to the IS, controlling its diffusion rate, most likely in a microtubule-dependent manner.

Ecm29 has been shown to negatively regulate the proteasome by inhibiting its ATPase activity, which is crucial to unfold and translocate target proteins into the catalytic core for degradation (De La Mota-Peynado et al., 2013). To determine whether Ecm29 silencing affected the activity of the proteasome, we measured the amount of ubiquitylated proteins and proteasome subunits in Ecm29-silenced and control B cells. Quantification by immunoblot of proteasome subunits: S4 for the regulatory

particle (19S), α-β for the catalytic core (20S), and LMP7 for the induced catalytic core (immune proteasome), showed no differences between control and Ecm29-silenced cells (**Supplementary Figures 2C,D**). These results indicate that in B cells, Ecm29 regulates the localization of the proteasome without significantly affecting its total mass or activity.

Ecm29 Regulates Actin Remodeling at the Synaptic Membrane and B Cell Spreading Responses

Having shown that Ecm29 regulates the distribution of the proteasome in B cells and considering that proteasome activity is crucial for actin remodeling at the centrosome and IS of B cells (Ibañez-Vega et al., 2019a), we sought to determine whether actin levels at these two regions were affected by Ecm29 depletion. To this end, we seeded control and Ecm29-silenced B cells onto antigen-coated coverslips and imaged them by confocal microscopy, measuring the spreading area, delimited by actin labeling. Unexpectedly and contrary to the effect of inhibiting proteasome activity (Ibañez-Vega et al., 2019a), we found that, after 30 and 60 min of activation, Ecm29-silenced cells displayed an increased spreading area, which was at least two-fold higher than control cells (**Figures 3A,B**). We next characterized actin dynamics at the synaptic interface of these cells by performing live imaging using TIRFM. For this purpose, control and Ecm29-silenced B cells expressing the actin fluorescent reporter LifeAct-mCherry were activated onto antigen-coated coverslips. Similar to our observations in fixed cells, Ecm29-silenced cells displayed an increased spreading response during activation, which was also approximately two-fold higher than control cells (**Figures 3C,D**). Under these conditions, we noticed that the spreading rate was also higher in Ecm29-silenced B cells (**Figure 3D**). Interestingly, these cells underwent continuous spreading, which was not followed by a stationary phase, generally observed in control cells after 10 min of activation, where spreading starts to slow down (**Figure 3D**). This observation suggests that Ecm29-silenced B cells sustain an uncontrolled spreading response without reaching a stationary phase or further contraction, as was previously shown by B cells interacting with membrane-tethered antigens (Fleire et al., 2006).

In T lymphocytes, immune synapse stability has been associated with forming symmetric synapse (Kumari et al., 2020). Given that Ecm29-silenced B cells displayed an uncontrolled spreading response, we investigated whether this was due to perturbed immune synapse stability. To this end, we quantified the IS symmetry during the spreading response in control and Ecm29-silenced B cells, measured as the aspect ratio of the spreading area. We found that the symmetry of the synapse in Ecm29-silenced cells was highly sustained compared to control cells (**Figure 3E**), suggesting that Ecm29 silencing enhances immune synapse stability in B cells.

Ecm29-silenced B cells also exhibited smaller lamellipodia, which could result from defects in actin polymerization, required to generate actin retrograde flow (Wang and Hammer, 2020). Thus, we sought to determine whether actin polymerization at lamellipodia, measured as the velocity of actin-retrograde flow, was also affected. For this purpose, we seeded LifeAct-mCherry expressing control and Ecm29-silenced B cells for 30 min in antigen-coated coverslips before performing live-cell imaging. We observed that the length of lamellipodia was significantly reduced in Ecm29-silenced B cells, which also showed a reduction in the velocity of actin-retrograde flow, compared to control cells (**Figures 4A,B**). Altogether these results highlight a role for Ecm29 in forming lamellipodia at the IS of B cells, and suggests that the proteasome close to the IS membrane could be regulating actin polymerization, probably, by the degradation of actin polymerizing factors, as was previously suggested (Hao et al., 2013; Ibañez-Vega et al., 2019a).

To further evaluate the impact of Ecm29 on actin polymerization at the IS, we seeded actin-GFP-expressing B cells, silenced or not for Ecm29, onto antigen-coated coverslips for 30 min and performed a Fluorescence Recovery After Photobleaching (FRAP) assay using TIRFM. This assay allowed us to quantify actin turnover at the synaptic interface, as an indirect measurement of actin polymerization, previously reported in B cells (Pauls et al., 2020). Indeed, Ecm29-silenced cells showed a reduction in fluorescence recovery velocity, expressed as the rate constant (k) (**Figures 4C–E**), suggesting that actin polymerization at the synapse is reduced under these conditions. To determine whether reduced actin polymerization at the IS in Ecm29-silenced cells translated into less F-actin accumulation at the synaptic interface, we activated B cells with antigen-coated beads and measured its accumulation at the antigen contact site. As expected, after different time points of activation, we observed reduced F-actin levels at the antigen contact site (bead) in Ecm29-silenced cells compared to control cells (**Figures 4F,G**). Considering that Ecm29-silenced cells accumulate more proteasome at the IS, this highlights its negative correlation with F-actin accumulation at the IS.

To further explore a functional link between proteasome and actin polymerization at the IS, we co-labeled F-actin (LifeAct-mCherry) and the 20S proteasome (5 nM Bsc2118-FL-Bodipy) in live cells activated on antigen-coated coverslips for 30 min and analyzed the synaptic interface by TIRFM. We found that structures labeled for the proteasome negatively correlated with F-actin fluorescence (**Supplementary Figures 5A–F,I**). This negative correlation was dependent on proteasome activity because pre-treatment with 5 μM MG-132 or high concentrations of Bsc2118-FL-Bodipy (100 nM), which inhibits proteasome activity, abolished this negative correlation. On the other hand, the silencing of Ecm29, did not affect this negative correlation (**Supplementary Figures 5G–I**). Altogether, these results suggest that the proteasome at the synaptic interface is associated with F-actin depletion, with functional repercussions in actin turnover and lamellipodia formation.

To determine how the proteasome negatively regulates actin accumulation at the IS of B cells, we evaluated whether the levels of actin polymerizing factors, which are targets of proteasome degradation (Schaefer et al., 2012), changed in Ecm29-silenced cells. The levels of actin polymerizing factors, Arp2, WASp, and HS1, which have been shown to play a role in B cells (Bolger-Munro et al., 2019; Roper et al., 2019) were quantified in control and Ecm29-silenced B cells, by immunoblot. We found reduced

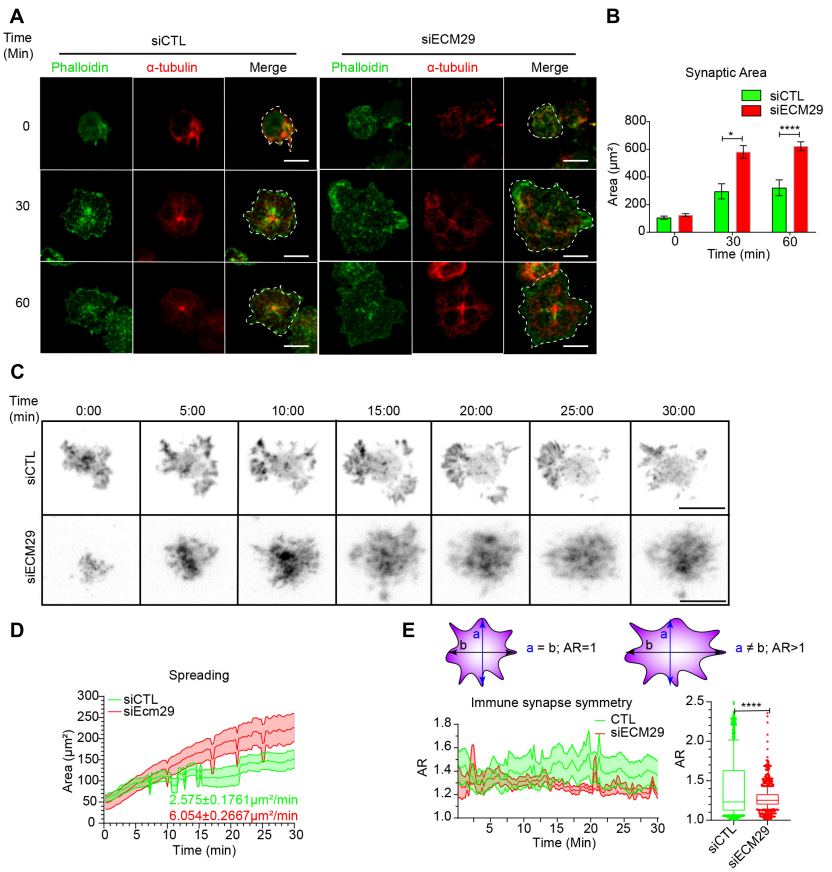

FIGURE 3 | Ecm29 silencing enhances B cell spreading responses: **(A)** Representative confocal images of control (siCTL) and Ecm29-silenced (siECM29) B cells activated for different time points (0, 30, and 60 min), stained with phalloidin (green) and α-Tubulin (red) are shown. **(B)** Quantification of the spreading area in **(A)**. $N = 3$. Cells > 40. **(C)** Representative Time-lapse images acquired by TIRFM of control and Ecm29-silenced B cells expressing LifeAct-mCherry (grayscale). **(D,E)** Quantification of the spreading area and aspect ratio (AR) and a schematic representation of AR values in **(C)**, respectively. The mean spreading velocity and mean AR are shown. $N = 10$. *$p < 0.05$. ****$p < 0.0001$. Kruskal–Wallis test with Dunn's test, and Mann-Whitney test was performed for all statistical analyses were performed. Mean with SEM bars **(B)**, lines **(D,E)**, and boxes and whiskers with 10% percentile **(E)** are shown. Scale bar = 10 μm.

levels of HS1 in Ecm29-silenced cells, whereas Arp2 or WASp remained unchanged (**Figures 4H,I**). Considering that HS1 is localized at the synaptic interface and the centrosome in B cells (Obino et al., 2016), our results suggest that, HS1 could be the main target of proteasome degradation at the synaptic interface during B cell activation, however, further studies are required to confirm this.

Ecm29 Silencing Enhances BCR Clustering and Signaling

Having shown that Ecm29 regulates actin polymerization at the IS, we next explored the role of Ecm29 in BCR signaling. F-actin depolymerization facilitates BCR diffusion at the IS, promoting receptor clustering, and signaling (Freeman et al., 2015; Tolar, 2017). Given that Ecm29 silencing reduced actin accumulation and turnover at the synapse, we evaluated whether the distribution of the BCR was affected under these conditions. Our results show that Ecm29-silenced cells displayed enhanced BCR accumulation at the center of the IS, especially after 30 min of activation, shown by the higher mean fluorescence (MFI) this region (the first quartile) (**Figures 5A,B**). This also translated into higher BCR downstream signaling where Erk phosphorylation levels, were higher in Ecm29-silenced cells compared to controls (**Figure 5C**). Thus, enhanced BCR clustering and signaling could result from unstable actin structures at the IS, increasing BCR mobility, as previously described (ref , Tolar, 2017). These observations suggest that the reduced actin polymerization at the IS in Ecm29-silenced B cells results in enhanced B cell activation. Considering that actin cytoskeleton remodeling is also important at the centrosome for antigen extraction and presentation (Obino et al., 2016; Ibañez-Vega et al., 2019a), we next evaluated whether Ecm29 silencing could affect centrosome repositioning upon BCR activation.

Ecm29 Regulates Centrosome Positioning at the IS

A hallmark of the B cell IS is the repositioning of the centrosome to the synaptic interface, which orchestrates the recruitment

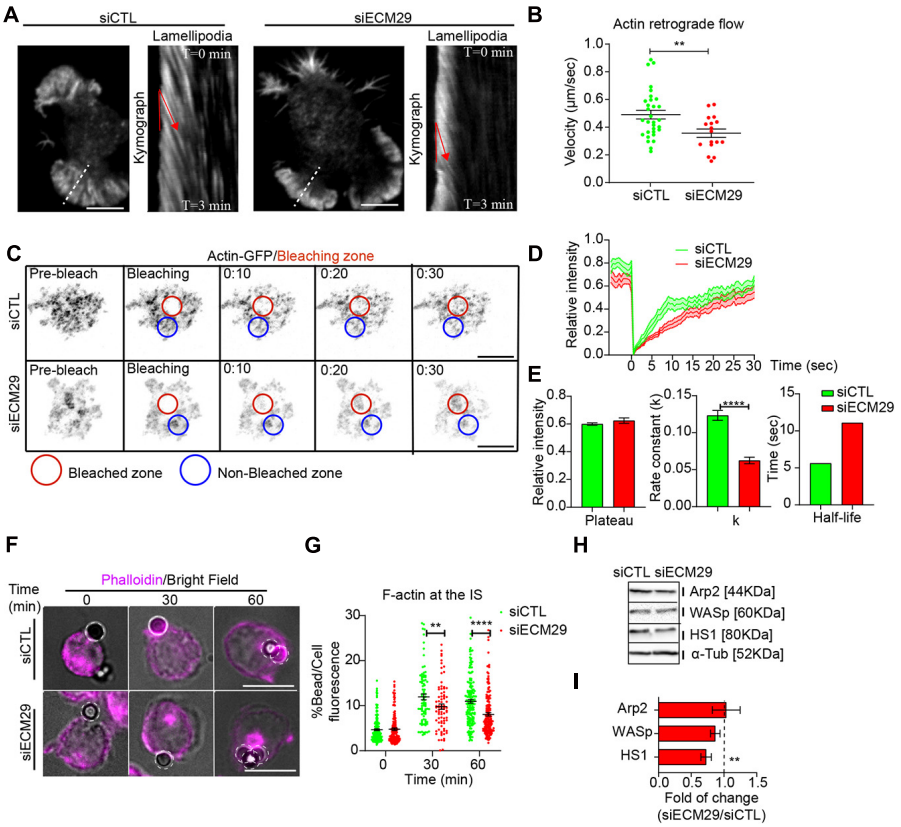

FIGURE 4 | Ecm29 silencing reduces actin dynamics and accumulation at the IS: **(A)** Representative TIRFM images of control (siCTL) and Ecm29-silenced (siECM29) B cells after 30 min of activation and their respective kymographs of lamellipodia (white dashed line). Red lines represent the actin retrograde flow angle. **(B)** Quantification of actin retrograde flow in **(A)**. $N = 17$. **(C)** Time-lapse FRAP-TIRFM images of control and Ecm29-silenced B cells expressing Actin-GFP (grayscale) after 30 min of activation. Red and blue circles represent the bleached and non-bleached zone, respectively. **(D,E)** Quantification of Fluorescence Recovery After Photobleaching of Actin-GFP, and associated parameters (plateau, k, and half-life). $N = 15$. **(F)** Representative epifluorescence images of control and Ecm29-silenced B cells activated with antigen-coated beads for different time points, labeled for F-actin (Phalloidin) are shown. **(G)** Quantification of F-actin accumulation at the bead in F. $N > 3$. Cells > 80. **(H)** Representative immunoblot of control and Ecm29-silenced B cells. Arp2, WASp, HS1, and α-Tub are shown. **(I)** Quantification of protein levels in **(E)**. $N > 4$. $^{**}p < 0.01$. $^{****}p < 0.0001$. A Mann–Whitney was performed. Mean with SEMs and individual experiments (points) **(A,G)**, and boxes with SEM **(I)** are shown. Scale bar = 10 µm.

of lysosomes to the IS, where they undergo local secretion to facilitate antigen extraction (Bellaiche et al., 2011). Centrosome repositioning to the synaptic interface requires depolymerization of perinuclear actin that maintains the centrosome linked to the nucleus (Obino et al., 2016). We previously described that proteasome activity is crucial for actin depletion at the centrosome to enable centrosome repositioning (Ibañez-Vega et al., 2019a). Thus, we asked whether silencing Ecm29 in B cells had a similar effect, given that it results in the mislocalization of the proteasome. For this purpose, we activated control and Ecm29-silenced B cells expressing Centrin-GFP on antigen-coated coverslips and measured the recruitment of the centrosome to the synapse after different time points of activation. As previously described, we found that the centrosome reached the proximity of the antigen-coated surface in control conditions, which we detected at the first and second Z-axis section of the fluorescence distribution graph (**Figures 6A,B**). Conversely, in Ecm29-silenced cells, the centrosome was not recruited to the IS, where the mean fluorescence of Centrin-GFP remained between the third and sixth Z fraction of the fluorescence distribution graph (**Figures 6A,C**). Next, we quantified the amount of actin at the centrosome in control and Ecm29-silenced cells. Our imaging analysis showed that Ecm29-silenced B cells exhibit defective actin clearance at the centrosome after 30 min of activation (**Figures 6D,E**), which most likely results from a decrease in proteasome activity associated with the centrosome of these cells (**Figures 2A,C** and **Supplementary Figure 2**). However, after later time points of activation (60 min), Ecm29-silenced B cells were able to deplete centrosome-associated actin to the levels of control cells, suggesting that complementary mechanisms involved in actin depletion could be taking place after longer periods of activation.

To confirm our results, we measured the distance between the centrosome and the nucleus in control and Ecm29 silenced B cells activated with antigen-coated beads. As expected, in Ecm29-silenced cells the centrosome remained opposed to the nucleus, confirming their deficiency to translocate their centrosome to the synaptic membrane (**Supplementary Figures 6A–C**).

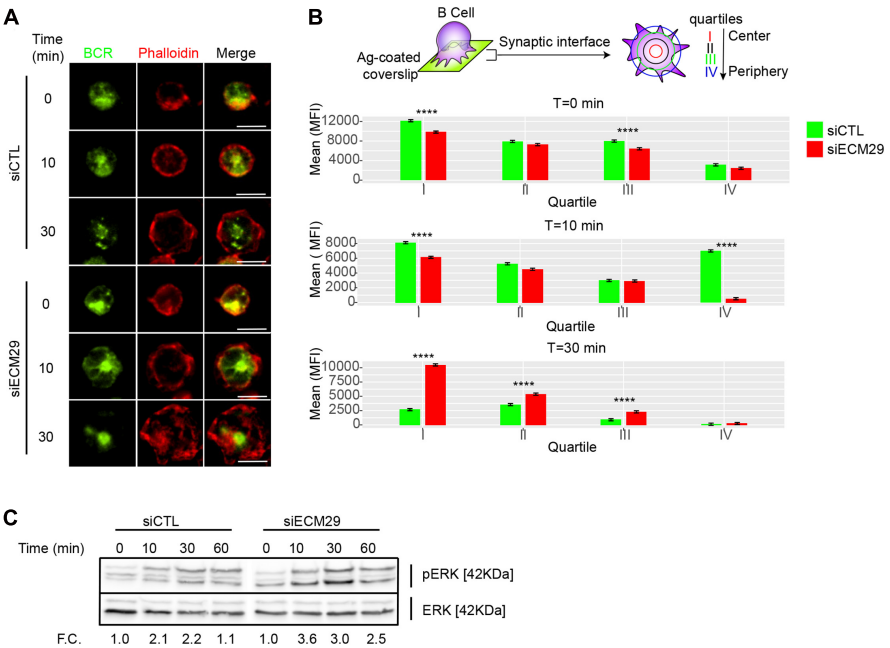

FIGURE 5 | Ecm29 silencing enhances BCR clustering and Erk phosphorylation: **(A)** Representative Epifluorescence images of control (siCTL) and Ecm29-silenced (siECM29) B cells, activated onto antigen-coated coverslips for different time points (0, 10, and 30 min), labeled for the BCR and F-actin (phalloidin). **(B)** Schematic representation of BCR distribution quantification, and the respective quantification of BCR accumulation in each quartile of the immune synapse in B cells shown in **(A)**. $N = 2$. Cells > 30. **(C)** Immunoblot of protein of control and Ecm29-silenced B cells activated for different time points (0, 10, 30, and 60 min). Phosphorylated Erk (pErk) and total Erk (Erk) are shown. F.C., Fold of change respect time 0 min. ****$p < 0.05$. Kruskal–Wallis test with Dunn's test was performed for all statistical analyses. Scale Bar = 10 μm.

Ecm29 Silencing Impairs Antigen Extraction and Presentation in B Cells

Defective centrosome repositioning to the IS impairs the recruitment and local secretion of lysosomes at the synaptic membrane, which can facilitate the extraction and processing of immobilized antigens (Bellaiche et al., 2011; Ibañez-Vega et al., 2019a). Therefore, we investigated the functional consequences of Ecm29 silencing on antigen extraction and presentation by B cells. To this end, we performed an antigen presentation assay using control or Ecm29-silenced B cells (**Figures 7A,B**). Our results show that B cells silenced for Ecm29 display defective antigen presentation and reduced cell surface expression of MHC-II, as evidenced by lower levels of loaded peptide presentation by Ecm29-silenced cells to T cells (**Figure 7B**). The defects in antigen presentation could result from impaired antigen extraction and possibly MHC-II trafficking to the cell membrane. To evaluate this possibility, we activated control or Ecm29 silenced B cells with OVA-antigen-coated beads for different time points and measured the amount of OVA fluorescence remaining on the beads as an indicator of antigen extraction. We found that Ecm29 silenced cells showed higher OVA-antigen levels on beads after activation compared to control cells, confirming that Ecm29-silenced B cells could not efficiently extract antigen (**Figures 7C,D**). Considering that antigen extraction relies on lysosome recruitment and secretion (Bellaiche et al., 2011), we also followed the distribution of lysosomes labeled for Lamp1 in activated B cells and noticed that Ecm29 displayed delayed recruitment of lysosomes to the IS (**Figures 7D,E**). Overall, these results suggest that lysosome trafficking to the IS depends on Ecm29, which promotes centrosome repositioning by depolymerizing actin within this region.

In summary, we put forward a novel mechanism involved in regulating the B cell immune synapse, where Ecm-29 dependent proteasome distribution orchestrates actin remodeling at the synaptic interface and the centrosome, thereby controlling key cellular functions such as lysosome trafficking and antigen extraction and presentation.

DISCUSSION

A functional immune synapse relies on actin remodeling at the synaptic membrane and the centrosome: The former promotes BCR clustering and downstream signaling (Freeman et al., 2015; Tolar, 2017; Spillane and Tolar, 2018), and the latter enables centrosome repositioning to the IS together with lysosomes, which, upon secretion, facilitate antigen extraction (Bellaiche et al., 2011; Obino et al., 2016; Ibañez-Vega et al., 2019a). Our work reveals that the localization of the proteasome at the synaptic interface and centrosome relies on Ecm29, which in turn regulates actin remodeling in both compartments; and, therefore, plays a pivotal role in immune synapse formation, antigen extraction, and presentation (**Figure 8**).

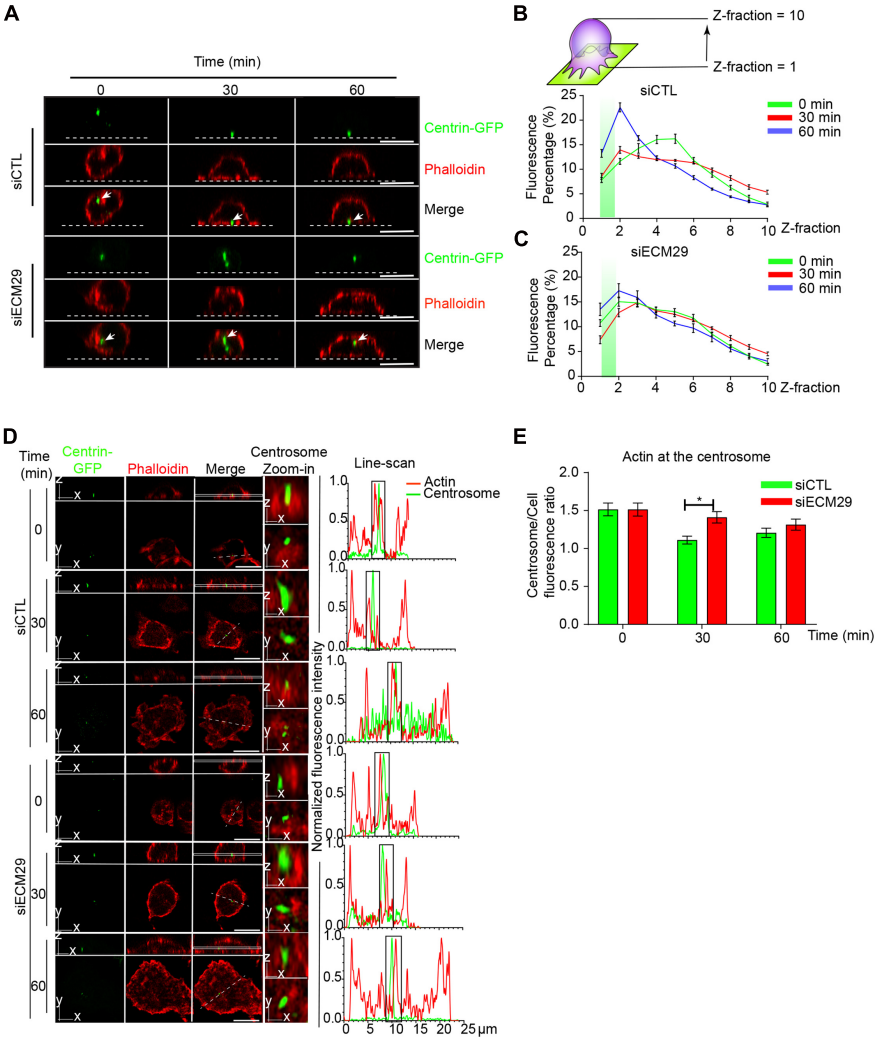

FIGURE 6 | Centrosome polarization and perinuclear actin clearance rely on Ecm29: **(A)** Representative X/Z confocal images of centrin-GFP expressing control (siCTL) and Ecm29-silenced (siECM29) B cells activated on antigen-coated coverslips for different time points, stained for F-actin, phalloidin are shown. White arrows indicate the centrosome. The white dashed line represents the position of the coverslip. **(B,C)** Quantification of centrosome fluorescence intensity along the Z dimension from the coverslip to the upper cell limit of control and Ecm29 silenced B cells, respectively. The green rectangle represents the synaptic Z area (between 1 and 2 Z-fraction), and the maximum value of the curve represents the localization of the centrosome in the Z dimension. $N = 2$. Cells > 19. **(D)** Representative Ayriscan images of centrin-GFP expressing control and Ecm29-silenced B cells activated on antigen-coated coverslips for different time points, labeled for F-actin, phalloidin. Magnifications of the centrosome (9 μm^2) and the fluorescence intensity distribution of centrin-GFP (green) and phalloidin (red) across the cell (dashed white lines) are shown. White rectangles represent the X/Y position for images in Z. **(E)** Quantification of actin at the centrosome in D. $N = 2$. Cells > 45. $^*p < 0.05$. Kruskal–Wallis test with Dunn's test, and Mann–Whitney test was performed for all statistical analyses. was performed for all statistical analyses. Mean with SEM lines **(B,C)** and bars **(E)** are shown. Scale bar = 10 µm.

A role of Ecm29 in regulating the localization of the proteasome has been previously reported in neurons (Otero et al., 2014; Lee et al., 2020), but has remained relatively unexplored in lymphocytes. The underlying mechanisms by which Ecm29 regulates the intracellular localization of the proteasome include: (1) promoting the interaction of the proteasome with motor proteins, such as kinesins and dyneins, which directly anchors the proteasome to microtubules, and is responsible for proteasome retrograde and anterograde movement (Hsu et al., 2015) (2) mediating the association of the proteasome to vesicles and favors its fast movement by hitch-hiking (Otero et al., 2014) and (3) promoting the association of the proteasome with Rab11 + recycling vesicles and organelles, such as Endoplasmic Reticulum and the centrosome (Gorbea et al., 2004, 2010). Our work suggests that Ecm29 mediates the association of the proteasome to microtubules and the centrosome in B cells; however, the molecular mechanisms involved in mobilizing the proteasome remain to be explored.

Interestingly, Ecm29 has also been described to act as a proteasome inhibitor and quality control protein, where its association to the proteasome inhibits the ATPase activity of the regulatory particle and stabilizes its interaction with the catalytic

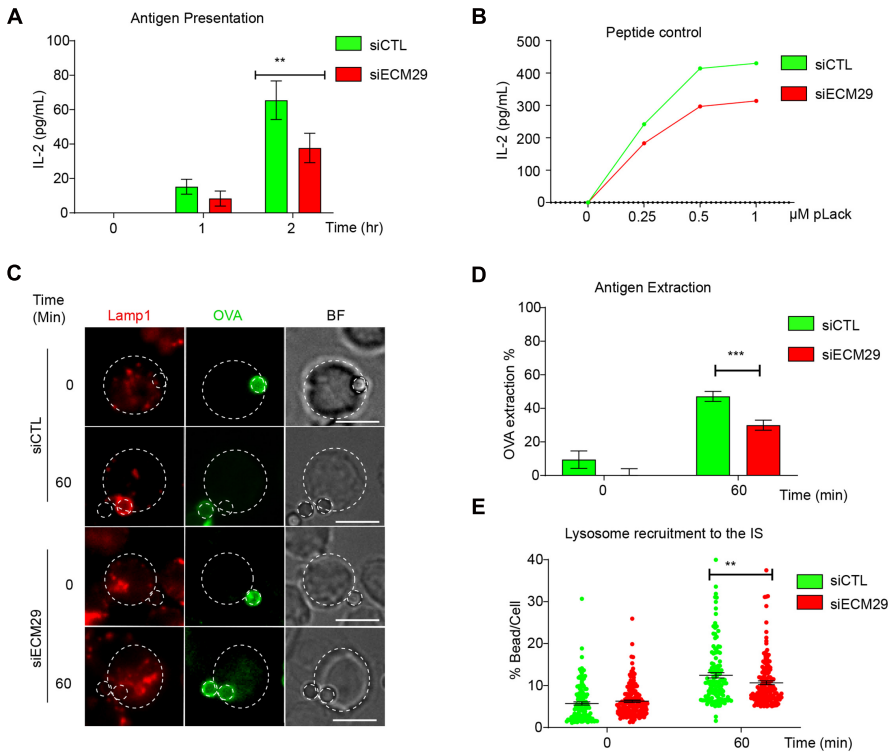

FIGURE 7 | Efficient antigen extraction and presentation requires Ecm29: **(A)** Antigen presentation assay for control (siCTL) and Ecm29 silenced (siECM9) B cells. Levels of IL-2 by T cells were quantified by ELISA. $N = 3$. **(B)** Representative graph of peptide controls for cells used in antigen presentation assays. **(C)** Representative images of control and Ecm29 silenced B cells activated with beads coated with anti-IgG + OVA in resting (0 min) and activating conditions (60 min). Lysosomes (Lamp1) and antigen (OVA) are shown. The white dashed circles delimit cell boundaries and bead. **(D,E)** Quantification of antigen extraction, measured as the amount of OVA extracted from the bead, and lysosome recruitment to the bead in **(C)**. $N = 4$. Cells > 82. $^{**}p < 0.01$. $^{***}p < 0.001$. Kruskal–Wallis test with Dunn's test, and Mann–Whitney test was performed for all statistical analyses was performed for all statistical analyses. Mean with SEM bars **(A,D)**, individual cells (points) **(E)** are shown. Scale bar = 10 µm.

core (Lehmann et al., 2010; De La Mota-Peynado et al., 2013; Haratake et al., 2016). However, we found that Ecm29 silencing did not affect overall levels of proteasome activity, measured as the accumulation of ubiquitylated proteins, which suggest that in B cells, Ecm29 regulates proteasome localization rather its activity. Despite of this, further analysis of how Ecm29 affects specific proteasome functions, such as degradation rate, ATPase activity, or specific protease activity, are needed to completely discard whether or not Ecm29 affects proteasome activity.

B cells silenced for Ecm29 displayed lower levels of proteasome at the centrosome, which correlated to increased F-actin at this level, suggesting that centrosome-associated proteasome could act as a negative regulator of actin polymerization within this region. This observation is consistent with our previous findings, where inhibition of proteasome activity also induced an accumulation of F-actin at the centrosome and defective actin clearance upon B cell activation, disabling centrosome repositioning to the synapse (Obino et al., 2016; Ibañez-Vega et al., 2019a). Accordingly, our results show that decreasing the proteasome at the centrosome, by silencing Ecm29, also leads to defective centrosome repositioning at the IS. As anticipated, defective centrosome polarization in Ecm29 silenced B cells correlated with poor lysosome recruitment to the IS and impaired antigen extraction and presentation. Thus, our results show that the proteasome pool associated to the centrosome regulates local proteostasis at this level, which is in the same line with previous observations suggesting that the centrosome acts as a platform for local UPS-mediated degradation (Vora and Phillips, 2016). Noticeably, at later time-points of activation, Ecm29-silenced B cells displayed reduced actin levels at the centrosome, which were comparable to control cells, suggesting other mechanisms might regulate actin at this stage. Such mechanisms could involve the local activation of actin-severing proteins, such as cofilin, which was previously associated to actin depletion in B cells (Freeman et al., 2015, 2018).

A striking observation reported here is that upon activation, Ecm29-silenced cells accumulated higher proteasome levels at the cortical and synaptic regions. Thus, it is tempting to speculate that Ecm29 favors the centrosomal localization of the proteasome, excluding it from the cell cortex and the IS. The molecular mechanisms underlying the cortical localization of the proteasome are not understood in lymphocytes. However, in neurons, adaptor proteins, such as GPM6A/B, were shown to mediate the interaction of the proteasome with the plasma membrane (Ramachandran and Margolis, 2017). Thus, it would

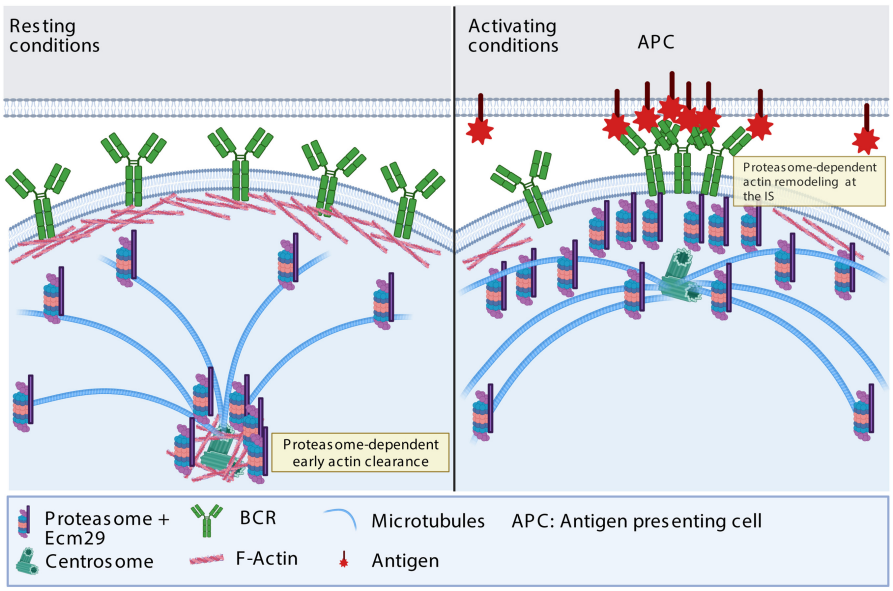

FIGURE 8 | Proposed model: In resting conditions, Ecm29 enhances proteasome localization at the centrosome. Upon activation, Ecm29 regulates the distribution of the proteasome at the synaptic interface. The subcellular localization of the proteasome between the centrosome and the immune synapse regulates actin remodeling in both compartments. At the centrosome, the proteasome facilitates early actin clearance and therefore centrosome translocation at the synapse, whereas at the immune synapse, the proteasome enhances actin remodeling by reducing its stability, thereby promoting cell spreading, BCR clustering and signaling. Further studies are required to determine which actin regulatory proteins are degraded by the proteasome, upon B cell activation and contribute to actin remodeling.

be interesting to address whether the mechanisms involved in the localization of cortical proteasome in neurons are shared by lymphocytes.

In addition to enhanced proteasome levels at the IS, Ecm29 silenced cells displayed reduced actin turnover and slower actin-retrograde flow at the synaptic interface, suggesting that actin polymerization at the IS was reduced within this zone. These observations are consistent with the general view of the proteasome as a negative regulator of actin polymerization (Schaefer et al., 2012; Hsu et al., 2015), where actin nucleating factors are selectively downregulated by the UPS (de la Fuente et al., 2007), thereby turning down actin polymerization. This idea is further supported by our observations, where we found that HS1 was decreased upon Ecm29 silencing, indicating that this protein could be targeted for proteasome degradation. Indeed, HS1 has five ubiquitin sites (K34, K60, K123, K192, and K239) (Hornbeck et al., 2012). In B cells, BCR activation triggers HS1 phosphorylation by Syk, and its subsequent recruitment to the IS, being crucial in the promotion of actin assembly at the IS (Hao et al., 2004; Obino et al., 2016). Thus, it is possible that silencing Ecm29, which results in increased levels of proteasome at the IS and enhanced HS1 degradation, could be responsible for poor actin accumulation at the synaptic interface, upon BCR activation. On the other hand, Ecm29 silencing did not alter WASp levels, which could be a consequence of its interaction with WASp interacting protein (WIP), which protects WASp from degradation and is also recruited to the IS of B cells (Keppler et al., 2018). Alternatively, the exacerbated spreading response and defective antigen extraction observed in Ecm29-silenced B cells, could also result from impaired Myosin II activity. Myosin II promotes contractile forces, which restrict cell spreading (Wakatsuki et al., 2003) and was also shown to exert pulling forces at the synaptic membrane of B lymphocytes to promote antigen extraction (Natkanski et al., 2013).

The actin cytoskeleton plays a critical role in BCR signaling by restricting its lateral diffusion and association with co-receptors (Tolar, 2017). Indeed, B cells treated with drugs that disrupt actin organization induce BCR signaling in the absence of ligand (Batista et al., 2010). Additionally, proteins belonging to the Ezrin-Radixin-Moesin Family (ERM family), which link the actin cytoskeleton to the plasma membrane, negatively regulate BCR lateral diffusion (Treanor et al., 2009; Liu et al., 2013; Tolar, 2017) and can be degraded by the proteasome (Grune et al., 2002). Interestingly, it has been reported that upon BCR activation, an early ubiquitylation response affects BCR downstream kinases, signaling components, such as LAT2, RAC1, CDC42, VAV1, and Ezrin (Satpathy et al., 2015). Thus, in addition to actin polymerizing factors, the proteasome at the IS could degrade proteins involved in BCR activation, as well as other factors that couple actin to the cell cortex, such as ezrin, and control membrane tension (Schaefer et al., 2012; Kelkar et al., 2020). Consequently, the larger spreading area displayed by Ecm29 silenced B cells, which accumulate more proteasome at the synaptic membrane, could result from a relaxed cortex or enhanced BCR signaling. Thus, the timely recruitment of the proteasome to the immune synapse is crucial to determine where and which proteins would be degraded.

Interestingly, microtubules drive the spreading response in fibroblasts, where the rapid growth of microtubules toward the cell borders is essential for isotropic spreading

(Tvorogova et al., 2018). In our study, we found that Ecm29-silenced B cells displayed a highly symmetric IS, which resembles an isotropic spreading response. Thus, it is tempting to speculate that the increased spreading response and the slow actin-retrograde flow in Ecm29-silenced B could allow microtubule growth toward the cell margins, which would lead to a sustained spreading and reduced actin-retrograde flow. Indeed, an analogous negative correlation between the actin cytoskeleton and microtubules was previously described at the centrosome, where the reduction of polymerized actin at the centrosome triggered an increased microtubule growth (Inoue et al., 2019). The role of the proteasome selectively degrading molecules that tune the microtubule-actin crosstalk at the synaptic membrane shall provide insights on how antigen extraction and processing are regulated at the B cell synapse.

In conclusion, our work reveals that the distribution of the proteasome, mediated by Ecm29, controls the formation of the IS by regulating actin dynamics at the centrosome and synaptic membrane. These new findings contribute to understanding how B lymphocytes efficiently manage to orchestrate complex actin cytoskeleton remodeling at these two levels and control the establishment of a polarized phenotype during IS formation.

MATERIALS AND METHODS

Cell Lines and Culture

The mouse lymphoma cell line IIA1.6, which is a FcγR-defective B cell line with the phenotype of quiescent mature B-cells (Lankar et al., 2002) and the LMR7.5 Lack T-cell hybridoma, which recognizes I-Ad-LACK$_{156-173}$ complexes, were cultured as previously described (Vascotto et al., 2007) in CLICK medium (RPMI 1640, 10% fetal bovine serum, 100 U/mL penicillin-streptomycin, 0.1% β-mercaptoethanol, and 2% sodium pyruvate. For proteasome inhibition, 5×10^6 B cells/mL were incubated with 5 μM MG-132 for 1 h at 37°C before functional analysis.

Antibodies and Reagents

We used rat anti-mouse LAMP1 (BD Bioscience, #553792, 1:200), rabbit anti-mouse α-Tubulin (Abcam, ab#6160, 1:200), rabbit anti-acetyl-α-Tubulin (Lys40; cell signaling, #5335, 1:200), rabbit anti-mouse γ-Tubulin (Abcam, #Ab11317, 1:1000), rabbit anti-mouse S4/19S RP (Abcam, #Ab223765, 1:100), rabbit anti-mouse αβ/20S proteasome (Abcam, #Ab22673, 1:200), anti-mouse Ecm29 (Abcam, #Ab28666, 1:100), mouse anti-mouse Ubiquitin P4D1 (Santa Cruz, #Sc-8017, 1:1000), anti-mouse anti-actin (cloneC4, ImmunO, #691001), rabbit anti-mouse Arp2 (Cellsignal, #5614, 1:500), goat anti-mouse IgGFab^2 (Jackson ImmunoResearch), rabbit anti-OVA (Sigma-Aldrich, #C6534, 1:500). For secondary antibodies: donkey anti-rabbit IgG-Alexa488 (LifeTech, 1:200), goat anti-rabbit IgG-Alexa546 (ThermoScientific, 1:200), Donkey anti-rat IgG-Alexa546 (ThermoScientific, 1:200), Donkey anti-rat-Alexa647 (ThermoScientific, 1:200), Phalloidin-Alexa-647 (Life Technology, #22287, 1:200), DAPI (Abcam). Ovalbumin and Nocodazole were purchased from Sigma-Aldrich, MG-132, and Epoxomicin were purchased from Merk (Millipore). Bsc2118-FL-Bodipy was kindly provided by Ulrike Kuckelkorn (Mlynarczuk-Bialy et al., 2014).

Cell Transfection

LifeAct-mCherry and αTubulin-mCherry plasmids were kindly provided by Ana Maria Lennon. For Ecm29, a silencing siRNA kit was purchased from Qiagen (1027416) and used as the combination of four different siRNA at 2.5 nM each one. As a control, we used a scrambled siRNA (Qiagen) at 10 nM. Nucleofector R T16 (Lonza, Gaithersburg, MD, United States) was used to electroporate 5×10^6 IIA1.6 B Lymphoma cells with 2 μg of plasmid DNA. After transfection, cells were cultured for 16 hrs before functional analysis.

Preparation of Ag-Coated Beads and AG-Coated Coverslips

Antigen-coated beads were prepared as previously described (Bellaiche et al., 2011). Briefly, ∼2×10^7 3-μm latex NH_2-beads (Polyscience, Eppelheim, Germany) were activated with 8% glutaraldehyde for four h at room temperature. Beads were washed with phosphate-buffered saline (PBS) and incubated overnight at 4°C with different ligands: using 100 μg/mL of either F(ab')2 goat anti-mouse immunoglobulin G (IgG), referred to as BCR-Ligand$^+$ or F(ab')2 goat anti-mouse IgM, referred to as BCR-Ligand$^-$ (MP Biomedical, Santa Ana, CA, United States). For antigen extraction assays, beads were coated with BCR-Ligand$^+$ or BCR-ligands$^-$ plus OVA 100 μg/mL. For antigen presentation assays, beads were coated with BCR$^+$ or BCR$^-$ ligands plus 100 μg/mL Lack protein. Antigen coverslips used to analyze the synaptic interface were coated with BCR-Ligand$^+$ overnight at 4°C in PBS.

Activation of B Cells With Ag-Coated Beads or Coverslips

Cells were plated on poly-L-Lysine–coated glass coverslips and activated with Ag-coated beads (1:1 ratio) for different time points in a cell culture incubator (37°C/5% CO_2) and then fixed in 4% paraformaldehyde (PFA) for 10 min at room temperature as previously described (Bellaiche et al., 2011). Fixed cells were incubated with antibodies in PBS-0.2% BSA-0.05% Saponin. In order to measure cell spreading, the B cell line was plated onto B220/anti-IgG, or anti-IgM coated glass coverslips, respectively, for different time points at 37°C in a cell culture incubator as previously described (Reversat et al., 2015).

Antigen Presentation Assay

Ag presentation assays were performed as previously described (Bellaiche et al., 2011). Briefly, IIA 1.6 (I-A^d) B cells were incubated with either Lack-BCR-Ligand$^+$ or BCR-Ligand$^-$ coated beads or different Lack peptide concentrations (Lack$_{156-173}$) for 1 h. Then Cells were washed with PBS, fixed in ice-cold PBS/0.01% glutaraldehyde for 1 min, and quenched with PBS/100 mM glycine. B cells were then incubated with Lack-specific LMR 7.5 T Cells in a 1:1 ratio for 4 h. Supernatants were collected, and interleukin-2 cytokine production was

measured using BD optiEA Mouse IL-2 ELISA set following the manufacturer's instructions (BD Biosciences).

Ag Extraction Assay

For antigen extraction assays, B cells incubated in a 1:1 ratio with BCR ligand^{+}-OVA-coated beads were plated on poly-Lys cover-slides at 37°C, fixed and stained for OVA. The amount of OVA remaining on the beads was calculated by establishing a fixed area around beads in contact with cells and measuring fluorescence on three-dimensional (3D) projections obtained from the sum of each plane (Details in "Image Analysis" section). The percentage of antigen extracted was estimated by the percentage of fluorescence intensity lost by the beads after 1 h.

Centrosome Isolation

Centrosome from B cells was isolated as previously described (Obino et al., 2016) with slight modifications. Briefly, B cells in resting conditions (CLICK-2% FBS) at 37°C/5%CO_2, were treated with adding 2 μM cytochalasin D (Merck Millipore) and 0.2 μM Nocodazole (Merck Millipore). Cells were washed in TBS (10 mM Tris-HCl 15 mM NaCl pH 7.5), then in 0.1X TBS supplemented with 8% sucrose and lysed in lysis buffer (1mM HEPES. 0.5% NP-40, 0.5 mM $MgCl_2$, 0.1% β-mercaptoethanol pH 7.2) supplemented with protease inhibitors for 15 min. Centrosomes were isolated from post-nuclear-supernatants by consecutive centrifugations at (1) 10,000 *g* for 30 min at 4°C on top of a 60% w/v sucrose cushion in gradient buffer (10 mM PIPES, 0.1% Triton X-100, 0.1% β-mercaptoethanol pH 7.2) and (2) 40,000 *g* for 60 min at 4°C on top of a discontinuous sucrose gradient (40–50–70% w/w). Finally, 12 fractions were recovered from the top to the bottom of the tube, and centrosome-containing fractions were detected by immunoblot γ-tubulin labeling.

Proteasome Activity

Protein extracts obtained from B cells were quantified and loaded onto black MaxiSorp 96 well plate (Nunc, Denmark) with proteasome substrate III fluorogenic (Calbiochem, Merck Millipore) diluted in Assay buffer (50 mM Tris-HCl pH: 7.2, 0.05 mM EDTA, 1 mM DTT). The plate was incubated for 1 h at 37°C, and then fluorescence was measured at 360/420 nm. All measurements were performed in triplicate.

Cell Imaging

For epifluorescence imaging, all Z-stack images were obtained with 0.5 microns between slices. Images were acquired in an epifluorescence microscope (Nikon Ti2Eclipse) with an X60/1.25NA and X100/1.3NA oil immersion objectives for bead and spreading assays, respectively. For confocal microscopy, images were acquired in a Nikon Ti2Eclipse inverted microscope with 60X/1.45NA oil immersion for bead and spreading assays, with a Z-stack of 0.5 microns. For Total internal reflection fluorescence microscopy (TIRFM), images were acquired in Nikon Ti2Eclipse inverted microscope with a 100x/1.50 NA oil immersion lens and an iXON Ultra EMCCD camera at 37°C. B-cells expressing LifeAct-mCherry were plated on Ag-coated glass chambers (Nunc^{TM} Lab-Tek^{TM} II). Images were acquired for 30 min at 15 s per frame for spreading assay and for 1 min at 0.75 s per frame for lysosome, proteasome, and actin retrograde flow tracking. For Ayriscan acquisition, images were obtained in the Zeiss LSM880 Airyscan Confocal microscope with a 63X/1.4NA oil immersion lens, with a Z-stack of 0.2 μm. The images were processed using Zeiss Black Zen software and analyzed with FIJI.

Fluorescence Recovery After Photobleaching in TIRFM (FRAP-TIRFM)

IIA1.6 cells were transfected with Actin-GFP together with scramble siRNA (siCTL) or ECM29-targeting siRNA (siECM29), and then allowed to spread onto antigen-coated coverslips for 30–40 min at 37°C in HEPES supplemented CLICK. Cells were then mounted on a stage-top incubator, and one central region was manually selected for photobleaching using a 405 nm laser (70% intensity, 100 ms, ND Stimulation unit), concurrent with Nikon TIRFM imaging. GFP signal intensity within the bleached zone was normalized to intensity values from an unbleached control region in the same cell. The curves were also y-transformed to (0,0) at $t = 0$ (bleaching event) so that individual recovery curves begin at the intensity minimum. Each recovery curve group was then fit to the following equation, with the constraint that $Y_0 = 0$: $Y = Y_0 + (\text{plateau-}Y_0)*(1\text{-}e^{-k*x})$. The rate constant (k) was derived by non-linear regression analysis using GraphPad Prism software.

Image Analysis

Image processing and analysis were performed with FIJI (ImageJ) software (Schindelin et al., 2012), as we previously described (Ibañez-Vega et al., 2019b). The centrosome was labeled with Centrin-GFP or α-Tubulin and determined by the brightest point where microtubules converged. Single-cell images shown in the figures were cropped from a larger field. Image brightness and contrast were manually adjusted. Centrosome polarity index was determined as previously described (Bellaiche et al., 2011). Briefly, we manually selected the location of the centrosome (Cent) and delimited the cell and bead borders to obtain the center of mass of both CMC (Cell mass center) and BMC (Bead mass center), respectively. The position of the centrosome was projected (CentProj) on the vector defined by the CMC-BMC axis. The centrosome polarity index was calculated by dividing the distance between the CMC and CentProj and the distance between CMC-BMC. The index ranges from −1 (anti-polarized) and +1 (fully polarized).

Proteasome recruitment to the IS in bead assays was quantified by dividing the fluorescence at the bead by the whole cell's fluorescence and then multiplying it by a factor of 100. For spreading assays, we manually delimited the border of the cell using a phalloidin label as a template (CellTemp); then, an ellipse was automatically determined (CenterTemp) at the center of CellTemp, which had a third of the CellTemp area. Next, the center's recruitment was calculated by dividing the fluorescence normalized by its area from CenterTemp and CellTemp, subtracting 1. Therefore, positive values mean

that the fluorescence is enriched at the center, and negative values, the opposite.

For actin quantification at the centrosome, we traced a circle with a 1μm radius with its center as the centrosome. The fluorescence at the centrosome (FCent) and its Area (ACent) were measured. The corresponding ratio gives the fluorescence density index (DCent = FCent/ACent). This value is divided by the density of the fluorescence of the entire cell (DCell). Values above 1 indicate an accumulation of the label at the centrosome compared to the whole cell. Whereas values below 1 indicate that there is a depletion at the centrosome compared to the whole cell.

For lysosome and proteasome tracking, we used the Trackmate plugin from FIJI (Schindelin et al., 2012), considering each spot with areas of 1 μm^2 and manually thresholded by the quality index.

The proteasome (Bsc2118-FL-Bodipy) fluorescence correlation with F-actin (LifeAct-mCherry) fluorescence of B cells seeded for 30 min in antigen-coated coverslips was automatically measured by a FIJI macros function. Briefly, the proteasome label was automatically detected by Analyze particle, and the proteasome and F-actin fluorescence were measured in each proteasome-spot (1 μm diameter circle). Next, each fluorescence signal was normalized by the total cell fluorescence in each frame to normalize fluorescence variation by LifeAct expression or Bsc2118-FL-Bodipy dosage. Then, the proteasome fluorescence and the related LifeAct fluorescence were arranged into discrete groups and graphed.

The spreading area of LifeAct-mCherry expressing B cells activated onto antigen-coated coverslips recorded by TIRFM was assessed by FIJI. Briefly, images were thresholded and binarized to detect cell boundaries automatically, and then cell areas were detected in each frame by Analyze particle plugin (FIJI). The spreading velocity was calculated by linear regression of area per time data. The asymmetry of the immune synapse was measured by the aspect ratio of each spreading area per frame, as previously described (Kumari et al., 2020).

Quantification of actin retrograde flow was performed as previously described (Jankowska and Burkhardt, 2017). Briefly, TIRFM recorded LifeAct-mCherry expressing B cells after 30 min of activation onto antigen-coated coverslips, were analyzed by FIJI, by reslicing two different lamellipodia structures per each cell, and manually drawing an angle at the edge of the lamellipodium. Each angle was transformed in microns per second, by converting the angle to radians (Rad-angle) and applying the following formula: V(μm/s) = tan(Rad_angle).

Quantification of BCR clustering at the IS center was performed by using an adaptation of the clock scan analysis plugin for Fiji (Dobretsov et al., 2017) implemented in a personalized macro with machine learning correction with the advanced Weka segmentation tool (Arganda-Carreras et al., 2017). Data obtained from the images was then curated and filtered using Rstudio. Briefly, outliers were eliminated using the IQR correction and the distribution of fluorescence (MFI) was divided into four quartiles, considering the distance from the center of mass of each cell to their correspondent periphery. Data was assessed for its normality using the Shapiro–Wilk test and multiple comparison tests were performed using ANOVA and *post hoc* tests (Tukey).

Statistical Analysis

Statistical analysis was performed with Prism (GraphPad Software) and RStudio. The *p*-values were calculated using different tests, as indicated in figure legends.

DATA AVAILABILITY STATEMENT

The original contributions presented in the study are included in the article/**Supplementary Material**, further inquiries can be directed to the corresponding author/s.

AUTHOR CONTRIBUTIONS

JI-V designed, performed, and analyzed most of the experiments, assembled the figures, and participated in the writing of the manuscript. FD performed the immunofluorescence and biochemical experiments and participated in the writing of the manuscript. JS helped to setup image quantification protocols. FG synthesized the lack peptide (Lack 156-173) used for all antigen presentation assays. JD helped with biochemical experiments. MY wrote the manuscript. MY and AS proposed the original hypothesis, designed the experiments, supervised and funded the overall research. All the authors contributed to the article and approved the submitted version.

FUNDING

MY was supported by a research grant from FONDECYT (1180900), AS was supported by a CONICYT Basal Financial Program AFB170005, JI-V was supported by a CONICYT PFCHA/Doctorado Nacional Chile/2015-21150566, and FD was supported by a CONICYT PFCHA/Doctorado Nacional Chile/2018-21191062.

ACKNOWLEDGMENTS

We are grateful to the Unidad de Microscopia Avanzada (UMA) of Pontificia Universidad Católica de Chile for its support in image acquisition.

SUPPLEMENTARY MATERIAL

The Supplementary Material for this article can be found online at: https://www.frontiersin.org/articles/10.3389/fcell.2021.650817/full#supplementary-material

Supplementary Figure 1 | Ecm29 cofractionates with the centrosome in B cells. **(A)** Representative immunoblot of centrosome fractions isolated from B cells in resting conditions, where γ-tubulin (centrosome) and Ecm29 were detected. **(B)** Representative confocal images of B cells in resting conditions, showing Centrin-GFP, γ-tubulin, and Golgi, and co-localization analysis. **(C)** Representative

confocal images of B cells in resting or activating conditions, showing Golgi, Centrin, and Ecm29, and line-scan analysis of each label across the cell. **(D)** Representative images of B cells in resting or activating conditions (60 min of activation) with antigen-coated beads, pretreated with DMSO as a control, 30 μM Nocodazole (NocZ) for 30 min. For activated B cells, drug treatment was performed after 30 min of activation. S4(19S RP), α-Tubulin, F-actin, and merge are shown. **(F)** Representative images of resting B cells or activated on antigen-coated coverslips (60 min of activation) pretreated with DMSO as a control, 30 μM Nocodazole (NocZ) for 30 min. For activated B cells, drug treatment was performed after 30 min of activation. Two sets of staining are shown: (1) S4(19S RP), α-Tubulin, F-actin, merge, and (2) Ecm29, α-Tubulin, F-actin, and merge, are shown. Scale Bar = 10 μm.

Supplementary Figure 2 | Ecm29 silencing does not affect levels of ubiquitylated proteins, but reduces proteasome levels at the centrosome in resting B cells. **(A)** Representative immunoblot of protein extracts obtained from resting B cells transfected with scrambled siRNA (siCTL) and Ecm29 targeted siRNA (siECM29). Ecm29 and BCR are shown. **(B)** Quantification Ecm29 levels in **(A)**. $N = 7$. **(C)** Representative immunoblot of control and Ecm29-silenced B cells in resting conditions, stained for Ubiquitin, Ecm29, S4 (19S), αβ (20S), LMP7, and actin. **(D)** Quantification of protein levels in **(C)**. $N > 3$. **(E)** Representative immunoblot of centrosome isolated fractions isolated from control and Ecm29-silenced B cells. S4 (19S) and γ-Tubulin are shown. Red rectangle indicates the centrosome-rich fractions. **(F,G)** Quantification of S4 (19S) protein levels ($N = 3$) and proteasome activity ($N = 2$) in centrosome-rich fractions in **(E)**, respectively. $^{**}p < 0.01$. Mann–Whitney test was performed for all statistical analyses. Mean with SEM bars are shown.

Supplementary Figure 3 | Live tracking of the proteasome shows it colocalizes with microtubules and is distributed across the IS. **(A)** Immunoblot of B cells treated with increasing concentrations of the specific proteasome probe (Bsc2118-FL-Bodipy) for 2 h, ubiquitin and actin labeling are shown. F.C., Fold of Change respect to the control (0 nM of Bsc2118-FL-Bodipy). **(B)** TIRFM Time-lapse and kymograph of α-Tubulin-mCherry (grayscale) expressing B cells probed with 5 nM Bsc2118-FL-Bodipy (Red). Black arrowheads indicate proteasome positive spots. Below: Table summarizing the colocalization of the proteasome (Bsc2118-FL-Bodipy) and α-Tubulin-mCherry. Overlap coefficient, k1, k2, Manders 1, and Manders 2, are shown. **(C)** Time-lapse images obtained by TIRFM of B cells labeled for proteasome (grayscale). The accumulation of proteasome tracks (right) is shown. The coldest colors represent the fastest tracks—Kymograph (below). Black arrowheads indicate proteasome positive spots at center and periphery. **(D)** Histogram of proteasome diffusion coefficient measured in **(C)**. $N = 2$, Cells > 30. Scale Bar = 10 μm.

Supplementary Figure 4 | Proteasome recruitment and distribution at the IS rely on Ecm29: **(A)** Representative Time-lapse images by TIRFM of control (siCTL) and Ecm29-silenced (siECM29) B cells after 30 min of activation on antigen-coated coverslips, probed with 5 nM Bsc2118-FL-Bodipy (gray scale). The cell boundary (black line) delimited by the LifeAct-mCherry signal (mask) and accumulation of tracks are shown. The coldest colors represent the fastest tracks. **(B–E)** Quantification of track displacement, track duration, track mean velocity, and the number of tracks of proteasomes at the IS of control or Ecm29 silenced B cells after 30 min of activation on antigen-coated coverslips. $N > 20$ Cells. $^{*}p < 0.05$, $^{**}p < 0.01$, $^{****}p < 0.0001$. Mann–Whitney test was performed. Scale Bar = 10 μm.

Supplementary Figure 5 | Proteasome arrival at the IS negatively regulates actin polymerization. **(A,C,E,G)** Representative TIRFM images of control, MG-132 pre-treated (5 μM for 1 h), Bsc2118-FL-Bodipy overdosed (100 nM), and Ecm29-silenced (siECM29) B cells. B cells were plated for 30 min onto antigen-coated coverslips and then recorded. LifeAct-mCherry (white) and proteasome (green [Bsc2118-FL-Bodipy]), magnifications proteasome spots (white dashed rectangles), together with their respective kymograph, are shown. White arrowheads indicate the proteasome arrival at the IS close to F-actin structures. **(B,D,F,H)** Quantification of the proteasome (green) and LifeAct-mCherry (Red) distribution at proteasome positive spots (white dashed line) and their distribution in time (Kymograph) showed on **(A,C,D,G)**, respectively. **(I)** Scheme illustrating the quantification rationale and results of the quantification of normalized fluorescence intensity correlation between Bsc2118-FL-Bodipy and LifeAct-mCherry, on Bsc2118-FL-Bodipy-positive spots of 1 μm in diameter shown in **(A,C,G,E)**. $N > 10$. $^{*}p < 0.05$. $^{**}p < 0.001$. $^{***}p < 0.0005$. $^{****}p < 0.0001$. Kruskal–Wallis test with Dunn's test was performed for all statistical analyses was performed. Each dot represents an independent positive Bsc2118-FL-Bodipy spot. Mean with SEM lines are shown. Scale Bar = 10 μm.

Supplementary Figure 6 | Centrosome-nucleus separation and centrosome recruitment to the IS is impaired in Ecm29-silenced B cells: (A) Representative Epifluorescence images of control (siCTL) and Ecm29-silenced (siECM29) B cells, activated with antigen-coated beads for different time points. Centrosome (Centrin-GFP) and nucleus (DAPI) are shown. The dashed line represents the distance between the centrosome-nucleus. A scheme depicting how the cell polarity index and the distance between the centrosome and nucleus were calculated, is shown. (B,C**)** Quantification of centrosome-nucleus distances and centrosome polarization in (A). $N > 3$. Cells > 116. Each dot represents an individual measurement (C). Mean with SEM lines (C) and bars (B) are shown. $^{***}p < 0.0005$. $^{****}p < 0.0001$. Kruskal–Wallis test with Dunn's test was performed. Scale Bar = 10 μm.

REFERENCES

Arganda-Carreras, I., Kaynig, V., Rueden, C., Eliceiri, K. W., Schindelin, J., Cardona, A., et al. (2017). Trainable weka segmentation: a machine learning tool for microscopy pixel classification. *Bioinformatics* 33, 2424–2426. doi: 10.1093/bioinformatics/btx180

Babich, A., Li, S., O'Connor, R. S., Milone, M. C., Freedman, B. D., and Burkhardt, J. K. (2012). F-actin polymerization and retrograde flow drive sustained PLCγ1 signaling during T cell activation. *J. Cell Biol.* 197, 775–787. doi: 10.1083/jcb.201201018

Batista, F. D., Treanor, B., and Harwood, N. E. (2010). Visualizing a role for the actin cytoskeleton in the regulation of B-cell activation. *Immunol. Rev.* 237, 191–204. doi: 10.1111/j.1600-065X.2010.00943.x

Bellaiche, Y., Gasman, S., Desdouets, C., Yuseff, M.-I., Darchen, F., Jauffred, B., et al. (2011). Polarized secretion of lysosomes at the B cell synapse couples antigen extraction to processing and presentation. *Immunity* 35, 361–374. doi: 10.1016/j.immuni.2011.07.008

Bolger-Munro, M., Choi, K., Scurll, J. M., Abraham, L., Chappell, R. S., Sheen, D., et al. (2019). Arp2/3 complex-driven spatial patterning of the BCR enhances immune synapse formation. BCR signaling and B cell activation. *eLife* 8:e44574. doi: 10.7554/elife.44574

Boyer, N. P., McCormick, L. E., Menon, S., Urbina, F. L., and Gupton, S. L. (2020). A pair of E3 ubiquitin ligases compete to regulate filopodial dynamics and axon guidance. *J. Cell Biol.* 219:e201902088. doi: 10.1083/jcb.201902088

Collins, G. A., and Goldberg, A. L. (2017). The logic of the 26S proteasome. *Cell* 169, 792–806. doi: 10.1016/j.cell.2017.04.023

Coux, O. (2002). Structure and functions of the 20S and 26S proteasomes. *Annu. Rev. Biochem.* 65, 801–847. doi: 10.1146/annurev.biochem.65.1.801

Dahlmann, B. (2016). Mammalian proteasome subtypes: their diversity in structure and function. *Arch. Biochem. Biophys.* 591, 132–140. doi: 10.1016/j.abb.2015.12.012

de la Fuente, M. A., Sasahara, Y., Calamito, M., Antón, I. M., Elkhal, A., Gallego, M. D., et al. (2007). WIP is a chaperone for Wiskott-Aldrich syndrome protein (WASP). *Proc. Natl. Acad. Sci. U S A.* 104, 926–931. doi: 10.1073/pnas.0610275104

De La Mota-Peynado, A., Lee, S. Y. C., Pierce, B. M., Wani, P., Singh, C. R., and Roelofs, J. (2013). The proteasome-associated protein Ecm29 inhibits proteasomal ATPase activity and in vivo protein degradation by the proteasome. *J. Biol. Chem.* 288, 29467–29481. doi: 10.1074/jbc.M113.491662

del Valle Batalla, F., Lennon-Dumenil, A. M., and Yuseff, M. I. (2018). Tuning B cell responses to antigens by cell polarity and membrane trafficking. *Mol. Immunol.* 101, 140–145. doi: 10.1016/j.molimm.2018.06.013

Dennis, M. K., Field, A. S., Burai, R., Ramesh, C., Whitney, K., Bologa, C. G., et al. (2012). Asymmetric proteasome segregation as a mechanism for unequal partitioning of the transcription factor T-bet during T lymphocyte division. *Immunity* 127, 358–366. doi: 10.1016/j.jsbmb.2011.07.002

Dikic, I. (2017). Proteasomal and autophagic degradation systems. *Annu. Rev. Biochem.* 86, 1–32. doi: 10.1146/annurev-biochem-061516-44908

Dobretsov, M., Petkau, G., Hayar, A., and Petkau, E. (2017). Clock scan protocol for image analysis: imagej plugins. *J. Vis. Exp.* 2017:55819. doi: 10.3791/55819

Fleire, S. J., Goldman, J. P., Carrasco, Y. R., Weber, M., Bray, D., and Batista, F. D. (2006). B cell ligand discrimination through a spreading and contraction response. *Science* 312, 738–741. doi: 10.1126/science.1123940

Freeman, S. A., Jaumouillé, V., Choi, K., Hsu, B. E., Wong, H. S., Abraham, L., et al. (2015). Toll-like receptor ligands sensitize B-cell receptor signalling by reducing actin-dependent spatial confinement of the receptor. *Nat. Commun.* 6:7015. doi: 10.1038/ncomms7168

Freeman, S. A., Mizuno, K., Roskelley, C. D., Gold, M. R., Lei, V., and Dang-Lawson, M. (2018). Cofilin-Mediated F-Actin severing is regulated by the rap GTPase and controls the cytoskeletal dynamics that drive lymphocyte spreading and BCR microcluster formation. *J. Immunol.* 187, 5887–5900. doi: 10.4049/jimmunol.1102233

Gil-Krzewska, A., Saeed, M. B., Oszmiana, A., Fischer, E. R., Lagrue, K., Gahl, W. A., et al. (2017). An actin cytoskeletal barrier inhibits lytic granule release from natural killer cells in chediak-higashi syndrome. *J. Allergy Clin. Immunol.* 142, 914–927.e6. doi: 10.1016/j.jaci.2017.10.040

Gorbea, C., Goellner, G. M., Teter, K., Holmes, R. K., and Rechsteiner, M. (2004). Characterization of mammalian Ecm29, a 26 S proteasome-associated protein that localizes to the nucleus and membrane vesicles. *J. Biol. Chem.* 279, 54849–54861. doi: 10.1074/jbc.M410444200

Gorbea, C., Pratt, G., Ustrell, V., Bell, R., Sahasrabudhe, S., Hughes, R. E., et al. (2010). A protein interaction network for Ecm29 links the 26 S proteasome to molecular motors and endosomal components. *J. Biol. Chem.* 285, 31616–31633. doi: 10.1074/jbc.M110.154120

Grune, T., Reinheckel, T., North, J. A., Li, R., Bescos, P. B., Shringarpure, R., et al. (2002). Ezrin turnover and cell shape changes catalyzed by proteasome in oxidatively stressed cells. *FASEB J.* 16, 1602–1610.

Hao, J. J., Carey, G. B., and Zhan, X. (2004). Syk-mediated tyrosine phosphorylation is required for the association of hematopoietic lineage cell-specific protein 1 with lipid rafts and B cell antigen receptor signalosome complex. *J. Biol. Chem.* 279, 33413–33420. doi: 10.1074/jbc.M313564200

Hao, Y. H., Doyle, J. M., Ramanathan, S., Gomez, T. S., Jia, D., Xu, M., et al. (2013). Regulation of WASH-dependent actin polymerization and protein trafficking by ubiquitination. *Cell* 152, 1051–1064. doi: 10.1016/j.cell.2013.01.051

Haratake, K., Sato, A., Tsuruta, F., and Chiba, T. (2016). KIAA0368 -deficiency affects disassembly of 26S proteasome under oxidative stress condition. *J. Biochem.* 159:mvw006. doi: 10.1093/jb/mvw006

Harwood, N. E., and Batista, F. D. (2010). Early events in B cell activation. *Annu. Rev. Immunol.* 28, 185–210. doi: 10.1146/annurev-immunol-030409-101216

Hornbeck, P. V., Kornhauser, J. M., Tkachev, S., Zhang, B., Skrzypek, E., Murray, B., et al. (2012). PhosphoSitePlus: a comprehensive resource for investigating the structure and function of experimentally determined post-translational modifications in man and mouse. *Nucleic Acids Res.* 40, D261–D270. doi: 10.1093/nar/gkr1122

Hsu, M., Guo, C., Liou, A. Y., Chang, T., Ng, M., Florea, B. I., et al. (2015). Stage-Dependent axon transport of proteasomes contributes to axon development. *Dev. Cell* 35, 418–431. doi: 10.1016/j.devcel.2015.10.018

Ibañez-Vega, J., Del Valle, Batalla, F., Saez, J. J., Soza, A., and Yuseff, M.-I. (2019a). Proteasome dependent actin remodeling facilitates antigen extraction at the immune synapse of B cells. *Front. Immunol.* 10:225. doi: 10.3389/fimmu.2019.00225

Ibañez-Vega, J., Fuentes, D., Lagos, J., Cancino, J., and Yuseff, M. I. (2019b). Studying organelle dynamics in B cells during immune synapse formation. *J. Vis. Exp.* 2019, 1–13. doi: 10.3791/59621

Inoue, D., Obino, D., Pineau, J., Farina, F., Gaillard, J., Guerin, C., et al. (2019). Actin filaments regulate microtubule growth at the centrosome. *EMBO J.* 38:e99630.

Jankowska, K. I., and Burkhardt, J. K. (2017). Analyzing actin dynamics at the immunological synapse. *Methods Mol Biol.* 1584, 7–29. doi: 10.1007/978-1-4939-6881-7_2

Kelkar, M., Bohec, P., and Charras, G. (2020). Mechanics of the cellular actin cortex: from signalling to shape change. *Curr. Opin. Cell Biol.* 66, 69–78. doi: 10.1016/j.ceb.2020.05.008

Keppler, S. J., Burbage, M., Gasparrini, F., Hartjes, L., Aggarwal, S., Massaad, M. J., et al. (2018). The lack of WIP binding to actin results in impaired B cell migration and altered humoral immune responses. *Cell Rep.* 24, 619–629. doi: 10.1016/j.celrep.2018.06.051

Kumari, S., Mak, M., Poh, Y., Tohme, M., Watson, N., Melo, M., et al. (2020). Cytoskeletal tension actively sustains the migratory T-cell synaptic contact. *EMBO J.* 39:e102783. doi: 10.15252/embj.2019102783

Kwak, K., Akkaya, M., and Pierce, S. K. (2019). B cell signaling in context. *Nat. Immunol.* 20, 963–969. doi: 10.1038/s41590-019-0427-429

Lankar, D., Vincent-Schneider, H., Briken, V., Yokozeki, T., Raposo, G., and Bonnerot, C. (2002). Dynamics of major histocompatibility complex class II compartments during B cell receptor-mediated cell activation. *J. Exp. Med.* 195, 461–472.

Laumonnerie, C., and Solecki, D. J. (2018). Regulation of polarity protein levels in the developing central nervous system. *J. Mol. Biol.* 430, 3472–3480. doi: 10.1016/j.jmb.2018.05.036

Lee, M., Liu, Y. C., Chen, C., Lu, C. H., Lu, S. T., Huang, T. N., et al. (2020). Ecm29-mediated proteasomal distribution modulates excitatory GABA responses in the developing brain. *J. Cell Biol.* 219:e201903033. doi: 10.1083/jcb.201903033

Lehmann, A., Niewienda, A., Jechow, K., Janek, K., and Enenkel, C. (2010). Ecm29 fulfils quality control functions in proteasome assembly. *Mol. Cell* 38, 879–888. doi: 10.1016/j.molcel.2010.06.016

Liu, C., Bai, X., Wu, J., Sharma, S., Upadhyaya, A., Dahlberg, C. I. M., et al. (2013). N-WASP is essential for the negative regulation of B cell receptor signaling. *PLoS Biol.* 11:e1001704. doi: 10.1371/journal.pbio.1001704

Liu, K., Jones, S., Minis, A., Rodriguez, J., Molina, H., and Steller, H. (2019). PI31 is an adaptor protein for proteasome transport in axons and required for synaptic development. *Dev. Cell* 50, 509–524.e10. doi: 10.1016/j.devcel.2019.06.009

Martín-Cófreces, N. B., Robles-Valero, J., Cabrero, J. R., Mittelbrunn, M., Gordón-Alonso, M., Sung, C. H., et al. (2008). MTOC translocation modulates IS formation and controls sustained T cell signaling. *J. Cell Biol.* 182, 951–962. doi: 10.1083/jcb.200801014

Mattila, P. K., Batista, F. D., and Treanor, B. (2016). Dynamics of the actin cytoskeleton mediates receptor cross talk: an emerging concept in tuning receptor signaling. *J. Cell Biol.* 212, 267–280. doi: 10.1083/jcb.201504137

Mlynarczuk-Bialy, I., Doeppner, T. R., Golab, J., Nowis, D., Wilczynski, G. M., Parobczak, K., et al. (2014). Biodistribution and efficacy studies of the proteasome inhibitor BSc2118 in a mouse melanoma model. *Transl. Oncol.* 7, 570–579. doi: 10.1016/j.tranon.2014.07.002

Natkanski, E., Lee, W. Y., Mistry, B., Casal, A., Molloy, J. E., and Tolar, P. (2013). B cells use mechanical energy to discriminate antigen affinities. *Science* 340, 1587–1590. doi: 10.1126/science.1237572

Obino, D., Farina, F., Malbec, O., Sáez, P. J., Maurin, M., Gaillard, J., et al. (2016). Actin nucleation at the centrosome controls lymphocyte polarity. *Nat. Commun.* 7:10969. doi: 10.1038/ncomms10969

Otero, M. G., Alloatti, M., Cromberg, L. E., Almenar-Queralt, A., Encalada, S. E., Pozo Devoto, V. M., et al. (2014). Fast axonal transport of the proteasome complex depends on membrane interaction and molecular motor function. *J. Cell Sci.* 127, 1537–1549. doi: 10.1242/jcs.140780

Pauls, S. D., Hou, S., and Marshall, A. J. (2020). SHIP interacts with adaptor protein Nck and restricts actin turnover in B cells. *Biochem. Biophys. Res. Commun.* 527, 207–212. doi: 10.1016/j.bbrc.2020.04.101

Pinto, M., Alves, P., Luis, M., Pedro, J., Ryu, H., Jeon, N., et al. (2016). The proteasome controls presynaptic differentiation through modulation of an on-site pool of polyubiquitinated conjugates. *J. Cell Biol.* 212, 789–801.

Ramachandran, K. V., and Margolis, S. S. (2017). A mammalian nervous-system-specific plasma membrane proteasome complex that modulates neuronal function. *Nat. Struct. Mol. Biol.* 24, 419–430. doi: 10.1038/nsmb.3389

Reversat, A., Yuseff, M.-I., Lankar, D., Malbec, O., Obino, D., Maurin, M., et al. (2015). Polarity protein Par3 controls B-cell receptor dynamics and antigen extraction at the immune synapse. *Mol. Biol. Cell* 26, 1273–1285. doi: 10.1091/mbc.E14-09-1373

Ritter, A. T., Asano, Y., Lippincott-Schwartz, J., Griffiths, G. M., Stinchcombe, J. C., Dieckmann, N. M. G., et al. (2015). Actin depletion initiates events leading to granule secretion at the immunological synapse. *Immunity* 42, 864–876. doi: 10.1016/j.immuni.2015.04.013

Roper, S. I., Wasim, L., Malinova, D., Way, M., Cox, S., and Tolar, P. (2019). B cells extract antigens using Arp2/3-generated actin foci interspersed with linear filaments. *eLife* 8:e48093. doi: 10.1101/792481

Satpathy, S., Wagner, S. A., Beli, P., Gupta, R., Kristiansen, T. A., Malinova, D., et al. (2015). Systems-wide analysis of BCR signalosomes and downstream phosphorylation and ubiquitylation. *Mol. Syst. Biol.* 11:22. doi: 10.15252/msb.20145880

Schaefer, A., Nethe, M., and Hordijk, P. L. (2012). Ubiquitin links to cytoskeletal dynamics, cell adhesion and migration. *Biochem. J.* 442, 13–25. doi: 10.1042/BJ20111815

Schindelin, J., Arganda-Carreras, I., Frise, E., Kaynig, V., Longair, M., Pietzsch, T., et al. (2012). Fiji: an open-source platform for biological-image analysis. *Nat. Methods* 9, 676–682. doi: 10.1038/nmeth.2019

Schmidt, C., Berger, T., Groettrup, M., and Basler, M. (2018). Immunoproteasome inhibition impairs T and B cell activation by restraining ERK signaling and proteostasis. *Front. Immunol.* 9:2386. doi: 10.3389/fimmu.2018.02386

Spillane, K. M., and Tolar, P. (2018). Mechanics of antigen extraction in the B cell synapse. *Mol. Immunol.* 101, 319–328. doi: 10.1016/j.molimm.2018.07.018

Tolar, P. (2017). Cytoskeletal control of B cell responses to antigens. *Nat. Rev. Immunol.* 17, 621–634. doi: 10.1038/nri.2017.67

Treanor, B., Depoil, D., Gonzalez-Granja, A., Barral, P., Weber, M., Dushek, O., et al. (2009). The membrane skeleton controls diffusion dynamics and signaling through the B cell receptor. *Immunity* 32, 187–199. doi: 10.1016/j.immuni.2009.12.005

Tvorogova, A., Saidova, A., Smirnova, T., and Vorobjev, I. (2018). Dynamic microtubules drive fibroblast spreading. *Biol. Open* 7:bio038968. doi: 10.1242/bio.038968

Vascotto, F., Lankar, D., Faure-André, G., Vargas, P., Diaz, J., Le Roux, D., et al. (2007). The actin-based motor protein myosin II regulates MHC class II trafficking and BCR-driven antigen presentation. *J. Cell Biol.* 176, 1007–1019. doi: 10.1083/jcb.200611147

Vora, S., and Phillips, B. (2016). The benefits of local depletion: the centrosome as a scaffold for ubiquitin-proteasome-mediated degradation. *Cell Cycle* 15, 2124–2134. doi: 10.1080/15384101.2016.1196306

Wakatsuki, T., Wysolmerski, R. B., and Elson, E. L. (2003). Mechanics of cell spreading: role of myosin II. *J. Cell Sci.* 116, 1617–1625. doi: 10.1242/jcs.00340

Wang, J. C., and Hammer, J. A. (2020). The role of actin and myosin in antigen extraction by B lymphocytes. *Semin. Cell Dev. Biol.* 102, 90–104. doi: 10.1016/j.semcdb.2019.10.017

Yi, J., Wu, X., Chung, A. H., Chen, J. K., Kapoor, T. M., and Hammer, J. A. (2013). Centrosome repositioning in T cells is biphasic and driven by microtubule end-on capture-shrinkage. *J. Cell Biol.* 202, 779–792. doi: 10.1083/jcb.201301004

Yuseff, M.-I., Pierobon, P., Reversat, A., and Lennon-Duménil, A.-M. (2013). How B cells capture, process and present antigens: a crucial role for cell polarity. *Nat. Rev. Immunol.* 13, 475–486. doi: 10.1038/nri3469

Conflict of Interest: The authors declare that the research was conducted in the absence of any commercial or financial relationships that could be construed as a potential conflict of interest.

frontiers in Cell and Developmental Biology

ORIGINAL RESEARCH
published: 20 May 2021
doi: 10.3389/fcell.2021.633099

cAMP Bursts Control T Cell Directionality by Actomyosin Cytoskeleton Remodeling

*Morgane Simao[1], Fabienne Régnier[1], Sarah Taheraly[1†], Achille Fraisse[1,2], Rachida Tacine[1], Marie Fraudeau[1†], Adam Benabid[1†], Vincent Feuillet[1†], Mireille Lambert[1], Jérôme Delon[1] and Clotilde Randriamampita[1]**

[1] Université de Paris, Institut Cochin, INSERM, CNRS, Paris, France, [2] Master de Biologie, École Normale Supérieure de Lyon, Université Claude Bernard Lyon I, Université de Lyon, Lyon, France

T lymphocyte migration is an essential step to mounting an efficient immune response. The rapid and random motility of these cells which favors their sentinel role is conditioned by chemokines as well as by the physical environment. Morphological changes, underlaid by dynamic actin cytoskeleton remodeling, are observed throughout migration but especially when the cell modifies its trajectory. However, the signaling cascade regulating the directional changes remains largely unknown. Using dynamic cell imaging, we investigated in this paper the signaling pathways involved in T cell directionality. We monitored cyclic adenosine 3′-5′ monosphosphate (cAMP) variation concomitantly with actomyosin distribution upon T lymphocyte migration and highlighted the fact that spontaneous bursts in cAMP starting from the leading edge, are sufficient to promote actomyosin redistribution triggering trajectory modification. Although cAMP is commonly considered as an immunosuppressive factor, our results suggest that, when transient, it rather favors the exploratory behavior of T cells.

Keywords: lymphocyte, migration, cAMP, actomyosin, chemokine

OPEN ACCESS

Edited by:
Balbino Alarcon, Consejo Superior de Investigaciones Científicas (CSIC), Spain

Reviewed by:
Yeh-Shiu Chu, National Yang-Ming University, Taiwan
Won Fen Wong, University of Malaya, Malaysia

***Correspondence:**
Clotilde Randriamampita
clotilde.randriamampita@inserm.fr

†Present address:
Sarah Taheraly, PSL Research University, Institut Curie, INSERM, Paris, France
Marie Fraudeau, Institut de Recherche Servier, Croissy, France
Adam Benabid, Department of Cell Biology, Institute for Biomedical Engineering, Faculty of Medicine, RWTH Aachen University, Aachen, Germany
Vincent Feuillet, Aix Marseille Université, CIML, INSERM, CNRS, Marseille, France

Specialty section:
This article was submitted to Cell Growth and Division, a section of the journal Frontiers in Cell and Developmental Biology

Received: *24 November 2020*
Accepted: *22 April 2021*
Published: *20 May 2021*

Citation:
Simao M, Régnier F, Taheraly S, Fraisse A, Tacine R, Fraudeau M, Benabid A, Feuillet V, Lambert M, Delon J and Randriamampita C (2021) cAMP Bursts Control T Cell Directionality by Actomyosin Cytoskeleton Remodeling. Front. Cell Dev. Biol. 9:633099. doi: 10.3389/fcell.2021.633099

INTRODUCTION

Fast and random motility of T lymphocytes is a prerequisite to perform efficient immune surveillance, as these cells need to scan the widest possible area in a short time within secondary lymphoid organs (Krummel et al., 2016). This motility is conditioned by the chemical (mainly chemokines) and physical (structural constraints) parameters specifically found in these confined environments. Even in the absence of physical obstacles, random migration is observed (see (Real et al., 2004) for instance), suggesting the existence of cell-intrinsic factors regulating the cell directionality.

T cells stimulated by chemokines lose their round shape within a few minutes, to acquire a clear polarized shape with a front, the lamellipodium, and a rear, the uropod. This asymmetry, required for their migration, is achieved by a rapid modification of their cytoskeleton (Moreau et al., 2018). In fact, chemokine stimulation triggers a rapid increase in polymerized actin (Real et al., 2007), especially branched actin which accumulates at the cell front giving the lamellipodium some highly dynamic properties adapted to the research strategy of T lymphocytes. Conversely, stable actin and actomyosin allow to maintain the structural shape of the cell body and to promote its contractility (Dupré et al., 2015; Chugh and Paluch, 2018). During T cell migration, continuous remodeling of

the cytoskeleton, such as the actin network, has to take place, especially each time cells modify their trajectory. Indeed, in this case, the cell slows down and its lamellipodium retracts, leading to the transient loss of cell asymmetry before being reestablished along another axis. Calcium has been clearly identified as the stop signal leading to lamellipodium retraction and migration inhibition when T cells encounter an antigen-presenting cell (Donnadieu et al., 1994; Dong et al., 2017). However, the signaling pathway involved in shape changes of chemokine-stimulated T cells during trajectory changes, remains unclear.

The role of cAMP upon migration remains confused depending on the cell types or the experimental conditions. In T lymphocytes, a negative effect of cAMP pathway has been known for a long time and is supported by different studies showing that agents inducing large increases in cAMP levels, such as forskolin, inhibitors of phosphodiesterases or prostaglandin E2, promote cell rounding and migration inhibition (Valitutti et al., 1993; Oppenheimer-Marks et al., 1994; Layseca-Espinosa et al., 2003; Dong et al., 2006). Interestingly, in other cell types, cAMP seems to play a more complex role in cell migration through its compartmentalization. In fibroblasts or epithelial cells, an increase of cAMP-activated protein kinase (PKA) activity at the leading edge has been reported to promote cell migration (Howe et al., 2005; Lim et al., 2008; McKenzie et al., 2020). Conversely, in neutrophils, local increases in cAMP promote uropod retraction through the regulation of the non-muscle myosin II by PKA (Liu et al., 2010). The development of powerful biosensors makes it possible to measure cAMP (Klarenbeek et al., 2011) at the subcellular level even in small cells such as lymphocytes and with a good temporal resolution, and therefore to revisit the role of cAMP in T cell migration.

Using dynamic cell imaging, we here investigate the signaling pathways involved in trajectory control during T cell migration. We demonstrate that transient spontaneous increases in intracellular cAMP are sufficient to drive T cell actomyosin reorganization, leading to paths modifications.

MATERIALS AND METHODS

Cells

CEM T cells were cultured in RPMI 1640, supplemented with 10% FCS, 2 mM L-Glutamine, 50 U/ml penicillin and 50 μg/ml streptomycin. When specified, cells were transfected by nucleofection (Amaxa Nucleofactor, Lonza) with 5 μg DNA for 5 millions of cells using the C-016 program. The cells were used the day after nucleofection.

Reagents

CXCL12 (recombinant human SDF1-α) was purchased from Peprotech (300-28A) and VCAM-1 (CD106 Fc chimera protein) from R&D Systems (862-VC-100). Calcium measurements were performed with Fura-2/AM (Molecular Probes, F1225). DMACM-caged 8-Br-cAMP was purchased from Biolog (D044). Nucleus labeling was performed with Hoechst (Molecular Probes, H1399). F-actin detection was performed by expressing the LifeAct-mCherry construct (gift from Dr. A. Benmerah). Myosin IIA was followed by expressing tagged form of Myosin Heavy Chain 9 (MyH9-GFP, gift from PJ Saez). Stable actin detection was performed with SiRActin (TebuBio, SC001) or with mRFP-Utrophin-CH (Addgene #64358).

Live Imaging Acquisition

For migration experiments, glass coverslips were coated with 1 μg/ml CXCL12 and 1 μg/ml VCAM-1 overnight at 4°C. After rinsing, coverslips were kept in mammalian saline buffer (140 mM NaCl, 5 mM KCl, 1 mM $CaCl_2$, 1 mM $MgCl_2$, 20 mM HEPES, and 11 mM glucose) supplemented with 5% FCS. Cells were deposited on coverslips just before image acquisition started. Live imaging experiments were performed at 37°C with a wide-field Nikon TE2000, equipped with a CMOS camera (ORCA-flash4.0 LT, Hamamatsu). Images were acquired every 10 s with Metafluor software.

Actin, Myosin, and Nucleus

For total polymerized actin detection, cells were transfected with LifeAct-mCherry construct. For stable actin detection, cells were transfected with Utrophin-CH-RFP. For non-muscle Myosin IIA detection, cells were transfected with MyH9-GFP construct. For stable actin labeling, cells were incubated for 1 h with 250 nM SiRActin in complete medium at 37°C. After rinsing, cells were deposited on coated coverslips. Nucleus labeling was performed with 4 min incubation, using 2 μg/ml Hoechst. Distribution of compounds was followed by 650 nm Excitation/700 nm Emission for SiRActin, 560 nm Excitation/645 nm Emission for LifeAct-mCherry, 485 nm Excitation/525 nm Emission for MyH9-GFP and 360 nm Excitation/440 nm Emission for Hoechst.

cAMP Measurements

For cAMP measurements, cells were transfected with the most sensitive version of TEpacVV [H187 (Klarenbeek et al., 2015)]. TEpacVV was a gift from Dr. K. Jalink (Netherlands Cancer Institute). Experiments were performed 24 h after transfection, as previously described (Conche et al., 2009). Briefly, when cAMP increases, the probe undergoes a conformational change that allows a decrease of energy transfer between a turquoise molecule (Excitation 436 nm, Emission 470 nm) and two Venus molecules (Excitation 500 nm, Emission 535 nm) (Klarenbeek et al., 2011); the energy transfer can be measured as a change in FRET (Excitation 436 nm, Emission 535 nm). Three images were acquired every 10 s: visible, Turquoise channel and FRET channel. The ratio R = Turquoise/FRET, which gives an estimate of cAMP concentration, was calculated with MetaFluor (Roper Scientific) after background subtraction. An increase of this ratio corresponds to an increase in cAMP concentration.

Calcium Measurements

For calcium experiments, cells were loaded with 500 nM Fura-2/AM for 20 min at 37°C. Excitation was performed alternatively at 350 and 380 nm and emission recorded at 510 nm. The ratio (Exc 350, Em510/Exc380, Em510) was calculated with MetaFluor (Roper Scientific) after background subtraction. For combined cAMP and Ca measurements, TEpacVV-transfected cells were

loaded only with 200 nM Fura-2/AM in order to minimize the crosstalk between the four fluorescence signals.

Image Analysis

Cell Roundness

This parameter was quantified with ImageJ software and corresponds to: $\frac{4 \times area}{\pi \times (major\ axis)^2}$. It is equal to 1 for a round cell and < 1 for a polarized one.

Front/Back Ratios

With Metamorph software, a 6–9 pixels wide scanline along the cell axis was drawn. The front/back ratio was then calculated by dividing the intensity at the front edge to the one measured at the back one.

Angles

Angle measurements were performed with ImageJ by drawing lines along the polarization axes observed between two consecutive lamellipodia formation.

Pearson Coefficient

In cells transfected with MyH9-GFP and labeled with SiRActin, Pearson Coefficient was measured on Fiji (ImageJ software, version 1.51 u) by using a macro containing the Coloc2 plugin. This coefficient measures the degree of overlap between two stainings and was used to quantify the degree of colocalization between MyH9-GFP and SiRActin staining. A Pearson Coefficient value of 0 means that there is no colocalization between the two stainings. By contrast, a Pearson Coefficient value of 1 means that there is a perfect colocalization between MyH9-GFP and SiRActin.

Kymographs

Kymographs have been performed with Metamorph software by drawing a line as wide as the cell along the migration axis.

Cross-Correlation

Cross-correlation was used to study the correlation between cAMP variations and cell shape (roundness). The Pearson correlation coefficient (ρ) between two time courses was computed as a function of time lag (τ):

$$\rho(\tau) = \frac{\sum[(x(i) - \overline{x}) \times \left(y(i \mp \tau) - \overline{y}\right)]}{\sqrt{\sum (x(i) - \overline{x})^2 \times \sum \left(y(i \mp \tau) - \overline{y}\right)^2}};$$

with x and y variables and $\overline{x}$ and $\overline{y}$ variable means.

Local Leading Edge Release of cAMP

CEM were incubated with 20 μM DMACM-caged 8-Br-cAMP for 3 h at 37°C. SiRActin (250 nM) was added to the medium during the last hour. Cells were rinsed and deposited on VCAM-1/CXCL12 coated coverslips for 30 min at 37°C. The experiment was performed by using an iMIC TILL Photonics microscope equipped with two cameras EMCCD (ANDOR Technology) and 60x objective (numerical aperture: 1.49) + 1.5 zoom. Images were acquired every 5 s. After four image acquisitions, the release of DMACM-caged 8-Br-cAMP was performed with a 405 nm laser (Toptica iBAEM 110 mV, 1 ms illumination, 100% power) by adjusting a 7 μm diameter region at the level of the leading edge of a migrating cell. For control experiments, a similar protocol was followed except that the cells were incubated with DMSO instead of caged-cAMP for the same duration.

Traction Force Microscopy

Traction force microscopy experiments were performed with the help of Cell Biomechanics facility of Cochin Institute.

Hydrogel Preparation

Hydrogels (∼700Pa) were prepared with acrylamide (3%, Sigma #A4058), bis-acrylamide (0.3%, Sigma #M1533-25), streptavidin-acrylamide (Invitrogen, S21379) and Flash Red 0.2 μm fluorescent beads (Bangs Laboratories, FSFR002). Streptavidin-acrylamide was used at 1/100,000 molecular ratio to acrylamide as previously described (Saitakis et al., 2017). After activation with TEMED and ammonium persulfate, 11 μl of the polymerization mix was added on a non-functionalized 12 mm diameter coverslip. A functionalized glass coverslip coated with silane (Sigma, 17-1330-01) was placed on top. Polymerization was performed at room temperature for 30 min.

Mechanical Properties of the Polyacrylamide Gels

Gels were unmolded by removing the non-functionalized coverslip. We then checked whether the bead distribution on the top surface was suitable for traction forces measurement (∼2000 beads per 512 × 512 pixels field). The Young Modulus was then calculated according to (Gross and Kress, 2017). In brief, tungsten carbide spheres with known radius (0.4 and 0.6 mm) and density (15,630 g/l) were deposited on the hydrogel surface. We then measured the gel deformation induced by the bead by acquiring z-images of the fluorescent beads embedded in the gel, focusing on the bottom and the top of the gel with an indentation of 0.2 μm. By using ImageJ, we measured the gel height and the collapse distance of the sphere. The Young Modulus was calculated by using a R code based on (Gross and Kress, 2017) (available on demand).

Functionalization of Hydrogel Surface

We used the specific biotin-streptavidin binding and anti-Fc/Fc binding to form a sandwich of macromolecules for the functionalization of polyacrylamide gels. All gel surfaces were incubated with 10 μg/ml of a goat anti-human IgG Fc biotinylated antibody (Abcam: ab97223) in PBS-BSA 0.2% overnight at 4°C. Gels were then incubated with 10 μg/ml recombinant human VCAM-1/CD106 Fc chimera in PBS-BSA 0.2% for 2 h at 37°C. We were not able to experimentally assess the VCAM-1 surface density, but theoretically calculated the density of streptavidin molecules on the gel. For this we used the three assumptions enunciated in Saitakis et al. (2017). In brief, (1) the volume of the hydrated gel (with culture medium) that we were able to calculate with the thickness and the coverslip diameter, is approximately 40% bigger than the initial volume of the polymerization mix (Hynd et al., 2007). (2) All the streptavidin-acrylamide molecules within the

polymerization mix polymerized within the gel. (3) Biotinylated anti-Fc antibody can access the first 10 nm of the gel (10 nm is the approximated size of the streptavidin molecule) due to their own size and the size of the pore reported in the literature (Trappmann et al., 2012). We then calculated that the theoretical surface density of streptavidin-acrylamide is 25 molecules/μm^2.

Traction Force Measurements

Traction force microscopy experiments were performed with 20x objective (numerical aperture 0.75) and 1.5 zoom. CXCL12-stimulated (100 ng/ml) cells were deposited on a VCAM-1-coated gel for 30 min at 37°C. Transmitted light and corresponding fluorescent images of beads and actin were acquired every 10 s using the MetaMorph software.

Force Image Analysis

We first aligned images of the fluorescent beads to correct the drift by using the ImageJ plugin Stack Reg. The forces were calculated by the method described in Martiel et al. (2015). Basically, the displacement field was calculated by Particle Image Velocimetry (PIV) plugin implemented in ImageJ. The PIV was performed through an iterative process. For each iteration, the displacement was calculated by the normalized correlation coefficient algorithm, so that an individual interrogation window was compared with a larger searching window. Each subsequent iteration took into account the displacement field measured previously. The resulting final grid size for the displacement field was 5.04 $\mu m \times 5.04$ μm with more than six beads per interrogation window on average. With the displacement field obtained by PIV analysis, the traction force field was reconstructed by the Fourier transform traction cytometry (FTTC) method (Martiel et al., 2015) with FTTC ImageJ plugin. The regularization parameter was set at 8×10^{-11} for all traction force reconstructions.

After this calculation, the forces along the cell body were isolated. The cell length was normalized by establishing that the cell front corresponds to 0% and the back to 100%. When specified (**Figures 1C**, **2D,E**), the forces along the cell axis were pooled.

Statistics

The statistical tests used for sample comparison are specified in the figure legends. In the figures, ns: not significant. They were performed with GraphPad software or RStudio.

RESULTS

Remodeling of Actin Cytoskeleton in Chemokine-Stimulated T Lymphocytes

Upon chemokine stimulation, T cells lose their symmetrical shape and become polarized. This modification can be visualized by depositing CEM T cells, a lymphoblastic cell line which expresses CXCR4, the receptor of the CXCL12 chemokine (C-X-C motif chemokine 12 or stromal cell derived factor 1), on a glass coverslip coated with the integrin VCAM-1 (vascular cell adhesion molecule 1) and CXCL12. In these conditions, cells randomly migrate at a speed of 6.19 $\pm$ 0.03 μm/min (N = 80 cells) (illustrated in **Supplementary Movie 1**). In order to follow in real time and at the subcellular level cytoskeleton reorganization, T cells were transfected with mCherry-tagged LifeAct, a peptide able to bind to F-Actin. As shown in **Figure 1A**, polymerized actin is observed mainly at the front of the cell which corresponds to newly polymerized actin, as previously described (Real et al., 2007). In order to distinguish this pool from stable actin which constitutes the main pool of F-actin in unstimulated cells, SiRActin [a fluorescent cell-permeable F-Actin binding compound (Milroy et al., 2012; Lukinavicius et al., 2014)] was used. Resting cells were incubated for 1 h with SiRActin, rinsed and then stimulated so that the newly polymerized actin was not labeled. In these conditions, we clearly observed that, contrary to total polymerized actin, the stable actin network was restricted to the back of the cell behind the nucleus (**Figure 1A** and **Supplementary Movie 2**). The distribution of the two actin networks was quantified by drawing a scanline along the antero-posterior axis of the cell and then by measuring the ratio of intensities between the front and the back as shown in the example presented in **Figure 1A**. A ratio superior to 1 indicates an accumulation at the cell front. A statistical difference was measured between the localization of these two actin networks: total polymerized actin accumulates at the cell front while stable actin mainly accumulates at the back (**Figure 1B**). We next wondered whether the polarization of actin networks could be correlated with a mechanical asymmetry during T cell migration. To answer this question, we used the dynamic Traction Force Microscopy technique (Nerger et al., 2017) which allows the forces developed by the cells upon migration on polyacrylamide (PAA) gels to be measured. T lymphocytes are fast-moving cells, therefore they are expected to develop low forces on their substrate. For this reason, we used soft PAA gels of about 700 Pa and measured how T cells were able to displace fluorescent beads embedded within the PAA gel while they migrate. As quantified in **Figure 1C** and illustrated in **Supplementary Figures 1A,C** and T cells clearly imprint centripetal forces with a maximum intensity at the back of the cells and minimal intensity at the front, as previously observed in neutrophils (Jannat et al., 2011). The intensity of the forces we measured was very low, i.e., 100 times smaller than what was measured in neutrophils on gels with comparable stiffness (Jannat et al., 2011). We can therefore conclude that, during migration, T lymphocytes adhere mainly, but poorly, where stable actin accumulates.

Actomyosin Relocalization Upon Trajectory Modification

The asymmetrical distribution of SiRActin remains stable upon migration. We thus investigated its behavior when cells retract their lamellipodium. This step is specifically required when cells round up and eventually change their direction. The example presented in **Supplementary Figures 2A,B** (kymograph and corresponding thumbnails) summarizes the different steps: upon migration, stable actin remains accumulated at the back of the cell (step 1) and (step 3); the retraction of the lamellipodium is accompanied by the relocalization of stable actin at the front

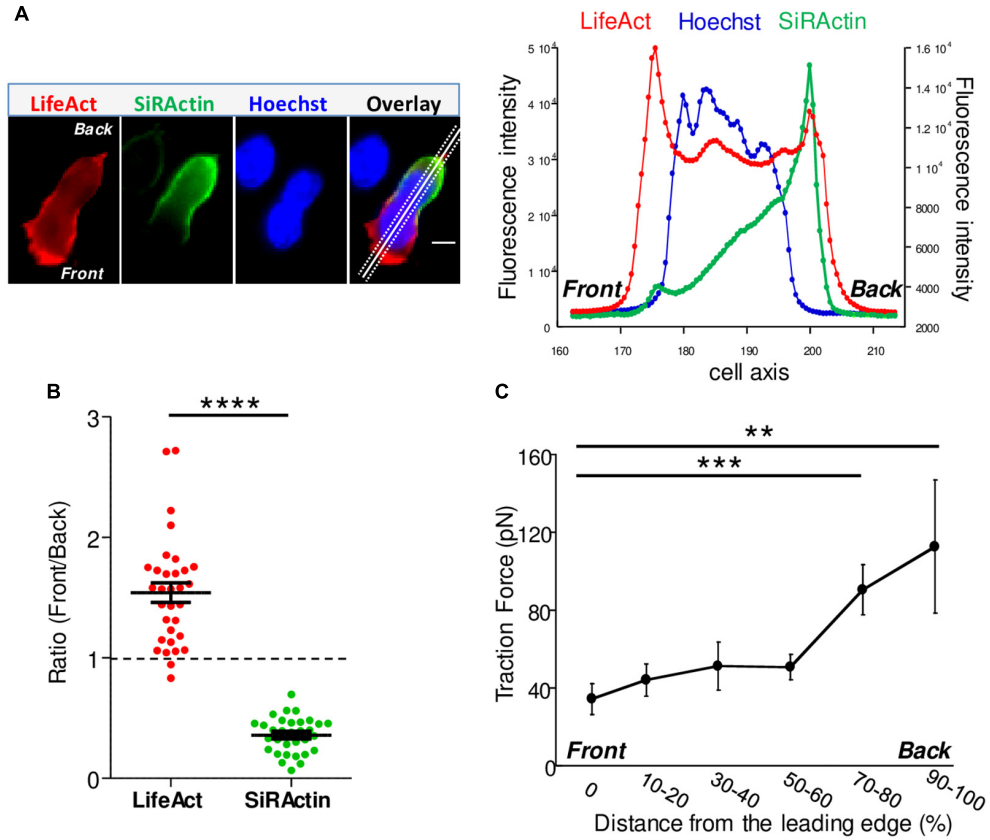

FIGURE 1 | Actin cytoskeleton asymmetry upon chemokine-stimulated T cells. **(A)** T cells were transfected with LifeAct-mCherry and labeled with SiRActin and Hoechst. After washing, the cells were deposited on a VCAM-1/CXCL12 coated coverslip. A typical distribution of total polymerized actin (LifeAct), stable actin network (SiRActin) and nucleus (Hoechst) is shown on the left panel and quantified along the scanline displayed on the overlay image (right panel). Images are from Movie 2. Scale bar = 10 μm. **(B)** Using similar scanlines as in A, the ratio between front and rear intensities was measured for total polymerized actin and stable actin networks. Mean ± SE (N = 31). The values obtained were statistically different (paired t-test, $^{****}p < 0.0001$, N = 32 cells). **(C)** The subcellular distribution of forces was measured in CXCL12-stimulated T cells upon migration on approximately 700 Pa gels coated with VCAM-1. The magnitude of these forces was significantly higher at the back of the cells compared to the front. The values of the forces expressed in picoNewton correspond to the mean of forces ± SE measured in 14 different cells. $^{***}p < 0.001$, $^{**}p < 0.01$ Kruskal-Wallis test.

where it rapidly accumulates (step 2) and (step 4). If the cell changes its direction (step 2), the stable actin will migrate entirely to this point which will constitute the new back of the migrating cell, as shown on the kymograph (**Supplementary Figure 2A**, red arrow). Conversely, if the cells round up (step 4) (yellow arrow), the stable actin will progressively redistribute homogeneously all around the cell membrane (step 5). The complete series of images is displayed in **Supplementary Movie 3**. The distribution of the stable actin is quantified on a series of cells during these different steps (**Figure 2A**): while, as previously shown in **Figure 1B**, it is clearly accumulated at the back upon migration (R = 0.35 ± 0.01, N = 85 events from 60 different cells), a transient accumulation at the front is observed during lamellipodium retraction (R = 1.89 ± 0.13, N = 53 events from 28 different cells) before it disperses around the membrane (R = 0.98 ± 0.04, N = 19 events from 16 different cells) when the cell rounds up. A similar relocalization of stable actin was observed when, having developed two lamellipodia, a cell retracts one of them (**Supplementary Figure 2C**). To confirm the results we obtained with SiRActin, we used another marker of stable actin, Utrophin-CH (Melak et al., 2017). In this case, a relocalization of stable actin network similar to the one detected with SiRActin is also observed upon lamellipodium retraction (**Supplementary Figures 3A,B**). Interestingly, non-muscle myosin-IIA [the main myosin isoform in T lymphocytes (Jacobelli et al., 2004)] displays a distribution similar to that of SiRActin as attested by Myosin Heavy Chain 9 (MyH9) localization upon migration, retraction and in round cells (**Figure 2B**). Indeed, MyH9 clearly accumulates at the cell back upon migration (R = 0.58 ± 0.03, N = 77 events from 42 different cells), relocalizes to the cell front during lamellipodium retraction (R = 2.09 ± 0.13, N = 69 events from 36 different cells) while it distributes uniformly when the cell rounds up (R = 1.02 ± 0.06, N = 20 events from 17 different cells). In these three configurations, a colocalization is observed between SiRActin and MyH9 distributions as shown in the example presented in **Supplementary Figure 2B** and **Supplementary Movie 4**. The strong correlation between the two markers is

attested by Pearson Coefficient (PC) $\geq$ 0.7 (PC = 0.70 $\pm$ 0.02, N = 39 events from 24 migratory cells; PC = 0.71 $\pm$ 0.03, N = 32 events from 21 cells retracting their lamellipodium; PC = 0.74 $\pm$ 0.05, N = 7 events from 7 cells rounding up) (**Figure 2C**). This result suggests that the stable actin network detected by SiRActin mainly corresponds to actomyosin. Lamellipodium retractions were associated with a modification of the cell shape: the cell rounds up before it eventually elongates in another direction. We therefore measured simultaneously over time, the relocalization of SiRActin to the lamellipodium (measurement of the front/back ratio along the cell axis) together with the cell roundness and quantified the delay between the two events. We observed that the accumulation of actin at the front starts at 8.7 $\pm$ 4.0 s (N = 38 cells) before the cells begin to round up, suggesting that the relocalization of the stable actin might drive the retraction of the lamellipodium. Finally, we examined whether the relocalization of stable actin was accompanied by a redistribution of the forces developed by the cells. As shown in **Figure 2D** and illustrated in **Supplementary Figures 1B,C**, once again the distribution of high intensity forces is similar to that of stable actin: upon retraction, contrary to migratory conditions, centripetal forces at the level of the lamellipodium, reached intensities similar to those observed at the back of the cell. The intensities at the cell front were statistically higher than those observed in migrating cells, while no differences were observed at the back (**Figure 2E**). Once the cells have rounded, forces can no longer be measured (**Supplementary Figure 1D**).

cAMP Variations Upon Trajectory Modification

We next wondered what the signaling pathway which triggers changes of direction and the simultaneous redistribution of the stable actin might be. Calcium has recently been associated with pausing upon confinement-induced T cell migration (Dong et al., 2017). Although, in our conditions, calcium (Ca) transients could sometimes be observed upon migration, they were neither systematic (**Supplementary Figure 4A**), nor associated with change of direction (**Supplementary Figure 4B**). We therefore focused on cAMP which has also been described as playing a role during migration (Howe, 2004). We used the very sensitive FRET biosensor, TEpacVV (Klarenbeek et al., 2011, 2015) to follow intracellular cAMP levels. As shown in the example presented in **Figure 3A** and **Supplementary Movie 5**, cAMP levels remained low upon migration, except at very specific moments when the cell stopped and eventually changed its direction. This can be visualized on the associated kymograph by the red zones corresponding to high cAMP levels. By zooming in on a change of direction (**Figure 3A**, white dotted rectangle), it appears that the cAMP increase starts at the cell front before invading the whole cell (**Figure 3B**). By combining cAMP and Ca measurements, we were able to demonstrate that no Ca variations could be detected in cells presenting some cAMP transients upon change of direction (**Supplementary Figure 4C**). The cellular heterogeneity in cAMP ratio was quantified by drawing scanlines along the antero-posterior axis of migrating cells. The front to back ratios were compared in cells which migrate, retract their lamellipodia or round up. While this ratio is equal to 1.00 $\pm$ 0.02 (N = 32 cells) upon migration, it increases up to 1.30 $\pm$ 0.03 (N = 32 cells) when the cells retract their lamellipodium before decreasing back to 1.00 $\pm$ 0.04 (N = 8 cells) once the cells have rounded up, meaning that lamellipodium retraction is associated with a local increase of cAMP at the cell front (**Figure 3C**). In our experimental conditions, some cells failed to migrate and went on repetitive elongation/retraction cycles (**Figures 3D–F**). Interestingly, these cells displayed cAMP oscillations (see **Supplementary Figure 5A** for two examples) with a very similar period from cell to cell (211.8 $\pm$ 11.7 s, N = 29 cells, **Supplementary Figure 5B**) and which is very regular for a given cell (**Supplementary Figure 5C**). These oscillations were associated with morphological changes corresponding to elongation/retraction cycles during which the level of cAMP starts to rise in the lamellipodium before invading the whole cell when it rounds up (**Figure 3D** and zoom in **Figure 3E**). The complete series of images is displayed in **Supplementary Movie 6**. In these cells, the antero-posterior ratio of cAMP was 1.05 $\pm$ 0.03 (N = 35 cells) upon elongation, increased to 1.38 $\pm$ 0.05 (N = 35 cells) upon retraction, before decreasing to 0.99 $\pm$ 0.03 (N = 32 cells) in round cells (**Figure 3F**). These values were very similar to those measured in migrating cells (**Figure 3C**). In order to quantify the coupling between cAMP level and the shape of the cells, the roundness was measured simultaneously with cAMP as in the example presented in **Figure 4A** (left panel). Clearly, the two parameters oscillate at the same frequency. However, an offset of 50 s is necessary in this example to synchronize cAMP levels and roundness (**Figure 4A**, right panel). A cross-correlation analysis was performed for a series of cells (see methods for details) and reveals that the most significant positive correlation between the two parameters (0.36 $\pm$ 0.05, N = 17 cells) is obtained with a 40–50 s temporal offset (**Figure 4B**). In other words, this result shows that cells start to round up 40 to 50 s after cAMP begins to rise.

In order to measure to what extent this event triggers a modification of cell trajectory, we measured the angle formed between the polarization axes observed between two consecutive lamellipodia separated by cAMP-induced lamellipodium retraction. As displayed on **Figure 3G**, the cells preferentially repolarize with an angle between 90° and 180° (Mean of 108.4 $\pm$ 4.7; N = 111 repolarization events from 37 cells) showing that cAMP transients favor directional changes.

Control of Stable Actin Relocalization by cAMP

To address the direct link between cAMP increase and stable actin recruitment, the two parameters were monitored simultaneously. As shown in the example presented in **Figure 5A** and in **Supplementary Movie 7**, a local increase of cAMP can first be observed in the lamellipodium which is followed by a recruitment of stable actin at this position. This observation has been quantified over time by measuring the front/back ratio for cAMP along a scanline together with the stable actin recruitment (**Figure 5A**, right panel) and the time lag was measured (gray arrow). The delay between the two events was 40.5 $\pm$ 3.6 s (N = 39

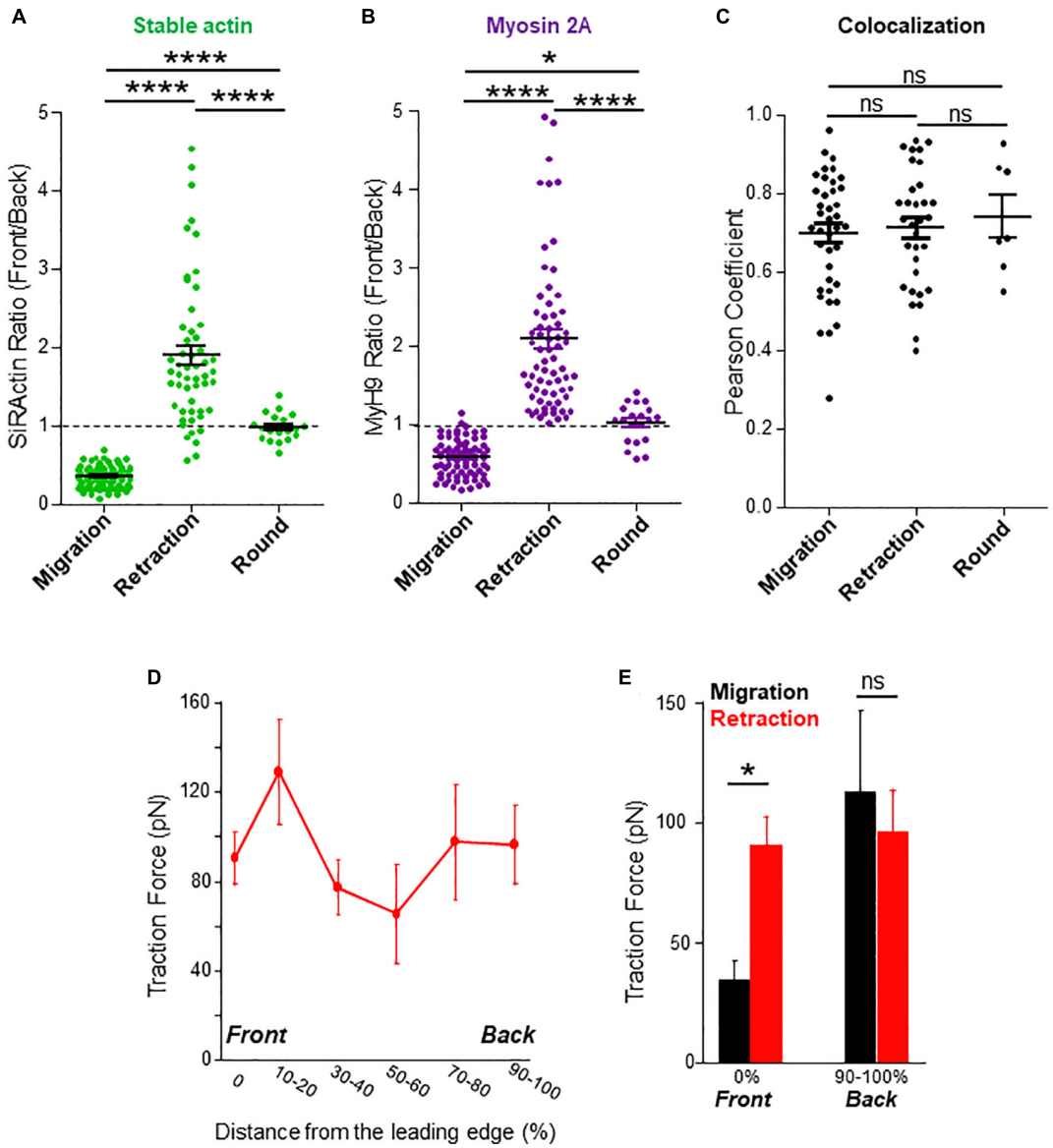

FIGURE 2 | Stable actin relocalization. **(A)** The front to back ratio of SiRActin intensities were measured by drawing a scanline along the cell axis of cells upon migration, while the lamellipodium retracted and once the cell had rounded up. Values correspond to the mean ± SE of 85 events from 60 different cells (migration), 53 events from 28 different cells (lamellipodium retraction) and 19 rounding events from 16 different cells (after retraction). Statistical analysis was performed through a one way ANOVA test with a Tukey post-test. ****$p < 0.0001$. **(B)** The front to back ratio of MyH9-GFP intensities were measured by drawing a scanline along the cell axis of cells upon migration, while the lamellipodium retracted and once the cell had rounded up. Values correspond to the mean ± SE of 77 events from 42 different cells (migration), 69 events from 36 different cells (lamellipodium retraction) and 20 rounding events from 17 different cells (after retraction). Statistical analysis was performed through a one way ANOVA test with a Tukey post-test. ****$p < 0.0001$, *$p < 0.05$. **(C)** In cells transfected with MyH9-GFP and labeled with SiRActin, Pearson coefficient was measured upon migration, while the lamellipodium retracted and once the cell had rounded up. Values correspond to the mean ± SE of 39 events from 24 different cells (migration), 32 events from 21 different cells (lamellipodium retraction) and seven rounding events from seven different cells (after retraction). Statistical analysis was performed through a one way ANOVA test with a Tukey post-test. ns: not significant. **(D)** Subcellular distribution of forces was measured in CXCL12-stimulated T lymphocytes upon lamellipodium retraction on approximately 700 Pa gels coated with VCAM-1. The values of the forces expressed in picoNewton correspond to the mean of forces ± SE measured in eight different cells retracting their lamellipodium. **(E)** Comparison of the values of the forces measured in 14 migrating cells (black) or in eight cells retracting their lamellipodium (red) at their front (0%) or their back (90–100%). *$p < 0.05$ Kruskal-Wallis test.

retraction events from 21 different cells, **Figure 5B**). This result indicates that the local increase in cAMP appears first, followed by the recruitment of stable actin. In order to establish with certainty the causal link between the two events, we artificially generated a local increase in cAMP in the lamellipodium by using a caged form of the nucleotide (DMACM-caged 8-Br-cAMP).

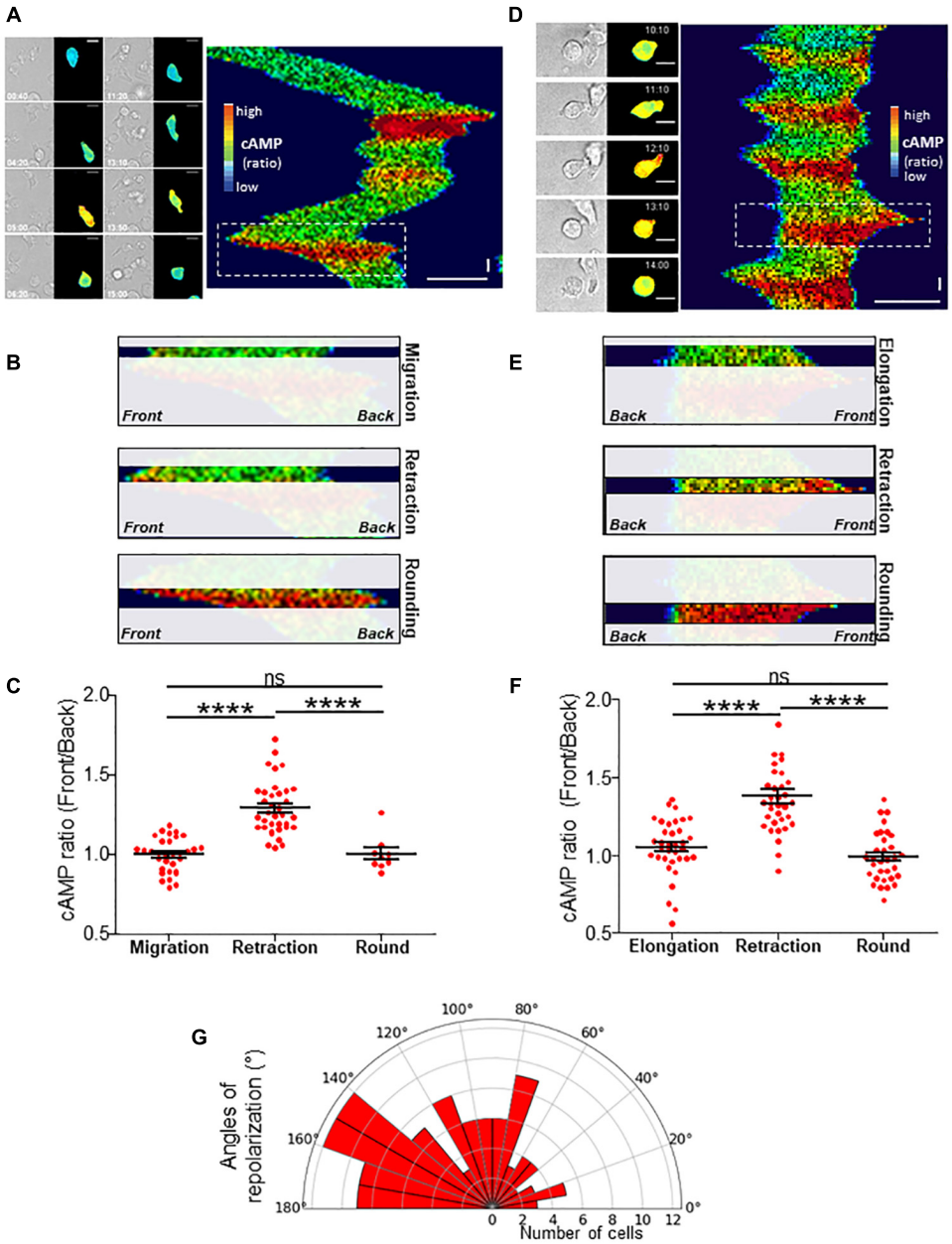

FIGURE 3 | cAMP variations upon migration. **(A)** Example of a TEpacVV-transfected T cell migrating on a CXCL12/VCAM-1-coated coverslip. The corresponding kymograph was established along the antero-posterior axis of the cell. The x axis corresponds to the average cAMP level along the cell while the y axis corresponds to time. cAMP levels were coded in false colors. The complete series of images is shown in **Supplementary Movie 5**. Horizontal scale bar = 10 μm, vertical scale bar = 1 min. **(B)** Zoom of the zone corresponding to the white rectangle in the kymograph presented in **(A)** illustrating that the increase of cAMP starts from the front before invading the whole cell. **(C)** Ratios of cAMP level from the front to the back of the cell were measured by drawing scanlines along antero-posterior axis in migrating cells, cells retracting their lamellipodium or after they rounded up. Values correspond to the mean ± SE of 32 events (migration), 36 events (retraction), 8 values (round cells after retraction) from 11 different cells. Statistical analysis was performed through a one way ANOVA test with a Tukey post-test. ****$p < 0.0001$. **(D)** Example of cAMP variations measured in a TEpacVV-transfected T cell displaying elongation/retraction cycles on a CXCL12/VCAM-1-coated coverslip. During recording, the cell presents 5 such cycles as displayed on the kymograph. The complete series of images is displayed in **Supplementary Movie 6**. Horizontal scale bar = 10 μm, vertical scale bar = 1 min. **(E)** Zoom of the zone corresponding to the white rectangle in the kymograph presented in **(D)** illustrating that the increase of cAMP starts at the front before invading the whole cell. **(F)** Ratios of front to back cAMP levels measured in cells displaying elongation/retraction cycles. Values correspond to the mean ± SE of 35 values (elongation), 35 values (lamellipodium retraction) and 32 values (round cells after retraction) from 9 different cells. Statistical analysis was performed through a one way ANOVA test with a Tukey post-test. ****$p < 0.0001$.**(G)** Polar distribution of repolarization angles. Values correspond to the angle formed between polarization axes observed between two consecutive lamellipodia separated by cAMP-induced lamellipodium retraction. Width of sectors = 10°. Values correspond to 111 measurements performed on 37 different cells.

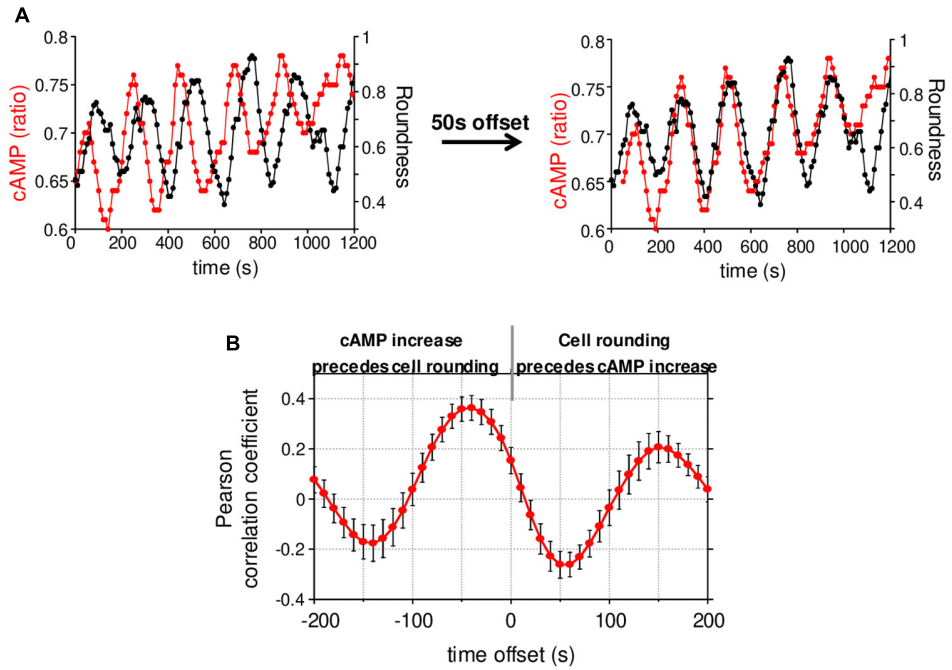

FIGURE 4 | cAMP variations and cell roundness. **(A)** Example of cAMP variations measured simultaneously with the cell roundness for the cell presented in **Figure 3D**. The shift of cAMP curve by 50 s allowed us to synchronize it with the cell roundness curve. **(B)** Cross-correlation between cAMP and cell roundness. A negative offset means cAMP increase precedes the cell rounding. Values correspond to the mean ± SE of cross-correlation coefficients measured on 17 cells displaying cAMP oscillations.

Unfortunately, this compound is weakly fluorescent and the release of a coumarin analog in addition to 8-Br-cAMP upon DMACM-caged 8-Br-cAMP uncaging, prevents us to measure simultaneously with our FRET biosensor, the rise in cAMP we trigger in these conditions. However, we can expect that the use of this compound allowed us to generate a transient rise in cAMP after illumination at 405 nm as we observed in a previous study (Conche et al., 2009) and to analyze its consequences on the distribution of stable actin, together with cell roundness. Illumination of the leading edge on a 7 μm diameter region induces the recruitment of SiRActin and a lamellipodium retraction when cells have been incubated with caged 8-Br-cAMP (**Figure 5C** and **Supplementary Movie 8**), but not in control conditions (**Supplementary Movie 9**). The frequency of retraction upon laser illumination was significantly higher in cells which had been loaded with caged-cAMP compared to control cells (**Figure 5D**). The retraction events observed in control cells probably correspond to illumination-induced or spontaneous retraction events. After cAMP-induced retraction, cells remain round or form a new lamellipodium in another direction (**Supplementary Movie 8**). As shown in **Figure 5E**, the accumulation of stable actin starts 35.2 ± 5.5 s (N = 23 cells) after cAMP release, while the lamellipodium begins to retract after 48.8 ± 6.5 s (N = 21 cells). This result demonstrates that a local increase in cAMP is sufficient to induce the recruitment of stable actin and the subsequent retraction of the lamellipodium. Interestingly, by generating an artificial increase in cAMP, the delays measured between the three steps (increase in cAMP/relocalization of stable actin/retraction of the lamellipodium) were very similar to those measured in chemokine-stimulated cells (**Figure 5F**), suggesting the involvement of a similar sequence of events in the two configurations and pointing out to cAMP as the upstream initial trigger of the whole sequence of cytoskeletal-driven morphological alterations responsible for directional changes in T cell migration.

DISCUSSION

T cell migration conditions an efficient immune response. The rapid and random displacement of these cells constitutes an important property for an optimization strategy for foreign antigen detection. Although anatomical constraints might impose T cell trajectory, we focus here on the influence of the chemical environment, i.e., chemokine, on T cell migration. We demonstrate that cell intrinsic factors are sufficient to promote random migration upon chemokine stimulation. Our results highlight a three step time sequence of signaling events, summarized in **Figure 5F**. Altogether, our results demonstrate that during T cell migration, a pool of actin corresponding to actomyosin displays an asymmetrical distribution. Surprisingly, this pool is mobile and sets the cell polarity: while it is restricted to the back of the cell upon migration, it is recruited at the lamellipodium upon cell rounding. We have shown that this redistribution is triggered by a rise in cAMP which starts at

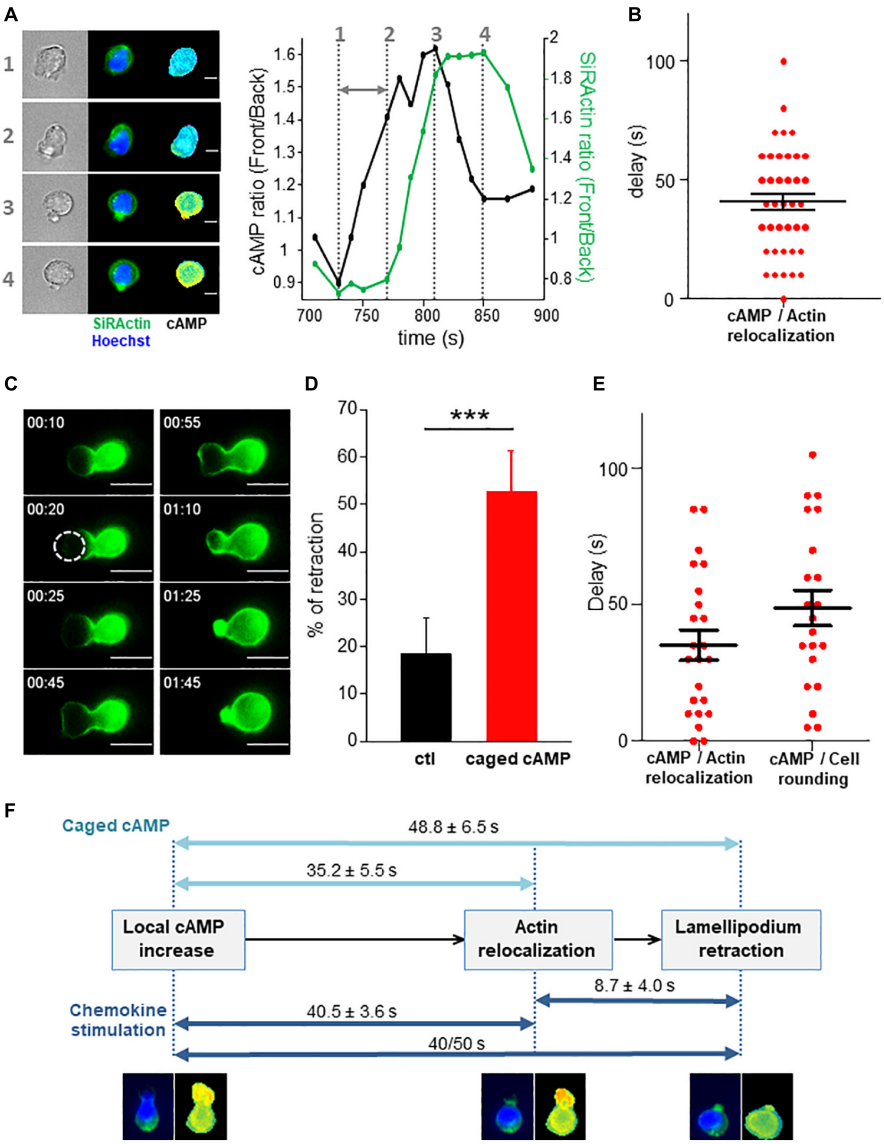

FIGURE 5 | cAMP increase drives stable actin relocalization. **(A)** Example of stable actin distribution recorded simultaneously with cAMP variations. The quantification of the two events is shown on the graph and the delay between the two is indicated by the gray arrow. The numbers show the times of the 4 steps. The complete series of images is shown in **Supplementary Movie 7**. Scale bar = 10 μm. **(B)** Delays between the beginning of cAMP increase and SiRActin relocalization measured as shown in (A). Values correspond to the mean ± SE of delays corresponding to 39 retraction events from 21 different cells. **(C)** Example of rounding up and actin relocalization induced by local release of cAMP after illumination at 405 nm. The cell was incubated previously with DMACM-caged 8-Br-cAMP and labeled with SiRActin. The size of the laser spot is indicated by the white circle. The complete series of images is shown in **Supplementary Movie 8**. Scale bar = 10 μm. **(D)** For each experiment, the frequency of lamellipodium retraction taking place within 2 min after illumination was quantified in cells pre-incubated with DMSO (ctl) or caged cAMP. Values correspond to the mean of nine independent experiments (6–21 cells/experiments). ***$p < 0.001$ paired *t*-test. **(E)** The delay between cAMP release and stable actin relocalization or increase of the roundness value was measured. For each cell, relocalization of SiRActin was measured over time as well as the roundness. The delay corresponds to the moment at which the values start to increase. Values correspond to the mean ± SE of 23 cells for actin relocalization and 21 for the roundness. **(F)** Summary of the three sequential steps leading to cell rounding: local increase in cAMP, recruitment of stable actin at the cell front cell, retraction of the lamellipodium leading to the rounding up of the cells. The delays measured in the different experiments are indicated. Dark blue: observation of migrating cells, light blue: artificial increase of cAMP induced by local photo-release of caged-cAMP.

the cell front before invading the whole cell. Interestingly, the cAMP-induced lamellipodium retraction is followed by the repolarization of the cells in another direction with a mean angle of about 110° and therefore promotes the exploratory behavior of the cells.

We may wonder what triggers cAMP bursts observed during T cell migration. The cells displaying repetitive elongation/retraction cycles as observed in some of our experiments might be a good model to address this issue. cAMP oscillations indicate that cells are able to synthetize and

degrade cAMP at high frequency (2.5 min). Surprisingly, the oscillation period is very similar from cell to cell, which suggests a universal cell-intrinsic cross-talk between adenylate cyclases and phosphodiesterases, the enzymes which, respectively, synthetize and degrade cAMP. One interesting possibility would be that cell deformation by itself, i.e., membrane stretching, could be the driving force of cAMP bursts. Indeed, the increase in membrane tension generated during migration (Pontes et al., 2017), might drive a cAMP increase, as suggested in other systems (Alenghat et al., 2009; McKenzie et al., 2020). In this context, the cAMP-induced recruitment of actomyosin would reduce this stretch by retracting the lamellipodium, and therefore inhibit the synthesis of cAMP. In parallel, cAMP increase *via* protein kinase A, one of the main targets of cAMP (Torres-Quesada et al., 2017), could activate phosphodiesterases (Gancedo, 2013) [such as PDE4 highly expressed in T cells (Sheth et al., 1997)] thus accelerating the cAMP decrease.

The link between cAMP and local recruitment of stable actin is another puzzling observation. As summarized in **Figure 5F**, a 40–50 s delay is necessary for stable actin to increase at the front after cAMP rise, suggesting that the link between the two events involves a multi-step signaling cascade which might involve PKA. Furthermore, upon lamellipodium retraction, we have observed a restricted zone of stable actin accumulation although the cAMP increase finally invades the whole cell. This suggests that a signal is generated very locally after cAMP increases. An interesting possibility would be the involvement of A Kinase anchoring proteins (AKAP), a family of proteins which would be able to convert the diffusible signal brought by cAMP into spatially restricted PKA activity (Dema et al., 2015).

Finally, the local recruitment of actomyosin at the lamellipodium results in its retraction within few seconds. Upon neutrophil migration, local increases in cAMP observed at the back of the cell have been reported to induce uropod retraction due to the regulation of non-muscle myosin IIA activity by PKA (Liu et al., 2010). Therefore, while cAMP promotes cell migration in neutrophils, it promotes exploratory behavior in T cells. Indeed, the local increase in cAMP is observed at the T cell front and promotes lamellipodium retraction (and then a change of trajectory) rather than at neutrophil back to promote uropod retraction (and therefore favoring migration). Furthermore, in T cells, retraction is due to cAMP-induced actomyosin relocalization rather than an increase in actomyosin activity as observed in neutrophils.

cAMP is generally considered as a messenger which dampens immune responses (Mosenden and Tasken, 2011). However, this statement must be qualified according to the characteristics of the cAMP increase. Indeed, for T cell activation, although high and sustained cAMP rises have been reported to inhibit TCR signaling such as calcium increase, lck activation or IL2 production (Henney and Lichtenstein, 1971; Tamir et al., 1996; Vang et al., 2001; Hermann-Kleiter et al., 2006; Daher et al., 2019), we have previously shown that T cell adhesion to antigen-presenting cells triggers a transient increase in cAMP which lowers the antigen detection threshold and therefore favors T cell responses (Conche et al., 2009). Concerning migration, similarly, high and sustained cAMP rises triggered by pharmacological drugs, PGE2 or β-adrenergic receptors stimulation, are known to inhibit T cell motility (Valitutti et al., 1993; Oppenheimer-Marks et al., 1994; Layseca-Espinosa et al., 2003; Dong et al., 2006). However, our present study highlights on the contrary that transient bursts in cAMP, by remodeling the actin cytoskeleton, might favor the exploratory behavior of T cells, a crucial step to mounting an efficient immune response. It might therefore be important to revisit the immunosuppressive effect of cAMP. Indeed, spatiotemporal and intensity control of cAMP signal is crucial for T cell properties: although sustained rise of cAMP may be inhibitory, transient increase of this messenger may, conversely, favor T cell responses.

DATA AVAILABILITY STATEMENT

The original contributions presented in the study are included in the article/**Supplementary Material**, further inquiries can be directed to the corresponding author/s.

AUTHOR CONTRIBUTIONS

MS, FR, ST, AF, RT, MF, AB, VF, JD, and CR performed experiments and analyzed data. ML helped with the experimental design of Traction Force Microscopy experiments. AF wrote R code for gel rigidity measurements. MS, JD, and CR designed experiments and wrote the manuscript. All authors contributed to the article and approved the submitted version.

FUNDING

This work was supported by Cochin Institute (PIC Program), Association pour la Recherche contre le Cancer (PJA 20131200379), CNRS, INSERM and Université de Paris. MS was supported by the Ministère de l'Enseignement Supérieur et de la Recherche.

ACKNOWLEDGMENTS

We thank G. Bismuth for helpful discussions and comments on the manuscript, Anna Mularski for helpful advice on Traction Force Microscopy, J. L. Martiel and Q. Tseng for ImageJ plugins for Traction Force Microscopy and advice, K. Jalink for TEpacVV construct, P. Saez for MyH9 construct, A. Benmerah for LifeAct construct, and the IMAG'IC facility for technical advice on local uncaging.

SUPPLEMENTARY MATERIAL

The Supplementary Material for this article can be found online at: https://www.frontiersin.org/articles/10.3389/fcell.2021.633099/full#supplementary-material

REFERENCES

Alenghat, F. J., Tytell, J. D., Thodeti, C. K., Derrien, A., and Ingber, D. E. (2009). Mechanical control of cAMP signaling through integrins is mediated by the heterotrimeric Galphas protein. *J. Cell. Biochem.* 106, 529–538. doi: 10.1002/jcb.22001

Chugh, P., and Paluch, E. K. (2018). The actin cortex at a glance. *J. Cell Sci.* 131:jcs186254. doi: 10.1242/jcs.186254

Conche, C., Boulla, G., Trautmann, A., and Randriamampita, C. (2009). T cell adhesion primes antigen receptor-induced calcium responses through a transient rise in adenosine 3',5'-cyclic monophosphate. *Immunity* 30, 33–43. doi: 10.1016/j.immuni.2008.10.020

Daher, C., Vimeux, L., Stoeva, R., Peranzoni, E., Bismuth, G., Wieduwild, E., et al. (2019). Blockade of beta-adrenergic receptors improves CD8(+) T-cell priming and cancer vaccine efficacy. *Cancer Immunol. Res.* 7, 1849–1863. doi: 10.1158/2326-6066.CIR-18-0833

Dema, A., Perets, E., Schulz, M. S., Deak, V. A., and Klussmann, E. (2015). Pharmacological targeting of AKAP-directed compartmentalized cAMP signalling. *Cell. Signal.* 27, 2474–2487. doi: 10.1016/j.cellsig.2015.09.008

Dong, H., Osmanova, V., Epstein, P. M., and Brocke, S. (2006). Phosphodiesterase 8 (PDE8) regulates chemotaxis of activated lymphocytes. *Biochem. Biophys. Res. Commun.* 345, 713–719. doi: 10.1016/j.bbrc.2006.04.143

Dong, T. X., Othy, S., Greenberg, M. L., Jairaman, A., Akunwafo, C., Leverrier, S., et al. (2017). Intermittent Ca(2+) signals mediated by Orai1 regulate basal T cell motility. *eLife* 6:e27827. doi: 10.7554/eLife.27827

Donnadieu, E., Bismuth, G., and Trautmann, A. (1994). Antigen recognition by helper T cells elicits a sequence of distinct changes of their shape and intracellular calcium. *Curr. Biol.* 4, 584–595. doi: 10.1016/s0960-9822(00)00130-5

Dupré, L., Houmadi, R., Tang, C., and Rey-Barroso, J. (2015). T Lymphocyte migration: an action movie starring the actin and associated actors. *Front. Immunol.* 6:586. doi: 10.3389/fimmu.2015.00586

Gancedo, J. M. (2013). Biological roles of cAMP: variations on a theme in the different kingdoms of life. *Biol. Rev. Camb. Philos. Soc.* 88, 645–668. doi: 10.1111/brv.12020

Gross, W., and Kress, H. (2017). Simultaneous measurement of the Young's modulus and the Poisson ratio of thin elastic layers. *Soft Matter* 13, 1048–1055. doi: 10.1039/c6sm02470j

Henney, C. S., and Lichtenstein, L. M. (1971). The role of cyclic AMP in the cytolytic activity of lymphocytes. *J. Immunol.* 107, 610–612.

Hermann-Kleiter, N., Thuille, N., Pfeifhofer, C., Gruber, T., Schafer, M., Zitt, C., et al. (2006). PKCtheta and PKA are antagonistic partners in the NF-AT transactivation pathway of primary mouse CD3+ T lymphocytes. *Blood* 107, 4841–4848. doi: 10.1182/blood-2005-10-4044

Howe, A. K. (2004). Regulation of actin-based cell migration by cAMP/PKA. *Biochim. Biophys. Acta* 1692, 159–174. doi: 10.1016/j.bbamcr.2004.03.005

Howe, A. K., Baldor, L. C., and Hogan, B. P. (2005). Spatial regulation of the cAMP-dependent protein kinase during chemotactic cell migration. *Proc. Natl. Acad. Sci. U.S.A.* 102, 14320–14325. doi: 10.1073/pnas.0507072102

Hynd, M. R., Frampton, J. P., Burnham, M. R., Martin, D. L., Dowell-Mesfin, N. M., Turner, J. N., et al. (2007). Functionalized hydrogel surfaces for the patterning of multiple biomolecules. *J. Biomed. Mater. Res. A* 81, 347–354. doi: 10.1002/jbm.a.31002

Jacobelli, J., Chmura, S. A., Buxton, D. B., Davis, M. M., and Krummel, M. F. (2004). A single class II myosin modulates T cell motility and stopping, but not synapse formation. *Nat. Immunol.* 5, 531–538. doi: 10.1038/ni1065

Jannat, R. A., Dembo, M., and Hammer, D. A. (2011). Traction forces of neutrophils migrating on compliant substrates. *Biophys. J.* 101, 575–584. doi: 10.1016/j.bpj.2011.05.040

Klarenbeek, J., Goedhart, J., van Batenburg, A., Groenewald, D., and Jalink, K. (2015). Fourth-generation epac-based FRET sensors for cAMP feature exceptional brightness, photostability and dynamic range: characterization of dedicated sensors for FLIM, for ratiometry and with high affinity. *PLoS One* 10:e0122513. doi: 10.1371/journal.pone.0122513

Klarenbeek, J. B., Goedhart, J., Hink, M. A., Gadella, T. W., and Jalink, K. (2011). A mTurquoise-based cAMP sensor for both FLIM and ratiometric read-out has improved dynamic range. *PLoS One* 6:e19170. doi: 10.1371/journal.pone.0019170

Krummel, M. F., Bartumeus, F., and Gerard, A. (2016). T cell migration, search strategies and mechanisms. *Nat. Rev. Immunol.* 16, 193–201. doi: 10.1038/nri.2015.16

Layseca-Espinosa, E., Baranda, L., Alvarado-Sanchez, B., Portales-Perez, D., Portillo-Salazar, H., and Gonzalez-Amaro, R. (2003). Rolipram inhibits polarization and migration of human T lymphocytes. *J. Invest. Dermatol.* 121, 81–87. doi: 10.1046/j.1523-1747.2003.12301.x

Lim, C. J., Kain, K. H., Tkachenko, E., Goldfinger, L. E., Gutierrez, E., Allen, M. D., et al. (2008). Integrin-mediated protein kinase A activation at the leading edge of migrating cells. *Mol. Biol. Cell* 19, 4930–4941. doi: 10.1091/mbc.e08-06-0564

Liu, L., Das, S., Losert, W., and Parent, C. A. (2010). mTORC2 regulates neutrophil chemotaxis in a cAMP- and RhoA-dependent fashion. *Dev. Cell* 19, 845–857. doi: 10.1016/j.devcel.2010.11.004

Lukinavicius, G., Reymond, L., D'Este, E., Masharina, A., Gottfert, F., Ta, H., et al. (2014). Fluorogenic probes for live-cell imaging of the cytoskeleton. *Nat. Methods* 11, 731–733. doi: 10.1038/nmeth.2972

Martiel, J. L., Leal, A., Kurzawa, L., Balland, M., Wang, I., Vignaud, T., et al. (2015). Measurement of cell traction forces with ImageJ. *Methods Cell Biol.* 125, 269–287. doi: 10.1016/bs.mcb.2014.10.008

McKenzie, A. J., Svec, K. V., Williams, T. F., and Howe, A. K. (2020). Protein kinase A activity is regulated by actomyosin contractility during cell migration and is required for durotaxis. *Mol. Biol. Cell* 31, 45–58. doi: 10.1091/mbc.E19-03-0131

Melak, M., Plessner, M., and Grosse, R. (2017). Actin visualization at a glance. *J. Cell Sci.* 130, 525–530. doi: 10.1242/jcs.189068

Milroy, L. G., Rizzo, S., Calderon, A., Ellinger, B., Erdmann, S., Mondry, J., et al. (2012). Selective chemical imaging of static actin in live cells. *J. Am. Chem. Soc.* 134, 8480–8486. doi: 10.1021/ja211708z

Moreau, H. D., Piel, M., Voituriez, R., and Lennon-Dumenil, A. M. (2018). Integrating physical and molecular insights on immune cell migration. *Trends Immunol.* 39, 632–643. doi: 10.1016/j.it.2018.04.007

Mosenden, R., and Tasken, K. (2011). Cyclic AMP-mediated immune regulation–overview of mechanisms of action in T cells. *Cell. Signal.* 23, 1009–1016. doi: 10.1016/j.cellsig.2010.11.018

Nerger, B. A., Siedlik, M. J., and Nelson, C. M. (2017). Microfabricated tissues for investigating traction forces involved in cell migration and tissue morphogenesis. *Cell. Mol. Life. Sci.* 74, 1819–1834. doi: 10.1007/s00018-016-2439-z

Oppenheimer-Marks, N., Kavanaugh, A. F., and Lipsky, P. E. (1994). Inhibition of the transendothelial migration of human T lymphocytes by prostaglandin E2. *J. Immunol.* 152, 5703–5713.

Pontes, B., Monzo, P., Gole, L., Le, A., Roux, L., Kosmalska, A. J., et al. (2017). Membrane tension controls adhesion positioning at the leading edge of cells. *J. Cell Biol.* 216, 2959–2977. doi: 10.1083/jcb.201611117

Real, E., Faure, S., Donnadieu, E., and Delon, J. (2007). Cutting edge: atypical PKCs regulate T lymphocyte polarity and scanning behavior. *J. Immunol.* 179, 5649–5652. doi: 10.4049/jimmunol.179.9.5649

Real, E., Kaiser, A., Raposo, G., Amara, A., Nardin, A., Trautmann, A., et al. (2004). Immature dendritic cells (DCs) use chemokines and intercellular adhesion molecule (ICAM)-1, but not DC-specific ICAM-3-grabbing nonintegrin, to stimulate CD4+ T cells in the absence of exogenous antigen. *J. Immunol.* 173, 50–60. doi: 10.4049/jimmunol.173.1.50

Saitakis, M., Dogniaux, S., Goudot, C., Bufi, N., Asnacios, S., Maurin, M., et al. (2017). Different TCR-induced T lymphocyte responses are potentiated by stiffness with variable sensitivity. *eLife* 6:e23190. doi: 10.7554/eLife.23190

Sheth, S. B., Chaganti, K., Bastepe, M., Ajuria, J., Brennan, K., Biradavolu, R., et al. (1997). Cyclic AMP phosphodiesterases in human lymphocytes. *Br. J. Haematol.* 99, 784–789. doi: 10.1046/j.1365-2141.1997.4803282.x

Tamir, A., Granot, Y., and Isakov, N. (1996). Inhibition of T lymphocyte activation by cAMP is associated with down-regulation of two parallel mitogen-activated protein kinase pathways, the extracellular signal-related kinase and c-Jun N-terminal kinase. *J. Immunol.* 157, 1514–1522.

Torres-Quesada, O., Mayrhofer, J. E., and Stefan, E. (2017). The many faces of compartmentalized PKA signalosomes. *Cell. Signal.* 37, 1–11. doi: 10.1016/j.cellsig.2017.05.012

Trappmann, B., Gautrot, J. E., Connelly, J. T., Strange, D. G., Li, Y., Oyen, M. L., et al. (2012). Extracellular-matrix tethering regulates stem-cell fate. *Nat. Mater.* 11, 642–649. doi: 10.1038/nmat3339

Valitutti, S., Dessing, M., and Lanzavecchia, A. (1993). Role of cAMP in regulating cytotoxic T lymphocyte adhesion and motility. *Eur. J. Immunol.* 23, 790–795. doi: 10.1002/eji.1830230403

Vang, T., Torgersen, K. M., Sundvold, V., Saxena, M., Levy, F. O., Skalhegg, B. S., et al. (2001). Activation of the COOH-terminal Src kinase (Csk) by cAMP-dependent protein kinase inhibits signaling through the T cell receptor. *J. Exp. Med.* 193, 497–507. doi: 10.1084/jem.193.4.497

Conflict of Interest: The authors declare that the research was conducted in the absence of any commercial or financial relationships that could be construed as a potential conflict of interest.

frontiers in Cell and Developmental Biology

MINI REVIEW
published: 08 June 2021
doi: 10.3389/fcell.2021.674572

Wiskott-Aldrich Syndrome Protein: Roles in Signal Transduction in T Cells

Jatuporn Ngoenkam[1], Pussadee Paensuwan[2], Piyamaporn Wipa[1], Wolfgang W. A. Schamel[3,4,5] and Sutatip Pongcharoen[6]**

[1] Department of Microbiology and Parasitology, Faculty of Medical Science, Naresuan University, Phitsanulok, Thailand, [2] Department of Optometry, Faculty of Allied Health Sciences, Naresuan University, Phitsanulok, Thailand, [3] Signalling Research Centers BIOSS and CIBSS, University of Freiburg, Freiburg, Germany, [4] Department of Immunology, Faculty of Biology, University of Freiburg, Freiburg, Germany, [5] Centre for Chronic Immunodeficiency (CCI), Freiburg University Clinics, University of Freiburg, Freiburg, Germany, [6] Department of Medicine, Faculty of Medicine, Naresuan University, Phitsanulok, Thailand

OPEN ACCESS

Edited by:
Esta Sterneck,
Center for Cancer Research, National Cancer Institute (NCI), Frederick, United States

Reviewed by:
Chaohong Liu,
Huazhong University of Science and Technology, China
Roberto Chiarle,
University of Turin, Italy

***Correspondence:**
Jatuporn Ngoenkam
jatupornn@nu.ac.th
Sutatip Pongcharoen
sutatipp@nu.ac.th

Specialty section:
This article was submitted to Cell Growth and Division, a section of the journal Frontiers in Cell and Developmental Biology

Received: 01 March 2021
Accepted: 17 May 2021
Published: 08 June 2021

Citation:
Ngoenkam J, Paensuwan P, Wipa P, Schamel WWA and Pongcharoen S (2021) Wiskott-Aldrich Syndrome Protein: Roles in Signal Transduction in T Cells. Front. Cell Dev. Biol. 9:674572. doi: 10.3389/fcell.2021.674572

Signal transduction regulates the proper function of T cells in an immune response. Upon binding to its specific ligand associated with major histocompatibility complex (MHC) molecules on an antigen presenting cell, the T cell receptor (TCR) initiates intracellular signaling that leads to extensive actin polymerization. Wiskott-Aldrich syndrome protein (WASp) is one of the actin nucleation factors that is recruited to TCR microclusters, where it is activated and regulates actin network formation. Here we highlight the research that has focused on WASp-deficient T cells from both human and mice in TCR-mediated signal transduction. We discuss the role of WASp in proximal TCR signaling as well as in the Ras/Rac-MAPK (mitogen-activated protein kinase), PKC (protein kinase C) and Ca^{2+}-mediated signaling pathways.

Keywords: WASp, T cell signaling, T cell activation, MAPK, PKC, calcium

INTRODUCTION

Wiskott-Aldrich syndrome (WAS) is a severe X-linked primary immunodeficiency caused by the mutations of the *WAS* gene on the X-chromosome. WAS is characterized by thrombocytopenia, eczema, increased susceptibility to infection and increased risk to develop autoimmune disease (Gallego et al., 1997; Bosticardo et al., 2009; Massaad et al., 2013). The *WAS* gene encodes the Wiskott-Aldrich syndrome protein (WASp), which is of the actin nucleation-promoting factor family. WASp is a cytosolic protein comprising 502 amino acids lacking intrinsic catalytic activity. Instead, WASp acts as scaffold protein that transduces a wide range of signals from cell surface receptors to mediate dynamic changes in the actin cytoskeleton in response to external stimuli (Sun et al., 2019). WASp is expressed exclusively in the hematopoietic cell lineages including T cells, B cells, natural killer (NK) cells, dendritic cells, macrophages, and platelets (Matalon et al., 2013). T cells isolated from WAS patient have a defect in actin reorganization in response to TCR-mediated stimulation (Gallego et al., 1997; Matalon et al., 2013). Furthermore, WASp has an essential role in signal transduction and effector functions of T cells.

Wiskott-Aldrich syndrome protein belongs to the WASp family of proteins consisting of WASp, neuronal (N)-WASp, and WAVE 1–3 and WASp and SCAR homolog (WASH) (Linardopoulou et al., 2007). Although, WASp and N-WASp share more than 50% sequence homology as well as

having similar protein binding partners and basic functions, these two proteins are not entirely redundant (Fried et al., 2014). In contrast to WASp, N-WASp is widely expressed in multiple tissues (Miki et al., 1996).

In this article, we review recent findings of WASp in TCR-mediated signal transduction. Since the adaptor protein non-catalytic region of tyrosine kinase (Nck) binds to WASp, we discuss the mechanisms of Nck-mediated WASp recruitment to the TCR whereby it may regulate the actin machinery and signal transduction in close proximity to the TCR.

WASp STRUCTURE AND ITS CHANGE DURING T CELL ACTIVATION

From the N- to the C-terminus, WASp contains a WASp homology 1 (WH1) domain (also known as EVH1, for ENA/VASP homology), a basic (B) domain, a GTPase-binding domain (GBD), a proline-rich domain (PRD), and a verprolin homology (V), cofilin (C) homology, and acidic region (A) (VCA domain) at the C-terminus (Zhang et al., 2009; **Figure 1A**). These distinct domains are required to mediate downstream signaling by binding to different cytoskeleton-regulating protein partners. More than 20 protein binding partners have been reported (Thrasher and Burns, 2010). Although, the structures of the WASp family members vary, the VCA domain is particularly conserved. The VCA domain interacts with actin and Arp2/3, whereas the PRD domain binds to various SH3 domain-containing proteins.

The first N-terminal WH1 domain is a binding site for a proline repeat motif present in the WASp interacting protein (WIP) (Volkman et al., 2002). WASp is constitutively associated with WIP. WIP regulates WASp activity and promotes WASp stability in resting T cell by protecting WASp from degradation by calpain and proteasome. It is also critical for localizing WASp to areas of actin polymerization (Chou et al., 2006; de la Fuente et al., 2007). In addition, the WH1 domain may act as a binding site for the Src family kinase Fyn and Lck in T cells (Sato et al., 2011; Matalon et al., 2013). Following the WH1 domain, the B domain is involved in the regulation of the WASp conformation, as it can bind the phosphoinositide PIP2 (phosphatidylinositol-4,5-bisphosphate) and acts in couple with the small GTPase Cdc42 to release of WASp from its auto-inhibited conformation toward the active conformation (Higgs and Pollard, 2000; Thrasher and Burns, 2010). The GBD domain can interact in *cis* with the C-terminal VCA domain, thereby inducing the closed autoinhibitory conformation (**Figure 1B**; Kim et al., 2000). Upon activation, the VCA domain is released from GBD as a consequence of the binding of GTP-bound Cdc42 to the WASp GBD. The PRD serves as the docking site for multiple protein binding partners that contain an SH3 domain such as Src and Tec family tyrosine kinases (Bunnell et al., 1996; Torres and Rosen, 2006) and the adaptor protein Nck (Rivera et al., 2004; Barda-Saad et al., 2005). Finally, after TCR engagement and the recruitment of GTP-bound Cdc42 to the WASp GBD, the released VCA region can interact with both monomeric actin (through the V region) and with the actin-related protein complex Arp2/3 (through the CA region) that work together to stimulate nucleation of branched actin filaments (**Figure 1B**; Symons et al., 1996; Miki and Takenawa, 1998; Blanchoin et al., 2000; Krause et al., 2000).

In resting T cells, WASp is mainly present in an autoinhibited conformation in the cytoplasm, in which the VCA domain interacts with a hydrophobic patch located within the GBD (**Figure 1B**). Upon TCR-mediated signaling, the kinase Zeta-associated protein of 70 kDa (ZAP-70) is recruited to the TCR and activated. Subsequently, it phosphorylates the adaptor protein Src homology 2 (SH2) domain-containing leukocyte protein of 76 kDa (SLP-76) that has a binding site for Nck and the guanine nucleotide exchange factor Vav-1. Nck is constitutively associated with WASp *via* the C-terminal SH3 domain of Nck binding to the PRD of WASp (Rivero-Lezcano et al., 1995; Paensuwan et al., 2015). Thus, Nck acts as a bridge to recruit WASp to the SLP-76 signaling complex. In association with SLP-76, Vav-1 mediates the exchange of GDP- to GTP-bound Cdc42, Rho family GTPases. GTP-bound Cdc42 then interacts with the WASp GBD, thereby releasing WASp from its auto-inhibited conformation, allowing VCA to bind to the Arp2/3 complex. Once bound to the VCA domain, Arp2/3 promotes the branching of the actin polymerization and rearrangement at the T cell-APC contact site (Zeng et al., 2003; Matalon et al., 2013). In addition, tyrosine 291 within WASp GBD can be phosphorylated by the Src family kinases Fyn and Lck (Badour et al., 2004; Torres and Rosen, 2006), which interact with the WASp WH1 domain (Sato et al., 2011). Phosphorylation of tyrosine 291 is essential for WASp activation (Cory et al., 2002; Badour et al., 2004). Thus, besides the recruitment of Cdc42 to WASp, WASp activation can be indicated by tyrosine 291 phosphorylation. Interestingly, phosphorylation of Y291 within WASp GBD domain also mediates WASp degradation by calpain and proteasome proteolysis (Watanabe et al., 2013; Sun et al., 2019).

INITIATION AND FOLLOWING PATHWAYS OF TCR SIGNALING

Following TCR engagement by its ligand peptide-MHC (pMHC), the TCR and its signaling molecules rapidly form microclusters where signaling is amplified and sustained (Seminario and Bunnell, 2008; Choudhuri and Dustin, 2010). The TCR is composed of the pMHC-binding TCRαβ heterodimer non-covalently associated with the non-variable signal transduction subunits CD3εγ, CD3εδ, and CD3ζζ (Kane et al., 2000; Alarcón et al., 2003). The TCRα and TCRβ chains have short cytoplasmic tails with no intrinsic capacity to mediate signal transduction. In contrast, the CD3 molecules serve as signal transducers by transferring information of TCR pMHC-binding to initiate signaling transduction (Hayes et al., 2003; Schamel et al., 2019). Each of the CD3 signaling subunits has cytoplasmic immunoreceptor tyrosine-based activation motifs (ITAMs) (Reth, 1989), one present in CD3ε, CD3δ, and CD3γ and three in CD3ζ. In addition, CD3ε has a proline-rich sequence

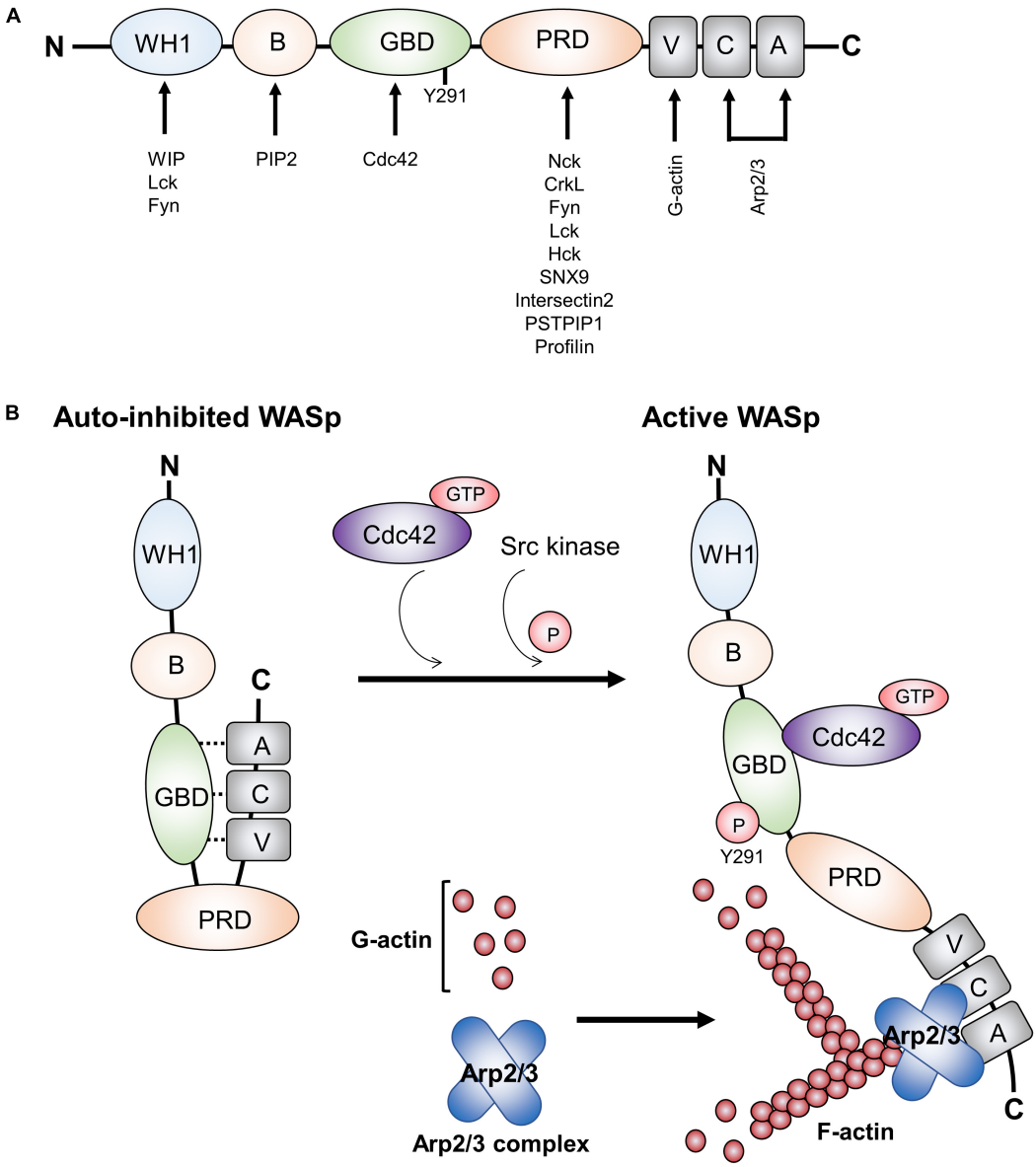

FIGURE 1 | Functional domains in WASp and WASp activation. **(A)** WASp contains various domains, which can bind proteins involved in TCR-mediated actin cytoskeleton remodeling and signal transduction. **(B)** WASp is in a closed auto-inhibited conformation in resting state due to its intracellular interaction between GBD and VCA domains. Upon TCR engagement, it mediates the binding of GTP-Cdc42 to the GBD domain, thereby releasing the VCA domain from GBD domain and changing the WASp structure into an opened conformation. In addition, WASp tyrosine 291 within GBD can be phosphorylated by the Src family kinases Fyn and Lck. Recruitment of GTP-Cdc42 to GBD and phosphorylation of WASp tyrosine 291 within GBD result in WASp activation. Subsequently, Arp2/3 and monomeric actin can bind the VCA domain, which induces a new actin branch. This figure was modified from Matalon et al. (2013). Wiskott-Aldrich syndrome protein–dynamic regulation of actin homeostasis: from activation through function and signal termination in T lymphocytes. Immunol. Rev. 256(1), 10–29; with a permission from John Wiley and Sons; license number 5065241058992.

(PRS) (Gil et al., 2002) and the receptor kinase (RK) motif (Hartl et al., 2020), which are required to regulate TCR activation. We will describe these two significant motifs in the next section.

T cell receptor engagement results in phosphorylation on tyrosine residues within the ITAMs, creating pairs of phosphotyrosines, which serve as docking sites for proteins containing SH2 domains such as ZAP-70. Following the binding of ZAP-70 to ITAMs, ZAP-70 phosphorylates LAT (linker for activation of T cells). Phosphorylated LAT recruits various enzymes and adaptor proteins to form multi-protein signaling complexes (Zhang et al., 1998). Recently, the formins mDia1 and mDia3 play a crucial role in F-actin polymerization, which facilitate LAT phosphorylation by ZAP-70 (Thumkeo et al., 2020). Phosphorylated LAT can bind to phospholipase Cγ1 (PLCγ1), phosphoinositide 3-kinase (PI3K), growth factor receptor-bound protein 2 (Grb2) and GRB2-related adaptor

downstream of Shc (Gads). Gads serves as a bridge to recruit SLP-76 to phospho-LAT, where SLP-76 is phosphorylated by ZAP-70. As described above, WASp is recruited to SLP-76 through Nck, where WASp can associate and activate Arp2/3 to promote actin filament formation (Wunderlich et al., 1999; Barda-Saad et al., 2005).

After the signaling complexes have formed, they are required to activate four pathways: Ras/Rac-mitogen-activated protein kinase (MAPK), protein kinase C (PKC), nuclear factor of κB (NF-κB) and Ca^{2+}-mediated signaling pathways, such as the nuclear factor of activated T cells (NFAT) pathway. The Ras pathway activates the extracellular receptor-activated kinase (Erk), a member of the MAP kinase family. The activated Erk translocates to the nucleus and phosphorylates its substrate Elk1. Phospho-Elk1 then stimulates the transcription of c-Fos, a component of the transcription factor the activation protein 1 (AP-1). In parallel with the Ras pathway, Rac is activated by Vav-1, thereby generating Rac-GTP. The active Rac-GTP activates another MAP kinase called c-Jun *N*-terminal kinase (Jnk). Once activation, Jnk then phosphorylates c-Jun, the second component of AP-1 (Smith-Garvin et al., 2009; Conley et al., 2016).

PLCγ1 bound to phospho-LAT is phosphorylated by ZAP-70 and the Tec family kinase Itk. Phosphorylated PLCγ1 catalyzes the hydrolysis of the plasma membrane phospholipid PIP2 generating two breakdown products, membrane-bound diacylglycerol (DAG) and inositol 1,4,5-trisphosphate (IP3) (Rhee and Bae, 1997; Braiman et al., 2006). DAG leads to the activation of PKCθ, which then mediates the activation and nuclear translocation of NF-κB. IP3 stimulates the increase in intracellular Ca^{2+}, which subsequently activates the transcription factor NFAT to translocate to the nucleus. In the nucleus, the transcription factors AP-1, NF-κB and NFAT bind to promotors of specific genes (Smith-Garvin et al., 2009). In the next section, we discuss WASp's function in proximal TCR signaling.

WASp's Role in Proximal TCR Signaling

Assembly of WASp to SLP-76 signalosome upon TCR engagement is a key step for WASp to mediate the branching of the actin cytoskeleton polymerization (Wunderlich et al., 1999; Barda-Saad et al., 2005). Furthermore, two more pathways of WASp recruitment to distinct cellular compartments in the vicinity of TCR-CD3 have been reported and are the points to be discussed in this section.

Ligand-binding to the TCR leads to the stabilization of the active conformation of the TCR (Gil et al., 2002; Minguet et al., 2007; Lee et al., 2015), in which the PRS, the RK motif and the ITAMs become exposed (Swamy et al., 2016; Hartl et al., 2020). In the active conformation the CD3ε PRS binds to the N-terminal SH3 domain of Nck, thus recruiting Nck to the TCR (Gil et al., 2002). Our recent work has suggested a role of actin polymerization in controlling Nck recruitment to CD3ε PRS (Wipa et al., 2020), although the exact mechanism remains enigmatic. At the same time Lck is recruited to the RK motif and the ITAMs can be phosphorylated (Hartl et al., 2020). Phosphorylation of CD3ε at the second ITAM tyrosine stabilizes the Nck-CD3ε interaction, since the SH2 domain of Nck can bind to the phospho-tyrosine (Paensuwan et al., 2016). This leaves the C-terminal SH3 domain of Nck free to interact with WASp. It has been found that WASp is constitutively associated with both Nck isoforms, Nck1 and Nck2, and both isoforms can associate with CD3ε (Gil et al., 2002). Indeed, we found that WASp can be recruited to the TCR upon TCR stimulation (Paensuwan et al., 2015; **Figure 2**), and this might be mediated by Nck. Thus, it was postulated that the direct recruitment of WASp to TCR-CD3 may also bring the effector molecules to TCR-CD3 that are essential for controlling the actin reorganization and signal transduction (Ngoenkam et al., 2018; **Figure 2**). Among these, GTP-Cdc42 has been found to be recruited to the T cell:APC contact site, where TCR, WASp and Vav-1 are accumulated (Cannon et al., 2001; Yokosuka and Saito, 2010). Localization of these proteins at the T cell:APC contact site supports the hypothesis of molecular machinery driven the actin polymerization at TCR. Further, recruitment of WASp to the TCR was relied on both the CD3 conformational change and partial CD3ε tyrosine phosphorylation (Paensuwan et al., 2015). This finding is coincident with the pattern of Nck recruitment to CD3ε following TCR triggering. This strengthens the possibility of Nck to mediate the recruitment of WASp to CD3ε. Further work is needed to assess the relative contributions of TCR-recruited WASp in regulating T cell activation. This finding may reveal the additional function of WASp besides its role in regulating actin polymerization such as controlling signal transduction in close proximity to the TCR.

Since WASp also binds to Lck (Matalon et al., 2013) recruitment of WASp to the TCR might help in phosphorylating the TCR. However, in WASp-deficient T cells phosphorylation of CD3ζ and ZAP-70 and total tyrosine proteins was undisturbed (Zhang et al., 1999), arguing against an important role of WASp in CD3 phosphorylation. It has been found in resting T cells that WASp is complexed with WIP (Ramesh et al., 1997), which directly interacts with the adaptor protein CrkL [CT10 regulator of kinase (Crk)-like] to form a CrkL-WIP-WASP complex. Following TCR ligation, CrkL, WIP and WASP were co-precipitated with ZAP-70 (Sasahara et al., 2002). Thus, a CrkL-WIP-WASP complex is recruited to ZAP-70 in response to TCR engagement to generate a ZAP-70-CrkL-WIP-WASp complex (Sasahara et al., 2002). Recruitment of this complex to the IS is mediated by the association of the CrkL SH2 domain to a phospho-tyrosine within interdomain B region of ZAP-70 (Chan et al., 1992). PKCθ then phosphorylates WIP thereby releasing WASp from WIP-mediated inhibition and then WASp is activated by membrane bound Cdc42 resulting in actin polymerization (Sasahara et al., 2002). Thus, besides *via* a SLP-76/Nck and a TCR/Nck complex, an alternative pathway of WASp recruitment to the IS is mediated by ZAP-70.

WASp's Role in the Ras/Rac-MAPK Pathway

In mammalian cells, there are three major members of MAPKs including Erk (Schaeffer and Weber, 1999), the p38 (Han and Ulevitch, 1999), and Jnk (Davis, 2000). Erk can be activated by Ras, while p38 and Jnk are activated by Rho family GTPases, including Rac and Cdc42 (Rincón et al., 2001). The nuclear target

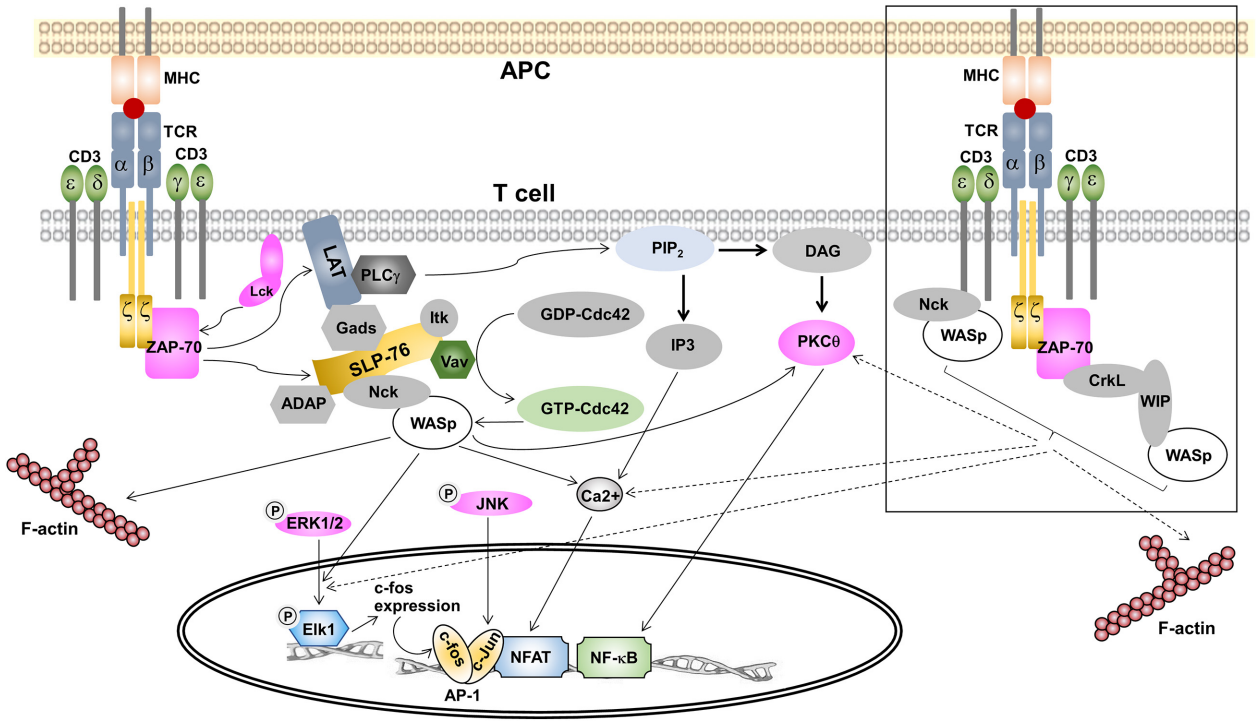

FIGURE 2 | The role of WASp in signal transduction in T cells. TCR ligation with pMHC triggers signal transduction within the cytoplasm of T cells. Once phosphorylated by ZAP-70, phospho-LAT recruits proteins to form the LAT/SLP-76 signalosome containing Nck and Vav. Vav activates the Rho GTPase Cdc42, which in turn interacts with WASp. This complex is recruited to the signalosome *via* Nck. In association with GTP-Cdc42, WASp is released from the auto-inhibited conformation and then initiates the ARP2/3-dependent F-actin polymerization. In Ras/Rac-MAPK pathway, WASp is essential for the translocation of phospho-Erk1/2 into the nucleus. Once in the nucleus, phospho-Erk1/2 phosphorylates Elk1, which then causes c-fos expression, a component of transcription factor AP-1. WASp was not required for the activation of Jnk, a kinase causing c-jun expression that is the second component of AP-1. In the PKC pathway, WASp contributes to PKCθ activation in response to low doses of antigen. Activated PKCθ is required for activation of transcription factor NF-κB and its nuclear translocation. For Ca^{2+}-mediated signaling, WASp is indispensable for intracellular Ca^{2+} mobilization, which is essential for NFAT translocation to the nucleus. In the squared box, two alternative pathways of WASp recruitment to TCR are shown. Firstly, WASp is constitutively associated with Nck and Nck-WASp is recruited to the TCR upon TCR ligation. Secondly, preformed CrkL-WIP-WASp is recruited to ZAP-70 following T cell activation. We propose that these two recent identified pools of WASp play a role in controlling actin polymerization and may contribute to the nuclear translocation of phospho-Erk1/2, PKCθ-mediated NF-κB activation and Ca^{2+} influx.

of these three MAP kinase members is the activation of the transcription factor AP-1.

T cells isolated from both WAS patient and WASp deficient (−/−) mice were unable to secrete IL-2 in response to TCR stimulation (Molina et al., 1993; Zhang et al., 1999; Cannon and Burkhardt, 2004). This impairment was not associated with TCR-proximal signaling since tyrosine phosphorylation of CD3ζ, ZAP-70, and total cellular protein detected in TCR-stimulated *WAS*$^{-/-}$ murine T cells were similar to those observed in the wild-type counterparts (Zhang et al., 1999). The IL-2 promotor is activated by the transcription factors NFAT, AP-1 and NF-κB. The activity of AP-1 and expression of c-Fos, but not c-Jun were markedly impaired in T cells from WASp$^{-/-}$ mice upon TCR stimulation (Cianferoni et al., 2005). Interestingly, upstream signaling proteins of AP-1 including Jnk, c-Jun, and Erk were normally phosphorylated. These results are consistent with previous studies showing that murine *WAS*$^{-/-}$ T cells exhibited normal phosphorylation of Erk and Jnk (Zhang et al., 1999). However, translocation of phosphorylated Erk into the nucleus and phosphorylation of its nuclear substrate, Elk1 were impaired. This phosphorylated nuclear Elk is responsible for activation of c-Fos, a component of the transcription factor AP-1 (Cianferoni et al., 2005). Thus, WASp is essential only for nuclear translocation of phospho-Erk, Elk1 phosphorylation and expression of c-Fos.

WASp's Role in PKC-Mediated Signaling

T cells express different PKC isoforms, including PKC-α, δ, ϵ, η, θ, and ζ (Brezar et al., 2015). PKCθ is the most studied isoform and is the first PKC family member that is recruited to the IS (Arendt et al., 2002). PKCθ plays a key role in a range of signaling cascades that ultimately leads to activation of downstream transcription factors NF-κB, NFAT, and AP-1 (Baier-Bitterlich et al., 1996; Sun et al., 2000; Pfeifhofer et al., 2003 Berg-Brown et al., 2004; Hayashi and Altman, 2007). In addition, PKCθ has been postulated to be involved TCR-induced actin polymerization through a process possibly mediated by WIP (Sasahara et al., 2002; Krzewski et al., 2006).

Once a ZAP-70-CrkL-WIP-WASp complex is formed at IS, PKCθ phosphorylates on WIP. This allows WASp to disengage from the WIP-WASp complex and to proceed its activation and function. As reported, PKCθ activation is dependent on Lck, Vav-1, ZAP-70, and SLP-76 (Sasahara et al., 2002). Thus, it has been proposed that the ZAP-70-CrkL-WIP pathway and PKCθ are the key players upstream of WASp activation (Sasahara et al., 2002). In keeping with this hypothesis, it was found that WASp-deficient T cells in response to antigen-specific APCs showed normal PKCθ polarization to the IS and stimulation of these cells with low doses of antigen caused diminished polarization of PKCθ (Cannon and Burkhardt, 2004), whereas activation with all peptide doses impaired IL-2 production in these cells. Thus, WASp is suggested to be the protein that can lower the threshold for organizing PKCθ at the IS. In addition, the roles of WASp on IS formation is proposed to be independent of its role in IL-2 production (Cannon and Burkhardt, 2004).

The data of WASp function in activation of NF-κB is scarce. However, it has been found that nuclear translocation and activity of NF-κB were normal in T cells from $WASp^{-/-}$ mice, whereas NFAT dephosphorylation and nuclear localization, nuclear AP-1 binding activity, and expression of c-Fos were all impaired (Cianferoni et al., 2005). Moreover, in the T helper 1 (Th1)-skewed cells, mutation of the VCA domain that is required for Arp2/3-dependent F-actin polymerization did not affect NF-κB-p65 nuclear translocation (Sadhukhan et al., 2014). Together, WASp is required for PKCθ activation in response to low doses of antigen, but WASp is not required NF-κB activation in T cells.

WASp's Role in Ca^{2+}-Mediated Signaling Pathways

T cell receptor engagement triggers the mobilization of Ca^{2+}, which is required for T cell activation, gene expression, motility, synapse formation, cytotoxicity, development, and differentiation (Feske, 2007). Once entered into the cells, Ca^{2+} activates calcineurin resulting in nuclear translocation of NFAT (Gwack et al., 2007). Peripheral lymphocytes exclusively express NFAT-1, NFAT-2, and NFAT-4 (Amasaki et al., 1998). T cells from WAS patients and WASp-deficient mice show defects in IL-2 production upon TCR-induced T cell activation. This was associated with a partial reduction in intracellular Ca^{2+} mobilization compared with wild-type cells, while phosphorylation of CD3ζ, ZAP-70, and Erk was normal (Zhang et al., 1999; Badour et al., 2004; Cannon and Burkhardt, 2004). WASp is required for the assembly of the IS structure, which is essential for optimal sustained calcium signaling (Calvez et al., 2011).

Consistent with mouse WASp-deficient T cells, $CD4^+$ and $CD8^+$ T cells from WAS patients secrete low levels of IL-2 as well as IFN-γ, and TNF-α in response to stimulation with anti-CD3 and anti-CD28 antibody (Trifari et al., 2006). Defective cytokine production is associated with the reduction of nuclear translocation of NFAT-1 in $CD4^+$ T cells, while a NFAT-1 and NFAT-2 reduction was observed in $CD8^+$ T cells (Trifari et al., 2006). Previous reports show that the WH1 domain of WASp plays an important role in TCR-induced NFAT-mediated transcription (Silvin et al., 2001). It has been proposed that WASp WH1 possibly binds WIP to initiate transcriptional NFAT activation. In addition, mutation of WASp WH2 domain (also known as the verprolin domain), which is essential for Arp2/3-mediated actin polymerization, did not inhibit NFAT activation. Thus, it is suggested that WASp is indispensable for NFAT activation in a manner that is independent of its function in Arp2/3-induced actin polymerization (Silvin et al., 2001). WASp may indirectly regulate TCR-mediated NFAT activation through binding with adaptor protein Nck, which subsequently binds the Pak serine/threonine kinase to promote TCR-mediated NFAT activation (Yablonski et al., 1998).

CONCLUSION REMARKS

Since WASp has been identified, accumulating pieces of evidence reveal the role of WASp as a nucleation-promoting factor that transform signals from cell surface receptors to actin cytoskeleton rearrangement. Intense research has uncovered the functional domains of WASp as well as its interacting partners, most of which are involved in controlling actin-filament formation. Previous model of WASp recruitment to IS following TCR ligation is relied on SLP-76/Nck complex. However, two alternative pathways of WASp recruitment to IS were identified which are mediated by TCR-Nck and ZAP-70-CrkL-WIP. These findings reveal different WASp pool existing in T cells and which pool contributing to regulate actin polymerization is still opened for investigation. The essential role of WASp in actin-dependent T cell activation has been continually reported. However, little is known about WASp in TCR-mediated signal transduction and T cell activation. WASp-deficient cells show normal in TCR-proximal signaling such as phosphorylation of CD3ζ and ZAP-70. However, they show a defect in nuclear translocation of phospho-Erk and decreased intracellular Ca^{2+} mobilization, the exact cause of which is not known. Diminishing these signaling events results in an impairment of AP-1 and NFAT activation and reduced of cytokine production. WASp is not involved translocation of Jnk and NF-κB. Interestingly, independent roles of WASp in NFAT activation and actin polymerization have been proposed. Thus, understanding of the role played by WASp in TCR signaling is one of the recent scientific interests to improve the knowledge of etiology of WASp and the treatment of WAS.

AUTHOR CONTRIBUTIONS

JN collected the data and drafted the manuscript. PW and PP helped in retrieving the data. WS and SP supervised and edited the manuscript. All authors contributed to the article and approved the submitted version.

FUNDING

SP has received research grants from the Thailand Science Research and Innovations (TSRI, grant no. BRG6180010) and

National Science, Research and Innovation Fund (NSRF, grant nos. R2564B011, R2564B012, and R2565B001). JN received research grants from Naresuan University (no. R2559B064), and the Thailand Research Fund (TRG5880030). This study was also supported by the German Research Foundation (DFG) through BIOSS—EXC294 and CIBSS—EXC 2189 to WS, SFB854 (B19 to WS) and SFB1381 (A9 to WS).

REFERENCES

Alarcón, B., Gil, D., Delgado, P., and Schamel, W. W. (2003). Initiation of TCR signaling: regulation within CD3 dimers. *Immunol. Rev.* 191, 38–46. doi: 10.1034/j.1600-065x.2003.00017.x

Amasaki, Y., Masuda, E. S., Imamura, R., Arai, K., and Arai, N. (1998). Distinct NFAT family proteins are involved in the nuclear NFAT-DNA binding complexes from human thymocyte subsets. *J. Immunol.* 160, 2324–2333.

Arendt, C. W., Albrecht, B., Soos, T. J., and Littman, D. R. (2002). Protein kinase C-theta: signalling from the center of the T-cell synapse. *Curr. Opin. Immunol.* 14, 323–330. doi: 10.1016/s0952-7915(02)00346-1

Badour, K., Zhang, J., Shi, F., Leng, Y., Collins, M., and Siminovitch, K. A. (2004). Fyn and PTP-PEST-mediated regulation of Wiskott-Aldrich syndrome protein (WASp) tyrosine phosphorylation is required for coupling T cell antigen receptor engagement to WASp effector function and T cell activation. *J. Exp. Med.* 199, 99–112. doi: 10.1084/jem.20030976

Baier-Bitterlich, G., Uberall, F., Bauer, B., Fresser, F., Wachter, H., Grunicke, H., et al. (1996). Protein kinase C-theta isoenzyme selective stimulation of the transcription factor complex AP-1 in T lymphocytes. *Mol. Cell. Biol.* 16, 1842–1850. doi: 10.1128/mcb.16.4.1842

Barda-Saad, M., Braiman, A., Titerence, R., Bunnell, S. C., Barr, V. A., and Samelson, L. E. (2005). Dynamic molecular interactions linking the T cell antigen receptor to the actin cytoskeleton. *Nat. Immunol.* 6, 80–89. doi: 10.1038/ni1143

Berg-Brown, N. N., Gronski, M. A., Jones, R. G., Elford, A. R., Deenick, E. K., Odermatt, B., et al. (2004). PKCtheta signals activation versus tolerance in vivo. *J. Exp. Med.* 199, 743–752. doi: 10.1084/jem.20031022

Blanchoin, L., Amann, K. J., Higgs, H. N., Marchand, J. B., Kaiser, D. A., and Pollard, T. D. (2000). Direct observation of dendritic actin filament networks nucleated by Arp2/3 complex and WASP/Scar proteins. *Nature* 404, 1007–1011. doi: 10.1038/35010008

Bosticardo, M., Marangoni, F., Aiuti, A., Villa, A., and Roncarolo, M. G. (2009). Recent advances in understanding the pathophysiology of Wiskott-Aldrich syndrome. *Blood* 113, 6288–6295. doi: 10.1182/blood-2008-12-115253

Braiman, A., Barda−Saad, M., Sommers, C. L., and Samelson, L. E. (2006). Recruitment and activation of PLC gamma 1 in T cells: a new insight into old domains. *EMBO J.* 25, 774–784. doi: 10.1038/sj.emboj.7600978

Brezar, V., Tu, W. J., and Seddiki, N. (2015). PKC-Theta in regulatory and effector T-cell functions. *Front. Immunol.* 13:530. doi: 10.3389/fimmu.2015.00530

Bunnell, S. C., Henry, P. A., Kolluri, R., Kirchhausen, T., Rickles, R. J., and Berg, L. J. (1996). Identification of Itk/Tsk Src homology 3 domain ligands. *J. Biol. Chem.* 271, 25646–25656. doi: 10.1074/jbc.271.41.25646

Calvez, R., Lafouresse, F., De Meester, J., Galy, A., Valitutti, S., and Dupré, L. (2011). The Wiskott-Aldrich syndrome protein permits assembly of a focused immunological synapse enabling sustained T-cell receptor signalling. *Haematologica* 96, 1415–1423. doi: 10.3324/haematol.2011.040204

Cannon, J. L., and Burkhardt, J. K. (2004). Differential roles for Wiskott-Aldrich syndrome protein in immune synapse formation and IL-2 production. *J. Immunol.* 173, 1658–1662. doi: 10.4049/jimmunol.173.3.1658

Cannon, J. L., Labno, C. M., Bosco, G., Seth, A., McGavin, M. H. K., Siminovitch, K. A., et al. (2001). WASP recruitment to the T cell:APC contact site occurs independently of Cdc42 activation. *Immunity* 15, 249–259. doi: 10.1016/S1074-7613(01)00178-9

Chan, A. C., Iwashima, M., Turck, C. W., and Weiss, A. (1992). ZAP- 70: a 70 kd protein-tyrosine kinase that associates with the TCR zeta chain. *Cell* 71, 649–662. doi: 10.1016/0092-8674(92)90598-7

Chou, H. C., Antón, I. M., Holt, M. R., Curcio, C., Lanzardo, S., Worth, A., et al. (2006). WIP regulates the stability and localization of WASP to podosomes in migrating dendritic cells. *Curr. Biol.* 16, 2337–2344. doi: 10.1016/j.cub.2006.10.037

Choudhuri, K., and Dustin, M. L. (2010). Signalling microdomains in T cells. *FEBS. Lett.* 584, 4823–4831. doi: 10.1016/j.febslet.2010.10.015

Cianferoni, A., Massaad, M., Feske, S., de la Fuente, M. A., Gallego, L., Ramesh, N., et al. (2005). Defective nuclear translocation of nuclear factor of activated T cells and extracellular signal-regulated kinase underlies deficient IL-2 gene expression in Wiskott-Aldrich syndrome. *J. Allergy Clin. Immunol.* 116, 1364–1371. doi: 10.1016/j.jaci.2005.09.006

Conley, J. M., Gallagher, M. P., and Berg, L. J. (2016). T cells and gene regulation: the switching on and turning up of genes after T cell receptor stimulation in CD8 T cells. *Front. Immunol.* 7:76. doi: 10.3389/fimmu.2016.00076

Cory, G. O., Garg, R., Cramer, R., and Ridley, A. J. (2002). Phosphorylation of tyrosine 291 enhances the ability of WASp to stimulate actin polymerization and filopodium formation. Wiskott-Aldrich Syndrome protein. *J. Biol. Chem.* 277, 45115–45121. doi: 10.1074/jbc.M203346200

Davis, R. J. (2000). Signal transduction by the JNK group of MAP kinases. *Cell* 103, 239–252. doi: 10.1016/s0092-8674(00)00116-1

de la Fuente, M. A., Sasahara, Y., Calamito, M., Antón, I. M., Elkhal, A., Gallego, M. D., et al. (2007). WIP is a chaperone for Wiskott-Aldrich syndrome protein (WASP). *Proc. Natl. Acad. Sci. U. S. A.* 104, 926–931. doi: 10.1073/pnas.0610275104

Feske, S. (2007). Calcium signalling in lymphocyte activation and disease. *Nat. Rev. Immunol.* 7, 690–702. doi: 10.1038/nri2152

Fried, S., Matalon, O., Noy, E., and Barda-Saad, M. (2014). WIP: more than a WASp-interacting protein. *J. Leukoc. Biol.* 96, 713–727. doi: 10.1189/jlb.2RU0314-162R

Gallego, M. D., Santamaria, M., Pena, J., and Molina, I. J. (1997). Defective actin reorganization and polymerization of Wiskott-Aldrich T cells in response to CD3-mediated stimulation. *Blood* 90, 3089–3097.

Gil, D., Schamel, W. W., Montoya, M., Sánchez-Madrid, F., and Alarcón, B. (2002). Recruitment of Nck by CD3 epsilon reveals a ligand-induced conformational change essential for T cell receptor signaling and synapse formation. *Cell* 109, 901–912. doi: 10.1016/s0092-8674(02)00799-7

Gwack, Y., Feske, S., Srikanth, S., Hogan, P. G., and Rao, A. (2007). Signalling to transcription: store-operated Ca2+ entry and NFAT activation in lymphocytes. *Cell Calcium* 42, 145–156. doi: 10.1016/j.ceca.2007.03.007

Han, J., and Ulevitch, R. J. (1999). Emerging targets for anti-inflammatory therapy. *Nat. Cell Biol.* 1, E39–E40. doi: 10.1038/10032

Hartl, F. A., Beck-Garcìa, E., Woessner, N. M., Flachsmann, L. J., Cárdenas, R. M. V., Brandl, S. M., et al. (2020). Noncanonical binding of Lck to CD3ε promotes TCR signaling and CAR function. *Nat. Immunol.* 21, 902–913. doi: 10.1038/s41590-020-0732-3

Hayashi, K., and Altman, A. (2007). Protein kinase C theta (PKCtheta): a key player in T cell life and death. *Pharmacol. Res.* 55, 537–544. doi: 10.1016/j.phrs.2007.04.009

Hayes, S. M., Shores, E. W., and Love, P. E. (2003). An architectural perspective on signalling by the pre-, alphabeta and gammadelta T cell receptors. *Immunol. Rev.* 191, 28–37. doi: 10.1034/j.1600-065x.2003.00011.x

Higgs, H. N., and Pollard, T. D. (2000). Activation by Cdc42 and PIP(2) of Wiskott-Aldrich syndrome protein (WASp) stimulates actin nucleation by Arp2/3 complex. *J. Cell. Biol.* 150, 1311–1320. doi: 10.1083/jcb.150.6.1311

Kane, L. P., Lin, J., and Weiss, A. (2000). Signal transduction by the TCR for antigen. *Curr. Opin. Immunol.* 12, 242–249. doi: 10.1016/s0952-7915(00)00083-2

Kim, A. S., Kakalis, L. T., Abdul-Manan, N., Liu, G. A., and Rosen, M. K. (2000). Autoinhibition and activation mechanisms of the Wiskott-Aldrich syndrome protein. *Nature* 404, 151–158. doi: 10.1038/35004513

Krause, M., Sechi, A. S., Konradt, M., Monner, D., Gertler, F. B., and Wehland, J. (2000). Fyn-binding protein (Fyb)/SLP-76-associated protein (SLAP), Ena/vasodilator-stimulated phosphoprotein (VASP) proteins and the Arp2/3 complex link T cell receptor (TCR) signalling to the actin cytoskeleton. *J. Cell. Biol.* 149, 181–194. doi: 10.1083/jcb.149.1.181

Krzewski, K., Chen, X., Orange, J. S., and Strominger, J. L. (2006). Formation of a WIP-, WASp-, actin-, and myosin IIA-containing multiprotein complex in activated NK cells and its alteration by KIR inhibitory signalling. *J. Cell Biol.* 173, 121–132. doi: 10.1083/jcb.200509076

Lee, M. S., Glassman, C. R., Deshpande, N. R., Badgandi, H. B., Parrish, H. L., Uttamapinant, C., et al. (2015). A mechanical switch couples T cell receptor triggering to the cytoplasmic juxtamembrane regions of CD3ζζ. *Immunity* 43, 227–239. doi: 10.1016/j.immuni.2015.06.018

Linardopoulou, E. V., Parghi, S. S., Friedman, C., Osborn, G. E., Parkhurst, S. M., and Trask, B. J. (2007). Human subtelomeric WASH genes encode a new subclass of the WASP family. *PLoS Genet.* 3:e237. doi: 10.1371/journal.pgen.0030237

Massaad, M. J., Ramesh, N., and Geha, R. S. (2013). Wiskott-Aldrich syndrome: a comprehensive review. *Ann. N. Y. Acad. Sci.* 1285, 26–43. doi: 10.1111/nyas.12049

Matalon, O., Reicher, B., and Barda-Saad, M. (2013). Wiskott-Aldrich syndrome protein–dynamic regulation of actin homeostasis: from activation through function and signal termination in T lymphocytes. *Immunol. Rev.* 256, 10–29. doi: 10.1111/imr.12112

Miki, H., Miura, K., and Takenawa, T. (1996). N-WASP, a novel actin-depolymerizing protein, regulates the cortical cytoskeletal rearrangement in a PIP2-dependent manner downstream of tyrosine kinases. *EMBO J.* 15, 5326–5335.

Miki, H., and Takenawa, T. (1998). Direct binding of the verprolin-homology domain in N-WASP to actin is essential for cytoskeletal reorganization. *Biochem. Biophys. Res. Commun.* 243, 73–78. doi: 10.1006/bbrc.1997.8064

Minguet, S., Swamy, M., Alarcón, B., Luescher, I. F., and Schamel, W. W. (2007). Full activation of the T cell receptor requires both clustering and conformational changes at CD3. *Immunity* 26, 43–54. doi: 10.1016/j.immuni.2006.10.019

Molina, I. J., Sancho, J., Terhorst, C., Rosen, F. S., and Remold-O'Donnell, E. (1993). T cells of patients with the Wiskott-Aldrich syndrome have a restricted defect in proliferative responses. *J. Immunol.* 151, 4383–4390.

Ngoenkam, J., Schamel, W. W., and Pongcharoen, S. (2018). Selected signalling proteins recruited to the T-cell receptor–CD3 complex. *Immunology* 153, 42–50. doi: 10.1111/imm.12809

Paensuwan, P., Hartl, F. A., Yousefi, O. S., Ngoenkam, J., Wipa, P., Beck-Garcia, E., et al. (2016). Nck binds to the T cell antigen receptor using its SH3.1 and SH2 domains in a cooperative manner, promoting TCR functioning. *J. Immunol.* 196, 448–458. doi: 10.4049/jimmunol.1500958

Paensuwan, P., Ngoenkam, J., Khamsri, B., Preechanukul, K., Sanguansermsri, D., and Pongcharoen, S. (2015). Evidence for inducible recruitment of Wiskott-Aldrich syndrome protein to T cell receptor-CD3 complex in Jurkat T cells. *Asian Pac. J. Allergy Immunol.* 33, 189–195. doi: 10.12932/AP0544.33.3.2015

Pfeifhofer, C., Kofler, K., Gruber, T., Tabrizi, N. G., Lutz, C., Maly, K., et al. (2003). Protein kinase C θ affects Ca2+ mobilization and NFAT activation in primary mouse T cells. *J. Exp. Med.* 197, 1525–1535. doi: 10.1084/jem.20020234

Ramesh, N., Antón, I. M., Hartwig, J. H., and Geha, R. S. (1997). WIP, a protein associated with wiskott-aldrich syndrome protein, induces actin polymerization and redistribution in lymphoid cells. *Proc. Natl. Acad. Sci. U. S. A.* 94, 14671–14676. doi: 10.1073/pnas.94.26.14671

Reth, M. (1989). Antigen receptor tail clue. *Nature* 338, 383–384. doi: 10.1038/338383b0

Rhee, S. G., and Bae, Y. S. (1997). Regulation of phosphoinositide-specific phospholipase C isozymes. *J. Biol. Chem.* 272, 15045–15048. doi: 10.1074/jbc.272.24.15045

Rincón, M., Flavell, R., and Davis, R. (2001). Signal transduction by MAP kinases in T lymphocytes. *Oncogene* 20, 2490–2497. doi: 10.1038/sj.onc.1204382

Rivera, G. M., Briceño, C. A., Takeshima, F., Snapper, S. B., and Mayer, B. J. (2004). Inducible clustering of membrane-targeted SH3 domains of the adaptor protein Nck triggers localized actin polymerization. *Curr. Biol.* 14, 11–22. doi: 10.1016/j.cub.2003.12.033

Rivero-Lezcano, O. M., Marcilla, A., Sameshima, J. H., and Robbins, K. C. (1995). Wiskott-Aldrich syndrome protein physically associates with Nck through Src homology 3 domains. *Mol. Cell. Biol.* 15, 5725–5731. doi: 10.1128/mcb.15.10.5725

Sadhukhan, S., Sarkar, K., Taylor, M., Candotti, F., and Vyas, Y. M. (2014). Nuclear role of WASp in gene transcription is uncoupled from its A.RP2/3-dependent cytoplasmic role in actin polymerization. *J. Immunol.* 193, 150–160. doi: 10.4049/jimmunol.1302923

Sasahara, Y., Rachid, R., Byrne, M. J., de la Fuente, M. A., Abraham, R. T., Ramesh, N., et al. (2002). Mechanism of recruitment of WASP to the immunological synapse and of its activation following TCR ligation. *Mol. Cell* 10, 1269–1281. doi: 10.1016/s1097-2765(02)00728-1

Sato, M., Sawahata, R., Takenouchi, T., and Kitani, H. (2011). Identification of Fyn as the binding partner for the WASP N-terminal domain in T cells. *Int. Immunol.* 23, 493–502. doi: 10.1093/intimm/dxr042

Schaeffer, H. J., and Weber, M. J. (1999). Mitogen-activated protein kinases: specific messages from ubiquitous messengers. *Mol. Cell. Biol.* 19, 2435–2444. doi: 10.1128/mcb.19.4.2435

Schamel, W. W., Alarcon, B., and Minguet, S. (2019). The TCR is an allosterically regulated macromolecular machinery changing its conformation while working. *Immunol. Rev.* 291, 8–25. doi: 10.1111/imr.12788

Seminario, M. C., and Bunnell, S. C. (2008). Signal initiation in T-cell receptor microclusters. *Immunol. Rev.* 221, 90–106. doi: 10.1111/j.1600-065X.2008.00593.x

Silvin, C., Belisle, B., and Abo, A. (2001). A role for Wiskott-Aldrich syndrome protein in T-cell receptor-mediated transcriptional activation independent of actin polymerization. *J. Biol. Chem.* 276, 21450–21457. doi: 10.1074/jbc.M010729200

Smith-Garvin, J. E., Koretzky, G. A., and Jordan, M. S. (2009). T cell activation. *Annu. Rev. Immunol.* 27, 591–619. doi: 10.1146/annurev.immunol.021908.132706

Sun, X., Wei, Y., Lee, P. P., Ren, B., and Liu, C. (2019). The role of WASp in T cells and B cells. *Cell Immunol.* 341:103919. doi: 10.1016/j.cellimm.2019.04.007

Sun, Z., Arendt, C. W., Ellmeier, W., Schaeffer, E. M., Sunshine, M. J., Gandhi, L., et al. (2000). PKC-theta is required for TCR-induced NF-kappa B activation in mature but not immature T lymphocytes. *Nature* 404, 402–407. doi: 10.1038/35006090

Swamy, M., Beck-Garcia, K., Beck-Garcia, E., Hartl, F. A., Morath, A., Yousefi, O. S., et al. (2016). A cholesterol-based allostery model of T cell receptor phosphorylation. *Immunity* 44, 1091–1101. doi: 10.1016/j.immuni.2016.04.011

Symons, M., Derry, J. M., Karlak, B., Jiang, S., Lemahieu, V., Mccormick, F., et al. (1996). Wiskott-Aldrich syndrome protein, a novel effector for the GTPase CDC42Hs, is implicated in actin polymerization. *Cell* 84, 723–734. doi: 10.1016/s0092-8674(00)81050-8

Thrasher, A. J., and Burns, S. O. (2010). WASP: a key immunological multitasker. *Nat. Rev. Immunol.* 10, 182–192. doi: 10.1038/nri2724

Thumkeo, D., Katsura, Y., Nishimura, Y., Kanchanawong, P., Tohyama, K., Ishizaki, T., et al. (2020). mDia1/3-dependent actin polymerization spatiotemporally controls LAT phosphorylation by Zap70 at the immune synapse. *Sci. Adv.* 6:eaay2432. doi: 10.1126/sciadv.aay2432

Torres, E., and Rosen, M. K. (2006). Protein-tyrosine kinase and GTPase signals cooperate to phosphorylate and activate Wiskott-Aldrich syndrome protein (WASP)/neuronal WASP. *J. Biol. Chem.* 281, 3513–3520. doi: 10.1074/jbc.M509416200

Trifari, S., Sitia, G., Aiuti, A., Scaramuzza, S., Marangoni, F., Guidotti, L. G., et al. (2006). Defective Th1 cytokine gene transcription in CD4+ and CD8+ T cells from Wiskott-Aldrich syndrome patients. *J. Immunol.* 177, 7451–7461. doi: 10.4049/jimmunol.177.10.7451

Volkman, B. F., Prehoda, K. E., Scott, J. A., Peterson, F. C., and Lim, W. A. (2002). Structure of the N-WASP EVH1 domain-WIP complex: insight into the molecular basis of Wiskott-Aldrich Syndrome. *Cell* 111, 565–576. doi: 10.1016/s0092-8674(02)01076-0

Watanabe, Y., Sasahara, Y., Ramesh, N., Massaad, M. J., Yeng Looi, C., Kumaki, S., et al. (2013). T-cell receptor ligation causes Wiskott-Aldrich syndrome protein degradation and F-actin assembly downregulation. *J. Allergy Clin. Immunol.* 132, 648–655.e1. doi: 10.1016/j.jaci.2013.03.046

Wipa, P., Paensuwan, P., Ngoenkam, J., Woessner, N. M., Minguet, S., Schamel, W. W., et al. (2020). Actin polymerization regulates recruitment of Nck to CD3ε upon T-cell receptor triggering. *Immunology* 159, 298–308. doi: 10.1111/imm.13146

Wunderlich, L., Faragó, A., Downward, J., and Buday, L. (1999). Association of Nck with tyrosine-phosphorylated SLP-76 in activated T lymphocytes. *Eur. J.*

Immunol. 29, 1068–1075. doi: 10.1002/(SICI)1521-4141(199904)29:04<1068::AID-IMMU1068<3.0.CO;2-P

Yablonski, D., Kane, L. P., Qian, D., and Weiss, A. (1998). A Nck-Pak1 signalling module is required for T-cell receptor-mediated activation of NFAT, but not of JNK. *EMBO J.* 17, 5647–5657. doi: 10.1093/emboj/17.19.5647

Yokosuka, T., and Saito, T. (2010). "The immunological synapse, TCR microclusters, and T cell activation," in *Immunological Synapse. Current Topics in Microbiology and Immunology*, vol 340, eds T. Saito and F. Batista (Berlin: Spinger), doi: 10/1007/978-3-642-03858-7_5

Zeng, R., Cannon, J. L., Abraham, R. T., Way, M., Billadeau, D. D., Bubeck-Wardenberg, J., et al. (2003). SLP-76 coordinates Nck-dependent Wiskott-Aldrich syndrome protein recruitment with Vav-1/Cdc42-dependent Wiskott-Aldrich syndrome protein activation at the T cell-APC contact site. *J. Immunol.* 171, 1360–1368. doi: 10.4049/jimmunol.171.3.1360

Zhang, J., Dong, B., and Siminovitch, K. A. (2009). Contributions of Wiskott-Aldrich syndrome family cytoskeletal regulatory adapters to immune regulation. *Immunol. Rev.* 232, 175–194. doi: 10.1111/j.1600-065X.2009.00846.x

Zhang, J., Shehabeldin, A., da Cruz, L. A., Butler, J., Somani, A. K., McGavin, M., et al. (1999). Antigen receptor-induced activation and cytoskeletal rearrangement are impaired in Wiskott-Aldrich syndrome protein-deficient lymphocytes. *J. Exp. Med.* 190, 1329–1342. doi: 10.1084/jem.190.9.1329

Zhang, W., Sloan-Lancaster, J., Kitchen, J., Trible, R. P., and Samelson, L. E. (1998). LAT: the ZAP-70 tyrosine kinase substrate that links T cell receptor to cellular activation. *Cell* 92, 83–92. doi: 10.1016/s0092-8674(00)80901-0

Conflict of Interest: The authors declare that the research was conducted in the absence of any commercial or financial relationships that could be construed as a potential conflict of interest.

frontiers in Cell and Developmental Biology

ORIGINAL RESEARCH
published: 10 June 2021
doi: 10.3389/fcell.2021.590655

Spectral Analysis of ATP-Dependent Mechanical Vibrations in T Cells

*Ishay Wohl and Eilon Sherman**

Racah Institute of Physics, The Hebrew University, Jerusalem, Israel

Mechanical vibrations affect multiple cell properties, including its diffusivity, entropy, internal content organization, and thus—function. Here, we used Differential Interference Contrast (DIC), confocal, and Total Internal Reflection Fluorescence (TIRF) microscopies to study mechanical vibrations in live (Jurkat) T cells. Vibrations were measured via the motion of intracellular particles and plasma membrane. These vibrations depend on adenosine triphosphate (ATP) consumption and on Myosin II activity. We then used spectral analysis of these vibrations to distinguish the effects of thermal agitation, ATP-dependent mechanical work and cytoskeletal visco-elasticity. Parameters of spectral analyses could be related to mean square displacement (MSD) analyses with specific advantages in characterizing intracellular mechanical work. We identified two spectral ranges where mechanical work dominated vibrations of intracellular components: 0–3 Hz for intracellular particles and the plasma-membrane, and 100–150 Hz for the plasma-membrane. The 0–3 Hz vibrations of the cell membrane that we measured in an experimental model of immune synapse (IS) are expected to affect the IS formation and function in effector cells. It may also facilitate immunological escape of extensively vibrating malignant cells.

Keywords: power of diffusion, mechanical fluctuations, malignancy, DFT, microscopy

OPEN ACCESS

Edited by:
Sudha Kumari, Massachusetts Institute of Technology, United States

Reviewed by:
Michael Loran Dustin, University of Oxford, United Kingdom
Dylan Myers Owen, University of Birmingham, United Kingdom
Noa B. Martin-Cofreces, Princess University Hospital, Spain

***Correspondence:**
Eilon Sherman
eilon.sherman@mail.huji.ac.il

Specialty section:
This article was submitted to Cell Growth and Division, a section of the journal Frontiers in Cell and Developmental Biology

Received: *02 August 2020*
Accepted: *27 April 2021*
Published: *10 June 2021*

Citation:
Wohl I and Sherman E (2021) Spectral Analysis of ATP-Dependent Mechanical Vibrations in T Cells. Front. Cell Dev. Biol. 9:590655. doi: 10.3389/fcell.2021.590655

INTRODUCTION

Mechanical work inside living cells plays a significant role in cell physiology (Huang and Ingber, 2005; Tee et al., 2010). For instance, direct transport of intracellular constituents is conducted by molecular motors such as kinesin, dynein and myosin II (Manfred and Woehlke, 2003). Other indirect intracellular motor activities may control important biophysical parameters, including intracellular diffusivity (Brangwynne et al., 2009; Guo et al., 2014), entropy (Wohl and Sherman, 2019) and phase partitioning of cell content (Wohl and Sherman, 2019). Indirect motor activity may include the incoherent fraction of mechanical forces that are applied by molecular motors on multiple sites on the cytoskeleton (Guo et al., 2014). Thus, these incoherent forces impact the cytoskeleton. The cytoskeleton is an elastic mesh (Mizuno et al., 2007), and thus it transfers those forces to intracellular constituents, e.g., vesicles and organelles that are embedded within or

Abbreviations: DIC, Differential interference contrast; TIRF, Total internal reflection fluorescence; ATP, Adenosine triphosphate; MSD, Mean square displacement; IS, Immune synapse; PM, Plasma membrane; TCR, T cell receptor; MHC, Major histocompatibility complex; APC, Antigen presenting cell; FBM, Fractional Brownian motion; RWF, Random walk on fractal; CTRW, Continues time random walk; PSD, Power spectral density; BD, Brownian diffusion; DFT, Discrete Fourier transform; SSE, Sum of squared errors; PDF, Probability density function; SD, standard deviation; ROI, Region of interest; ASD, Amplitude spectral density; PFA, Paraformaldehyde; ANOVA, Analysis of Variance.

adjacent to it. Applied forces on the cytoskeleton from tension generation by cortical actin may also influence the mechanical activity of the cytoskeleton (Chugh and Paluch, 2018).

Notably, mechanical work generates forces that are non-thermal and depend on ATP consumption. As a result of these forces, the cytoskeleton transfers mechanical work and augments the diffusion of intracellular particles (Brangwynne et al., 2009; Guo et al., 2014). It also increases intracellular entropy and decreases the partition of the intracellular content, as in liquid-liquid phase separation (LLPS) (Wohl and Sherman, 2019).

The plasma membrane (PM) is physically connected to the cortical actin (Salbreux et al., 2012). Thus, both thermal and active fluctuations of the actin mesh translate into corresponding fluctuations of the PM. In the case of T cells (studied here), their activation is an outstanding example of the significance of such PM fluctuations and their effect on cell biology and decision-making. T cells get activated upon specific triggering of their T-cell antigen receptor (TCR). Such triggering occurs when TCRs recognize their cognate ligands, namely antigens, presented on the major histocompatibility complex (pMHC) on the surface of antigen presenting cells (APCs) (Chakraborty and Weiss, 2014). Recently, it has been shown that the interactions between the TCR-pMHC and TCR activation depend on repeatedly applied perpendicular forces (Huppa et al., 2010; Ma and Finkel, 2010). Thus, the fluctuations described in this study could significantly contribute to the effective rates of TCR engagement and triggering, specificity of antigen recognition and cell activation.

Here, we aimed to study intracellular diffusion and intracellular mechanical work, as they occur in T cells. Specifically, the impact of non-equilibrium forces on intracellular particles motion enables the investigation of those forces by analyzing the dynamics of these particles. Intracellular diffusion motion is usually characterized as anomalous diffusion, for which the mean square displacement (MSD) is not linearly correlated to the time-lag of measurements (Granek and Pierrat, 1999; Caspi et al., 2000). The MSD equation is $\langle \Delta r^2 \rangle = K_\alpha t^\alpha$, where K_α is the diffusion coefficient and α is the diffusion power. Finding these specific anomalous diffusion parameters does not usually facilitate the identification of the main cellular mechanisms that explains those results. The reason is that different underlying mechanisms may lead to similar anomalous diffusion K_α and α results (e.g., Golan and Sherman, 2017).

Three main mathematical models have been defined in relation to different cellular mechanisms that may govern the intracellular anomalous diffusion, including visco-elasticity, diffusion and percolation in a crowded environment and medium with traps or energetic disorder (Meroz et al., 2013). Fractional Brownian motion (FBM) is a model that is characterized by long-range temporal correlations and relates to diffusion motion in visco-elastic media. The model of Random walk on a fractal (RWF) enables to characterize diffusion motion or percolation in fractal media, such as crowded environment. Through the Continues Time Random Walk (CTRW) model, the particle diffusion is hindered by trapping events and binding interactions. The motion of the particle is characterized by a broad distribution of waiting times between jumps. In a wider definition, this model also applies to a medium with energetic disorder (Meroz et al., 2013).

The diffusion motion patterns of a particle that is stuck in a trap and will randomly gain enough energy to jump to another location may be similar to the diffusion motion patterns of a free particle that randomly gains a large amount of mechanical energy that will cause it to jump to a relatively remote location. Both situations are described by the CTRW model. Accordingly, the impact of mechanical energy on intracellular diffusion is likely to cause the anomalous diffusion patterns to better match that model. A distinctive difference between the CTRW model and the other FBM or RWF models is that the CTRW model describes a non-ergodic process, while FBM and RWF describe ergodic processes (Jeon et al., 2011; Meroz et al., 2013). Accordingly, if a break in ergodicity could be demonstrated while analyzing diffusion motion in living cells, it is reasonable to assume that in that situation the CTRW model and its related underlying mechanisms are dominant and better explain the cellular condition (Meroz et al., 2013).

Following that, an analytic framework of intracellular diffusion motion that combines the effects of spatial fluctuations with ergodicity breaking should clearly capture the impact of intracellular mechanical work on the anomalous diffusion. Such an analysis should be able to discern underlying mechanisms of intracellular diffusion motion that may yield similar anomalous diffusion parameters (K_α and α) but differ in their ergodicity.

The power spectral density (PSD) analysis of a wide range of time-dependent parameters was studied in many fields of science, including physics, biophysics, geology, weather science, etc. (Krapf et al., 2018). Often, the PSD has the form: $\mu_s(f,\infty) = A/f^\beta$ (Krapf et al., 2018). This prevalent PSD function has been defined analytically for diverse situations including chaotic Hamiltonian systems (Geisel et al., 1987), periodically driven bi-stable systems (Shneidman et al., 1994), fluctuations of a phase-separating interface (Delfino and Squarcini, 2016), Brownian Diffusion (BD) (Krapf et al., 2018), and multiple models of anomalous diffusion (Krapf et al., 2018, 2019; Sposini et al., 2019). Except from theoretical studies, PSD of diffusion motion was investigated mainly in simulations and basic experimental setups incorporating quantum dots (Houel et al., 2015) or trajectories of tracers in artificial crowded fluids (Weiss, 2013), but not in live cells. When investigating vibrations in live cells, a combined contribution to the PSD of two components has to be considered: First, a homogenous and random (white-noise-like) contribution due to thermal forces. Second, a periodic or incoherent contribution due to inhomogeneous mechanical work. The second component is naturally related to a break in ergodicity and could be more readily distinguished while analyzing intracellular modes of vibration utilizing PSD calculations.

Spectral analysis of the dynamics live cells constituents may have the advantage of providing better insight into the biophysical mechanisms behind their anomalous diffusion and ergodicity breaking, especially in regard to intracellular mechanical work.

Here, we utilized a relatively simple spectral analysis framework for the exploration of intracellular diffusion and

intracellular mechanical work. This framework is based on Discrete Fourier Transform (DFT) of temporal position changes of intracellular constituents. This framework then serves to analyze the intracellular diffusion of intracellular particles (e.g., vesicles or other small organelles) and fluctuations of cell diameter in live Jurkat cells, before and after ATP depletion. From the PSD results of the motion of cell constituents, we define parameters that reflect intracellular mechanical work. We show that cells under normal (physiological) conditions are active and produce significant extent of mechanical work. This work is diminished in the same cells that become non-active after ATP depletion. Next, we explore intracellular mechanical work over a wide spectrum of time-scales and frequencies. We identified two spectral ranges where mechanical work dominated vibrations of intracellular components: 0–3 Hz for intracellular particles and the plasma-membrane, and 100–150 Hz for the plasma-membrane. Such vibrations of the cell membrane are expected to affect the formation and function of the immune synapse by effector cells. Thus, we studied the membrane vibrations of Jurkat cells in an experimental model of the immune synapse using total internal reflection fluorescence (TIRF) microscopy. Indeed, we identified ATP-dependent membrane fluctuations at the model synapse, esp. below 3 Hz. These mechanical fluctuations of the cell membrane may also affect T cell recognition of extensively vibrating malignant cells. We expect that spectral analysis of intracellular vibrations and motion will become a useful tool for characterizing cell condition and activity in health and disease.

RESULTS

Spectral Analysis of Temporal Fluctuations of Large Intracellular Particles Is Related to Intracellular Diffusivity and Intracellular Mechanical Work

The cytoskeleton is an elastic polymeric mesh that spans the intracellular volume with a mesh size of around 50 nm (Guo et al., 2014). The elastic cytoskeleton mesh is surrounded by a crowded viscous intracellular gel-like medium. These two constituents largely make the two-component visco-elastic cellular content (Brangwynne et al., 2009). Notably, the mechanical response of the intracellular medium is mainly elastic and less viscous (Guo et al., 2014) with low Reynolds number (Cartwright et al., 2009). The energy due to vibrations in this elastic cytoskeleton has the value of: $E_{mechanical} = 0.5kA^2 + E_{loss}$, where E_{loss} is the (relatively small) dissipated energy, k is the equivalent spring constant of the system, and A is the amplitude of the motion. Monitoring movements of an intracellular particle (like a vesicle) that is significantly larger than the cytoskeleton mesh size (50 nm) can reveal the movements of the adjacent cytoskeleton mesh. Spectral analysis of this particle movement (i.e., its change in position over time) will express multiple modes of vibrations of the adjacent cytoskeleton mesh. Each vibration mode of this mesh has a mechanical energy level of approximately 0.5 kA^2. The integral of the spectrum of vibrations represents the approximated total mechanical energy of the measured part of the cytoskeleton mesh in the specified spectral range. Monitoring movements of multiple intracellular particles and averaging the spectral analysis results of these movements enable insight into the mechanical energy and work of the entire cytoskeleton and cellular system.

Thermal agitation forces and incoherent intracellular mechanical forces (which are a by-product of directed forces that are utilized for cell physiology), both act on the cytoskeleton. Together, they contribute to the cytoskeletal modes of vibrations. These vibration modes can then be revealed by monitoring embedded particles inside the mesh for their diffusion motion. Spectral analysis of the diffusion motion of these particles can be related to the modes of vibration and mechanical energy of the adjacent cytoskeleton.

In order to explore these relations we consider the diffusion motion of an intracellular particle embedded in the elastic cytoskeleton mesh as illustrated in **Figure 1**. The change in particle position over time could be analyzed by DFT to produce the particle's amplitudes of spatial fluctuations for the corresponding spatial dimensions (x or y). These amplitudes of spatial fluctuations represent the different modes of vibrations that determine the combined mechanical energy of the particle and adjacent elastic cytoskeletal mesh.

To further investigate these spectral amplitudes of spatial fluctuations, we consider the three following aspects:

1. The summation (integral) of all powers (the squared amplitudes), which relates to the total mechanical energy of the particle-elastic mesh system in the specified spectral range. Each power represents a specific amplitude of vibration (*A or Amplitude*) and its corresponding mode of mechanical energy (namely, $E_{mechanical} = 0.5\,kA^2$).
2. The vibration spectrum is fitted with a power equation for each set of spectral results for each cell and condition:

$$Amplitude_{estimated} = a/(frequency)^b \quad (1)$$

   The relation of a and b parameters of the power fit to the diffusion and mechanical work characteristic are further studied below.
3. The extent to which the actual spectrum of amplitudes fits to the model equation of estimated power. In other words, we quantify the magnitude of the sum of squared errors (SSE) that relates the spectrum to its power fit equation. Then, the correlations of SSE values to the intracellular diffusion and mechanical work characteristic are investigated.

A general diffusion process can be characterized by its typical probability density function (PDF) of translocations for each corresponding time-lag, and following that, by the statistics of MSDs. First we analyze the condition of Brownian diffusion, for which $\alpha = 1$. The PDF of translocation for each time-lag in this case is Gaussian. We simulated the movement of particles undergoing normal diffusion with different diffusion coefficients (represented by the different standard deviations of the PDF of translocation Gaussians; **Figures 2A–D**). In this simulation, calculating the spectra of amplitudes of fluctuations (of position changes in time) reveals that the compatibility of a power fit model to these spectral results is high. It also shows that the a

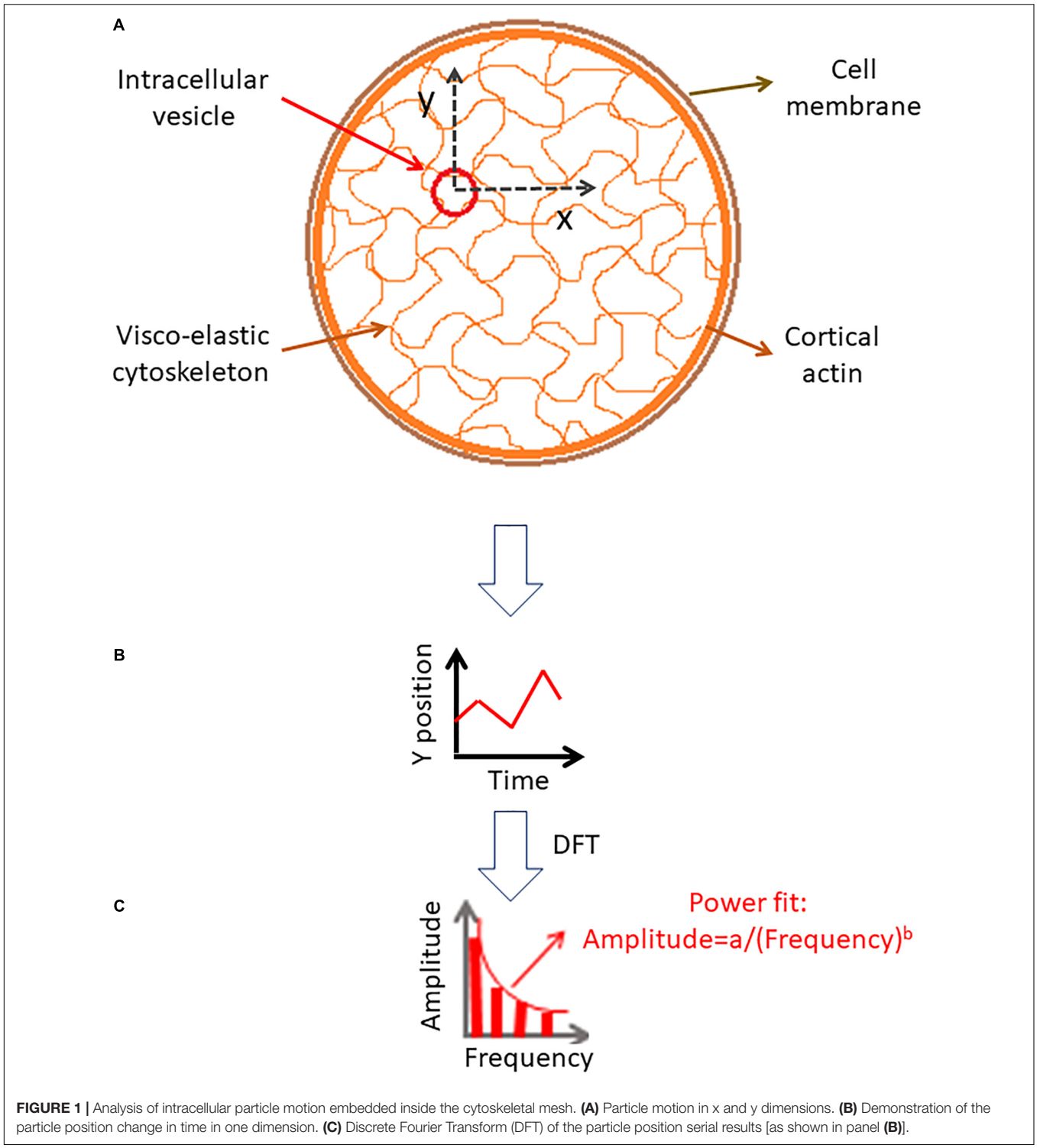

FIGURE 1 | Analysis of intracellular particle motion embedded inside the cytoskeletal mesh. **(A)** Particle motion in x and y dimensions. **(B)** Demonstration of the particle position change in time in one dimension. **(C)** Discrete Fourier Transform (DFT) of the particle position serial results [as shown in panel **(B)**].

parameter of the power fit [$Amplitude_{estimated} = a/(frequency)^b$] is correlated to the standard deviation (SD) of PDF of translocations (**Figure 2E**) and accordingly, to diffusivity. Following this simulation of normal diffusion we conclude that the SSE of the power fit is also correlated to the SD of PDF of translocations and diffusivity (**Figure 2F**).

The characteristic PDF of a diffusing particle (along with its parameters K_α and α) can be related to the spectral analysis results of its position changes in time. For an ergodic diffusion process, the PDF of translocations in a time-lag that corresponds to the interval between measurements reveals the statistic of the sequential translocation steps of that diffusive object. Knowing

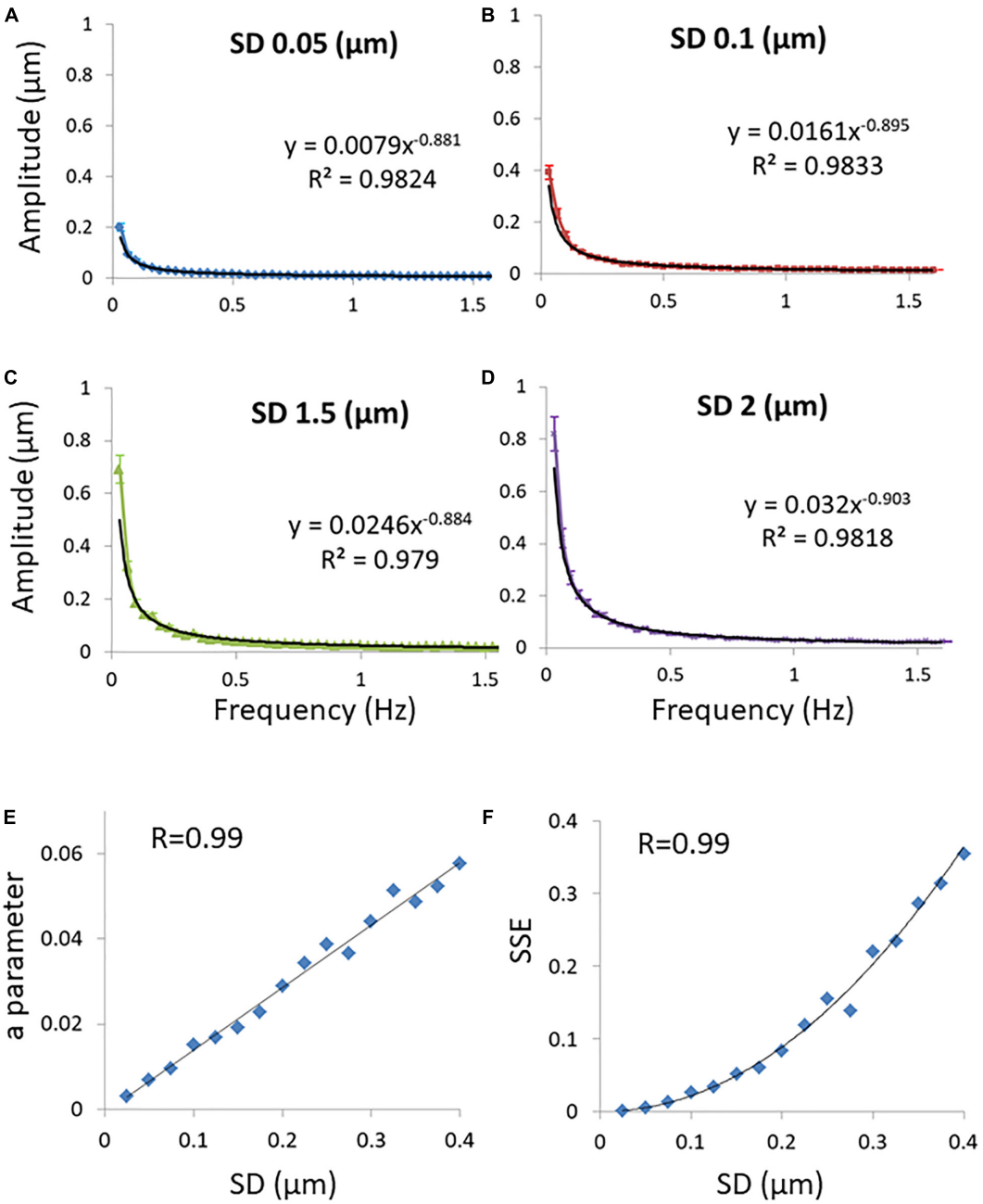

FIGURE 2 | Simulations results. **(A)** Discrete Fourier Transform (DFT) of a simulated particle position change in time when the probability density function's (PDF) of translocations are Gaussian and the SD of translocations is 0.05 μm. Power fit parameters of the DFT results are added. **(B)** The same as **(A)** except that the SD of translocations is 0.1 μm. **(C)** The same as **(A)** except that the SD of translocations is 0.15 μm. **(D)** The same as **(A)** except that the SD of translocations is 0.2 μm. 50 simulations were performed for each condition described in panels **(A–D)**. **(E)** The correlation between the SD of translocations and the *a* parameter of the power fit results ($y = ax^b$) in each condition of SD. **(F)** The correlation between the SD's of translocations and the sum of squared errors (SSE) of the power fit in each condition of SD. Error bars in panels **(A–D)** are SEM.

this statistic of translocations does not allow us to reconstruct the exact trajectory of that particle during measurements. Still, one can anticipate the different amplitudes of spatial fluctuations and their correspondent statistical frequencies from the given PDF of translocations. The knowledge of the different amplitudes of spatial fluctuation with their corresponding frequencies of occurrence is generally equivalent to the results of the DFT analysis of the position fluctuations of that same particle over time. In this analysis, the different frequency-dependent amplitudes of the DFT represent the different amplitudes of the particle's spatial fluctuations (i.e., translocations). Similarly, the corresponding frequencies of these amplitudes (in the

DFT) represent the equivalent probability of occurrence of these translocations (in the PDF). Thus, it is expected that the DFT results of this particle diffusion movements will be related to its PDF of translocations and accordingly, to its diffusion parameters.

Following that, the possible analytical relations between the DFT power fit parameters a and b and the PDF parameters K_α and α in conditions that included anomalous or non-ergodic diffusion were explored and described in **Supplementary Material**. Power fit parameter a was found to be correlated to the PDF parameter K_α (this compatible with the simulation experiment results presented in **Figure 2E**) while b parameter of the power fit was found to be correlated to the PDF α parameter in anomalous ergodic diffusion process. In a non-ergodic diffusion processes with a brake in symmetry that correlation between b parameter and α is expected to break also. Parameter b as being more sensitive to the brake in symmetry of the diffusion process will increase more in comparison to α .

In living cells: the applied forces that relate to intracellular mechanical work may be directional in contrary to the perfect random and symmetric thermal forces or the elastic forces of the relatively symmetric cytoskeleton mesh. Those forces due to intracellular mechanical work will break the ergodicity and the symmetry of the affected diffusion motion in cells. Following that, the high b values in this condition of non-equilibrium non-ergodic process may be the result of two contributions to b. The first contribution to b relates to large translocations (α) and the shape of the PDF. This adds to a second contribution to large translocations that relates to the breaking of ergodicity and symmetry due to mechanical work.

To summarize the expected influence on the a and b parameters of the power fit by adding mechanical work to the cellular system:

- The a parameter increases due to the increase in K_α and diffusivity associated with active cells.
- Values of b also increase due to the increase in α (power of diffusion), while added mechanical work breaks ergodicity and further increases b values.

According to these arguments, the product value of $a \cdot b$ could be used to differentiate active cells from non-active ones.

In an ergodic diffusion process, SSE values of the power fit formula that fit the spectral amplitudes of position temporal fluctuations are correlated to diffusivity, as demonstrated in **Figure 2F**. This result may be explained by the assumption that in a more dynamic system the errors from expected values should be more significant. As the dynamics of the system or variance of translocations is higher, the variance of variance (or the forth moment) will be higher as well. It is reasonable to assume that in an active, non-ergodic system the applied forces are not perfectly random and symmetric as thermal forces. Accordingly, the amplitudes spectrum in this case will be less "smooth." Thus, the SSE values of the power fit will increase further relative to the basic levels of SSE values due to the degree of dynamics of the particles and errors of measurements.

Spectral Analysis of Intracellular Particles Position Fluctuations in Jurkat T Lymphocytes Before and After ATP Depletion

In this section, we present the results of the spectral analysis of position fluctuations in time of intracellular particles in Jurkat T lymphocytes, each cell before and after ATP depletion. Specifically, we explore the relations of these results to diffusion parameters (K_α and α) that were calculated for the same cells and conditions. Depletion of cellular ATP was induced by 30 min incubation with 0.2 μM of the mitochondrial complex 1 inhibitor Rotenone (Sigma-Aldrich,St. Louis, MO, United States) together with 10 mM glycolysis inhibitor 2-deoxy-D-glucose (Sigma-Aldrich,St. Louis, MO, United States) (Guo et al., 2014). For the visualization and monitoring of intracellular objects, including vesicles, we employed Differential Interference Contrast (DIC) microscopy (**Supplementary Figure 1a**). Cells were imaged repeatedly every 0.3 s, with a total of 100 images acquired for each cell. For intracellular particle tracking we utilized the ImageJ plugin MultiTracker (Kuhn lab, the University of Texas at Austin) (Wohl and Sherman, 2019; Wohl et al., 2019). First, the x and y positions of each identified particle at each point of time (determined by the MultiTracker plug in) were recorded (**Supplementary Figures 1b–e**). Then, the DFT of these time-dependent position changes were calculated for each spatial dimension. The average DFT amplitudes of all moving particles in each cell under each condition were determined for the x and y spatial dimensions. A fit to a model of power series ($y = a/x^b$) was conducted for the DFT amplitudes results such that the parameters a, b, and SSE of the power fit could be obtained. See section "Materials and Methods" for further details on imaging and analyses.

From the position results of the detected intracellular particles, we also calculated the MSD values for time-lags form 0.3 to 3 s (with a 0.3 s gradual increase). The average MSD values were determined for that series of time-lags for each cell before and after ATP depletion. These values were fitted to a model of power series to determine the corresponding K_α and α values for the underlying diffusion process in these cells.

As expected, the K_α and α values were higher in the normal active cells, as compared to the same cells after ATP depletion (K_α: 0.023 $\mu m^2/s$ vs. 0.013 $\mu m^2/s$ with $p < 10^{-4}$. α: 0.924 vs. 0.809, with $p < 10^{-3}$).

To estimate ergodicity in the cells, we employed a basic principle which implies that in an ergodic system the distribution of translocations of a specific trajectory is not dependent on its spatial location. Following that, the distributions of translocations of all trajectories in a perfectly ergodic system are similar. In our experiment, the distribution of translocations of each trajectory or a particle is reflected by this particle's MSD results. Evaluating the heterogeneity of all particles MSD results in a cell (SD of MSD results in that cell) will produce an estimation of the ergodic level in that cell system (Krapf et al., 2018). When we compared in that way the level of ergodicity in the active cells to the level in the same cells after ATP depletion, we found (as expected) that the level of ergodicity in active

normal cells is lower than in non-active ATP-depleted cells (SD of MSD's = 0.026 μm^2 in normal cells vs. SD of MSD's = 0.018 μm^2 in ATP-depleted cells, $p = 0.01$).

We summarize in **Figure 3** the results of the DFT analysis of particles position changes in living Jurkat cells before ATP depletion and DFT results of the same living cells after ATP depletion (that inhibits cellular active mechanical work). As expected: *a*, *b*, *SSE*, and the *sum of all powers* are all higher in active live cells as compared to the same cells after ATP depletion.

Next, we evaluated the ability of these parameters, derived from spectral analysis of position fluctuations, to capture different aspects of particle motion, esp. in comparison to the prevalent anomalous diffusion parameters K_α and α. Specifically, we studied the correlation between these two groups of parameters, as shown in **Figure 4**.

Strikingly, the two groups of parameters were significantly correlated in ATP-depleted cells (**Figures 4A,C,E,G**). In non-active cells, most of mechanical forces are thermal and random. Thus, we expect that: the *a* parameter will be related to K_α, the *b* parameter will be related to α and *SSE* of the fit to the amplitudes will be related to the *SSE* of fit to the MSD values (as discussed in the previous section).

On the other hand, for cells before ATP depletion, there was no correlation between *b* and α probably due to the break in ergodicity (as also discussed above). These cells were physiologically intact and active, and produced mechanical work. Therefore, the *b* parameter values may express the break in ergodicity that is typical for living active cells.

Moreover, in active cells the correlation between *SSE* of the fit of amplitudes and the *SEE* of the fit of MSD's also seemed to break. This is probably due to the addition of forces that relates to intracellular mechanical work. These forces may act in a similar time-scale and frequencies to our observations and may directly influence the spectrum of position fluctuations related to these frequencies.

The *sum of powers* of the spectral analysis was found to be correlated to the *sum of all MSD* values under both cell conditions (**Figures 4G,H**). The sum of powers of the particles' spatial fluctuations over time may represent a summation of all modes of vibrations (in this time-scale) of these particles that are embedded in an elastic medium. Therefore, this summation of all powers relates to the total mechanical energy of this system, namely the mechanical work plus thermal energy when the system is under non-equilibrium. It relates only to thermal energy when the system is in equilibrium. The sum of MSD values represents the diffusivity of these particles. The mechanical energy and diffusivity are expected to be correlated in cellular systems both under equilibrium and non-equilibrium conditions, as shown in a previous work (Wohl and Sherman, 2019).

Next, we further wanted to test if these new parameters, which relate to the amplitudes or powers of temporal position fluctuations, have a better discriminative ability to differentiate between active working cells and non-active ATP-depleted cells in comparison to the classical diffusion parameters of K_α *and* α. We analyzed the t-statistic results that have been obtained while using each parameter to differentiate the two physiological conditions (**Figure 5**). The t-statistic values of each parameter when comparing normal active cells to the same cells after ATP depletion reflect the discriminative strength of that parameter to create two groups of results that are statistically diverse. The t-statistic values of the new parameters are higher than the t-statistic values of classical diffusion parameters. This difference is statistically significant as summarized in **Figure 5**. The discriminative ability or t-statistic of the parameter for ergodic estimation alone is the lowest (**Figure 5**; left bar).

We conclude that the new DFT-derived parameters may detect better the increase in mechanical energy that characterizes active and physiologically normal cells (in contrast to non-active ATP-depleted ones), in comparison to the classical diffusion parameters of K_α *and* α.

Spectral Analysis of Temporal Fluctuations in Cell Diameter Before and After ATP Depletion

In active cells the mechanical work of the elastic cytoskeleton augments the motion of intracellular particles (Mizuno et al., 2007; Brangwynne et al., 2009; Guo et al., 2014; Wohl and Sherman, 2019). By that it increases the amplitude of the particles' modes of vibrations and mechanical energy. This mechanical work of the elastic cytoskeleton mesh on particles that are embedded within must have a co-effect on the dynamics of the elastic mesh borders, which are intimately related to the cell membrane. In other words, the actively vibrating and elastic cytoskeletal mesh that augments the motion of embedded particles will also produce matching vibrations of its boundaries, which are mechanically coupled to the cell membrane by the cortical actin (schematically illustrated in **Figure 6A**; Salbreux et al., 2012; Chugh and Paluch, 2018). Following that, we hypothesized that monitoring fluctuations in cell diameter should exhibit similar spectral patterns to the spatial fluctuations of intracellular particles.

In order to test this hypothesis we first highlighted the cell membrane via fluorescent staining of CD45, an abundant surface glycoprotein in T cells (Donovan and Koretzky, 1993). Then we conducted fast and repetitive line-scans across the cell membrane at its apparent mid-section by confocal scanning microscopy (**Figure 6B**). Acquisition time for a single line-scan was 2 ms, using a pixel width of 50 nm. The repetitive line-scans could then be presented as a kymograph (**Figure 6C**). Cell membrane position was determined according to the pixel with the highest intensity. Cell diameter fluctuations were analyzed in each Jurkat cell before and 30 minute after ATP depletion. After DFT analysis, average amplitudes of each frequency were calculated for each experimental condition. The data were then smoothed using a moving average window of 10 data points in the spectra (i.e., 5 Hz). The average amplitudes of 14 Jurkat cells, each cell before and after ATP depletion, are presented in **Figure 7**. As a control, the average amplitudes of 20 Jurkat cells after fixation are presented as well. As can be seen in **Figure 7A** there are two distinct frequencies ranges for power fit: <3 Hz and >3 Hz. The first range of frequencies (<3 Hz) is compatible with the range of frequencies that have been explored in the previous section, utilizing repeated DIC images of intracellular particles.

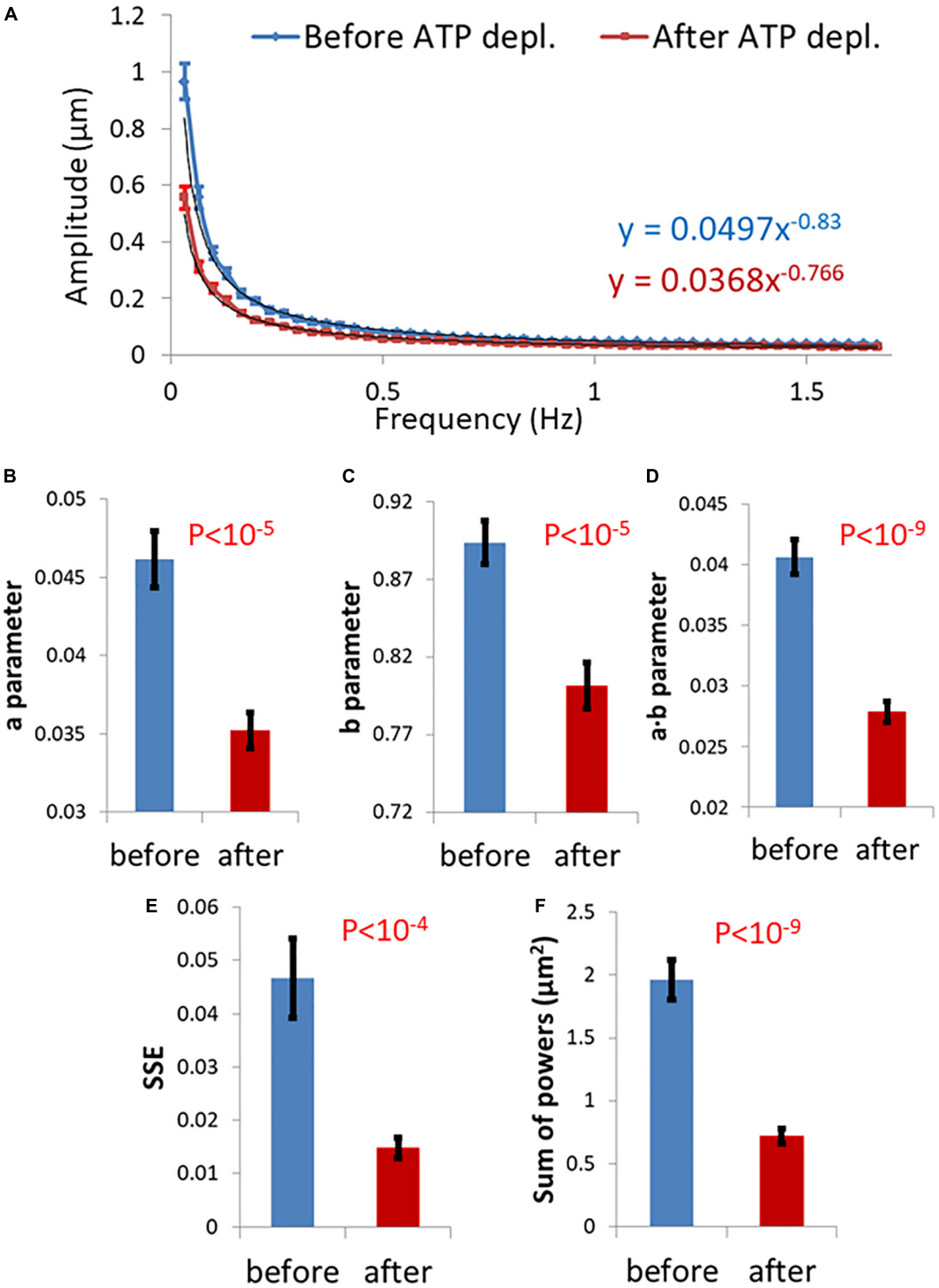

FIGURE 3 | Differential Interference Contrast (DIC) microscopy results of intracellular particles motion in live cells before and after adenosine triphosphate (ATP) depletion analyzed by amplitude spectral density (ASD) and power spectral density (PSD). **(A)** ASD analysis results in (n = 29) cells before (blue line) and after (red line) ATP depletion and the corresponding power fit parameters. **(B–E)** Power fit parameters: a, b, $a{\cdot}b$, and *SSE* for the ASD analysis results in the cells [in **(A)**] before and after ATP depletion. **(F)** Power fit parameter "*Sum of powers*" for the PSD analysis results in the cells [in **(A)**] before and after ATP depletion. Error bars in panels **(A–F)** are SEM.

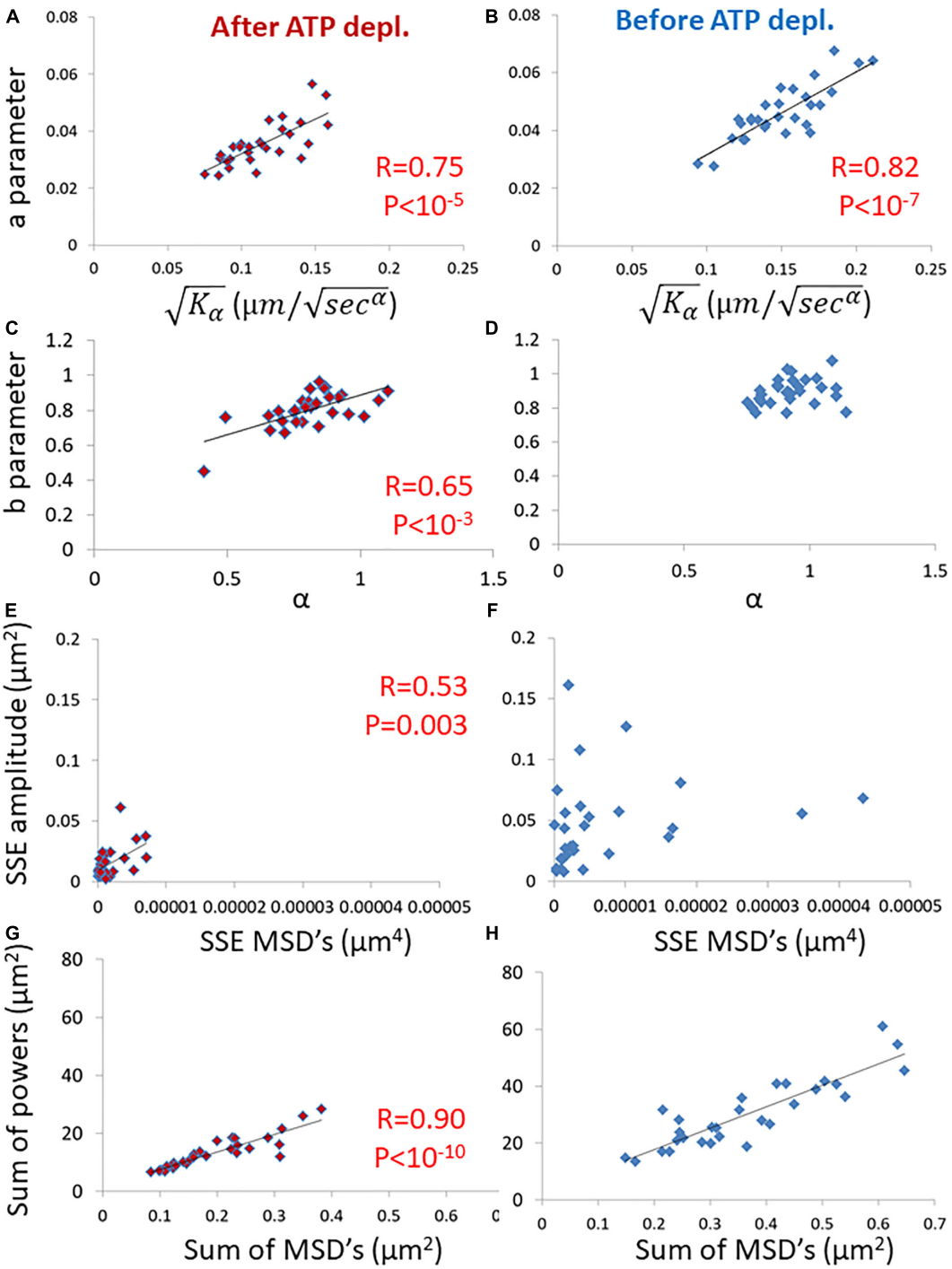

FIGURE 4 | Correlation of amplitude spectral density (ASD)/ power spectral density (PSD) parameters and mean square displacement (MSD) parameters in live cells before and after adenosine triphosphate (ATP) depletion. **(A)** The correlation between the *a* parameter of ASD analysis and $\sqrt{K_\alpha}$ of MSD analysis in ATP-depleted cells. Analyses relate to DIC microscopy results of intracellular particles motion of shown in **Figure 3** (n = 29). **(B)** The correlation between the *a* parameter of ASD analysis and $\sqrt{K_\alpha}$ of MSD analysis in cells before ATP depletion. **(C)** The correlation between the *b* parameter of ASD analysis and α of MSD analysis in ATP depleted cells. **(D)** The correlation between the *b* parameter of ASD analysis and α of MSD analysis in cells before ATP depletion. **(E)** The correlation between the SSE parameter of ASD analysis and SSE of power fit to MSD analysis in ATP depleted cells. **(F)** The correlation between the SSE parameter of ASD analysis and the sum of squared errors (SSE) of power fit to MSD analysis in cells before ATP depletion. **(G)** The correlation between "Sum of powers" parameter of PSD analysis and sum of MSD's parameter (from MSD analysis) in ATP depleted cells. **(H)** The correlation between "Sum of powers" parameter of PSD analysis and sum of MSD's parameter (from MSD analysis) in cells before ATP depletion. *R*- and *P*-values of significant correlations are presented in the corresponding correlations images.

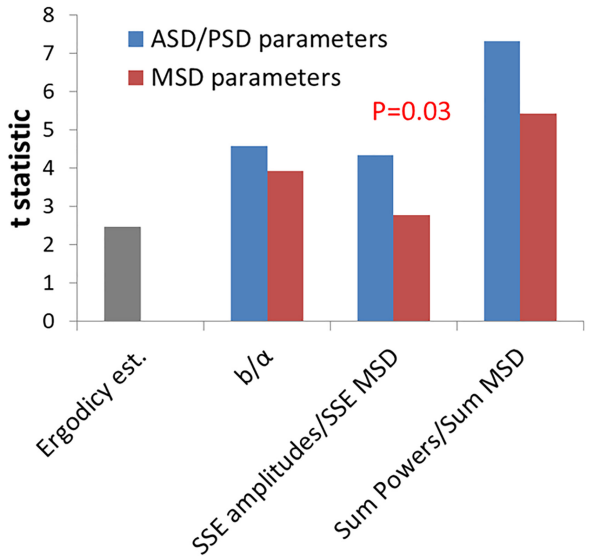

FIGURE 5 | Comparing the discrimination power of power spectral density (PSD)/amplitude spectral density (ASD) vs. mean square displacement (MSD) analyses for intracellular mechanical work. T-statistics values for the difference between cells before ATP depletion and the same cells after ATP depletion according to the two groups of parameters: ASD/PSD analysis based parameters in compare to MSD analysis based parameters. Corresponding parameters from the two groups are compared: the *b* parameter vs. α, sum of squared errors (SSE) of amplitudes vs. SSE of MSD's, and "Sum of powers" vs. Sum of MSD's. The t-statistics value for the ergodic test (described in "Results" section) is also presented. The *P*-values for the difference in t-statistics values between ASD/PSD parameters and the corresponding MSD parameters was calculated according to *t*-test for paired two samples and was found to be 0.03.

Concentrating on amplitudes in the frequency range <3 Hz (**Figure 7B**) reveals that these amplitude-spectra are similar to the amplitude-spectra obtained for DIC images of intracellular particles. According to **Figure 7E**, the *sum of powers* parameter is reduced after ATP depletion and the power fit parameters, namely *SSE* and $a \cdot b$, are also reduced (**Figures 7C,D**). As could be assumed, it seems that the elastic cytoskeleton modes of vibrations that augment the motion of large intracellular particles (meaning, larger than the mesh size) also impact the motion of the borders of that elastic mesh that are adjacent to the cell membrane. In that way, modes of vibration of the cell diameter relate to modes of vibration of intracellular particles. Both of these vibration types reflect intracellular mechanical work that is done on the elastic cytoskeleton.

Inspecting the Higher Frequencies in the Power Spectra of the Cell Diameter Fluctuations Before and After ATP Depletion

Our fast confocal imaging of the cell diameter and its fluctuations enabled us to examine also the modes of vibration of this diameter at relatively high frequencies. Specifically, we studied the amplitudes of fluctuations of cell diameter at 50–200 Hz in cells before and after ATP depletion and also in fixed cells (**Figure 8**). From these results, it seems that in the frequency range between 100 and 150 Hz, the amplitudes are less random relative to the amplitudes in the other frequency ranges.

In an ideally viscous medium in equilibrium, the spectrum of thermal forces on a particle is equivalent to white noise and independent of frequency. Thus, the power spectrum of spatial fluctuations of such a particle should be completely random and non-correlated. If correlations in the particle motion appear due to extra thermal forces, as elastic forces in the medium or forces due to mechanical work, then the amplitude spectrum of that particle motion is expected to be less random. Autocorrelation analysis of the amplitude spectra will lead to higher values and a decrease in decay with increased frequency lags. Therefore, autocorrelation analysis may differentiate an amplitude-spectrum that is more typical to ideal Brownian process or to noise from an amplitude-spectrum that is more typical to elastic forces or mechanical work.

Following this concept, three ranges of frequencies of the amplitude-spectra of the cells were analyzed for autocorrelation: 50–100 Hz, 100–150 Hz, and 150–200 Hz. In each range of frequencies, the average autocorrelation results for each lag, for each cell and for each cellular condition are presented in **Figure 9**. According to **Figure 9A**, at the 50–100 Hz range, the decay of the autocorrelation function was similar and pronounced for the fixed cells, normal and ATP-depleted cells. At the next frequencies range of 100–150 Hz, the fixed and ATP-depleted cells have similar and more pronounced decay relative to the autocorrelation function decay of normal cells. At the last frequencies range of 150–200 Hz, the decay was similar and pronounced under all cells conditions.

We assume that in ATP-depleted cells no significant mechanical work is produced. Following that assumption, it seems that the difference in the decay between normal and ATP-depleted cells in 100–150 Hz may be due to a larger extent of mechanical work in normal active cells that reduces the randomness of their amplitudes of vibrations. If elasticity was the main contributing factor in this frequency range, the decay of autocorrelation in fixed cells and ATP-depleted cells are not expected to be similar. This is since the mechanical characteristics of the intracellular medium are very different under these two conditions. Last, at the frequency ranges of 50–100 Hz and 150–200 Hz, autocorrelation decay functions under all conditions are pronounced and similar. This indicates that the measured powers in this frequency range may represent thermal agitation or noise of the measurement system.

Differences in the shape of the amplitude-spectra (**Figure 8**, compare panels b with c and d) and related autocorrelation analyses (**Figure 9B**) suggest that intracellular mechanical work can be observed and related primarily to the 100–150 Hz frequency range.

Fluctuations of Jurkat Cell Membrane in a Model of an Immune Synapse

So far, we have described intracellular fluctuations as captured by the motion of intracellular particles or by the cell boundaries. The fluctuations of the cell membrane may have an impact

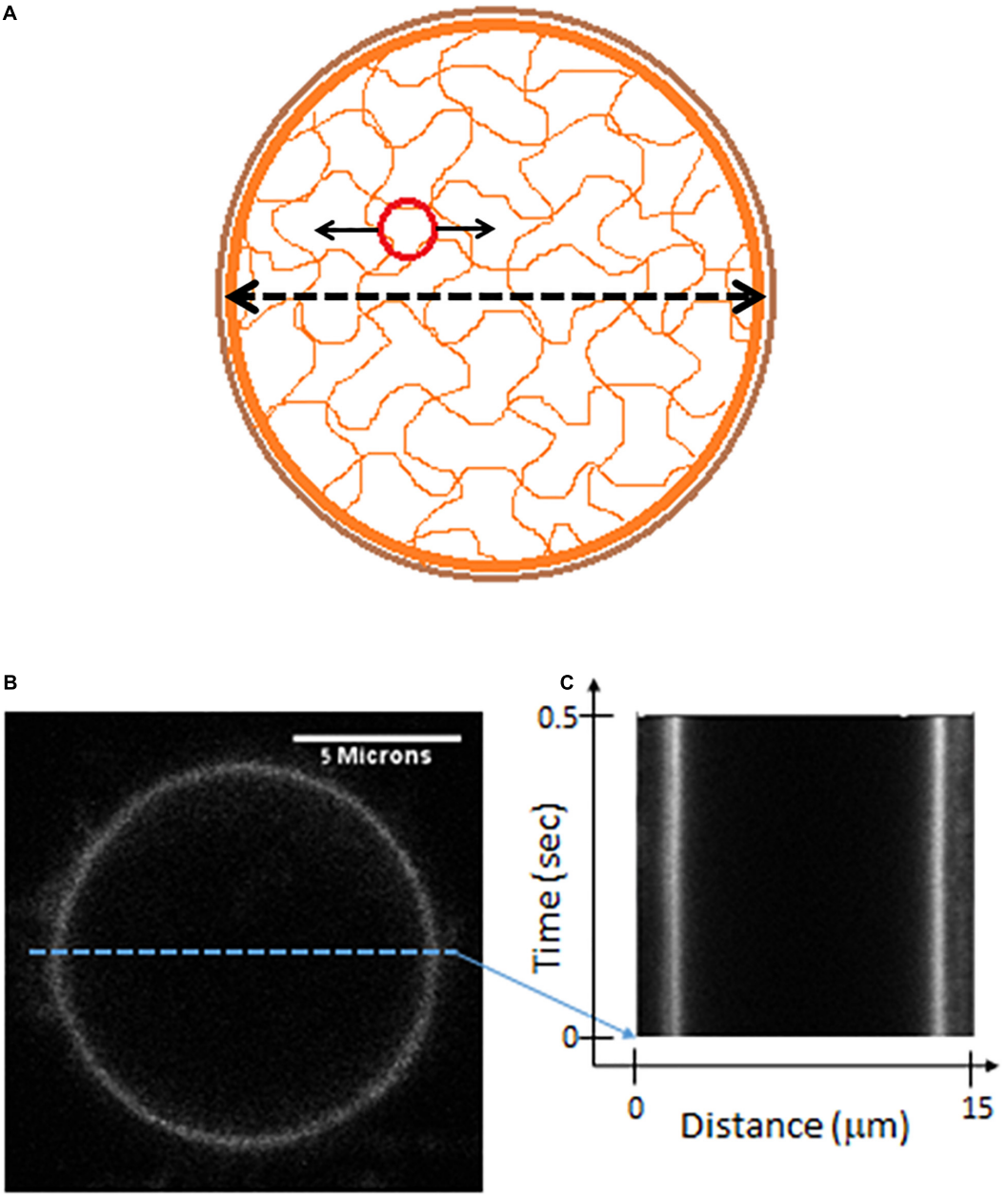

FIGURE 6 | Live cells Measurements of cell diameter fluctuations. **(A)** A scheme of the cell showing mechanical relations of its constituents. The possible mechanical relation between intracellular cytoskeleton fluctuations (that may be detected by the motion of imbedded particles) and the fluctuations of cytoskeleton borders or the cortical actin (that may be detected by following changes in cell diameter). **(B)** Confocal imaging of a live Jurkat cells, stained with CD45. **(C)** A kymograph showing fast (2 ms) and repetitive line-scans across the cell membrane at its apparent mid-section, as shown in panel **(B)**.

on the formation and function of the immune synapse that forms between T cells and antigen presenting cells (APCs) (Huppa et al., 2010; Ma and Finkel, 2010). To study such a possible impact, we measured fluctuations of Jurakt cells at their interface with coverslips coated with αCD3ε antibodies. Such coverslips often serve as a model for the immune synapse, as the cells spread on the coverslips and get robustly activated (Balagopalan et al., 2011). The membrane of the cells was stained with an αCD45 primary antibody, labeled with Alexa647 and imaged by time-lapse TIRF microscopy. Imaging in TIRF enabled sub-diffraction sensitivity of the intensity signal to membrane fluctuations along the Z-axis (perpendicular to the interface) (Balagopalan et al., 2011). For each cell, 1,000 images were captured in a time lag of 4.8 ms between each sequential image. Live cells were measured without and after ATP depletion (as described in the section "Materials and Methods"), while fixed cells served for control. In each cell, we chose for analysis a squared region of interest (ROI) of 121 pixels at

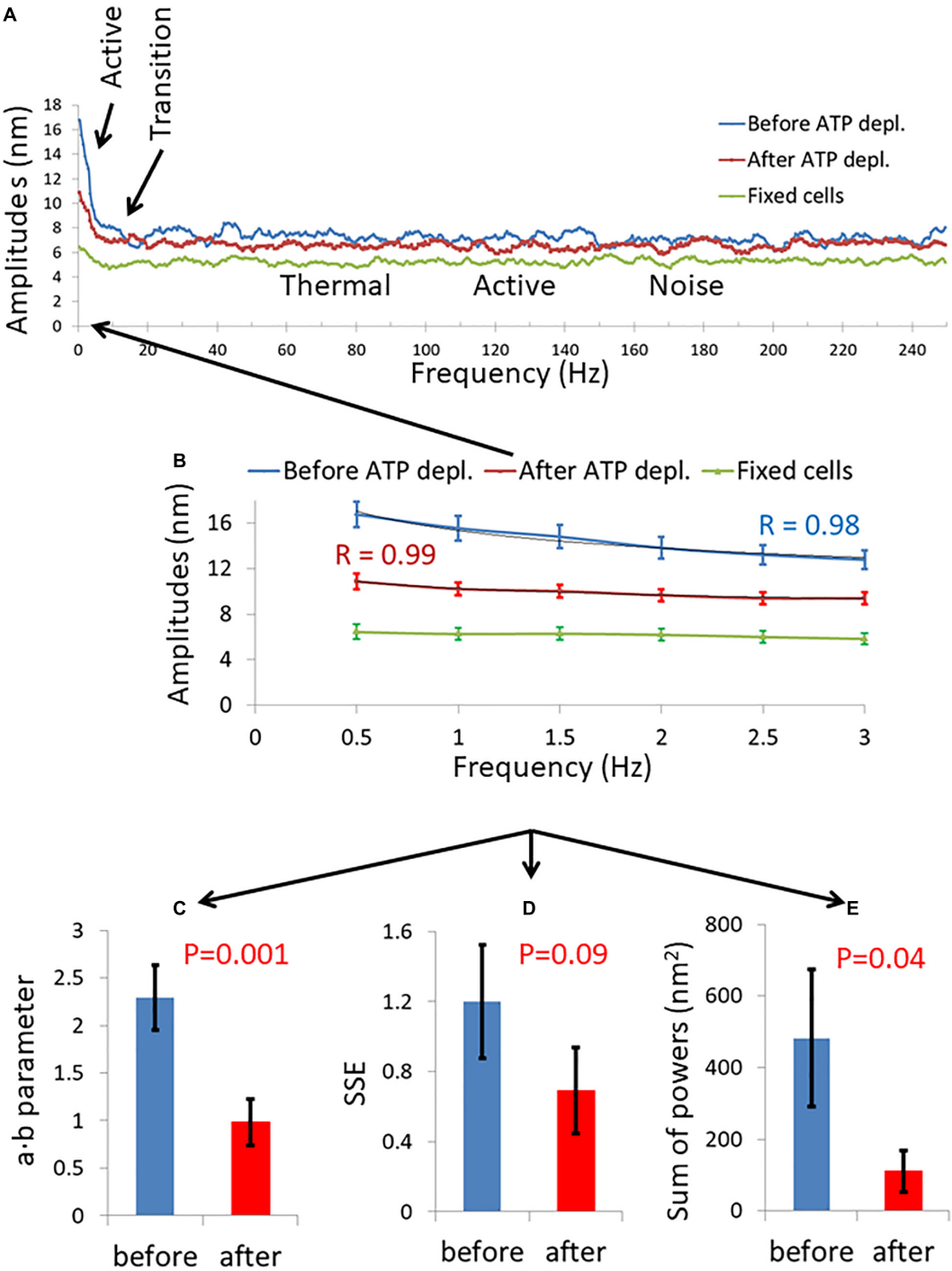

FIGURE 7 | Amplitude spectral density (ASD) and power spectral density (PSD) analysis results of live cells diameter fluctuations before and after adenosine triphosphate (ATP) depletion. **(A)** Average ASD analysis results in cells before (blue line) and after (red line) ATP depletion. Control average ASD results of 20 fixed cells are also presented (green line). Specific ranges of frequencies according to their dominant mechanism of fluctuations are highlighted. *N* = 14 cells. **(B)** Focusing on ASD results in the frequencies range of 0–3 Hz out of the total frequencies range presented in image **(A)**. R values for the power fit to the ASD results are also presented. **(C)** Average power fit parameter *a*·*b* results of the ASD analysis presented in image **(B)** before and after ATP depletion. **(D)** Average power fit parameter sum of squared errors (SSE) results of the ASD analysis presented in image **(B)** before and after ATP depletion. **(E)** Average power fit parameter "Sum of powers" results of the PSD analysis before and after ATP depletion. Error bars in **(B–E)** are SEM.

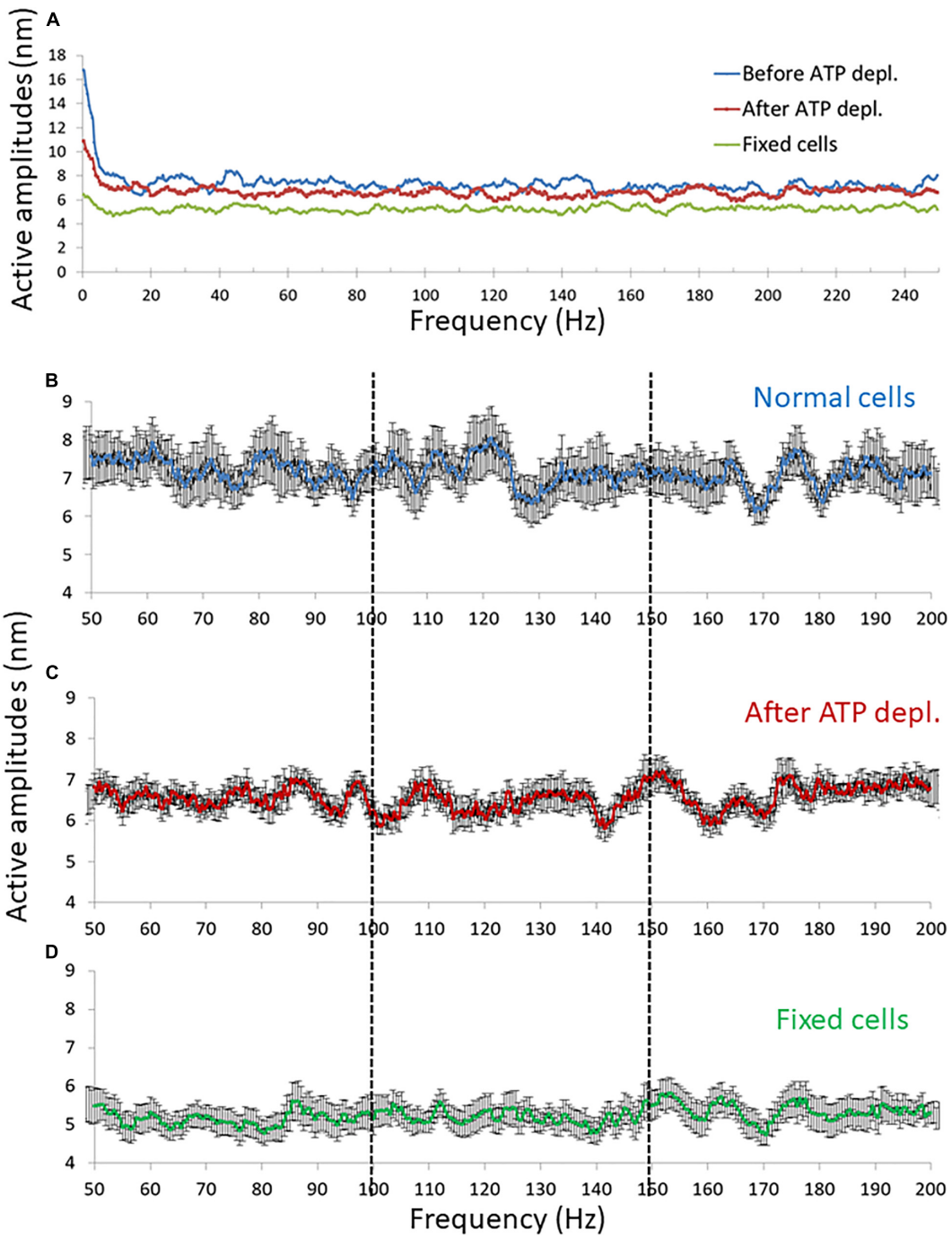

FIGURE 8 | Amplitude spectral density (ASD) results in high frequencies (>50 Hz). **(A)** Average ASD results in normal non-treated cells (*N* = 14), adenosine triphosphate (ATP) depleted cells (*N* = 14) and dead fixated cells (*N* = 20). **(B–D)** Average ASD results in the frequencies range between 50 and 200 Hz in normal non-treated cells **(B)**, ATP depleted cells **(C)**, and fixated dead cells **(D)**. Error bars in panels **(B–D)** are SEM.

the cell interface with the coverslip (see section "Materials and Methods"). The temporal fluctuations of the normalized fluorescence intensities were analyzed by DFT for each pixel in that ROI. The amplitudes were then averaged for each frequency for all the pixels of an ROI. The averaged DFT results of each ROI (or cell) could then be compared between cells and conditions and analyzed by the power fit parameters as presented in **Figure 10**.

The amplitude spectral density (ASD) results for frequencies >3 Hz (and up to 100 Hz) were similar for normal cells and cells after fixation (**Figure 10A**; green and blue curves). Measured fluctuations in fixed cells were likely due

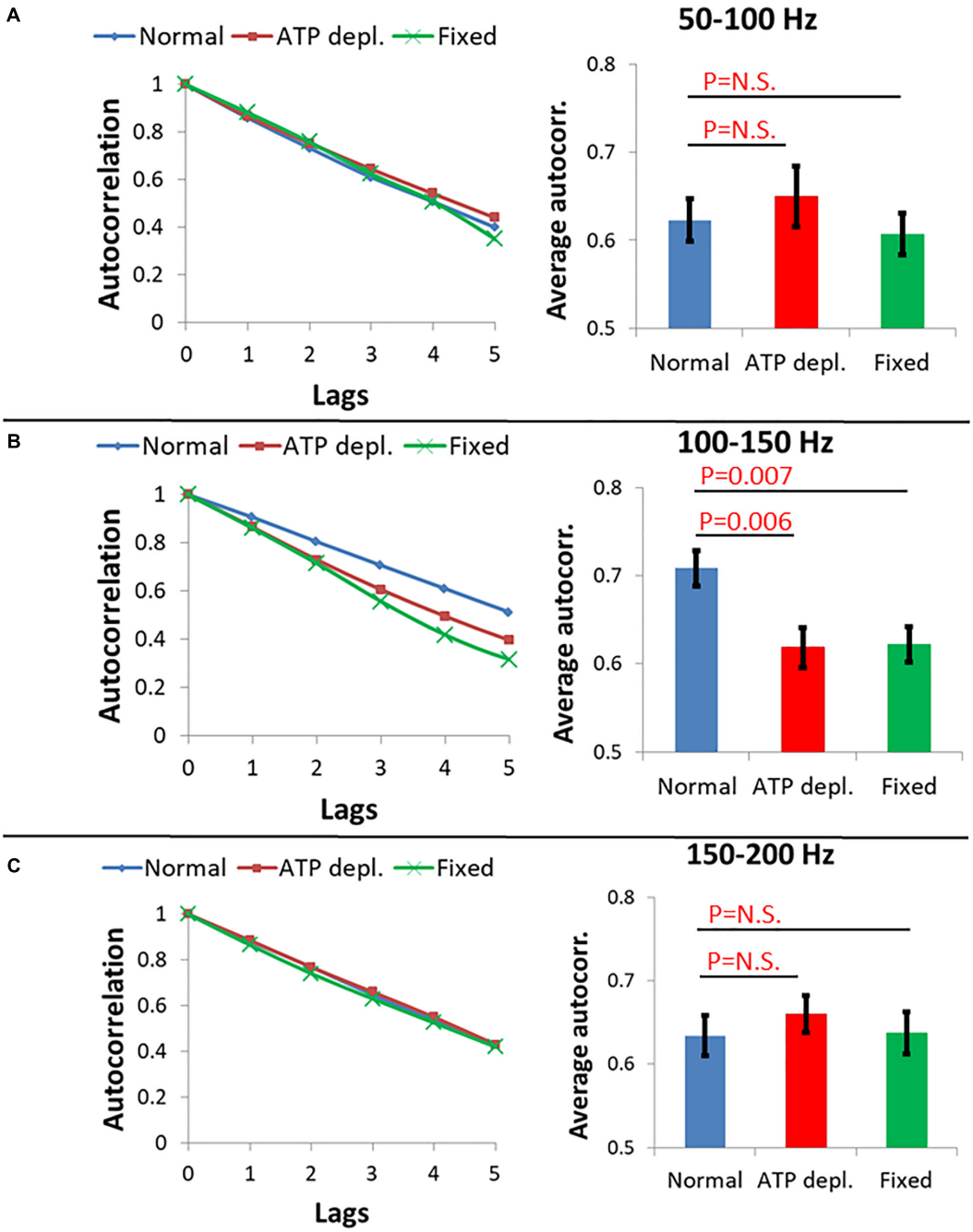

FIGURE 9 | Average autocorrelation results of Amplitude spectral density (ASD) analysis. **(A)** Average autocorrelation results of ASD in normal non-treated cells (*N* = 14), adenosine triphosphate (ATP) depleted cells (*N* = 14) and dead fixated cells (*N* = 20) in the frequencies range between 50 and 100 Hz. Results relate to the spectral data in **Figure 8**. On the right the average autocorrelation values of 1–5 lags in each cellular condition with their SD of mean are presented. **(B)** Average autocorrelation results of ASD in the normal non-treated cells, ATP depleted cells and dead fixated cells in the frequencies range between 100 and 150 Hz. On the right the average autocorrelation values of 1–5 lags in each cellular condition with their SD of mean are presented. **(C)** Average autocorrelation results of ASD in the normal non-treated cells, ATP depleted cells and dead fixated cells in the frequencies range between 150 and 200 Hz. On the right the average autocorrelation values of 1–5 lags in each cellular condition with their SD of mean are presented.

to thermal motion and noise of the measurement system. The thermal fluctuations depend on the mechanical properties (as elasticity or stiffness) of the measured system. In our synapse model, the stiffness of the coverslip governed the mechanical properties of the system and the related thermal motion in fixed and live normal cells. Otherwise, and as expected, we could not detect active fluctuations at that frequency range in live cells (see **Figure 7A**). The relatively higher level of thermal fluctuations

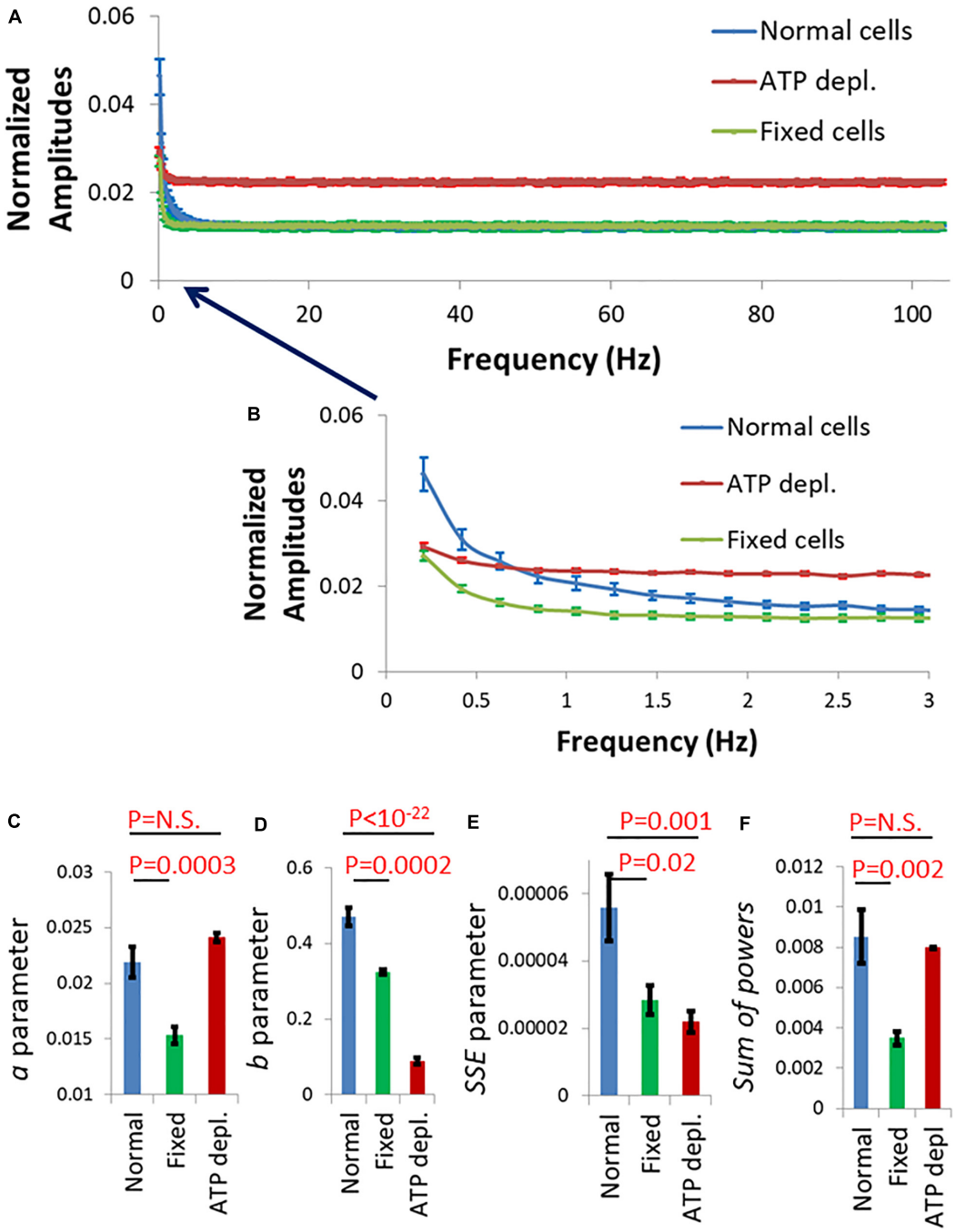

FIGURE 10 | Fluctuation of Jurkat cell membrane in a model of the immune synapse imaged by TIRF microscopy. **(A)** Discrete Fourier Transform (DFT) results of fluctuations of normalized intensity of anti-CD45 antibodies labeled with Alexa647, which highlighted the plasma membrane of Jurkat cells. The cells adhered to coverslips coated with anti-CD3ε. Amplitudes of normal cells (*N* = 30) are in blue, adenosine triphosphate (ATP) depleted cells (*N* = 33) are in red and fixed cells (*N* = 24) are in green. **(B)** Frequency range of 0–3 Hz of the amplitudes in **(A)**. Power fit parameters: *a* **(C)**, *b* **(D)**, sum of squared errors (*SSE*) **(E)**, and *Sum of powers* **(F)** results of the amplitudes presented in **(B)**. Error bars in panels **(A–F)** are SEM.

in ATP-depleted cells is probably due to an interruption of the immune synapse and some disconnection of cells from the stiff αCD3-coated coverslip.

At frequencies <3 Hz, membrane fluctuations were significantly higher in normal active cells than in fixed cells and in ATP-depleted cells (**Figure 10B**; compare blue curve to green and red curves). Also, the power fit parameters were significantly higher in normal cells relative to fixed cells (**Figures 10C–F**). Due to the suggested partial disconnection of the ATP depleted cells from the coverslip their thermal/baseline

fluctuations were higher and that increased their *a* and *sum of powers* parameters values (**Figures 10C,F**). Parameters *b* and *SSE* are less sensitive to the extent of adhesion of the cells to the coverslip since they depend mostly on the shape of the power-fit curve. Thus, *b* and *SSE* capture better the conditions of low intracellular mechanical work in those ATP depleted cells. These results suggest that ATP-dependent cytoskeletal motion significantly contribute to membrane fluctuations at low (<3 Hz) frequencies; and that these fluctuations directly modify the interface of the cells with a TCR-activating surface that mimics the immune synapse.

DISCUSSION

Here we studied active modes of vibrations of the cytoskeleton and plasma membrane in lymphocytes. Specifically, we analyzed spatial fluctuations of intracellular particles and of the cell diameter utilizing DFT analysis. The cytoskeletal motion was studied by monitoring the motion of intracellular large particles, larger than the cytoskeleton mesh size of around 50 nm (Guo et al., 2014). Such particles are typically embedded inside the cytoskeleton (Luby-Phelps, 2000). Their motion reflects cytoskeletal fluctuations due to the mechanical coupling between these particles and the surrounding elastic mesh. Cytoskeletal fluctuations could then be also reflected in fluctuations of the cell membrane and its diameter. The amplitudes of vibration of the cytoskeleton were related theoretically and experimentally to the extent of intracellular mechanical work. We could further compare mechanical vibrations in physiologically intact cells in comparison to ATP-depleted cells or cells after treatment with blebbistatin. Focusing on relative changes in the results under these various conditions largely cancels out possible contribution of extracellular effects, which are unchanged between these measurements.

The extent of mechanical vibrations in lymphocytes, especially the mechanical vibrations of the plasma membrane, could significantly impact the immune synapse (Huppa et al., 2010; Ma and Finkel, 2010). Thus, we demonstrated the existence of active, ATP-dependent vibrations of the cell membrane of Jurkat T cells after spreading and activation in an experimental model of an immune synapse. In that way, the extent of cellular mechanical vibrations may influence the ability of T lymphocytes to create stable immune synapse and to generate adequate immune response.

There are two main approaches to characterize the complex intracellular medium. If viewed as a highly complex solution, then the motion of intracellular particles could be naturally analyzed in terms of time-dependent translocations and diffusivity. Still the intracellular content can also be viewed as a two component elastic gel; i.e., an elastic polymeric mesh made of the actin cytoskeleton, immersed in crowded viscous gel. In this case, the medium would be more intuitively analyzed in terms of the spectrum of its vibrations.

The random motion of particles has been theoretically and experimentally investigated through their modes of vibration using PSD analysis. The PSD analysis is classically calculated by first performing a Fourier transform of each individual trajectory x(t) [or y(t)] over the finite observation time T and then averaging the spectral results for a statistical ensemble of all possible trajectories (Krapf et al., 2019). In some theoretical types of anomalous diffusion this analysis is not integrable. In such cases, the PSD analysis was adopted to use the Fourier transform of the autocorrelation function of the random process, since autocorrelation is integrable. This enabled to characterize the spectral contents of that non-integrable process according to Wiener–Khinchin theorem (Sposini et al., 2019). In our experiments, the number of measurements was relatively large (100), yet finite. Thus, the particles' displacement results were analyzed by DFT, while the conversion to the autocorrelation function seemed unnecessary. In each cell the results of many particles or trajectories were averaged (average number of trajectories for a cell was 39 with SD of 16) which enabled us to rely on a statistical ensemble for the amplitude spectral density (ASD) or PSD calculations, as in the classic way for calculation of these spectra.

In the case of Brownian motion the relation between powers of fluctuations and the related frequencies could be described by a power-law equation in the form:

$$\mu_s = \frac{cK_\alpha}{f^2} \tag{2}$$

where μ_s stands for the power, f is the related frequency, K_α stands for the diffusion coefficient and c is a constant (Krapf et al., 2019). From that equation the amplitude of fluctuations, A_s can be defined as

$$A_s = \frac{\sqrt{cK_\alpha}}{f^1} \tag{3}$$

In the case of FBM sub-diffusion, when $\alpha < 1$, the power of the frequency (f) is changed to $\alpha+1$ (compare to a value of 2 in Brownian motion) (Krapf et al., 2019; Sposini et al., 2019).

Our experimental results in living cells follow these theoretical equations. Indeed, we find that the PSD (or ASD) results can be accurately fitted with a power-law equation (Eq. 1). The parameter *a* derived from the fits to the experimental amplitudes were linearly correlated to the square root of diffusivity and K_α results (**Figures 4A,B**). This is expected from the theoretical relation $a = \sqrt{cK_\alpha}$. The values of the power *b* of the fit to the ASD results were relatively close to 1, as suggested by Eq. 3 for FBM. Nevertheless, the differences of *b* from 1 may be attributed to the major differences between intracellular motion and Brownian motion due to elasticity, fractal media, mechanical work and break in ergodicity (Luby-Phelps, 2000; Meroz et al., 2013; Guo et al., 2014).

Aside from the fit parameters of *a* and *b*, we considered two additional parameters: *SSE* of the power fit and *sum of powers* of the PSD analysis. We found that all of these ASD- and PSD-related parameters were sensitive to intracellular mechanical work. This work augmented the cytoskeletal vibrations via a non-ergodic process.

We found that the ASD- and PSD-related parameters could better distinguish mechanically active cells from non-active ATP-depleted cells, as compared to the regular MSD-based anomalous

diffusion parameters (**Figure 5**). The lower sensitivity of the MSD-based anomalous diffusion parameter α to respond to intracellular mechanical work may be related to fact that ATP-depletion reduces the elasticity of the cytoplasm of living cells. Accordingly, the value of α in ATP-depleted cells may be influenced by two opposing effects: First, an increase in α value due to the decrease in elasticity upon ATP depletion (Guo et al., 2014); Second, a decrease in α due to the decrease in motivated random forces (Brangwynne et al., 2009). On the other hand, the corresponding parameter *b* of the ASD analysis is influenced also by the break in ergodicity that accompanies the increase in intracellular mechanical work. This sensitivity of *b* to non-ergodic processes may improve its ability to detect the effect of the increase in intracellular dynamics, associated with intracellular mechanical work.

Incoherent forces due to intracellular mechanical work may be applied at different locations on the cytoskeleton, each with its own frequency. Such forces are expected to make the ASD results of cytoskeletal fluctuations more complex, lowering the quality of a fit to a relatively simple power-law model. In this situation the system could be characterized as having relatively high energetic disorder, which directly relates to lower ergodicity. In contrast, ASD results of the same network experiencing only thermal forces (i.e., "white noise" forces that don't have any frequency preference) will more accurately follow a fit of a power-law model. Accordingly, *SSE* values are higher in normal active cells in comparison to non-active ATP-depleted cells. Again, these differences are due to the addition of mechanical forces and break in ergodicity in active cells. Measuring the parameter of *Sum-of-powers* is a relatively direct way to evaluate the mechanical energy of the vibrating system—in this case the cytoskeleton.

The calculation procedure of the ASD or PSD fluctuation parameters seems to be simpler and more automatic in comparison to the calculation of MSD parameters. MSD analyses require taking statistical measurements of multiple displacement results that relate to different time-lags for each particle.

The cytoskeletal vibrations could be monitored by motion of particles that are embedded within it but also by the motion of it borders- namely, the cortical actin and the adjacent cell membrane. Analyzing fluctuations in cell diameter by ASD and PSD calculations that were conducted in the same cells before and after ATP-depletion revealed compatible results with the ASD and PSD analysis of intracellular particles motion. The power fit parameters of cell diameter fluctuations $a \cdot b$ and the *sum of powers* were higher in normal active cells, as compared to the same cells after ATP depletion.

Our confocal microscope line-scan imaging of fluctuations of the cell diameter enabled to conduct ASD analyses over a wide range of frequencies. Thus, we could define several specific ranges of frequencies, each with a dominant underlying mechanism (**Figure 7A**). These mechanisms control the amplitude of the cytoskeletal fluctuations in their related spectral range, as follows: At 0–3 Hz cytoskeletal fluctuations are governed by incoherent fraction of ATP-dependent molecular motors (such as myosin II) forces, as suggested by Guo et al. (2014). This mechanism may also explain our DIC results of the motion of intracellular particles that were measured in similar lower frequencies (**Figure 3**). To further support this suggested mechanism we conducted similar experiments to those presented in **Figure 3** with cells treated with the myosin II inhibitor blebbistatin (**Supplementary Figure 2**). The effects on intracellular motion of blebbistatin treatment and ATP depletion were similar (compare **Figure 3** and **Supplementary Figure 2**). These findings support the role of myosin II motors in the generation of our described intracellular mechanical work and active motion. At the successive range of frequencies below 100 Hz, thermal agitation dominates. This was also suggested by Guo et al. (2014), and is also supported by our current findings (**Figure 9A**). Interestingly, analysis of cell diameter fluctuations at 100–150 Hz indicated that active, ATP-dependent mechanical fluctuations likely dominate in this frequency range. We propose that active mechanical tension fluctuations and tension generation of the cortical actin may explain these results (Wohl et al., 2020), but this assumption requires further validation.

We note that the T cell surface is covered with mobile microvilli. Microvilli mobility has been shown to depend on actin remodeling, and occurs over time scales of seconds to tens-of-seconds (Cai et al., 2017). Since our measurements of cell diameter relies on the identification of a stain of the plasma membrane, they could in principle capture some of the microvilli dynamics and interfere with our diameter measurements. However, our spectra are focused on relatively faster processes (of 0.5–3 Hz) than actin remodeling (Walker et al., 2020). Moreover, we show in previous studies that our measured spectra correlate with forces and volume changes that occur at the borders of the cell with similar spectra to our current measurements (Wohl et al., 2020). These findings support that active cell fluctuations dominate our measured spectra. Still, a possible contribution from microvilli dynamics on our measurements cannot be completely ruled out at the lowest frequencies.

TCR activation has been shown to be a dynamic process, in which the TCR-pMHC bond is repeatedly ruptured and reconnected by perpendicular forces to the immune synapse plane. Rupture forces acting on the TCR-CD3-pMHC bond promote conformational changes of the TCR chains that promote TCR activation (Ma and Finkel, 2010). Specifically, these conformational changes enables exposure and phosphorylation of immunoreceptor tyrosine-based activation motifs (ITAMs) on the TCR intracellular chains and further propagation of T cell activation signals (Hwang et al., 2020). Here, we have shown that cytoskeleton vibrations may result in corresponding vibrations of the cell diameter and plasma membrane. The matching of the TCR-CD3-pMHC bond strength and pulling forces at the synapse could enable specificity of the TCR response. Repeated triggering of the TCR by cell vibrations could further provide sensitivity and specificity to this response (Ma and Finkel, 2010). The described force strength and frequency through this process are around 10 pN and 1 Hz (Limozin et al., 2019). According to our results of cell diameter fluctuations (**Figure 7B**), the perpendicular component of the cell membrane fluctuations at 1 Hz has an amplitude of ∼16 nm. From previous AFM measurements (Wohl et al., 2020), the tension fluctuations of the (Jurkat) cell surface at 1 Hz have an amplitude of ∼0.001 μN/μm. Multiplying the

tension fluctuations of 0.001 μN/μm and spatial movements of 16 nm produces forces of ∼16 pN due to this motion. Thus, we conclude that the scales of forces and frequencies related to our measured membrane fluctuations are suitable for activating engaged TCRs at the immune synapse. In that way, lymphocyte vibrations may control or interfere with the T cells' ability to respond to important immunological stimuli.

Here, we studied intracellular and membrane vibrations in Jurkat cells that originated from human leukemic T cells. Malignant cells typically have increased active mechanical fluctuations at relatively low frequencies (below 3 Hz) (Lau et al., 2003; Guo et al., 2014). They also have a softer surface (Xu et al., 2012; Hayashi and Iwata, 2015), which depends mainly on the degree of cortical actin tension. If indeed fluctuations of the T cell membrane contribute to sensitivity and specificity of TCR-pMHC interactions, these properties of (non-adherent) malignant cells could hinder the ability of the T cell to properly recognize and react against the malignant cells. Specifically, the T cell may not be able to accurately evaluate the affinity of the TCR-pMHC bond, and to create repeated and sufficient TCR deformations for maximal triggering of the TCR. By this mechanism, transformed cells may escape immune surveillance and killing by cytotoxic T cells (this mechanism is illustrated in **Figure 11**).

We conclude that spectral analysis (either ASD or PSD) may provide a simple and effective technique to study active cellular vibrations and the overall mechanical activity of cells. Active vibrations of the cell membrane may influence lymphocyte ability to respond to immunological cues and may further enable malignant cells to escape immunological surveillance.

MATERIALS AND METHODS

Materials

Complete Medium (medium): RPMI-1640, DMEM medium, heat-inactivated fetal calf serum (FCS), penicillin, streptomycin, glutamine, sodium pyruvate, and HEPES obtained from Biological Industries (Kibbutz Beit Haemek, Israel). Rotenone and 2-deoxy-d-glucose from Sigma-Aldrich (St. Louis, MO, United States). CD45 proteins were purchased from BioLegend. Anti-human CD3 from eBioscience Inc. (Thermo Fisher Scientific). Blebbistatin was purchased from Sigma-Aldrich (St. Louis, MO, United States).

Cell Line

Jurkat (human leukemic) E6.1 ($CD4^+$) T cells were a kind gift from the Samelson lab at the NIH. Jurkat cells were maintained in RPMI-1640 medium supplemented with 10% FCS, 100 U/ml penicillin, 100 μg/ml streptomycin, 2% glutamine, 2% sodium pyruvate and 2% HEPES. Cells were maintained in completely humidified air with 5% CO2 at 37°C.

Immunostaining

CD45 proteins were labeled using mouse anti-human primary antibodies conjugated to Alexa647 fluorophore (BioLegend, 304056). Labeling procedure followed the manufacturers' protocols. Briefly, 0.5 μg of mouse anti human anti-CD45 monoclonal antibody conjugated to Alexa647 was added to 500×10^3 cells suspended in FACS buffer for 45 min on ice. Cells were then washed in phosphate buffered saline (PBS) for three times and suspended in imaging buffer (RPMI without phenol red, 10% FBS, 25 mM HEPES).

Sample Preparation

Coverslip preparation was as follows: coverslips (#1.5 glass chambers, iBidi) were washed with acidic ethanol at room temperature (RT) for 10 min and dried at 37°C for 1 h. Coverslips were than incubated at RT for 15 min with 0.01% poly-L-lysine (Sigma) diluted in water. This was followed by washing and drying of the coverslips at 37°C for 1 h. For the immune synapse model experiment the poly-L-lysine covered coverslips were incubated for 2 h at 37°C with 10 μg/ml anti CD3 antibodies diluted in PBS. Than the chambers were washed three times with PBS and left with PBS till the application of cells. Finally, cells were suspended in imaging buffer at a concentration of 1 million and 100,000–500,000 cells and were applied onto coverslips.

Cells Fixation

Paraformaldehyde (PFA) 4% was added to the cells medium while on the coverslips in a ratio of 3/2 for 45 min incubation afterword all liquid were gently aspirated and replaced with imaging buffer (RPMI without phenol red, 10% FBS, 25 mM HEPES).

Treatment of Jurkat Cells With Blebbistatin or Rotenone and 2-Deoxy-D-Glucose

Upon completion of measurements in all the cells and after recording the location of each cell, blebbistatin 10 μM or Rotenone 0.2 μM and 10 mM 2-deoxy-d-glucose were added to the cells medium. The samples were than incubated for 30 min on the microscope stage. At the end of incubation, each cell was measured again according to its recorded location. We excluded from analysis moving cells that may have changed their location during measurements.

Microscope

Differential interference contrast (DIC) image stacks were taken with FV-1200 confocal microscope (Olympus, Japan) equipped with an environmental incubator (temperature and CO2) using a 60×/1.42 oil objective.

Confocal microscopy: Jurkat cells were imaged using an Abberior Expertline confocal/STED microscope (Abberior Instruments, Göttingen, Germany), mounted on a TiE Nikon microscope and operated by the Imspector software (v0.13.11885; Abberior Instruments, Göttingen, Germany). The cells were excited using a 638 mn pulsed laser (90 ps) 2 mW/cm2 at 50% power for x-t live cell experiments. Samples were imaged with a (CFI-SR-HP) Apochromat TIRF X100 NA 1.49 oil immersion objective (Nikon Instruments). Image stacks were generated by taking 1,000 serial images with acquisition time of 2 ms for frames of unidirectional 300 pixels (50 nm pixel size, 5 μs pixel dwell time). The reflection light was detected using an APD with

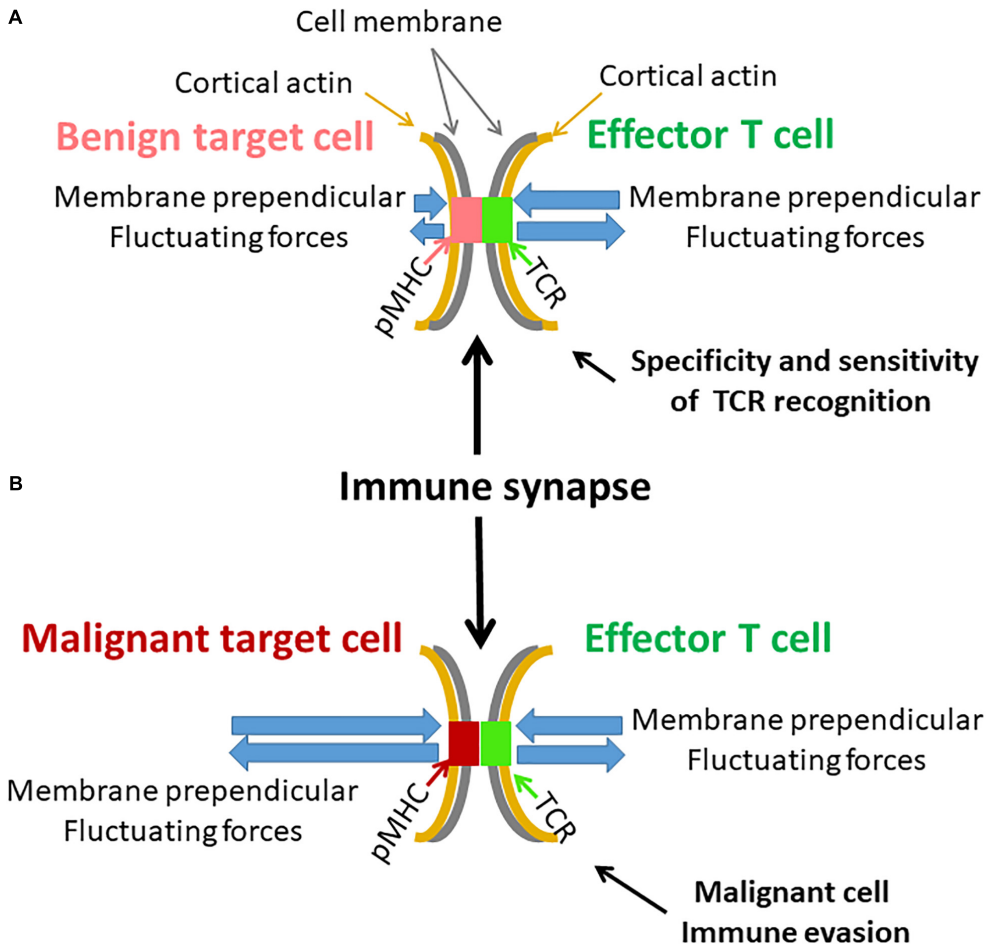

FIGURE 11 | Possible effects of cell membrane fluctuations on T cell function. **(A)** An illustration of an immune synapse between an effector T cell with its specific TCR and a benign target cell with a complimentary pMHC. Both cell membranes and their attached cortical actin are mechanically vibrating but to a different extent. Resultant perpendicular forces act on the TCR-pMHC complex, leading to its modified lifetime. The benign target cell membrane is relatively firm and stable. The more pronounced membrane fluctuations of the effector T cell could effectively produce repeated and precise rupture forces on the TCR-pMHC complex to generate effective cellular response. **(B)** A similar illustration of an immune synapse between effector T cell and a malignant target cell. The malignant target cell membrane and its underlying cortical actin are less firm and fluctuate more relative to benign cells [as in panel **(A)**]. The fluctuations of the effector T cell are milder relative to the membrane fluctuations of the malignant target cell. Thus, the TCR-pMHC complex is subject to incoherent forces, abrogating precise and organized activation of the TCR and the effector T cell. This may further lead to possible immune evasion of the malignant cell.

a band-pass filter of 650–720 nm and a pinhole setting of 1.1 Airy units. Each line was scanned once.

TIRF microscopy: Jurkat cells were imaged using a TiE Nikon microscope. The cells were excited using a 647 mn pulsed laser (90 ps) at 2 mW/cm^2 (20% power). Samples were imaged using a (CFI-SR-HP) Apochromat TIRF X100, NA of 1.49, oil-immersion objective (Nikon Instruments). Image stacks were generated by taking 1,000 serial images with an acquisition time of 4.8 ms per individual frames of 128 × 128 pixels (160 nm pixel size). The reflection light was detected using an avalanche photodiode (APD) with a band-pass filter of 650–720 nm.

TIRF images analysis: In each cell, a squared ROI of 121 pixels was chosen at the cell interface with the coverslip. Fluorescence intensity of each pixel in each image was normalized by dividing its intensity with the average intensity of that time-dependent image. The temporal fluctuations of the normalized fluorescence intensities were analyzed by DFT for each pixel in a ROI. The amplitudes of the DFT analyzes were then averaged for each frequency for all the pixels of an ROI to obtain the averaged DFT results of each ROI (or cell) in each condition.

MSD Calculations

Jurkat cells were measured using a microscope in DIC mode, utilizing × 60 magnification and conditions that were described in detail in the previous sections. The measurements included repeated measurements every 0.3 s over a time window of 30 s. This measurement time allowed us to effectively avoid the constrains of the limited cell size (up to ∼10 μm) on diffusion. The cell image stacks were first converted to 8-bit images and thresholded (yielding binary images) to segment individual entities for tracking. **Supplementary Figure 1** shows an example of DIC imaging of a representative Jurkat cell, before and after

thresholding, on which particle tracking analysis was performed.

We defined thresholding levels according to the histogram of gray levels of the images. We noticed that a small range of thresholding values (in gray levels) were appropriate for segmentation, since too narrow threshold values caused fragmentation of the objects into isolated pixels, whereas threshold values that were too wide resulted in object contour thickening and unification. Analyzing the size distribution of the segmented objects, revealed that most of these objects were in the size range of intracellular vesicles or organelles (0.15 to ∼1.17 μm, average diameter 0.5 μm). Particles diameter were similar in cells before and after ATP depletion.

Further analyses of MSD statistics and fitting ("one term power series model fit") were carried out using Matlab R2017b (MathWorks). Calculations of MSD values of intracellular objects were performed using the ImageJ plugin MultiTracker (The Kuhn lab; The University of Texas at Austin).

Statistical Analyses

The acquired data was exported to Excel spreadsheets (Microsoft Office Professional plus 2010, Microsoft Inc., Redmond, Washington, United States) for graph and table presentation and for statistical analysis with Real Statistic Resource pack. Significance of differences between groups was calculated using Analysis of Variance (ANOVA) single factor function or *t*-test for paired two samples, with statistical significance set at $p < 0.05$.

The experimental results are shown from same-day experiments. The results were verified to be similar to those of 1–2 additional independent experiments (which are not shown).

DATA AVAILABILITY STATEMENT

The original contributions presented in the study are included in the article/**Supplementary Material**, further inquiries can be directed to the corresponding author/s.

AUTHOR CONTRIBUTIONS

ES supervised the research. ES and IW designed the research and wrote the manuscript. IW performed the research. Both authors contributed to the article and approved the submitted version.

FUNDING

This research was supported by Grant No. 1761/17 from the Israeli Science Foundation.

ACKNOWLEDGMENTS

We thank Naomi Book (The Silberman Institute at HUJI) for her assistance with DIC microscopy.

SUPPLEMENTARY MATERIAL

The Supplementary Material for this article can be found online at: https://www.frontiersin.org/articles/10.3389/fcell.2021.590655/full#supplementary-material

REFERENCES

Balagopalan, L., Sherman, E., Barr, V. A., and Samelson, L. E. (2011). Imaging techniques for assaying lymphocyte activation in action. *Nat. Rev. Immunol.* 11, 21–33. doi: 10.1038/nri2903

Brangwynne, C. P., Koenderink, G. H., Mackintosh, F. C., and Weitz, D. A. (2009). Intracellular transport by active diffusion. *Trends Cell Biol.* 19, 423–427.

Cai, E., Marchuk, K., Beemiller, P., Beppler, C., Rubashkin, M. G., Weaver, V. M., et al. (2017). Visualizing dynamic microvillar search and stabilization during ligand detection by T cells. *Science* 356:eaal3118. doi: 10.1126/science.aal3118

Cartwright, J. H. E., Piro, O., and Tuval, I. (2009). Fluid dynamics in developmental biology?: moving fluids that shape ontogeny. *HFSP J.* 3, 77–93. doi: 10.2976/1.3043738

Caspi, A., Granek, R., and Elbaum, M. (2000). Enhanced diffusion in active intracellular transport. *Phys. Rev. Lett.* 85, 5655–5658. doi: 10.1103/physrevlett.85.5655

Chakraborty, A. K., and Weiss, A. (2014). Insights into the initiation of TCR signaling. *Nat. Immunol.* 15, 798–807. doi: 10.1038/ni.2940

Chugh, P., and Paluch, E. K. (2018). The actin cortex at a glance. *J. Cell Sci.* 131:jcs186254.

Delfino, G., and Squarcini, A. (2016). Long range correlations generated by phase separation. Exact results from field theory. *J. High Energy Phys.* 11:119.

Donovan, J. A., and Koretzky, G. A. (1993). CD45 and the immune response. *J. Am. Soc. Nephrol.* 4, 976–985. doi: 10.1681/asn.v44976

Geisel, T., Zacherl, A., and Radons, G. (1987). Generic 1/f noise in chaotic hamiltonian dynamics. *Phys. Rev. Lett.* 59:2503.

Golan, Y., and Sherman, E. (2017). Resolving mixed mechanisms of protein subdiffusion at the T cell plasma membrane. *Nat. Commun.* 8:15851.

Granek, R., and Pierrat, S. (1999). Enhanced transverse diffusion in active biomembranes. *Phys. Rev. Lett.* 83, 872–875. doi: 10.1103/physrevlett.83.872

Guo, M., Ehrlicher, A. J., Jensen, M. H., Renz, M., Moore, J. R., Goldman, R. D., et al. (2014). Probing the stochastic, motor-driven properties of the cytoplasm using force spectrum microscopy. *Cell* 158, 822–832. doi: 10.1016/j.cell.2014.06.051

Hayashi, K., and Iwata, M. (2015). Stiffness of cancer cells measured with an AFM indentation method. *J. Mech. Behav. Biomed. Mater.* 49, 105–111. doi: 10.1016/j.jmbbm.2015.04.030

Houel, J., Doan, Q. T., Cajgfinger, T., Ledoux, G., Amans, D., Aubret, A., et al. (2015). Autocorrelation analysis for the unbiased determination of power-law exponents in single-quantum-dot blinking. *ACS Nano* 9, 886–893. doi: 10.1021/nn506598t

Huang, S., and Ingber, D. E. (2005). Cell tension, matrix mechanics, and cancer development. *Cancer Cell* 8, 175–176. doi: 10.1016/j.ccr.2005.08.009

Huppa, J. B., Axmann, M., Mörtelmaier, M. A., Lillemeier, B. F., Newell, E. W., Brameshuber, M., et al. (2010). TCR-peptide-MHC interactions in situ show accelerated kinetics and increased affinity. *Nature* 463, 963–967. doi: 10.1038/nature08746

Hwang, J. R., Byeon, Y., Kim, D., and Park, S. G. (2020). Recent insights of T cell receptor-mediated signaling pathways for T cell activation and development. *Exp. Mol. Med.* 52, 750–761. doi: 10.1038/s12276-020-0435-8

Jeon, J. H., Tejedor, V., Burov, S., Barkai, E., Selhuber-Unkel, C., Berg-Sørensen, K., et al. (2011). In vivo anomalous diffusion and weak ergodicity breaking of lipid granules. *Phys. Rev. Lett.* 106, 28–30.

Krapf, D., Lukat, N., Marinari, E., Metzler, R., Oshanin, G., Selhuber-Unkel, C., et al. (2019). Spectral content of a single non-brownian trajectory. *Phys. Rev. X* 9:11019.

Krapf, D., Marinari, E., Metzler, R., Oshanin, G., Xu, X., and Squarcini, A. (2018). Power spectral density of a single Brownian trajectory: what one can and cannot learn from it. *New J. Phys.* 20:23029.

Lau, A. W. C., Hoffman, B. D., Davies, A., Crocker, J. C., and Lubensky, T. C. (2003). Microrheology, stress fluctuations, and active behavior of living cells. *Phys. Rev. Lett.* 91, 1–4.

Limozin, L., Bridge, M., Bongrand, P., Dushek, O., van der Merwe, P. A., and Robert, P. T. C. R. (2019). –pMHC kinetics under force in a cell-free system show no intrinsic catch bond, but a minimal encounter duration before binding. *Proc. Natl. Acad. Sci. U.S.A.* 116, 16943–16948. doi: 10.1073/pnas.1902141116

Luby-Phelps, K. (2000). Cytoarchitecture and physical properties of cytoplasm: volume, viscosity, diffusion, intracellular surface area. *Int. Rev. Cytol.* 192, 189–221. doi: 10.1016/s0074-7696(08)60527-6

Ma, Z., and Finkel, T. H. (2010). T cell receptor triggering by force. *Trends Immunol.* 31, 1–6. doi: 10.1016/j.it.2009.09.008

Manfred, S., and Woehlke, G. (2003). Molecular motors. *Nature* 422, 45–55.

Meroz, Y., Sokolov, I. M., and Klafter, J. (2013). Test for determining a subdiffusive model in ergodic systems from single trajectories. *Phys. Rev. Lett.* 110, 1–4. doi: 10.1017/etds.2020.96

Mizuno, D., Tardin, C., Schmidt, C. F., and MacKintosh, F. C. (2007). Nonequilibrium mechanics of active cytoskeletal networks. *Science* 315, 370–373. doi: 10.1126/science.1134404

Salbreux, G., Charras, G., and Paluch, E. (2012). Actin cortex mechanics and cellular morphogenesis. *Trends Cell Biol.* 22, 536–545. doi: 10.1016/j.tcb.2012.07.001

Shneidman, V. A., Jung, P., and Hänggi, P. (1994). Power spectrum of a driven bistable system. *Europhys. Lett.* 26:571. doi: 10.1209/0295-5075/26/8/003

Sposini, V., Metzler, R., and Oshanin, G. (2019). Single-Trajectory spectral analysis of scaled Brownian motion. *New J. Phys.* 21:73043.

Tee, S. Y., Bausch, A. R., and Janmey, P. A. (2010). The mechanical cell. *Curr. Biol.* 19, R745–R748.

Walker, M., Rizzuto, P., Godin, M., and Pelling, A. E. (2020). Structural and mechanical remodeling of the cytoskeleton maintains tensional homeostasis in 3D microtissues under acute dynamic stretch. *Sci. Rep.* 10:7696.

Weiss, M. (2013). Single-particle tracking data reveal anticorrelated fractional Brownian motion in crowded fluids. *Phys. Rev. E Stat. Nonlin. Soft Matter Phys.* 88:010101.

Wohl, I., and Sherman, E. (2019). ATP-dependent diffusion entropy and homogeneity in living cells. *Entropy* 21, 962–980. doi: 10.3390/e21100962

Wohl, I., Yakovian, O., Razvag, Y., Reches, M., and Sherman, E. (2020). Fast and synchronized fluctuations of cortical actin negatively correlate with nucleoli liquid–liquid phase separation in T cells. *Eur. Biophys. J.* 49, 409–423. doi: 10.1007/s00249-020-01446-9

Wohl, I., Zurgil, N., Hakuk, Y., Sobolev, M., and Deutsch, M. (2019). Discrimination of leukemic Jurkat cells from normal lymphocytes via novo label – free cytometry based on fluctuation of image gray values. *Eur. Biophys. J.* 48, 267–275. doi: 10.1007/s00249-019-01351-w

Xu, W., Mezencev, R., Kim, B., Wang, L., McDonald, J., and Sulchek, T. (2012). Cell stiffness is a biomarker of the metastatic potential of ovarian cancer cells. *PLoS One* 7:e46609. doi: 10.1371/journal.pone.0046609

Conflict of Interest: The authors declare that the research was conducted in the absence of any commercial or financial relationships that could be construed as a potential conflict of interest.

frontiers in Cell and Developmental Biology

ORIGINAL RESEARCH
published: 14 June 2021
doi: 10.3389/fcell.2021.646077

WASp Is Crucial for the Unique Architecture of the Immunological Synapse in Germinal Center B-Cells

Yanan Li[1,2,3], Anshuman Bhanja[3], Arpita Upadhyaya[4,5], Xiaodong Zhao[1,2] and Wenxia Song[3]*

[1] Department of Rheumatology and Immunology, Children's Hospital of Chongqing Medical University, Chongqing, China, [2] Ministry of Education Key Laboratory of Child Development and Disorders, Chongqing Key Laboratory of Child Infection and Immunity, China International Science and Technology Cooperation Base of Child Development and Critical Disorders, National Clinical Research Center for Child Health and Disorders, Chongqing, China, [3] Department of Cell Biology and Molecular Genetics, University of Maryland, College Park, College Park, MD, United States, [4] Department of Physics, University of Maryland, College Park, College Park, MD, United States, [5] Institute for Physical Science and Technology, University of Maryland, College Park, College Park, MD, United States

B-cells undergo somatic hypermutation and affinity maturation in germinal centers. Somatic hypermutated germinal center B-cells (GCBs) compete to engage with and capture antigens on follicular dendritic cells. Recent studies show that when encountering membrane antigens, GCBs generate actin-rich pod-like structures with B-cell receptor (BCR) microclusters to facilitate affinity discrimination. While deficiencies in actin regulators, including the Wiskott-Aldrich syndrome protein (WASp), cause B-cell affinity maturation defects, the mechanism by which actin regulates BCR signaling in GBCs is not fully understood. Using WASp knockout (WKO) mice that express Lifeact-GFP and live-cell total internal reflection fluorescence imaging, this study examined the role of WASp-mediated branched actin polymerization in the GCB immunological synapse. After rapid spreading on antigen-coated planar lipid bilayers, GCBs formed microclusters of phosphorylated BCRs and proximal signaling molecules at the center and the outer edge of the contact zone. The centralized signaling clusters localized at actin-rich GCB membrane protrusions. WKO reduced the centralized micro-signaling clusters by decreasing the number and stability of F-actin foci supporting GCB membrane protrusions. The actin structures that support the spreading membrane also appeared less frequently and regularly in WKO than in WT GCBs, which led to reductions in both the level and rate of GCB spreading and antigen gathering. Our results reveal essential roles for WASp in the generation and maintenance of unique structures for GCB immunological synapses.

Keywords: B-lymphocytes, germinal center, actin, WASp, signal transduction, immunological synapse

OPEN ACCESS

Edited by:
Balbino Alarcon, Consejo Superior de Investigaciones Científicas (CSIC), Spain

Reviewed by:
Jonathan Michael Lee, University of Ottawa, Canada
Deniz Saltukoglu, University of Freiburg, Germany

****Correspondence:***
Xiaodong Zhao
zhaoxd530@aliyun.com

Specialty section:
This article was submitted to Cell Growth and Division, a section of the journal Frontiers in Cell and Developmental Biology

Received: *24 December 2020*
Accepted: *17 May 2021*
Published: *14 June 2021*

Citation:
Li Y, Bhanja A, Upadhyaya A, Zhao X and Song W (2021) WASp Is Crucial for the Unique Architecture of the Immunological Synapse in Germinal Center B-Cells. Front. Cell Dev. Biol. 9:646077. doi: 10.3389/fcell.2021.646077

INTRODUCTION

B-cell-mediated antibody responses provide essential immune protection against infectious diseases. Antibodies and antibody responses have been explored as immune therapies and preventatives for cancer, immune disorders, and infectious diseases. Upon encountering cognate antigen, mature B-cells in B-cell follicles of the secondary lymphoid organs are activated through the B-cell antigen receptor (BCR) to proliferate, leading to the formation of germinal centers (GCs). B-cells undergo somatic hypermutation in immunoglobulin genes of the BCR in the dark zone

(DZ) of GCs. Germinal center B-cells (GCBs) with mutated BCRs then migrate to the light zone (LZ), where GCBs compete with each other to engage and capture antigen through their clonal-specific BCRs (Chan and Brink, 2012; Shlomchik and Weisel, 2012; Victora and Nussenzweig, 2012). BCR's ability to transduce signals and capture antigens is essential for GCBs to survive and differentiate into memory B-cells that mediate rapid and robust recall antibody responses and long-lived plasma cells that maintain the levels of protective antibodies (Gitlin et al., 2014; Turner et al., 2018; Shlomchik et al., 2019).

Deficiencies of actin regulators responsible for generating branched actin structures cause concurrent immune deficiencies and autoimmune diseases in humans. These actin regulators include ARPC1B, a hematopoietic-specific ARPC1 isoform of Arp2/3 complex that nucleates branched actin (Kuijpers et al., 2017; Volpi et al., 2019), and a hematopoietic-specific member of the branched actin nucleation promoting factors, Wiskott-Aldrich syndrome protein (WASp), which activates Arp2/3 (Padrick and Rosen, 2010). The immune disorders caused by deficiencies of these two actin regulators share some common characteristics, including microthrombocytopenia, immunodeficiency, eczema, and increased risk of malignancies and autoimmune manifestations (Notarangelo et al., 2008; Kuijpers et al., 2017; Volpi et al., 2019). While the impact of ARPC1B deficiency on B-cells is unknown, and the role of WASp in B-cell mediated antibody responses has been studied. Both WASp-deficient patients and mouse models, including germline and B-cell specific knockout, exhibit defects in mounting antibody responses to infections and immunizations. However, their B-cell development and B-cell differentiation into GCBs, memory B-cells, and plasmablasts are relatively normal (Becker-Herman et al., 2011; Recher et al., 2012; Simon et al., 2014). Moreover, both WAS patients and mice develop a wide range of autoreactive IgM and IgG as well as germinal centers in the absence of antigenic challenges. In chimeric mouse models with wild type (WT) T-cells, both WASp-deficient transitional B-cells and GCBs show hyper-responsiveness to BCR cross-linking and enrichment of self-reactive populations (Becker-Herman et al., 2011; Kolhatkar et al., 2015). These indicate a regulatory role of WASp-mediated branched actin in GCBs, where high-affinity antigen-specific B-cells are selected and autoreactive B-cells are eliminated.

The activation of B-cells from all subsets is initiated by the binding of the BCR to antigens. In GCs, B-cells encounter antigens on the surface of follicular dendritic cells or soluble antigen diffusing into GCs (Batista and Harwood, 2009; Cyster, 2010). Binding multivalent antigens triggers BCR aggregation in lipid rafts (Cheng et al., 1999; Sohn et al., 2008), and membrane antigens induce the formation of immunological synapses (ISs) at the contact zone between GCBs and antigen-presenting membranes. Src kinases, which constitutively reside in lipid rafts, phosphorylate the tyrosines of immunoreceptor tyrosine-based activation motifs (ITAMs) in the cytoplasmic domains of CD79a and/or CD79b, the signaling component of the BCR (Reth, 1992). The phosphorylated ITAM provides a docking site for the SH2 domain of the tyrosine kinase Syk. ITAM binding leads to Syk phosphorylation and activation. Syk then activates multiple downstream signaling pathways, including phosphatidylinositol-3 kinase, phospholipase Cγ2, and Bruton's tyrosine kinase (Dal Porto et al., 2004; Kwak et al., 2019). Following signaling activation, several phosphatases, including SH2-containing tyrosine phosphatase 1 (SHP1) and SH2-containing phosphatidylinositol-5 phosphatase 1 (SHIP1), are recruited to ISs, leading to signal attenuation (Brauweiler et al., 2000; Franks and Cambier, 2018).

B-cell affinity maturation in GCs is antigen-driven, indicating the crucial role of BCR-antigen engagement and subsequent signaling (Mesin et al., 2016; Cirelli and Crotty, 2017; Shlomchik et al., 2019). Compared to naïve B-cells with no previous antigen experience, BCR signaling in GCBs is relatively attenuated, associated with increased activation of the phosphatases SHP and SHIP (Khalil et al., 2012; Shlomchik et al., 2019). Such attenuated BCR signaling likely increases the GCB activation threshold and their ability to distinguish between high- and low-affinity antigens (Kwak et al., 2018). Signaling activation promotes BCR internalization and intracellular transport of antigens for processing and presentation to follicular T-helper cells (Liu et al., 2013b; Avalos and Ploegh, 2014; Hoogeboom and Tolar, 2016). B-cells can capture both soluble antigens and antigens associated with APCs. Internalization of membrane-associated antigens requires higher-affinity BCRs than soluble antigens, enhancing the B-cell affinity discrimination of antigens (Batista and Neuberger, 2000).

The role of the actin cytoskeleton in BCR signaling of naïve B-cells has been extensively studied. Upon encountering cognate antigens with multi-valency or those associated with membranes, the earliest signaling triggers transient actin depolymerization, releasing surface BCRs from restraints to lateral mobility imposed by the cortical actin network (Treanor et al., 2010; Freeman et al., 2011). Following the initial depolymerization, actin polymerizes rapidly, driving BCR clustering—the formation, growth, and merging of BCR microclusters (Harwood and Batista, 2011; Song et al., 2013; Tolar, 2017). When interacting with membrane-associated antigens, actin polymerization mediates B-cell spreading, expanding the contact zone between B-cells and antigen-presenting surfaces and driving surface BCRs to the contact zone, which amplifies BCR signaling. Following spreading, B-cells undergo actin-dependent contraction (Fleire et al., 2006). In addition to facilitating the gathering of antigen-engaged BCRs to form ISs, this contraction promotes BCR signaling attenuation (Liu et al., 2013a; Seeley-Fallen et al., 2014). Branched actin polymerization, mediated by WASp and its ubiquitous homolog neuronal (N)-WASp, is essential for B-cell spreading and signaling amplification. However, N-WASp but not WASp facilitates B-cell contraction and signaling attenuation. B-cell-specific N-WASp deletion in mice also induces GCs without immunization and autoantibody production (Liu et al., 2013a). Therefore, WASp and N-WASp activated branched actin polymerization is involved in both BCR signaling amplification and attenuation in naive B-cells.

While deficiencies in actin regulators significantly impact GCBs, the exact role of the actin cytoskeleton in GCB BCR signaling has not been fully understood. Recent studies have shown a unique architecture of the GCB IS formed on

antigen-presenting membranes. Distinct from the relatively smooth membrane contact of naive B-cells, GCBs generate actin- and ezrin-rich pod-like structures to contact antigen-presenting surfaces, which leads to the formation of less centralized BCR microclusters (Nowosad et al., 2016; Kwak et al., 2018). The stability of this specialized IS depends on BCR antigen-binding affinity, consequently enhancing GCBs' ability to distinguish antigen affinity (Kwak et al., 2018). The unique pod-like structure of GCB ISs and the particular impact of deficiencies in actin regulators for branched actin on GCs suggest a distinct role of the actin cytoskeleton in GCB ISs.

This study examined the mechanism by which WASp promoted polymerization of branched actin in the formation of GCB ISs, using WASp knockout mice expressing Lifeact-GFP that binds to F-actin and total internal reflection fluorescence microscopy. Here, we show that when interacting with planar lipid bilayers coated with a high density of Fab' fragment of anti-BCR antibody, WT GCBs form centralized BCR signaling microclusters at plasma membrane protrusions. These centralized signaling microclusters are surrounded by regions of low signaling, in contact with the antigen-presenting membrane. Branched actin generated by WASp is required for the formation and stabilization of the unique membrane structure of the GCB ISs by generating and sustaining actin networks that support plasma membrane protrusions as well as interactions with antigen-presenting membranes in the periphery of the IS.

MATERIALS AND METHODS

Animals

Wild type (WT, C57BL/6) and WASp knockout (WKO) mice on a C57BL/6 background were purchased from Jackson Laboratories (Cat# 000664 and 019458). A lack of WASp expression in WKO mice was verified using western blotting (**Supplementary Figure 1**). Lifeact-GFP mice on a C57BL/6 background were kindly provided by Dr. Roberto Weigert's laboratory in National Cancer Institute, Maryland, United States. WKO mice expressing Lifeact-GFP were generated by crossing WKO and Lifeact-GFP mice. All work involving animals was approved by the Institutional Animal Care and Use Committee at the University of Maryland.

Germinal Center B-Cells (GCBs)

WT and WKO mice with or without expressing Lifeact-GFP were immunized intraperitoneally with sheep red blood cells (SRBC) (Innovative Research Cat# ISHRBC10P) twice 7 days apart and euthanized at 7 days following the second immunization. Splenocytes were released from the spleens using frosted glass slides and filtered through 40 μm cell strainer (Thermo Fisher, Cat# 22-363-547). Red blood cells were lysed using ACK lysing buffer (Gibico Cat# 10492-01). GCBs were enriched using a negative selection method based on a published protocol (Cato et al., 2011). Briefly, splenocytes were incubated with biotinylated anti-CD43 (eBioscience Cat# 13-0431-82), anti-CD11c (eBioscience Cat# 13-0114-81), and anti-IgD (Southern Biotech Cat# 112008) antibodies. After washing, cells were incubated with anti-biotin microbeads (Miltenyi Biotec Cat# 130-090-485) and went through a LS column (Miltenyi Biotec Cat# 130-042-401) according to the manufacture's recommended protocol. Cells eluted from LS columns were collected as enriched GCBs.

Western Blotting

Western blotting was used to verify WASp-deficiency in WKO mice. Splenocytes from WT and WKO mice were lysed, and cell lysates were analyzed by western blotting, probing for WASp (Santa Cruz Cat# 365859). The blots were stripped and probed for GAPDH (Proteintech Cat# HRP-60004) as loading controls.

Flow Cytometry

To determine the purity of enriched GCBs and compare the sizes and the surface BCR levels of GCBs from WT and WKO mice, splenocytes and isolated GCBs were stained with antibodies specific to B220 (Biolegend Cat# 103236), GL7 (Invitrogen Cat# 12-5902-82), CD95 (BD Biosciences Cat# 557653), and IgG (Biolegend Cat# 405315) and analyzed by a BD FACS Canto II flow cytometer (BD Sciences) and Flowjo software.

Planar Lipid Bilayers (PLBs)

Mono-biotinylated Fab' (mB-Fab' or Fab') was generated from the $F(ab')_2$ fragment of anti-mouse IgM + G antibody (Jackson ImmunoResearch Cat# 115-006-068) using a previously published protocol (Peluso et al., 2003). mB-Fab' was conjugated with Alex Fluor (FA) 546 using a labeling kit (Thermo Fisher Cat# A10237) according to the manufacturer's protocol. The PLB was prepared using liposomes made by sonicating 1,2-dioleoyl-sn-Glycero-3-phosphocholine and 1,2-dioleoyl-sn-Glycero-3-phosphoethanolamine-cap-biotin (Avanti Polar Lipids Cat# 850375 and 870273) in a 100:1 molar ratio in PBS (Sohn et al., 2008). Coverslip chambers (Thermo Fisher Cat# 155411) were incubated with the liposomes before coating with 1 μg/ml streptavidin (Jackson ImmunoResearch Cat# 016-000-084) and followed by 2 μg/ml AF546-mB-Fab' mixed with 8 μg/ml mB-Fab' (Fab'-PLB). For a non-stimulation control, biotinylated holo-transferrin (TF; 16 μg/ml, Jackson ImmunoResearch Cat# 015-060-050) binds Tf receptors on GCBs but does not activate the BCR was used to substitute the mB-Fab' (Tf-PLB). To analyze surface BCRs on GCBs interacting with Tf-PLB, surface BCRs were labeled with non-biotinylated AF546-Fab' on ice before incubating with TF-PLBs.

Total Internal Reflection Fluorescence Microscopy (TIRF) and Image Analysis

Images were acquired using a TIRF microscope (NIKON Eclipse Ti-E TIRF, 63 × 1.49NA oil objective). Interference reflection images (IRM) and AF488 and AF546 images were acquired sequentially. To identify light-zone and dark-zone GCBs, enriched GCBs were stained with AF488-anti-CD86 (Invitrogen Cat# 53-0869-42) and PE-anti-CXCR4 (Invitrogen Cat# 12-9991-82) and then incubated with Fab'-PLBs for 5 min at 37°C before fixation with 4% paraformaldehyde. Cells with high levels of CD86 staining and low levels of CXCR4 staining

were identified as light-zone GCB. After initial characterization, enriched GCBs were pre-stained with anti-CXCR4 antibodies before incubating with Fab'-PLB for all the experiments, and cells with no or low level of CXCR4 staining were identified as light-zone GCBs.

To analyze signaling and F-actin in GCBs, enriched GCBs were incubated with Fab'-PLBs or Tf-PLBs at 37°C for varying lengths of time, fixed with 4% paraformaldehyde, permeabilized with 0.05% saponin, and stained with antibodies specific for phospho-CD79a Y182 (Cell Signaling Technology Cat# 14732), phospho-SHIP1 Y1020 (Cell Signaling Technology Cat# 3941), phospho-SHP1 Y536 (Abcam Cat# ab51171), phospho-Syk (Y525/Y526) (Cell Signaling Technology Cat# 2710), phospho-Akt (S473) (Cell Signaling Technology Cat# 4060), or AF488-phalloidin (Cytoskeleton Cat# PHDG1). Cell contact area, the total (TFI) and mean fluorescence intensity (MFI) in the cell contact zone, and fluorescence intensity (FI) along lines across cells were determined based on IRM and TIRF images using NIH ImageJ.

For live-cell imaging, GCBs expressing Lifeact-GFP were incubated with Fab'-PLBs at 37°C, 5% CO_2, and imaged by TIRF, acquiring one frame every 2 s. Cell contact area, the TFI, and the MFI in the cell contact zone were determined based on IRM and TIRF images analyzed with custom-made codes using MATLAB software (The MathWorks, Inc., Natick, MA, United States). Increasing rates of the cell contact area and the MFI of AF546-Fab' or Lifeact-GFP in the contact zone were determined using the slopes of the contact area or MFI vs. time plots and linear regression. Kymographs of time-lapse images were generated using NIH ImageJ.

For the analysis of BCR-Fab' cluster growth, one randomly selected kymograph was generated for each cell from time-lapse images using NIH ImageJ. AF546-Fab' clusters, which were visually distinguishable and trackable for at least 7 min, were identified by visual inspection. Five such AF546-Fab' clusters were randomly selected from each kymograph. The FI along each cluster track in kymographs was measured.

Phalloidin and Lifeact-GFP foci in individual cells were identified visually and manually, aided by intensity maps generated using NIH ImageJ. The MFI of all identifiable foci and the MFI of the entire contact zone of individual cells were determined using NIH ImageJ manually. F-actin foci were identified when the MFI of phalloidin foci was 2-folds or the MFI of Lifeact-GFP foci was 1.5-fold of their MFI in the cell contact zone. The relative lifetime of actin foci was determined by the duration that individual actin foci can be detected in a kymograph. The width ratio of the adherent regions, the wider side relative to the narrower side, in individual cells was determined using a randomly selected kymograph per cell generated using time-lapse IRM images and an average of four time points: 3, 5, 7, and 10 min.

Statistical Analysis

Statistical significance was assessed using unpaired, two-tailed Student's *t*-tests (Prism-GraphPad software) when only two groups were compared, and one-way ANOVA when 3 or more groups were compared. All data were presented as the mean ± SD (standard deviation).

RESULTS

WASp-Deficiency Alters the Architecture of Germinal Center B-Cell Immunological Synapses

To examine germinal center B-cell (GCB) immunological synapses (ISs), we isolated GCBs from sheep red blood cell (SRBC)-immunized mice (**Supplementary Figure 2**). GCBs were incubated with planar lipid bilayers (PLBs) coated with Alexa Fluor 546-conjugated and unconjugated monobiotinylated Fab' fragment of anti-mouse IgM + G antibody (Fab'-PLB) or biotinylated transferrin (Tf-PLB) through biotin–streptavidin interactions (Liu et al., 2011). The Fab'-PLB elicits a maximal level of B-cell receptor (BCR) activation in naïve B-cells (Liu et al., 2011, 2012, 2013a,b; Seeley-Fallen et al., 2014). Cells were fixed at different times after the incubation and stained for phosphorylated CD79a (pCD79a), indicating activated BCRs, phosphorylated Syk (pSyk), and Akt (pAkt) as activated proximal signaling molecules, and phosphorylated SHIP1 (pSHIP1) and SHP1 (pSHP1) as activated inhibitory signaling molecules. We image the GCB plasma membrane regions that contact the PLB (contact zone) using interference reflection microscopy (IRM) and total internal reflection fluorescence microscopy (TIRF) as surface BCRs in the contact zone can directly engage Fab'-PLB. We focused on the light zone (LZ) GCBs, as the LZ is where most GCBs encounter antigen on follicular dendritic cells. We distinguished LZ GCBs among enriched GCB based on their relatively low levels of CXCR4 staining (**Supplementary Figure 3**; Allen et al., 2004). Phosphorylated CD79a was detected in the contact zone of both wild type (WT) and WASp knockout (WKO) LZ GCBs (**Figure 1A**) but not in the contact zone of GCBs interacting with Tf-PLB (**Supplementary Figure 4**). Both the mean fluorescence intensity (MFI) and the total fluorescence intensity (TFI) of pCD79a in the contact zone of individual LZ GCBs increased over time, peaked after ∼5 and ∼9 min incubation, respectively, and persisted at least for 20 min (**Figures 1A,B**). Compared to WT GCBs, the pCD79a MFI and TFI were significantly reduced in WKO GCBs (**Figures 1A,B**). The MFI and TFI of pSyk, pAkt, pSHIP1, and pSHP1 all increased in the contact zone of LZ GCBs over time (**Supplementary Figure 5**). The MFI and TFI of pSyk increased similarly as pCD79a, while the MFI and TFI of pAkt, pSHIP1, and pSHP1 peaked at 7, 3, and 3 min, respectively, and decreased afterward (**Supplementary Figure 5**). Compared to WT GCBs, WKO GCBs had significantly decreased levels of pSyk and pSHP1 but increased levels of pSHIP1 with no change in the level of pAkt in the contact zone (**Figures 1C,D** and **Supplementary Figure 5**).

In the contact zone of WT LZ GCBs, pCD79a and pSyk were primarily detected as numerous puncta in the central area (**Figures 1E,F**, upper panels, green arrows in the FI line profile) and the outer edge of the contact zone (**Figures 1E,F**, upper panels, black arrows in the FI line profile). The central

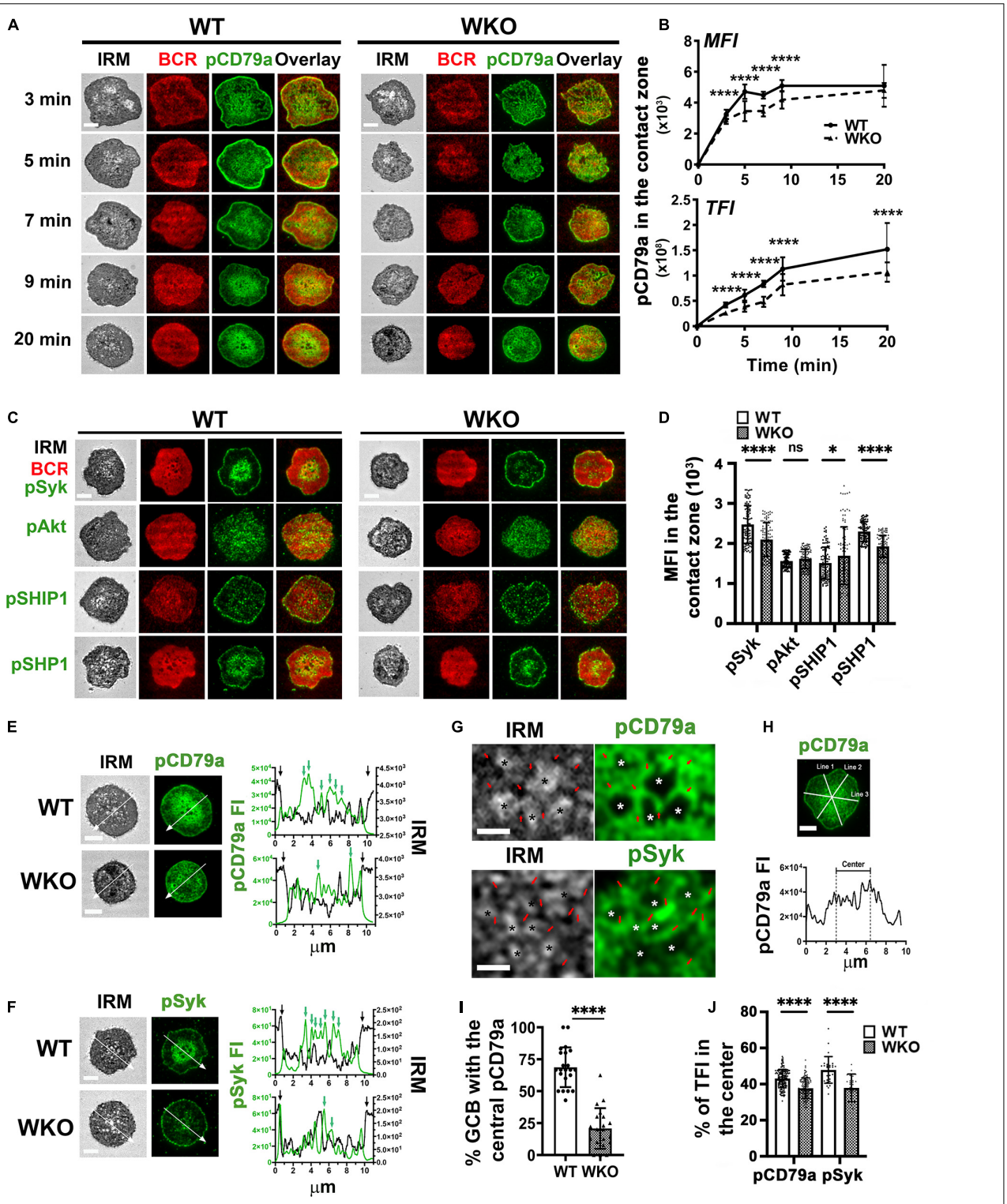

FIGURE 1 | WASp knockout (WKO) reduces BCR signaling and distorts the immunological synapse (IS) of light-zone germinal center B-cells (LZ GCBs). GCBs isolated from sheep red blood cells (SRBC)-immunized wild type (WT) and WKO mice were incubated with Alexa Fluor (AF) 546-conjugated monobiotinylated Fab'-anti-mouse IgM + G tethered planar lipid bilayers (Fab'-PLB) at 37°C and fixed at different times, permeabilized, stained for phosphorylated CD79a (pCD79a), Syk (pSyk), Akt (pAkt), SHIP1 (pSHIP1), or SHP1 (pSHP1). The GCB plasma membrane contacting Fab'-PLB (contact zone) was imaged by an interference reflection microscope (IRM) and a total internal reflection fluorescence microscope (TIRF). **(A)** Representative IRM and TIRF images of WT and WKO GCBs stained for pCD79a at 3, 5, 7, 9, and 20 min. **(B)** The mean fluorescence intensity (MFI) and the total fluorescence intensity (TFI) of the pCD79a in the contact zone at

(Continued)

FIGURE 1 | Continued
different times were quantified by NIH ImageJ. The results were the average (± SD) of > 60 individual cells per condition from six independent experiments. **(C)** Representative IRM and TIRF images of WT and WKO GCBs stained for pSyk, pAkt, pSHIP1, or pSHP1 at 7 min. **(D)** The MFI of pSyk, pAkt, pSHIP1, and pSHP1 in the contact zone at 7 min was measured using NIH ImageJ. Data points represent individual cells. **(E,F)** Representative IRM and TIRF images of WT and WKO stained for pCD79a **(E)** and pSyk **(F)** at 20 min and the FI and the IRM density along the lines. In the line profiles, black arrows indicate the outer edge of the contact zone. Green arrows indicate pCD79a or pSyk FI peaks. **(G)** Enlarged representative IRM and TIRF images of the central regions in the WT GCBs stained for pCD79a and pSyk shown in **(E,F)**. Stars, plasma membrane areas that pulled away from Fab'-PLB. Red arrows, plasma membrane areas that were in close contact with Fab'-PLB. **(H)** GCBs with centralized pCD79a staining in the contact zone were identified using three randomly selected FI line profiles per cell. **(I)** Percentages of GCBs with the centralized pCD79a staining. Data points represent individual images at 5 min. **(J)** The percentages of pCD79a FI and pSyk FI in the central region indicated in **(H)**. Data points represent individual cells. Scale bars, 3 μm. The results were the average (± SD) of > 60 individual cells per condition. $n = 3\sim4$. $^{*}p < 0.05$ and $^{****}p < 0.0001$, unpaired Student's *t*-test or one-way ANOVA.

pCD79a- and pSyk-rich area was surrounded by a pCD79a- and pSyk-poor region (**Figures 1A,C,E,F**). Staining of pSHP1 in the contact zone exhibited similar patterns as pCD79a and pSyk, but pAkt appeared as scattered puncta, and pSHIP1 was primarily located at the outer edge of the contact zone (**Figure 1C**). WKO disrupted the centralized organization of pCD79a (**Figure 1E**) and pSyk (**Figure 1F**) but did not affect the organization of the inhibitory signaling molecules pSHIP1 and pSHP1 (**Figure 1C**). IRM images and their intensity line profiles exhibited variability in the central part of the contact area (**Figures 1E–G**, left panels). We have previously shown a monotonic relationship between IRM intensity and membrane height (Lam Hui et al., 2012). The dark IRM intensities represent close apposition of the cell membrane to Fab'-PLB within the TIRF detection field, while the light IRM intensities represent the cell membrane apposition away from Fab'-PLB and the TIRF defection field. Thus, the IRM intensity variation indicates protrusions of the GCB plasma membrane in contact with the PLB (**Figures 1E–G**, left panels). The overlay of IRM intensity and pCD79a or pSyk FI line profiles showed that signaling puncta were located at the central protrusions that closely contacted Fab'-PLB, but much less in the membrane area surrounding the central protrusions even though it also interacted with F-ab'-PLB (**Figures 1E,F**, green arrows and **Figure 1G**, red arrows). While WKO GCBs also formed similar membrane protrusions in the contact zone, they were not centralized and less organized and associated with fewer signaling puncta (**Figures 1E,F**). We quantified this unique signaling organization of the GCB ISs by determining the percentage of LZ GCBs with central enrichment of pCD79a (**Figure 1I**) and the percentage of pCD79a or pSyk FI in the central area compared to the entire contact zone in individual cells (**Figure 1J**), using three randomly selected FI line profiles per cell (**Figure 1H**). Nearly 70% of WT LZ GCBs had such a central pCD79a organization compared to ∼20% of WKO LZ GCBs (**Figure 1I**). There was a significantly higher percentage of pCD79a and pSyk FI in the central area of the WT GCB contact zone compared to that in WKO GCBs (**Figure 1J**). Taken together, these data suggest that WASp is critical for the unique architecture of GCB ISs.

WASp Promotes GCB Spreading on Antigen-Presenting Surfaces

B-cells undergo actin-driven spreading when interacting with antigen-presenting surfaces, increasing the contact area (Fleire et al., 2006). We utilized IRM to examine the role of WASp in GCB spreading. LZ GCBs were incubated with Fab'-PLB and then either imaged after fixing at different times or imaged live by IRM. IRM images of fixed cells showed that GCBs started to bind Fab'-PLB within 1 min, rapidly spread, and reached the maximal contact area at 3 min (**Figures 2A,B**). Live-cell imaging was initiated when GCBs landed on the Fab'-PLB, and it took GCBs less than 2 min to reach maximal spreading (**Figures 2C,D** and **Supplementary Video 1**). WKO GCBs spread significantly less than WT GCBs (**Figures 2A–D** and **Supplementary Video 1**). In contrast to the contraction of naïve B-cells following spreading (Fleire et al., 2006), both WT and WKO GCBs maintained the maximal contact area for at least 20 min (**Figures 2A–D**). To analyze GCB spreading kinetics, we measured the initial GCB spreading rate using the slopes of the contact area vs. time plots and linear regression (**Figure 2E**). We found that WKO GCBs spread significantly slower than WT GCBs (**Figures 2E,F**), in addition to showing a reduction in the maximal contact area. Flow cytometry analysis showed that WT and WKO GCBs had similar forward scattering (**Supplementary Figure 6**), indicating that the reduced spreading rate and area of WKO GCBs were not caused by a reduction in the sizes of WKO GCBs. We also noticed that WKO GCBs took a few seconds longer than WT GCBs to transition from landing to binding to Fab'-PLB (**Figure 2G**). The times for cell landing and binding were determined using time-lapse images of IRM. IRM detects a shadow when a cell lands on Fab'-PLB but is not close enough to bind, and when the cell binds to Fab'-PLB, the shadow in IRM images became dark. These data suggest that WASp is required for optimal kinetics and extent of GCB spreading.

WASp Facilitates Antigen Gathering and BCR-Antigen Microcluster Growth

Upon interacting with antigen on presenting surfaces, antigen-engaged BCRs aggregate into microclusters, leading to signaling activation (Depoil et al., 2009; Tolar et al., 2009). To examine the role of WASp during this process in GCBs, we determined the relative amount of AF546-Fab' gathered in the contact zone of individual cells and in individual microclusters, as well as their rates of increase. As AF546-Fab' tethered on PLB clusters only when engaging surface BCRs (**Supplementary Figure 4**; Liu et al., 2012), AF546-Fab' clustering reflects surface BCR clustering. GCBs were incubated with Fab'-PLB and either imaged after fixation at different times or imaged live by TIRF. The MFI and TFI of AF546-Fab' of fixed WT and WKO GCBs peaked at 3∼5 min (**Figures 3A–C**), later than the time (< 3 min)

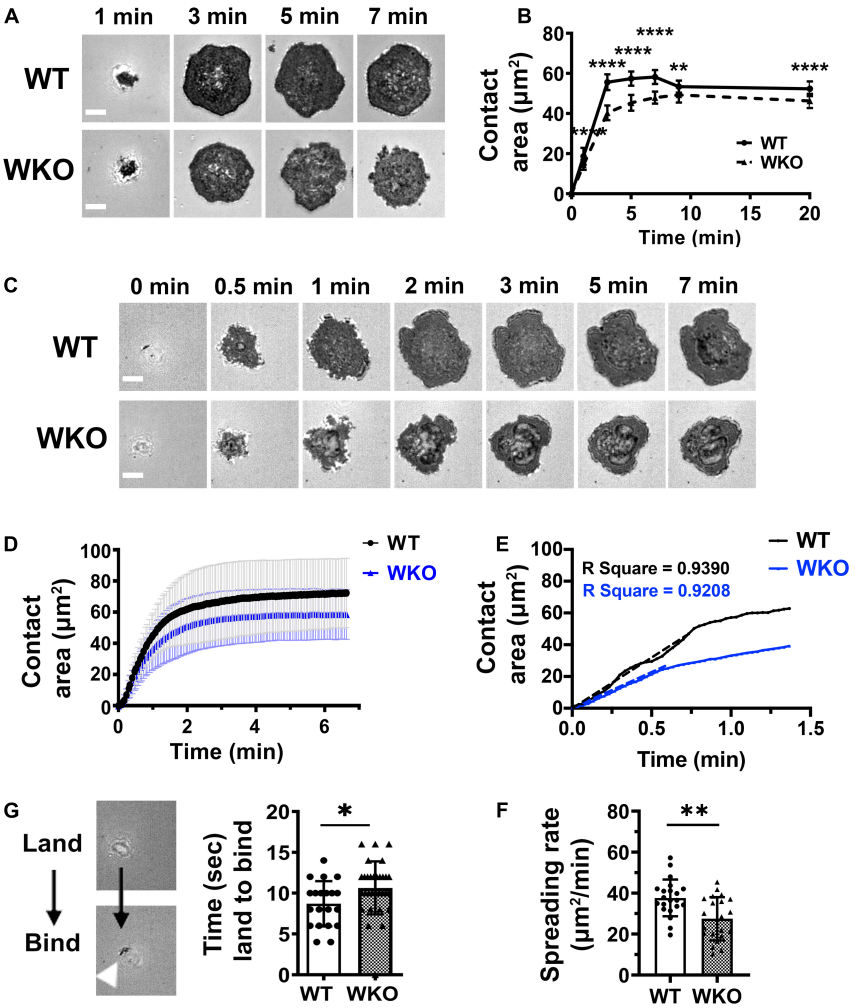

FIGURE 2 | WASp contributes to GCB spreading on Fab'-PLB. GCBs isolated from SRBC-immunized mice were incubated with Fab'-PLB and either imaged after fixation **(A,B)** or live **(C–F)** by IRM. **(A)** Representative IRM images of WT and WKO GCBs fixed at indicated times. **(B)** Contact areas of fixed GCBs on Fab'-PLB over time were measured using NIH-ImageJ. The results were the average (± SD) of > 100 individual cells per condition from 7 independent experiments. **(C)** Representative time-lapse IRM images of WT and WKO GCBs. **(D)** Contact areas of WT and WKO GCBs over time using time-lapse IRM images and NIH ImageJ. The results were the average (± SD) of 20∼30 individual cells per condition from four independent experiments. **(E)** Initial spreading rates of individual GCBs were determined using the slopes of their contact area vs. time curves by linear regression. Shown is an example. **(F)** Spreading rates of WT and WKO GCBs on Fab'-PLB. **(G)** Representative IRM images (left panels) of a cell that just landed on (white shadow) or started binding (dark spots) to Fab'-PLB. The time between cell landing on and binding to Fab'-PLB (right). Data points represent individual cells. Shown are the averages (± SD) of 20∼30 individual cells for each condition. $n = 4$. Scale bars, 3 μm. $^{*}p < 0.05$, $^{**}p < 0.01$, and $^{****}p < 0.0001$, unpaired Student's t-test or one-way ANOVA.

when GCBs reached the maximal spreading (**Figure 2B**). WKO significantly reduced the MFI and TFI of AF546-Fab' in the GCB contact zone (**Figures 3A–C**). Live-cell imaging confirmed the reduction of AF-546-Fab' MFI in the WKO GCB contact zone (**Figures 3D,E** and **Supplementary Video 2**). Kinetic analysis of time-lapse images showed a drastic reduction in the rate of increase of AF546-Fab' MFI in the WKO GCB contact zone, compared to WT GCBs (**Figures 3D–F**). We used kymographs from individual cells to analyze trackable AF546-Fab' microclusters and measured their FI over time (**Figure 3G**, arrows). The FI of individual AF546-Fab' microclusters in both WT and WKO GCBs peaked in less than 2 min and appeared to saturate as the intensity levels were mostly unchanged, at least for the next 5 min (**Figure 3H**). Furthermore, most Fab'-BCR microclusters barely moved and could therefore be tracked for several minutes in individual kymographs (**Figure 3G**), suggesting that they are relatively immobile. The FI and rate of increase of FI in individual AF546-Fab' microclusters in WKO GCBs were significantly lower than those in WT GCBs (**Figures 3G–I**). To determine if the reductions observed in WKO GCBs were due to a decrease in surface levels of the BCR, we stained splenocytes from immunized mice for BCR (IgG), B-cell (B220), and GCB (GL7 and CD95) markers. Flow cytometry analysis showed that the IgG level on WKO GCBs was not reduced but rather slightly increased, compared to WT GCBs (**Supplementary Figure 7**). Thus, our results suggest that

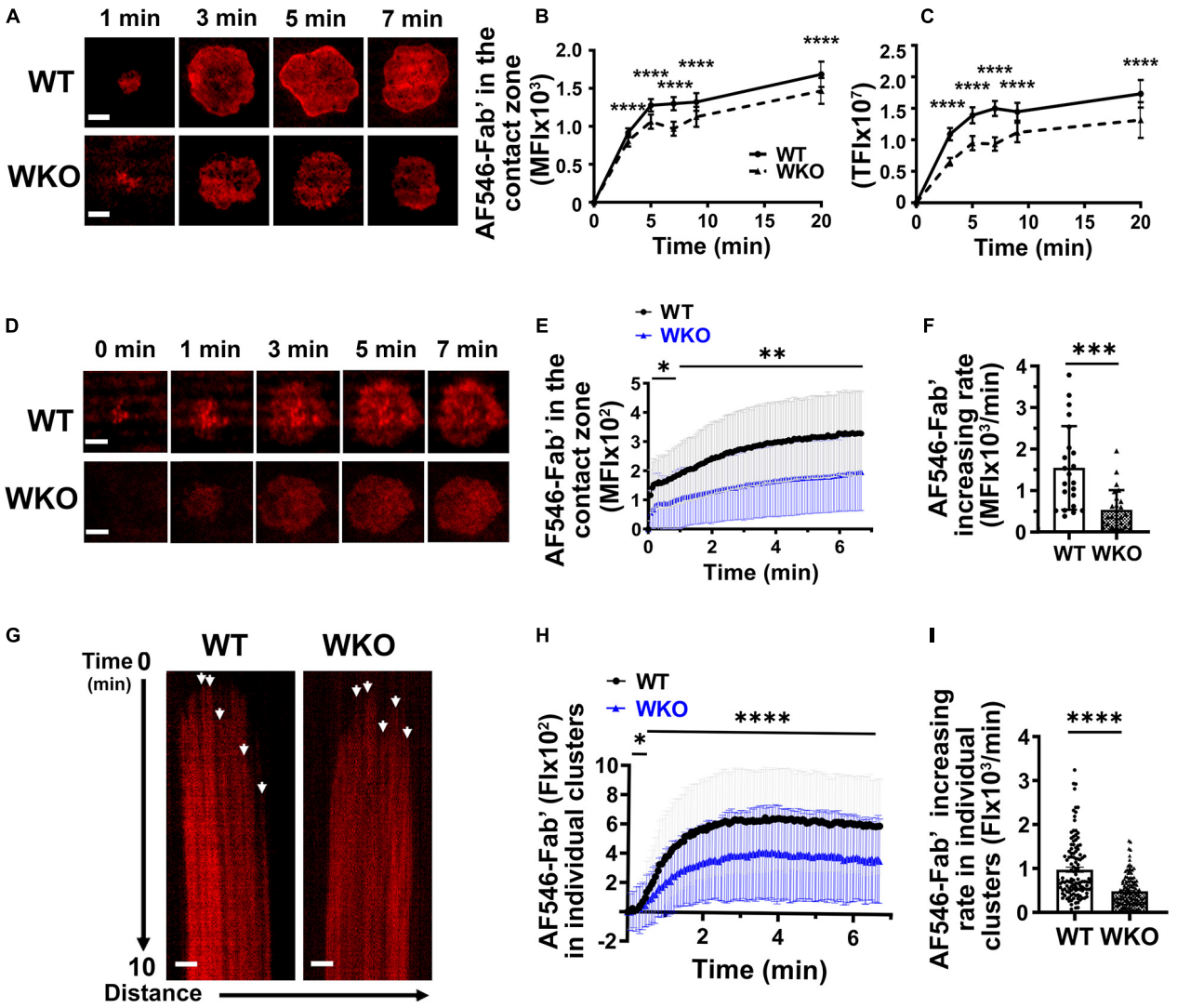

FIGURE 3 | WASp promotes BCR clustering in response to Fab'-PLB. GCBs isolated from SRBC-immunized WT and WKO mice were incubated with AF546-Fab'-PLB and were imaged either after fixation at varying times or live using TIRF. **(A)** Representative AF546-Fab' images of GCBs fixed at 1, 3, 5, and 7 min. **(B,C)** The MFI **(B)** and TFI **(C)** of AF546-Fab' in the contact zone of fixed GCBs over time using NIH ImageJ. **(D)** Representative time-lapse AF546-Fab' images of WT and WKO GCBs. **(E)** MFI of AF546-Fab' in the GCB contact zone over time. **(F)** Increasing rates of AF546-Fab' MFI in the contact zone of individual GCBs were determined using slops of AF546-Fab' vs. time plots and linear regression, as shown in **Figure 2E**. Data points represent individual cells. **(G)** Representative kymographs generated using AF546-Fab' time-lapse images of the WT and WKO GCB contact zone using NIH ImageJ. White arrows, the starts of individual AF546-Fab' clusters. **(H)** The FI of AF546-Fab' in individual clusters over time using kymographs and NIH ImageJ. **(I)** Increasing rates of AF546-Fab' FI in individual clusters were analyzed as described in **Figure 2E**. Data points represent individual clusters. Scale bars, 3 μm. The results were the averages (± SD) of 22∼100 individual cells **(B,C,E)**, or > 120 BCR clusters and 5 clusters per kymograph per cell **(H)** for each condition. $n = 4\sim7$. $^{**}p < 0.01$, $^{***}p < 0.001$, and $^{****}p < 0.0001$, unpaired Student's *t*-test or one-way ANOVA.

WASp facilitates antigen gathering by promoting the growth of antigen-engaged BCR microclusters.

WASp Is Required for the Formation and Stabilization of Actin Foci Supporting Centralized Membrane Protrusions

WASp is an actin nucleation-promoting factor that activates Arp2/3-mediated polymerization of branched actin (Padrick and Rosen, 2010). We evaluated the contribution of WASp to actin reorganization during GCB response to antigen-presenting surfaces using phalloidin staining and GCBs from Lifeact-GFP-expressing mice. Both phalloidin and Lifeact-GFP bind to F-actin, but phalloidin staining requires cell fixation and membrane permeabilization (Riedl et al., 2008; Melak et al., 2017). Analysis of TIRF images showed that the MFI of phalloidin staining in the contact zone of GCBs fixed at different times increased rapidly upon interacting with Fab'-PLB and peaked before 1 min (**Figures 4A,B**). The MFI of Lifeact-GFP in the contact zone of GCBs imaged live rose relatively slowly

(**Figures 4C,D** and **Supplementary Video 3**). However, the MFI of both phalloidin and Lifeact-GFP in the contact zone of WKO GCBs were significantly reduced, compared to those of WT GCBs (**Figures 4A–D** and **Supplementary Video 3**). Furthermore, the initial rate of increase of Lifeact-GFP in the WKO GCB contact zone was significantly slower than that in the WT GCB contact zone (**Figure 4E**). Thus, WASp is primarily involved in the rapid accumulation of F-actin in the GCB contact zone.

Previous studies have shown that the GCB IS consists of actin-rich protrusions engaging antigen on presenting surfaces (Nowosad et al., 2016; Kwak et al., 2018). Consistent with these early findings, we found F-actin puncta, as observed by phalloidin staining, concentrated at the central area of the WT GCB contact zone (**Figure 5A**), where signaling puncta were also located (**Figure 1**). The overlay of phalloidin FI and IRM intensity line profiles showed the colocalization of F-actin foci with the darker regions of IRM images, where the GCB membrane was in close apposition to antigen-presenting surfaces (**Figures 5A,B**, green arrows). However, we did not detect such F-actin foci at the GCB membrane area surrounding the central protrusions even though the IRM intensity showed its interaction with Fab'-PLB (**Figures 5A,B**). We identified local regions of actin

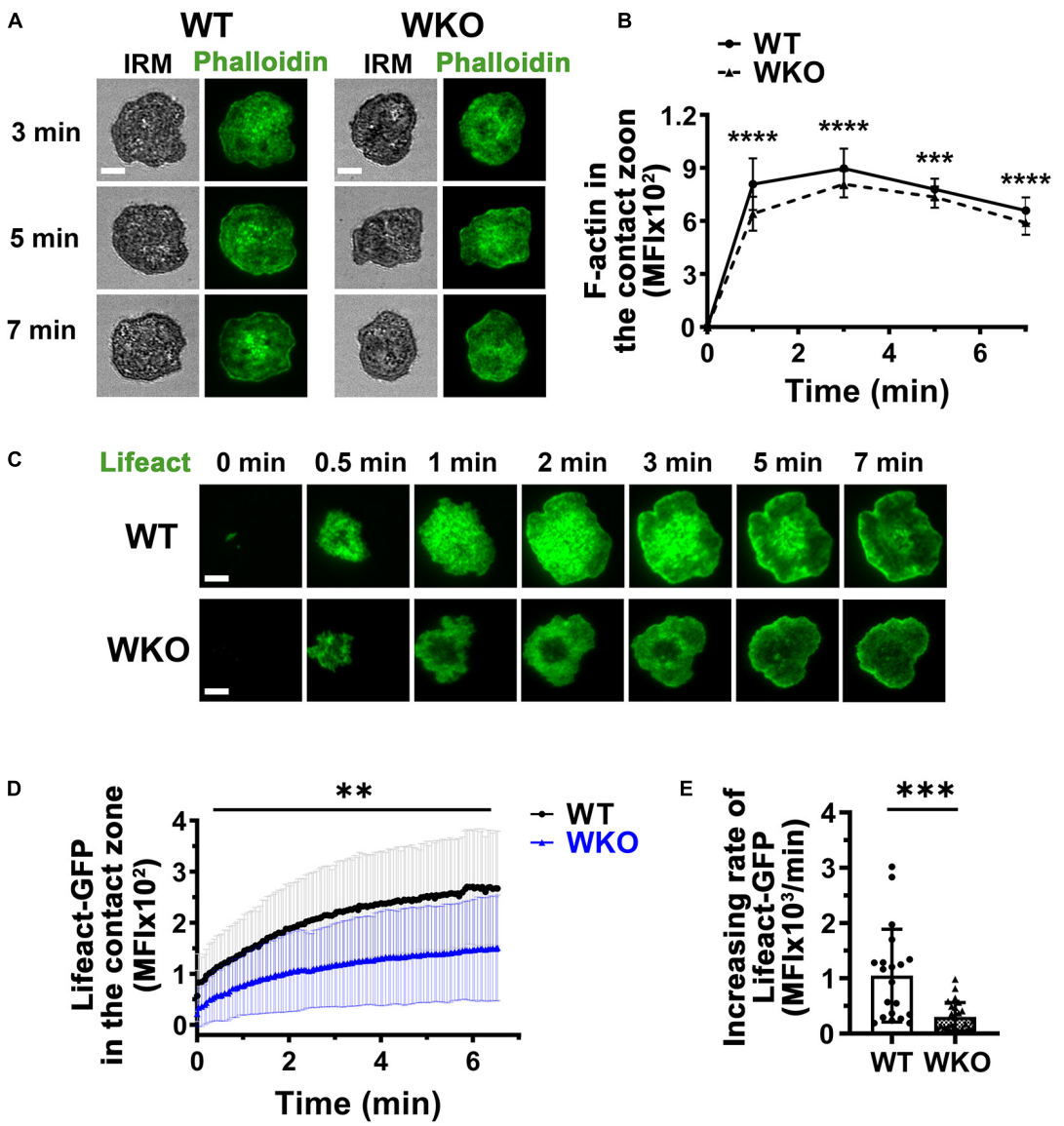

FIGURE 4 | WASp is involved in F-actin accumulation in the GCB contact zone. **(A,B)** GCBs isolated from SRBC-immunized WT and WKO mice were incubated with Fab'-PLB, fixed, permeabilized, stained for F-actin with phalloidin, and imaged using IRM and TIRF. Shown are representative images **(A)** and the MFI of phalloidin in the GCB contact zone at different times **(B)**. **(C–E)** GCBs isolated from SRBC-immunized WT and WKO mice expressing Lifeact-GFP were incubated with Fab'-PLB and imaged live using TIRF. Shown are representative time-lapse TIRF images of Lifeact-GFP **(C)**, the MFI of Lifeact-GFP in the contact zone over time **(D)**, and the increasing rates of Lifeact-GFP MFI, measured as illustrated in **Figure 2E**. Data points represent individual cells. Scale bars, 3 μm. The results were the average (± SD) of 22∼50 individual cells per condition. $n = 4$. $^{**}p < 0.01$, $^{***}p < 0.001$, and $^{****}p < 0.0001$, unpaired Student's *t*-test or one-way ANOVA.

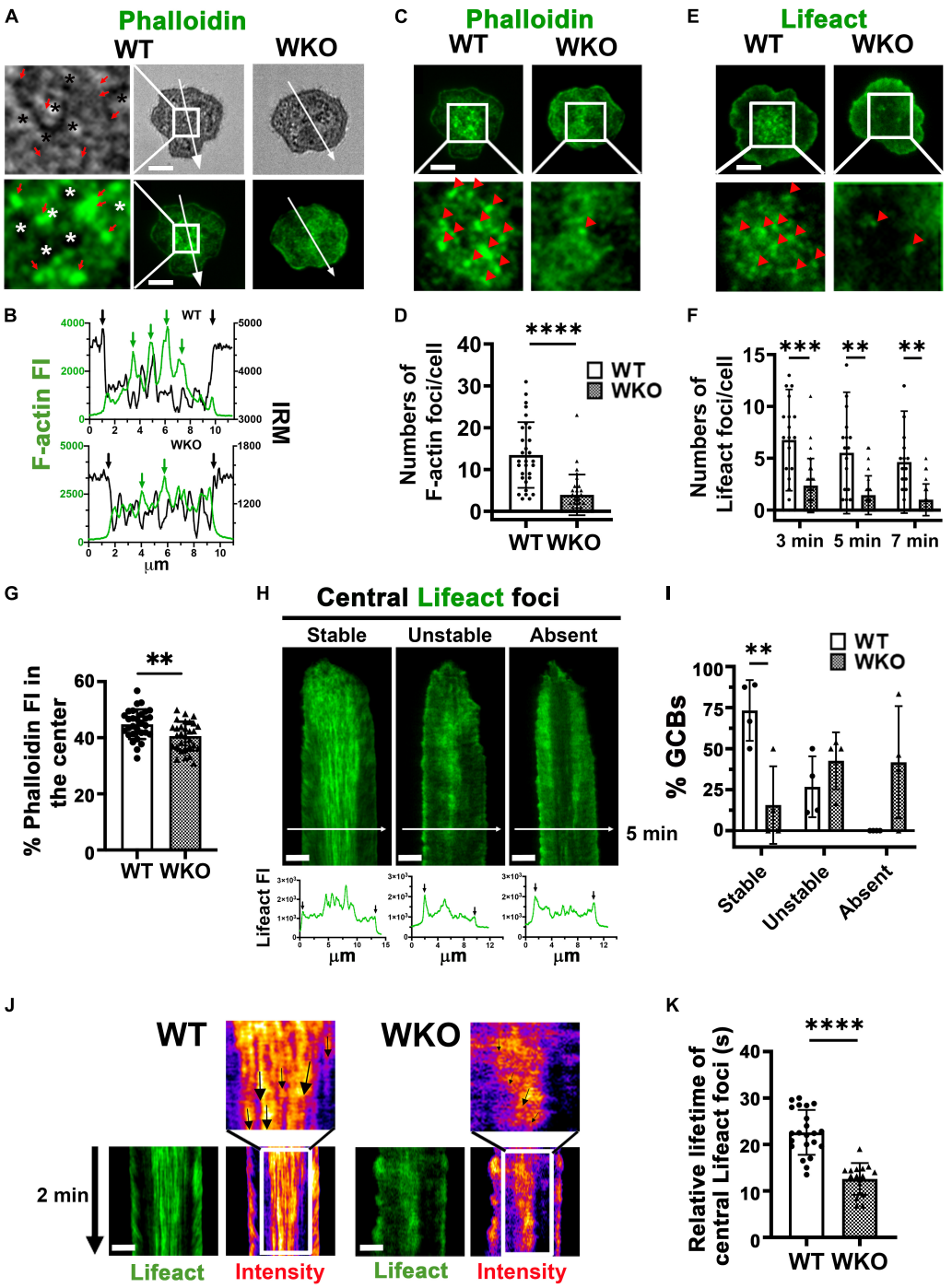

FIGURE 5 | WASp is required for generating stable F-actin foci at the centralized membrane protrusions in the GCB contact zone. GCBs isolated from SRBC-immunized WT and WKO mice expressing or not Lifeact-GFP were incubated with Fab'-PLB and either fixed, permeabilized, stained with phalloidin and imaged, or imaged live using IRM and TIRF. **(A)** Representative IRM and TIRF images of phalloidin staining of WT and WKO GCBs at 7 min and enlarged images of the central area in the WT GCB contact zone (left panels). Star *, the plasma membrane areas pulled away from Fab'-PLB. Red arrows, the plasma membrane areas were in close contact with Fab'-PLB. **(B)** The FI of phalloidin staining and the density of IRM image along the arrowed lines of WT (top) and WKO (bottom) cells in **(A)**. **(C)** Representative images of fixed GCBs stained with phalloidin and their central area of the contact zone at 7 min. Red arrowheads, phalloidin stained F-actin foci identified by the MFI of individual foci that were 2 folds higher than the MFI of the entire contact zone. **(D)** The number of phalloidin-stained F-actin foci per GCB contact zone at 7 min. Data points represent individual cells. **(E)** Representative images of Lifeact-GFP expressing GCBs and their enlarged central area of the contact zone at 7 min. Red arrowheads, Lifeact-GFP F-actin foci identified by the MFI of individual foci that were 1.5 fold higher than the MFI of the entire contact zone. **(F)** The number of Lifeact-GFP foci per GCB contact zone at 3, 5, and 7 min. Data points represent individual cells. **(G)** Percentages of the phalloidin FI in the

(Continued)

FIGURE 5 | Continued
central area relative to the phalloidin TFI in the contact zone. Data points represent individual cells. **(H)** Representative kymographs generated from time-lapse images of Lifeact-GFP GCBs by TIRF and Lifeact-GFP FI line profiles at 5 min (white arrow lines) to show three phenotypes: stable, unstable, and no central Lifeact foci. Black arrows in line profiles indicate the outer edges of the GCB contact zone. **(I)** Percentages of cells with stable, unstable, and no Lifeact foci in the center of the contact zone. Data points represent independent experiments. **(J)** Representative kymographs of Lifeact-GFP-expressing GCBs and their intensity heat maps from 4 to 6 min. Arrows, tracks of individual Lifeact-GFP actin foci. **(K)** The relative lifetime of Lifeact-GFP F-actin foci was measured by the duration of individual foci that could be tracked in a randomly selected kymograph. Data points represent individual cells, averages of 3 foci per cell. Scale bars, 3 μm. The results were the average (± SD) of 20∼30 individual cells per condition. $n = 3\sim4$. $^{**}p < 0.01$, $^{***}p < 0.001$, and $^{****}p < 0.0001$, unpaired Student's *t*-test or one-way ANOVA.

enrichment as F-actin foci close to Fab'-PLB if their phalloidin (**Figure 5C**) and Lifeact-GFP (**Figure 5E**) MFI was 2 and 1.5 folds higher than the MFI of phalloidin and Lifeact-GFP over the entire contact zone, respectively. We found a significantly higher number of such F-actin foci in the center of the WT than the WKO contact zone (**Figures 5A–F**). This reduced number of F-actin foci was associated with a decrease in the percentage of phalloidin staining in the center of the WKO GCB contact zone compared to that in the WT GCB contact zone (**Figure 5G**). We examined the formation of these centralized actin foci using kymographs generated from time-lapse images of GCBs expressing Lifeact-GFP (**Figure 5H**). We found that ∼70% of WT GCBs formed F-actin foci during the first minute of interaction with antigen-presenting surfaces. These F-actin foci gradually became centralized and were detected up to 20 min (Stable) (**Figure 5H**, left panels, and **Figure 5I**). In the remainder of WT GCBs, F-actin foci formed but did not persist for very long (Unstable) (**Figure 5H**, middle panels, and **Figure 5I**). In contrast, only ∼14% of WKO GCBs formed stable central F-actin foci (**Figure 5I**). We did not detect any centralized F-actin foci in ∼43% WKO GCBs (**Figure 5H**, right panels, and **Figure 5I**). The remainder of the WKO GCBs exhibited unstable F-actin foci (**Figure 5H**, middle panels, and **Figure 5I**). We evaluated the relative lifetime of F-actin foci by measuring the duration of individual F-actin foci that could be detected in randomly selected GCB kymographs and their intensity heat maps (**Figure 5J**, arrows). The relative lifetime of F-actin foci in WKO GCBs was much shorter than those in WT GCBs (**Figures 5J,K**). These data indicate that WASp is essential for the generation and stabilization of centralized F-actin foci supporting the GCB membrane protrusions that engage antigen on presenting surfaces.

WASp Contributes to the Actin Cytoskeleton Supporting the Lamellipodia and the Adherent Region Surrounding the Central Protrusions

In addition to the centralized F-actin foci, we observed actin structures at the outer edge of the contact zone, supporting the spreading membrane (**Figure 6A** and **Supplementary Video 3**). We determined their relative lifetime using kymographs generated from time-lapse images of Lifeact-GFP-expressing GCBs (**Figure 6A**) as described for the relative lifetime of central F-actin foci. Similar to the central F-actin foci, the actin structures at the outer edge of the WKO GCB contact zone had significantly shorter lifetimes than those of WT GCBs (**Figure 6B**). We further measured the number of Lifeact-GFP FI peaks per minute (**Figures 6C,D**) and the standard deviation of the time between two Lifeact-GFP peaks (**Figures 6C,E**) using kymographs to reflect the frequency and the regularity of this actin structure at the leading edge of the spreading membrane. We found that the Lifeact-GFP FI peaks appeared at the outer edge of the WKO GCB contact zone much less frequently and with less regularity than those in WT GCBs (**Figures 6C–E**). To examine the impact of such changes in the actin cytoskeleton caused by WKO on the interaction of GCBs with antigen-presenting surfaces, we analyzed time-lapse IRM images using kymographs (**Figure 6F**). In the contact zone of WT GCBs, we observed a ∼2 μm wide dark region (indicating adhesion of the GCB plasma membrane to antigen-presenting surfaces) surrounding the centralized protrusions after reaching maximal spread area (**Figure 6F**, top panels, red arrows). The width of this adherent region in WKO GCBs appeared to be more variable over time and more asymmetrical than in WT GCBs (**Figure 6F**, bottom panels, red arrows). To examine this adherent region closely, we determined the width ratio of the adherent region at two opposite sides in individual contact zones at 3, 5, 7, and 10 min (**Figure 6G**) and the fold change in the width of the adherent region between 5 and 7 min (**Figure 6H**). WKO GBCs displayed significantly higher ratios of the adherent region width between the two sides of individual contact zones (**Figure 6G**) and significantly greater fold changes between 5 and 7 min (**Figure 6H**) than WT GCBs. These results suggest that WKO destabilizes this adherent region. Thus, WASp contributes to the actin cytoskeletal network that maintains the adhesion of GCBs to antigen-presenting surfaces, thereby stabilizing the IS.

DISCUSSION

Germinal centers are critical for selecting high-affinity antigen-specific B-cells and eliminating non-specific B-cells generated during somatic hypermutation (Victora and Nussenzweig, 2012; Mesin et al., 2016). A lack of antibody responses to vaccinations and infections and an accumulation of autoantibodies in WAS patients and mouse models suggest a failure of GCBs in the affinity maturation process (Notarangelo et al., 2008; Bosticardo et al., 2009; Becker-Herman et al., 2011). This study has revealed that WASp is essential for building the unique architecture of the GCB IS. WASp is responsible for generating and stabilizing actin structures that support and maintain membrane protrusions in the center of the GCB IS. WASp also contributes to the actin structures that drive GCB spreading and adhesion to antigen-presenting surfaces, stabilizing the GCB IS. GCBs rely on this unique architecture of the IS to discriminate the affinity of antigen

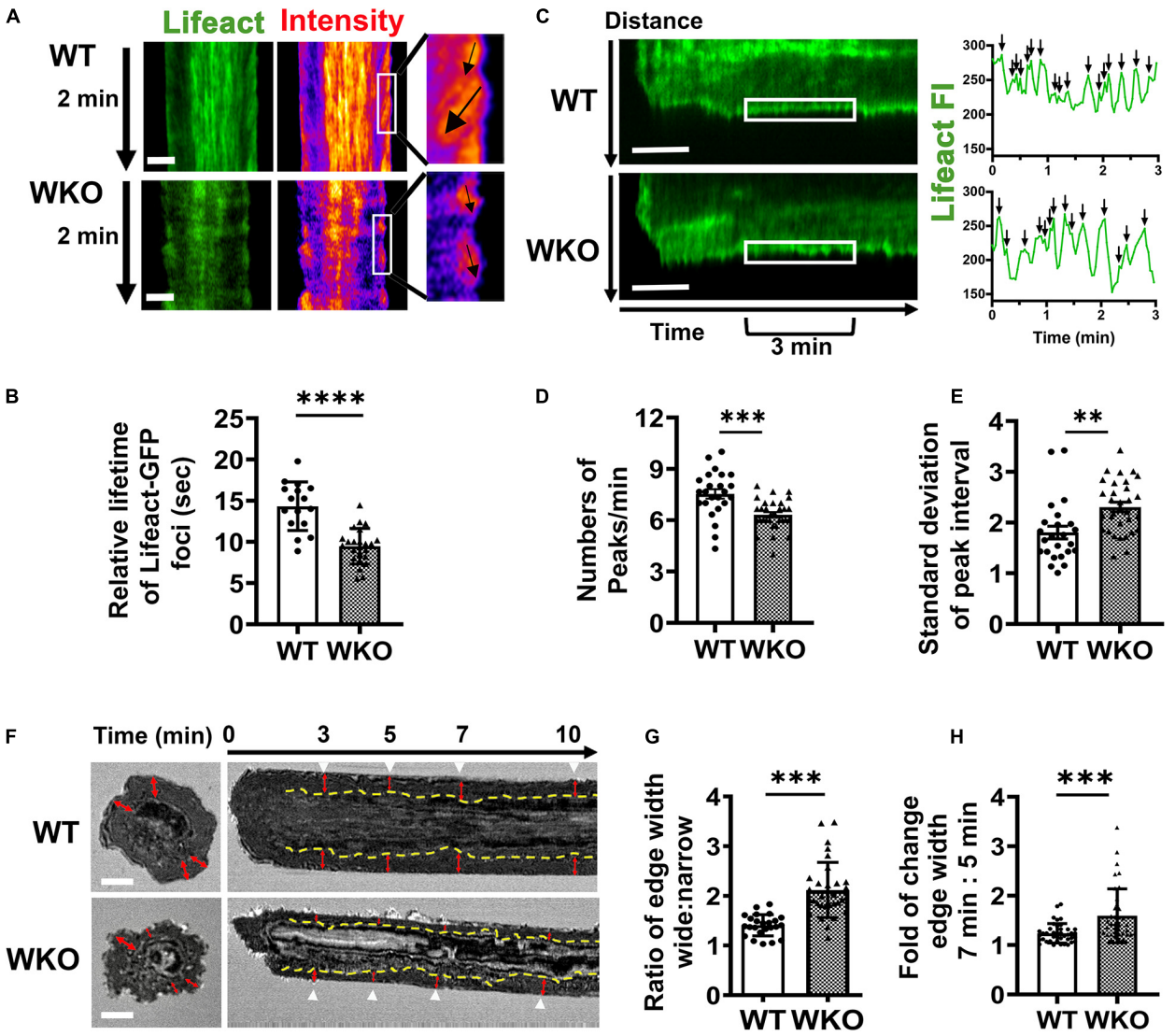

FIGURE 6 | WASp is required for the formation of a steady adherent region surrounding the central signalosome. GCBs isolated from SRBC-immunized Lifeact-GFP mice were incubated with Fab'-PLB and imaged live using IRM and TIRF. **(A)** Representative kymographs from 2.5 to 4.5 min and their intensity heat maps generated from Lifeact-GFP time-lapse images. White box, peripheral regions for 1 min. Black arrows, tracks of Lifeact foci at an edge region. **(B)** Relative lifetimes of Lifeact-GFP foci were evaluated by the duration of Lifeact-GFP foci detected in randomly selected kymographs. Data points represent individual cells, the average of 8∼10 Lifeact foci tracks per cell. **(C)** Representative Lifeact-GFP kymographs (from the center to the periphery of the contact zone). White box, peripheral regions between 3 and 6 min. FI in the peripheral region (white box) over time was shown in the right panels. Black arrows, individual Lifeact-GFP FI peaks. **(D)** Numbers of Lifeact-GFP FI peaks per min between 3 and 6 min. **(E)** Standard deviation (SD) of time intervals between peaks. **(F)** Representative IRM images at 7 min and kymographs generated from time-lapse IRM images of WT and WKO GCBs. Yellow dashed lines indicate the border between the periphery and center regions of the contact zone based on IRM density. Red arrows indicate the width of the periphery area. White arrow, time. **(G)** The ratio of the periphery width at the wider side relative to the narrow side. Data points represent the average of the ratios at 3, 5, 7, and 10 min in individual cells. **(H)** The fold of change in the periphery width between 5 and 7 min. Data points represent individual cells. Scale bars, 3 μm. The results were the average (± SD) of 20∼30 individual cells per condition. $n = 4$. $^{**}p < 0.01$, $^{***}p < 0.001$, and $^{****}p < 0.0001$, unpaired Student's *t*-test or one-way ANOVA.

presented on the surface of antigen-presenting cells, activate BCR signaling, and capture antigen for processing and presentation (Nowosad et al., 2016; Kwak et al., 2018).

Recent studies have shown that GCBs from human tonsils and mouse spleens engage membrane antigen through actin-rich pod-like membrane protrusions and form BCR microclusters at the tips of these protrusions (Nowosad et al., 2016; Kwak et al., 2018). This organization is different from the naïve B-cell IS. The naïve B-cell plasma membrane interacting with antigen-presenting surfaces is relatively smooth, allowing BCR microclusters to merge into a central cluster. In contrast, the pod-like membrane protrusions prohibit BCR microclusters from growing and merging. This unique GCB IS architecture has been shown to provide GCBs an enhanced ability to sense

their binding affinity to antigen, as the stability of pod-like membrane protrusions increases with antigen affinity (Nowosad et al., 2016; Kwak et al., 2018). Using high-resolution IRM and TIRF imaging, this study extends these findings by showing that these membrane protrusions concentrate in the center of the GCB contact zone and are relatively stable when GCBs interact with PLB coated with a relatively high density of Fab' fragment of anti-IgM + G antibody. As PLBs provide high-avidity binding to surface BCRs, the centralized, stable protrusions probably reflect the IS characteristics in GCBs interacting with high-affinity antigen. How antigen affinity and the stiffness of antigen-presenting surfaces influence the GCB IS architecture remains an interesting question.

This study further shows that activated signaling molecules, including both positive (CD79, Syk, and Akt) and negative (SHP1) signaling molecules, appear at the protrusions at similar times. The peak levels of phosphorylated CD79a and Syk persist at least for 20 min. In contrast, stimulatory kinases in naïve B-cells interacting with the same type of Fab'-PLB are first activated and then down-regulated by activated phosphatases (Liu et al., 2011, 2013a; Seeley-Fallen et al., 2014). Our findings are consistent with the previous observation that the activity of phosphatases is enhanced in GCBs (Khalil et al., 2012) and increases at similar times as stimulatory kinases in response to antigenic stimulation (Kwak et al., 2018). Together, these data suggest that the phosphatases SHP1 and SHIP1 work with stimulatory kinases to regulate the level of persistent BCR signaling in germinal center B-cells rather than deactivate BCR signaling in naïve B-cells. We also noticed that stimulatory kinases and inhibitory phosphatases distribute differentially at the membrane protrusions, even though they are activated in GCBs simultaneously. Activated CD79, Syk, and SHP1 fill the contact region of the membrane protrusions and the outer edge of the contact zone, while activated Akt and SHIP1 appear as puncta, sparsely decorating the membrane protrusions and the outer edge of the contact zone, respectively. These observations suggest that GCBs organize signaling molecules into distinct microclusters and maintain them for persistent signaling through pod-like membrane protrusions. However, our studies using TIRF were limited to the GCB contact membrane. High-resolution three-dimensional imaging is required for fully visualizing and characterizing the organization of GCB signalosomes.

WASp has been shown to have B-cell intrinsic roles in the germinal center, causing GCB hyper-proliferation and plasma cell differentiation in WASp-deficient mouse models (Becker-Herman et al., 2011). However, the cellular mechanism by which WASp regulates GCB affinity maturation remains elusive. WASp activates the actin nucleation factor Arp2/3, downstream of Cdc42 and phosphatidylinositol-4,5-biphosphates (Bi and Zigmond, 1999; Padrick and Rosen, 2010). Activated Arp2/3 polymerizes branched actin filaments, which are known to drive lamellipodia of migrating and spreading cells (Bisi et al., 2013; Alekhina et al., 2017). Therefore, it is not surprising to find that WASp contributes significantly to GCB spreading on antigen-presenting surfaces, particularly the spreading kinetics. WASp plays a similar role in naïve B-cells (Liu et al., 2013a). Spreading expands B-cell contact with antigen-presenting surfaces, amplifying BCR clustering and signaling (Fleire et al., 2006; Harwood and Batista, 2010).

In addition to its role in GCB spreading, the new finding of this study is that WASp is essential for the formation and stabilization of pod-like membrane protrusions, the unique membrane structures of the GCB IS. WASp is responsible for the generation and/or extended lifetime of actin foci that support the membrane protrusions at the center of the GCB contact zone, as both the number of actin foci and their relative lifetime are reduced in WKO GCBs. This finding suggests that actin structures supporting pod-like membrane protrusions are based on branched actin networks. Furthermore, WASp is also required for the stability and regularity of branched actin structures at the outer edge of the GCB contact membrane after rapid spreading. These actin structures, which appear to be tread milling, function to maintain the GCB contact area and the GCB adherence to antigen-presenting surfaces surrounding the centralized membrane protrusions. The role of these actin structures in GCBs is opposite to what was observed in naïve B-cells, where actin at the outer edge of the contact zone drives B-cell contraction following spreading, which promotes signaling attenuation (Liu et al., 2013a; Seeley-Fallen et al., 2014). This functional difference in the actin cytoskeleton between GCBs and naïve B-cells likely contributes to their distinct BCR signaling signatures and a heightened ability of GCBs to distinguish antigen-binding affinity compared to naïve B-cells (Khalil et al., 2012; Nowosad et al., 2016; Kwak et al., 2018; Luo et al., 2019). The role of WASp in the generation and maintenance of actin structures supporting the unique architecture of the GCB IS may explain the defective germinal center reaction in WAS patients and mouse models. WASp-deficiency causes GCBs to generates less and/or relatively unstable membrane protrusions, which likely reduces the ability of GCBs to distinguish antigen-binding affinity, causing failures in selecting high-affinity antigen-specific B-cells.

The reductions in BCR phosphorylation, BCR clustering, and cell spreading in WKO GCBs compared to WT GCBs suggest that WASp promotes BCR activation by increasing cell spreading and BCR clustering at the contact zone. These findings are similar to what we observed in WKO native B-cells (Liu et al., 2013a), suggesting a common role for WASp in naïve B-cells and GCBs, besides its GCB-specific functions. Using single molecule imaging, we have recently shown that the mobility of surface BCRs is significantly lower in WKO native B-cells than in WT naïve B cells (Rey-Suarez et al., 2020), implying that WASp promotes BCR clustering by mobilizing BCRs on the B-cell surface. Interestingly, along with the reduced BCR clustering and activation in WKO GCBs, the levels of two major phosphatases in the contact zone are differentially altered, with pSHIP1 increasing and pSHP1 decreasing, suggesting that WASp differentially regulates these two phosphatases. The implication of such opposing alterations of SHIP1 and SHP1 activation in

WKO GCBs is unknown. We have also noticed that the impact of WASp-deficiency on the organization of micro-signaling clusters is much more than its effect on the level of BCR proximal signaling. This is likely the result of the saturated strength of activation by a relatively high-density of Fab' on PLB, overcoming signaling defects caused by WASp deficiency. Future studies with graded antigen density and affinity will further reveal the mechanism by which WASp regulates GCB affinity maturation.

The moderate reduction in cell spreading, BCR clustering, and signaling in WKO GCBs indicates that WASp is not essential for BCR signaling in GCBs. The WASp family has additional members, including N-WASp and WAVE, which can all activate Arp2/3-mediated branched actin polymerization (Padrick and Rosen, 2010; Oda and Eto, 2013; Alekhina et al., 2017). We have previously shown that both WASp and N-WASp are required for cell spreading, BCR clustering, and signaling in naïve B-cells. Naïve B-cells from WASp and N-WASp (B-cell-specific) double knockout mice fail to spread, cluster surface BCRs, and activate BCRs when interacting with the same Fab'-PLB (Liu et al., 2013a). These results suggest that N-WASp can functionally compensate for the lack of WASp in GCBs but cannot exclude WAVE's possible roles in GCBs. How these actin nucleation promoting factors work together in GCBs to facilitate affinity maturation is a subject of our future interest.

In summary, this study has identified a role for WASp and WASp-activated branched actin polymerization in the generation and maintenance of the unique architecture of the GCB IS. This unique architecture is essential for GCBs to discriminate antigen-binding affinity for the selection of high-affinity antigen-specific B-cells to mount antibody responses. The defective GCB IS architecture provides a cellular mechanism by which WASp deficiency causes immune disorders.

DATA AVAILABILITY STATEMENT

The original contributions presented in the study are included in the article/**Supplementary Material**, further inquiries can be directed to the corresponding author/s.

ETHICS STATEMENT

The animal study was reviewed and approved by the Institutional Animal Care and Use Committee (IACUC) at the University of Maryland (College Park, MD, United States) and Chongqing Medical University (Chongqing, China).

AUTHOR CONTRIBUTIONS

YL, WS, AU, and XZ established the study design and provided the research strategy. YL and AB performed the experiments and the data analysis. YL and WS prepared and wrote the manuscript. All authors read and approved the manuscript.

FUNDING

This work was supported by the US National Institute of Health grant R01 GM064625 to WS. YL was supported by National Science Foundation of China grant #8161001201 to XZ. AU was supported by the US National Science Foundation grant PHY 1915534.

ACKNOWLEDGMENTS

We thank Drs. A. Beaven (CBMG Imaging Core, University of Maryland) and K. Class (CBMG Flow Cytometry Core, University of Maryland) for assistance with confocal microscopy and flow cytometry and members of the Song and Zhao laboratories for helpful discussions.

SUPPLEMENTARY MATERIAL

The Supplementary Material for this article can be found online at: https://www.frontiersin.org/articles/10.3389/fcell.2021.646077/full#supplementary-material

REFERENCES

Alekhina, O., Burstein, E., and Billadeau, D. D. (2017). Cellular functions of Wasp family proteins at a glance. *J. Cell* Sci. 130, 2235–2241. doi: 10.1242/jcs.199570

Allen, C. D., Ansel, K. M., Low, C., Lesley, R., Tamamura, H., Fujii, N., et al. (2004). Germinal center dark and light zone organization is mediated by CXCR4 and CXCR5. *Nat. Immunol.* 5, 943–952. doi: 10.1038/ni1100

Avalos, A. M., and Ploegh, H. L. (2014). Early BCR Events and Antigen Capture, Processing, and Loading on MHC Class II on B Cells. *Front. Immunol.* 5:92. doi: 10.3389/fimmu.2014.00092

Batista, F. D., and Harwood, N. E. (2009). The who, how and where of antigen presentation to B cells. *Nat. Rev. Immunol.* 9, 15–27. doi: 10.1038/nri2454

Batista, F. D., and Neuberger, M. S. (2000). B cells extract and present immobilized antigen: implications for affinity discrimination. *EMBO J.* 19, 513–520. doi: 10.1093/emboj/19.4.513

Becker-Herman, S., Meyer-Bahlburg, A., Schwartz, M. A., Jackson, S. W., Hudkins, K. L., Liu, C., et al. (2011). WASp-deficient B cells play a critical, cell-intrinsic role in triggering autoimmunity. *J. Exp. Med.* 208, 2033–2042. doi: 10.1084/jem.20110200

Bi, E., and Zigmond, S. H. (1999). Actin polymerization: where the WASP stings. *Curr. Biol.* 9, R160–R163.

Bisi, S., Disanza, A., Malinverno, C., Frittoli, E., Palamidessi, A., and Scita, G. (2013). Membrane and actin dynamics interplay at lamellipodia leading edge. *Curr. Opin. Cell Biol.* 25, 565–573. doi: 10.1016/j.ceb.2013.04.001

Bosticardo, M., Marangoni, F., Aiuti, A., Villa, A., and Grazia Roncarolo, M. (2009). Recent advances in understanding the pathophysiology of Wiskott-Aldrich syndrome. *Blood* 113, 6288–6295. doi: 10.1182/blood-2008-12-115253

Brauweiler, A. M., Tamir, I., and Cambier, J. C. (2000). Bilevel control of B-cell activation by the inositol 5-phosphatase SHIP. *Immunol. Rev.* 176, 69–74.

Cato, M. H., Yau, I. W., and Rickert, R. C. (2011). Magnetic-based purification of untouched mouse germinal center B cells for ex vivo manipulation and biochemical analysis. *Nat. Protoc.* 6, 953–960. doi: 10.1038/nprot.2011.344

Chan, T. D., and Brink, R. (2012). Affinity-based selection and the germinal center response. *Immunol. Rev.* 247, 11–23. doi: 10.1111/j.1600-065X.2012.01118.x

Cheng, P. C., Dykstra, M. L., Mitchell, R. N., and Pierce, S. K. (1999). A role for lipid rafts in B cell antigen receptor signaling and antigen targeting. *J. Exp. Med.* 190, 1549–1560.

Cirelli, K. M., and Crotty, S. (2017). Germinal center enhancement by extended antigen availability. *Curr. Opin. Immunol.* 47, 64–69. doi: 10.1016/j.coi.2017.06.008

Cyster, J. G. (2010). B cell follicles and antigen encounters of the third kind. *Nat. Immunol.* 11, 989–996. doi: 10.1038/ni.1946

Dal Porto, J. M., Gauld, S. B., Merrell, K. T., Mills, D., Pugh-Bernard, A. E., and Cambier, J. (2004). B cell antigen receptor signaling 101. *Mol. Immunol.* 41, 599–613. doi: 10.1016/j.molimm.2004.04.008

Depoil, D., Weber, M., Treanor, B., Fleire, S. J., Carrasco, Y. R., Harwood, N. E., et al. (2009). Early events of B cell activation by antigen. *Sci. Signal.* 2:pt1. doi: 10.1126/scisignal.263pt1

Fleire, S. J., Goldman, J. P., Carrasco, Y. R., Weber, M., Bray, D., and Batista, F. D. (2006). B cell ligand discrimination through a spreading and contraction response. *Science* 312, 738–741. doi: 10.1126/science.1123940

Franks, S. E., and Cambier, J. C. (2018). Putting on the Brakes: regulatory Kinases and Phosphatases Maintaining B Cell Anergy. *Front. Immunol.* 9:665. doi: 10.3389/fimmu.2018.00665

Freeman, S. A., Lei, V., Dang-Lawson, M., Mizuno, K., Roskelley, C. D., and Gold, M. R. (2011). Cofilin-mediated F-actin severing is regulated by the Rap GTPase and controls the cytoskeletal dynamics that drive lymphocyte spreading and BCR microcluster formation. *J. Immunol.* 187, 5887–5900. doi: 10.4049/jimmunol.1102233

Gitlin, A. D., Shulman, Z., and Nussenzweig, M. C. (2014). Clonal selection in the germinal centre by regulated proliferation and hypermutation. *Nature* 509, 637–640. doi: 10.1038/nature13300

Harwood, N. E., and Batista, F. D. (2010). Early events in B cell activation. *Annu. Rev. Immunol.* 28, 185–210. doi: 10.1146/annurev-immunol-030409-101216

Harwood, N. E., and Batista, F. D. (2011). The cytoskeleton coordinates the early events of B-cell activation. *Cold Spring Harb. Perspect. Biol.* 3:a002360. doi: 10.1101/cshperspect.a002360

Hoogeboom, R., and Tolar, P. (2016). Molecular Mechanisms of B Cell Antigen Gathering and Endocytosis. *Curr. Top. Microbiol. Immunol.* 393, 45–63. doi: 10.1007/82_2015_476

Khalil, A. M., Cambier, J. C., and Shlomchik, M. J. (2012). B cell receptor signal transduction in the GC is short-circuited by high phosphatase activity. *Science* 336, 1178–1181. doi: 10.1126/science.1213368

Kolhatkar, N. S., Brahmandam, A., Thouvenel, C. D., Becker-Herman, S., Jacobs, H. M., Schwartz, M. A., et al. (2015). Altered BCR and TLR signals promote enhanced positive selection of autoreactive transitional B cells in Wiskott-Aldrich syndrome. *J. Exp. Med.* 212, 1663–1677. doi: 10.1084/jem.20150585

Kuijpers, T. W., Tool, A. T. J., van der Bijl, I., de Boer, M., van Houdt, M., de Cuyper, I. M., et al. (2017). Combined immunodeficiency with severe inflammation and allergy caused by ARPC1B deficiency. *J. Allergy Clin. Immunol.* 140, 273–277.e10. doi: 10.1016/j.jaci.2016.09.061

Kwak, K., Akkaya, M., and Pierce, S. K. (2019). B cell signaling in context. *Nat. Immunol.* 20, 963–969. doi: 10.1038/s41590-019-0427-9

Kwak, K., Quizon, N., Sohn, H., Saniee, A., Manzella-Lapeira, J., Holla, P., et al. (2018). Intrinsic properties of human germinal center B cells set antigen affinity thresholds. *Sci. Immunol.* 3:eaau6598. doi: 10.1126/sciimmunol.aau6598

Lam Hui, K., Wang, C., Grooman, B., Wayt, J., and Upadhyaya, A. (2012). Membrane dynamics correlate with formation of signaling clusters during cell spreading. *Biophys. J.* 102, 1524–1533. doi: 10.1016/j.bpj.2012.02.015

Liu, C., Bai, X., Wu, J., Sharma, S., Upadhyaya, A., Dahlberg, C. I., et al. (2013a). N-WASP is essential for the negative regulation of B cell receptor signaling. *PLoS Biol.* 11:e100170. doi: 10.1371/journal.pbio.1001704

Liu, C., Fallen, M. K., Miller, H., Upadhyaya, A., and Song, W. (2013b). The actin cytoskeleton coordinates the signal transduction and antigen processing functions of the B cell antigen receptor. *Front. Biol.* 8:475–485. doi: 10.1007/s11515-013-1272-0

Liu, C., Miller, H., Hui, K. L., Grooman, B., Bolland, S., Upadhyaya, A., et al. (2011). A balance of Bruton's tyrosine kinase and SHIP activation regulates B cell receptor cluster formation by controlling actin remodeling. *J. Immunol.* 187, 230–239. doi: 10.4049/jimmunol.1100157

Liu, C., Miller, H., Orlowski, G., Hang, H., Upadhyaya, A., and Song, W. (2012). Actin reorganization is required for the formation of polarized B cell receptor signalosomes in response to both soluble and membrane-associated antigens. *J. Immunol.* 188, 3237–3246. doi: 10.4049/jimmunol.1103065

Luo, W., Hawse, W., Conter, L., Trivedi, N., Weisel, F., Wikenheiser, D., et al. (2019). The AKT kinase signaling network is rewired by PTEN to control proximal BCR signaling in germinal center B cells. *Nat. Immunol.* 20, 736–746. doi: 10.1038/s41590-019-0376-3

Melak, M., Plessner, M., and Grosse, R. (2017). Actin visualization at a glance. *J. Cell Sci.* 130, 525–530. doi: 10.1242/jcs.189068

Mesin, L., Ersching, J., and Victora, G. D. (2016). Germinal Center B Cell Dynamics. *Immunity* 45, 471–482. doi: 10.1016/j.immuni.2016.09.001

Notarangelo, L. D., Miao, C. H., and Ochs, H. D. (2008). Wiskott-Aldrich syndrome. *Curr. Opin. Hematol.* 15, 30–36. doi: 10.1097/MOH.0b013e3282f30448

Nowosad, C. R., Spillane, K. M., and Tolar, P. (2016). Germinal center B cells recognize antigen through a specialized immune synapse architecture. *Nat. Immunol.* 17, 870–877. doi: 10.1038/ni.3458

Oda, A., and Eto, K. (2013). WASPs and WAVEs: from molecular function to physiology in hematopoietic cells. *Semin. Cell Dev. Biol.* 24, 308–313. doi: 10.1016/j.semcdb.2013.03.002

Padrick, S. B., and Rosen, M. K. (2010). Physical mechanisms of signal integration by WASP family proteins. *Annu. Rev. Biochem.* 79, 707–735. doi: 10.1146/annurev.biochem.77.060407.135452

Peluso, P., Wilson, D. S., Do, D., Tran, H., Venkatasubbaiah, M., Quincy, D., et al. (2003). Optimizing antibody immobilization strategies for the construction of protein microarrays. *Anal. Biochem.* 312, 113–124. doi: 10.1016/s0003-2697(02)00442-6

Recher, M., Burns, S. O., de la Fuente, M. A., Volpi, S., Dahlberg, C., and Walter, J. E. (2012). B cell-intrinsic deficiency of the Wiskott-Aldrich syndrome protein (WASp) causes severe abnormalities of the peripheral B-cell compartment in mice. *Blood* 119, 2819–2828. doi: 10.1182/blood-2011-09-379412

Reth, M. (1992). Antigen receptors on B lymphocytes. *Annu. Rev. Immunol.* 10, 97–121. doi: 10.1146/annurev.iy.10.040192.000525

Rey-Suarez, I., Wheatley, B. A., Koo, P., Bhanja, A., Shu, Z., Mochrie, S., et al. (2020). WASP family proteins regulate the mobility of the B cell receptor during signaling activation. *Nat. Commun.* 11:439. doi: 10.1038/s41467-020-14335-8

Riedl, J., Crevenna, A. H., Kessenbrock, K., Yu, J. H., Neukirchen, D., Bista, M., et al. (2008). Lifeact: a versatile marker to visualize F-actin. *Nat. Methods* 5, 605–607. doi: 10.1038/nmeth.1220

Seeley-Fallen, M. K., Liu, L. J., Shapiro, M. R., Onabajo, O. O., Palaniyandi, S., Zhu, X., et al. (2014). Actin-binding protein 1 links B-cell antigen receptors to negative signaling pathways. *Proc. Natl. Acad. Sci. U. S. A.* 111, 9881–9886. doi: 10.1073/pnas.1321971111

Shlomchik, M. J., Luo, W., and Weisel, F. (2019). Linking signaling and selection in the germinal center. *Immunol. Rev.* 288, 49–63. doi: 10.1111/imr.12744

Shlomchik, M. J., and Weisel, F. (2012). Germinal center selection and the development of memory B and plasma cells. *Immunol. Rev.* 247, 52–63. doi: 10.1111/j.1600-065X.2012.01124.x

Simon, K. L., Anderson, S. M., Garabedian, E. K., Moratto, D., Sokolic, R. A., and Candotti, F. (2014). Molecular and phenotypic abnormalities of B lymphocytes in patients with Wiskott-Aldrich syndrome. *J. Allergy Clin. Immunol.* 133, 896–9.e4. doi: 10.1016/j.jaci.2013.08.050

Sohn, H. W., Tolar, P., and Pierce, S. K. (2008). Membrane heterogeneities in the formation of B cell receptor-Lyn kinase microclusters and the immune synapse. *J. Cell Biol.* 182, 367–379. doi: 10.1083/jcb.200802007

Song, W., Liu, C., Seeley-Fallen, M. K., Miller, H., Ketchum, C., and Upadhyaya, A. (2013). Actin-mediated feedback loops in B-cell receptor signaling. *Immunol. Rev.* 256, 177–189. doi: 10.1111/imr.12113

Tolar, P. (2017). Cytoskeletal control of B cell responses to antigens. *Nat. Rev. Immunol.* 17, 621–634. doi: 10.1038/nri.2017.67

Tolar, P., Hanna, J., Krueger, P. D., and Pierce, S. K. (2009). The constant region of the membrane immunoglobulin mediates B cell-receptor clustering and signaling in response to membrane antigens. *Immunity* 30, 44–55. doi: 10.1016/j.immuni.2008.11.007

Treanor, B., Depoil, D., Gonzalez-Granja, A., Barral, P., Weber, M., Dushek, O., et al. (2010). The membrane skeleton controls diffusion dynamics and signaling through the B cell receptor. *Immunity* 32, 187–199. doi: 10.1016/j.immuni.2009.12.005

Turner, J. S., Ke, F., and Grigorova, I. L. (2018). B Cell Receptor Crosslinking Augments Germinal Center B Cell Selection when T Cell Help Is Limiting. *Cell Rep.* 25, 1395–1403.e4. doi: 10.1016/j.celrep.2018.10.042

Victora, G. D., and Nussenzweig, M. C. (2012). Germinal centers. *Annu. Rev. Immunol.* 30, 429–457. doi: 10.1146/annurev-immunol-020711-075032

Volpi, S., Cicalese, M. P., Tuijnenburg, P., Tool, A. T. J., Cuadrado, E., Abu-Halaweh, M., et al. (2019). A combined immunodeficiency with severe infections, inflammation, and allergy caused by ARPC1B deficiency. *J. Allergy Clin. Immunol.* 143, 2296–2299. doi: 10.1016/j.jaci.2019.02.003

Conflict of Interest: The authors declare that the research was conducted in the absence of any commercial or financial relationships that could be construed as a potential conflict of interest.

frontiers in Cell and Developmental Biology

REVIEW
published: 24 June 2021
doi: 10.3389/fcell.2021.665519

Actin Dynamics at the T Cell Synapse as Revealed by Immune-Related Actinopathies

Loïc Dupré[1,2,3]*, *Kaan Boztug*[1,4,5,6,7] *and Laurène Pfajfer*[1,2,3,4]

[1] Ludwig Boltzmann Institute for Rare and Undiagnosed Diseases (LBI-RUD), Vienna, Austria, [2] Department of Dermatology, Medical University of Vienna, Vienna, Austria, [3] Toulouse Institute for Infectious and Inflammatory Diseases (INFINITy), INSERM, CNRS, Toulouse III Paul Sabatier University, Toulouse, France, [4] St. Anna Children's Cancer Research Institute (CCRI), Vienna, Austria, [5] CeMM Research Center for Molecular Medicine of the Austrian Academy of Sciences, Vienna, Austria, [6] Department of Pediatrics and Adolescent Medicine, Medical University of Vienna, Vienna, Austria, [7] St. Anna Children's Hospital, Department of Pediatrics and Adolescent Medicine, Medical University of Vienna, Vienna, Austria

The actin cytoskeleton is composed of dynamic filament networks that build adaptable local architectures to sustain nearly all cellular activities in response to a myriad of stimuli. Although the function of numerous players that tune actin remodeling is known, the coordinated molecular orchestration of the actin cytoskeleton to guide cellular decisions is still ill defined. T lymphocytes provide a prototypical example of how a complex program of actin cytoskeleton remodeling sustains the spatio-temporal control of key cellular activities, namely antigen scanning and sensing, as well as polarized delivery of effector molecules, via the immunological synapse. We here review the unique knowledge on actin dynamics at the T lymphocyte synapse gained through the study of primary immunodeficiences caused by mutations in genes encoding actin regulatory proteins. Beyond the specific roles of individual actin remodelers, we further develop the view that these operate in a coordinated manner and are an integral part of multiple signaling pathways in T lymphocytes.

Keywords: T lymphocytes, immune-related actinopathies, actin cytoskeleton remodeling, immunological synapse, actin binding proteins, primary immunodeficiencies

OPEN ACCESS

Edited by:
Sudha Kumari, Massachusetts Institute of Technology, United States

Reviewed by:
Raif Geha, Boston Children's Hospital and Harvard Medical School, United States
Andres Alcover, Institut Pasteur, France

***Correspondence:**
Loïc Dupré
loic.dupre@rud.lbg.ac.at

Specialty section:
This article was submitted to Cell Growth and Division, a section of the journal Frontiers in Cell and Developmental Biology

Received: *08 February 2021*
Accepted: *06 April 2021*
Published: *24 June 2021*

Citation:
Dupré L, Boztug K and Pfajfer L (2021) Actin Dynamics at the T Cell Synapse as Revealed by Immune-Related Actinopathies. Front. Cell Dev. Biol. 9:665519. doi: 10.3389/fcell.2021.665519

PREAMBLE

The actin cytoskeleton provides a structural basis to sustain, not only cell shape remodeling, but also nearly every dynamic cellular process. The actin cytoskeleton is endowed with highly dynamic and adaptable properties. Indeed, multiple actin networks that are uniquely assembled coexist within cells, occupying specific locations and exerting specialized cellular processes (Blanchoin et al., 2014; Lappalainen, 2016). These distinct networks are governed by different dosage of the multiple molecular activities that tune actin dynamics (Pollard, 2016). Interestingly, the diversity of actin-driven processes reflects the multiplicity of dynamic activities shared among all cells, as well as the numerous specialized activities at work in individual cell subsets. This notion applies particularly to the hematopoietic system, which is composed of cells with highly diversified and specialized activities that rely on actin dynamics.

In particular, T cells assemble the immunological synapse (IS), an adhesive structure that is the site of complex actin network organization and dynamics. As such the T cell synapse provides a prototypical example of how the actin cytoskeleton sustains the coordination of key cellular activities, including adhesion, receptor patterning and control of secretory events, to name a few.

The requirement of actin cytoskeleton integrity for productive T cell/APC encounter and for the assembly of key signaling networks has been established along with the characterization of the IS (Billadeau et al., 2007). Recent studies have started to apply resolutive approaches to uncover some of the complexity of actin remodeling at this highly specialized structure. The current notion is that of multiple supportive roles for the actin cytoskeleton at the T cell synapse. From a spatial perspective, sub-networks have been identified, with specific interactions with receptor clusters that display specific patterning. From a temporal perspective, actin remodeling supports a sequence of events that are particularly crucial to tune T cell activation and function.

The many facets of actin cytoskeleton remodeling are supported by a multiplicity of molecular actors that integrate complex stimuli into adapted actin responses. Research in this field has been shaped by the discovery of rare deficiencies, which highlight the role of specific molecules in the function of immune cells. In particular actin-related primary immunodeficiencies (PID) might be considered as models to investigate the tuning of T cell activation and function by the actin cytoskeleton. This review covers our current understanding of the molecular control of actin cytoskeleton remodeling at the T cell IS via the prism of actin-related PID. By now, approximately 20 PID entities due to actin defects (so called actinopathies) have been identified (Burns et al., 2017; Janssen and Geha, 2019; Tangye et al., 2019). These rare pathologies provide unique models to reveal the physiological role of actin regulators in human T cells in the context of natural environmental challenges.

Here we provide a review on actin dynamics and sub-networks supporting the T cell IS. We then highlight how the elucidation of actin-related PID has led to fundamental discoveries about the molecular regulation of the actin cytoskeleton at the T cell IS. Then, we try to integrate knowledge from individual studies around key aspects of actin dynamics at T cell IS. In particular, we discuss recent research about how actin regulators coordinate their activities to assemble specific actin networks. We also discuss how distinct actin networks may combine their function to control the sequential steps of the T cell IS.

CONTROL OF THE T CELL IMMUNOLOGICAL SYNAPSE BY THE ACTIN CYTOSKELETON

Multilayered Activities of the Actin Cytoskeleton at the Immunological Synapse

Through its intrinsic remodeling properties, the actin cytoskeleton provides a structural basis for the dynamic and polymorphic architecture of the IS. The fact that actin cytoskeleton integrity is necessary to establish dynamic and prolonged contacts between T cells and antigen-presenting cells (APC) (Valitutti et al., 1995; Delon et al., 1998) was actually recognized prior to the characterization of the molecular organization of the IS (Monks et al., 1998; Grakoui et al., 1999). Following these early observations, a wealth of studies has contributed to the current notion that the actin cytoskeleton exerts multiple tasks during the T cell/APC interaction. These tasks may be split as those operating at the cellular scale (**Figure 1A**) and those operating at the mesoscale (**Figure 1B**). At the cellular scale, the actin cytoskeleton promotes a morphological transition from an elongated shape characterizing migrating lymphocytes to a round-up shape following adhesion to the APC and migration arrest (Negulescu et al., 1996). The stop signal is delivered through TCR evoked phosphorylation of myosin IIA, which inactivates the contractile machinery responsible for rapid motility (Jacobelli et al., 2004). The actin cytoskeleton then sustains the formation of lateral membrane protrusions that scan the surface of the APC (Tskvitaria-Fuller et al., 2003). At the mesoscale, it is remarkable that the local architecture of the actin cytoskeleton differs along the radial layers of the IS (recently reviewed in Roy and Burkhardt, 2018; Hammer et al., 2019). The first identified sub-structure has been the dynamic ring-like structure at the periphery of the synapse, which is enriched in branched F-actin and corresponds to a radial lamellipodium sought to stabilize the IS (Bunnell et al., 2001). Quite distinctly, the center of the T/APC contact is characterized by a relative depletion of F-actin. Although it had initially been considered a region deprived of F-actin (Stinchcombe et al., 2006), improved resolution has revealed that the IS center is sustained by an actin network with loose reticulation. The partial depletion of F-actin at the IS center is reached within one minute of IS assembly so that it has been proposed to initiate key subsequent events (Ritter et al., 2015). These include the polarization of the MTOC (Stinchcombe et al., 2006) and the delivery of secretory vesicles such as lytic granules (Brown et al., 2011; Rak et al., 2011). Beyond these distinct F-actin subdomains, actin cytoskeleton integrity is essential to assembly of TCR microclusters and signaling platforms (Campi et al., 2005). Furthermore actin dynamics is characterized by an inward flow promoting the centripetal transport of receptor microclusters (Varma et al., 2006; Kaizuka et al., 2007). Interestingly, differential coupling of surface receptors promotes molecular segregation into distinct domains, such as TCR (cSMAC) and LFA-1 (pSMAC). The actin cytoskeleton is also playing an active role in TCR endocytosis and recycling (McGavin et al., 2001). It may seem puzzling how the actin cytoskeleton drives so many distinct activities in the confined space of the IS. Such functional multiplicity and diversification relies on the ability of the actin cytoskeleton to build local networks of specific filament length, density and reticulation. As we will see in the following chapter dedicated to natural deficiencies in actin regulatory proteins, these local networks are governed by specific molecular activities. The plethora of activities sustained by the actin cytoskeleton is also intimately related to the dynamic nature of such networks and the recycling nature of actin remodeling. Another key property of the actin cytoskeleton is its ubiquitous ability to interact with membranes, receptor complexes and organelles. The actin cytoskeleton is indeed endowed with the capacity to adapt its structure to the encountered physical constrains. Those considerations regarding the actin cytoskeleton remodeling properties certainly are not restricted to the IS and apply in

numerous other cellular processes. However, the IS provides a prototypical example of how multiple layers of physical and biochemical events can be coordinated in a restricted space. We will review in the next sections the current knowledge on the actin-controlled IS events at the cellular and meso-scales.

Actin Control of the Immunological Synapse at the Cellular Scale: Shape, Symmetry, and Polarity

Shape Remodeling Along the Immunological Synapse Life Cycle

The IS is established very rapidly upon recognition of cognate APC. It is driven by a spreading behavior over the surface of the APC (**Figure 1A**), which is sustained by actin polymerization generating forces to appose the membrane of the T cell to that of the APC. Then T cells further emit a radial extension beyond the cell body, in the form of an undulating lamellipodium. Actin remodeling is among the most early molecular activity downstream of TCR stimulation, as shown by a recent phosphoproteomic analysis (Locard-Paulet et al., 2020). This is in line with early findings that the initial actin cytoskeleton response precedes calcium flux (Delon et al., 1998). Actin-driven membrane dynamics seems to operate through successive steps. The application of lattice light-sheet microscopy has allowed gaining high spatial and temporal resolution to study the transition from migration to IS assembly and maturation (Ritter et al., 2015). Upon contact of migrating murine $CD8^+$ T cells with APC, a collapse of the uropod is first observed, while actin-based ruffles and projections emerging from the leading edge move in a reward actin flow toward the back of the cell. Rapidly then the central part of the IS harbors a relatively poor content in F-actin. The TCR molecules, initially at the uropod, accumulate within 2 min of target cell interaction initially via lateral translocation and in a second wave via the intracellular vesicle pool. With a further delay of 6 min in average, the MTOC repolarizes from the uropod to the center of the IS. When CTLs detach from the target cell, they reverse their polarity by initiating an actin-rich lamellipodia at the distal pole, with the centrosome, granules, and TCR relocalizing to the newly formed uropod (Ritter et al., 2015).

The Different Shades of Immunological Synapses

The IS is usually depicted as a « model synapse », with perfectly radial organization, important spreading and clear-cut segregation of sub-domains. However, there is a wide dispersion in IS shapes and symmetries across T cell populations and depending on stimulation systems. A majority of the work assessing T cell IS organization is based on planar APC substitutes, by either coating stimulatory molecules on glass or plastic or by embedding stimulatory molecules in lipid bilayers. These systems obviously present the advantage of being able to control stimulatory molecule identity and density as well as to image the IS with high resolution. In the context of T cell/APC interactions, differences in IS assembly are expected due to ligand composition and densities, ligand dynamics and anchorage, surface structure and biophysical properties. There are multiple shades between the migratory behavior of T cells and the full arrest upon cognate APC encounter, reflecting the fact that T cells scanning for antigens are sensing concurrent stop and go signals such as chemokines (Dustin, 2004; Viola et al., 2006). This has led to the concept that T cells may assemble either stable synapse or motile IS, named "kinapses" (Dustin, 2008). This would match the notion that T cell/DC encounters might be highly heterogenous in length, from few minutes to hours (Gunzer et al., 2000; Mempel et al., 2004; Miller et al., 2004).

The existence of intermediate states infers that migration and IS conformation might not be drastically opposing behaviors. As proposed by Dustin, stabilization of the IS might not correspond to a shut-down of the motility machinery but rather a symmetrization of force-generating structures to balance forces and hold the cell in contact with the APC (Dustin, 2008). IS turnover and T cell detachment would then result from a mechanism of symmetry breaking. This view is comforted by the fact that migrating CTL and those forming conjugates have remarkably similar actin dynamics, including projections forming at the leading edge and actin flowing rearward toward the uropod (Ritter et al., 2015). The attractive notion about this view is that graded tuning of stabilization might provide a mechanism to adjust T cell scanning and resulting activation.

In vivo imaging of tagged TCR in naïve T cells provided evidence that TCR clustering and internalization is not strictly dependent on the establishment of stable contacts with APC (Friedman et al., 2010). Using *in situ* cytometry, Moreau et al. have found that TCR-pMHC affinity controls T cell motility during antigen recognition *in vivo*. In particular in the context of intermediate affinity ligands, kinapses are the predominant form of APC contacts and are able to sustain strong TCR signals (Moreau et al., 2012). Actin remodeling, in particular via the Arp2/3 complex, appears necessary to drive the stop behavior leading to stable IS, but dispensable for the partial deceleration characteristic of the kinapse (Moreau et al., 2015). This suggests that distinct actin remodeling patterns tune the « appetite » of T cells to the antigenic stimulus by favoring motile scanning of APC with low stimulatory capacity and full arrest on highly stimulatory APC.

Actin Control of the Immunological Synapse at the Mesoscale: Local Meshworks, Receptor Clusters, Organelle Traffic

Local Actin Networks and Meshworks

One key to the understanding of the plethora of functions sustained by the actin cytoskeleton at the IS is its organization in discrete dynamic networks (recently reviewed by Hammer et al., 2019). These networks correspond to substructures that are not unique *per se* to T cells, but that are arranged in a unique fashion at the T cell IS (**Figure 1B**). The most prominent networks comprise a lamellipodium that tend to arrange radially, a lamellar connecting the lamellipodium to the cell body and multiple actin foci distributed at the IS interface. These networks are segregated in space but are also structurally distinct as they are shaped by different actin filament length and branching degree.

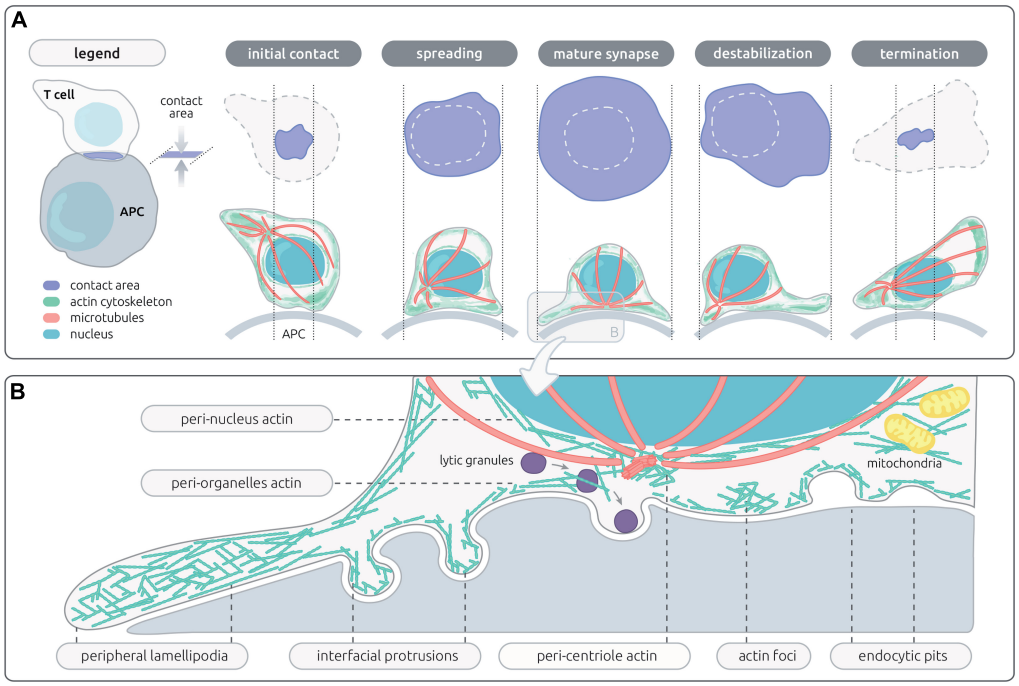

FIGURE 1 | Actin networks sustaining T cell synapse shape and microarchitecture. **(A)** Schematic representation of the en-face and side views of the contact area between a T cell and an antigen-presenting cell (APC). The successive steps of the IS life cycle are depicted, from initial T cell/APC contact to termination of the IS. The contact area, actin cytoskeleton, microtubules and nucleus are represented with the indicated colors. **(B)** Schematic representation of the microarchitecture of a mature IS, corresponding to a transversal view of the contact between a $CD8^+$ T cell and a target cell. This representation assembles the different actin networks described so far in the context of lymphocyte activation, including those proximal to the plasma membrane and those associated with inner organelles of the cell.

Synapse assembly and maturation is supported by the sequential organization of these distinct networks, as recently revealed by live 3D STED of Jurkat T cells (Fritzsche et al., 2017). The first step of spreading is supported by the ruffles decorating resting cells, which is followed by assembly of a flat undulating lamellipodium supported of a dense actin filament meshwork. Within a few minutes, the lamellipodium starts contracting. Below the cell body, both a cortical network as well as a cytoplasmic network can be distinguished and are separated from the lamellipodium by a ring enriched in myosin-II. Remarkably, both an inward-growing ramified actin network and an outward-growing lamellipodial network co-exist Jurkat T cells forming 2D synapses. The relative importance of these networks as well as their dynamic properties seem, however, to differ between Jurkat T cells and primary T cells (Colin-York et al., 2020), and possibly among different T cell subsets.

Beyond those dynamic networks that sustain the main subdomains of the IS, the actin cytoskeleton sustains different types of membrane protrusions. It has been long appreciated that T cells are covered with actin-rich microvilli that represent the first surface T cells use to scan their environment. Recent studies point to the importance of these tiny structures as structural units to preassemble receptors and proximal signaling molecules and as structural basis for the "palpation" of the APC surface and scanning of pMHC complexes by the TCR (Jung et al., 2016; Cai et al., 2017; Ghosh et al., 2020). Although the apposition of the plasma membrane from the T cell and the APC is depicted as flat, there is evidence for indentations in the form of podosome-like structures. This applies to antigen-experienced T cells inspecting the surface of endothelial cells and APC (Carman et al., 2007; Sage et al., 2012) and to CTL interacting with target cells (Tamzalit et al., 2019). How actin dependent microvilli and larger membrane indentations may relate to the underlying dynamics actin cortex is currently unclear.

Receptor Patterning and Signaling via Differential Coupling to the Centripetal Actin Flow

The centripetal actin flow has been established as a key driver of cell surface receptor dynamics at the IS. Via differential anchorage to the cortical actin, receptors are transported towards the IS center at different rates (reviewed in Beemiller and Krummel, 2010). This transport mechanism allows the typical molecular patterning of the IS characterized by the positioning of TCR at the cSMAC, adhesion molecules as a ring at the pSMAC and exclusion of large molecules such as CD45 at the dSMAC. The centripetal movement of TCR microclusters is a key rheostat to T cell activation since it provides a balance between sustained TCR signaling and TCR internalization/degradation (Lee et al., 2003; Barda-Saad et al., 2005; Campi et al., 2005; Varma et al., 2006). Interestingly the cSMAC may accommodate both signaling and degradation depending on antigen quality (Cemerski et al., 2008). Whether this is related to distinct rates of actin-driven TCR internalization has not been elucidated. Beyond this large-scale molecular segregation, the anchorage

to the actin cytoskeleton allows for force generation, which is an integral mechanism of receptor activation applying to the TCR, integrins and probably many co-receptors (Bashour et al., 2014; Das et al., 2015; Hu and Butte, 2016; Li and Springer, 2017). Remarkably, antigen unbinding kinetics have recently been shown to impact the actin retrograde flow velocity, in such a way that T cells appear to normalize TCR force generation across various antigens (Colin-York et al., 2019). Such feedback mechanism would allow T cells to widen the range of antigens able to evoke productive TCR engagement. While TCR are held in the cSMAC of mature IS, the active conformation of integrins is confined to the pSMAC (Comrie et al., 2015). The differential motility behavior of TCR and integrins in relation to the underlying actin cytoskeleton probably reflects distinct mechanical coupling. This is supported by the observation that TCR is associated to actin foci (Kumari et al., 2015), while LFA-1 clusters appear to align with the lamella-like region of the IS, which presents with a high acto-myosin activity, taking the shape of linear filaments organized into concentric arcs in Jurkat T cells (Murugesan et al., 2016). This receptor-specific coupling is supported by the identification of distinct actin machineries for TCR and LFA- 1 clusters (driven respectively by Arp2/3 and formins) (Tabdanov et al., 2015). A further layer of regulation arises from the fact that engagement of integrins may constrain the centripetal actin flow, thereby altering signaling microcluster motion and TCR signaling (Nguyen et al., 2008; Jankowska et al., 2018).

Engagement of costimulatory molecules such as CD28 has since the first descriptions of the IS been appreciated to promote actin polarization as well as redistribution of receptors towards the T cell:APC interface (Wülfing and Davis, 1998). The actin remodeling activity of CD28 has recently been shown to operate via the stimulation of WAVE2 and cofilin (Roybal et al., 2016). A further example of how co-receptors impact molecular organization at the IS via their anchorage to the actin cytoskeleton is given by CD2, which assembles as a corolla towards the edge of the IS via its cytoplasmic tail involved in F-actin coupling. At this site, CD2 has been recently proposed to capture other costimulatory molecules, such as CD28, ICOS, CD226 and SLAM-F1 (Demetriou et al., 2020). CD2 is also involved in the localization of the inhibitory receptor PD-1 at the IS, as well as its negative impact on signaling. Interestingly, PD-1 blocks the TCR-induced stop signal (Fife et al., 2009), reinforcing the notion that co-receptors modulate T cell activity at least in part via the regulation of IS assembly and stability. As stated above, such regulation is expected to operate via specific coupling to the actin cytoskeleton, as further exemplified by a recent study showing that PD-1 promotes actin remodeling at the IS via cofilin, coronin and Arp2/3 (Ambler et al., 2020).

The ERM (Ezrin/Radixin/Moesin) protein family stems as particularly relevant to the coupling of T cell surface receptors to the cortical actin. Indeed these proteins crosslink transmembrane proteins and actin filament upon conformational activation that is initiated locally by PIP2 (Fehon et al., 2010; McClatchey, 2014). In T lymphocytes, only ezrin and moesin are expressed (Shaffer et al., 2009), and are involved in migration, adherence, and IS formation. In particular, ezrin and moesin have been shown to drive CD43 clearing from the center of the IS (Allenspach et al., 2001; Delon et al., 2001), to regulate TCR patterning (Roumier et al., 2001), as well as to contribute to signaling microcluster dynamics and patterning (Lasserre et al., 2010). ERM proteins have also been recently described as effective sensor at the initial stage of TCR signaling (Ghosh et al., 2020). More precisely, T cells possess thin actin rich structures called microvilli, enriched in TCR, CD2, coreceptors, LAT and Lck molecules as well as phosphorylated EMR protein (Brown et al., 2003; Ghosh et al., 2020). The TCR molecules are indeed localized at the microvilli thanks to their interaction with the ERM proteins and microvilli then act as hubs for TCR signaling.

In conclusion, the dynamic and adjustable scaffold provided by the cortical actin network at the IS sustains key biophysical properties essential for antigen sensing and signal integration via the TCR, integrins and numerous co-receptors. It sustains molecular transport and force exertion during receptor scanning, as well as molecular segregation for signal organization, amplification and termination.

Actin-Microtubule Interplay at the Immunological Synapse

A key event in the regulation of T cell polarity in the context of IS assembly is the translocation of the centrosome from the uropod towards the T cell/APC interface (Geiger et al., 1982). As explained above, this event occurs rapidly after the partial clearance of F-actin from the IS center (Ritter et al., 2015). The actin and microtubule cytoskeletons are coordinated at the IS via a bidirectional interplay. MTOC translocation to the IS depends on phosphorylation of PLC–g1 (Quann et al., 2009), which is stimulated by F-actin polymerization (Babich et al., 2012). Reversely, centrioles play a key role for shaping F-actin remodeling at the IS since their genetic deletion leads to impaired formation of the F-actin peripheral ring and loss of F-actin-dependent force exertion towards the target cells in the context of CTL (Tamzalit et al., 2020). Below the IS, some of the microtubules irradiating from the MTOC distribute parallel to the synapse plane and appear to anchor in the peripheral actin ring. Such anchorage has been proposed to assist MTOC polarization towards the IS center and to be regulated by microtubule linkers such as IQGAP-1 and ezrin (Kuhn and Poenie, 2002; Lasserre et al., 2010). An additional layer of coordination between the actin and tubulin cytoskeletons might be provided by the F-actin cloud surrounding the centrosome. This distinct centrosomal actin network dependent on the Arp2/3 activity and has recently been characterized in the context of B cells in which it controls the polarization of the centrosome to the IS and regulates microtubule growth (Obino et al., 2016; Inoue et al., 2019). This network is also relevant to the T cell IS, where its disassembly is a prerequisite to MTOC polarization (Bello-Gamboa et al., 2020).

Actin Dynamics Controlling Endocytic and Exocytic Events at the T Cell Synapse

Endocytic and exocytic events occurring at the IS are key to fuel receptors and signaling molecules, to regulate receptor

endocytosis, degradation and recycling, as well as to control the polarized delivery of effector molecules such as lytic molecules, cytokines and chemokines (recently reviewed in Mastrogiovanni et al., 2020). The traffic of vesicular compartments within the cell and at the plasma membrane depends on highly complex and specialized molecular machineries, as well as the coordinated action of the actin and microtubule cytoskeletons. This applies to the assembly of TCR microsclusters, which depend at least in part from intracellular pools of TCR and signaling molecules such as Lck and LAT (Balagopalan et al., 2018). It also applies to the internalization and endosomal trafficking of multiple key receptors. A clear illustration of the role played by specific actin remodeling in the endosome-to-membrane recycling processes is provided by the finding that T cells lacking the Arp2/3 activator WASH fail to maintain surface levels of the TCR, CD28, LFA-1 and GLUT1, as a result of a collapse of the endosomal compartment (Piotrowski et al., 2013).

The role of the cytoskeleton in the control of the polarized delivery of lytic granule content to the IS has been a matter of debate. The prevalent model has been that, upon TCR activation, lytic granules cluster around the centrosome so that centrosome translocation to the IS brings the core of the lytic granules towards the center of the IS (Ritter et al., 2015). The apposition of the centrosome to the plasma membrane may even sustain direct delivery of lytic granules for membrane docking and fusion (Stinchcombe et al., 2006). However, the dependency of lytic granule polarized secretion to centrosome reorientation is not that strict as evidenced by studies showing that the centrosome might be dispensable for the directional secretion of lytic granules (Bertrand et al., 2013; Tamzalit et al., 2020). CTL are particularly dependent on the assembly of a tight junction at the synapse with target cells via the LFA-1 belt at the pSMAC which has been proposed to act as a seal to confine lytic granule content delivery towards the target cell (Somersalo et al., 2004; Le Floc'h et al., 2013). At the cSMAC, F-actin is not deprived as initially sought but assembled into an Arp2/3-dependent branched network, which acts as a filter to regulate lytic granule exocytosis. Degranulation is indeed dependent on local F-actin meshwork clearances controlled via coronin-1A activity (Mace and Orange, 2014). Lytic granule presence and such clearances might not be coordinated, but rather stochastic clearance formation and disappearance appear to provide a mechanism to increase the probability for granule exocytosis (Carisey et al., 2018). Furthermore CTL apply mechanical force against the target cell. This is coordinated in time and space with lytic granule secretion and allows boosting the lytic activity of perforin (Basu et al., 2016). Interestingly, once degranulation of lytic granules has occurred, actin density recovers across the synapse as a mechanism to halt further secretion (Ritter et al., 2017).

A key effector function of T cells is their ability to produce and secrete a vast array of cytokines, whose nature depends on the specification of T cells towards differentiated subsets. Interestingly, cytokines might be secreted at the IS in a polarized manner or released multi-directionally (Huse et al., 2006), implying that distinct secretory machinery are responsible for the delivery of cytokines in targeted versus diffusive modalities. The dependency of cytokine secretion to the actin cytoskeleton machinery has not been investigated as thoroughly as for lytic granules. Cytokines transit from the Golgi apparatus to the plasma membrane through distinct vesicles. Secretion of cytokines by $CD4^+$ T cells requires Cdc42-driven actin remodeling but not MTOC polarization (Chemin et al., 2012). In particular defective polarized secretion of IFN-γ was related to a reduced ability of Cdc42-silenced T cells to deplete F-actin at the center of the IS established with super-antigen-pulsed B cells. Whether local actin clearance is regulated as for lytic granules is currently unknown. It is tempting to speculate that cytokine release might be differentially controlled by the actin cytoskeleton, depending on vesicle types and T cell subsets in a way to balance polarized versus diffusive secretion, that may correspond to distinct biological scopes (selective activation of DC and help to B cells via polarized cytokine delivery, versus bystander activation and diffusive delivery of inflammatory mediators).

In addition to the controlled release of effector molecules, TCR stimulation induces the release at the synapse of extracellular microvesicles containing TCR, CD40L, ICAOS and tetraspanins (Blanchard et al., 2002; Choudhuri et al., 2014). Such event may buffer T cell activation and modulate DC stimulation and B cell help. Cytotoxic lymphocytes have recently been shown to also release supramolecular attack particles as autonomous killing entities (Bálint et al., 2020). Whether the synaptic release of these various extracellular microvesicles depends on the actin cytoskeleton remains to be defined.

Additional Cytoplasmic Pools of Actin Assist Positioning and Dynamics of Major Organelles

Immunological synapse assembly is accompanied by cytoskeleton-dependent mitochondrial redistribution towards the T cell-APC interface. This localization allows maintaining Ca^{2+} influx across the plasma membrane and downstream activation (Quintana et al., 2007). Furthermore, platinum replica electron microscopy has recently revealed that mitochondria are embedded in a dynamic actin-Myosin-II cytoskeleton network assisting constriction and fission (Yang and Svitkina, 2019). Such events are key to regulate metabolic switches along T cell differentiation and reactivation (Buck et al., 2016). Whether such events occur at and are dependent on the IS is currently unknown.

Nuclear A-type lamins that form the nuclear lamina have been found to be upregulated in activated T cells and to promote F-actin polymerization via the linker of nucleoskeleton and cytoskeleton (LINC). Furthermore lamin-A expression was associated with TCR clustering and increased signaling (González-Granado et al., 2014). A structural link between the nucleus and the IS via a lamin-A-LINK-actin axis might provide a mechanism allowing direct transmission of mechanical forces from the plasma membrane to the nucleus. Whether this might modulate T cell transcriptional activity as reported in other cellular models (Wang et al., 2009) remains to be investigated.

MOLECULAR CONTROL OF ACTIN REMODELING AT THE IMMUNOLOGICAL SYNAPSE VIA THE PRISM OF ACTIN-RELATED PIDS

T Cell Immunological Synapse Defects Caused by Deficiencies in the Actin-Binding Proteins ARPC1B, HEM1, WASP, WIP, and WDR1

As described above, distinct but interconnected actin networks sustain IS assembly and dynamics (**Figure 2**, central panel). The molecular machinery that orchestrates this complex combination of local actin networks has started to be elucidated. In particular, research on actin-related PID is pointing to the molecules that play an essential role in this process and helps bridging molecular defects at the IS to downstream impairments in T cell function (see **Table 1**). To date, T cell synapse defects have been characterized in 5 PIDs caused by defects in actin-binding proteins (ARPC1B, HEM1, WASP, WIP, and WDR1), with the overall finding that the corresponding proteins play non-redundant roles at the IS. As summarized in **Figure 2**, we review here current knowledge on the molecular activities of these 5 regulators, in terms of actin remodeling and T cell IS microarchitecture.

WASP Deficiency

The Wiskott-Aldrich syndrome (WAS) is an X-linked PID characterized by microthrombocytopenia, eczema, recurrent infections and increased risk of autoimmune manifestations and malignancies (Ochs and Thrasher, 2006). This severe disorder is caused by a combination of cellular defects in all hematopoietic cell subsets, in accordance with the expression profile of the corresponding protein WASP. However, intrinsic defects of T cell subsets expressing non-functional mutated WASP or lacking WASP, including effector $CD4^+$ T cells (Trifari et al., 2006) and $CD8^+$ T cells (De Meester et al., 2010), Treg (Adriani et al., 2007; Humblet-Baron et al., 2007; Maillard et al., 2007; Marangoni et al., 2007) and Tfh (Zhang et al., 2016) are sought to contribute to susceptibility to infections, tumors and auto-immune manifestations described to occur at high frequency in WAS patients. In addition, there is a clear selective advantage of $WASP^+$ cells over $WASP^-$ cells in patients with de novo corrective mutation (Ariga et al., 2001; Wada et al., 2001; Trifari et al., 2010). This observation has contributed to build the rational for the implementation of gene therapy, which is now proposed as an alternative to HSC-T for the treatment of WAS (Aiuti et al., 2013). WASP has been recognized early as an effector of Cdc42 promoting actin polymerization via the Arp2/3 complex (Symons et al., 1996; Machesky and Insall, 1998). WASP has been among the first actin regulators to be identified as a key regulator of IS assembly (Dupré et al., 2002; Orange et al., 2002; Sasahara et al., 2002). Follow-up studies have helped understanding that WASP is predominantly involved in the stabilization of the IS, rather than its initial assembly (Sims et al., 2007). T cells derived from WAS patients appear indeed to assemble kinapses rather than synapses when contacting APC (Calvez et al., 2011). This bias towards kinapses has been attributed to an inability to mediate the stop signal, especially in the context of APC presenting low antigen concentrations (Cannon and Burkhardt, 2004; Lafouresse et al., 2012). Interestingly, the motile synapses of WASP-deficient T cells have been associated to dispersed TCR triggering and erratic calcium flux, which may underline biased defects in Th1 cytokine via delayed NFAT-1 nuclear translocation and defective T-bet induction (Cianferoni et al., 2005; Trifari et al., 2006; Taylor et al., 2010; Calvez et al., 2011). WASP appears to play a direct role in TCR signal organization since it promotes the assembly of dense actin foci associated with TCR microclusters, together with Arp2/3 (Kumari et al., 2015). Such TCR-driven actin foci may provide a platform for TCR signalosome organization and concomitantly a structure to potentiate interaction with the APC via invadopodia-like membrane protrusions. Indeed, in the absence of WASP, TCR-driven actin foci assembly and phosphorylation of the mechanosensory molecule CasL are severely impaired (Kumari et al., 2015). WASP was also shown to mediate via Nck the cross-linking to the actin cytoskeleton of molecular condensates containing the key signaling molecules LAT, Grb2, Sos1, and SLP-76 (Ditlev et al., 2019). Those condensates were shown to dependent on actin coupling for their centripetal diffusion at the dSMAC, while they seemed to uncouple form WASP to cross the pSMAC presumably because of heightened formin activity. Such molecular condensates might be associated to the WASP-dependent actin foci.

Inability of WASP-deficient T cells to maintain stable IS is also relevant to $CD8^+$ T cells. WAS $CD8^+$ T cells display reduced killing activity while their ability to secrete lytic granules is maintained (De Meester et al., 2010). Live microscopy recording of CTL and target cell interactions revealed a delay in the ability of WASP-deficient CTL to deliver the lethal hit (Houmadi et al., 2018). WASP-deficient CTL were observed by TIRF microscopy to form unstable synapses in association with an actin cytoskeleton meshwork of reduced density. At the nanoscale, WASP-deficiency was associated with reduced number and molecular density of LFA-1 nanoclusters. At the cellular scale, this was associated with a reduced ability to maintaining the LFA-1 adhesive ring (Houmadi et al., 2018), which plays a key role in $CD8^+$ T cells to allow polarized delivery of lytic granule content (Somersalo et al., 2004). Interestingly, the role of WASP in controlling IS stability also applies in the context of IS turnover, a poorly studied step of the IS life cycle (Kumari et al., 2020). IS decay has indeed been shown to be directly related to the degradation of WASP as part of ubiquitination and proteolysis mechanisms. This suggests that WASP may act as a molecular timer in the context of T cell stimulation, with its activation leading to actin foci assembly and IS stabilization, but also programming it for degradation with IS destabilization as a consequence.

WIP Deficiency

Wiskott-Aldrich syndrome protein (WASP)-interacting protein (WIP) was initially identified with a yeast two-hybrid system aiming at identifying WASP partners (Ramesh et al., 1997). WIP

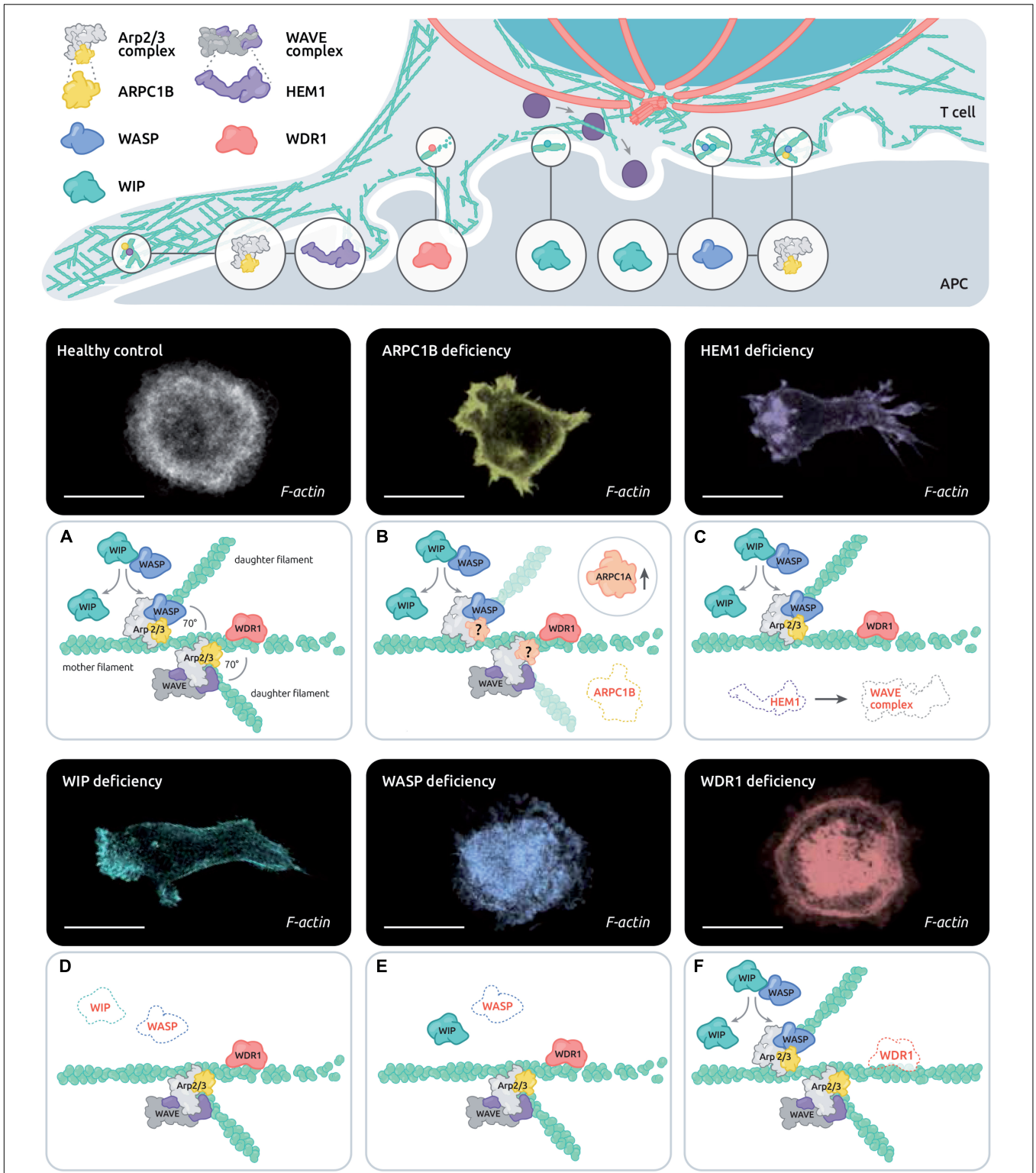

FIGURE 2 | Control of actin remodeling at the T cell synapse by the disease-related actin-binding proteins ARPC1B, HEM1, WASP, WIP and WDR1. The upper scheme depicts the estimated distribution of PID associated actin-binding proteins in the various actin networks of the IS. The lower panels combine representative T cells stained with phalloidin and the corresponding molecular alterations in the context of healthy T cells **(A)**, ARPC1B deficiency **(B)**, HEM1 deficiency **(C)**, WASP deficiency **(D)**, WIP deficiency **(E)**, and WDR1 deficiency **(F)**. Scale bar: 10 μm.

TABLE 1 | Inventory of immune-related actinopathies and associated T cell synapse defects.

Actin-related inborn errors of immunity				T cell synapse defects			
Gene	**Protein**	**Initial description**	**Clinical symptoms**	**Patient T cells**	**References**	**Cellular and murine models**	**References**
ACTB	β-actin	Nunoi et al., 1999	Mental retardation, recurrent bacterial and viral infections	n.t.		n.t.	
ARHGEF1	ARHGEF1	Bouafia et al., 2019	Airways infections, defective antibody production	n.t.		n.t.	
ARPC1B	ARPC1B	Kahr et al., 2017; Kuijpers et al., 2017; Somech et al., 2017	Failure to thrive, platelet abnormalities, eczema, infections, vasculitis, hepatosplenomegaly, thrombocytopenia	Deficient cell spreading during IS assembly and formation of spike-like structures	Brigida et al., 2018	CK666 treatment induces collapse of branched actin network and increases linear actin filaments	Murugesan et al., 2016
CARMIL2	CARMIL2	Sorte et al., 2016; Wang et al., 2016; Schober et al., 2017	Malignancy (EBV+), IBD, recurrent skin and upper airway infections, failure to thrive	n.t.		No modification of IS formation, but absence of CD28-CARMIL2-CARM1 colocalization	Liang et al., 2013; Roncagalli et al., 2016
CDC42	Cdc42	Takenouchi et al., 2015; Gernez et al., 2019; Lam et al., 2019; Szczawinska-Poplonyk et al., 2020	Autoinflammation, HLH, malignant lymphoproliferation	n.t.		Impaired actin remodeling at the IS	Chemin et al., 2012
CORO1A	Coronin-1A	Shiow et al., 2008	Bacterial and viral infections, aggressive EBV-associated B cell lymphoproliferation, T cell lymphopenia, T-B+ SCID	n.t.		Increase of WASP and ARP2/3 at the IS area, accumulation of F-actin	Föger et al., 2006; Mugnier et al., 2008
DIAPH1	DIAPH1/mDIA1	Kaustio et al., 2021	seizures, cortical blindness, microcephaly syndrome (SCBMS), mitochondrial dysfunction and immunodeficiency	Reduced adhesion and MTOC polarization to the IS, attenuated mitochondrial calcium	Kaustio et al., 2021	Centrosome polarization, spatiotemporal control of Zap70-dependent LAT phosphorylation	Gomez et al., 2007; Thumkeo et al., 2020
DEF6	DEF6	Serwas et al., 2019	Severe autoimmune manifestations, recurrent infections	n.t.		Impaired actin polymerization upon TCR activation, defective ZAP-70 polarization at the IS area	Fanzo et al., 2006
DOCK2	DOCK2	Dobbs et al., 2015	Severe invasive bacterial and viral infections	n.t.		Defect in IS formation and size, impaired TCR and lipid raft translocation upon TCR engagement	Sanui et al., 2003; Le Floc'h et al., 2013
DOCK8	DOCK8	Engelhardt et al., 2009; Zhang et al., 2009, 8	Upper airway infections, susceptibility to viral infection	n.t.		Defective IS formation and reduction of LFA-1 recruitment at the IS area	Randall et al., 2011
NCKAP1L	HEM1	Castro et al., 2020; Cook et al., 2020; Salzer et al., 2020	Fever, recurrent bacterial and viral skin infections, severe respiratory tract infections, poor antibody responses, autoimmune manifestations	Dismorphic IS structure, preserved actin foci, LFA-1 activation and conjugate formation towards target cells	Cook et al., 2020; Salzer et al., 2020	Impaired localization of LFA-1 and β1 integrins at the IS	Nolz et al., 2007
MKL1	MKL1	Record et al., 2015	Severe bacterial infections, skin abscesses	n.t.		n.t.	
MSN	MOESIN	Lagresle-Peyrou et al., 2016	Eczema, episodic bacterial and VZV infections, lymphopenia	No alteration of IS	Lagresle-Peyrou et al., 2016	Treatment with calyculin A induces inhibition of TCR clustering, absence of F-actin exclusion	Ilani et al., 2007
MYH9	Myosin IIA	Seri et al., 2003	MHY9-related diseases: May-Hegglin anomaly, Sebastian syndrome, Fechtner syndrome, and Epstein syndrome; mild macrothrombocytopenia, leukocyte inclusions	n.t.		Failure to assemble pSMAC and cSMAC, defective IS stability, modification of TCR microcluster velocity and directionality	Ilani et al., 2009; Kumari et al., 2012; Yi et al., 2012
NIK	NIK	Willmann et al., 2014	CVID, recurrent bacterial and viral infections, candidiasis	n.t.		Decreased expression of proteins involved in IS formation and F-actin dynamics	Lacher et al., 2018
PSTPIP1	PSTPIP1	Wise et al., 2002	Oligoarticular pyogenic arthritis, acne, pyoderma gangrenosum-like lesions	Defective IS assembly and stability	Janssen et al., 2018	Defect of IS assembly	Badour et al., 2003
RAC2	RAC2	Ambruso et al., 2000	Lymphopenia, recurrent respiratory infections, poor wound healing, leukocytosis	n.t.		n.t.	
RASGRP1	RASGRP1	Salzer et al., 2016; Winter et al., 2018	Severe pneumonia, failure to thrive, EBV susceptibility	n.t.		n.t.	

(Continued)

TABLE 1 | Continued

		Actin-related inborn errors of immunity		T cell synapse defects			
Gene	**Protein**	**Initial description**	**Clinical symptoms**	**Patient T cells**	**References**	**Cellular and murine models**	**References**
RHOG	RhoG	Kalinichenko et al., 2021	HLH features, fever, cytopenia, low hemoglobin	Decreased F-actin density at the IS	Kalinichenko et al., 2021	n.t.	
RHOH	RhoH	Crequer et al., 2012b	Persistent EV-HPV infections, skin lesions	n.t.		RhoH overexpression increases conjugate formation; defective recruitment of Lck and ZAP70	Chae et al., 2010; Baker et al., 2012
STK4/MST1	MST1	Crequer et al., 2012a; Nehme et al., 2012	Recurrent infections, EBV infections, skin lesions and infections	n.t.		Decrease IS formation and stability, severe reduction of T-APC stable contacts, mislocalization of kindlin3 at the IS	Tomiyama et al., 2013; Kondo et al., 2017
WAS	WASP	Derry et al., 1994	Thrombocytopenia, eczema, T cell lymphopenia, recurrent bacterial and viral infections	Aberrant actin protrusions, unstable IS, reduced LFA1 clustering	Dupré et al., 2002; Calvez et al., 2011; Houmadi et al., 2018	Unstable IS	Sims et al., 2007
WDR1	WDR1	Kuhns et al., 2016; Standing et al., 2017; Pfajfer et al., 2018	Autoinflammation, skin and airway infections	Actin accumulation and disorganized IS structure	Pfajfer et al., 2018	n.t.	
WIPF1	WIP	Lanzi et al., 2012	Eczema, T lymphopenia, thrombocytopenia,	Aberrant spreading in the context of the IS	Pfajfer et al., 2017	n.t.	

n.t., not tested.

deficiency in humans appears to be extremely rare. The few identified patients with WIP deficiency carry severe mutations leading to undetectable protein expression (Lanzi et al., 2012; Pfajfer et al., 2017). WIP deficient patients present with a WAS-like phenotype, including eczema, T cell lymphopenia and recurrent infections. Because WIP acts as a chaperone for WASP (de la Fuente et al., 2007), WIP deficiency leads to defective expression of WASP, which explains the partial overlap of phenotypes between the 2 deficiencies. $CD8^+$ T cells and NK cells from WIP-deficient patients harbor cytotoxic defects that are related to defective contact with target cells. WIP-deficient $CD8^+$ T cells display a very aberrant actin organization in the context of IS assembly, which suggests additional defects than those caused by the lack of WASP (Pfajfer et al., 2017). The actin network in WIP deficient T cells is poorly reticulated indicating reduced Arp2/3-dependent actin branching activity. A possible explanation for this severe phenotype is the dual role of WIP in promoting Arp2/3 activation via WASP and cortactin (Kinley et al., 2003). In the context of the IS, WIP is enriched in the peripheral lamellipodia and along the cell body cortex. Structured illumination microscopy revealed that it distributes as tiny patches that intermingled the reticulated actin network of the IS periphery (Pfajfer et al., 2017), in agreement with a role in promoting densely reticulated actin networks via Arp2/3 branching.

ARPC1B Deficiency

ARPC1B is part of the Arp2/3 complex, which is the molecular unit that promotes the branching of new actin filaments on the side of mother filaments. The ARPC1 subunit exists under 2 isoforms, ARPC1A and ARPC1B. The ARPC1B subunit is exclusively expressed in the hematopoietic lineage. The discovery of ARPC1B deficiency in humans is fairly recent (Kahr et al., 2017; Kuijpers et al., 2017; Somech et al., 2017). Patients suffer from combined immunodeficiency, allergy and inflammation. In particular patients are subject to severe and prolonged lung viral infections. A number of these patients also display severe bleeding and skin vasculitis (Volpi et al., 2019). Comparably to WASP deficiency ARPC1B deficiency impacts thrombocyte development, leading to microthrombocytes, as well as neutrophil motility (Volpi et al., 2019). ARPC1B also plays a crucial role in the T cell compartment since patients harbor defects in T cell proliferation, migration, and cytotoxic activity and T_{REG} functions (Brigida et al., 2018). Upon IS assembly in healthy T cells, the Arp2/3 complex polarizes to the peripheral lamellipodia (Brigida et al., 2018). In ARPC1B deficient patients, T cells fail to emit a lamellipodia structure. They instead emit aberrant actin-rich structures, including spikes and long filopodia-like structures, both in the context of 2D IS and contact with APC (Brigida et al., 2018; Randzavola et al., 2019). As a result of such defective IS, T cells from ARPC1B deficient patients form less stable conjugates and kill less efficiently. Additionally to its role in driving IS assembly via the lamellipodium, ARPC1B has been proposed to control the recycling of key molecules such as the TCR, CD8 and GLUT1, via the retromer and the WASH complex (Randzavola et al., 2019). Accordingly the $CD8^+$ T cells from an ARPC1B deficient patient

were found to express low levels TCR, CD8 and GLUT1, implying that the functional defects of these cells arise from a complex combination of defects of multiple actin networks. This is in line with the pleiotropic activity of the Arp2/3 complex in multiple specialized actin networks.

HEM1 Deficiency

Hematopoietic Protein 1 (HEM1), which is encoded by the ***NCKAP1L*** gene, is part of the pentameric WAVE complex, which represents an alternative activator of the Arp2/3 complex in parallel to WASP. Comparably to WASP, HEM1 is an hematopoietic specific protein reinforcing the notion that immune cells are equipped with distinct activators of the Arp2/3 complex. The WAVE complex exists in an autoinhibitory state in the cytoplasm. Its activation depends on the coincident activity of prenylated Rac1 and association to membranes containing acidic phospholipids (Lebensohn and Kirschner, 2009). In particular the 3D opening of WAVE2 frees its VCA domain, which promotes interaction with the Arp2/3 complex and drives actin branching. HEM1 deficiency in humans has been described recently in 3 independent studies (Castro et al., 2020; Cook et al., 2020; Salzer et al., 2020). Patient-derived T cells display reduced F-actin density associated with a dysmorphic IS structure. These cells fail to assemble the typical actin ring and instead display an excess of spikes proposed to be formin-dependent. However, HEM1-deficient T cells still possess actin foci, suggesting that WASP activity is maintained in these cells. The WAVE complex appears to locate primarily at the periphery of the lamellipodia, implying that its main function is to promote lamellipodia growth via Arp2/3. Previous studies in mice with WAVE2 deficiency have pointed to the role of the WAVE complex in CRAC-mediated calcium entry (Nolz et al., 2006) and integrin activation (Nolz et al., 2007). Whether this applies to HEM1 deficient human T cells remains to be explored. Although Hem1-deficient $CD8^+$ T cells display severe IS defects, this does not appear to translate in cytotoxic T cell dysfunction, at least as measured *in vitro*. Interestingly, these cells appear to secrete abnormally high amount of lytic molecules following non-specific activation via IL-2 or PMA/ionomycin, probably as a result of the poorly structured cortical actin network whose filtering function might be altered (Cook et al., 2020). However, in the context of specific activation via the TCR, lytic granules secretion in HEM1-deficient cells is similar to that of control cells. It is therefore possible that in the context of HEM1-deficient $CD8^+$ T cells, cytotoxic activity might be maintained because facilitated secretion compensates for the aberrantly organized IS. Following TCR stimulation HEM1-deficient T cells harbor defects in upregulation of activation markers and reduction of proliferation and cytokine production (Cook et al., 2020). However such defects might not be solely explained by defective IS. Indeed, in addition to actin remodeling defects, the absence of the HEM1 protein causes a defective activation of the mTORC2/AKT pathway, with HEM1 activating mTORC2 enzymatic activity independently from its association to the WAVE complex. The relative contribution of actin-dependent and actin independent functions of HEM1 to the T cell defects remains to be elucidated.

WDR1 Deficiency

WD Repeat Domain 1 (WDR1, also referred as AIP1 for Actin-Interacting Protein 1) acts in concert with cofilin and coronin to promote actin filament disassembly via a severing activity. This process is essential for fast actin filament turnover (Kotila et al., 2019). WDR1 deficiency is a recently described PID which leads to inflammation, multiple respiratory tract infections and impact both innate and adaptive immunity (Kuhns et al., 2016; Standing et al., 2017; Pfajfer et al., 2018). Regarding the lymphoid compartment, the B cells are more affected by the WDR1 mutants than T cell compartment, depicted by a paucity of B cell in the bone marrow and in the periphery. While T cell development seems to be normal in patients, WDR1 deficiency results in a reduction of the T_{FH} subset, most likely due to B cell lymphopenia (Pfajfer et al., 2018). T cells, but also neutrophils, monocytes and B cells, present an accumulation of F-actin content, more probably due to a defect in actin severing/depolymerization, as it has been described in mice (Kile et al., 2007). In the context of the IS, WDR1-deficient T cells harbor a variety of actin-rich structures usually not encountered in healthy primary T cells, such as actin arcs, actin spikes and large actin condensates (Pfajfer et al., 2018). Some of those actin structures and in particular arcs are reminiscent of the formin-dependent structures described to predominantly occur in Jurkat T cells (Murugesan et al., 2016). This suggests that reduced actin turnover in WDR1-deficient T cells might shift the equilibrium between the Arp2/3-driven branching and formin-driven elongation activities, in favor of the latter. Unexpectedly however, only minor alterations of T cell activation were detected in the primary T cells isolated from the studied WDR1-deficient patients. A mild reduction of the calcium response upon TCR activation was measured, while proliferation, motility, cytotoxicity and TCR internalization were preserved (Pfajfer et al., 2018). Of note WDR1 deficiency appeared to more severely affect the B cell compartment. Why WDR1 deficiency differentially affects the activation and differentiation of T cells and B cells is currently unknown.

We have reviewed above how natural deficiencies are contributing to revealing the role of key individual actin-binging proteins in T cell IS assembly. From these studies, it emerges that the corresponding proteins play non-redundant function in IS assembly, with their deficiencies leading to characteristic defects. It is particularly striking that HEM1 and WIP are required for IS spreading via lamellipodia extension, while WASP seems to be particularly involved in IS stability and turn-over. WDR1 deficiency highlights distinct requirements of T and B cell IS of actin turn-over for IS function. Can the comparative analysis of these actinopathies tell us about how IS controls T cell activation and function? Interestingly $CD8^+$ T cells from these patients display distinct IS defects but also a wide range of cytotoxic impairment (from non-affected in HEM1 deficiency, to mildly reduced in WAS to more severely affected in WIP and ARPC1B deficiencies). The precise nature of the actin cytoskeleton alterations rather than the apparent severity of IS morphology seems to account for functional outcome. In addition, complex combinations of defects (such as discussed for HEM1 deficiency) renders prediction of how

IS impairments may translate in defective function difficult to make.

Immunological Synapse Defects in Additional Actin Related Deficiencies

Beyond the 5 actin-related PIDs described in detail above, additional 15 monogenic immunodeficiencies related to the actin remodeling machinery have been characterized to date (**Figure 3** and **Table 1**). This includes deficiency in the actin-binding proteins coronin-1A (Shiow et al., 2008), moesin (Lagresle-Peyrou et al., 2016) and CARMIL2 (Sorte et al., 2016; Wang et al., 2016; Schober et al., 2017). In addition, a point mutation in the β-actin gene (*ACTB*) itself has been reported in a single patient presenting with immunodeficiency, thrombocytopenia, but also intellectual and developmental impairments (Nunoi et al., 1999). More upstream in the actin remodeling machinery, deficiencies in the Rho GTPases Rac2 (Ambruso et al., 2000), RhoH (Crequer et al., 2012b), Cdc42 (Takenouchi et al., 2015; Gernez et al., 2019; Lam et al., 2019; Szczawinska-Poplonyk et al., 2020) and RhoG (Kalinichenko et al., 2021) have been characterized in patients with various forms of immunodeficiency. Actin-related PIDs also include deficiencies in the GTPase regulators DOCK2 (Dobbs et al., 2015), DOCK8 (Engelhardt et al., 2009; Zhang et al., 2009), DEF6 (Serwas et al., 2019) and ARHGEF1 (Bouafia et al., 2019). Finally, deficiencies in more indirect regulators of actin cytoskeleton dynamics have been associated to PID entities. This includes CD2BP1/PSTPIP1 (Wise et al., 2002), MST1/STK4 (Crequer et al., 2012a; Nehme et al., 2012), NIK (Willmann et al., 2014), MKL1 (Record et al., 2015) and RasGRP1 (Salzer et al., 2016; Winter et al., 2018). These PID-related proteins build a molecular network that covers key aspects of the actin remodeling machinery (**Figure 3**). Given the fundamental role of the actin cytoskeleton in sustaining multiple processes occurring at the IS, it is conceivable that most of the above-listed PID-related regulators concur to drive actin dynamics in the context of the T cell IS. Indeed, complementary studies in murine models or model cell lines are pointing to the contribution of multiple additional molecular actors, as depicted in **Figure 3**. For some of the actin-related PIDs, it should be noted that IS defects in NK cells and B cells have also been characterized, although these are not covered in the present review. We focus below on the 3 actin-binding proteins coronin-1A, moesin and CARMIL2.

Coronin-1A Deficiency

Coronin-1A is an hematopoietic cell-specific member of the conserved coronin family, which binds F-actin via WD repeat domains. Coronin-1A interacts with the Arp2/3 complex and inhibits its activity (Humphries et al., 2002). It also promotes

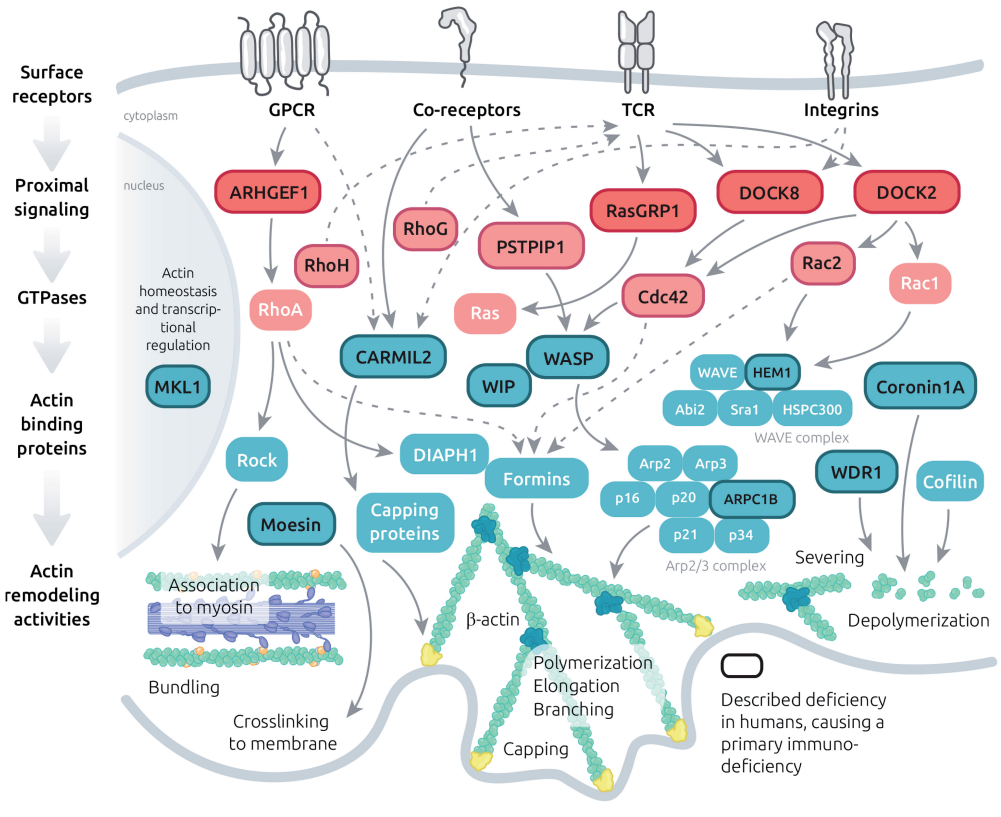

FIGURE 3 | Molecular machinery controlling actin dynamics in T cells. Schematic view of the major signaling events leading to actin cytoskeleton remodeling downstream key T cell surface receptors. The represented molecules include GTPase regulators, GTPases and actin binding proteins with diversified actin remodeling activities. A focus is made on molecules which have been implicated in PID (dark letters and lines) and on their interactors.

actin disassembly in association with cofilin and WDR1. Mutations in *CORO1A*, the gene that encodes coronin-1A, lead to a severe form of PID with life-threatening infections and EBV-driven lymphoproliferation (Shiow et al., 2008; Moshous et al., 2013). This deficiently particularly affects the T cell compartment with severe T cell lymphopenia related to impaired egress from the thymus, in line with the role of coronin-1A in T cell trafficking (Föger et al., 2006). Beyond this defect, peripheral T cells have been shown to depend on coronin-1A for Ca^{2+} mobilization from intracellular stores (Mueller et al., 2008). This activity depends on coronin-1A interaction with PLC-γ1 and might be independent from its actin remodeling one. Furthermore coronin-1A has been shown to regulate cAMP levels in peripheral T cells (Jayachandran et al., 2019), reinforcing the notion that this protein exerts actin-independent functions in T cells. How the actin-dependent function of coronin-1A might regulate T cell IS assembly and dynamics has started to be investigated in $CD4^+$ murine cells (Britton et al., 2017). In those cells, PKCθ keeps coronin-1A in a phosphorylated inhibitory state at the IS center. Where at the T cell IS and when coronin-1A may exerts its Arp2/3 inhibitory and actin disassembly activities still remain open questions. The actin-related role of coronin-1A at the IS has been clarified in more detail in the context of NK cells. In particular the study of a coronin-1A-deficient patient has highlighted that coronin-1A is indispensable for NK cell cytotoxic activity (Mace and Orange, 2014). Such defect was found to be related to a defective deconstruction of the cortical actin meshwork, which is required for lytic granule secretion. Whether a similar process is operating in cytotoxic T cells has not been explored yet.

Moesin Deficiency

As introduced above, the ERM proteins crosslink the actin cytoskeleton to the plasma membrane So far, only moesin among the ERM family has been reported to be associated with primary immunodeficiencies. Human moesin deficiency affects particularly the T cell compartment, resulting in T cell proliferation and migratory defects (Lagresle-Peyrou et al., 2016; Delmonte et al., 2017). Moesin-deficient human T cells fail to exclude CD43 molecules (Lagresle-Peyrou et al., 2016). Indeed, upon TCR activation, moesin is dephosphorylated, and loses its ability to binds CD43 molecules, which are not anchored to the actin cytoskeleton anymore (Delon et al., 2001; Ilani et al., 2007). CD43 molecules are then supposedly more motile and are excluded from the IS area. After roughly 20 min after TCR activation, moesin molecules have been rephosphorylated, resulting in a rapid reattachment of CD43 molecules at the pSMAC, leading to the stable localization of CD43 molecules at this site (Delon et al., 2001; Brown et al., 2003). It remains to be investigated which other molecules might be affected in their dynamics relocation in the context of moesin deficiency. How the anchoring function of moesin affects downstream signaling events and globally controls T cell activation and function remains to be explored.

CARMIL2 Deficiency

CARMIL2 (also known as RLTPT in mice) is a capping protein expressed in the lymphoid compartment. Patients carrying CARMIL2 mutations present recurrent upper airway infection and are more susceptible to EBV infection leading to disseminated EBV^+ smooth muscle tumors (SMT) (Schober et al., 2017). CARMIL2 deficiency leads to a combined immunodeficiency, in which the T cell compartment is particularly affected. This is explained by the critical role of CARMIL2 in mediating CD28-evoked costimulation. In mirror with mice study (Liang et al., 2013), CARMIL2 deficiency leads to defective T_{REG} development as well as defective CD28-mediated T cell function (cytokine production, proliferation). In addition, T cells present a defective migration capacity and directionality due an abnormal actin structure at the leading edge (Schober et al., 2017). So far, the role of CARMIL2 protein in IS assembly has not been explored. A mice study described a defect of PKCθ clustering in T cells where Rltpr is mutated to block the CD28 signaling pathway (Liang et al., 2013). This shows that in normal T cells, PKCθ is recruited at the IS following TCR engagement, and is dependent of the CD28-CD80 binding and Rltpr. However, reported CARMIL2-deficient patients did not show defective PKCθ phosphorylation upon TCR stimulation.

Formins as Important Regulators of the T Cell Synapse

Beyond the molecules studied in the context of actin-related PIDs, additional actin regulators have been shown to be involved in IS assembly and regulation. A particularly pivotal role in actin cytoskeleton remodeling is played by the formin family comprises 15 members in mammals that promote linear actin filament polymerization by recruiting profilin-bound actin monomers and protecting elongated actin filaments from proteins with anti-capping activity (Breitsprecher and Goode, 2013). Formins play essential roles in cell migration, adhesion, and cell-cell interactions. As such they are particularly relevant to sustaining immune cell function. T cells express at least 2 members of the formin family, Diaphanous-related formin-1 (mDIA1, DIAPH1), and Formin-like 1 (FMNL1, FRL1) (Gomez et al., 2007). Interestingly, mDIA1 and FMNL1 carry GTPase-binding domains for RhoA and Cdc42, respectively (Schönichen and Geyer, 2010), suggesting distinct connectivity to acto-myosin and actin remodeling activities. Studies in mDIA1 KO mice have revealed the role of mDIA1 in promoting T cell emigration from the thymus and recruitment into peripheral tissues (Vicente-Manzanares et al., 2003; Eisenmann et al., 2007; Sakata et al., 2007). More recently, FMNL1 has been shown to mediate effector T cell trafficking to inflammatory sites in the context of T cell-mediated autoimmunity, by promoting actin polymerization at the back of the nucleus to help T cells overcome restrictive barriers (Thompson et al., 2020). In the context of the T cell IS both mDIA1 and FMNL1 contribute to the reorientation of the MTOC and their deletion in $CD8^+$ T cells reduces cytotoxic activity (Gomez et al., 2007). These 2 formins appear to have distinct localization in the lamellipodium of T cells

forming the IS. Moreover, FMNL1 and mDIA1 are enriched around the MTOC, arranging into tight ring and starburst patterns, respectively (Gomez et al., 2007). This suggests that mDIA1 and FMNL1 play complementary roles in driving MTOC polarization in T cells upon cognate APC encounter. Whether these roles are exerted directly or via the peri-centriole actin network described recently at the B cell synapse (Obino et al., 2016) remains to be investigated. A further layer of complexity regarding formin activities in the context of T cell activation is the existence of 3 FMNL1 isoforms (FMNL1α/β/γ) with distinct C-term domains that appear to distribute differentially at the MTOC, actin cortex and golgi apparatus (Colón-Franco et al., 2011; Bello-Gamboa et al., 2020). Recently, mDIA1 and mDIA3 were found to play a key role at the T cell IS by controlling a very early step of TCR signaling. Indeed ablation of these formins in murine $CD8^+$ T cells affected the localization of phosphorylated Zap70 and downstream LAT phosphorylation (Thumkeo et al., 2020). These formins were shown to also be indispensable for IS spreading, peripheral F-actin ring formation and TCR microcluster centralization. These findings point to the very proximal roles for F-actin remodeling in the context of TCR-driven antigen recognition, as discussed in chapter 1.

There is to date no reported PID entity that would be caused by genetic alterations in genes encoding formins. However, homozygous loss of *DIAPH1* (the gene that encodes DIAPH1/mDIA1), which was initially reported to cause is causing seizures, cortical blindness, and microcephaly syndrome in humans (Ercan-Sencicek et al., 2015), has recently been reported to be associated with lymphocyte maturation and function impairments, as well as increased risk of B cell lymphoma (Kaustio et al., 2021). The immune cell defects included defective T cell IS assembly, in particular MTOC polarization, in agreement with earlier cell biology studies. The severity of the neurological manifestations related to the role of mDia1 in brain development have initially masked immune system deficiency in the affected patients. Furthermore, a gain-of-function variant in *DIAPH1* was reported to cause hearing loss associated to macrothrombocytopenia and mild neutropenia (Stritt et al., 2016). Lymphocyte function was reported to be abnormal in these patients. It is possible that specific mutations in additional formin isoforms with preponderant expression in the hematopoietic system will be identified as causative in yet undiagnosed PIDs or complex syndromes.

ACTIN REMODELING PROGRAM SUSTAINING IMMUNOLOGICAL SYNAPSE ASSEMBLY AND TURNOVER

The Actin Remodeling Machinery in the Context of T Cell Activation

The knowledge gained through the study of individual actinopathies and complementary models is providing the notion that actin regulators play non-redundant activities in the context of T cell activation and function (as illustrated in **Figure 2**). Beyond the study of single deficiencies, a yet poorly studied question is that of the coordination at work among such regulators. Indeed, actin cytoskeleton homeostasis relies on a coherent molecular program to guarantee coexistence of multiple actin networks, their adaptability to stimuli and their turnover. Actin regulators are integral to the signaling events provoked upon engagement of the TCR, integrins, coreceptors, chemokine receptors (**Figure 3**) and probably nearly any T cell surface receptor. In a global atlas of TCR signaling, the earliest signaling events have recently been mapped to proteins belonging to the term "guanine nucleotide releasing factors," "GTPase activation," "cell projection," "cytoskeleton," and "actin binding" (Locard-Paulet et al., 2020). This makes sense given that actin remodeling is required for synapse initiation and spreading, as well as to drive receptor patterning. As illustrated in **Figure 3**, the layers connecting surface receptors to the various actin remodeling activities encompass proximal signaling molecules, GTPase regulators, GTPases and actin binding proteins. The hierarchical orchestration of this signaling network in time and space is barely understood. Beside basic studies conducted in various cellular models, studies on the immune-related actinopathies presented above have started to provide original insight into specific facets of the molecular interplay sculpting the actin remodeling ensemble (in **Figure 3**, molecules related to PID have been highlighted). We will focus in the next chapter on the molecular details about the WIP-WASP-DOCK8 interaction, since more knowledge has been accumulated for this area of the actin remodeling network (at least in the context of T cells). It provides a glimpse into the nature of the connectivity between TCR stimulation and actin remodeling.

Complex Coordination Among Actin Regulators: Focus on WIP-WASP-DOCK8

As explained above, WIP has initially been described as a chaperone for WASP. Accordingly, WIP-deficient T cells have been reported to fail expressing WASP, both in mice models and corresponding patients (de la Fuente et al., 2007; Lanzi et al., 2012; Pfajfer et al., 2017). The loss of WASP expression in the context of WIP deficiency can be explained by the fact that WIP protects WASP from ubiquitination and its degradation by the proteasome and calpain (Chou et al., 2006; de la Fuente et al., 2007). In addition to protecting WASP from degradation, WIP has been shown in non-hematopoietic cells to act as a link between Nck and N-WASP (Donnelly et al., 2013), the homologue of WASP in non-hematopoietic cells. This positions WIP as a molecule capable to connect signaling events proximal to receptors to WASP/N-WASP-dependent actin remodeling. The hierarchy of connections between TCR stimulation and actin remodeling and the pivotal role of WIP has been recently revealed by a phosphoproteomic approach showing that WIP phosphorylation events are among the earliest marks upon TCR stimulation (Locard-Paulet et al., 2020). Indeed, WIP belongs to a cluster of signaling molecules with very rapid but transient phosphorylation, with Serine 268 and 330 phosphorylated as early as 15 sec after TCR stimulation. Interestingly Serine 340 of WIP is phosphorylated at a later time point and in a prolonged

manner. This suggests a chronological orchestration of signaling events along the steps of IS maturation. Those molecular marks are not within the WASP interaction domain and may not directly impact WIP activity towards WASP. Rather, PKCθ phosphorylation of WIP at S488 has been proposed as a mediator of is accompanied by the dissociation of the WIP/WASP complex dissociation, which is a pre-requisite required for WASP activation (Sasahara et al., 2002; Fried et al., 2014b).

A further layer of complexity of the WIP-WASP pathway relates to the WASP-independent functions of WIP. T cell synapse defects appear to be more severe in WIP-deficiency as they are in WASP-deficiency (Calvez et al., 2011; Pfajfer et al., 2017), although these 2 deficiencies have not formally been compared side by side with similar models and stimulations. The distinct severity of IS defects (as well as other defects in T cells and other cell types, as reviewed in Fried et al., 2014a) can be explained by the fact that the function of WIP is not limited to protecting WASP from degradation. Because of its structure and abundance of proline residues, WIP indeed interacts with multiple proteins including additional actin-related proteins, beyond WASP. This includes cortactin that promotes Arp/2/3-dependent actin polymerization (Kinley et al., 2003). Furthermore, T cells from mice that express a WIP mutant that lacks the capacity to bind actin without affecting WASP levels display decreased cellular F-actin content, a disorganized actin cytoskeleton, impaired chemotaxis and *in vivo* homing (Massaad et al., 2014). Together, these data suggest that WIP controls lymphocyte motility independently from its WASP stabilization function, possibly via its capacity to bind actin directly and to interact with Nck and cortactin (Antón and Jones, 2006).

The interaction of WASP and WIP occurs as part of a molecular complex also including the upstream regulator DOCK8, as shown in T cells by co-immunoprecipitation assays (Janssen et al., 2016). Interestingly WIP bridges DOCK8 to WASP and to actin via distinct molecular domains. Therefore WIP acts as a scaffold with actin affinity, on which WASP and DOCK8 can dock. Such molecular complex assembly allows WASP activation by the GEF activity of DOCK8 (via Cdc42), at the proximity to actin structures in a way to control local remodeling. The DOCK8 mutant (S1827P in DHR2 domain) with loss of GEF activity for Cdc42 but preserved binding to WIP and WASP was used to show that the control of WASP activity is via its GEF activity (Janssen et al., 2016). In the context of LFA-1 activation, the WIP-WASP-DOCK8 complex can associate with talin to bind to the β chain of LFA-1, which promotes actin anchorage and conformational activation (Ham et al., 2013).

Deficiencies in WASP, WIP and DOCK8 share multiple impairments in T cell function, albeit to a different degree. This indicates that although these proteins belong to a common signaling pathway downstream TCR activation, they are additionally endowed with independent activities. Indeed, DOCK8 exerts WASP-independent functions, such as through its association with STAT3, which explains occurrence of Hyper-IgE in DOCK8-deficient individuals (Zhang et al., 2009). Along the same line, WIP exerts WASP-independent functions, such as through cortactin, which may explain higher severity of WIP deficiency as compared to that of WASP.

Actin Homeostasis Is Driven by Competition Among Actin Networks

The coexistence of dynamic actin networks within the cell has been proposed to be tuned by a global treadmilling process, in which a steady-state amount of polymerizable actin monomers is established by the dynamics of each network (Carlier and Shekhar, 2017). In that context, specific triggers might result in differential partitioning of actin to distinct networks via the relative activation of Rho GTPases. This view is supported by the notion of competition as a basic principle to determine the size of distinct actin networks (Burke et al., 2014; Lomakin et al., 2015; Antkowiak et al., 2019). In particular, this seems to apply to the cortical actin, which has been shown to be regulated by the activities of the Arp2/3 complex and formins, as competitive actin nucleators (Bovellan et al., 2014).

Such concept of competition at the basis of actin homeostasis is important to fully apprehend some of the cellular defects in patients with actinopathies. For example, we found that aberrant spikes and elongated protrusions dynamically assembled at the periphery of ARPC1B-deficient T cells in the context of TCR/LFA-1 activation result from an imbalanced actin dynamics in favor of formins (Brigida et al., 2018). Indeed patient-derived T cells treated with the pan-formin inhibitor SMIFH2 displayed a collapse of the aberrant protrusions. It should be noted, however, that such treatment did not restore normal assembly of the synapse, pointing to the required intrinsic activity of Arp2/3 to drive IS assembly by favoring lamellipodia extension. This observation is in line with a previous work showing that Arp2/3 inhibition in Jurkat cells results in the emission of formin-dependant actin spikes (Murugesan et al., 2016). This data also illustrates that the consequence of a given molecular deficiency might be the combination of the loss of the intrinsic function of the considered actor together with indirect compensatory effects. Another level of co-regulation is illustrated by compensatory mechanisms that might arise in the context of actin-regulator deficiencies. Indeed, ARPC1B deficiency has recently been shown to be accompanied by a molecular compensation via ARPC1A (Randzavola et al., 2019). Why ARPC1A expression does not rescue the function of ARPC1B deficient immune cells remains to be investigated.

Integration of Concurrent Stimuli by the Actin Remodeling Machinery

Individual studies on actin-related PIDs have been able to pinpoint defects in available cellular models and have focused on a few stimuli. We currently lack information on the selectivity (or ubiquity) of actin remodelers in mediating the activity of the multiple receptors that decorate T cells and contribute to the regulation of migration, adhesion and activation. If one considers WASP, for which more substantial knowledge has been accumulated, studies with patient-derived T cells collectively indicate that it is involved in transmitting activation via multiple receptors including the TCR (Molina et al., 1993; Dupré et al., 2002), CD28 (Badour et al., 2007), integrins (Lafouresse et al., 2012; Houmadi et al., 2018) and chemokine receptors (Haddad et al., 2001). However, the involvement of WASP

downstream of many costimulatory or inhibitory receptors has not been explored. Beyond WASP, whether actin regulators tend to share their activity downstream multiple receptors or to operate selectively is currently unknown. Anyway, we favor the view that each T cell triggering (with nature of receptors engaged and strength of engagement as variables) will lead to an adapted remodeling of the local actin networks sustaining the IS. Given the segregation of receptors in distinct areas of the IS that are sustained by distinct cortical actin reticulation, it is tempting to speculate that the different receptors establish distinct crosstalk with the actin cytoskeleton and its remodeling machinery. This notion is supported by the evidence that receptors are organized into distinct membrane subdomains that establish specific connections to the actin cytoskeleton. Indeed, TCR clusters are associated with dense actin foci, which are driven by WASP and Arp2/3 activities (Kumari et al., 2015). In a complementary study, LFA-1 was shown to associate to an actin network regulated by the formin FHOD1 (Tabdanov et al., 2015). Very interestingly, LFA-1 adhesion was shown to mediate actomyosin forces via its associated network, which were necessary to reinforce TCR-associated actin foci. This shows not only that receptors are embedded in specific local actin environments that they shape upon triggering, but also that receptor interplay operates at least in part via connections of these local actin networks. The spatial range at which such crosstalk might operate is currently unknown and will require dedicated micropatterning and imaging approaches, coupled to biosensors able to capture local molecular activities.

CONCLUDING REMARKS

Approaching the molecular control of IS actin dynamics and sub-networks via the prism of actin-related PID has taught us a lot in recent years. Indeed such natural defects have pointed to key molecules, which deficiency translates into pathological states. Beyond the initial studies on actin dynamics that have made use of drugs with crude effects on actin dynamics, understanding of fine molecular control of actin remodeling through precise actin regulators has greatly deepen our understanding of actin homeostasis. With the deployment of genome sequencing, multiple new entities have been discovered recently and will continue to be discovered. Not only does PID research provide molecular pathways of interest, but it also fosters fundamental research in the sense that elucidation of complex deficiencies often challenges the limits of current knowledge.

The morphological analysis of the IS of T cells from patients with deficiencies in WASP, WIP, WDR1, RasGRP1, ARPC1B, and HEM1 reveal distinct roles of individual actin regulators in shaping IS microarchitecture. Together, these data point to the non-overlapping activities of multiple actin regulators during T cell activation, calling for a comprehensive and systematic analysis of T cell signaling in these unique models. Such goal would require better standardization of the current approaches, in particular regarding morphological analysis of the IS (Mace and Orange, 2015; Jankowska et al., 2018). Improving approaches to characterize IS defects might in turn benefit diagnostic efforts and accelerate discovery of yet undiagnosed PIDs related with actin remodeling.

AUTHOR CONTRIBUTIONS

LD and LP wrote the manuscript and conceptualized the figures. KB provided intellectual input and edited the manuscript. All authors contributed to the article and approved the submitted version.

ACKNOWLEDGMENTS

We wish to thank Tatjana Hirschmugl (Scillustration, Graz, and Vienna, Austria) for design and production of the artwork. This work received support from WWTF (*PrecisePID* project LS16-060 to LD and KB) and CNRS (International Research Project *SysTact* to LD).

REFERENCES

Adriani, M., Aoki, J., Horai, R., Thornton, A. M., Konno, A., Kirby, M., et al. (2007). Impaired in vitro regulatory T cell function associated with Wiskott-Aldrich syndrome. *Clin. Immunol.* 124, 41–48. doi: 10.1016/j.clim.2007.02.001

Aiuti, A., Biasco, L., Scaramuzza, S., Ferrua, F., Cicalese, M. P., Baricordi, C., et al. (2013). Lentiviral hematopoietic stem cell gene therapy in patients with Wiskott-Aldrich syndrome. *Science* 341:1233151. doi: 10.1126/science.1233151

Allenspach, E. J., Cullinan, P., Tong, J., Tang, Q., Tesciuba, A. G., Cannon, J. L., et al. (2001). ERM-dependent movement of CD43 defines a novel protein complex distal to the immunological synapse. *Immunity* 15, 739–750. doi: 10.1016/s1074-7613(01)00224-2

Ambler, R., Edmunds, G. L., Tan, S. L., Cirillo, S., Pernes, J. I., Ruan, X., et al. (2020). PD-1 suppresses the maintenance of cell couples between cytotoxic T cells and target tumor cells within the tumor. *Sci. Signal* 13:eaau4518. doi: 10.1126/scisignal.aau4518

Ambruso, D. R., Knall, C., Abell, A. N., Panepinto, J., Kurkchubasche, A., Thurman, G., et al. (2000). Human neutrophil immunodeficiency syndrome is associated with an inhibitory Rac2 mutation. *PNAS* 97, 4654–4659. doi: 10.1073/pnas.080074897

Antkowiak, A., Guillotin, A., Sanders, M. B., Colombo, J., Vincentelli, R., and Michelot, A. (2019). Sizes of actin networks sharing a common environment are determined by the relative rates of assembly. *PLoS Biol.* 17:e3000317. doi: 10.1371/journal.pbio.3000317

Antón, I. M., and Jones, G. E. (2006). WIP: a multifunctional protein involved in actin cytoskeleton regulation. *Eur. J. Cell Biol.* 85, 295–304. doi: 10.1016/j.ejcb.2005.08.004

Ariga, T., Kondoh, T., Yamaguchi, K., Yamada, M., Sasaki, S., Nelson, D. L., et al. (2001). Spontaneous *In Vivo* reversion of an inherited mutation in the wiskott-aldrich syndrome. *J. Immunol.* 166, 5245–5249. doi: 10.4049/jimmunol.166.8.5245

Babich, A., Li, S., O'Connor, R. S., Milone, M. C., Freedman, B. D., and Burkhardt, J. K. (2012). F-actin polymerization and retrograde flow drive sustained PLCγ1 signaling during T cell activation. *J. Cell Biol.* 197, 775–787. doi: 10.1083/jcb.201201018

Badour, K., McGavin, M. K. H., Zhang, J., Freeman, S., Vieira, C., Filipp, D., et al. (2007). Interaction of the Wiskott-Aldrich syndrome protein with sorting nexin 9 is required for CD28 endocytosis and cosignaling in T cells. *Proc. Natl. Acad. Sci. U. S. A.* 104, 1593–1598. doi: 10.1073/pnas.0610543104

Badour, K., Zhang, J., Shi, F., McGavin, M. K. H., Rampersad, V., Hardy, L. A., et al. (2003). The Wiskott-Aldrich Syndrome Protein Acts Downstream of CD2 and the CD2AP and PSTPIP1 Adaptors to Promote Formation of the Immunological Synapse. *Immunity* 18, 141–154. doi: 10.1016/S1074-7613(02)00516-2

Baker, C. M., Comrie, W. A., Hyun, Y.-M., Chung, H.-L., Fedorchuk, C. A., Lim, K., et al. (2012). Opposing roles for RhoH GTPase during T-cell migration and activation. *PNAS* 109, 10474–10479. doi: 10.1073/pnas.1114214109

Balagopalan, L., Yi, J., Nguyen, T., McIntire, K. M., Harned, A. S., Narayan, K., et al. (2018). Plasma membrane LAT activation precedes vesicular recruitment defining two phases of early T-cell activation. *Nat. Commun.* 9:2013. doi: 10.1038/s41467-018-04419-x

Bálint, Š, Müller, S., Fischer, R., Kessler, B. M., Harkiolaki, M., Valitutti, S., et al. (2020). Supramolecular attack particles are autonomous killing entities released from cytotoxic T cells. *Science* 368, 897–901. doi: 10.1126/science.aay9207

Barda-Saad, M., Braiman, A., Titerence, R., Bunnell, S. C., Barr, V. A., and Samelson, L. E. (2005). Dynamic molecular interactions linking the T cell antigen receptor to the actin cytoskeleton. *Nat. Immunol.* 6, 80–89. doi: 10.1038/ni1143

Bashour, K. T., Gondarenko, A., Chen, H., Shen, K., Liu, X., Huse, M., et al. (2014). CD28 and CD3 have complementary roles in T-cell traction forces. *Proc. Natl. Acad. Sci. U. S. A.* 111, 2241–2246. doi: 10.1073/pnas.1315606111

Basu, R., Whitlock, B. M., Husson, J., Le Floc'h, A., Jin, W., Oyler-Yaniv, A., et al. (2016). Cytotoxic T Cells Use Mechanical Force to Potentiate Target Cell Killing. *Cell* 165, 100–110. doi: 10.1016/j.cell.2016.01.021

Beemiller, P., and Krummel, M. F. (2010). Mediation of T-Cell Activation by Actin Meshworks. *Cold Spring Harb. Perspect. Biol.* 2:a002444. doi: 10.1101/cshperspect.a002444

Bello-Gamboa, A., Velasco, M., Moreno, S., Herranz, G., Ilie, R., Huetos, S., et al. (2020). Actin reorganization at the centrosomal area and the immune synapse regulates polarized secretory traffic of multivesicular bodies in T lymphocytes. *J. Extracell Ves.* 9:1759926. doi: 10.1080/20013078.2020.1759926

Bertrand, F., Müller, S., Roh, K.-H., Laurent, C., Dupré, L., and Valitutti, S. (2013). An initial and rapid step of lytic granule secretion precedes microtubule organizing center polarization at the cytotoxic T lymphocyte/target cell synapse. *Proc. Natl. Acad. Sci. U. S. A.* 110, 6073–6078. doi: 10.1073/pnas.1218640110

Billadeau, D. D., Nolz, J. C., and Gomez, T. S. (2007). Regulation of T-cell activation by the cytoskeleton. *Nat. Rev. Immunol.* 7, 131–143. doi: 10.1038/nri2021

Blanchard, N., Lankar, D., Faure, F., Regnault, A., Dumont, C., Raposo, G., et al. (2002). TCR activation of human T cells induces the production of exosomes bearing the TCR/CD3/zeta complex. *J. Immunol.* 168, 3235–3241. doi: 10.4049/jimmunol.168.7.3235

Blanchoin, L., Boujemaa-Paterski, R., Sykes, C., and Plastino, J. (2014). Actin dynamics, architecture, and mechanics in cell motility. *Physiol. Rev.* 94, 235–263. doi: 10.1152/physrev.00018.2013

Bouafia, A., Lofek, S., Bruneau, J., Chentout, L., Lamrini, H., Trinquand, A., et al. (2019). Loss of ARHGEF1 causes a human primary antibody deficiency. *J. Clin. Invest.* 129, 1047–1060. doi: 10.1172/JCI120572

Bovellan, M., Romeo, Y., Biro, M., Boden, A., Chugh, P., Yonis, A., et al. (2014). Cellular Control of Cortical Actin Nucleation. *Curr. Biol.* 24, 1628–1635. doi: 10.1016/j.cub.2014.05.069

Breitsprecher, D., and Goode, B. L. (2013). Formins at a glance. *J. Cell Sci.* 126, 1–7. doi: 10.1242/jcs.107250

Brigida, I., Zoccolillo, M., Cicalese, M. P., Pfajfer, L., Barzaghi, F., Scala, S., et al. (2018). T-cell defects in patients with ARPC1B germline mutations account for combined immunodeficiency. *Blood* 132, 2362–2374. doi: 10.1182/blood-2018-07-863431

Britton, G. J., Ambler, R., Clark, D. J., Hill, E. V., Tunbridge, H. M., McNally, K. E., et al. (2017). PKCθ links proximal T cell and Notch signaling through localized regulation of the actin cytoskeleton. *eLife* 6:e20003. doi: 10.7554/eLife.20003

Brown, A. C. N., Oddos, S., Dobbie, I. M., Alakoskela, J.-M., Parton, R. M., Eissmann, P., et al. (2011). Remodelling of Cortical Actin Where Lytic Granules Dock at Natural Killer Cell Immune Synapses Revealed by Super-Resolution Microscopy. *PLoS Biol.* 9:e1001152. doi: 10.1371/journal.pbio.1001152

Brown, M. J., Nijhara, R., Hallam, J. A., Gignac, M., Yamada, K. M., Erlandsen, S. L., et al. (2003). Chemokine stimulation of human peripheral blood T lymphocytes induces rapid dephosphorylation of ERM proteins, which facilitates loss of microvilli and polarization. *Blood* 102, 3890–3899. doi: 10.1182/blood-2002-12-3807

Buck, M. D., O'Sullivan, D., Klein Geltink, R. I., Curtis, J. D., Chang, C.-H., Sanin, D. E., et al. (2016). Mitochondrial Dynamics Controls T Cell Fate through Metabolic Programming. *Cell* 166, 63–76. doi: 10.1016/j.cell.2016.05.035

Bunnell, S. C., Kapoor, V., Trible, R. P., Zhang, W., and Samelson, L. E. (2001). Dynamic actin polymerization drives T cell receptor-induced spreading: a role for the signal transduction adaptor LAT. *Immunity* 14, 315–329. doi: 10.1016/s1074-7613(01)00112-1

Burke, T. A., Christensen, J. R., Barone, E., Suarez, C., Sirotkin, V., and Kovar, D. R. (2014). Homeostatic actin cytoskeleton networks are regulated by assembly factor competition for monomers. *Curr. Biol.* 24, 579–585. doi: 10.1016/j.cub.2014.01.072

Burns, S. O., Zarafov, A., and Thrasher, A. J. (2017). Primary immunodeficiencies due to abnormalities of the actin cytoskeleton. *Curr. Opin. Hematol.* 24, 16–22. doi: 10.1097/MOH.0000000000000296

Cai, E., Marchuk, K., Beemiller, P., Beppler, C., Rubashkin, M. G., Weaver, V. M., et al. (2017). Visualizing dynamic microvillar search and stabilization during ligand detection by T cells. *Science* 356, eaal3118. doi: 10.1126/science.aal3118

Calvez, R., Lafouresse, F., De Meester, J., Galy, A., Valitutti, S., and Dupré, L. (2011). The Wiskott-Aldrich syndrome protein permits assembly of a focused immunological synapse enabling sustained T-cell receptor signaling. *Haematologica* 96, 1415–1423. doi: 10.3324/haematol.2011.040204

Campi, G., Varma, R., and Dustin, M. L. (2005). Actin and agonist MHC-peptide complex-dependent T cell receptor microclusters as scaffolds for signaling. *J. Exp. Med.* 202, 1031–1036. doi: 10.1084/jem.20051182

Cannon, J. L., and Burkhardt, J. K. (2004). Differential Roles for Wiskott-Aldrich Syndrome Protein in Immune Synapse Formation and IL-2 Production. *J. Immunol.* 173, 1658–1662. doi: 10.4049/jimmunol.173.3.1658

Carisey, A. F., Mace, E. M., Saeed, M. B., Davis, D. M., and Orange, J. S. (2018). Nanoscale Dynamism of Actin Enables Secretory Function in Cytolytic Cells. *Curr. Biol.* 28, 489–502.e. doi: 10.1016/j.cub.2017.12.044

Carlier, M.-F., and Shekhar, S. (2017). Global treadmilling coordinates actin turnover and controls the size of actin networks. *Nat. Rev. Mol. Cell Biol.* 18, 389–401. doi: 10.1038/nrm.2016.172

Carman, C. V., Sage, P. T., Sciuto, T. E., de la Fuente, M. A., Geha, R. S., Ochs, H. D., et al. (2007). Transcellular Diapedesis Is Initiated by Invasive Podosomes. *Immunity* 26, 784–797. doi: 10.1016/j.immuni.2007.04.015

Castro, C. N., Rosenzwajg, M., Carapito, R., Shahrooei, M., Konantz, M., Khan, A., et al. (2020). NCKAP1L defects lead to a novel syndrome combining immunodeficiency, lymphoproliferation, and hyperinflammation. *J. Exp. Med.* 217, e20192275. doi: 10.1084/jem.20192275

Cemerski, S., Das, J., Giurisato, E., Markiewicz, M. A., Allen, P. M., Chakraborty, A. K., et al. (2008). The balance between T cell receptor signaling and degradation at the center of the immunological synapse is determined by antigen quality. *Immunity* 29, 414–422. doi: 10.1016/j.immuni.2008.06.014

Chae, H.-D., Siefring, J. E., Hildeman, D. A., Gu, Y., and Williams, D. A. (2010). RhoH Regulates Subcellular Localization of ZAP-70 and Lck in T Cell Receptor Signaling. *PLoS One* 5:e13970. doi: 10.1371/journal.pone.0013970

Chemin, K., Bohineust, A., Dogniaux, S., Tourret, M., Guégan, S., Miro, F., et al. (2012). Cytokine secretion by CD4+ T cells at the immunological synapse requires Cdc42-dependent local actin remodeling but not microtubule organizing center polarity. *J. Immunol.* 189, 2159–2168. doi: 10.4049/jimmunol.1200156

Chou, H.-C., Antón, I. M., Holt, M. R., Curcio, C., Lanzardo, S., Worth, A., et al. (2006). WIP Regulates the Stability and Localization of WASP to Podosomes in Migrating Dendritic Cells. *Curr. Biol.* 16, 2337–2344. doi: 10.1016/j.cub.2006.10.037

Choudhuri, K., Llodrá, J., Roth, E. W., Tsai, J., Gordo, S., Wucherpfennig, K. W., et al. (2014). Polarized release of TCR-enriched microvesicles at the T cell immunological synapse. *Nature* 507, 118–123. doi: 10.1038/nature12951

Cianferoni, A., Massaad, M., Feske, S., de la Fuente, M. A., Gallego, L., Ramesh, N., et al. (2005). Defective nuclear translocation of nuclear factor of activated T cells and extracellular signal-regulated kinase underlies deficient IL-2 gene expression in Wiskott-Aldrich syndrome. *J. Allergy Clin. Immunol.* 116, 1364–1371. doi: 10.1016/j.jaci.2005.09.006

Colin-York, H., Javanmardi, Y., Skamrahl, M., Kumari, S., Chang, V. T., Khuon, S., et al. (2019). Cytoskeletal Control of Antigen-Dependent T Cell Activation. *Cell Rep.* 26, 3369–3379.e. doi: 10.1016/j.celrep.2019.02.074

Colin-York, H., Kumari, S., Barbieri, L., Cords, L., and Fritzsche, M. (2020). Distinct actin cytoskeleton behaviour in primary and immortalised T-cells. *J. Cell Sci.* 133:jcs232322. doi: 10.1242/jcs.232322

Colón-Franco, J. M., Gomez, T. S., and Billadeau, D. D. (2011). Dynamic remodeling of the actin cytoskeleton by FMNL1γ is required for structural maintenance of the Golgi complex. *J. Cell Sci.* 124, 3118–3126. doi: 10.1242/jcs.083725

Comrie, W. A., Babich, A., and Burkhardt, J. K. (2015). F-actin flow drives affinity maturation and spatial organization of LFA-1 at the immunological synapse. *J. Cell Biol.* 208, 475–491. doi: 10.1083/jcb.201406121

Cook, S. A., Comrie, W. A., Poli, M. C., Similuk, M., Oler, A. J., Faruqi, A. J., et al. (2020). HEM1 deficiency disrupts mTORC2 and F-actin control in inherited immunodysregulatory disease. *Science* 369, 202–207. doi: 10.1126/science.aay5663

Crequer, A., Picard, C., Patin, E., D'Amico, A., Abhyankar, A., Munzer, M., et al. (2012a). Inherited MST1 Deficiency Underlies Susceptibility to EV-HPV Infections. *PLoS One* 7:e44010. doi: 10.1371/journal.pone.0044010

Crequer, A., Troeger, A., Patin, E., Ma, C. S., Picard, C., Pedergnana, V., et al. (2012b). Human RHOH deficiency causes T cell defects and susceptibility to EV-HPV infections. *J. Clin. Invest.* 122, 3239–3247. doi: 10.1172/JCI62949

Das, D. K., Feng, Y., Mallis, R. J., Li, X., Keskin, D. B., Hussey, R. E., et al. (2015). Force-dependent transition in the T-cell receptor β-subunit allosterically regulates peptide discrimination and pMHC bond lifetime. *Proc. Natl. Acad. Sci. U. S. A.* 112, 1517–1522. doi: 10.1073/pnas.1424829112

de la Fuente, M. A., Sasahara, Y., Calamito, M., Antón, I. M., Elkhal, A., Gallego, M. D., et al. (2007). WIP is a chaperone for Wiskott-Aldrich syndrome protein (WASP). *Proc. Natl. Acad. Sci. U. S. A.* 104, 926–931. doi: 10.1073/pnas.0610275104

De Meester, J., Calvez, R., Valitutti, S., and Dupré, L. (2010). The Wiskott-Aldrich syndrome protein regulates CTL cytotoxicity and is required for efficient killing of B cell lymphoma targets. *J. Leuk. Biol.* 88, 1031–1040. doi: 10.1189/jlb.0410197

Delmonte, O. M., Biggs, C. M., Hayward, A., Comeau, A. M., Kuehn, H. S., Rosenzweig, S. D., et al. (2017). First Case of X-Linked Moesin Deficiency Identified After Newborn Screening for SCID. *J. Clin. Immunol.* 37, 336–338. doi: 10.1007/s10875-017-0391-9

Delon, J., Bercovici, N., Liblau, R., and Trautmann, A. (1998). Imaging antigen recognition by naive CD4+ T cells: compulsory cytoskeletal alterations for the triggering of an intracellular calcium response. *Eur. J. Immunol.* 28, 716–729. doi: 10.1002/(SICI)1521-4141(199802)28:02<716::AID-IMMU716<3.0.CO;2-E

Delon, J., Kaibuchi, K., and Germain, R. N. (2001). Exclusion of CD43 from the Immunological Synapse Is Mediated by Phosphorylation-Regulated Relocation of the Cytoskeletal Adaptor Moesin. *Immunity* 15, 691–701. doi: 10.1016/S1074-7613(01)00231-X

Demetriou, P., Abu-Shah, E., Valvo, S., McCuaig, S., Mayya, V., Kvalvaag, A., et al. (2020). A dynamic CD2-rich compartment at the outer edge of the immunological synapse boosts and integrates signals. *Nat. Immunol.* 21, 1232–1243. doi: 10.1038/s41590-020-0770-x

Derry, J. M., Ochs, H. D., and Francke, U. (1994). Isolation of a novel gene mutated in Wiskott-Aldrich syndrome. *Cell* 78, 635–644. doi: 10.1016/0092-8674(94)90528-2

Ditlev, J. A., Vega, A. R., Köster, D. V., Su, X., Tani, T., Lakoduk, A. M., et al. (2019). A composition-dependent molecular clutch between T cell signaling condensates and actin. *eLife* 8:e42695. doi: 10.7554/eLife.42695

Dobbs, K., Domínguez Conde, C., Zhang, S.-Y., Parolini, S., Audry, M., Chou, J., et al. (2015). Inherited DOCK2 Deficiency in Patients with Early-Onset Invasive Infections. *N. Engl. J. Med.* 372, 2409–2422. doi: 10.1056/NEJMoa1413462

Donnelly, S. K., Weisswange, I., Zettl, M., and Way, M. (2013). WIP Provides an Essential Link between Nck and N-WASP during Arp2/3-Dependent Actin Polymerization. *Curr. Biol.* 23, 999–1006. doi: 10.1016/j.cub.2013.04.051

Dupré, L., Aiuti, A., Trifari, S., Martino, S., Saracco, P., Bordignon, C., et al. (2002). Wiskott-Aldrich syndrome protein regulates lipid raft dynamics during immunological synapse formation. *Immunity* 17, 157–166. doi: 10.1016/s1074-7613(02)00360-6

Dustin, M. L. (2004). Stop and Go Traffic to Tune T Cell Responses. *Immunity* 21, 305–314. doi: 10.1016/j.immuni.2004.08.016

Dustin, M. L. (2008). T-cell activation through immunological synapses and kinapses. *Immunol. Rev.* 221, 77–89. doi: 10.1111/j.1600-065X.2008.00589.x

Eisenmann, K. M., West, R. A., Hildebrand, D., Kitchen, S. M., Peng, J., Sigler, R., et al. (2007). T cell responses in mammalian diaphanous-related formin mDia1 knock-out mice. *J. Biol. Chem.* 282, 25152–25158. doi: 10.1074/jbc.M703243200

Engelhardt, K. R., McGhee, S., Winkler, S., Sassi, A., Woellner, C., Lopez-Herrera, G., et al. (2009). Large deletions and point mutations involving the dedicator of cytokinesis 8 (DOCK8) in the autosomal-recessive form of hyper-IgE syndrome. *J. Allergy Clin. Immunol.* 124, 1289–1302.e. doi: 10.1016/j.jaci.2009.10.038

Ercan-Sencicek, A. G., Jambi, S., Franjic, D., Nishimura, S., Li, M., El-Fishawy, P., et al. (2015). Homozygous loss of DIAPH1 is a novel cause of microcephaly in humans. *Eur. J. Hum. Genet.* 23, 165–172. doi: 10.1038/ejhg.2014.82

Fanzo, J. C., Yang, W., Jang, S. Y., Gupta, S., Chen, Q., Siddiq, A., et al. (2006). Loss of IRF-4–binding protein leads to the spontaneous development of systemic autoimmunity. *J. Clin. Invest.* 116, 703–714. doi: 10.1172/JCI24096

Fehon, R. G., McClatchey, A. I., and Bretscher, A. (2010). Organizing the cell cortex: the role of ERM proteins. *Nat. Rev. Mol. Cell Biol.* 11, 276–287. doi: 10.1038/nrm2866

Fife, B. T., Pauken, K. E., Eagar, T. N., Obu, T., Wu, J., Tang, Q., et al. (2009). Interactions between PD-1 and PD-L1 promote tolerance by blocking the TCR-induced stop signal. *Nat. Immunol.* 10, 1185–1192. doi: 10.1038/ni.1790

Föger, N., Rangell, L., Danilenko, D. M., and Chan, A. C. (2006). Requirement for coronin 1 in T lymphocyte trafficking and cellular homeostasis. *Science* 313, 839–842. doi: 10.1126/science.1130563

Fried, S., Matalon, O., Noy, E., and Barda–Saad, M. (2014a). WIP: more than a WASp-interacting protein. *J. Leuk. Biol.* 96, 713–727. doi: 10.1189/jlb.2RU0314-162R

Fried, S., Reicher, B., Pauker, M. H., Eliyahu, S., Matalon, O., Noy, E., et al. (2014b). Triple-color FRET analysis reveals conformational changes in the WIP-WASp actin-regulating complex. *Sci. Signal* 7:ra60. doi: 10.1126/scisignal.2005198

Friedman, R. S., Beemiller, P., Sorensen, C. M., Jacobelli, J., and Krummel, M. F. (2010). Real-time analysis of T cell receptors in naive cells in vitro and in vivo reveals flexibility in synapse and signaling dynamics. *J. Exp. Med.* 207, 2733–2749. doi: 10.1084/jem.20091201

Fritzsche, M., Fernandes, R. A., Chang, V. T., Colin-York, H., Clausen, M. P., Felce, J. H., et al. (2017). Cytoskeletal actin dynamics shape a ramifying actin network underpinning immunological synapse formation. *Sci. Adv.* 3:e1603032. doi: 10.1126/sciadv.1603032

Geiger, B., Rosen, D., and Berke, G. (1982). Spatial relationships of microtubule-organizing centers and the contact area of cytotoxic T lymphocytes and target cells. *J. Cell Biol.* 95, 137–143. doi: 10.1083/jcb.95.1.137

Gernez, Y., Jesus, A. A., de, Alsaleem, H., Macaubas, C., Roy, A., et al. (2019). Severe autoinflammation in 4 patients with C-terminal variants in cell division control protein 42 homolog (CDC42) successfully treated with IL-1β inhibition. *J. Aller. Clin. Immunol.* 144, 1122–1125.e. doi: 10.1016/j.jaci.2019.06.017

Ghosh, S., Di Bartolo, V., Tubul, L., Shimoni, E., Kartvelishvily, E., Dadosh, T., et al. (2020). ERM-Dependent Assembly of T Cell Receptor Signaling and Co-stimulatory Molecules on Microvilli prior to Activation. *Cell Rep.* 30, 3434–3447.e. doi: 10.1016/j.celrep.2020.02.069

Gomez, T. S., Kumar, K., Medeiros, R. B., Shimizu, Y., Leibson, P. J., and Billadeau, D. D. (2007). Formins Regulate the Actin-Related Protein 2/3 Complex-Independent Polarization of the Centrosome to the Immunological Synapse. *Immunity* 26, 177–190. doi: 10.1016/j.immuni.2007.01.008

González-Granado, J. M., Silvestre-Roig, C., Rocha-Perugini, V., Trigueros-Motos, L., Cibrián, D., Morlino, G., et al. (2014). Nuclear envelope lamin-A couples actin dynamics with immunological synapse architecture and T cell activation. *Sci. Signal* 7:ra37. doi: 10.1126/scisignal.2004872

Grakoui, A., Bromley, S. K., Sumen, C., Davis, M. M., Shaw, A. S., Allen, P. M., et al. (1999). The immunological synapse: a molecular machine controlling T cell activation. *Science* 285, 221–227. doi: 10.1126/science.285.5425.221

Gunzer, M., Schäfer, A., Borgmann, S., Grabbe, S., Zänker, K. S., Bröcker, E. B., et al. (2000). Antigen presentation in extracellular matrix: interactions of T cells with dendritic cells are dynamic, short lived, and sequential. *Immunity* 13, 323–332. doi: 10.1016/s1074-7613(00)00032-7

Haddad, E., Zugaza, J. L., Louache, F., Debili, N., Crouin, C., Schwarz, K., et al. (2001). The interaction between Cdc42 and WASP is required for SDF-1-induced T-lymphocyte chemotaxis. *Blood* 97, 33–38. doi: 10.1182/blood.v97.1.33

Ham, H., Guerrier, S., Kim, J., Schoon, R. A., Anderson, E. L., Hamann, M. J., et al. (2013). Dedicator of Cytokinesis 8 Interacts with Talin and Wiskott-Aldrich Syndrome Protein To Regulate NK Cell Cytotoxicity. *J. Immunol.* 190, 3661–3669. doi: 10.4049/jimmunol.1202792

Hammer, J. A., Wang, J. C., Saeed, M., and Pedrosa, A. T. (2019). Origin Organization, Dynamics, and Function of Actin and Actomyosin Networks at the T Cell Immunological Synapse. *Annu. Rev. Immunol.* 37, 201–224. doi: 10.1146/annurev-immunol-042718-041341

Houmadi, R., Guipouy, D., Rey-Barroso, J., Vasconcelos, Z., Cornet, J., Manghi, M., et al. (2018). The Wiskott-Aldrich Syndrome Protein Contributes to the Assembly of the LFA-1 Nanocluster Belt at the Lytic Synapse. *Cell Rep.* 22, 979–991. doi: 10.1016/j.celrep.2017.12.088

Hu, K. H., and Butte, M. J. (2016). T cell activation requires force generation. *J. Cell Biol.* 213, 535–542. doi: 10.1083/jcb.201511053

Humblet-Baron, S., Sather, B., Anover, S., Becker-Herman, S., Kasprowicz, D. J., Khim, S., et al. (2007). Wiskott-Aldrich syndrome protein is required for regulatory T cell homeostasis. *J. Clin. Invest.* 117, 407–418. doi: 10.1172/JCI29539

Humphries, C. L., Balcer, H. I., D'Agostino, J. L., Winsor, B., Drubin, D. G., Barnes, G., et al. (2002). Direct regulation of Arp2/3 complex activity and function by the actin binding protein coronin. *J. Cell Biol.* 159, 993–1004. doi: 10.1083/jcb.200206113

Huse, M., Lillemeier, B. F., Kuhns, M. S., Chen, D. S., and Davis, M. M. (2006). T cells use two directionally distinct pathways for cytokine secretion. *Nat. Immunol.* 7, 247–255. doi: 10.1038/ni1304

Ilani, T., Khanna, C., Zhou, M., Veenstra, T. D., and Bretscher, A. (2007). Immune synapse formation requires ZAP-70 recruitment by ezrin and CD43 removal by moesin. *J. Cell Biol.* 179, 733–746. doi: 10.1083/jcb.200707199

Ilani, T., Vasiliver-Shamis, G., Vardhana, S., Bretscher, A., and Dustin, M. L. (2009). T cell antigen receptor signaling and immunological synapse stability require myosin IIA. *Nat. Immunol.* 10, 531–539. doi: 10.1038/ni.1723

Inoue, D., Obino, D., Pineau, J., Farina, F., Gaillard, J., Guerin, C., et al. (2019). Actin filaments regulate microtubule growth at the centrosome. *EMBO J.* 38:e99630. doi: 10.15252/embj.201899630

Jacobelli, J., Chmura, S. A., Buxton, D. B., Davis, M. M., and Krummel, M. F. (2004). A single class II myosin modulates T cell motility and stopping, but not synapse formation. *Nat. Immunolo.* 5, 531–538. doi: 10.1038/ni1065

Jankowska, K. I., Williamson, E. K., Roy, N. H., Blumenthal, D., Chandra, V., Baumgart, T., et al. (2018). Integrins Modulate T Cell Receptor Signaling by Constraining Actin Flow at the Immunological Synapse. *Front. Immunol.* 9:25. doi: 10.3389/fimmu.2018.00025

Janssen, E., and Geha, R. S. (2019). Primary immunodeficiencies caused by mutations in actin regulatory proteins. *Immunol. Rev.* 287, 121–134. doi: 10.1111/imr.12716

Janssen, E., Tohme, M., Hedayat, M., Leick, M., Kumari, S., Ramesh, N., et al. (2016). A DOCK8-WIP-WASp complex links T cell receptors to the actin cytoskeleton. *J. Clin. Invest.* 126, 3837–3851. doi: 10.1172/JCI85774

Janssen, W. J. M., Grobarova, V., Leleux, J., Jongeneel, L., van Gijn, M., van Montfrans, J. M., et al. (2018). Proline-serine-threonine phosphatase interacting protein 1 (PSTPIP1) controls immune synapse stability in human T cells. *J. Allergy Clin. Immunol.* 142, 1947–1955. doi: 10.1016/j.jaci.2018.01.030

Jayachandran, R., Gumienny, A., Bolinger, B., Ruehl, S., Lang, M. J., Fucile, G., et al. (2019). Disruption of Coronin 1 Signaling in T Cells Promotes Allograft Tolerance while Maintaining Anti-Pathogen Immunity. *Immunity* 50, 152–165.e. doi: 10.1016/j.immuni.2018.12.011

Jung, Y., Riven, I., Feigelson, S. W., Kartvelishvily, E., Tohya, K., Miyasaka, M., et al. (2016). Three-dimensional localization of T-cell receptors in relation to microvilli using a combination of superresolution microscopies. *PNAS* 113, E5916–E5924. doi: 10.1073/pnas.1605399113

Kahr, W. H. A., Pluthero, F. G., Elkadri, A., Warner, N., Drobac, M., Chen, C. H., et al. (2017). Loss of the Arp2/3 complex component ARPC1B causes platelet abnormalities and predisposes to inflammatory disease. *Nat. Commun.* 8:14816. doi: 10.1038/ncomms14816

Kaizuka, Y., Douglass, A. D., Varma, R., Dustin, M. L., and Vale, R. D. (2007). Mechanisms for segregating T cell receptor and adhesion molecules during immunological synapse formation in Jurkat T cells. *Proc. Natl. Acad. Sci. U. S. A.* 104, 20296–20301. doi: 10.1073/pnas.0710258105

Kalinichenko, A., Perinetti Casoni, G., Dupre, L., Trotta, L. C., Huemer, J., Galgano, D., et al. (2021). RhoG deficiency abrogates cytotoxicity of human lymphocytes and causes hemophagocytic lymphohistiocytosis. *Blood* 137, 2033–2045. doi: 10.1182/blood.2020008738

Kaustio, M., Nayebzadeh, N., Hinttala, R., Tapiainen, T., Åström, P., Mamia, K., et al. (2021). Loss of DIAPH1 causes SCBMS, combined immunodeficiency and mitochondrial dysfunction. *J. Allergy Clin. Immunol.* 12:656. doi: 10.1016/j.jaci.2020.12.656 [Online ahead of print]

Kile, B. T., Panopoulos, A. D., Stirzaker, R. A., Hacking, D. F., Tahtamouni, L. H., Willson, T. A., et al. (2007). Mutations in the cofilin partner Aip1/Wdr1 cause autoinflammatory disease and macrothrombocytopenia. *Blood* 110, 2371–2380. doi: 10.1182/blood-2006-10-055087

Kinley, A. W., Weed, S. A., Weaver, A. M., Karginov, A. V., Bissonette, E., Cooper, J. A., et al. (2003). Cortactin interacts with WIP in regulating Arp2/3 activation and membrane protrusion. *Curr. Biol.* 13, 384–393. doi: 10.1016/s0960-9822(03)00107-6

Kondo, N., Ueda, Y., Kita, T., Ozawa, M., Tomiyama, T., Yasuda, K., et al. (2017). NDR1-Dependent Regulation of Kindlin-3 Controls High-Affinity LFA-1 Binding and Immune Synapse Organization. *Mol. Cell Biol.* 37, e424–e416. doi: 10.1128/MCB.00424-16

Kotila, T., Wioland, H., Enkavi, G., Kogan, K., Vattulainen, I., Jégou, A., et al. (2019). Mechanism of synergistic actin filament pointed end depolymerization by cyclase-associated protein and cofilin. *Nat. Commun.* 10:5320. doi: 10.1038/s41467-019-13213-2

Kuhn, J. R., and Poenie, M. (2002). Dynamic polarization of the microtubule cytoskeleton during CTL-mediated killing. *Immunity* 16, 111–121. doi: 10.1016/s1074-7613(02)00262-5

Kuhns, D. B., Fink, D. L., Choi, U., Sweeney, C., Lau, K., Priel, D. L., et al. (2016). Cytoskeletal abnormalities and neutrophil dysfunction in WDR1 deficiency. *Blood* 128, 2135–2143. doi: 10.1182/blood-2016-03-706028

Kuijpers, T. W., Tool, A. T. J., Bijl, I., van der, Boer, M., de, et al. (2017). Combined immunodeficiency with severe inflammation and allergy caused by ARPC1B deficiency. *J. Allergy Clin. Immunol.* 140, 273–277.e. doi: 10.1016/j.jaci.2016.09.061

Kumari, S., Depoil, D., Martinelli, R., Judokusumo, E., Carmona, G., Gertler, F. B., et al. (2015). Actin foci facilitate activation of the phospholipase C-γ in primary T lymphocytes via the WASP pathway. *eLife*. 4:e04953. doi: 10.7554/eLife.04953

Kumari, S., Mak, M., Poh, Y.-C., Tohme, M., Watson, N., Melo, M., et al. (2020). Cytoskeletal tension actively sustains the migratory T-cell synaptic contact. *EMBO J.* 39:e102783. doi: 10.15252/embj.2019102783

Kumari, S., Vardhana, S., Cammer, M., Curado, S., Santos, L., Sheetz, M. P., et al. (2012). T Lymphocyte Myosin IIA is Required for Maturation of the Immunological Synapse. *Front. Immunol.* 3:230. doi: 10.3389/fimmu.2012.00230

Lacher, S. M., Thurm, C., Distler, U., Mohebiany, A. N., Israel, N., Kitic, M., et al. (2018). NF-κB inducing kinase (NIK) is an essential post-transcriptional regulator of T-cell activation affecting F-actin dynamics and TCR signaling. *J. Autoimmun.* 94, 110–121. doi: 10.1016/j.jaut.2018.07.017

Lafouresse, F., Cotta-de-Almeida, V., Malet-Engra, G., Galy, A., Valitutti, S., and Dupré, L. (2012). Wiskott-Aldrich syndrome protein controls antigen-presenting cell-driven CD4+ T-cell motility by regulating adhesion to intercellular adhesion molecule-1. *Immunology* 137, 183–196. doi: 10.1111/j.1365-2567.2012.03620.x

Lagresle-Peyrou, C., Luce, S., Ouchani, F., Soheili, T. S., Sadek, H., Chouteau, M., et al. (2016). X-linked primary immunodeficiency associated with hemizygous mutations in the moesin (MSN) gene. *J. Allergy Clin. Immunol.* 138, 1681–1689.e. doi: 10.1016/j.jaci.2016.04.032

Lam, M. T., Coppola, S., Krumbach, O. H. F., Prencipe, G., Insalaco, A., Cifaldi, C., et al. (2019). A novel disorder involving dyshematopoiesis, inflammation, and HLH due to aberrant CDC42 function. *J. Exp. Med.* 216, 2778–2799. doi: 10.1084/jem.20190147

Lanzi, G., Moratto, D., Vairo, D., Masneri, S., Delmonte, O., Paganini, T., et al. (2012). A novel primary human immunodeficiency due to deficiency in the

WASP-interacting protein WIP. *J. Exp. Med.* 209, 29–34. doi: 10.1084/jem.20110896

Lappalainen, P. (2016). Actin-binding proteins: the long road to understanding the dynamic landscape of cellular actin networks. *MBOC* 27, 2519–2522. doi: 10.1091/mbc.e15-10-0728

Lasserre, R., Charrin, S., Cuche, C., Danckaert, A., Thoulouze, M.-I., de Chaumont, F., et al. (2010). Ezrin tunes T-cell activation by controlling Dlg1 and microtubule positioning at the immunological synapse. *EMBO J.* 29, 2301–2314. doi: 10.1038/emboj.2010.127

Le Floc'h, A., Tanaka, Y., Bantilan, N. S., Voisinne, G., Altan-Bonnet, G., Fukui, Y., et al. (2013). Annular PIP3 accumulation controls actin architecture and modulates cytotoxicity at the immunological synapse. *J. Exp. Med.* 210, 2721–2737. doi: 10.1084/jem.20131324

Lebensohn, A. M., and Kirschner, M. W. (2009). Activation of the WAVE complex by coincident signals controls actin assembly. *Mol. Cell* 36, 512–524. doi: 10.1016/j.molcel.2009.10.024

Lee, K.-H., Dinner, A. R., Tu, C., Campi, G., Raychaudhuri, S., Varma, R., et al. (2003). The immunological synapse balances T cell receptor signaling and degradation. *Science* 302, 1218–1222. doi: 10.1126/science.1086507

Li, J., and Springer, T. A. (2017). Integrin extension enables ultrasensitive regulation by cytoskeletal force. *Proc. Natl. Acad. Sci. U. S. A.* 114, 4685–4690. doi: 10.1073/pnas.1704171114

Liang, Y., Cucchetti, M., Roncagalli, R., Yokosuka, T., Malzac, A., Bertosio, E., et al. (2013). The lymphoid lineage–specific actin-uncapping protein Rltpr is essential for costimulation via CD28 and the development of regulatory T cells. *Nat. Immunol.* 14, 858–866. doi: 10.1038/ni.2634

Locard-Paulet, M., Voisinne, G., Froment, C., Goncalves Menoita, M., Ounoughene, Y., Girard, L., et al. (2020). LymphoAtlas: a dynamic and integrated phosphoproteomic resource of TCR signaling in primary T cells reveals ITSN2 as a regulator of effector functions. *Mol. Syst. Biol.* 16:e9524. doi: 10.15252/msb.20209524

Lomakin, A. J., Lee, K.-C., Han, S. J., Bui, D. A., Davidson, M., Mogilner, A., et al. (2015). Competition for actin between two distinct F-actin networks defines a bistable switch for cell polarization. *Nat. Cell Biol.* 17, 1435–1445. doi: 10.1038/ncb3246

Mace, E. M., and Orange, J. S. (2014). Lytic immune synapse function requires filamentous actin deconstruction by Coronin 1A. *Proc. Natl. Acad. Sci. U. S. A.* 111, 6708–6713. doi: 10.1073/pnas.1314975111

Mace, E. M., and Orange, J. S. (2015). Insights into primary immune deficiency from quantitative microscopy. *J. Allergy Clin. Immunol.* 136, 1150–1162. doi: 10.1016/j.jaci.2015.03.049

Machesky, L. M., and Insall, R. H. (1998). Scar1 and the related Wiskott–Aldrich syndrome proteinWASP, regulate the actin cytoskeleton through the Arp2/3 complex. *Curr. Biol.* 8, 1347–1356. doi: 10.1016/S0960-9822(98)00015-3

Maillard, M. H., Cotta-de-Almeida, V., Takeshima, F., Nguyen, D. D., Michetti, P., Nagler, C., et al. (2007). The Wiskott-Aldrich syndrome protein is required for the function of CD4+CD25+Foxp3+ regulatory T cells. *J. Exp. Med.* 204, 381–391. doi: 10.1084/jem.20061338

Marangoni, F., Trifari, S., Scaramuzza, S., Panaroni, C., Martino, S., Notarangelo, L. D., et al. (2007). WASP regulates suppressor activity of human and murine CD4(+)CD25(+)FOXP3(+) natural regulatory T cells. *J. Exp. Med.* 204, 369–380. doi: 10.1084/jem.20061334

Massaad, M. J., Oyoshi, M. K., Kane, J., Koduru, S., Alcaide, P., Nakamura, F., et al. (2014). Binding of WIP to actin is essential for T cell actin cytoskeleton integrity and tissue homing. *Mol. Cell Biol.* 34, 4343–4354. doi: 10.1128/MCB.00533-14

Mastrogiovanni, M., Juzans, M., Alcover, A., and Di Bartolo, V. (2020). Coordinating Cytoskeleton and Molecular Traffic in T Cell Migration Activation, and Effector Functions. *Front. Cell Dev. Biol.* 8:591348. doi: 10.3389/fcell.2020.591348

McClatchey, A. I. (2014). ERM proteins at a glance. *J. Cell Sci.* 127, 3199–3204. doi: 10.1242/jcs.098343

McGavin, M. K., Badour, K., Hardy, L. A., Kubiseski, T. J., Zhang, J., and Siminovitch, K. A. (2001). The intersectin 2 adaptor links Wiskott Aldrich Syndrome protein (WASp)-mediated actin polymerization to T cell antigen receptor endocytosis. *J. Exp. Med.* 194, 1777–1787. doi: 10.1084/jem.194.12.1777

Mempel, T. R., Henrickson, S. E., and Von Andrian, U. H. (2004). T-cell priming by dendritic cells in lymph nodes occurs in three distinct phases. *Nature* 427, 154–159. doi: 10.1038/nature02238

Miller, M. J., Safrina, O., Parker, I., and Cahalan, M. D. (2004). Imaging the single cell dynamics of CD4+ T cell activation by dendritic cells in lymph nodes. *J. Exp. Med.* 200, 847–856. doi: 10.1084/jem.20041236

Molina, I. J., Sancho, J., Terhorst, C., Rosen, F. S., and Remold-O'Donnell, E. (1993). T cells of patients with the Wiskott-Aldrich syndrome have a restricted defect in proliferative responses. *J. Immunol.* 151, 4383–4390.

Monks, C. R., Freiberg, B. A., Kupfer, H., Sciaky, N., and Kupfer, A. (1998). Three-dimensional segregation of supramolecular activation clusters in T cells. *Nature* 395, 82–86. doi: 10.1038/25764

Moreau, H. D., Lemaître, F., Garrod, K. R., Garcia, Z., Lennon-Duménil, A.-M., and Bousso, P. (2015). Signal strength regulates antigen-mediated T-cell deceleration by distinct mechanisms to promote local exploration or arrest. *PNAS* 112, 12151–12156. doi: 10.1073/pnas.1506654112

Moreau, H. D., Lemaître, F., Terriac, E., Azar, G., Piel, M., Lennon-Dumenil, A.-M., et al. (2012). Dynamic in situ cytometry uncovers T cell receptor signaling during immunological synapses and kinapses in vivo. *Immunity* 37, 351–363. doi: 10.1016/j.immuni.2012.05.014

Moshous, D., Martin, E., Carpentier, W., Lim, A., Callebaut, I., Canioni, D., et al. (2013). Whole-exome sequencing identifies Coronin-1A deficiency in 3 siblings with immunodeficiency and EBV-associated B-cell lymphoproliferation. *J. Allergy Clin. Immunol.* 131, 1594–1603.e. doi: 10.1016/j.jaci.2013.01.042

Mueller, P., Massner, J., Jayachandran, R., Combaluzier, B., Albrecht, I., Gatfield, J., et al. (2008). Regulation of T cell survival through coronin-1-mediated generation of inositol-1,4,5-trisphosphate and calcium mobilization after T cell receptor triggering. *Nat. Immunol.* 9, 424–431. doi: 10.1038/ni1570

Mugnier, B., Nal, B., Verthuy, C., Boyer, C., Lam, D., Chasson, L., et al. (2008). Coronin-1A Links Cytoskeleton Dynamics to TCRαβ-Induced Cell Signaling. *PLoS One* 3:e3467. doi: 10.1371/journal.pone.0003467

Murugesan, S., Hong, J., Yi, J., Li, D., Beach, J. R., Shao, L., et al. (2016). Formin-generated actomyosin arcs propel T cell receptor microcluster movement at the immune synapse. *J. Cell Biol.* 215, 383–399. doi: 10.1083/jcb.201603080

Negulescu, P. A., Krasieva, T. B., Khan, A., Kerschbaum, H. H., and Cahalan, M. D. (1996). Polarity of T cell shape, motility, and sensitivity to antigen. *Immunity* 4, 421–430. doi: 10.1016/s1074-7613(00)80409-4

Nehme, N. T., Schmid, J. P., Debeurme, F., André-Schmutz, I., Lim, A., Nitschke, P., et al. (2012). MST1 mutations in autosomal recessive primary immunodeficiency characterized by defective naive T-cell survival. *Blood* 119, 3458–3468. doi: 10.1182/blood-2011-09-378364

Nguyen, K., Sylvain, N. R., and Bunnell, S. C. (2008). T cell costimulation via the integrin VLA-4 inhibits the actin-dependent centralization of signaling microclusters containing the adaptor SLP-76. *Immunity* 28, 810–821. doi: 10.1016/j.immuni.2008.04.019

Nolz, J. C., Gomez, T. S., Zhu, P., Li, S., Medeiros, R. B., Shimizu, Y., et al. (2006). The WAVE2 Complex Regulates Actin Cytoskeletal Reorganization and CRAC-Mediated Calcium Entry during T Cell Activation. *Curr. Biol.* 16, 24–34. doi: 10.1016/j.cub.2005.11.036

Nolz, J. C., Medeiros, R. B., Mitchell, J. S., Zhu, P., Freedman, B. D., Shimizu, Y., et al. (2007). WAVE2 regulates high-affinity integrin binding by recruiting vinculin and talin to the immunological synapse. *Mol. Cell Biol.* 27, 5986–6000. doi: 10.1128/MCB.00136-07

Nunoi, H., Yamazaki, T., Tsuchiya, H., Kato, S., Malech, H. L., Matsuda, I., et al. (1999). A heterozygous mutation of β-actin associated with neutrophil dysfunction and recurrent infection. *PNAS* 96, 8693–8698. doi: 10.1073/pnas.96.15.8693

Obino, D., Farina, F., Malbec, O., Sáez, P. J., Maurin, M., Gaillard, J., et al. (2016). Actin nucleation at the centrosome controls lymphocyte polarity. *Nat. Commun.* 7:10969. doi: 10.1038/ncomms10969

Ochs, H. D., and Thrasher, A. J. (2006). The Wiskott-Aldrich syndrome. *J. Allergy Clin. Immunol.* 117, 725–738. doi: 10.1016/j.jaci.2006.02.005

Orange, J. S., Ramesh, N., Remold-O'Donnell, E., Sasahara, Y., Koopman, L., Byrne, M., et al. (2002). Wiskott–Aldrich syndrome protein is required for NK cell cytotoxicity and colocalizes with actin to NK cell-activating immunologic synapses. *Proc. Natl. Acad. Sci. U. S. A.* 99, 11351–11356. doi: 10.1073/pnas.162376099

Pfajfer, L., Mair, N. K., Jiménez-Heredia, R., Genel, F., Gulez, N., Ardeniz, Ö, et al. (2018). Mutations affecting the actin regulator WD repeat-containing protein 1 lead to aberrant lymphoid immunity. *J. Allergy Clin. Immunol.* 142, 1589–1604.e. doi: 10.1016/j.jaci.2018.04.023

Pfajfer, L., Seidel, M. G., Houmadi, R., Rey-Barroso, J., Hirschmugl, T., Salzer, E., et al. (2017). WIP deficiency severely affects human lymphocyte architecture during migration and synapse assembly. *Blood* 130, 1949–1953. doi: 10.1182/blood-2017-04-777383

Piotrowski, J. T., Gomez, T. S., Schoon, R. A., Mangalam, A. K., and Billadeau, D. D. (2013). WASH Knockout T Cells Demonstrate Defective Receptor Trafficking Proliferation, and Effector Function. *Mol. Cell. Biol.* 33, 958–973. doi: 10.1128/MCB.01288-12

Pollard, T. D. (2016). Actin and Actin-Binding Proteins. *Cold Spring Harb. Perspect. Biol.* 8:a018226. doi: 10.1101/cshperspect.a018226

Quann, E. J., Merino, E., Furuta, T., and Huse, M. (2009). Localized diacylglycerol drives the polarization of the microtubule-organizing center in T cells. *Nat. Immunol.* 10, 627–635. doi: 10.1038/ni.1734

Quintana, A., Schwindling, C., Wenning, A. S., Becherer, U., Rettig, J., Schwarz, E. C., et al. (2007). T cell activation requires mitochondrial translocation to the immunological synapse. *PNAS* 104, 14418–14423. doi: 10.1073/pnas.0703126104

Rak, G. D., Mace, E. M., Banerjee, P. P., Svitkina, T., and Orange, J. S. (2011). Natural Killer Cell Lytic Granule Secretion Occurs through a Pervasive Actin Network at the Immune Synapse. *PLoS Biol.* 9:e1001151. doi: 10.1371/journal.pbio.1001151

Ramesh, N., Antón, I. M., Hartwig, J. H., and Geha, R. S. (1997). WIP, a protein associated with wiskott-aldrich syndrome protein, induces actin polymerization and redistribution in lymphoid cells. *Proc. Natl. Acad. Sci. U. S. A.* 94, 14671–14676. doi: 10.1073/pnas.94.26.14671

Randall, K. L., Chan, S. S.-Y., Ma, C. S., Fung, I., Mei, Y., Yabas, M., et al. (2011). DOCK8 deficiency impairs CD8 T cell survival and function in humans and mice. *J. Exp. Med.* 208, 2305–2320. doi: 10.1084/jem.20110345

Randzavola, L. O., Strege, K., Juzans, M., Asano, Y., Stinchcombe, J. C., Gawden-Bone, C. M., et al. (2019). Loss of ARPC1B impairs cytotoxic T lymphocyte maintenance and cytolytic activity. *J. Clin. Invest.* 129, 5600–5614. doi: 10.1172/JCI129388

Record, J., Malinova, D., Zenner, H. L., Plagnol, V., Nowak, K., Syed, F., et al. (2015). Immunodeficiency and severe susceptibility to bacterial infection associated with a loss-of-function homozygous mutation of MKL1. *Blood* 126, 1527–1535. doi: 10.1182/blood-2014-12-611012

Ritter, A. T., Asano, Y., Stinchcombe, J. C., Dieckmann, N. M. G., Chen, B.-C., Gawden-Bone, C., et al. (2015). Actin depletion initiates events leading to granule secretion at the immunological synapse. *Immunity* 42, 864–876. doi: 10.1016/j.immuni.2015.04.013

Ritter, A. T., Kapnick, S. M., Murugesan, S., Schwartzberg, P. L., Griffiths, G. M., and Lippincott-Schwartz, J. (2017). Cortical actin recovery at the immunological synapse leads to termination of lytic granule secretion in cytotoxic T lymphocytes. *Proc. Natl. Acad. Sci. U. S. A.* 114, E6585–E6594. doi: 10.1073/pnas.1710751114

Roncagalli, R., Cucchetti, M., Jarmuzynski, N., Grégoire, C., Bergot, E., Audebert, S., et al. (2016). The scaffolding function of the RLTPR protein explains its essential role for CD28 co-stimulation in mouse and human T cells. *J. Exp. Med.* 213, 2437–2457. doi: 10.1084/jem.20160579

Roumier, A., Olivo-Marin, J. C., Arpin, M., Michel, F., Martin, M., Mangeat, P., et al. (2001). The membrane-microfilament linker ezrin is involved in the formation of the immunological synapse and in T cell activation. *Immunity* 15, 715–728. doi: 10.1016/s1074-7613(01)00225-4

Roy, N. H., and Burkhardt, J. K. (2018). The Actin Cytoskeleton: A Mechanical Intermediate for Signal Integration at the Immunological Synapse. *Front. Cell Dev. Biol.* 6:116. doi: 10.3389/fcell.2018.00116

Roybal, K. T., Buck, T. E., Ruan, X., Cho, B. H., Clark, D. J., Ambler, R., et al. (2016). Computational spatiotemporal analysis identifies WAVE2 and Cofilin as joint regulators of costimulation-mediated T cell actin dynamics. *Sci. Signal.* 9:rs3. doi: 10.1126/scisignal.aad4149

Sage, P. T., Varghese, L. M., Martinelli, R., Sciuto, T. E., Kamei, M., Dvorak, A. M., et al. (2012). Antigen recognition is facilitated by invadosome-like protrusions formed by memory/effector T cells. *J. Immunol.* 188, 3686–3699. doi: 10.4049/jimmunol.1102594

Sakata, D., Taniguchi, H., Yasuda, S., Adachi-Morishima, A., Hamazaki, Y., Nakayama, R., et al. (2007). Impaired T lymphocyte trafficking in mice deficient in an actin-nucleating protein, mDia1. *J. Exp. Med.* 204, 2031–2038. doi: 10.1084/jem.20062647

Salzer, E., Cagdas, D., Hons, M., Mace, E. M., Garncarz, W., Petronczki, ÖY., et al. (2016). RASGRP1 deficiency causes immunodeficiency with impaired cytoskeletal dynamics. *Nat. Immunol.* 17, 1352–1360. doi: 10.1038/ni.3575

Salzer, E., Zoghi, S., Kiss, M. G., Kage, F., Rashkova, C., Stahnke, S., et al. (2020). The cytoskeletal regulator HEM1 governs B cell development and prevents autoimmunity. *Sci. Immunol.* 5:eabc3979. doi: 10.1126/sciimmunol.abc3979

Sanui, T., Inayoshi, A., Noda, M., Iwata, E., Stein, J. V., Sasazuki, T., et al. (2003). DOCK2 regulates Rac activation and cytoskeletal reorganization through interaction with ELMO1. *Blood* 102, 2948–2950. doi: 10.1182/blood-2003-01-0173

Sasahara, Y., Rachid, R., Byrne, M. J., de la Fuente, M. A., Abraham, R. T., Ramesh, N., et al. (2002). Mechanism of recruitment of WASP to the immunological synapse and of its activation following TCR ligation. *Mol. Cell.* 10, 1269–1281. doi: 10.1016/s1097-2765(02)00728-1

Schober, T., Magg, T., Laschinger, M., Rohlfs, M., Linhares, N. D., Puchalka, J., et al. (2017). A human immunodeficiency syndrome caused by mutations in CARMIL2. *Nat. Commun.* 8:14209. doi: 10.1038/ncomms14209

Schönichen, A., and Geyer, M. (2010). Fifteen formins for an actin filament: a molecular view on the regulation of human formins. *Biochim. Biophys. Acta* 1803, 152–163. doi: 10.1016/j.bbamcr.2010.01.014

Seri, M., Pecci, A., Di Bari, F., Cusano, R., Savino, M., Panza, E., et al. (2003). MYH9-related disease: May-Hegglin anomaly Sebastian syndrome, Fechtner syndrome, and Epstein syndrome are not distinct entities but represent a variable expression of a single illness. *Medicine* 82, 203–215. doi: 10.1097/01.md.0000076006.64510.5c

Serwas, N. K., Hoeger, B., Ardy, R. C., Stulz, S. V., Sui, Z., Memaran, N., et al. (2019). Human DEF6 deficiency underlies an immunodeficiency syndrome with systemic autoimmunity and aberrant CTLA-4 homeostasis. *Nat. Commun.* 10:3106. doi: 10.1038/s41467-019-10812-x

Shaffer, M. H., Dupree, R. S., Zhu, P., Saotome, I., Schmidt, R. F., McClatchey, A. I., et al. (2009). Ezrin and moesin function together to promote T cell activation. *J. Immunol.* 182, 1021–1032. doi: 10.4049/jimmunol.182.2.1021

Shiow, L. R., Roadcap, D. W., Paris, K., Watson, S. R., Grigorova, I. L., Lebet, T., et al. (2008). The actin regulator coronin 1A is mutant in a thymic egress-deficient mouse strain and in a patient with severe combined immunodeficiency. *Nat. Immunol.* 9, 1307–1315. doi: 10.1038/ni.1662

Sims, T. N., Soos, T. J., Xenias, H. S., Dubin-Thaler, B., Hofman, J. M., Waite, J. C., et al. (2007). Opposing effects of PKCtheta and WASp on symmetry breaking and relocation of the immunological synapse. *Cell* 129, 773–785. doi: 10.1016/j.cell.2007.03.037

Somech, R., Lev, A., Lee, Y. N., Simon, A. J., Barel, O., Schiby, G., et al. (2017). Disruption of Thrombocyte and T Lymphocyte Development by a Mutation in ARPC1B. *J. Immunol.* 199, 4036–4045. doi: 10.4049/jimmunol.1700460

Somersalo, K., Anikeeva, N., Sims, T. N., Thomas, V. K., Strong, R. K., Spies, T., et al. (2004). Cytotoxic T lymphocytes form an antigen-independent ring junction. *J. Clin. Invest.* 113, 49–57. doi: 10.1172/JCI19337

Sorte, H. S., Osnes, L. T., Fevang, B., Aukrust, P., Erichsen, H. C., Backe, P. H., et al. (2016). A potential founder variant in CARMIL2/RLTPR in three Norwegian families with warts, molluscum contagiosum, and T-cell dysfunction. *Mol. Genet. Genomic Med.* 4, 604–616. doi: 10.1002/mgg3.237

Standing, A. S. I., Malinova, D., Hong, Y., Record, J., Moulding, D., Blundell, M. P., et al. (2017). Autoinflammatory periodic fever, immunodeficiency, and thrombocytopenia (PFIT) caused by mutation in actin-regulatory gene WDR1. *J. Exp. Med.* 214, 59–71. doi: 10.1084/jem.20161228

Stinchcombe, J. C., Majorovits, E., Bossi, G., Fuller, S., and Griffiths, G. M. (2006). Centrosome polarization delivers secretory granules to the immunological synapse. *Nature* 443, 462–465. doi: 10.1038/nature05071

Stritt, S., Nurden, P., Turro, E., Greene, D., Jansen, S. B., Westbury, S. K., et al. (2016). A gain-of-function variant in DIAPH1 causes dominant macrothrombocytopenia and hearing loss. *Blood* 127, 2903–2914. doi: 10.1182/blood-2015-10-675629

Symons, M., Derry, J. M. J., Karlak, B., Jiang, S., Lemahieu, V., McCormick, F., et al. (1996). Wiskott–Aldrich Syndrome Protein, a Novel Effector for the

GTPase CDC42Hs Is Implicated in Actin Polymerization. *Cell* 84, 723–734. doi: 10.1016/S0092-8674(00)81050-8

Szczawinska-Poplonyk, A., Ploski, R., Bernatowska, E., and Pac, M. (2020). A Novel CDC42 Mutation in an 11-Year Old Child Manifesting as Syndromic Immunodeficiency, Autoinflammation, Hemophagocytic Lymphohistiocytosis, and Malignancy: A Case Report. *Front. Immunol.* 11:318. doi: 10.3389/fimmu.2020.00318

Tabdanov, E., Gondarenko, S., Kumari, S., Liapis, A., Dustin, M. L., Sheetz, M. P., et al. (2015). Micropatterning of TCR and LFA-1 ligands reveals complementary effects on cytoskeleton mechanics in T-cells. *Integr. Biol.* 7, 1272–1284. doi: 10.1039/c5ib00032g

Takenouchi, T., Kosaki, R., Niizuma, T., Hata, K., and Kosaki, K. (2015). Macrothrombocytopenia and developmental delay with a de novo CDC42 mutation: Yet another locus for thrombocytopenia and developmental delay. *Am. J. Med. Genet. A* 167A, 2822–2825. doi: 10.1002/ajmg.a.37275

Tamzalit, F., Tran, D., Jin, W., Boyko, V., Bazzi, H., Kepecs, A., et al. (2020). Centrioles control the capacity, but not the specificity, of cytotoxic T cell killing. *Proc. Natl. Acad. Sci. U. S. A.* 117, 4310–4319. doi: 10.1073/pnas.1913220117

Tamzalit, F., Wang, M. S., Jin, W., Tello-Lafoz, M., Boyko, V., Heddleston, J. M., et al. (2019). Interfacial actin protrusions mechanically enhance killing by cytotoxic T cells. *Sci. Immunol.* 4:aav5445. doi: 10.1126/sciimmunol.aav5445

Tangye, S. G., Bucciol, G., Casas-Martin, J., Pillay, B., Ma, C. S., Moens, L., et al. (2019). Human inborn errors of the actin cytoskeleton affecting immunity: way beyond WAS and WIP. *Immunol. Cell Biol.* 97, 389–402. doi: 10.1111/imcb.12243

Taylor, M. D., Sadhukhan, S., Kottangada, P., Ramgopal, A., Sarkar, K., D'Silva, S., et al. (2010). Nuclear Role of WASp in the Pathogenesis of Dysregulated TH1 Immunity in Human Wiskott-Aldrich Syndrome. *Sci. Transl. Med.* 2, ra44–ra37. doi: 10.1126/scitranslmed.3000813

Thompson, S. B., Sandor, A. M., Lui, V., Chung, J. W., Waldman, M. M., Long, R. A., et al. (2020). Formin-like 1 mediates effector T cell trafficking to inflammatory sites to enable T cell-mediated autoimmunity. *eLife*. 9:e58046. doi: 10.7554/eLife.58046

Thumkeo, D., Katsura, Y., Nishimura, Y., Kanchanawong, P., Tohyama, K., Ishizaki, T., et al. (2020). mDia1/3-dependent actin polymerization spatiotemporally controls LAT phosphorylation by Zap70 at the immune synapse. *Sci. Adv.* 6:eaay2432. doi: 10.1126/sciadv.aay2432

Tomiyama, T., Ueda, Y., Katakai, T., Kondo, N., Okazaki, K., and Kinashi, T. (2013). Antigen-specific suppression and immunological synapse formation by regulatory T cells require the Mst1 kinase. *PLoS One* 8:e73874. doi: 10.1371/journal.pone.0073874

Trifari, S., Scaramuzza, S., Catucci, M., Ponzoni, M., Mollica, L., Chiesa, R., et al. (2010). Revertant T lymphocytes in a patient with Wiskott-Aldrich syndrome: analysis of function and distribution in lymphoid organs. *J. Allergy Clin. Immunol.* 125, 439.e–448.e. doi: 10.1016/j.jaci.2009.11.034

Trifari, S., Sitia, G., Aiuti, A., Scaramuzza, S., Marangoni, F., Guidotti, L. G., et al. (2006). Defective Th1 Cytokine Gene Transcription in CD4+ and CD8+ T Cells from Wiskott-Aldrich Syndrome Patients. *J. Immunol.* 177, 7451–7461. doi: 10.4049/jimmunol.177.10.7451

Tskvitaria-Fuller, I., Rozelle, A. L., Yin, H. L., and Wülfing, C. (2003). Regulation of Sustained Actin Dynamics by the TCR and Costimulation as a Mechanism of Receptor Localization. *J. Immunol.* 171, 2287–2295. doi: 10.4049/jimmunol.171.5.2287

Valitutti, S., Müller, S., Cella, M., Padovan, E., and Lanzavecchia, A. (1995). Serial triggering of many T-cell receptors by a few peptide–MHC complexes. *Nature* 375, 148–151. doi: 10.1038/375148a0

Varma, R., Campi, G., Yokosuka, T., Saito, T., and Dustin, M. L. (2006). T cell receptor-proximal signals are sustained in peripheral microclusters and terminated in the central supramolecular activation cluster. *Immunity* 25, 117–127. doi: 10.1016/j.immuni.2006.04.010

Vicente-Manzanares, M., Rey, M., Pérez-Martínez, M., Yáñez-Mó, M., Sancho, D., Cabrero, J. R., et al. (2003). The RhoA Effector mDia Is Induced During T Cell Activation and Regulates Actin Polymerization and Cell Migration in T Lymphocytes. *J. Immunol.* 171, 1023–1034. doi: 10.4049/jimmunol.171.2.1023

Viola, A., Contento, R. L., and Molon, B. (2006). T cells and their partners: The chemokine dating agency. *Trends Immunol.* 27, 421–427. doi: 10.1016/j.it.2006.07.004

Volpi, S., Cicalese, M. P., Tuijnenburg, P., Tool, A. T. J., Cuadrado, E., Abu-Halaweh, M., et al. (2019). A combined immunodeficiency with severe infections, inflammation, and allergy caused by ARPC1B deficiency. *J. Allergy Clin. Immunol.* 143, 2296–2299. doi: 10.1016/j.jaci.2019.02.003

Wada, T., Schurman, S. H., Otsu, M., Garabedian, E. K., Ochs, H. D., Nelson, D. L., et al. (2001). Somatic mosaicism in Wiskott–Aldrich syndrome suggests in vivo reversion by a DNA slippage mechanism. *PNAS* 98, 8697–8702. doi: 10.1073/pnas.151260498

Wang, N., Tytell, J. D., and Ingber, D. E. (2009). Mechanotransduction at a distance: mechanically coupling the extracellular matrix with the nucleus. *Nat. Rev. Mol. Cell. Biol.* 10, 75–82. doi: 10.1038/nrm2594

Wang, Y., Ma, C. S., Ling, Y., Bousfiha, A., Camcioglu, Y., Jacquot, S., et al. (2016). Dual T cell- and B cell-intrinsic deficiency in humans with biallelic RLTPR mutations. *J. Exp. Med.* 213, 2413–2435. doi: 10.1084/jem.20160576

Willmann, K. L., Klaver, S., Doğu, F., Santos-Valente, E., Garncarz, W., Bilic, I., et al. (2014). Biallelic loss-of-function mutation in NIK causes a primary immunodeficiency with multifaceted aberrant lymphoid immunity. *Nat. Commun.* 5:5360. doi: 10.1038/ncomms6360

Winter, S., Martin, E., Boutboul, D., Lenoir, C., Boudjemaa, S., Petit, A., et al. (2018). Loss of RASGRP1 in humans impairs T-cell expansion leading to Epstein-Barr virus susceptibility. *EMBO Mol. Med.* 10, 188–199. doi: 10.15252/emmm.201708292

Wise, C. A., Gillum, J. D., Seidman, C. E., Lindor, N. M., Veile, R., Bashiardes, S., et al. (2002). Mutations in CD2BP1 disrupt binding to PTP PEST and are responsible for PAPA syndrome, an autoinflammatory disorder. *Hum. Mol. Genet.* 11, 961–969. doi: 10.1093/hmg/11.8.961

Wülfing, C., and Davis, M. M. (1998). A receptor/cytoskeletal movement triggered by costimulation during T cell activation. *Science* 282, 2266–2269. doi: 10.1126/science.282.5397.2266

Yang, C., and Svitkina, T. M. (2019). Ultrastructure and dynamics of the actin-myosin II cytoskeleton during mitochondrial fission. *Nat. Cell. Biol.* 21, 603–613. doi: 10.1038/s41556-019-0313-6

Yi, J., Wu, X. S., Crites, T., and Hammer, J. A. (2012). Actin retrograde flow and actomyosin II arc contraction drive receptor cluster dynamics at the immunological synapse in Jurkat T cells. *Mol. Biol. Cell.* 23, 834–852. doi: 10.1091/mbc.E11-08-0731

Zhang, Q., Davis, J. C., Lamborn, I. T., Freeman, A. F., Jing, H., Favreau, A. J., et al. (2009). Combined Immunodeficiency Associated with DOCK8 Mutations. *N. Engl. J. Med.* 361, 2046–2055. doi: 10.1056/NEJMoa0905506

Zhang, X., Dai, R., Li, W., Zhao, H., Zhang, Y., Zhou, L., et al. (2016). Abnormalities of follicular helper T-cell number and function in Wiskott-Aldrich syndrome. *Blood* 127, 3180–3191. doi: 10.1182/blood-2015-06-652636

Conflict of Interest: The authors declare that the research was conducted in the absence of any commercial or financial relationships that could be construed as a potential conflict of interest.

frontiers in Cell and Developmental Biology

ORIGINAL RESEARCH
published: 09 July 2021
doi: 10.3389/fcell.2021.647063

The Actin-Disassembly Protein Glia Maturation Factor γ Enhances Actin Remodeling and B Cell Antigen Receptor Signaling at the Immune Synapse

Nikola Deretic[†§], Madison Bolger-Munro[†‡§], Kate Choi[†], Libin Abraham[†] and Michael R. Gold[*†]*

Department of Microbiology and Immunology, Life Sciences Institute, University of British Columbia, Vancouver, BC, Canada

Signaling by the B cell antigen receptor (BCR) initiates actin remodeling. The assembly of branched actin networks that are nucleated by the Arp2/3 complex exert outward force on the plasma membrane, allowing B cells to form membrane protrusions that can scan the surface of antigen-presenting cells (APCs). The resulting Arp2/3 complex-dependent actin retrograde flow promotes the centripetal movement and progressive coalescence of BCR microclusters, which amplifies BCR signaling. Glia maturation factor γ (GMFγ) is an actin disassembly-protein that releases Arp2/3 complex-nucleated actin filaments from actin networks. By doing so, GMFγ could either oppose the actions of the Arp2/3 complex or support Arp2/3 complex-nucleated actin polymerization by contributing to the recycling of actin monomers and Arp2/3 complexes. We now show that reducing the levels of GMFγ in human B cell lines via transfection with a specific siRNA impairs the ability of B cells to spread on antigen-coated surfaces, decreases the velocity of actin retrograde flow, diminishes the coalescence of BCR microclusters into a central cluster at the B cell-APC contact site, and decreases APC-induced BCR signaling. These effects of depleting GMFγ are similar to what occurs when the Arp2/3 complex is inhibited. This suggests that GMFγ cooperates with the Arp2/3 complex to support BCR-induced actin remodeling and amplify BCR signaling at the immune synapse.

Keywords: B cell, actin, B cell receptor, immune synapse, signal transduction, cell spreading, glia maturation factor-γ

OPEN ACCESS

Edited by:
Sudha Kumari,
Massachusetts Institute of Technology, United States

Reviewed by:
Jonathan Michael Lee,
University of Ottawa, Canada
Katherine Pfister,
University of Pittsburgh, United States

****Correspondence:***
Madison Bolger-Munro
madison.bolger-munro@ist.ac.at
Michael R. Gold
mgold@mail.ubc.ca

†ORCID:
Nikola Deretic
orcid.org/0000-0002-3313-2814
Madison Bolger-Munro
orcid.org/0000-0002-8176-4824
Kate Choi
orcid.org/0000-0002-7959-1944
Libin Abraham
orcid.org/0000-0002-4725-3502
Michael R. Gold
orcid.org/0000-0003-1222-3191

‡Present address:
Madison Bolger-Munro,
Institute of Science and Technology of Austria, Klosterneuburg, Austria

§These authors have contributed equally to this work

Specialty section:
This article was submitted to Cell Growth and Division, a section of the journal Frontiers in Cell and Developmental Biology

Received: *29 December 2020*
Accepted: *07 June 2021*
Published: *09 July 2021*

Citation:
Deretic N, Bolger-Munro M, Choi K, Abraham L and Gold MR (2021) The Actin-Disassembly Protein Glia Maturation Factor γ Enhances Actin Remodeling and B Cell Antigen Receptor Signaling at the Immune Synapse. Front. Cell Dev. Biol. 9:647063. doi: 10.3389/fcell.2021.647063

INTRODUCTION

Activated B cells contribute to health and disease by producing antibodies, secreting pro- and anti-inflammatory cytokines, and presenting antigens (Ags) to T cells (Conley et al., 2009; Shen and Fillatreau, 2015; Cashman et al., 2019; Cyster and Allen, 2019; Meffre and O'Connor, 2019). B cell activation is initiated by the binding of Ags to the B cell Ag receptor (BCR), which

Abbreviations: Ag, antigen; APC, antigen-presenting cell; Arp, actin-related protein; BCR, B cell antigen receptor; BSA, bovine serum albumin; cSMAC, central supramolecular activation cluster; F-actin, filamentous actin; FCS, fetal calf serum; GMF, glia maturation factor; HEL, hen egg lysozyme; Ig, immunoglobulin; ITAM, immunoreceptor tyrosine-based activation motif; mHBS, modified HEPES-buffered saline; pCD79, phosphorylated CD79; PFA, paraformaldehyde; TIRF, total internal reflection fluorescence; WASp, Wiskott-Aldrich Syndrome protein.

triggers signaling pathways that regulate gene expression, cell metabolism, cell cycle progression, and cytoskeletal organization (Packard and Cambier, 2013; Li et al., 2018; Jellusova, 2020). BCR signaling induces reorganization of the actin cytoskeleton, which can be readily visualized *in vitro* when B cells are plated on a rigid substrate coated with Ags or with antibodies against the membrane immunoglobulin (Ig) subunit of the BCR. Under these conditions, B cells spread in a radial manner, forming a peripheral ring of branched filamentous actin (F-actin) that generates broad, outwardly moving lamellipodial protrusions (Freeman et al., 2011). At the same time, the central region of the Ag contact site is depleted of F-actin via the action of actin-disassembly proteins such as cofilin (Freeman et al., 2011). Many actin-regulatory proteins are targets of BCR signaling (Tolar, 2017) and mutations in actin regulators such as Wiskott-Aldrich Syndrome protein (WASp), Arpc1B, Hem1/NCKAP1L, and Wdr1 result in autoimmune or immunodeficiency syndromes that have been termed actinopathies (Kile et al., 2007; Kahr et al., 2017; Kuijpers et al., 2017; Brigida et al., 2018; Candotti, 2018; Pfajfer et al., 2018; Randzavola et al., 2019; Volpi et al., 2019; Cook et al., 2020; Sprenkeler et al., 2020). Hence, identifying proteins that link the BCR to actin remodeling can provide new insights into B cell activation and dysfunction.

Although B cells can be activated by soluble Ags, they are activated most efficiently by Ags that are displayed on the surface of Ag-presenting cells (APCs) (Batista and Harwood, 2009; Cyster, 2010; Heesters et al., 2016). Follicular dendritic cells, dendritic cells, and subcapsular sinus macrophages can capture Ags and concentrate them on their surface in an intact form that can be recognized by B cells (Heesters et al., 2016). When B cells bind Ags that are mobile within a membrane, BCR signaling stimulates rapid remodeling of the actin cytoskeleton, as well as actin-dependent spatial reorganization of BCRs and other membrane proteins, leading to formation of an immune synapse (Harwood and Batista, 2011; Song et al., 2014).

The actin remodeling that drives immune synapse formation enhances the ability of membrane-bound Ags to stimulate BCR signaling and B cell activation (Depoil et al., 2008; Bolger-Munro et al., 2019). Initial BCR signaling initiates transient, localized disassembly of the submembrane actin mesh (Freeman et al., 2011). This removes actin-based diffusion barriers and the resulting increase in BCR mobility within the plasma membrane enables them to form BCR microclusters (Treanor et al., 2010, 2011; Freeman et al., 2011). BCR clustering leads to phosphorylation of the immunoreceptor tyrosine-based activation motifs (ITAMs) within the CD79a/b (Igα/Igβ) subunit of the BCR (Dal Porto et al., 2004; Abraham et al., 2016). Subsequent recruitment of the Syk tyrosine kinase and other signaling proteins to the BCR leads to the formation of microcluster-based signaling complexes termed microsignalosomes (Weber et al., 2008; Treanor et al., 2009). Concomitantly, actin polymerization at the cell periphery allows B cells to extend membrane protrusions across the surface of the APC in order to encounter more Ag and form additional BCR microclusters (Fleire et al., 2006; Bolger-Munro et al., 2019). The B cell then retracts these membrane protrusions, promoting the centripetal movement and coalescence of BCR microclusters (Fleire et al., 2006; Bolger-Munro et al., 2019). BCR-Ag microclusters ultimately coalesce into a central supramolecular activation complex (cSMAC), a distinguishing feature of an immune synapse. cSMAC formation may facilitate the internalization of BCR-Ag complexes, which allows B cells to present Ags to T cells and elicit critical second signals for activation (Yuseff et al., 2013; Nowosad et al., 2016).

There are two major modes of actin network assembly (Kadzik et al., 2020). Formin proteins mediate linear actin polymerization, which generates thin membrane protrusions such as filopodia. In contrast, the assembly of branched actin networks, which is initiated by the actin-related protein (Arp) 2/3 complex, drives the formation of broad lamellipodial protrusions. When activated by WASp or other nucleation-promoting factors, the Arp2/3 complex binds to the side of an actin filament and nucleates the formation of a new actin branch that grows at a 70° angle from the mother filament.

We have shown that the Arp2/3 complex plays a major role in BCR-induced actin remodeling, immune synapse formation, and APC-induced BCR signaling (Bolger-Munro et al., 2019). When the Arp2/3 complex is inhibited or depleted, B cells exhibit impaired spreading on immobilized anti-Ig antibodies. We also showed that Arp2/3 complex-dependent actin retrograde flow, a consequence of membrane-proximal actin polymerization being opposed by the elastic resistance of the plasma membrane, is required for the initial centripetal movement of BCR microclusters and for cSMAC formation. Importantly, this Arp2/3 complex-dependent movement and coalescence of BCR microclusters amplifies BCR signaling and promotes B cell activation. These findings suggest that other proteins that regulate Arp2/3 complex-nucleated actin polymerization are also likely to be important for B cell spreading and APC-induced B cell responses.

The remodeling of actin networks involves the cooperative actions of actin assembly and disassembly factors. In lamellipodia, Arp2/3 complex-dependent actin polymerization depends on actin-disassembly factors such as cofilin, coronins, and glia maturation factor γ (GMFγ) (Goode et al., 2018; Kadzik et al., 2020). These proteins disassemble older segments of actin filaments, releasing actin monomers that can then be loaded with ATP and used for new actin polymerization. This coupling of actin depolymerization and polymerization is referred to as treadmilling (Carlier and Shekhar, 2017).

The role of GMFγ in B cells, and in immune synapse formation, has not been investigated. In *S. pombe*, disrupting *Gmf1*, the gene encoding the homolog of GMFγ, results in reduced actin turnover and defects in actin organization (Ydenberg et al., 2015). GMFγ also regulates actin dynamics in immune cells. GMFγ depletion reduces the migration of neutrophils, T cells, and monocytes toward chemoattractants (Aerbajinai et al., 2011, 2016; Lippert and Wilkins, 2012). In *in vitro* assays, GMFγ can inhibit Arp2/3 complex activity and also debranch actin networks by causing the release of the Arp2/3 complex and daughter filament from the mother filament (Gandhi et al., 2010; Nakano et al., 2010; Ydenberg et al., 2013; Sokolova et al., 2017). These activities could position GMFγ as an inhibitor of processes that depend on Arp2/3 complex-nucleated

actin polymerization. Alternatively, GMFγ-mediated release of Arp2/3 complex-bound filaments from the actin network could sustain Arp2/3 complex-dependent processes by enabling the recycling of both Arp2/3 complexes and actin monomers (Goode et al., 2018). Given its potential role as either a positive or negative regulator of Arp2/3 complex-dependent actin polymerization, we tested the hypothesis that GMFγ regulates BCR-induced actin remodeling, immune synapse formation, and APC-induced BCR signaling.

MATERIALS AND METHODS

B Cell Lines

The Ramos human IgM$^+$ B cell line was obtained from ATCC (#CRL-1596). Raji D1.3 B cells, which express a transgenic hen egg lysozyme (HEL)-specific BCR were a gift from Dr. Bebhinn Treanor (University of Toronto, Toronto, Canada). A population of Raji D1.3 B cells with high expression of the D1.3 IgM-BCR was obtained by FACS sorting the cells after staining with rat anti-mouse IgM-FITC (Invitrogen, #11-5790-81, 1:200 dilution). Cells were cultured in RPMI-1640 supplemented with 10% heat-inactivated fetal calf serum (FCS), 1 mM sodium pyruvate, 2 mM glutamine, and 50 μM β-mercaptoethanol. All cells were confirmed to be mycoplasma-negative.

siRNA-Mediated Depletion of GMFγ

Using the Ingenio electroporation kit (Mirus, #MIR50118) and an Amaxa Nucleofector (program O-006 for Ramos B cells; program M-013 for Raji D1.3 B cells), 3×10^6 cells were transiently transfected with 2 μg of either control non-targeting siRNA (Silencer Select Negative Control #2, Ambion, #4390846) or siRNA directed against human GMFγ (GMFG Silencer Select Pre-designed siRNA, Ambion, #4392420). Where indicated, the cells were co-transfected with 1 μg of the pmaxGFP plasmid (Lonza, #D-00069). Transfected cells were cultured for 48–72 h before being used in experiments. The levels of GMFγ and actin (loading control) in siRNA-transfected cells were analyzed by immunoblotting with a rabbit antibody against human GMFγ (Proteintech, #13625-1-AP, 1:500; overnight at 4°C) or a monoclonal β-actin antibody (Santa Cruz, #sc-47778, 1:5000; 1 h at room temperature), followed by horseradish peroxidase-conjugated goat anti-rabbit IgG (Bio-Rad, #170-6515; 1:3,000) or goat anti-mouse IgG (Bio-Rad, #170-6516; 1:3,000). Bands were detected by ECL (Azure Biosystems, #AC2101), then imaged and quantified using a Li-Cor C-DiGit imaging system.

Analysis of Cell Surface BCR Levels and Cell Size by Flow Cytometry

To assess cell surface BCR levels, 10^6 B cells were resuspended in 50 μL ice-cold FACS buffer (PBS with 2% FCS), and then stained on ice for 30 min with Alexa Fluor 647-conjugated goat anti-human IgM Fab fragments (Jackson ImmunoResearch, #109-607-043, 1:200) or with rat anti-mouse IgM FITC (Invitrogen, #11-5790-81, 1:200) to detect the D1.3 BCR. Flow cytometry was performed using an LSRII-561 cytometer (Becton Dickinson Biosciences). Data were analyzed using FlowJo software (Treestar Inc.) using forward and side scatter to gate on single intact cells. Forward scatter was used as a relative measure of cell size.

Analysis of B Cell Spreading, GMFγ Localization, and Actin Dynamics

Glass coverslips (12-mm diameter, Thermo Fisher Scientific, #12-545-80) were coated with either 2.5 μg/cm^2 donkey anti-human IgM (Jackson ImmunoResearch, #709-005-073) or 0.22 μg/cm^2 HEL (NANOCS, #LSN-BN-1) for 30 min at room temperature and then blocked with 2% bovine serum albumin (BSA) in PBS for 30 min at room temperature. After being resuspended in modified HEPES-buffered saline (mHBS; 25 mM HEPES, pH 7.2, 125 mM NaCl, 5 mM KCl, 1 mM $CaCl_2$, 1 mM Na_2HPO_4, 1 mg/mL glucose, 1 mM sodium pyruvate, 2 mM glutamine, 50 μM β-mercaptoethanol) with 2% FCS, 5×10^4 B cells were added to the coverslips. After 3–30 min at 37°C, the cells were fixed with 4% paraformaldehyde (PFA) for 10 min at room temperature and then permeabilized with 0.1% Triton X-100 in PBS for 3 min. F-actin was visualized by staining with rhodamine-phalloidin (Thermo Fisher, #R415, 1:400 in PBS + 2% BSA) for 30 min at room temperature. Where indicated, the fixed cells were blocked with PBS + 2% BSA for 30 min, stained for 1 h at room temperature with rabbit anti-human GMFγ (Proteintech, #13625-1-AP, 1:200 in PBS + 2% BSA), washed, and then incubated for 30 min at room temperature with Alexa Fluor-647-conjugated goat anti-rabbit IgG (Thermo Fisher Scientific, #A21244, 1:400 in PBS + 2% BSA) plus rhodamine-phalloidin. Coverslips were mounted onto slides using ProLong Diamond anti-fade reagent (Thermo Fisher Scientific, #P36965). Images of the B cell-coverslip interface were captured using a spinning disk confocal microscope (Intelligent Imaging Innovations) consisting of an inverted Zeiss Axiovert 200M microscope with a 100× 1.45 NA oil Plan-Fluor objective lens and a QuantEM 512SC Photometrics camera. Cell area was quantified using Fiji software (Schindelin et al., 2012). Radial fluorescence intensity profiles were generated with a custom macro that utilizes Fiji software together with the Radial Profile Extended plug-in[1]. This plug-in is based on an algorithm originally developed by Baggethun[2], which yields a plot of the normalized integrated intensities around concentric circles, as a function of the distance from a center point. The integrated intensity is the sum of the fluorescence intensity values for the pixels around a circle of radius x, divided by the number of these pixels that are part of the image (i.e., not outside the cell). This value is then normalized to the maximal integrated intensity for any circle from that cell. The radial coordinates for each cell are expressed as normalized distances from the center.

For live-cell imaging at 37°C, Raji D1.3 B cells were transfected with a plasmid encoding F-tractin-GFP (Johnson and Schell, 2009), along with either control siRNA or GMFγ siRNA, and then cultured for 72 h. Cells (2×10^5 in 100 μL mHBS + 2% FCS) were added to coverslips that had been coated with

[1]http://questpharma.u-strasbg.fr/html/radial-profile-ext.html

[2]Baggethun P. 2009. Image analysis: radial profile plot https://www.researchgate.net/publication/317704672_Image_analysis_Radial_profile_plot

2.5 μg/cm^2 donkey anti-human IgM and allowed to spread for 5 min. The cell-coverslip contact site was then imaged by total internal reflection fluorescence (TIRF) microscopy. Images of GFP-expressing cells were acquired every 2 s for 15 min using an Olympus IX81 inverted microscope equipped with a 150× NA 1.45 TIRF objective, a high performance electron multiplier charge-coupled device camera (Photometrics Evolve), and real-time data acquisition software (Metamorph). Fiji software was used to generate kymographs.

APC-Induced cSMAC Formation and BCR Signaling

B cell-APC interactions were analyzed as described previously (Wang et al., 2018; Bolger-Munro et al., 2019). COS-7 cells (ATCC, #CRL-1651) were transiently transfected with a plasmid encoding the mHEL-HaloTag Ag. The mHEL-HaloTag protein consists of the complete HEL protein fused to the transmembrane and cytosolic domains of the H-2K^b protein, with the HaloTag protein fused to the C-terminus of the H-2K^b cytosolic domain (Wang et al., 2018). The mHEL-HaloTag-expressing COS-7 cells were cultured for 24 h before adding 2.2 × 10^4 cells to glass coverslips that had been coated with 5 μg/mL fibronectin, and then culturing the cells for an additional 24 h. After washing the COS-7 cells with PBS, the mHEL-HaloTag Ag was labeled with Janelia Fluor 549 HaloTag ligand (Promega, #GA1110, 1:20,000 dilution in 200 μL mHBS + 2% FCS) for 15 min at 37°C. siRNA-transfected Raji D1.3 cells (5 × 10^5 cells in 100 μL mHBS + 2% FCS) were added to the COS-7 APCs for 3–30 min at 37°C. The cells were then fixed with 4% PFA for 10 min, permeabilized with 0.1% Triton X-100 in PBS for 3 min, and blocked with PBS + 2% BSA for 30 min, all at room temperature. The cells were stained for 1 h at room temperature with an antibody that recognizes the phosphorylated CD79 ITAMs (pCD79; Cell Signaling Technologies, #5173, 1:200 in PBS + 2% BSA), washed, and then incubated for 30 min at room temperature with PBS + 2% BSA containing Alexa Fluor-647-conjugated goat anti-rabbit IgG (Thermo Fisher Scientific, #A21244, 1:400) plus Alexa Fluor 488-conjugated phalloidin (Thermo Fisher Scientific, #A12379, 1:400). After mounting the coverslips onto slides, the B cell-APC interface was imaged by spinning disk confocal microscopy. For each B cell, custom Fiji macros[3] were used to quantify the total amount of pCD79 fluorescence and mHEL-HaloTag Ag fluorescence present in clusters at the B cell-APC interface, as well as the Ag fluorescence intensity for each microcluster on an individual B cell (Bolger-Munro et al., 2019, 2021). Briefly, the mean background fluorescence intensity per pixel was calculated and subtracted from all pixel values by using the rolling ball background subtraction ImageJ plug-in with the radius of the rolling ball set to 10 pixels. A binary image was then generated using Otsu thresholding. Cluster segmentation was performed using the "Analyze Particles" function in FIJI with clusters defined as being > 0.05 μm^2. Masks generated in this way were then mapped onto the original image for quantification of pixel intensity. Pixel intensities within the mask were summed to determine the total fluorescence intensity that was present in clusters for each cell. As defined previously, a cell was deemed to have formed a cSMAC when > 90% of the Ag fluorescence had been gathered into one or two clusters at the center of the synapse (Bolger-Munro et al., 2019).

[3]https://github.com/mbolgermunro/FIJImacros/blob/master/APC_analyser_MBM.ijm

BCR Signaling in Response to Soluble Anti-IgM

Raji D1.3 B cells (3 × 10^6 in 100 μL mHBS) were stimulated at 37°C with 20 μg/mL goat anti-mouse IgM (Jackson ImmunoResearch, #115-005-020) to engage the D1.3 BCR. Ramos B cells were stimulated with 20 μg/mL donkey anti-human IgM (Jackson ImmunoResearch, #709-005-073). Reactions were stopped, and cells lysed, by adding 30 μL RIPA buffer (30 mM Tris-HCl, pH 7.4, 150 mM NaCl, 1% Igepal (Sigma-Aldrich), 0.5% sodium deoxycholate, 0.1% SDS, 2 mM EDTA) with 3X protease and phosphatase inhibitors (3 mM phenylmethylsulfonyl fluoride, 30 μg/mL leupeptin, 3 μg/mL aprotinin, 3 μg/mL pepstatin A, 75 mM β-glycerophosphate, 3 mM Na_3MoO_4, 3 mM Na_3VO_4). After 15 min on ice with intermittent mixing, insoluble material was removed by centrifugation. Cell lysates (20 μg protein) were separated by SDS-PAGE and then analyzed by immunoblotting with antibodies that recognize the phosphorylated CD79 ITAMs (pCD79; Cell Signaling Technologies, #5173, 1:000; overnight at 4°C), human GMFγ (Proteintech, #13625-1-AP, 1:500; overnight at 4°C) or β-actin (Santa Cruz, #sc-47778, 1:5,000; 1 h at room temperature), followed by horseradish peroxidase-conjugated goat anti-rabbit IgG (Bio-Rad, #170-6515; 1:3,000) or goat anti-mouse IgG (Bio-Rad, #170-6516; 1:3,000). After ECL detection, blots were quantified and imaged using a Li-Cor C-DiGit imaging system.

Statistical Analysis

Two-tailed paired *t*-tests were used to compare mean values for matched sets of samples. The Mann-Whitney *U*-test was used to compare ranked values in samples with many cells and high variability (e.g., dot plots for immunofluorescence signaling data). Outliers were identified using Robust Regression and Outlier Removal (ROUT) in GraphPad Prism with Q set to 1% (Motulsky and Brown, 2006).

RESULTS

Depleting GMFγ Reduces B Cell Spreading on Immobilized Anti-IgM or Ag

To assess the role of GMFγ in B cells, we transfected the Ramos and Raji D1.3 human B cell lines with either GMFγ-specific siRNA or a control non-targeting siRNA. Representative GMFγ immunoblots are shown in **Figures 1A,B**. Quantification of immunoblots from 17 independent experiments showed that transfection with GMFγ siRNA reduced the level of GMFγ protein to 25–50% of that in control siRNA-transfected cells. This partial depletion of GMFγ could result in underestimating the contributions of GMFγ to B cell responses. Partial

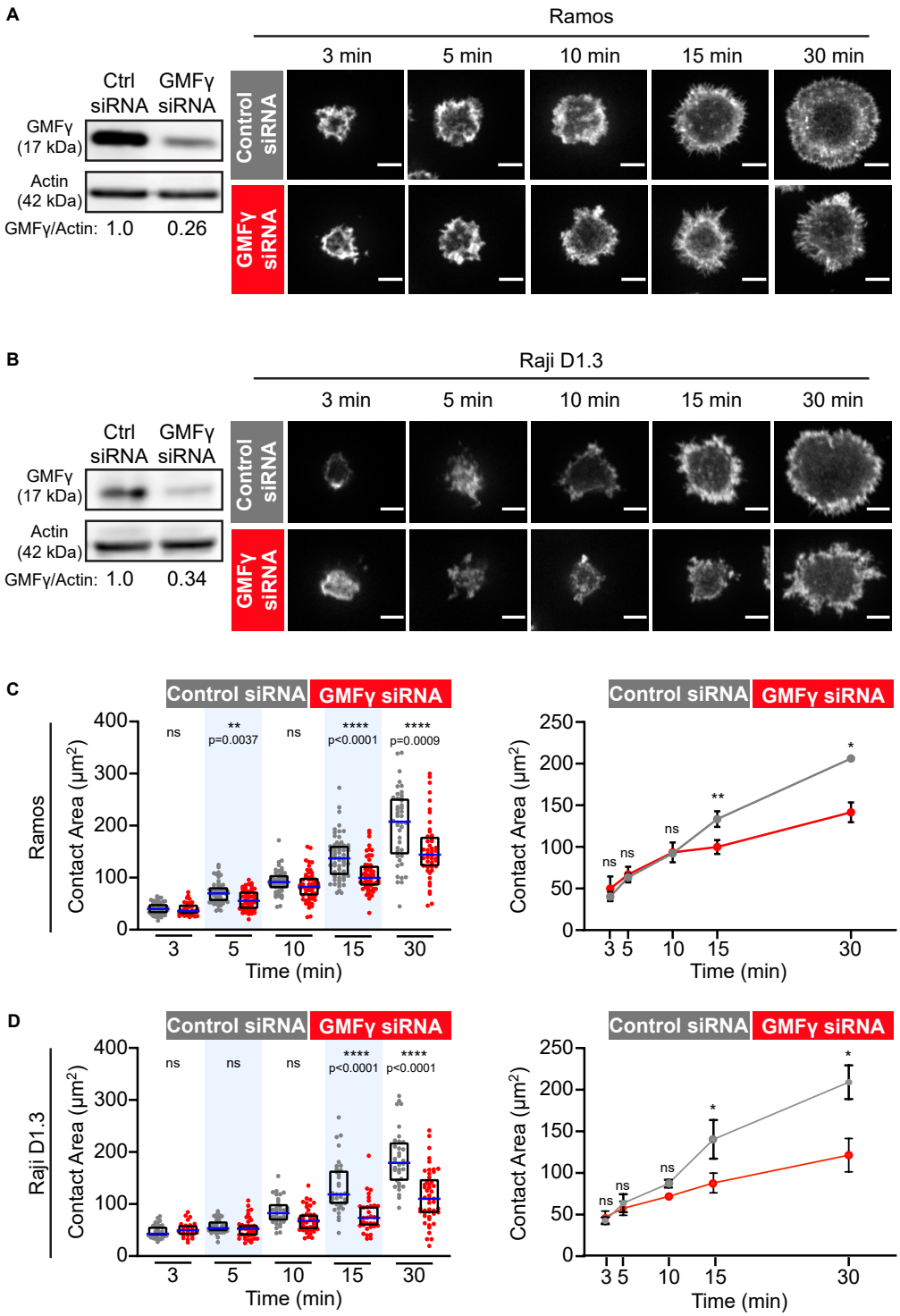

FIGURE 1 | Depleting GMFγ reduces B cell spreading on immobilized anti-Ig. **(A,B)** Ramos B cells **(A)** or Raji D1.3 B cells **(B)** were transfected with control non-targeting siRNA or GMFγ siRNA. Immunoblots (left panels) show GMFγ levels in cell extracts, with actin as a loading control. The transfected B cells were added to anti-IgM-coated-coverslips and allowed to spread for the indicated times before being stained with rhodamine-phalloidin. Representative confocal microscopy images are shown (right panels). Scale bars: 5 μm. **(C,D)** For each B cell, the cell area was quantified using the actin staining to define the cell edge. The left panels show data from representative experiments. Each dot represents one cell. The median (blue line) and interquartile ranges (black box) for > 30 cells are shown for each time point. *p*-values were determined using the Mann-Whitney *U*-test. The right panels show the mean ± SEM of the median cell areas from three independent experiments. Where no error bars are shown, they were smaller than the symbols. *p*-values were determined using paired two-tailed *t*-tests. $^{****}p < 0.0001$; $^{**}p < 0.01$; $^{*}p \leq 0.05$; ns, not significant ($p > 0.05$).

depletion of GMFγ has been reported in a number of other studies that have employed GMFγ siRNA as a loss-of-function approach (Lippert and Wilkins, 2012; Wang et al., 2014; Aerbajinai et al., 2016, 2019).

GMFγ has been implicated in the recycling of receptors back to the cell surface after endocytosis (Lippert and Wilkins, 2012; Aerbajinai et al., 2013, 2016) and depleting GMFγ in macrophages increases cell surface levels of Toll-like receptor 4 (Aerbajinai et al., 2013). Therefore, prior to assessing the role of GMFγ in BCR-induced actin remodeling, we tested whether GMFγ depletion altered BCR surface expression. Cell surface BCR levels in GMFγ siRNA-transfected Ramos B cells were 95 ± 6% of those in control siRNA-transfected cells (mean ± SEM for the mean fluorescence intensities from 5 experiments) (**Supplementary Figure 1A**). In Raji D1.3 B cells, GMFγ siRNA transfection reduced cell surface levels of the endogenous human BCR to 79 ± 4% of those in control siRNA-transfected cells (mean ± SEM for 5 experiments) and the transfected D1.3 BCR to 76 ± 2% of control cell levels (mean ± SEM for 4 experiments) (**Supplementary Figure 1B**). The reduced BCR cell surface expression in Raji D1.3 cells was not due to a decrease in cell size as control and GMFγ-depleted cells had similar mean forward scatter values (**Supplementary Figure 1**). Importantly, compared to control cells, GMFγ siRNA-transfected Ramos and Raji D1.3 B cells did not exhibit a reduction in initial BCR signaling (CD79 phosphorylation) in response to soluble anti-Ig antibodies. This finding is discussed in more detail in the last paragraph of the results section.

When B cells encounter anti-Ig antibodies or Ags that have been immobilized on rigid surfaces, BCR signaling stimulates actin remodeling that drives radial B cell spreading. This spreading is substantially reduced or altered when either cofilin or the Arp2/3 complex is inhibited (Freeman et al., 2011; Bolger-Munro et al., 2019, 2021). Hence, this assay is a robust platform for identifying proteins that regulate peripheral actin dynamics in B cells. To test whether GMFγ regulates BCR-induced actin remodeling and B cell spreading, control siRNA- and GMFγ siRNA-transfected B cells were added to anti-IgM-coated coverslips and allowed to spread for 3–30 min. Because the incomplete knockdown of GMFγ could be due to some cells not taking up the siRNA, we co-transfected the B cells with a GFP-encoding plasmid and then analyzed only GFP-expressing cells. The cell periphery was visualized by staining F-actin and the cell area in the confocal plane closest to the coverslip was quantified using Fiji software. Ramos and Raji D1.3 B cells that had been transfected with GMFγ siRNA exhibited relatively normal initial cell spreading at 3–10 min (**Figure 1**). However, compared to control siRNA-transfected cells, GMFγ-depleted Ramos and Raji D1.3 B cells had significantly reduced contact areas at the 15 and 30 min time points (**Figure 1**). These findings suggest that GMFγ is a positive regulator of sustained B cell spreading.

Because the Raji D1.3 B cells express a transfected HEL-specific BCR in addition to their endogenous BCR, we were able to extend these studies to Ag-induced B cell spreading. Recent work has shown that occupancy of the Ag-binding sites in the BCR may activate the BCR in a different manner than anti-Ig antibodies that cluster BCRs (Volkmann et al., 2016; Shen et al., 2019). We found that depleting GMFγ impaired the ability of Raji D1.3 B cells to spread on HEL-coated coverslips, with significant and consistent reductions in the median spreading areas at the 15 and 30 min time points compared to control siRNA-transfected cells (**Figure 2**). Thus, GMFγ is important for sustained B cell spreading on both anti-Ig and Ag.

GMFγ Abuts the Inner Face of the Peripheral Actin Ring and Contributes to Actin Retrograde Flow

The radial spreading of B cells in response to immobilized BCR ligands is characterized by the formation of a peripheral branched actin network that drives lamellipodial protrusion. Persistent outward movement of lamellipodia is associated with actin treadmilling in which actin-disassembly factors dismantle older segments of the peripheral actin network that are further from the plasma membrane, allowing components to be recycled for new actin assembly at the plasma membrane (Carlier and Shekhar, 2017). *In vitro*, GMFγ preferentially releases older actin branches where the Arp2/3-bound ATP has been hydrolyzed to ADP (Boczkowska et al., 2013; Pandit et al., 2020). To gain insight into how GMFγ regulates peripheral actin dynamics during B cell spreading we imaged the localization of the endogenous GMFγ protein, relative to actin structures, in Ramos B cells that were plated on immobilized anti-Ig (**Figure 3**). As the B cells spread, they formed a distinct peripheral F-actin ring surrounding a central actin-depleted region. GMFγ was present in this central region of the cell and abutted the interior face of the peripheral F-actin ring (**Figures 3A,B**). In contrast, GMFγ appeared to be relatively under-represented in the outer portion of the peripheral actin ring, which is presumably close to the plasma membrane.

To quantitatively assess the spatial distribution of GMFγ relative to the peripheral actin ring, we generated radial fluorescence intensity profiles in which the normalized integrated fluorescence intensity is plotted vs. the relative distance from the center of the cell (x = 0) to the edge of the cell (x = 1.0). Briefly, the algorithm generates a series of concentric circles around the center of the cell and then determines the average fluorescence intensity for the pixels along the perimeter of each circle. This integrated intensity is then normalized to the maximal integrated intensity (defined as 1.0) for any circle from that cell, and plotted vs. the relative distance from the center of the cell. **Figure 3B** shows a representative example for an individual cell that had spread on immobilized anti-IgM for 30 min. In **Figure 3C**, Ramos B cells were allowed to spread on immobilized anti-IgM for 10, 15, or 30 min and the averaged radial fluorescence intensity profiles for 78–129 cells per time point are shown. The peripheral actin ring that forms in spreading B cells coincided with a distinct peak of the actin radial fluorescence intensity, which was close to the edge of the cell (**Figures 3B,C**). Importantly, this analysis showed that the peak of GMFγ fluorescence intensity was consistently closer to the center of the cell than the peak of actin fluorescence (**Figures 3B,C**). Although GMFγ was abundant in the center of the cells, GMFγ levels were substantially lower where the actin fluorescence peaked. These findings are consistent with a model

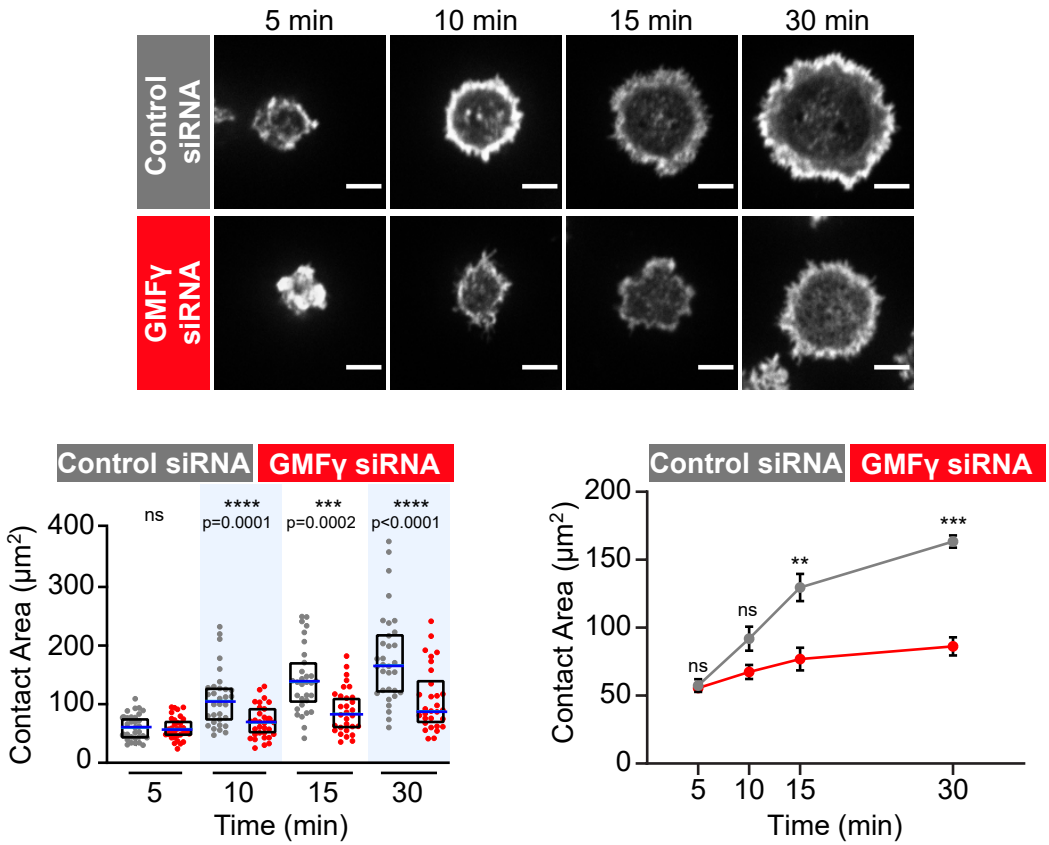

FIGURE 2 | Depleting GMFγ reduces B cell spreading on immobilized HEL. Raji D1.3 B cells that had been transfected with either control siRNA or GMFγ siRNA were added to coverslips coated with 0.22 μg/cm^2 HEL and allowed to spread for the indicated times. Representative confocal microscopy images of cells stained with rhodamine-phalloidin are shown. Scale bars: 5 μm. The cell area was quantified using the actin staining to define the cell edge. In the dot plot (left graph), each dot represents one cell, the median (blue line) and interquartile ranges (black box) for > 30 cells are shown for each time point, and *p*-values were determined using the Mann-Whitney *U*-test. The line graph on the right shows the mean ± SEM of the median cell areas from three independent experiments. Where no error bars are shown, they were smaller than the symbols. *p*-values were determined using paired two-tailed *t*-tests. ****$p < 0.0001$; ***$p < 0.001$; **$p < 0.01$; ns, not significant ($p > 0.05$).

in which GMFγ disassembles older portions of the peripheral actin network that are closer to the center of the cell. At the same time, the reduced levels of GMFγ at the leading edge would allow Arp2/3 complex-nucleated branched actin polymerization to drive outward expansion of lamellipodia.

The outward forces generated by actin polymerization at the plasma membrane are opposed by the elastic resistance of the membrane. The resulting inward forces result in retrograde flow of the peripheral actin network. When B cells interact with Ags that are mobile within a membrane, this actin retrograde flow promotes the initial centralization and progressive coalescence of BCR microclusters, which amplifies microcluster-based BCR signaling (Bolger-Munro et al., 2019). Because actin disassembly supports on-going actin polymerization at the plasma membrane, we asked whether GMFγ contributes to the generation of actin retrograde flow in B cells. To assess this, real-time imaging of peripheral F-actin structures was carried out in Raji D1.3 B cells that were transfected with control siRNA or GMFγ siRNA along with cDNA encoding F-tractin-GFP, a fusion protein that binds F-actin. This allowed us to visualize the centripetal movement of peripheral actin structures (**Figure 4A** and **Supplementary Movies 1, 2**). We then used kymograph analysis to calculate the inward velocity of distinct actin structures from multiple cells (**Figure 4B**). This analysis showed that the median velocity of the actin retrograde flow was reduced by 38% when the cells were transfected with GMFγ siRNA, as compared to control siRNA-transfected cells (**Figure 4C**). Thus, GMFγ contributes to the peripheral actin dynamics that result in actin retrograde flow.

Depleting GMFγ Reduces APC-Induced cSMAC Formation and BCR Signaling at the Immune Synapse

When B cells encounter APCs displaying Ags that can bind to their BCR, BCR-Ag microclusters form rapidly and begin to coalesce. Arp2/3 complex-dependent actin retrograde flow is required for the initial centripetal movement of BCR-Ag microclusters, which amplifies microcluster-based BCR signaling and promotes the microcluster coalescence that leads to cSMAC formation (Bolger-Munro et al., 2019). Because

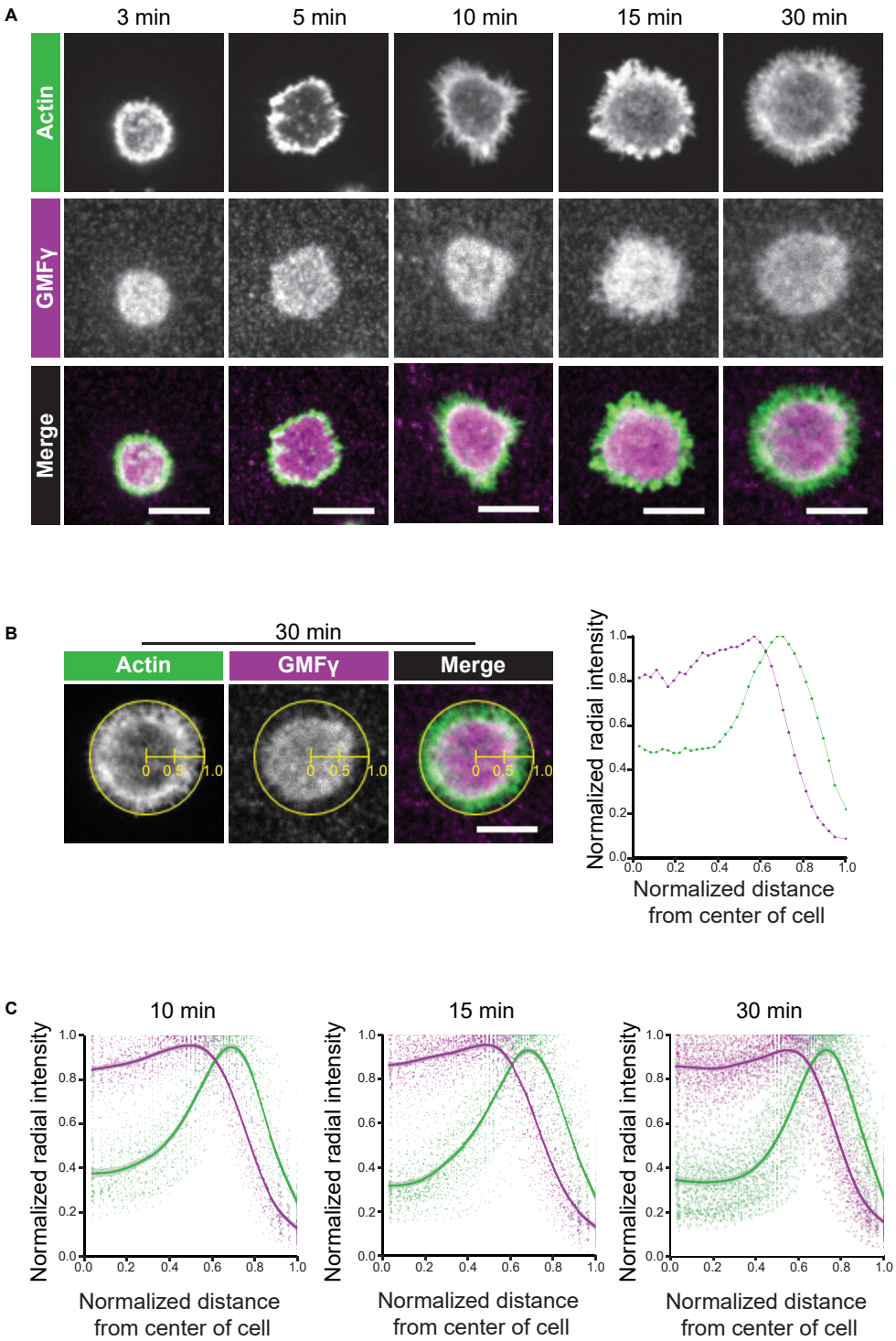

FIGURE 3 | GMFγ abuts the inner face of the peripheral actin ring. Ramos B cells were allowed to spread for 3–30 min on anti-IgM-coated coverslips before being stained with an anti-GMFγ antibody plus rhodamine-phalloidin. **(A)** Representative confocal microscopy images. Scale bars: 10 μm. **(B)** Example of actin and GMFγ radial fluorescence intensity profiles for an individual cell. The ImageJ Radial Profile Extended plug-in generates concentric circles with radii corresponding to different distances from the center of the cell and then calculates the average fluorescence intensity per pixel around the perimeter of each circle. This integrated radial intensity value is normalized to the maximal value for any circle from that cell (defined as 1.0) and is plotted vs. its relative distance between the center of the cell ($x = 0$) and the edge of the cell ($x = 1$). The graph (right panel) shows the radial intensity profiles for GMFγ (purple) and F-actin (green) for the cell shown in the left three panels, which had spread on immobilized anti-IgM for 30 min. **(C)** The averaged radial fluorescence intensity profiles for 78–129 cells per time point are shown for cells that had spread on anti-IgM for 10, 15, or 30 min in one of 4 independent experiments. For each relative distance, the dots are the values for individual cells. The solid lines and corresponding gray contours are the generalized additive model and standard error of the smoothing estimate.

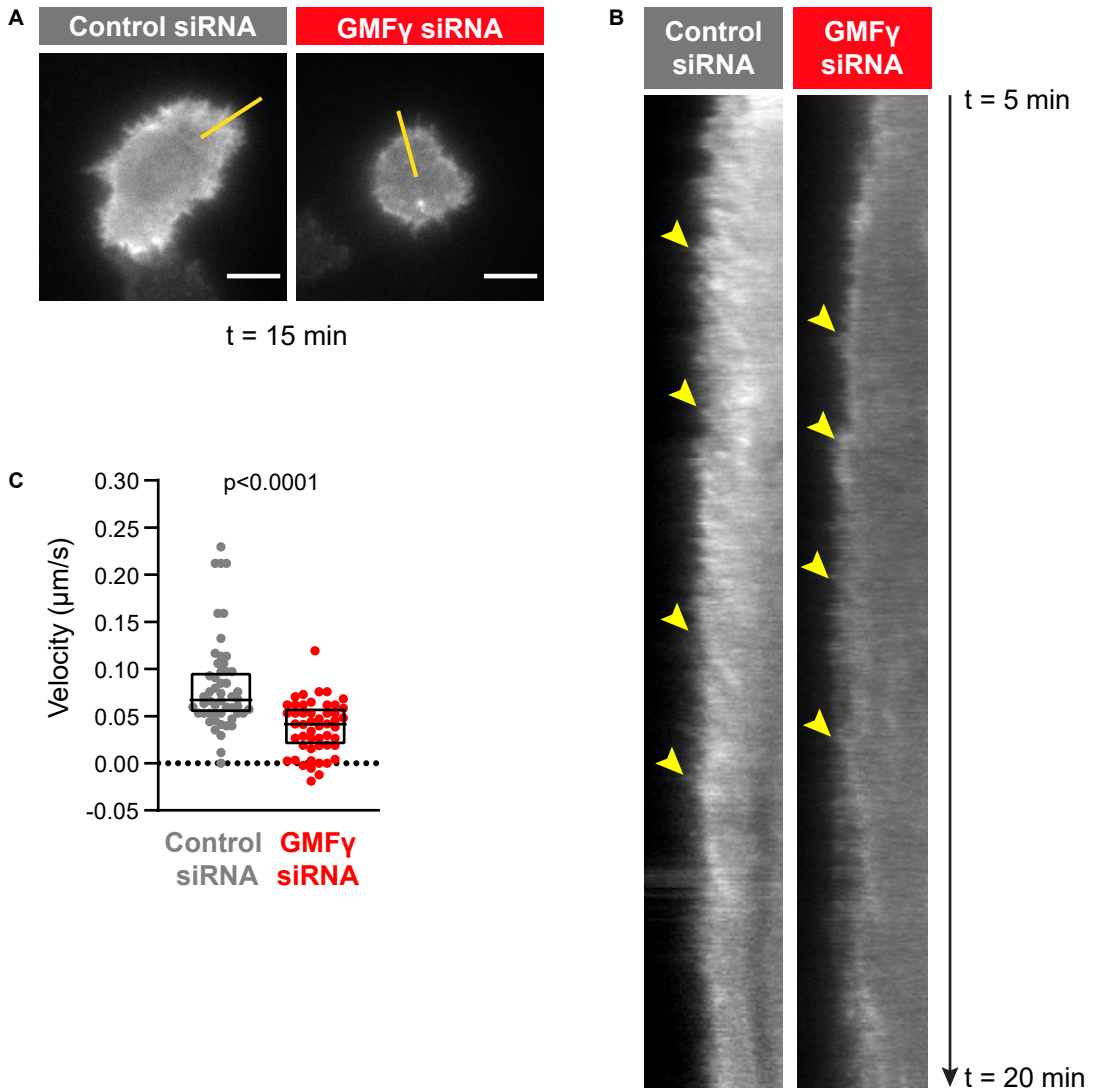

FIGURE 4 | Depleting GMFγ reduces the velocity of actin retrograde flow. Raji D.3 B cells that had been co-transfected with F-tractin-GFP cDNA and either control siRNA or GMFγ siRNA were added to anti-human IgM-coated coverslips and allowed to spread for 5 min. The cells were then imaged by TIRF microscopy at 2 s intervals for 15 min (t = 5 min to t = 20 min). Video recordings of representative cells are shown in **Supplementary Movie 1** (control siRNA) and **Supplementary Movie 2** (GMFγ siRNA). **(A)** Still images of the control siRNA- and GMFγ siRNA-transfected cells shown in **Supplementary Movies 1, 2** at t = 15 min. Scale bars: 5 μm. **(B)** Kymographs were generated along the yellow lines in **(A)**. Arrowheads indicate the starting points of representative actin tracks for which centripetal velocities were determined. **(C)** The centripetal velocity ($\Delta x/\Delta t$) was calculated for individual actin tracks on the kymographs. Each dot on the graph is an individual actin track. The velocity was determined for 52 tracks from 9 cells (control siRNA) or 51 tracks from 11 cells (GMFγ siRNA). The Mann-Whitney U-test was used to calculate the p-value.

GMFγ supports the Arp2/3 complex-dependent spreading of B cells on immobilized BCR ligands, we asked whether it is also important for APC-induced immune synapse formation and BCR signaling. To test this, HEL-specific Raji D1.3 B cells were transfected with either control or GMFγ siRNA and then allowed to interact with adherent APCs expressing the mHEL-HaloTag Ag, a transmembrane form of HEL that can be fluorescently labeled (Wang et al., 2018; Bolger-Munro et al., 2019). After 3–30 min, the cells were fixed and stained with an antibody to the phosphorylated CD79a/CD79b ITAMs in order to detect this essential initial event in BCR signaling. Imaging the B cell-APC interface allowed us to visualize BCR-Ag microclusters, monitor their coalescence into a cSMAC, and quantify the amount of pCD79 and mHEL-HaloTag fluorescence that is present in clusters. As shown in previous studies, the gathering of membrane-bound Ags into microclusters that can be detected by diffraction-limited microscopy is due to BCR binding. These Ag clusters align with BCR clusters on the B cell, and clusters of activated BCRs (i.e., those in which CD79 is phosphorylated or to which the Syk protein kinase has been

recruited) overlap extensively with the Ag clusters (Depoil et al., 2008). Hence, Ag clusters that align with pCD79 clusters are believed to be clusters of BCR-bound Ags in which Ag binding has initiated BCR signaling.

We found that depleting GMFγ did not affect the formation of BCR-Ag microclusters but reduced their coalescence into a cSMAC. Both control siRNA- and GMFγ siRNA-transfected Raji D1.3 B cells rapidly formed BCR-Ag microclusters throughout the B cell-APC contact site and, on average, gathered similar amounts of Ag into clusters (**Figures 5A,B**). Over time, the BCR microclusters in the majority of the control cells coalesced to form a large central cluster. In contrast, a greater number of the GMFγ siRNA-transfected cells failed to form a large central cluster and the Ag fluorescence was instead distributed among multiple small clusters. This difference in microcluster coalescence can be seen by comparing the Ag clusters in the images of control vs. GMFγ siRNA-transfected cells at the 15 min time point in **Figure 5A**. To more rigorously compare the extent of microcluster coalescence in different cell populations, we applied a quantitative analysis that we developed previously (Bolger-Munro et al., 2019). We determine the amount of Ag fluorescence associated with each discrete Ag cluster on an individual B cell and define cSMAC formation as > 90% of the clustered Ag fluorescence being contained in 1 or 2 clusters. This analysis showed that when control siRNA-transfected cells were added to APCs for 30 min, ∼60% of the cells in 5 independent experiments formed a cSMAC (**Figure 5C**). In contrast, when GMFγ was depleted, only ∼40% of the cells formed a cSMAC after 30 min (**Figure 5C**). Data from a representative experiment are presented in **Figure 6**, which shows the distribution of Ag fluorescence among clusters on individual cells and depicts the number of clusters required to contain > 90% of the Ag fluorescence. This analysis showed that a greater percent of control siRNA-transfected Raji D1.3 B cells formed cSMACs, i.e., gathered > 90% of the Ag fluorescence into one or two clusters, compared to the GMFγ siRNA-transfected cells. Thus, the progressive coalescence of BCR-Ag microclusters that leads to cSMAC formation is reduced when GMFγ is depleted.

The growth and coalescence of BCR-Ag microclusters, as well as their centripetal movement, amplify microcluster-based BCR signaling (Ketchum et al., 2014; Bolger-Munro et al., 2019). To determine whether GMFγ contributes to this signal amplification, we first quantified for each B cell the total amount of pCD79 fluorescence present in clusters at the B cell-APC interface. When GMFγ was depleted from Raji D1.3 cells, the amount of clustered pCD79 per cell was significantly reduced, compared to control siRNA-transfected cells (**Figure 5D**). This reduction in APC-induced BCR signaling was especially pronounced at the earliest time points, i.e., at 3, 5, and 10 min after adding the B cells to the APCs. In five independent experiments, the median pCD79 levels at the 3 min and 10 time points were reduced by more than 50% when GMFγ was depleted. Hence, GMFγ is a positive regulator of microcluster-based BCR signaling at the immune synapse. For each B cell, we also divided the total amount of pCD79 fluorescence present in clusters at the B cell-APC interface by the total amount of Ag fluorescence in clusters. This reflects the amount of BCR signaling generated per unit of Ag that has been gathered into microclusters, a ratio that we define as "signal amplification." When GMFγ was depleted, the magnitude of this BCR signal amplification was significantly reduced at the 3, 5, and 10 min time points (**Figure 5E**). Thus, GMFγ is a positive regulator of BCR signaling amplification, which is associated with the actin-dependent centripetal movement and coalescence of BCR-Ag microclusters.

In contrast to APC-bound Ags, where Ag binding occurs only at a polarized cell-cell contact site, BCR signaling in response to uniformly distributed soluble BCR ligands is much less dependent on actin dynamics and organization (Bolger-Munro et al., 2019). Consistent with this, we found that reducing the levels of GMFγ in Raji D1.3 B cells had no effect on CD79 phosphorylation in response to soluble anti-Ig antibodies (**Figure 7A**). Similar results were obtained in Ramos B cells (**Figure 7B**). Thus, GMFγ enhances BCR signaling in response to APC-bound Ags (**Figure 5**) but appears to be dispensable for responses to soluble BCR ligands. This indicates that GMFγ is not a direct regulator of BCR signaling but instead regulates actin dynamics that amplify BCR signaling responses to spatially restricted Ag arrays, such as those on the surface of APCs.

DISCUSSION

Actin-disassembly proteins play a central role in remodeling actin networks and also fuel actin polymerization by liberating actin monomers from filaments. Hence, the complex changes in actin dynamics and architecture that drive immune synapse formation are likely to depend on the actions of actin-disassembly proteins. In this study we show that GMFγ supports the ability of B cells to spread across anti-Ig- and Ag-coated surfaces, enhances cSMAC formation at the B cell-APC contact site, and amplifies APC-induced BCR signaling. The lamellipodial protrusion that drives B cell spreading on rigid substrates, as well as the coalescence of BCR microclusters into a cSMAC in response to APC-bound Ags, is driven by Arp2/3 complex-dependent actin polymerization. Hence, GMFγ is a positive regulator of BCR-induced actin remodeling that works in concert with the Arp2/3 complex.

In vitro biochemical studies had suggested that GMFγ can antagonize Arp2/3 complex function. At high concentrations, which may be non-physiological, GMFγ can bind to the Arp2/3 complex and cause a conformational change that prevents the nucleation of new actin filaments that branch off from the mother filament (Sokolova et al., 2017). However, at lower concentrations, GMFγ primarily causes debranching, releasing both the Arp2/3 complex and the daughter filament from the mother filament (Gandhi et al., 2010; Ydenberg et al., 2013). The released daughter filaments would have exposed pointed ends, which are sites of actin filament disassembly (Pollard, 2016; Goode et al., 2018). The resulting actin monomers can be converted to the polymerization-competent ATP-bound form by profilin (Kotila et al., 2018). Profilin-actin complexes can then bind to membrane-associated nucleation promoting factors such as WASp, which can interact with actin filament-associated Arp2/3 complexes. This allows the direct delivery of actin

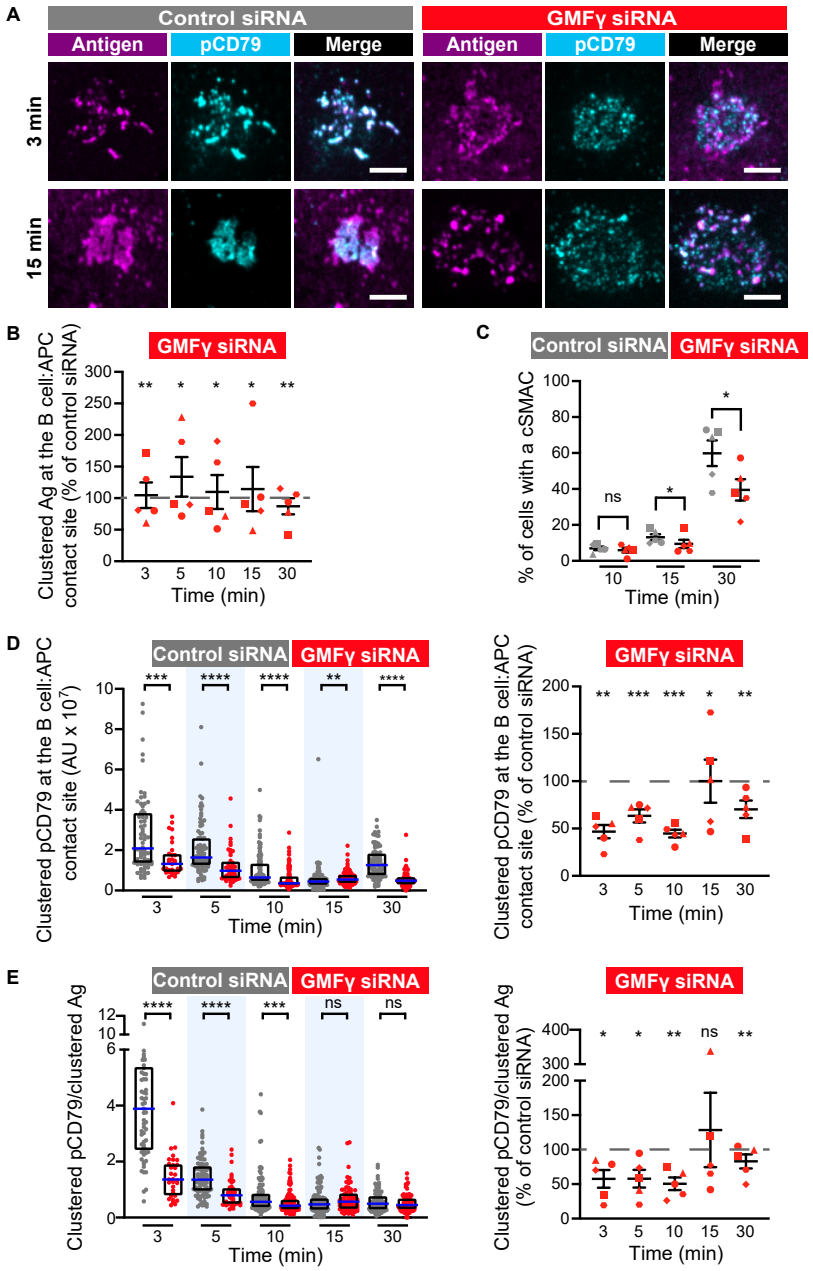

FIGURE 5 | Depleting GMFγ reduces cSMAC formation and proximal BCR signaling at the immune synapse. Raji D1.3 B cells were transfected with either control siRNA or GMFγ siRNA and added to COS-7 APCs expressing the mHEL-HaloTag Ag (magenta). The cells were fixed at the indicated times and stained with an antibody that recognizes the phosphorylated CD79 ITAMs (pCD79, cyan). The B cell-APC interface was imaged by spinning disk microscopy. **(A)** Representative images from one of five independent experiments. Scale bars: 5 μm. **(B)** The total fluorescence intensity of the mHEL-HaloTag Ag that had been gathered into clusters at the B cell-APC contact site was quantified for each B cell and the median values were calculated for each time point. Each symbol on the graph represents the median value for the GMFγ knockdown cells, expressed as a percent of the median value for the control siRNA-transfected cells for the same time point in the same experiment. The differently shaped symbols represent five independent experiments. Paired *t*-tests were used to calculate *p*-values. **(C)** The percent of cells that had formed a cSMAC, defined as > 90% of the total Ag fluorescence intensity being contained in one or two clusters, is graphed. The different symbols represent independent experiments. Paired *t*-tests were used to calculate *p*-values. **(D)** The total fluorescence intensity of pCD79 that was present in clusters at the B cell-APC contact site was quantified for each B cell. The left panel shows representative data from one experiment. Each dot is one cell. $n > 31$ cells per condition. The median (blue line) and interquartile ranges (black box) are shown. The Mann-Whitney *U*-test was used to calculate *p*-values. The right panel shows the results from five independent experiments, presented as in **(B)**, with n > 30 cells per condition in each experiment. Each symbol represents a single experiment in which the median pCD79 fluorescence intensity for GMFγ-depleted cells is expressed as a percent of the corresponding median value for the control cells. Paired *t*-tests were used to calculate *p*-values. **(E)** For each B cell represented in **(D)**, the total fluorescence intensity of clustered pCD79 was divided by the total fluorescence intensity of the clustered mHEL-HaloTag Ag. The median (blue line) and interquartile ranges (black box) are shown. The data are presented as in **(B,D)**. $^{****}p < 0.0001$; $^{***}p < 0.001$; $^{**}p < 0.01$; $^{*}p \leq 0.05$; ns, not significant ($p > 0.05$).

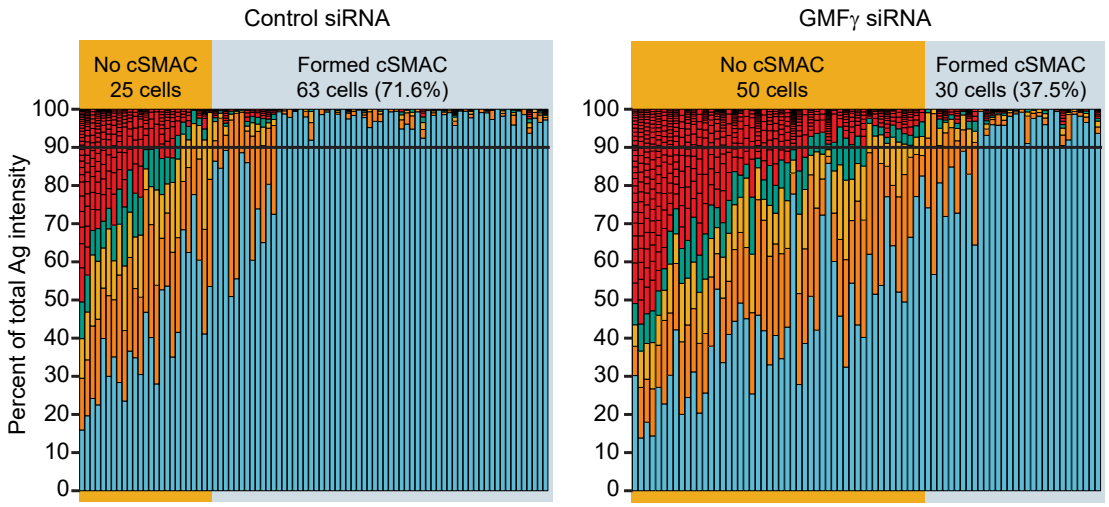

FIGURE 6 | Depleting GMFγ reduces the percent of cells that form a cSMAC. Raji D1.3 B cells that had been transfected with control siRNA or GMFγ siRNA were added to mHEL-HaloTag-expressing COS-7 APCs. The cells were fixed after 30 min and the B cell-APC interface was imaged by spinning disk microscopy. The stacked bar plots show the fraction of the total Ag fluorescence intensity in individual clusters. Each bar represents one cell and each colored segment within a bar represents a single Ag cluster. The size of the colored segment is proportional to the fraction of the cell's total Ag fluorescence intensity that is contained within that cluster. Cells in which > 90% of the total Ag fluorescence intensity (black horizontal lines) was contained in 1–2 clusters were deemed to have formed a cSMAC. The data are from one of the 5 independent experiments that are compiled in **Figure 5C**.

monomers to the Arp2/3 complex and their assembly into new branches (Mullins et al., 2018). In addition to providing actin monomers to fuel Arp2/3 complex-dependent actin polymerization, GMFγ-mediated debranching releases Arp2/3 complexes from existing filaments, allowing them to nucleate new actin branches and promote actin polymerization. Because the amount of nucleation-competent ATP-bound Arp2/3 complexes may be limiting within cells, recycling of Arp2/3 complexes is thought to be important for the sustained assembly of dendritic actin networks and the formation of lamellipodia. The role of GMFγ in promoting Arp2/3 complex release and recycling within lamellipodia is supported by studies in fibroblasts showing that the amount of Arp2/3 complex present in lamellipodia is increased when the related GMFβ protein is depleted and decreased when GMFβ is overexpressed (Haynes et al., 2015). Hence, instead of opposing Arp2/3 complex function, GMF proteins may be important for sustaining Arp2/3 complex-dependent processes.

Our findings support the idea that GMFγ works in concert with the Arp2/3 complex in B cells. The radial spreading of B cells on immobilized Ags, which is driven by Arp2/3 complex-dependent actin polymerization, was significantly impaired when GMFγ was depleted. The difference in the substrate contact area between control and GMFγ-depleted B cells becomes progressively larger over time, suggesting that the GMFγ-depleted cells may run out of polymerization-competent actin monomers or free Arp2/3 complexes. In other cell types, GMFγ is also a positive regulator of processes that require actin polymerization such as membrane ruffling, leading edge protrusion, and cell migration (Ikeda et al., 2006; Aerbajinai et al., 2011, 2016; Lippert and Wilkins, 2012; Poukkula et al., 2014). GMFγ preferentially releases older actin branches where the Arp2/3-bound ATP has been hydrolyzed to ADP (Boczkowska et al., 2013; Pandit et al., 2020). This fits with the actin treadmilling model for lamellipodial protrusion in which older segments of the actin network that are further from the membrane are disassembled into monomers, which can then be recycled and used for Arp2/3 complex-nucleated actin polymerization at the plasma membrane (Carlier and Shekhar, 2017). Consistent with this model, when B cells spread on immobilized BCR ligands and formed broad lamellipodia, we found that GMFγ abutted, and perhaps overlapped somewhat, with the inner face of the peripheral actin ring. Importantly, GMFγ was present at much lower amounts in the outer portion of this leading edge than elsewhere in the cell. This may allow the Arp2/3 complex to nucleate actin polymerization at the plasma membrane, and drive the outward expansion of lamellipodia, with less opposition from GMFγ.

We have previously shown that Arp2/3 complex-dependent actin polymerization generates actin retrograde flow at the cell periphery, which drives the initial centralization of BCR-Ag microclusters and promotes their coalescence (Bolger-Munro et al., 2019). This amplifies microcluster-based BCR signaling and leads to cSMAC formation. We found that depleting GMFγ significantly decreased the velocity of actin retrograde flow and reduced cSMAC formation. By providing a source of polymerization-competent actin monomers and recycled Arp2/3 complexes, GMFγ may help sustain the peripheral actin polymerization that generates actin retrograde flow and drives the progressive coalescence of BCR-Ag microclusters. The formation of larger BCR clusters enhances BCR signaling (Ketchum et al., 2014) and we showed that GMFγ helps amplify BCR signaling at the B cell-APC contact site, as assessed by the amount of pCD79 per unit of clustered Ag. The contribution

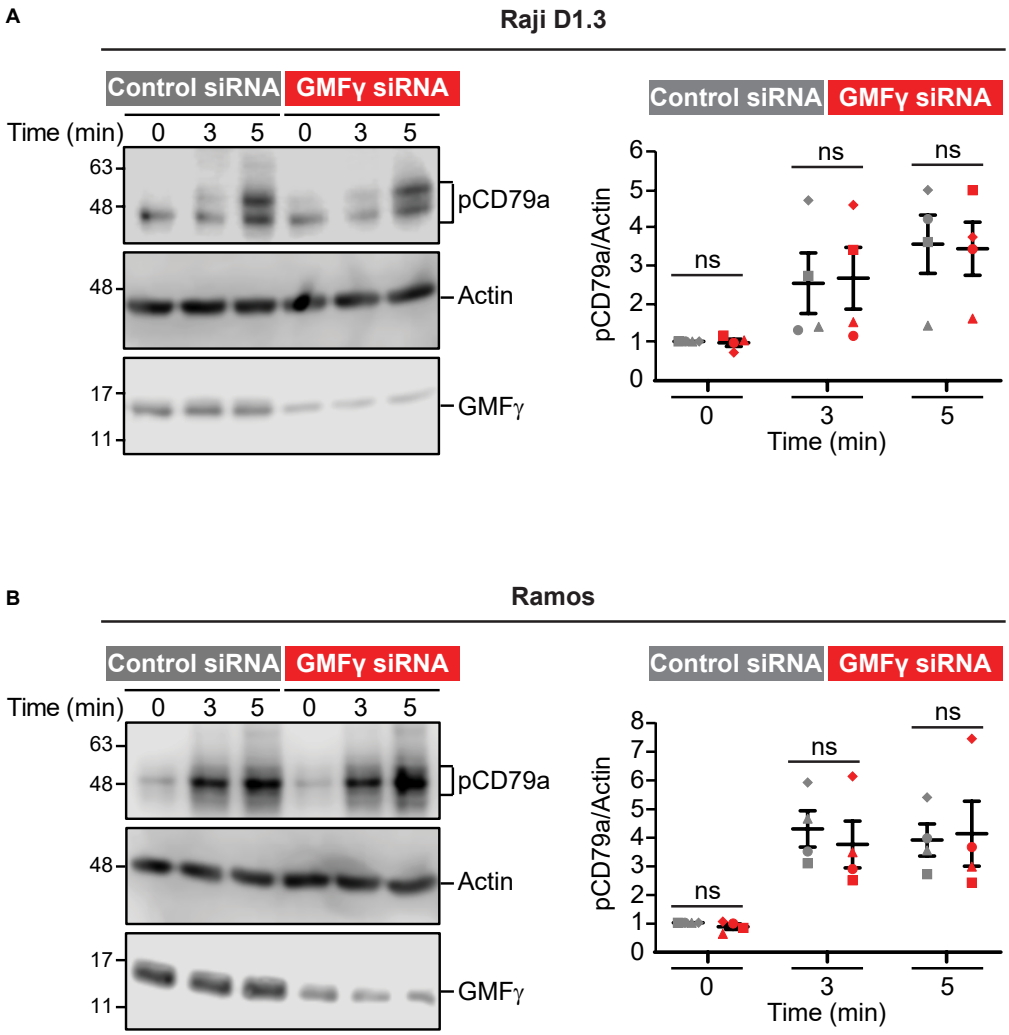

FIGURE 7 | Depleting GMFγ does not impair CD79 phosphorylation induced by soluble anti-Ig antibodies. Cells were transfected with either control siRNA or GMFγ siRNA. **(A)** Raji D1.3 B cells were stimulated with 20 μg/mL goat anti-mouse IgM to initiate signaling through the D1.3 BCR. **(B)** Ramos B cells were stimulated with donkey anti-human IgM. Cell lysates were analyzed by immunoblotting with antibodies that recognize the phosphorylated CD79a ITAM (pCD79a), actin (loading control), or GMFγ. The left panels show a representative experiment. The right panels show results from 4 independent experiments. For each sample, the pCD79a band intensity was divided by the corresponding actin band intensity (loading control). The resulting ratios were normalized to that for the 0 min control siRNA cell sample (defined as 1.0) in the same experiment. On the graph, each of the four experiments is indicated by a different symbol. The bars show the mean ± SEM. Paired *t*-tests were used to calculate *p*-values. ns, not significant ($p > 0.05$).

of GMFγ to actin retrograde flow at the immune synapse may also help amplify microcluster-based BCR signaling. The BCR is a mechanosensitive receptor (Shaheen et al., 2019) and the retrograde flow of actin structures could exert force on BCR microclusters that amplify BCR signaling. Overall, our findings are consistent with the idea that GMFγ works in concert with the Arp2/3 complex to enhance BCR microcluster coalescence and microcluster-based BCR signaling at the B cell-APC immune synapse.

Because Ags larger than ∼70 kDa cannot freely diffuse into the B cell follicles within lymphoid organs, APCs play a critical role in B cell responses to larger Ags such as microbial pathogens (Batista and Harwood, 2009; Cyster, 2010; Heesters et al., 2016). In the lymph nodes, a specialized subpopulation of macrophages that line the subcapsular sinus utilizes cell surface lectins, complement receptors, and Fc receptors to capture bacteria, viruses, and immune complexes that are present in the incoming lymphatic fluid. These subcapsular sinus macrophages are in contact with the B cell follicle and can transport the captured Ag from its lumenal side to the side facing the B cell follicle, where they present the Ag to B cells. The Ag can also be shuttled from the subcapsular sinus macrophage to follicular dendritic cells in the center of the B cell follicle (Phan et al., 2007, 2009). Follicular dendritic cells are specialized APCs that produce chemokines that attract B cells (Heesters et al., 2014). B cell interactions with Ag-bearing follicular dendritic cells are essential for the germinal center response that leads to affinity maturation of the antibody response and Ig class switching

(Heesters et al., 2016). The important physiological role of APC-mediated B cell activation provides a strong rationale for identifying the cytoskeletal regulators that amplify BCR signaling at the immune synapse, a process that allows small amounts of APC-bound Ag to activate B cells. Indeed, Batista and colleagues showed that 100-fold lower concentrations of Ag are required for B cell activation when the Ag is presented on an APC than when it is in a soluble form (Batista et al., 2001). The unique role of actin dynamics in APC-induced B cell activation is highlighted by the observation that the Arp2/3 complex (Bolger-Munro et al., 2019), the Cdc42 activator DOCK8 (Randall et al., 2009; Sun et al., 2018), and CD19 (Depoil et al., 2008), a transmembrane protein that recruits the Rac/Cdc42 activator Vav, are important for B cell responses to membrane-bound Ags but are all dispensable for responses to soluble Ag. Consistent with this, we showed that reducing GMFγ levels impaired BCR signaling in response to APC-bound Ag but not soluble Ag.

BCR signaling is critical for B cell development and the magnitude of BCR signaling determines whether Ag encounter results in B cell activation, as opposed to the deletion or silencing of potentially self-reactive B cells (Cashman et al., 2019; Meffre and O'Connor, 2019; Tan et al., 2019). Autoimmunity can result from excessive BCR signaling as well as failures to eliminate self-reactive B cells in which BCR signaling is reduced. Indeed, many immunodeficiency syndromes in which immune responses to Ag challenge are impaired are associated with autoimmunity and the production of self-reactive antibodies (Cashman et al., 2019; Meffre and O'Connor, 2019; Tan et al., 2019). By amplifying microcluster-based BCR signaling in response to APC-bound Ags, actin remodeling may modulate the Ag density thresholds that determine whether a B cell-APC encounter leads to B cell activation or tolerance. Hence, it is not surprising that mutations in a number of actin-regulatory proteins lead to actinopathies, immune dysregulation syndromes characterized by autoimmunity as well as immune deficiency that results in recurring microbial infections (Sprenkeler et al., 2020). Reduced BCR signaling in response to cell-associated Ags could compromise the ability to delete self-reactive B cells, allowing them to be activated under certain conditions. Conversely, B cell responses to bacteria and viruses are particularly dependent on APCs and impaired BCR signaling to microbial Ags that are captured by APCs may result in deficient immunity to infection. Indeed, the ability of APC-bound Ags to induce B cell proliferation and activation is reduced when the Arp2/3 complex is inhibited (Bolger-Munro et al., 2019). This suggests that actin-regulatory proteins that work in concert with the Arp2/3 complex, such as GMFγ, may also influence the threshold for B cell activation and tolerance.

There are two GMF genes in vertebrate genomes, GMFβ and GMFγ. The two GMF proteins are 82% identical in amino acid sequence, have similar 3-dimensional structures, and both can mediate actin debranching (Goode et al., 2018). Like GMFγ, GMFβ also regulates lamellipodial actin dynamics, at least in fibroblasts (Haynes et al., 2015). RNA-Seq data suggest that both GMFs are expressed in B cells[4]. Whether GMFβ also contributes to BCR-induced actin remodeling, B cell spreading, cSMAC formation, or APC-induced BCR signaling remains to be determined. Nevertheless, we showed that selectively reducing the levels of GMFγ was sufficient to impair all of these actin-dependent processes. The debranching activity of GMF proteins may also be regulated by phosphorylation. *In vitro*, recombinant GMFγ with a phosphomimetic S2E mutation exhibits a greatly reduced affinity for ADP-bound Arp2/3 complex (Boczkowska et al., 2013). This suggests that there could be dynamic regulation of GMF-mediated debranching that is coordinated with the initiation and termination of lamellipodial protrusion or other actin-dependent processes.

GMFγ is one of many actin-disassembly proteins that contribute to the spatiotemporal regulation of actin dynamics and remodeling. Cofilin and related actin-severing proteins are essential for actin network remodeling (Kadzik et al., 2020). Like GMFγ, cofilin preferentially disassembles older portions of peripheral actin networks that are further from the plasma membrane (Bernstein and Bamburg, 2010). In lamellipodia, the actions of the Arp2/3 complex and cofilin are tightly coupled with cofilin-dependent recycling of actin monomers and Arp2/3 complexes sustaining actin treadmilling (Carlier and Shekhar, 2017). We have shown that cofilin and its co-factor Wdr1 are critical regulators of actin dynamics and organization in B cells, and are important for B cell spreading as well as the actin-dependent amplification of BCR signaling at the immune synapse (Freeman et al., 2011; Bolger-Munro et al., 2021). In contrast to cofilin, capping proteins and their interactors regulate actin monomer depolymerization at the barbed ends of filaments (Edwards et al., 2014). In particular, twinfilin substantially increases the rate of barbed end depolymerization (Hilton et al., 2018) and depleting twinfilin decreases actin turnover dynamics at the leading edge (Hakala et al., 2021). Finally, GMFγ, coronins, and arpin regulate actin dynamics by targeting the Arp2/3 complex (Sokolova et al., 2017). These proteins bind to different sites on the Arp2/3 complex and, *in vitro*, they all induce the Arp2/3 complex to assume an "open" conformation that cannot nucleate branched actin polymerization. This suggests that they may have partly overlapping functions. GMFγ, coronins, and arpin can also act in additive or synergistic manners. However, only GMFγ catalyzes actin debranching by binding to the Arp2/3 complex and causing the dissociation of the Arp2/3 complex that bridges the daughter filament to the mother filament (Sokolova et al., 2017). Together, this network of Arp2/3 complex regulators may enable precise spatial and temporal regulation of branched actin polymerization and the architecture of dendritic actin networks.

Because GMFγ, coronins, and arpin may regulate the Arp2/3 complex in a cooperative manner, it is not surprising that depleting GMFγ has less dramatic effects on B cell spreading and B cell responses to APCs than what we observed when the Arp2/3 complex was depleted or inhibited (Bolger-Munro et al., 2019). The role of arpin in B cells has not been examined. Coronins are multifunctional proteins that regulate multiple aspects of immune cell function (Tokarz-Deptula et al., 2016). Coronin 1 is important for T cell homeostasis as well as TCR- and BCR-induced Ca^{2+} responses (Mueller et al., 2008;

[4]http://rstats.immgen.org/Skyline/skyline.html

Combaluzier et al., 2009; Siegmund et al., 2011). However, the role of coronin 1 in actin-dependent processes in B cells remains unexplored. Because actin dynamics amplify APC-induced BCR signaling, dissecting the contributions of different actin-disassembly proteins may provide new insights into the regulation of B cell activation.

DATA AVAILABILITY STATEMENT

The raw data supporting the conclusions of this article will be made available by the authors, without undue reservation.

AUTHOR CONTRIBUTIONS

MB-M and ND conceived and designed the experiments. ND, KC, LA, and MB-M performed the experiments. ND, MB-M, KC, and MG analyzed the results. ND, MB-M, and MG wrote the manuscript with input from KC. MG was the principal investigator of the study. All authors contributed to the article and approved the submitted version.

FUNDING

This work was supported by grants PJT-152946 and PJT-166196 (to MG) from the Canadian Institutes of Health Research. MB-M was supported by a 4-year fellowship and a Friedman Award for Scholars in Health from the University of British Columbia. ND was supported by an Undergraduate Summer Research Award from the Natural Sciences and Engineering Research Council (NSERC) of Canada.

ACKNOWLEDGMENTS

We thank the UBC Life Sciences Institute Imaging Facility and the UBC Flow Cytometry Facility. We thank May Dang-Lawson for laboratory and technical support.

SUPPLEMENTARY MATERIAL

The Supplementary Material for this article can be found online at: https://www.frontiersin.org/articles/10.3389/fcell.2021.647063/full#supplementary-material

REFERENCES

Abraham, L., Wang, J. C., Bolger-Munro, M., and Gold, M. R. (2016). Structure, function, and spatial organization of the B cell receptor (BCR). *Encycloped. Immunobiol.* 2, 40–54. doi: 10.1016/B978-0-12-374279-7.05005-0

Aerbajinai, W., Ghosh, M. C., Liu, J., Kumkhaek, C., Zhu, J., Chin, K., et al. (2019). Glia maturation factor-gamma regulates murine macrophage iron metabolism and M2 polarization through mitochondrial ROS. *Blood Adv.* 3, 1211–1225. doi: 10.1182/bloodadvances.2018026070

Aerbajinai, W., Lee, K., Chin, K., and Rodgers, G. P. (2013). Glia maturation factor-gamma negatively modulates TLR4 signaling by facilitating TLR4 endocytic trafficking in macrophages. *J. Immunol.* 190, 6093–6103. doi: 10.4049/jimmunol.1203048

Aerbajinai, W., Liu, L., Chin, K., Zhu, J., Parent, C. A., and Rodgers, G. P. (2011). Glia maturation factor-gamma mediates neutrophil chemotaxis. *J. Leukoc. Biol.* 90, 529–538. doi: 10.1189/jlb.0710424

Aerbajinai, W., Liu, L., Zhu, J., Kumkhaek, C., Chin, K., and Rodgers, G. P. (2016). Glia maturation factor-gamma regulates monocyte migration through modulation of beta1-integrin. *J. Biol. Chem.* 291, 8549–8564. doi: 10.1074/jbc.M115.674200

Batista, F. D., and Harwood, N. E. (2009). The who, how and where of antigen presentation to B cells. *Nat. Rev. Immunol.* 9, 15–27. doi: 10.1038/nri2454

Batista, F. D., Iber, D., and Neuberger, M. S. (2001). B cells acquire antigen from target cells after synapse formation. *Nature* 411, 489–494. doi: 10.1038/35078099

Bernstein, B. W., and Bamburg, J. R. (2010). ADF/cofilin: a functional node in cell biology. *Trends Cell Biol.* 20, 187–195. doi: 10.1016/j.tcb.2010.01.001

Boczkowska, M., Rebowski, G., and Dominguez, R. (2013). Glia maturation factor (GMF) interacts with Arp2/3 complex in a nucleotide state-dependent manner. *J. Biol. Chem.* 288, 25683–25688. doi: 10.1074/jbc.C113.493338

Bolger-Munro, M., Choi, K., Cheung, F., Liu, Y. T., Dang-Lawson, M., Deretic, N., et al. (2021). The Wdr1-LIMK-cofilin axis controls B cell antigen receptor-Induced actin remodeling and signaling at the immune synapse. *Front. Cell Dev. Biol.* 9:649433. doi: 10.3389/fcell.2021.649433

Bolger-Munro, M., Choi, K., Scurll, J., Abraham, L., Chappell, R. S., Sheen, D., et al. (2019). Arp2/3 complex-driven spatial patterning of the BCR enhances immune synapse formation, BCR signaling and B cell activation. *eLife* 8:e44574. doi: 10.7554/eLife.44574

Brigida, I., Zoccolillo, M., Cicalese, M. P., Pfajfer, L., Barzaghi, F., Scala, S., et al. (2018). T-cell defects in patients with ARPC1B germline mutations account for combined immunodeficiency. *Blood* 132, 2362–2374. doi: 10.1182/blood-2018-07-863431

Candotti, F. (2018). Clinical manifestations and pathophysiological mechanisms of the Wiskott-Aldrich syndrome. *J. Clin. Immunol.* 38, 13–27. doi: 10.1007/s10875-017-0453-z

Carlier, M.-F., and Shekhar, S. (2017). Global treadmilling coordinates actin turnover and controls the size of actin networks. *Nat. Rev. Molec. Cell Biol.* 18, 389–401. doi: 10.1038/nrm.2016.172

Cashman, K. S., Jenks, S. A., Woodruff, M. C., Tomar, D., Tipton, C. M., Scharer, C. D., et al. (2019). Understanding and measuring human B-cell tolerance and its breakdown in autoimmune disease. *Immunol. Rev.* 292, 76–89. doi: 10.1111/imr.12820

Combaluzier, B., Mueller, P., Massner, J., Finke, D., and Pieters, J. (2009). Coronin 1 is essential for IgM-mediated Ca2+ mobilization in B cells but dispensable for the generation of immune responses in vivo. *J. Immunol.* 182, 1954–1961. doi: 10.4049/jimmunol.0801811

Conley, M. E., Dobbs, A. K., Farmer, D. M., Kilic, S., Paris, K., Grigoriadou, S., et al. (2009). Primary B cell immunodeficiencies: comparisons and contrasts. *Annu. Rev. Immunol.* 27, 199–227. doi: 10.1146/annurev.immunol.021908.132649

Cook, S. A., Comrie, W. A., Poli, M. C., Similuk, M., Oler, A. J., Faruqi, A. J., et al. (2020). HEM1 deficiency disrupts mTORC2 and F-actin control in inherited immunodysregulatory disease. *Science* 369, 202–207. doi: 10.1126/science.aay5663

Cyster, J. G. (2010). B cell follicles and antigen encounters of the third kind. *Nat. Immunol.* 11, 989–996. doi: 10.1038/ni.1946

Cyster, J. G., and Allen, C. D. C. (2019). B cell responses: cell interaction dynamics and decisions. *Cell* 177, 524–540. doi: 10.1016/j.cell.2019.03.016

Dal Porto, J. M., Gauld, S. B., Merrell, K. T., Mills, D., Pugh-Bernard, A. E., and Cambier, J. (2004). B cell antigen receptor signaling 101. *Mol. Immunol.* 41, 599–613. doi: 10.1016/j.molimm.2004.04.008

Depoil, D., Fleire, S., Treanor, B. L., Weber, M., Harwood, N. E., Marchbank, K. L., et al. (2008). CD19 is essential for B cell activation by promoting B cell receptor-antigen microcluster formation in response to membrane-bound ligand. *Nat. Immunol.* 9, 63–72. doi: 10.1038/ni1547

Edwards, M., Zwolak, A., Schafer, D. A., Sept, D., Dominguez, R., and Cooper, J. A. (2014). Capping protein regulators fine-tune actin assembly dynamics. *Nat. Rev. Mol. Cell Biol.* 15, 677–689. doi: 10.1038/nrm3869

Fleire, S. J., Goldman, J. P., Carrasco, Y. R., Weber, M., Bray, D., and Batista, F. D. (2006). B cell ligand discrimination through a spreading and contraction response. *Science* 312, 738–741. doi: 10.1126/science.1123940

Freeman, S. A., Lei, V., Dang-Lawson, M., Mizuno, K., Roskelley, C. D., and Gold, M. R. (2011). Cofilin-mediated F-actin severing is regulated by the Rap GTPase and controls the cytoskeletal dynamics that drive lymphocyte spreading and BCR microcluster formation. *J. Immunol.* 187, 5887–5900. doi: 10.4049/jimmunol.1102233

Gandhi, M., Smith, B. A., Bovellan, M., Paavilainen, V., Daugherty-Clarke, K., Gelles, J., et al. (2010). GMF is a cofilin homolog that binds Arp2/3 complex to stimulate filament debranching and inhibit actin nucleation. *Curr. Biol.* 20, 861–867. doi: 10.1016/j.cub.2010.03.026

Goode, B. L., Sweeney, M. O., and Eskin, J. A. (2018). GMF as an actin network remodeling factor. *Trends Cell Biol.* 28, 749–760. doi: 10.1016/j.tcb.2018.04.008

Hakala, M., Wioland, H., Tolonen, M., Kotila, T., Jegou, A., Romet-Lemonne, G., et al. (2021). Twinfilin uncaps filament barbed ends to promote turnover of lamellipodial actin networks. *Nat. Cell Biol.* 23, 147–159. doi: 10.1038/s41556-020-00629-y

Harwood, N. E., and Batista, F. D. (2011). The cytoskeleton coordinates the early events of B-cell activation. *Cold Spring Harb. Perspect. Biol.* 3:a002360. doi: 10.1101/cshperspect.a002360

Haynes, E. M., Asokan, S. B., King, S. J., Johnson, H. E., Haugh, J. M., and Bear, J. E. (2015). GMFbeta controls branched actin content and lamellipodial retraction in fibroblasts. *J. Cell Biol.* 209, 803–812. doi: 10.1083/jcb.201501094

Heesters, B. A., Myers, R. C., and Carroll, M. C. (2014). Follicular dendritic cells: dynamic antigen libraries. *Nat. Rev. Immunol.* 14, 495–504. doi: 10.1038/nri3689

Heesters, B. A., van der Poel, C. E., Das, A., and Carroll, M. C. (2016). Antigen presentation to B cells. *Trends Immunol.* 37, 844–854. doi: 10.1016/j.it.2016.10.003

Hilton, D. M., Aguilar, R. M., Johnston, A. B., and Goode, B. L. (2018). Species-specific functions of twinfilin in actin filament depolymerization. *J. Mol. Biol.* 430, 3323–3336. doi: 10.1016/j.jmb.2018.06.025

Ikeda, K., Kundu, R. K., Ikeda, S., Kobara, M., Matsubara, H., and Quertermous, T. (2006). Glia maturation factor-gamma is preferentially expressed in microvascular endothelial and inflammatory cells and modulates actin cytoskeleton reorganization. *Circ. Res.* 99, 424–433. doi: 10.1161/01.RES.0000237662.23539.0b

Jellusova, J. (2020). Metabolic control of B cell immune responses. *Curr. Opin. Immunol.* 63, 21–28. doi: 10.1016/j.coi.2019.11.002

Johnson, H. W., and Schell, M. J. (2009). Neuronal IP3 3-kinase is an F-actin-bundling protein: Role in dendritic targeting and regulation of spine morphology. *Mol. Biol. Cell* 20, 5166–5180. doi: 10.1091/mbc.E09-01-0083

Kadzik, R. S., Homa, K. E., and Kovar, D. R. (2020). F-actin cytoskeleton network self-organization through competition and cooperation. *Annu. Rev. Cell Dev. Biol.* 36, 35–60. doi: 10.1146/annurev-cellbio-032320-094706

Kahr, W. H., Pluthero, F. G., Elkadri, A., Warner, N., Drobac, M., Chen, C. H., et al. (2017). Loss of the Arp2/3 complex component ARPC1B causes platelet abnormalities and predisposes to inflammatory disease. *Nat. Commun.* 8:14816. doi: 10.1038/ncomms14816

Ketchum, C., Miller, H., Song, W., and Upadhyaya, A. (2014). Ligand mobility regulates B cell receptor clustering and signaling activation. *Biophys. J.* 106, 26–36. doi: 10.1016/j.bpj.2013.10.043

Kile, B. T., Panopoulos, A. D., Stirzaker, R. A., Hacking, D. F., Tahtamouni, L. H., Willson, T. A., et al. (2007). Mutations in the cofilin partner Aip1/Wdr1 cause autoinflammatory disease and macrothrombocytopenia. *Blood* 110, 2371–2380. doi: 10.1182/blood-2006-10-055087

Kotila, T., Kogan, K., Enkavi, G., Guo, S., Vattulainen, I., Goode, B. L., et al. (2018). Structural basis of actin monomer re-charging by cyclase-associated protein. *Nat. Commun.* 9:1892. doi: 10.1038/s41467-018-04231-7

Kuijpers, T. W., Tool, A. T. J., van der Bijl, I., de Boer, M., van Houdt, M., de Cuyper, I. M., et al. (2017). Combined immunodeficiency with severe inflammation and allergy caused by ARPC1B deficiency. *J. Allergy Clin. Immunol.* 140:e210. doi: 10.1016/j.jaci.2016.09.061

Li, J., Yin, W., Jing, Y., Kang, D., Yang, L., Cheng, J., et al. (2018). The coordination between B cell receptor signaling and the actin cytoskeleton during B cell activation. *Front. Immunol.* 9:3096. doi: 10.3389/fimmu.2018.03096

Lippert, D. N., and Wilkins, J. A. (2012). Glia maturation factor gamma regulates the migration and adherence of human T lymphocytes. *BMC Immunol.* 13:21. doi: 10.1186/1471-2172-13-21

Meffre, E., and O'Connor, K. C. (2019). Impaired B-cell tolerance checkpoints promote the development of autoimmune diseases and pathogenic autoantibodies. *Immunol. Rev.* 292, 90–101. doi: 10.1111/imr.12821

Motulsky, H. J., and Brown, R. E. (2006). Detecting outliers when fitting data with nonlinear regression - a new method based on robust nonlinear regression and the false discovery rate. *BMC Bioinformatics* 7:123. doi: 10.1186/1471-2105-7-123

Mueller, P., Massner, J., Jayachandran, R., Combaluzier, B., Albrecht, I., Gatfield, J., et al. (2008). Regulation of T cell survival through coronin-1-mediated generation of inositol-1,4,5-trisphosphate and calcium mobilization after T cell receptor triggering. *Nat. Immunol.* 9, 424–431. doi: 10.1038/ni1570

Mullins, R. D., Bieling, P., and Fletcher, D. A. (2018). From solution to surface to filament: actin flux into branched networks. *Biophys. Rev.* 10, 1537–1551. doi: 10.1007/s12551-018-0469-5

Nakano, K., Kuwayama, H., Kawasaki, M., Numata, O., and Takaine, M. (2010). GMF is an evolutionarily developed Adf/cofilin-super family protein involved in the Arp2/3 complex-mediated organization of the actin cytoskeleton. *Cytoskeleton* 67, 373–382. doi: 10.1002/cm.20451

Nowosad, C. R., Spillane, K. M., and Tolar, P. (2016). Germinal center B cells recognize antigen through a specialized immune synapse architecture. *Nat. Immunol.* 17, 870–877. doi: 10.1038/ni.3458

Packard, T. A., and Cambier, J. C. (2013). B lymphocyte antigen receptor signaling: initiation, amplification, and regulation. *F1000Prime Rep* 5:40. doi: 10.12703/P5-40

Pandit, N. G., Cao, W., Bibeau, J., Johnson-Chavarria, E. M., Taylor, E. W., Pollard, T. D., et al. (2020). Force and phosphate release from Arp2/3 complex promote dissociation of actin filament branches. *Proc. Natl. Acad. Sci. U S A.* 117, 13519–13528. doi: 10.1073/pnas.1911183117

Pfajfer, L., Mair, N. K., Jimenez-Heredia, R., Genel, F., Gulez, N., Ardeniz, O., et al. (2018). Mutations affecting the actin regulator WD repeat-containing protein 1 lead to aberrant lymphoid immunity. *J. Allergy Clin. Immunol.* 142:e1511. doi: 10.1016/j.jaci.2018.04.023

Phan, T. G., Gray, E. E., and Cyster, J. G. (2009). The microanatomy of B cell activation. *Curr. Opin. Immunol.* 21, 258–265. doi: 10.1016/j.coi.2009.05.006

Phan, T. G., Grigorova, I., Okada, T., and Cyster, J. G. (2007). Subcapsular encounter and complement-dependent transport of immune complexes by lymph node B cells. *Nat. Immunol.* 8, 992–1000. doi: 10.1038/ni1494

Pollard, T. D. (2016). Actin and actin-binding proteins. *Cold Spring Harb. Perspect. Biol.* 8:a018226. doi: 10.1101/cshperspect.a018226

Poukkula, M., Hakala, M., Pentinmikko, N., Sweeney, M. O., Jansen, S., Mattila, J., et al. (2014). GMF promotes leading-edge dynamics and collective cell migration in vivo. *Curr. Biol.* 24, 2533–2540. doi: 10.1016/j.cub.2014.08.066

Randall, K. L., Lambe, T., Johnson, A. L., Treanor, B., Kucharska, E., Domaschenz, H., et al. (2009). Dock8 mutations cripple B cell immunological synapses, germinal centers and long-lived antibody production. *Nat. Immunol.* 10, 1283–1291. doi: 10.1038/ni.1820

Randzavola, L. O., Strege, K., Juzans, M., Asano, Y., Stinchcombe, J. C., Gawden-Bone, C. M., et al. (2019). Loss of ARPC1B impairs cytotoxic T lymphocyte maintenance and cytolytic activity. *J. Clin. Invest.* 129, 5600–5614. doi: 10.1172/JCI129388

Schindelin, J., Arganda-Carreras, I., Frise, E., Kaynig, V., Longair, M., Pietzsch, T., et al. (2012). Fiji: an open-source platform for biological-image analysis. *Nat. Methods* 9, 676–682. doi: 10.1038/nmeth.2019

Shaheen, S., Wan, Z., Haneef, K., Zeng, Y., Jing, W., and Liu, W. (2019). B cell mechanosensing: a mechanistic overview. *Adv. Immunol.* 144, 23–63. doi: 10.1016/bs.ai.2019.08.003

Shen, P., and Fillatreau, S. (2015). Antibody-independent functions of B cells: a focus on cytokines. *Nat. Rev. Immunol.* 15, 441–451. doi: 10.1038/nri3857

Shen, Z., Liu, S., Li, X., Wan, Z., Mao, Y., Chen, C., et al. (2019). Conformational change within the extracellular domain of B cell receptor in B cell activation upon antigen binding. *eLife* 8:42271. doi: 10.7554/eLife.42271

Siegmund, K., Zeis, T., Kunz, G., Rolink, T., Schaeren-Wiemers, N., and Pieters, J. (2011). Coronin 1-mediated naive T cell survival is essential for the development of autoimmune encephalomyelitis. *J. Immunol.* 186, 3452–3461. doi: 10.4049/jimmunol.1003491

Sokolova, O. S., Chemeris, A., Guo, S., Alioto, S. L., Gandhi, M., Padrick, S., et al. (2017). Structural basis of Arp2/3 complex inhibition by GMF, coronin, and arpin. *J. Mol. Biol.* 429, 237–248. doi: 10.1016/j.jmb.2016.11.030

Song, W., Liu, C., and Upadhyaya, A. (2014). The pivotal position of the actin cytoskeleton in the initiation and regulation of B cell receptor activation. *Biochim. Biophys. Acta* 1838, 569–578. doi: 10.1016/j.bbamem.2013.07.016

Sprenkeler, E. G. G., Webbers, S. D. S., and Kuijpers, T. W. (2020). When actin is not actin' like it should: a new category of distinct primary immunodeficiency disorders. *J. Innate Immun.* 13, 3–25. doi: 10.1159/000509717

Sun, X., Wang, J., Qin, T., Zhang, Y., Huang, L., Niu, L., et al. (2018). Dock8 regulates BCR signaling and activation of memory B cells via WASP and CD19. *Blood Adv.* 2, 401–413. doi: 10.1182/bloodadvances.2017007880

Tan, C., Noviski, M., Huizar, J., and Zikherman, J. (2019). Self-reactivity on a spectrum: A sliding scale of peripheral B cell tolerance. *Immunol. Rev.* 292, 37–60. doi: 10.1111/imr.12818

Tokarz-Deptula, B., Malinowska, M., Adamiak, M., and Deptula, W. (2016). Coronins and their role in immunological phenomena. *Cent. Eur. J. Immunol.* 41, 435–441. doi: 10.5114/ceji.2016.65143

Tolar, P. (2017). Cytoskeletal control of B cell responses to antigens. *Nat. Rev. Immunol.* 17, 621–634. doi: 10.1038/nri.2017.67

Treanor, B., Depoil, D., Bruckbauer, A., and Batista, F. D. (2011). Dynamic cortical actin remodeling by ERM proteins controls BCR microcluster organization and integrity. *J. Exp. Med.* 208, 1055–1068. doi: 10.1084/jem.20101125

Treanor, B., Depoil, D., Gonzalez-Granja, A., Barral, P., Weber, M., Dushek, O., et al. (2010). The membrane skeleton controls diffusion dynamics and signaling through the B cell receptor. *Immunity* 32, 187–199. doi: 10.1016/j.immuni.2009.12.005

Treanor, B., Harwood, N. E., and Batista, F. D. (2009). Microsignalosomes: spatially resolved receptor signalling. *Biochem. Soc. Trans.* 37, 1014–1018. doi: 10.1042/BST0371014

Volkmann, C., Brings, N., Becker, M., Hobeika, E., Yang, J., and Reth, M. (2016). Molecular requirements of the B-cell antigen receptor for sensing monovalent antigens. *EMBO J.* 35, 2371–2381. doi: 10.15252/embj.201694177

Volpi, S., Cicalese, M. P., Tuijnenburg, P., Tool, A. T. J., Cuadrado, E., Ahanchian, H., et al. (2019). A combined immunodeficiency with severe infections, inflammation and allergy caused by ARPC1B deficiency. *J. Allergy Clin. Immunol.* 143, 2296–2299. doi: 10.1016/j.jaci.2019.02.003

Wang, J. C., Bolger-Munro, M., and Gold, M. R. (2018). Imaging the Interactions Between B Cells and Antigen-Presenting Cells. *Methods Mol. Biol.* 1707, 131–161. doi: 10.1007/978-1-4939-7474-0_10

Wang, T., Cleary, R. A., Wang, R., and Tang, D. D. (2014). Glia maturation factor-gamma phosphorylation at Tyr-104 regulates actin dynamics and contraction in human airway smooth muscle. *Am. J. Respir. Cell Mol. Biol.* 51, 652–659. doi: 10.1165/rcmb.2014-0125OC

Weber, M., Treanor, B., Depoil, D., Shinohara, H., Harwood, N. E., Hikida, M., et al. (2008). Phospholipase C-gamma2 and Vav cooperate within signaling microclusters to propagate B cell spreading in response to membrane-bound antigen. *J. Exp. Med.* 205, 853–868. doi: 10.1084/jem.20072619

Ydenberg, C. A., Johnston, A., Weinstein, J., Bellavance, D., Jansen, S., and Goode, B. L. (2015). Combinatorial genetic analysis of a network of actin disassembly-promoting factors. *Cytoskeleton* 72, 349–361. doi: 10.1002/cm.21231

Ydenberg, C. A., Padrick, S. B., Sweeney, M. O., Gandhi, M., Sokolova, O., and Goode, B. L. (2013). GMF severs actin-Arp2/3 complex branch junctions by a cofilin-like mechanism. *Curr. Biol.* 23, 1037–1045. doi: 10.1016/j.cub.2013.04.058

Yuseff, M. I., Pierobon, P., Reversat, A., and Lennon-Dumenil, A. M. (2013). How B cells capture, process and present antigens: a crucial role for cell polarity. *Nat. Rev. Immunol.* 13, 475–486. doi: 10.1038/nri3469

Conflict of Interest: The authors declare that the research was conducted in the absence of any commercial or financial relationships that could be construed as a potential conflict of interest.

frontiers in Cell and Developmental Biology

ORIGINAL RESEARCH
published: 23 July 2021
doi: 10.3389/fcell.2021.673446

Increasing LFA-1 Expression Enhances Immune Synapse Architecture and T Cell Receptor Signaling in Jurkat E6.1 Cells

Chiara Cassioli[1†], Stefan Balint[2†], Ewoud B. Compeer[2], James H. Felce[2], Alessandra Gamberucci[3], Chiara Della Bella[4], Suet Ling Felce[5], Jlenia Brunetti[6], Salvatore Valvo[2], Daniela Pende[7], Mario M. D'Elios[4], Lorenzo Moretta[8], Michael L. Dustin[2] and Cosima T. Baldari[1]**

[1] Department of Life Sciences, University of Siena, Siena, Italy, [2] Kennedy Institute of Rheumatology, University of Oxford, Oxford, United Kingdom, [3] Department of Molecular and Developmental Medicine, University of Siena, Siena, Italy, [4] Department of Experimental and Clinical Medicine, University of Florence, Florence, Italy, [5] Nuffield Department of Medicine, University of Oxford, Oxford, United Kingdom, [6] Department of Medical Biotechnologies, University of Siena, Siena, Italy, [7] IRCCS Ospedale Policlinico San Martino, Genova, Italy, [8] Pediatric Hospital Bambino Gesù, Rome, Italy

The Jurkat E6.1 clone has been extensively used as a powerful tool for the genetic and biochemical dissection of the TCR signaling pathway. More recently, these cells have been exploited in imaging studies to identify key players in immunological synapse (IS) assembly in superantigen-specific conjugates and to track the dynamics of signaling molecules on glass surfaces coated with activating anti-CD3 antibodies. By comparison, Jurkat cells have been used only scantily for imaging on supported lipid bilayers (SLBs) incorporating laterally mobile TCR and integrin ligands, which allow to study synaptic rearrangements of surface molecules and the fine architecture of the mature IS, likely due to limitations in the assembly of immune synapses with well-defined architecture. Here we have explored whether upregulating the low levels of endogenous LFA-1 expression on Jurkat E6.1 cells through transduction with CD11a- and CD18-encoding lentiviruses can improve IS architecture. We show that, while forced LFA-1 expression did not affect TCR recruitment to the IS, E6.1 LFA-1^{high} cells assembled better structured synapses, with a tighter distribution of signaling-competent TCRs at the center of the IS. LFA-1 upregulation enhanced protein phosphotyrosine signaling on SLBs but not at the IS formed in conjugates with SEE-pulsed APCs, and led to the constitutive formation of an intracellular phosphotyrosine pool co-localizing with endosomal CD3ζ. This was paralleled by an increase in the levels of p-ZAP-70 and p-Erk both under basal conditions and following activation, and in enhanced Ca^{2+} mobilization from intracellular stores. The enhancement in early signaling E6.1 LFA-1^{high} cells did not affect expression of the early activation marker CD69 but led to an increase in IL-2 expression. Our results highlight a new role for LFA-1 in the core architecture of the IS that can be exploited to study the spatiotemporal redistribution of surface receptors on SLBs, thereby extending the potential of E6.1 cells and their derivatives for fine-scale imaging studies.

Keywords: cSMAC, TCR signaling, supported lipid bilayer (SLB), Jurkat cell, LFA-1

OPEN ACCESS

Edited by:
Sudha Kumari, Massachusetts Institute of Technology, United States

Reviewed by:
John Hammer, National Institutes of Health (NIH), United States
Navin Kumar Verma, Nanyang Technological University, Singapore
Francisco Sanchez-Madrid, Autonomous University of Madrid, Spain

***Correspondence:**
Michael L. Dustin
michael.dustin@kennedy.ox.ac.uk
Cosima T. Baldari
baldari@unisi.it

† These authors have contributed equally to this work

Specialty section:
This article was submitted to Cell Growth and Division, a section of the journal Frontiers in Cell and Developmental Biology

Received: *27 February 2021*
Accepted: *21 June 2021*
Published: *23 July 2021*

Citation:
Cassioli C, Balint S, Compeer EB, Felce JH, Gamberucci A, Della Bella C, Felce SL, Brunetti J, Valvo S, Pende D, D'Elios MM, Moretta L, Dustin ML and Baldari CT (2021) Increasing LFA-1 Expression Enhances Immune Synapse Architecture and T Cell Receptor Signaling in Jurkat E6.1 Cells. Front. Cell Dev. Biol. 9:673446. doi: 10.3389/fcell.2021.673446

INTRODUCTION

T cell immunological synapses (IS) are specialized cell-cell junctions between T cells and antigen presenting cells (APC) that are stable, demarcated by adhesion molecules and mediate vectoral cell–cell communication through a synaptic cleft (Dustin and Colman, 2002). Kupfer described the classical architecture of T-cell activation by APCs organized into supramolecular activation clusters (SMACs) with a ring of adhesive LFA-1-ICAM1 interactions forming the peripheral (p)SMAC and a central cluster of TCR in the central (c)SMAC (Monks et al., 1998), which together define the IS (Norcross et al., 1984; Dustin and Springer, 1998). The dynamic formation of ISs were first observed with supported lipid bilayers (SLB) presenting laterally mobile ICAM-1 and pMHC complexes, which enable formation of SMACs through a T cell autonomous process (Grakoui et al., 1999). Not only does LFA-1 mediate key interactions in the pSMAC, but the higher level of LFA-1 expression on memory versus naïve CD8 T cells is associated with more stable IS (Mayya et al., 2018), although this correlation has not been further tested for causality. In addition to lateral movement of LFA-1 and TCR in the plane of the plasma membrane, vesicular trafficking also plays a key role in IS formation (Onnis and Baldari, 2019; Mastrogiovanni et al., 2020). Early IS formation studies with cellular or SLB-based antigen presentation required use of primary T cells from transgenic mice. The use of readily available cell lines such as Jurkat would be advantageous for a number of reasons.

The acute T cell leukemia-derived Jurkat cell line has represented a robust tool to study T cell signaling, allowing for the biochemical and genetic identification of key players in the TCR signaling cascade (Abraham and Weiss, 2004). Jurkat cells activated by the Raji B lymphoblastoid cell line and staphylococcal superantigen E (SEE) have been useful, but do not provide fine resolution of IS structures (Blanchard et al., 2002). Jurkat cells have also been instrumental in reconstructing the dynamics of signaling molecules following TCR triggering when plated on glass surfaces coated with activating anti-CD3 antibodies through live imaging of transfected fluorescent reporters (Bunnell et al., 2001, 2002), which has been further refined with speckle microscopy (Kaizuka et al., 2007) and super-resolution methods (Fritzsche et al., 2017). This system led to the discovery that an F-actin ring is formed as T cells spread on surfaces with central clearance of F-actin (Bunnell et al., 2001). This central F-actin clearance with the formation of gaps in the mesh is a defining characteristic of the secretory domain that is critical for effector function (Ritter et al., 2015, 2017). A major intrinsic limitation of this approach is that, since the activating antibodies are immobile, the cells are unable to reorganize surface receptors and integrins to form the characteristic SMAC-based architecture of an IS and the method is only used to model early events in T-cell activation. The general strategy to efficiently incorporate laterally mobile antibodies into SLBs (Carrasco et al., 2004) made it possible to present laterally mobile anti-CD3 and ICAM1 to generate a Jurkat based IS model, however, in this setting TCR microclusters interspersed with LFA-1 clusters (Kaizuka et al., 2007, 2009; Murugesan et al., 2016; Chen et al., 2017), which are instead better separated with a more compact central TCR cluster in primary $CD4^+$ T cells (Grakoui et al., 1999; Varma et al., 2006; Kumari et al., 2015).

Here, we have sought to improve IS architecture using an engineered Jurkat subline. Several clones have been derived from the original Jurkat line (**Table 1**). The most widely used to dissect TCR signaling is clone E6.1 (Weiss et al., 1984), from which subclones lacking individual TCR/CD3 components, integrin subunits or signaling molecules, such as Lck, ZAP-70, LAT, SLP-76, PLCγ, or CARMA-1, have been derived by mutagenesis (Abraham and Weiss, 2004). The basis for the less defined architecture of the IS formed by Jurkat E6.1 cells is not clear, but could include low levels of the integrin LFA-1 (CD11a/CD18) or associated co-factors such as talin and paxillin (Harburger and Calderwood, 2009). This limits the suitability of Jurkat E6.1 cells to track the dynamics of protein reorganization during IS assembly using SLB-based live imaging. Here we investigate whether increasing LFA-1 expression in Jurkat E6.1 cells can improve the architecture of ISs in the SLB setting. The results show that forcing increased LFA-1 surface expression by lentiviral transduction enhanced TCR segregation to the center of the cSMAC and local phosphotyrosine signaling. Forced LFA-1 expression did not enhance either the efficiency of TCR or tyrosine phosphoprotein accumulation at the IS formed by E6.1 cells in the setting of SEE-specific conjugates, but improved their ability to signal in response to TCR engagement, leading to increased IL-2 expression. Additionally, forced LFA-1 expression enhanced basal TCR signaling and accumulation of tyrosine phosphoproteins at $CD3\zeta^+$ endosomes. The results highlight a new role for LFA-1 in the core architecture of the IS formed by E6.1 cells that can be exploited to study the spatiotemporal redistribution of surface receptors on SLBs, thereby extending the potential of E6.1 cells and their derivatives for the study of T cell autonomous IS formation.

MATERIALS AND METHODS

Cells and Lentiviral Transduction

Cells lines included Jurkat T cell clones E6.1 (Weiss et al., 1984) (obtained from ATCC) and JA3 (Moretta et al., 1985), and Raji B cells. A E6-1 line expressing high levels of LFA-1 was obtained by transduction with lentiviruses encoding LFA-1 subunits CD11a and CD18. Expression vectors for CD11a and CD18 were generated by insertion of their respective full-length genes into the lentiviral expression vector pHR. Genes were synthesized including terminal STOP codons and flanked by a 5′ *Mlu*I restriction exonuclease site and GCCACC Kozak sequence, and a 3′ *Not*I restriction site (GeneArt Gene Synthesis, ThermoFisher Scientific). Fragments were inserted into pHR vector via *Mlu*I + *Not*I restriction digestion and ligation by T4 DNA ligase. Lentiviruses were produced in HEK 293T

TABLE 1 | Jurkat cell genealogy.

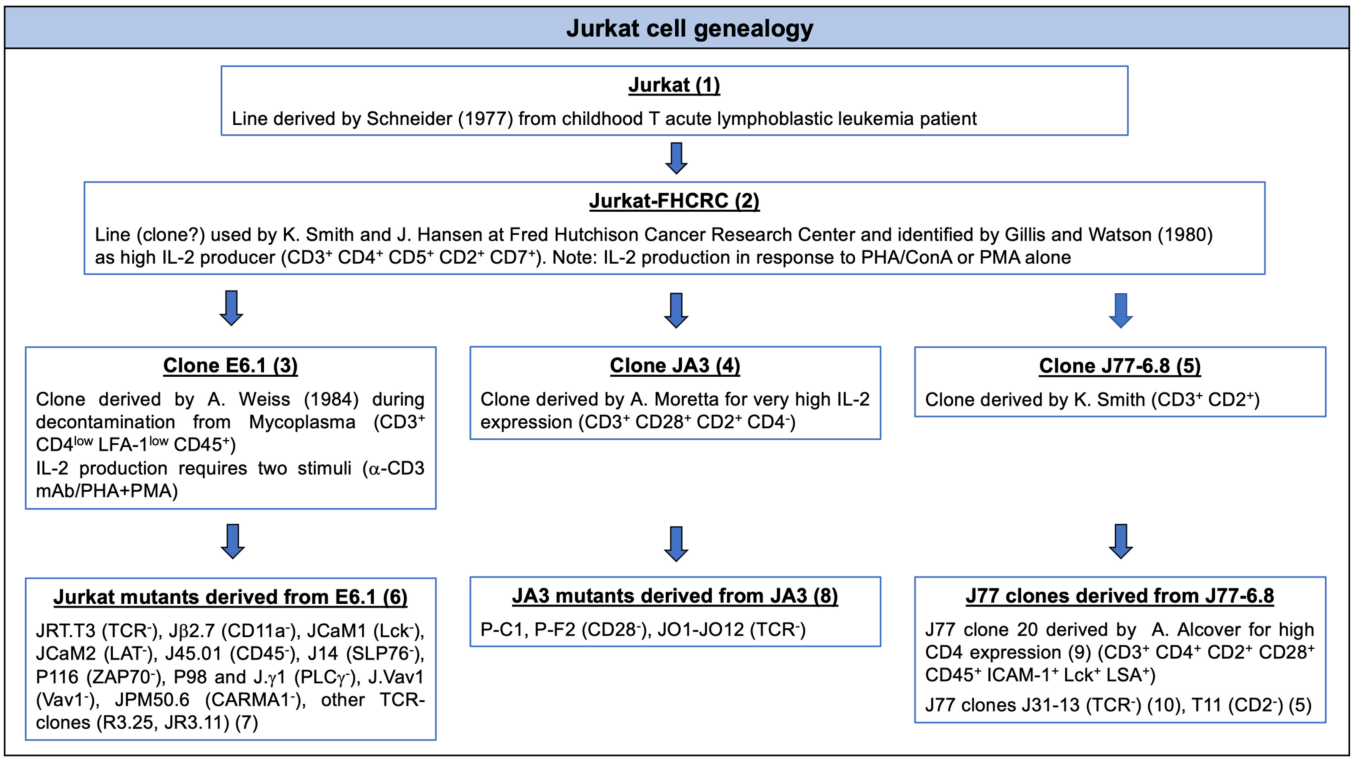

(1) Schneider et al. (1977) Int J Cancer 19, 621.6

(2) Gillis and Watson (1980) J Exp Med 152, 1709-1719 (mentions gift Jurkat-FHCRC_w/o ref)

(3) Weiss et al. (1984) J Immunol 133, 123-128

(4) Moretta et al. (1985) J Exp Med 162, 823-838

(5) Moingeon et al. (1988) J Exp Med 168, 2077-2090 (mentions gift J77-6.8 w/o ref and generation of clones)

(6) Abraham and Weiss (2004) Nat Rev Immunol 4, 301-308

(7) Rubin et al. (2000) Scand J Immunol 52, 173-183

(8) Moretta et al. (1987) Proc Natl Acad Sci USA 84, 1654-1658

(9) Alcover et al. (1988) EMBO J 7, 1973-1977

(10) Danielian et al. (1992) Eur J Immunol 22, 2915-2921

cells at 3 × 10^5/ml, 2 ml/well in 6-well plates in DMEM (#11960044) + 10% FBS (#15595309), 1% Glu (#25030-024), 1% Pen/Strep (#15140-122), all from Thermo Scientific. GeneJuice transfection was performed with vectors pHR-CD11a and pHR-CD18, pP8.91, and pMD.G. After 3 days of culture, supernatant was removed, spun at 500g for 5 min and passed through a 0.45 μm syringe filter. This virus solution was mixed with polybrene and spun down with Jurkat cells at 800 g for 90 min (RT, dec 6, acc 4). Cells were grown for >48 h at 37°C, 5% CO_2 and passaged twice before stocks were frozen. Transduction efficiency was near 100% such that no selection was necessary. Experiments were performed with E6.1 LFA1^{high} cells from two transductions and the transduced cells were not used more than 10 passages. We used the validated ATCC E6.1 as a control for experiments in this paper. We note that E6.1 cells transduced with LifeAct-GFP (Fritzsche et al., 2017) and CXCR4-HaloTag (Felce et al., 2020) using the same lentiviral system showed no change in LFA-1 expression or IS organization compared to the untransduced ATCC E6.1 cells (unpublished observations).

Cells were cultured in RPMI 1640 medium (Life Technologies, #31870074) supplemented with 10% (vol/vol) FBS, 2 mM L-glutamine and 50 U/ml of Penicillin-Streptomycin at a max density of 1.5 × 10^6/ml.

RNA-seq Analysis

Raw counts for publicly deposited RNA-seq datasets (as used in Felce et al., 2021; Jurkat E6.1: GEO: GSE145453, Expression Atlas: E-MTAB-2706, GEO: GSE93435; Primary T cells: GEO: GSE122735, NCBI SRA: SRP026389, Expression Atlas: E-MTAB-3827) were normalized for gene length and *ACTB* mRNA counts. Fold difference was calculated as the mean normalized count in Jurkat samples relative to each primary T cell sample.

Flow Cytometry

To assess surface expression of CD11a and CD3ε on Jurkat cells, 0.25 × 10^6 cells/sample were washed and blocked with

2% FBS/PBS for 30 min at 4°C and then stained with anti-CD3ε-Alexa Fluor 488 (BioLegend, #317310) and anti-CD11a (ThermoFisher, #MA11A10) conjugated in house with Alexa Fluor 647 (ThermoFisher, #A20006), at 10 μg/mL for 30 min at 4°C. Finally, cells were washed three times in 2% FBS/PBS, fixed in 2% PFA/PBS, analyzed by LSRFortesa (BD Biosciences) with BD FACSDiva software and plotted using FlowJo version 10.

Flow cytometric analysis of surface CD69 was carried out using FITC anti-CD69, clone FN50 (BioLegend, #310904) at 1 μg/ml for 30 min at 4°C. Samples were analyzed with Guava Easy Cyte Cytometer (Millipore) and plotted using FlowJo version 6.1.1.

IL-2 intracellular staining flow cytometry was carried out using APC-labeled anti-human IL-2, clone MQ1-17H12 (BioLegend, #500310), at 0.125 μg/5 × 10^5 cells. Samples were analyzed using a Becton Dickinson FACS CANTO II with BD FACSDiva 6.0 software.

For all experiments unstained cells and isotype controls were performed for background correction and gating.

SLBs Preparation and Use

Planar Supported Lipid Bilayers (SLBs) were formed as previously described (Saliba et al., 2019). In brief, glass coverslips were cleaned with piranha solution (30% H_2O_2 and 70% H_2SO_4), rinsed extensively, dried, negatively charged through plasma cleaning, and assembled with a six-channel sticky-Slide VI 0.4 (Ibidi, #80608). SLBs were formed by filling each channel with a suspension of small unilamellar vesicles composed of 1,2-dioleoyl-*sn*-glycero-3-[*N*-(5-amino-1-carboxypentyp) succinyl] (12.5% mol) and 1,2-dioleoyl-*sn*-glycero-3-phosphoethanolamine-*N*-cap biotinyl (0.05% mol) in 1,2-dioleoyl-*sn*-glycero-3-phosphocholine at a total lipid concentration of 0.4 mM (Avanti Polar Lipids). SLBs were blocked with 5% casein (Sigma-Aldrich) in PBS containing 100 μM $NiSO_4$. His-tagged proteins were incubated on bilayers for additional 20 min to obtain histidine-tagged–conjugated mouse ICAM1 at 200 molecules/μm^2, histidine-tagged–conjugated UCHT1-Fab′ fragments at 30 molecules/μm^2, and histidine-tagged–conjugated human CD80 at 100 molecules/μm^2. Unbound proteins were flushed out with HEPES Buffered Salin Solution supplemented with 0.1% Human Serum Albumin (Calbiochem). Protein concentrations required to achieve desired densities on bilayers were calculated from calibration curves constructed from flow-cytometric measurements of bead-SLB, compared with reference beads containing known numbers of the appropriate fluorescent dyes (Bangs Laboratories). Bilayers were continuous liquid disordered phase as determined by fluorescence recovery after photobleaching with a 10 μm-bleach spot on an FV1200 confocal microscope (Olympus).

Jurkat cells were incubated at 37°C on SLB containing fluorescently labeled ICAM1-Alexa Fluor-405 and UCHT1-Fab'-CF568 and unlabeled CD80. After 15 min of incubation cells were fixed with 4% electron microscopy grade formaldehyde in PBS for 30 min at RT and washed three times with PBS. For intracellular staining, fixed cells were permeabilized and blocked with 0.01% Triton X-100 (Sigma-Aldrich, #X100-5ML) in blocking buffer (5% BSA/PBS) for 1 h at RT, washed three times with PBS, and stained with anti-CD3ζ Alexa Fluor-647 (SantaCruz, #SC-1239 AF647), anti-pTyr Alexa Fluor-488 (Biolegend, #309306) at 10 μg/mL in 5% BSA/PBS for 1 h at RT followed by three times washing with PBS. Cells were also stained with Alexa Fluor-405 Phalloidin (Thermo Fisher Scientific, # A30104) to highlight actin cytoskeleton.

Conjugate Formation

Conjugates between Jurkat cells and SEE-pulsed Raji B cells were carried out as previously described (Finetti et al., 2009). Raji cells were pulsed for 2 h with 10 μg/ml SEE (Toxin Technology, Sarasota, FL, United States) and labeled with 10 μM Cell Tracker Blue (Molecular Probes) for the last 20 min. Conjugates between T cells and unpulsed B cells were used as negative controls. SEE-pulsed or unpulsed Raji B cells were mixed with Jurkat T cells (1:1) and conjugates analyzed 15 min after their formation. Samples were allowed to adhere for 15 min on poly-L-lysine (Sigma-Aldrich)-coated wells of diagnostic microscope slides (ThermoFisher Scientific), then fixed by immersion in methanol for 10 min at -20°C. Following fixation, samples were washed in PBS and incubated with anti-pTyr (Cell Signaling, #8954) at 10 μg/mL and anti-CD3ζ at 15 μg/mL (SantaCruz, #sc-1239) in PBS 1X overnight at 4°C. After washing in PBS, samples were incubated for 45 min at room temperature with anti-rabbit Alexa-Fluor-488- and anti-mouse Alexa-Fluor-555-labeled secondary antibodies (ThermoFisher Scientific, #A11008 and #A211422, respectively).

Fluorescence Microscopy

TIRFM was performed on an Olympus IX83 inverted microscope equipped with a 4-line (405, 488, 561, and 640 nm laser) illumination system. The system was fitted with an Olympus UApON 150 × 1.45 NA objective, and a Photomertrics Evolve delta EMCCD camera to provide Nyquist sampling. Analysis of TIRFM images was performed with ImageJ (National Institute of Health). Mean fluorescence intensities of ICAM-1, CD3ε, CD3ζ, pTyr and phalloidin were calculated as the sum of intensities in each pixel in the cell spreading area divided by the spreading area of the corresponding cell. The spreading area was determined by thresholding the IRM (Interference Reflection Microscopy) images of each cell.

Intensity compactness of CD3ε clusters represents how compact the intensity signal from each CD3ε cluster is within the defined area. If the CD3ε clusters are concentrated around the center of the defined area, the intensity compactness is closer to 1. If the CD3ε clusters are more sparsely and heterogeneously distributed within the defined area, the value goes toward 0. The area to calculate the intensity of compactness was defined by the cSMAC of Jurkat cells. The ImageJ plugin to calculate the intensity compactness was kindly provided by Prof. Jérémie Rossy (Biotechnology Institute Thurgau, University of Konstanz, Switzerland).

Confocal microscopy imaging of Jurkat cells on SLB was carried out on a Zeiss LSM980 (Zeiss, Germany) using a 63 × 1.40 NA oil immersion objective. Cells were stained as for TIRF microscopy and 3D confocal imaging was carried out at 200 nm z-steps. The orthogonal views and 3D reconstruction of images was performed using ImageJ (National Institute of Health).

Confocal microscopy of cell–cell conjugates was carried out on a Zeiss LSM700 (Zeiss, Germany) using a 63x/1.40 oil immersion objective. Images were acquired with pinholes opened to obtain 0.8 μm-thick sections. Detectors were set to detect an optimal signal below the saturation limits. Images were processed with Zen 2009 image software (Carl Zeiss, Jena, Germany). The quantitative co-localization analysis of pTyr with CD3ζ in E6.1 LFA-1^{high} cells was performed on median optical sections using ImageJ and JACoP plug-in to determine Manders' coefficient M1 (Manders et al., 1992). Scoring of conjugates for pTyr clustering at the IS was based on the concentration of the respective staining solely at the T-cell:APC contact. The recruitment index of pTyr was calculated as either the relative fluorescence at the T-cell:APC contact site compared to the mean fluorescence of three membrane regions with the same area outside of the contact (**Figure 3B**) or the relative fluorescence at the T-cell:APC contact site compared to the entire cell, either excluding (**Figure 3D**) or including (**Figure 3C**) the fluorescence of the constitutive intracellular pTyr pool. 3D confocal imaging of conjugates was carried out on a Leica TCS SP8 (Leica, Germany) at 220 nm z-steps. The orthogonal views and 3D reconstruction of images were performed using ImageJ (NIH).

Cell Activation for Immunoblot and Flow Cytometric Analysis of Activation Markers

For immunoblot experiments 12-well plates were coated with 5 μg/ml of anti-CD3ε mAb, clone OKT3 (BioLegend, #317302) and 1 μg/ml of ICAM1 Fc (R&D System, #720-IC) in PBS 1X overnight at 4°C or for 2 h at 37°C, followed by extensive rinse with PBS 1X. Cells (2.5×10^6 cells/sample) were pelleted, resuspended in serum-free RPMI-1640 at the density of 1×10^6 cells/ml, then seeded on non-activating (ICAM-1) or activating (ICAM-1 + anti-CD3ε) plates and incubated for 5 or 20 min at 37°C, 5% CO_2. Unstimulated samples were included as negative controls.

For the quantification of T-cell activation Jurkat cells (0.15×10^6 cells/sample) seeded on either plate-bound anti-CD3ε or anti-CD3ε + ICAM-1 and incubated for 16 h at 37°C, 5% CO_2. Surface CD69 was quantified by flow cytometry. T cells activated with 100 ng/ml PMA and 500 ng/ml A23187 were used as positive control. For IL-2 measurements, 10^6 cells were activated on plate-bound anti-CD3ε mAb, clone OKT3 (BioLegend, #317302) and anti-CD28 mAb, clone CD28.2, all at 5 μg/ml in PBS 1X (BioLegend, #302902) for 6 h. After 1 h incubation, the protein transport inhibitor cocktail containing brefeldin A and monensin (eBioscience, #00-4980-93) was added (2 μl/ml). Membrane permeabilization was done by BD cytofix/cytoperm fixation/permeabilization kit (BD Bioscience, #554714) according to the manufacturer's protocol prior to processing samples for flow cytometry.

Immunoblots

Cells (2.5×10^6 cells/sample) were pelleted, washed twice in ice-cold PBS and lysed in 25 μl lysis buffer (1% Triton X-100 in 20 mM Tris-HCl, pH 8.0, 150 mM NaCl) in the presence of Protease Inhibitor Cocktail Set III (Calbiochem) and 0.2 mg of the phosphatase inhibitor sodium orthovanadate (Sigma-Aldrich). Quantification of total protein content was carried out using the Quantum Protein Assay Kit according to manufacturer's protocol (EuroClone). Post-nuclear supernatants were denatured in 4X Bolt™ LDS Sample Buffer (Invitrogen) supplemented with 10X Bolt™ LDS Sample Buffer (Invitrogen) for 5 min at 100°C. Proteins were subjected to SDS-PAGE on Bolt™ Bis-Tris Mini Protein Gels (Invitrogen) and transferred to nitrocellulose (GE HealthCare) under wet conditions. Blocking was performed in 5% non-fat dry milk in PBS 0.02% Tween-20. Membranes were incubated with anti-p-ZAP70 Y319 (Cell Signaling, #2701) and anti-p-Erk1/2 T202/Y204 (Cell Signaling, #9101) primary antibodies at RT followed by secondary horseradish-peroxidase (HRP)-conjugated antibodies for 45 min at RT. Secondary antibodies were detected by using SuperSignal™ West Pico Plus Chemiluminescent Substrates (ThermoFisher Scientific). Membranes were stripped with ReBlot Plus Mild Antibody Stripping Solution 10X (Chemicon) and reprobed with anti-ZAP70 (Merck Millipore, #05-253) and anti-Erk2 (SantaCruz, #sc-1647) control antibodies. Blots were scanned using a laser densitometer (ET-M2170; EPSON, Suwa, Yapan) and quantified using ImageJ (NIH).

[Ca^{2+}] Measurements

Jurkat cells were loaded with the fluorescent calcium indicator Fura- 2 acetoxymetyl ester (Fura-2/AM) to evaluate changes of cytosolic free calcium concentration as described (Gamberucci et al., 1994). Briefly, after Fura-2-AM (3 μM) loading for 30 min at RT, the cells were maintained in medium (140 mM NaCl, 5.4 mM KCl, 1 mM MgCl2, 1 mM $CaCl_2$, 10 mM glucose, 15 mM Hepes buffer, pH 7.4). Aliquots were rapidly centrifuged and resuspended in fresh nominally Ca^{2+} free medium at the density of 2×10^6 cells/1 ml: cytosolic Ca^{2+} basal levels were obtained by adding Na-ethylene glycol bis(B-amino ethyl ether)-N,N,N0,N0 tetraacetic acid (EGTA) to nominally Ca^{2+} free medium to eliminate possible calcium traces; reticular Ca^{2+} was evaluated after depletion of the stores with anti-CD3ε mAb, clone OKT3 at 1.3 μg/ml (BioLegend, #317302) followed by cross-linking with anti-mouse IgG at 10 μg/ml. The subsequent Ca^{2+} influx through the plasma membrane channels was evaluated by re-adding 1.7 mM $CaCl_2$.

Fura-2 fluorescence was measured using a Varian Cary Eclipse fluorescence spectrophotometer (Palo Alto, CA, United States) (excitation wavelengths, 340 and 380 nm; emission, 510 nm) equipped with magnetic stirring and temperature control set at 35°C. At the end of each experiment, digitonin (20 mg/ml) and EGTA (10 mM) (Sigma-Aldrich) were added in order to measure maximal (Rmax) and minimal (Rmin) ratio (340/380) fluorescence values, respectively. The equation $[Ca^{2+}]_i = (R\text{-}R_{min})/(R_{max}\text{-}R)Sf^*Kd$ was used to convert the Fura-2 ratio values to intracellular calcium concentrations.

Total $[Ca^{2+}]_i$ release over time was quantified by measuring the Area Under the Curve (AUC) that represents the area enclosed under the curve of the $[Ca^{2+}]_i$ versus the time for 4 min after OKT3 addition; AUC was calculated using GraphPad Prism version 7.00 (La Jolla, CA, United States).

Statistics

The number of repeats and the number of cells analyzed is specified in each figure legend. Statistical analyses were performed using GraphPad Software (La Jolla, CA, United States). Pairwise or multiple comparisons among values with normal distribution were carried out by using Student's *t*-test (paired or unpaired) and one-way ANOVA with Tukey's *post hoc* test, whereas values without Gaussian distribution were analyzed with Mann–Whitney test or Kruskal–Wallis test. Statistical significance was defined as: ns $p > 0.05$, $^{*}p \leq 0.05$, $^{**}p \leq 0.01$, $^{***}p \leq 0.001$, $^{****}p \leq 0.0001$.

RESULTS

Forced LFA-1 Expression in E6.1 Cells Improves TCR Segregation to the cSMAC Center

Transcriptomic comparison of E6.1 cells against primary $CD4^{+}$ T cells using RNA-seq (public datasets as used in Felce et al., 2021) revealed that primary T cells have 8.7 ± 5.5 times more *ITGAL* mRNA (encoding CD11a) and 7.1 ± 2.6 times more *ITG2B* mRNA (encoding CD18) than E6.1 cells. To investigate whether the amount of surface LFA-1 influences the core architecture of the IS formed by two most commonly used Jurkat cell lines, E6.1 (Weiss et al., 1984) and JA3 (Moretta et al., 1985), we first measured the surface expression levels of CD11a and CD3ε by flow cytometry. Surface expression levels of CD11a on both cell lines were comparable (**Figure 1A** and **Supplementary Figure 1A**). Both lines displayed comparable levels of surface CD3ε and showed the presence of a $CD3\varepsilon^{low}$ population that was more abundant among JA3 cells (**Supplementary Figure 1B**).

To assess the bull's eye pattern of the mature IS architecture, cells were plated on SLB containing an agonistic anti-CD3ε (UCHT1) Fab′ fragment labeled with CF568 and the LFA-1 ligand ICAM-1 directly conjugated with Alexa Fluor-405, and analyzed by total internal reflection fluorescence microscopy (TIRFM) (**Figure 1B** and **Supplementary Figures 2A,B**). Cells were plated for 15 min, a time point at which, in primary T cells, the TCR and LFA-1 have segregated into the cSMAC and pSMAC, respectively. Slightly higher levels of CD3ε were observed at the interface of JA3 cells compared to E6.1 cells with SLB, as measured by mean fluorescence intensity (MFI) of the UCHT1 signal at the SLB (**Figure 1C**). This small increase was due to the smaller cell spreading area of JA3 cells (**Supplementary Figure 3**). Of note, similar to E6.1 cells, JA3 cells formed an ICAM-1 ring, which can only be elicited in the presence of a strong TCR signal, indicating that the presence of a more abundant population of $CD3\varepsilon^{low}$ among JA3 cells does not compromise their ability to assemble immune synapses. The levels of LFA-1 measured by mean fluorescence intensity of ICAM-1 on SLBs were not significantly different between E6.1 and JA3 (**Figure 1D**), supporting the results obtained by flow cytometry (**Figure 1A** and **Supplementary Figure 1A**). Hence both Jurkat cell lines have similar capability of CD3 transport that underlies TCR spatial organization and signaling at the IS (Onnis and Baldari, 2019). However, by assessing the images in **Figure 1B** and **Supplementary Figures 2A,B**, JA3 cells formed more compact and tighter CD3-enriched cSMACs within the ICAM-1-enriched ring compared to E6.1 cells. This was confirmed by measuring intensity compactness to quantify the distribution of CD3ε clusters within the cSMAC of E6.1 and JA3 cells (see section "Materials and Methods" for description). We observed significant differences between the two cell lines, with CD3ε clusters showing a lower compactness in E6.1 cells compared to JA3 cells (**Figure 1E**).

As mentioned above, primary T cells have approximately 9 times more LFA-1 than E6.1 Jurkat cells and are known to form compact CD3ε-enriched cSMAC (Demetriou et al., 2020). To directly address whether increasing LFA-1 levels could improve cSMAC formation in E6.1 cells, we transduced these cells with lentiviruses encoding human CD11a and CD18, generating the E6.1 LFA-1^{high} line. E6.1 LFA-1^{high} cells expressed higher levels of surface LFA-1 compared to both parental E6.1 cells (∼2-fold) and JA3 cells (∼3-fold), as assessed by flow cytometry (**Figure 1A** and **Supplementary Figure 1A**). CD3ε surface levels were comparable across Jurkat cell lines (**Supplementary Figure 1B**).

To analyze TCR compartmentalization at the cSMAC, E6.1 LFA-1^{high} cells were plated on SLBs as for E6.1 and JA3, and analyzed by TIRFM (**Figure 1B** and **Supplementary Figure 2C**). As expected, forced LFA-1 expression in E6.1 cells increased the amount of ICAM-1-engaged LFA-1 on SLBs (**Figure 1D**). E6.1 LFA-1^{high} cells formed a tight and compact CD3ε-enriched cSMAC within the ICAM-1-enriched ring (**Figures 1B,E** and **Supplementary Figure 2C**), with a similar cell spreading area (**Supplementary Figure 3**) but an increase in the levels of CD3ε at the interface with the SLB compared to E6.1 cells (**Figure 1C**). Together, these data demonstrate that LFA-1 enhances the efficiency of TCR recruitment to the cSMAC and facilitates the formation of the core IS architecture.

Increasing LFA-1 Expression in E6.1 Cells Improves Phosphotyrosine Signaling at the IS Formed on Activating SLBs but Not in SEE-Specific Cell Conjugates

To understand whether the increased levels of LFA-1 can enhance signaling, we measured the accumulation of tyrosine phosphoproteins at the IS formed in the SLB setting. E6.1, E6.1 LFA-1^{high} and JA3 cells were plated on SLBs containing an agonistic anti-CD3ε (UCHT1) Fab' fragment labeled with CF568 and the LFA-1 ligand ICAM-1 directly conjugated with Alexa Fluor-405 for 15 min and analyzed by TIRFM (**Figure 2A** and **Supplementary Figure 4**). After fixation and permeabilization, cells were stained with directly conjugated primary antibodies against anti-CD3ζ Alexa Fluor-647, anti-phosphotyrosine (pTyr) Alexa-Fluor-488, and phalloidin Alexa Fluor-405 to visualize the underlying actin cytoskeleton (**Figure 2A** and **Supplementary Figure 4**). Again, JA3 cells had smaller spreading areas (**Figure 2B**) with levels of CD3ε and CD3ζ accumulation comparable to E6.1 and E6.1 LFA-1^{high} cells, while accumulation was higher in E6.1 LFA-1^{high} cells compared to E6.1 cells

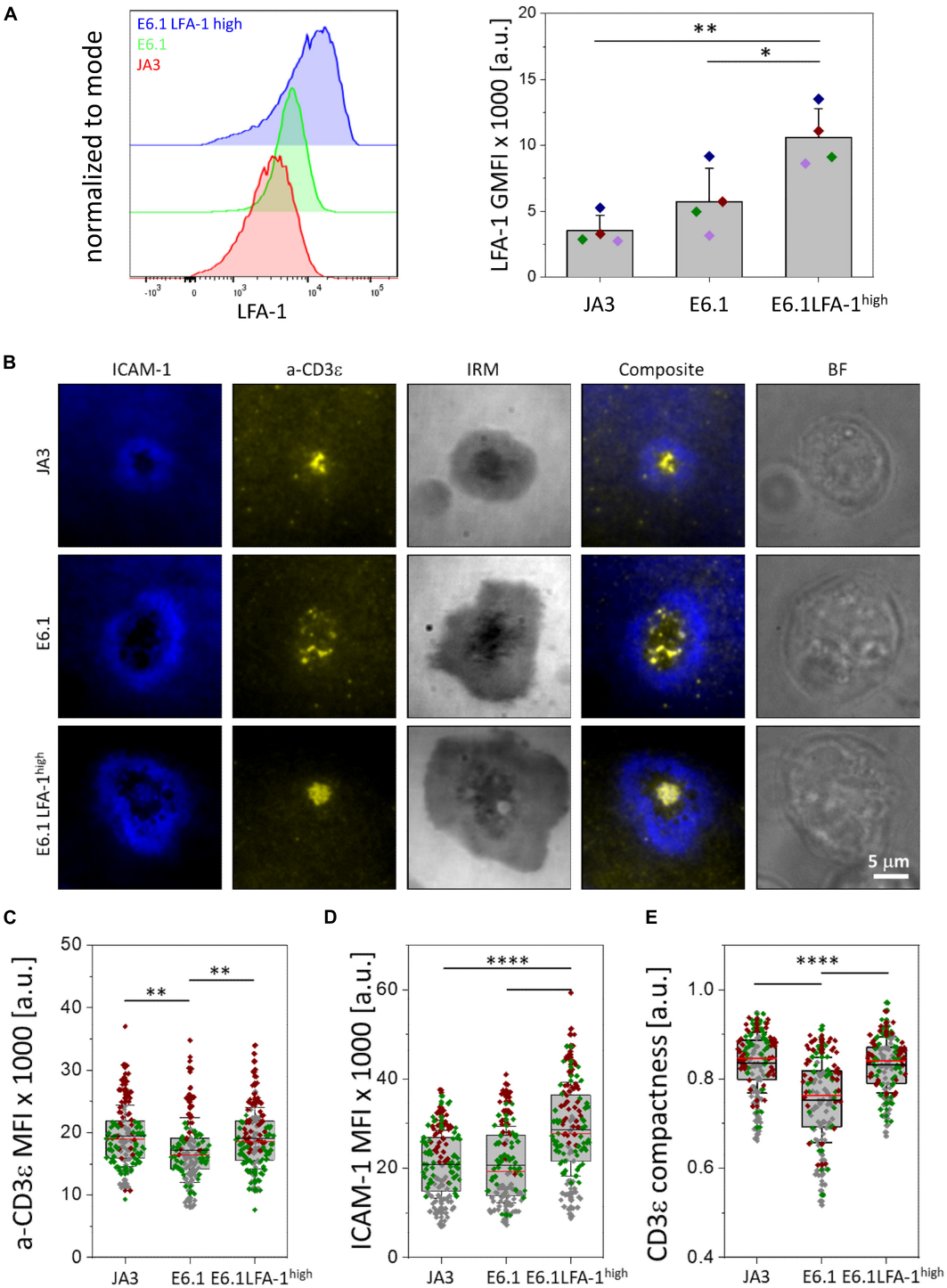

FIGURE 1 | Increasing LFA-1 expression in E6.1 cells improves TCR segregation to the cSMAC center. **(A)** Flow cytometric analysis of surface expression of LFA-1 (CD11a) on JA3, E6.1 and E6.1 LFA-1^{high} Jurkat cells. Representative FACS plots of LFA-1 are shown. The histogram shows GMFI of LFA-1 (mean ± SD). **(B)** Representative TIRFM images of E6.1, E6.1 LFA-1^{high} or JA3 Jurkat cells interacting with activating [ICAM1-AF405 (blue) + anti-CD3ε UCHT1-CF568 Fab' (yellow)] SLBs for 15 min. IRM, interference reflection microscopy; BF, bright field. Scale bar, 5 µm. **(C,D)** Quantification of the corresponding mean fluorescent intensity (MFI) of anti-CD3ε **(C)** and ICAM-1 **(D)** from the different Jurkat lines as in **(B)**. **(E)** Quantification of the CD3ε compactness at the cSMAC from the experiment in **(B)**. Horizontal lines and error bars represent mean ± SD (black line) and median (red line). Gray boxes represent 25-75 percentile. Data are from minimum of 120 cells from three independent experiments; each dot represents a cell; each color represents an independent experiment. One-way analysis of variance (ANOVA) with Tukey's *post hoc* test. Only significant differences are shown. *$p < 0.05$; **$p < 0.01$; ****$p < 0.0001$.

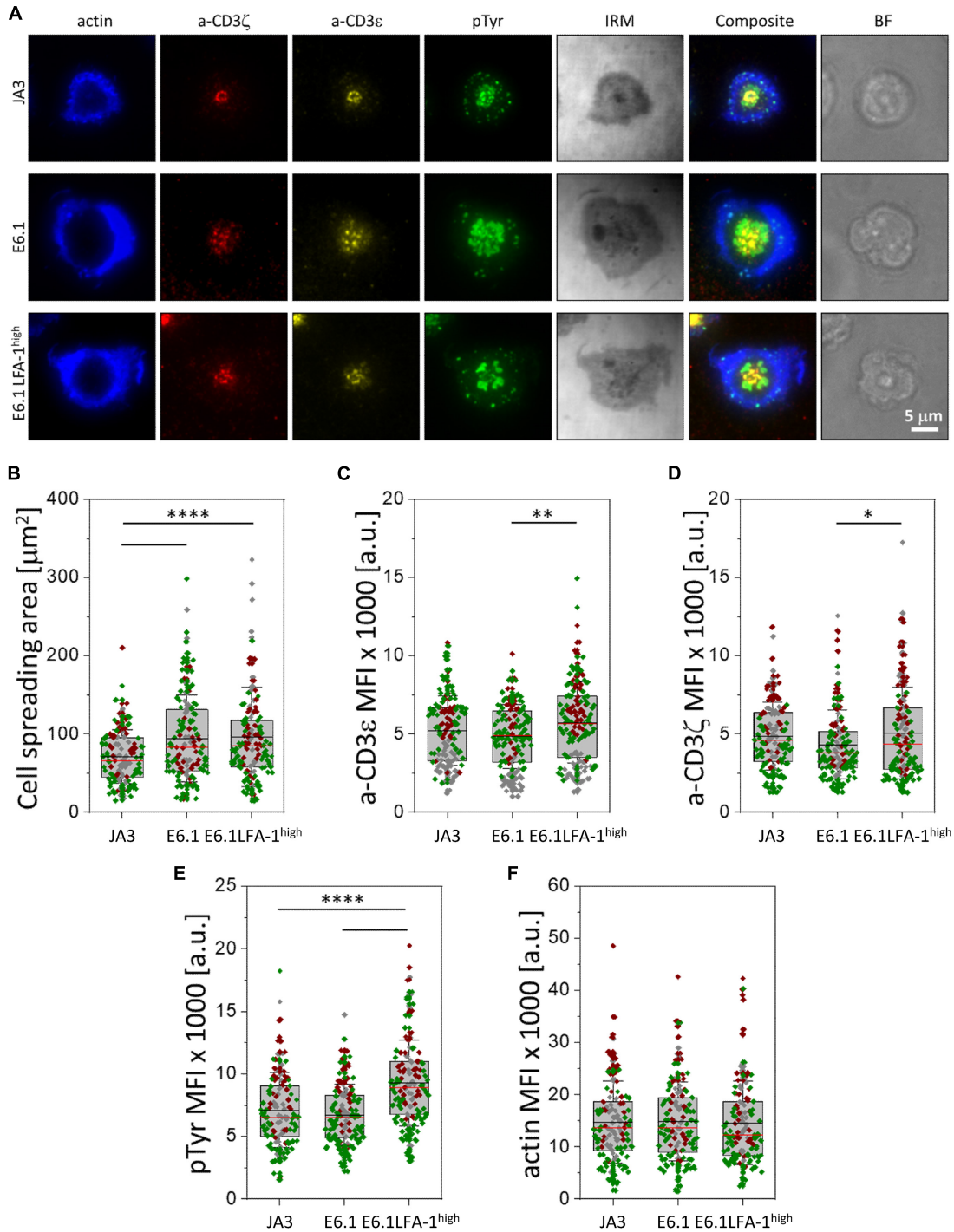

FIGURE 2 | Increasing LFA-1 expression in E6.1 cells improves phosphotyrosine signaling at the cSMAC. **(A)** Representative TIRFM images of E6.1, E6.1 LFA-1^{high} or JA3 Jurkat cells interacting with activating [ICAM1 + anti-CD3ε UCHT1-CF568 Fab' (yellow)] SLB for 15 min. Cells were permeabilized and stained with directly conjugated primary antibodies against anti-CD3ζ-AF647 (red), anti-phosphotyrosine [pTyr-AF488 (green)]; the cell actin cytoskeleton was labeled with phalloidin-AF405 (blue). IRM, interference reflection microscopy; BF, bright field. Scale bar, 5 µm. **(B)** Quantification of cell spreading area of different Jurkat cell lines on activating SLB as in **(A)**. Corresponding mean fluorescent intensity (MFI) of anti-CD3ε **(C)**, anti-CD3ζ **(D)**, anti-pTyr **(E)** and actin **(F)** from different Jurkat cell lines as in **(A)**. Horizontal lines and error bars represent mean ± SD (black line) and median (red line). Gray box represents 25–75 percentile. Data are from minimum of 130 cells from three independent experiments; each dot represents a cell; each color represents an independent experiment. One-way analysis of variance (ANOVA) with Tukey's *post hoc* test. Only significant differences are shown. *$p < 0.05$; **$p < 0.01$; ****$p < 0.0001$.

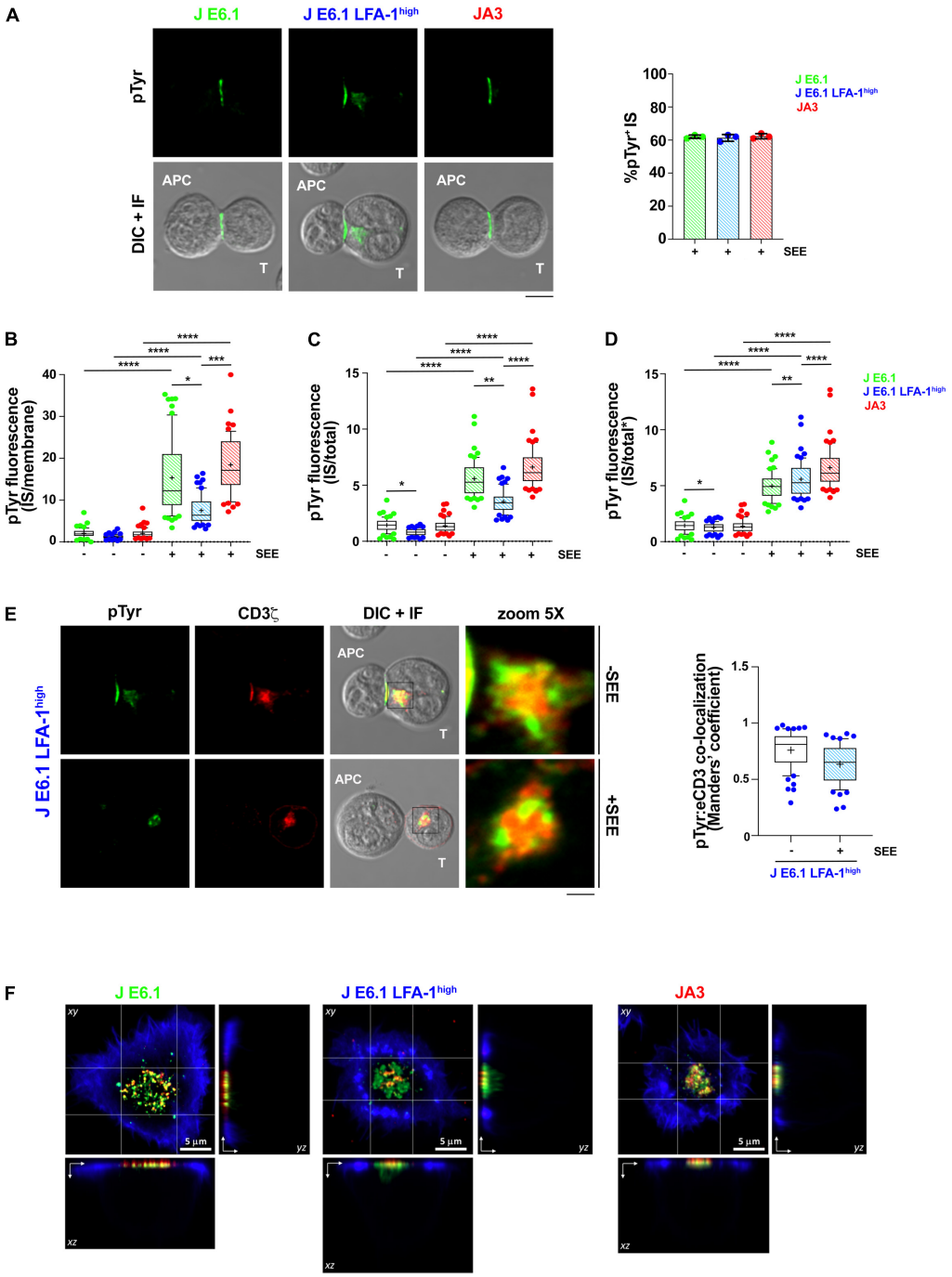

FIGURE 3 | Increasing LFA-1 expression in E6.1 cells does not improve phosphotyrosine signaling at the IS in conjugates with SEE-loaded APCs.
(A) Immunofluorescence analysis of tyrosine phosphoproteins (pTyr) in 15-min conjugates of E6.1, E6.1 LFA-1^{high} or JA3 Jurkat cells and SEE-pulsed Raji cells (APC). Representative images are shown. The histogram shows the percentage (mean ± SD) of conjugates with pTyr staining at the T-cell:APC contact (right; unpaired Student's *t*-test; $n > 40$ conjugates/sample from three independent experiments). **(B)** Quantification of the relative mean fluorescence intensity (MFI) of anti-pTyr at the IS membrane versus the mean of anti-pTyr MFIs measured at three different membrane regions of the same size outside of the T-cell:APC contact (mean ± SD; Kruskal–Wallis test; $n \geq 20$ conjugates/sample from three independent experiments). Graph boxes represent 10–90 percentile and the mean is shown as "+." **(C)** Quantification of the relative mean fluorescence intensity (MFI) of anti-pTyr at the IS membrane versus the MFI of the whole T cell (total) (mean ± SD; Kruskal–Wallis test; $n \geq 20$ conjugates/sample from three independent experiments). Graph boxes represent 10–90 percentile and the mean is shown as "+." **(D)** Quantification of the relative mean fluorescence intensity (MFI) of anti-pTyr at the IS membrane versus the MFI of the whole T cell excluding the intracellular pTyr pool in E6.1 LFA-1^{high} cells (total*) (mean ± SD; Kruskal–Wallis test; $n \geq 20$ conjugates/sample from three independent experiments). Graph boxes represent

(Continued)

FIGURE 3 | Continued
10–90 percentile and the mean is shown as "+." **(E)** Immunofluorescence analysis of 15-min conjugates of E6.1, E6.1 LFA-1^{high} or JA3 cells and Raji cells (APC) in the presence or absence of SEE. Cells were co-stained with anti-pTyr and anti-CD3ζ antibodies. Representative images of E6.1 LFA-1^{high} cells are shown (representative xy images of E6.1 and JA3 cells are shown in **Supplementary Figure 5A**, orthogonal views from 3D confocal images are shown in **Supplementary Figure 5B** and 3D reconstructions of representative z-stacks in videos 1–3). The histogram shows the quantification (mean ± SD) of the co-localization of intracellular pTyr^{+} pool and endosomal CD3ζ (eCD3) in E6.1 LFA-1^{high} cells (Manders' coefficient) (mean ± SD; Kruskal–Wallis test; $n \geq 20$ conjugates/sample from three independent experiments). Graph boxes represent 10–90 percentile and the mean is shown as "+." Scale bar, 5 μm. Only significant differences are shown. $^{*}p < 0.05$; $^{**}p < 0.01$; $^{***}p < 0.001$; $^{****}p < 0.0001$. **(F)** Representative xy and orthogonal views from 3D confocal images of E6.1, E6.1 LFA-1^{high} or JA3 Jurkat cells interacting with activating [ICAM1 + anti-CD3ε UCHT1-CF568 Fab' (red)] SLB for 15 min (3D reconstructions of representative z-stacks are shown in **Supplementary Videos 4–6**). Cells were permeabilized and stained with directly conjugated primary antibodies against anti-phosphotyrosine [pTyr-AF488 (green)] and the cell actin cytoskeleton was labeled with phalloidin-AF405 (blue). Scale bar, 5 μm.

(**Figures 2C,D**). Quantification of the TIRFM images revealed higher pTyr levels in E6.1 LFA-1^{high} cells compared to parental E6.1 (**Figure 2E**), likely due to their more compact cSMAC. PTyr signaling in E6.1 LFA-1^{high} cells was also more efficient compared to JA3 cells (**Figure 2E**). In all Jurkat lines the underlying actin cytoskeleton formed an actin ring, which is a marker of cell activation, and LFA-1 overexpression did not alter the amount of actin at the SLB contact (**Figure 2F**).

To further understand whether the ability of LFA-1 to influence the architecture of the IS in the SLB setting translates into enhanced signaling in cell-cell conjugates, we compared E6.1, E6.1 LFA-1^{high} and JA3, cells in the classical context of SEE-specific conjugates. Jurkat cells were mixed with SEE-pulsed Raji cells (used as APC) for 15 min and the accumulation of tyrosine phosphoproteins at the T-cell:APC interface was measured by confocal microscopy. All Jurkat lines showed a comparable proportion of pTyr-positive conjugates (**Figure 3A** and **Supplementary Figure 5**). Unexpectedly, as opposed to the SLB setting, the accumulation of tyrosine phosphoproteins at the synaptic membrane upon activation was lower in E6.1 LFA-1^{high} cells compared to E6.1 cells, both when calculating the ratio of the membrane pTyr signal versus the average of three similarly sized regions of the non-synaptic membrane, and when calculating the ratio of the membrane pTyr signal versus the total cellular pTyr signal (**Figures 3B,C**). This suggests that in the more complex setting of cell-cell conjugates other integrins or costimulatory receptors contribute to the accumulation of tyrosine phosphoproteins at the IS. Remarkably, as opposed to parental E6.1 cells, E6.1 LFA-1^{high} cells displayed a vesicular pTyr pool that localized just beneath the synaptic membrane in the majority of conjugates and was present also in the absence of SEE (**Figure 3A** and **Supplementary Figure 5**). The pTyr^{+} pool was not observed in JA3 cells, which displayed pTyr accumulation at the synaptic membrane comparable to E6.1 cells (**Figure 3A** and **Supplementary Figures 5,6A**). Of note, when the signal of the constitutive intracellular pTyr pool was subtracted from the total cellular pTyr signal, the accumulation of tyrosine phosphoproteins at the synaptic membrane of E6.1 LFA-1^{high} cells was not significantly different from E6.1 of JA3 cells (**Figure 3D** and **Supplementary Videos 1–3**). Interestingly, the vesicular pTyr^{+} pool unique to E6.1 LFA-1^{high} cells co-localized with the intracellular pool of CD3ζ (**Figure 3E**, **Supplementary Figures 6A–C**, and **Supplementary Videos 1–3**).

To better visualize the accumulation of tyrosine phosphoproteins at the IS of E6.1, E6.1 LFA-1^{high} and JA3 cells, we performed 3D confocal imaging on SLBs. Visualization of all three cell lines by their corresponding orthogonal views revealed the presence of the internal pTyr pool only in E6.1 LFA-1^{high} cells (**Figure 3F** and **Supplementary Videos 4–6**). Together, these results suggest that the redistribution of tyrosine phosphoproteins into a synaptic and subsynaptic pool in E6.1 LFA-1^{high} cells is a consequence of forced LFA-1 expression.

Increasing LFA-1 Expression in E6.1 Cells Enhances TCR Signaling and IL-2 Expression

To explore the outcome of the peculiar subcellular compartmentalization of tyrosine phosphoproteins in E6.1 LFA-1^{high} cells we carried out an immunoblot analysis on E6.1 and E6.1 LFA-1^{high} cells plated for 5 min or 20 min on glass-immobilized ICAM-1 in the presence or absence of anti-CD3ε mAb (clone OKT3). Interestingly, E6.1 LFA-1^{high} cells, either unstimulated or plated on ICAM-1 alone, had high basal levels of both p-ZAP-70 and p-Erk when compared to both E6.1 and JA3 cells (**Figures 4A–C** and **Supplementary Figure 7**). Signaling was enhanced in the presence of anti-CD3ε mAb at 5 min and further enhanced at 20 min in all cell lines (**Figures 4A–C**). Activated E6.1 LFA-1^{high} cells displayed significantly higher levels of p-ZAP-70 and p-Erk compared to E6.1 cells, suggesting that forced LFA-1 expression improves early signaling (**Figures 4A–C**; blue vs. green dot histograms). Interestingly, activated JA3 cells (red dot histograms) displayed lower levels of p-ZAP-70 and p-Erk in response to stimulation compared to the other cell lines, but also had the lowest levels of basal signaling (**Figures 4A–C**), making them the best responders.

To further investigate the potential impact of forced LFA-1 expression on early signaling in E6.1 cells, we measured Ca^{2+} mobilization from intracellular stores. Cells were loaded with the fluorescent Ca^{2+} indicator Fura-2/AM and Ca^{2+} flux was measured by fluorimetry either under resting conditions or following TCR cross-linking in Ca^{2+}-free medium. The kinetics of intracellular Ca^{2+} mobilization was comparable between the two E6.1 cell lines, however total intracellular Ca^{2+} released over time was higher E6.1 LFA-1^{high} cells (**Figure 4D**). Total intracellular Ca^{2+} released over time was also higher in JA3 cells, but Ca^{2+} was released faster, reached a higher peak and returned rapidly to baseline compared to the E6.1 lines (**Figure 4D**, histogram), again highlighting JA3 cells as good responders.

To assess how these differences in early signaling influence the downstream biological response, we carried out a flow cytometric analysis of the activation marker CD69 on the three

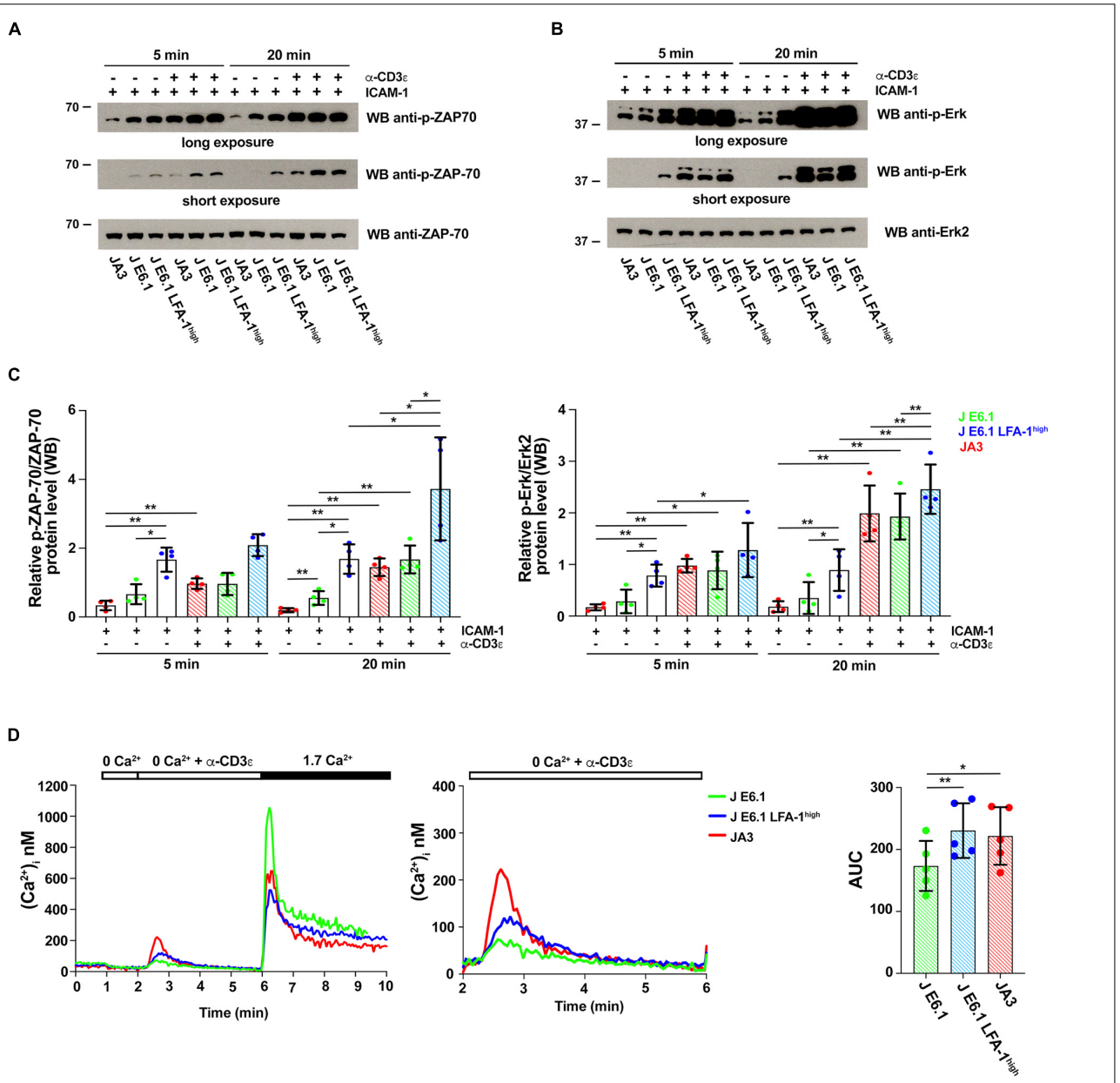

FIGURE 4 | Increasing LFA-1 expression in E6.1 cells affects early signaling events. **(A,B)** Immunoblot analysis with anti-p-ZAP-70 **(A)** or anti-p-Erk1/2 **(B)** antibodies of lysates from E6.1, E6.1 LFA-1^{high} or JA3 Jurkat cells plated on glass-immobilized ICAM-1 in the presence or absence of anti-CD3ε mAb, clone OKT3 for 5 or 20 min. Anti-ZAP-70 and anti-Erk2 antibodies were used as respective loading controls. Representative blots are shown. The migration of molecular mass markers is indicated. **(C)** Quantification of the relative levels of p-ZAP-70 and p-Erk1/2, normalized to the respective loading control (mean ± SD; paired Student's *t*-test; $n = 4$). Only significant differences are shown. $^{*}p < 0.05$; $^{**}p < 0.01$. **(D)** $[Ca^{2+}]_i$ mobilization in Fura-2/AM-loaded Jurkat cells. Cells were stimulated with anti-CD3ε mAb, clone OKT3 followed by anti-mouse IgG in Ca^{2+}-free buffer to evaluate Ca^{2+} release followed by re-addition of 1.7 mM Ca^{2+} to evoke Ca^{2+} influx (left); a magnification of anti-CD3ε mAb (clone OKT3) + anti-mouse IgG-induced Ca^{2+} release is shown on the right. The histogram shows AUC values to quantify anti-CD3ε mAb-induced Ca^{2+} release (mean ± SD; paired Student's *t*-test; $n = 5$). Only significant differences are shown. $^{*}p < 0.05$; $^{**}p < 0.01$.

Jurkat lines activated under the same conditions for 16 h. CD69 expression in the two E6.1 lines showed a bimodal distribution, with a $CD69^{low}$ and a $CD69^{high}$ population, the former being larger in E6.1 LFA-1^{high} cells (**Figures 5A,B**). The mean fluorescence intensity of CD69 in the $CD69^{high}$ population was however comparable between E6.1 and E6.1 LFA-1^{high} cells (**Figure 5C**), indicating that fewer E6.1 LFA-1^{high} cells responded to the stimulation compared to E6.1 cells, but that these cells were equally efficient in expressing CD69. Activated JA3 cells displayed a homogeneous distribution of CD69, and both the percentage of $CD69^{+}$ cells and the mean fluorescence intensity of CD69 were lower compared

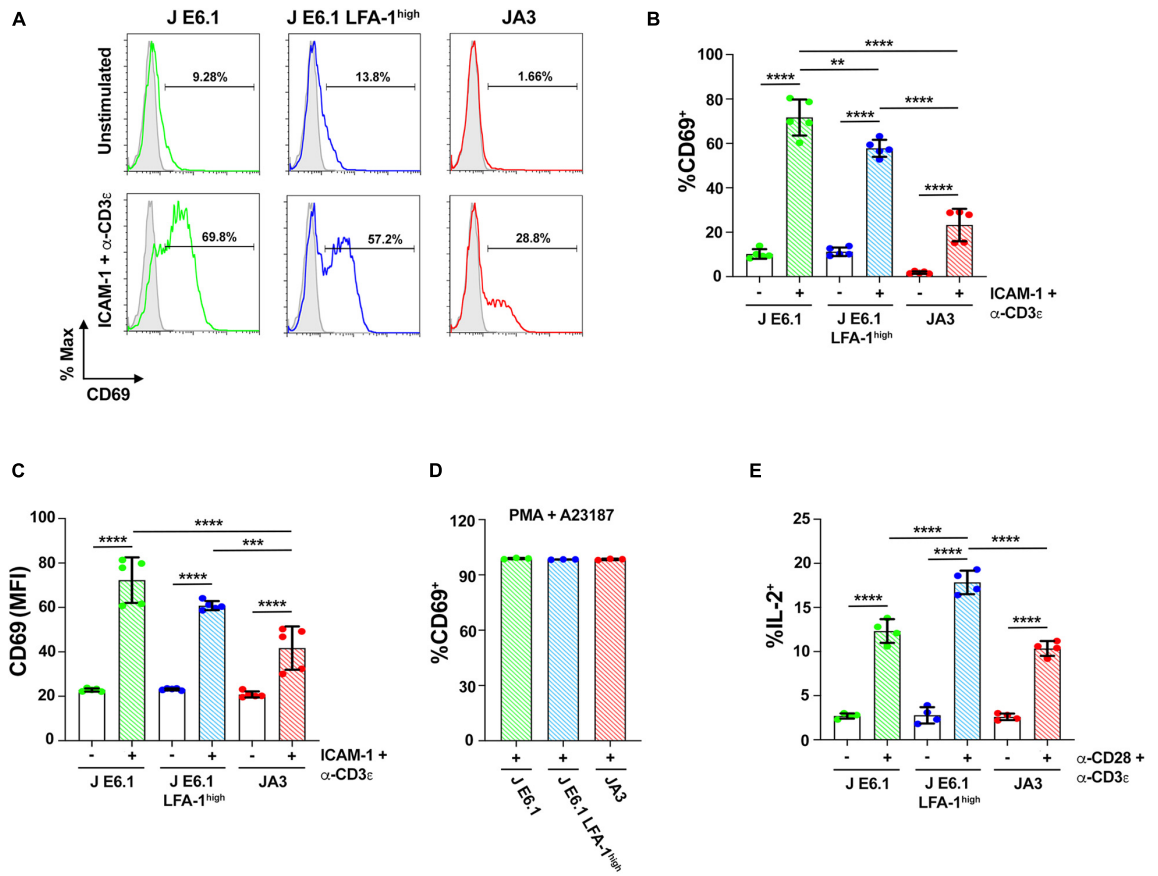

FIGURE 5 | Increasing LFA-1 expression in E6.1 cells improves IL-2 expression. **(A)** Representative FACS profiles of CD69 staining in E6.1, E6.1 LFA-1^{high} or JA3 Jurkat cells either unstimulated or plated on glass-immobilized ICAM-1 and anti-CD3ε mAb, clone OKT3 for 16 h. **(B,C)** Histograms showing the percentage (%) of CD69^{+} cells **(B)** and CD69 MFI **(C)** among cells activated as in **(A)** (mean ± SD; One-Way ANOVA test; $n \geq 3$). **(D)** Histogram showing the percentage (%) of CD69^{+} cells among JA3, E6.1 and E6.1 LFA-1^{high} Jurkat cells stimulated for 16 h with a combination of 100 ng/ml PMA and 500 ng/ml A23187 (mean ± SD; One-Way ANOVA test; $n = 3$). **(E)** Intracellular staining flow cytometry of E6.1, E6.1 LFA-1^{high} or JA3 Jurkat cells stimulated for 6 h on immobilized anti-CD3ε, clone OKT3 and anti-CD28 mAb. A cocktail of brefeldin A and monensin was added in the last 1 h of culture. Cells were permeabilized and stained with anti-IL-2 mAb and the percentage (%) of IL-2^{+} cells was quantified by flow cytometry. Only significant differences are shown. $^{**}p < 0.01$; $^{***}p < 0.001$; $^{****}p < 0.0001$.

to both E6.1 and E6.1 LFA-1^{high} cells (**Figures 5A–C**). Of note, unstimulated JA3 cells had a very low basal frequency of CD69^{+} cells compared to the two E6.1 lines, consistent with the low levels of basal signaling (**Figure 5B**). No difference was observed when cells were stimulated pharmacologically using a combination of the phorbol ester PMA and the calcium ionophore A23187, which bypass TCR signaling (**Figure 5D**), indicating that the intracellular signaling machinery downstream of the TCR is functional in all cell lines.

We extended the study to a later biological readout of T cell activation, namely IL-2 expression, which has more stringent requirements compared to CD69 (Testi et al., 1989). The frequency of IL-2 expressing cells activation was measured by intracellular staining flow cytometry. The frequency of IL-2^{+} cells was higher among E6.1 LFA-1^{high} cells compared to E6.1 cells, with the lowest frequency among JA3 cells (**Figure 5E**), suggesting a correlation between the levels of p-ZAP-70/p-Erk achieved in response to early signaling and the expression of IL-2.

DISCUSSION

Similar to all immortalized cell lines, Jurkat cells do not fully recapitulate the features of their primary CD4^{+} counterparts. The differences must be kept in mind when extrapolating concepts from the results obtained using this T cell model, and validation in primary T cells is mandatory. For example, loss-of-function mutations in the genes encoding the lipid phosphatases PTEN and SHIP-1 make Jurkat E6.1 cells unsuitable for studies on PI3 kinase signaling (Shan et al., 2000; Freeburn et al., 2002; Gioia et al., 2018). Additionally, because the cognate peptide-MHC ligand of the Jurkat TCR is unknown, activation must be carried out using surrogate ligands, namely agonistic anti-CD3 antibodies or SEE (Kappler et al., 1989). The signaling pathways triggered by these agonists reproduce closely, but not completely, the pathway triggered by peptide-MHC (Zamoyska, 2006). Nonetheless, Jurkat cells remain a robust tool easily amenable to genetic manipulation and biochemical studies that is extensively used to provide working hypotheses

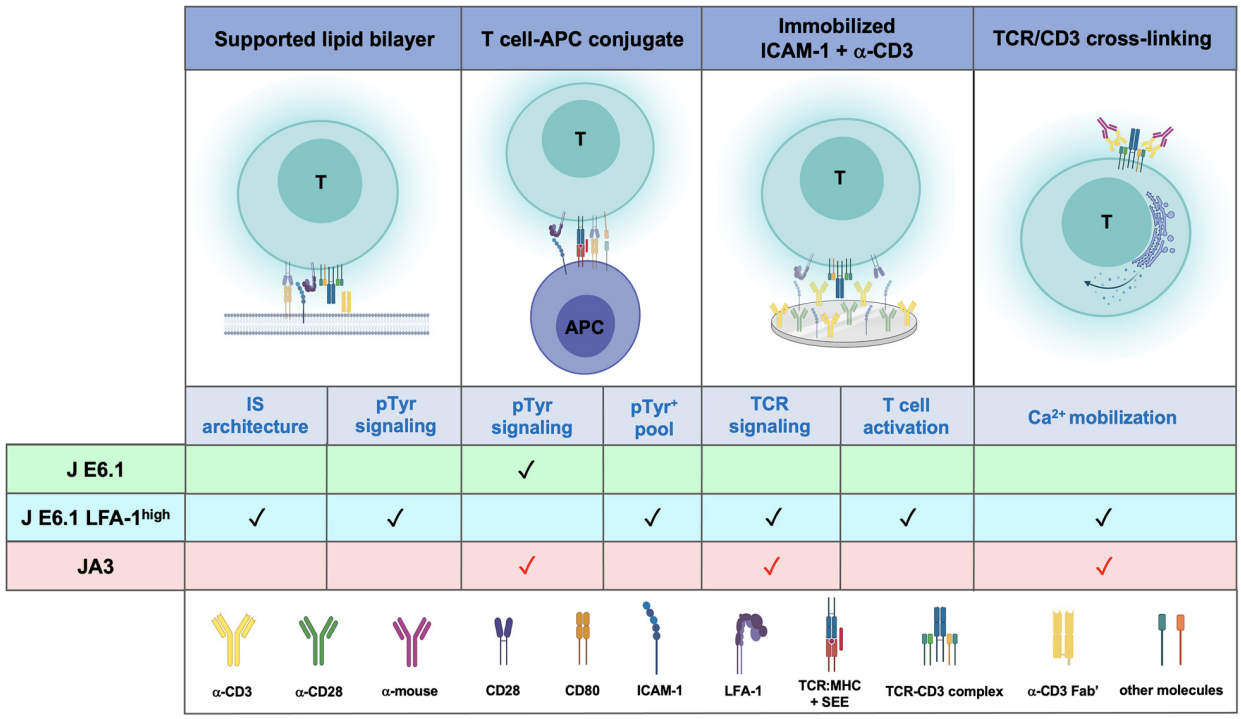

FIGURE 6 | Comparative performance of E6.1, E6.1 LFA-1^{high} and JA3 cells in IS architecture, TCR signaling and T-cell activation. Schematic representation of experimental settings used for testing the performance of the three Jurkat lines. The symbol "✓" indicates the best responder between E6.1 and E6.1 LFA-1^{high} cells. The symbol "✓" indicates experimental settings in which JA3 cells are good responders. The figure was generated with BioRender.com.

to test *ex vivo* on primary T cells or *in vivo* in genetically engineered mice.

Supported lipid bilayers have become established as a versatile tool to visualize T cell autonomous aspects of IS dynamics at nanometer to micrometer scales (Dustin, 2010). The SLB mimics an APC in many aspects, but the T cell alone drives the nanometer to micrometer scale process of microcluster and SMAC formation. Incorporating into the basic setting of a TCR ligand (pMHC or anti-CD3 Fab'), an integrin ligand (e.g., ICAM-1) and other molecules that bind co-stimulatory or co-inhibitory receptors has brought to light subdomain organization of the classic SMACs characterized by the segregation of specific receptors, as recently shown for CD2 and CD28 (Demetriou et al., 2020). While Jurkat cells have been widely exploited for studies of IS assembly in the setting of SEE-specific cell-cell conjugates, to date their use for imaging studies on SLBs has been limited. However, the results have demonstrated that, notwithstanding the less compact distribution of TCR clusters at the cSMAC and subtle differences in the actin cytoskeleton architecture compared to quiescent primary $CD4^+$ T cells (Murugesan et al., 2016; Colin-York et al., 2019), this model can be exploited as a convenient toolkit to analyze the dynamics of protein segregation during IS formation (Kaizuka et al., 2007, 2009). Our data show that, by compensating for the low expression of LFA-1 in the most extensively used Jurkat T cell clone E6.1, it is possible to enhance the ability of these cells to form well-structured immune synapses. In particular, while both E6.1 cells and their LFA-1^{high} counterparts effectively segregate the TCR, LFA-1 and F-actin in the respective SMACs, LFA-1 enhances the compartmentalization of the TCR to the cSMAC. This finding recapitulates in human T cells the finding that LFA-1 is dispensable for cSMAC formation in OVA-specific mouse $CD4^+$ cells (Graf et al., 2007). Hence engineered LFA-1^{high} Jurkat E6.1 cells are a valuable model to study the redistribution of signaling molecules during IS assembly in the context of LFA-1 signaling and LFA-1-mediated adhesion using the SLB setting. The improvement in IS architecture associated with increased LFA-1 expression in E6.1 may impact also effector function requiring directed secretion of soluble factors (Huse et al., 2006) or extracellular vesicle budding (Choudhuri et al., 2014). Similarly, expression of CD40L in E6.1 cells could be studied not only in terms of transcription and surface expression, but also in terms of directed budding of TCR and CD40L positive synaptic ectosomes in the cSMAC (Saliba et al., 2019).

Surprisingly, while increasing LFA-1 expression in E6.1 cells improved their performance in the SLB system, neither conjugate formation nor pTyr signaling was enhanced in E6.1 LFA-1^{high} cells stimulated with SEE-pulsed APCs. This suggests that E6.1 cells may exploit other integrins or accessory surface receptors for TCR co-stimulation to compensate for the low

levels of LFA-1, and indeed we found that the efficiency and extent of tyrosine phosphoprotein accumulation in E6.1 cells, but not in E6.1 LFA-1^{high} cells, relies in part on CD2 (unpublished results). Intriguingly, E6.1 LFA-1^{high} cells show a peculiar pattern of tyrosine phosphoprotein distribution at the IS, with a lower accumulation at the synaptic membrane compared to E6.1 cells concomitant with the presence of an intracellular pool that colocalizes with endosomal CD3ζ. This pool was present also in conjugates formed in the absence of SEE, albeit under these conditions it was not polarized at the T-cell:APC contact. This observation suggests that E6.1 LFA-1^{high} cells may have some constitutive activation due to enhanced TCR tonic signaling. This is supported by the enhanced basal activation of ZAP-70 and Erk observed in these cells. A basal endosomal accumulation of signaling-competent tyrosine-phosphorylated CD3ζ in Jurkat cells has been previously reported (Yudushkin and Vale, 2010). Although no information of LFA-1 expression was included in this study, we speculate that the Jurkat clone used may have been LFA-1^{high}.

Interestingly, when comparing specific steps of the TCR signaling cascade in E6.1 and E6.1 LFA-1^{high} cells, forced LFA-1 expression showed an enhancing effect on the signaling readouts used, with an increase in the levels of p-ZAP-70 and p-Erk in response to activation and an increase in intracellular Ca^{2+} mobilization. This correlates with a higher expression of a late activation marker, IL-2, while expression of CD69 among responder cells was comparable. We can speculate that the signals elicited by the TCR in this setting are sufficient to activate maximal CD69 expression in E6.1 cells independently of the levels of surface LFA-1. This may not apply to IL-2 expression, which has more stringent requirements compared to CD69 (Testi et al., 1989). It is noteworthy that E6.1 LFA-1^{high} cells show a clear bimodal pattern of CD69 expression, with a substantial increase in the CD69-negative population. We could hypothesize that the high basal ZAP-70 and Erk activation in E6.1 LFA-1^{high} cells makes them partially anergic, such that not all cells are able to respond.

Interestingly, our results show that the JA3 clone, which was derived from the same Jurkat line as E6.1 cells (Moretta et al., 1985), has unique features compared to both E6.1 and E6.1 LFA-1^{high} cells. Despite expressing LFA-1 at levels comparable to E6.1 cells, JA3 cells form well-structured synapses displaying a tight segregation of the TCR to the cSMAC. Differences can also be detected in early signaling, with lower levels of p-ZAP-70 and p-Erk in response to activation compared to the two E6.1 lines but also very low basal signaling, which makes them better responders. Additionally, the kinetics of their Ca^{2+} response is faster. Nevertheless, similar to the E6.1 lines, the levels of CD69 and IL-2 expression in activated JA3 cells appear to correlate with the amount of activated p-ZAP-70 and p-Erk, making them the weakest CD69 and IL-2 expressers among the three Jurkat lines analyzed. These differences may be accounted for in part by the specific constellation of mutations accumulated in the selection process of the E6.1 and JA3 clones.

CONCLUSION

Our data extend the exploitability of Jurkat E6.1 cells by providing a strategy to make them more amenable to imaging IS formation in the SLB setting. This would potentially allow reduction of animal use and further reduce the need for primary T cells in studies on IS architecture and its abnormalities in disease. The improvement in IS architecture of E6.1 cells resulting from forced LFA-1 expression entails, however, an enhancement in basal signaling. JA3 cells, which have the "cleanest" background, could complement E6.1 cells for signaling studies to fully exploit the Jurkat paradigm of T cell signaling (**Figure 6**).

DATA AVAILABILITY STATEMENT

The raw data supporting the conclusions of this article will be made available by the authors, without undue reservation.

AUTHOR CONTRIBUTIONS

All the authors listed have made a substantial, direct and intellectual contribution to the work, and approved it for publication. CC, SB, EBC, JHF, AG, CDB, SLF, and JB performed the experimental work. CC and SB prepared the figures. SV, DP, MMD'E, and LM contributed essential reagents.

FUNDING

This work was carried out with the support of AIRC (IG-2017 – ID 20148) and Ministero dell'Istruzione, dell'Università e della Ricerca (Grant PRIN bando 2017 – 2017FS5SHL) to CTB. SB and EBC are supported by ERC AdG 670930 to MLD. MLD is supported by the Kennedy Trust for Rheumatology Research. MLD and CTB are supported by ERC Synergy Grant 951329.

ACKNOWLEDGMENTS

The authors wish to thank Lina Chen, Elke Kurz, and Heather Rada for keeping the bilayer platform and producing histidine-tagged recombinant proteins UCHT1-Fab' fragment and ICAM-1.

SUPPLEMENTARY MATERIAL

The Supplementary Material for this article can be found online at: https://www.frontiersin.org/articles/10.3389/fcell.2021.673446/full#supplementary-material

REFERENCES

Abraham, R. T., and Weiss, A. (2004). Jurkat T cells and development of the T-cell receptor signalling paradigm. *Nat. Rev. Immunol.* 4, 301–308. doi: 10.1038/nri1330

Alcover, A., Alberini, C., Acuto, O., Clayton, L. K., Transy, C., Spagnoli, G. C., et al. (1988). Interdependence of CD3-Ti and CD2 activation pathways in human T lymphocytes. *EMBO J.* 7, 1973-1977.

Blanchard, N., Di Bartolo, V., and Hivroz, C. (2002). In the immune synapse, ZAP-70 controls T cell polarization and recruitment of signaling proteins but not formation of the synaptic pattern. *Immunity* 17, 389–399. doi: 10.1016/s1074-7613(02)00421-1

Bunnell, S. C., Hong, D. I., Kardon, J. R., Yamazaki, T., Mcglade, C. J., Barr, V. A., et al. (2002). T cell receptor ligation induces the formation of dynamically regulated signaling assemblies. *J. Cell Biol.* 158, 1263–1275. doi: 10.1083/jcb.200203043

Bunnell, S. C., Kapoor, V., Trible, R. P., Zhang, W., and Samelson, L. E. (2001). Dynamic actin polymerization drives T cell receptor-induced spreading: a role for the signal transduction adaptor LAT. *Immunity* 14, 315–329. doi: 10.1016/s1074-7613(01)00112-1

Carrasco, Y. R., Fleire, S. J., Cameron, T., Dustin, M. L., and Batista, F. D. (2004). LFA-1/ICAM-1 interaction lowers the threshold of B cell activation by facilitating B cell adhesion and synapse formation. *Immunity* 20, 589–599. doi: 10.1016/s1074-7613(04)00105-0

Chen, B. M., Al-Aghbar, M. A., Lee, C. H., Chang, T. C., Su, Y. C., Li, Y. C., et al. (2017). The Affinity of Elongated Membrane-Tethered Ligands Determines Potency of T Cell Receptor Triggering. *Front. Immunol.* 8:793. doi: 10.3389/fimmu.2017.00793

Choudhuri, K., Llodra, J., Roth, E. W., Tsai, J., Gordo, S., Wucherpfennig, K. W., et al. (2014). Polarized release of T-cell-receptor-enriched microvesicles at the immunological synapse. *Nature* 507, 118–123. doi: 10.1038/nature12951

Colin-York, H., Kumari, S., Barbieri, L., Cords, L., and Fritzsche, M. (2019). Distinct actin cytoskeleton behaviour in primary and immortalised T-cells. *J. Cell Sci.* 133:jcs232322.

Danielian, S., Alcover, A., Polissard, L., Stefanescu, M., Acuto, O., Fischer, S., et al. (1992). Both T cell receptor (TcR)-CD3 complex and CD2 increase the tyrosine kinase activity of p56lck. CD2 can mediate TcR-CD3-independent and CD45-dependent activation of p56lck. *Eur. J. Immunol.* 22, 2915-2921. doi: 10.1002/eji.1830221124

Demetriou, P., Abu-Shah, E., Valvo, S., Mccuaig, S., Mayya, V., Kvalvaag, A., et al. (2020). A dynamic CD2-rich compartment at the outer edge of the immunological synapse boosts and integrates signals. *Nat. Immunol.* 21, 1232–1243. doi: 10.1038/s41590-020-0770-x

Dustin, M. L. (2010). Insights into function of the immunological synapse from studies with supported planar bilayers. *Curr. Top. Microbiol. Immunol.* 340, 1–24. doi: 10.1007/978-3-642-03858-7_1

Dustin, M. L., and Colman, D. R. (2002). Neural and immunological synaptic relations. *Science* 298, 785–789. doi: 10.1126/science.1076386

Dustin, M. L., and Springer, T. A. (1988). Lymphocyte function-associated antigen-1 (LFA-1) interaction with intercellular adhesion molecule-1 (ICAM-1) is one of at least three mechanisms for lymphocyte adhesion to cultured endothelial cells. *J. Cell Biol.* 107, 321–331. doi: 10.1083/jcb.107.1.321

Felce, J. H., Parolini, L., Sezgin, E., Cespedes, P. F., Korobchevskaya, K., Jones, M., et al. (2020). Single-Molecule, Super-Resolution, and Functional Analysis of G Protein-Coupled Receptor Behavior Within the T Cell Immunological Synapse. *Front. Cell Dev. Biol.* 8:608484. doi: 10.3389/fcell.2020.608484

Felce, S. L., Farnie, G., Dustin, M. L., and Felce, J. H. (2021). RNA-Seq analysis of early transcriptional responses to activation in the leukaemic Jurkat E6.1 T cell line [version 2; peer review: 2 approved with reservations]. *Wellcome Open Res.* 5:42. doi: 10.12688/wellcomeopenres.15748.2

Finetti, F., Paccani, S. R., Riparbelli, M. G., Giacomello, E., Perinetti, G., Pazour, G. J., et al. (2009). Intraflagellar transport is required for polarized recycling of the TCR/CD3 complex to the immune synapse. *Nat. Cell Biol.* 11, 1332–1339. doi: 10.1038/ncb1977

Freeburn, R. W., Wright, K. L., Burgess, S. J., Astoul, E., Cantrell, D. A., and Ward, S. G. (2002). Evidence that SHIP-1 contributes to phosphatidylinositol 3,4,5-trisphosphate metabolism in T lymphocytes and can regulate novel phosphoinositide 3-kinase effectors. *J. Immunol.* 169, 5441–5450. doi: 10.4049/jimmunol.169.10.5441

Fritzsche, M., Fernandes, R. A., Chang, V. T., Colin-York, H., Clausen, M. P., Felce, J. H., et al. (2017). Cytoskeletal actin dynamics shape a ramifying actin network underpinning immunological synapse formation. *Sci. Adv.* 3:e1603032. doi: 10.1126/sciadv.1603032

Gamberucci, A., Innocenti, B., Fulceri, R., Banhegyi, G., Giunti, R., Pozzan, T., et al. (1994). Modulation of Ca2+ influx dependent on store depletion by intracellular adenine-guanine nucleotide levels. *J. Biol. Chem.* 269, 23597–23602. doi: 10.1016/s0021-9258(17)31557-0

Gillis, S., and Watson, J. (1980). Biochemical and biological characterization of lymphocyte regulatory molecules. V. Identification of an interleukin 2-producing human leukemia T cell line. *J. Exp. Med.* 152, 1709–1719. doi: 10.1084/jem.152.6.1709

Gioia, L., Siddique, A., Head, S. R., Salomon, D. R., and Su, A. I. (2018). A genome-wide survey of mutations in the Jurkat cell line. *BMC Genomics* 19:334. doi: 10.1186/s12864-018-4718-6

Graf, B., Bushnell, T., and Miller, J. (2007). LFA-1-mediated T cell costimulation through increased localization of TCR/class II complexes to the central supramolecular activation cluster and exclusion of CD45 from the immunological synapse. *J. Immunol.* 179, 1616–1624. doi: 10.4049/jimmunol.179.3.1616

Grakoui, A., Bromley, S. K., Sumen, C., Davis, M. M., Shaw, A. S., Allen, P. M., et al. (1999). The immunological synapse: a molecular machine controlling T cell activation. *Science* 285, 221–227. doi: 10.1126/science.285.5425.221

Harburger, D. S., and Calderwood, D. A. (2009). Integrin signalling at a glance. *J. Cell Sci.* 122, 159–163. doi: 10.1242/jcs.018093

Huse, M., Lillemeier, B. F., Kuhns, M. S., Chen, D. S., and Davis, M. M. (2006). T cells use two directionally distinct pathways for cytokine secretion. *Nat. Immunol.* 7, 247–255. doi: 10.1038/ni1304

Kaizuka, Y., Douglass, A. D., Vardhana, S., Dustin, M. L., and Vale, R. D. (2009). The coreceptor CD2 uses plasma membrane microdomains to transduce signals in T cells. *J. Cell Biol.* 185, 521–534. doi: 10.1083/jcb.200809136

Kaizuka, Y., Douglass, A. D., Varma, R., Dustin, M. L., and Vale, R. D. (2007). Mechanisms for segregating T cell receptor and adhesion molecules during immunological synapse formation in Jurkat T cells. *Proc. Natl. Acad. Sci. U. S. A.* 104, 20296–20301. doi: 10.1073/pnas.0710258105

Kappler, J., Kotzin, B., Herron, L., Gelfand, E. W., Bigler, R. D., Boylston, A., et al. (1989). V beta-specific stimulation of human T cells by staphylococcal toxins. *Science* 244, 811–813. doi: 10.1126/science.2524876

Kumari, S., Depoil, D., Martinelli, R., Judokusumo, E., Carmona, G., Gertler, F. B., et al. (2015). Actin foci facilitate activation of the phospholipase C-γ in primary T lymphocytes via the WASP pathway. *Elife* 4:e04953.

Manders, E. M., Stap, J., Brakenhoff, G. J., Van Driel, R., and Aten, J. A. (1992). Dynamics of three-dimensional replication patterns during the S-phase, analysed by double labelling of DNA and confocal microscopy. *J. Cell Sci.* 103, 857–862. doi: 10.1242/jcs.103.3.857

Mastrogiovanni, M., Juzans, M., Alcover, A., and Di Bartolo, V. (2020). Coordinating Cytoskeleton and Molecular Traffic in T Cell Migration, Activation, and Effector Functions. *Front. Cell Dev. Biol.* 8:591348. doi: 10.3389/fcell.2020.591348

Mayya, V., Judokusumo, E., Abu Shah, E., Peel, C. G., Neiswanger, W., Depoil, D., et al. (2018). Durable Interactions of T Cells with T Cell Receptor Stimuli in the Absence of a Stable Immunological Synapse. *Cell Rep.* 22, 340–349. doi: 10.1016/j.celrep.2017.12.052

Moingeon, P., Alcover, A., Clayton, L. K., Chang, H. C., Transy, C., and Reinherz, E. L. (1988). Expression of a functional CD3-Ti antigen/MHC receptor in the absence of surface CD2. Analysis with clonal Jurkat cell mutants. *J. Exp. Med.* 168, 2077–2090. doi: 10.1084/jem.168.6.2077

Monks, C. R., Freiberg, B. A., Kupfer, H., Sciaky, N., and Kupfer, A. (1998). Three-dimensional segregation of supramolecular activation clusters in T cells. *Nature* 395, 82–86. doi: 10.1038/25764

Moretta, A., Pantaleo, G., Lopez-Botet, M., and Moretta, L. (1985). Involvement of T44 molecules in an antigen-independent pathway of T cell activation. Analysis of the correlations to the T cell antigen-receptor complex. *J. Exp. Med.* 162, 823–838. doi: 10.1084/jem.162.3.823

Moretta, A., Poggi, A., Olive, D., Bottino, C., Fortis, C., Pantaleo, G., et al. (1987). Selection and characterization of T-cell variants lacking molecules involved in T-cell activation (T3 T-cell receptor, T44, and T11): analysis of the functional relationship among different pathways of activation. *Proc. Natl. Acad. Sci. U.S.A.* 84, 1654–1658. doi: 10.1073/pnas.84.6.1654

Murugesan, S., Hong, J., Yi, J., Li, D., Beach, J. R., Shao, L., et al. (2016). Formin-generated actomyosin arcs propel T cell receptor microcluster movement at the immune synapse. *J. Cell Biol.* 215, 383–399. doi: 10.1083/jcb.201603080

Norcross, M. A. (1984). A synaptic basis for T-lymphocyte activation. *Ann. Immunol. (Paris).* 135D, 113–134. doi: 10.1016/s0769-2625(84)81105-8

Onnis, A., and Baldari, C. T. (2019). Orchestration of Immunological Synapse Assembly by vesicular trafficking. *Front. Dev. Cell Biol.* 7:110. doi: 10.3389/fcell.2019.00110

Ritter, A. T., Asano, Y., Stinchcombe, J. C., Dieckmann, N. M., Chen, B. C., and Gawden-Bone, C. (2015). Actin depletion initiates events leading to granule secretion at the immunological synapse. *Immunity* 42, 864–876. doi: 10.1016/j.immuni.2015.04.013

Ritter, A. T., Kapnick, S. M., Murugesan, S., Schwartzberg, P. L., Griffiths, G. M., and Lippincott-Schwartz, J. (2017). Cortical actin recovery at the immunological synapse leads to termination of lytic granule secretion in cytotoxic T lymphocytes. *Proc. Natl. Acad. Sci. U. S. A.* 114, E6585–E6594.

Rubin, B., Llobera, R., Gouaillard, C., Alcover, A., and Arnaud, J. (2000). Dissection of the role of CD3gamma chains in profound but reversible T-cell receptor down-regulation. *Scand. J. Immunol.* 52, 173–183. doi: 10.1046/j.1365-3083.2000.00767.x

Saliba, D. G., Cespedes-Donoso, P. F., Balint, S., Compeer, E. B., Korobchevskaya, K., Valvo, S., et al. (2019). Composition and structure of synaptic ectosomes exporting antigen receptor linked to functional CD40 ligand from helper T cells. *Elife* 8:e47528.

Schneider, U., Schwenk, H. U., and Bornkamm, G. (1977). Characterization of EBV-genome negative "null" and "T" cell lines derived from children with acute lymphoblastic leukemia and leukemic transformed non-Hodgkin lymphoma. *Int. J. Cancer* 19, 621–626. doi: 10.1002/ijc.2910190505

Shan, X., Czar, M. J., Bunnell, S. C., Liu, P., Liu, Y., Schwartzberg, P. L., et al. (2000). Deficiency of PTEN in Jurkat T cells causes constitutive localization of Itk to the plasma membrane and hyperresponsiveness to CD3 stimulation. *Mol. Cell Biol.* 20, 6945–6957. doi: 10.1128/mcb.20.18.6945-6957.2000

Testi, R., Phillips, J. H., and Lanier, L. L. (1989). T cell activation via Leu-23 (CD69). *J. Immunol.* 143, 1123–1128.

Varma, R., Campi, G., Yokosuka, T., Saito, T., and Dustin, M. L. (2006). T cell receptor-proximal signals are sustained in peripheral microclusters and terminated in the central supramolecular activation cluster. *Immunity* 25, 117–127. doi: 10.1016/j.immuni.2006.04.010

Weiss, A., Wiskocil, R. L., and Stobo, J. D. (1984). The role of T3 surface molecules in the activation of human T cells: a two-stimulus requirement for IL 2 production reflects events occurring at a pre-translational level. *J. Immunol.* 133, 123–128.

Yudushkin, I. A., and Vale, R. D. (2010). Imaging T-cell receptor activation reveals accumulation of tyrosine-phosphorylated CD3ζ in the endosomal compartment. *Proc. Natl. Acad. Sci. U. S. A.* 107, 22128–22133. doi: 10.1073/pnas.1016388108

Zamoyska, R. (2006). Superantigens: supersignalers? *Sci Stke* 2006:e45.

Conflict of Interest: The authors declare that the research was conducted in the absence of any commercial or financial relationships that could be construed as a potential conflict of interest.

Publisher's Note: All claims expressed in this article are solely those of the authors and do not necessarily represent those of their affiliated organizations, or those of the publisher, the editors and the reviewers. Any product that may be evaluated in this article, or claim that may be made by its manufacturer, is not guaranteed or endorsed by the publisher.

frontiers in Cell and Developmental Biology

REVIEW
published: 05 August 2021
doi: 10.3389/fcell.2021.682294

Journey to the Center of the Cell: Cytoplasmic and Nuclear Actin in Immune Cell Functions

Julien Record[1†], Mezida B. Saeed[1*†], Tomas Venit[2], Piergiorgio Percipalle[2,3] and Lisa S. Westerberg[1*]*

[1] Department of Microbiology, Tumor and Cell Biology, Karolinska Institute, Stockholm, Sweden, [2] Science Division, Biology Program, New York University Abu Dhabi (NYUAD), Abu Dhabi, United Arab Emirates, [3] Department of Molecular Biosciences, The Wenner-Gren Institute, Stockholm University, Stockholm, Sweden

OPEN ACCESS

Edited by:
Sudha Kumari,
Massachusetts Institute of Technology, United States

Reviewed by:
Oliver T. Fackler,
Heidelberg University, Germany
Loïc Dupré,
Institut National de la Santé et de la Recherche Médicale (INSERM), France

***Correspondence:**
Julien Record
Julien.Record@ki.se
Mezida B. Saeed
Mezida.Bedru.Saeed@ki.se
Lisa S. Westerberg
Lisa.Westerberg@ki.se

† These authors have contributed equally to this work

Specialty section:
This article was submitted to Cell Growth and Division, a section of the journal Frontiers in Cell and Developmental Biology

Received: 18 March 2021
Accepted: 06 July 2021
Published: 05 August 2021

Citation:
Record J, Saeed MB, Venit T, Percipalle P and Westerberg LS (2021) Journey to the Center of the Cell: Cytoplasmic and Nuclear Actin in Immune Cell Functions. Front. Cell Dev. Biol. 9:682294. doi: 10.3389/fcell.2021.682294

Actin cytoskeletal dynamics drive cellular shape changes, linking numerous cell functions to physiological and pathological cues. Mutations in actin regulators that are differentially expressed or enriched in immune cells cause severe human diseases known as primary immunodeficiencies underscoring the importance of efficienct actin remodeling in immune cell homeostasis. Here we discuss recent findings on how immune cells sense the mechanical properties of their environement. Moreover, while the organization and biochemical regulation of cytoplasmic actin have been extensively studied, nuclear actin reorganization is a rapidly emerging field that has only begun to be explored in immune cells. Based on the critical and multifaceted contributions of cytoplasmic actin in immune cell functionality, nuclear actin regulation is anticipated to have a large impact on our understanding of immune cell development and functionality.

Keywords: immune cells, actin, nucleus, mechanosensing, cytoplasm

Abbreviations: Arp2/3, actin related protein complex 2/3; BCR, B cell receptor; BMDCs, bone marrow derived dendritic cells; CDK, cyclin-dependent kinase; DC, dendritic cell; Dock8, dedicator of cytokinesis 8; ER, endoplasmic reticulum; F-actin, filamentous actin; FAK, focal adhesion kinase; G-actin, globular actin; GAP, GTPase activating protein; GEF, guanine exchange factor; Hem-1, hematopoietic protein 1; ICAM-1, intercellular adhesion molecule 1; JMY, junction-mediating and regulatory; KASH, Klarsicht, ANC-1, Syne homology; LAT, linker of activation; LINC, linker of nucleoskeleton and cytoskeleton; LFA-1, lymphocyte function-associated antigen 1; MCM proteins, minichromosome maintenance (MCM) proteins; mDia, mammalian Diaphanous-related; MHC, major histocompatibility (classes I and II); MICAL, Molecules Interacting with CasL; MLC, myosin light chain; MRTF-A/MKL1, myocardin related transcription factor A/megakaryoblastic leukemia 1; MsrB, methionine sulfoxide reductase; MTOC, microtubule-organizing center; NES, nuclear export signal; NM1, nuclear myosin 1; NLS, nuclear localization signal; NPC, nuclear pore complex; NPF, nucleation promoting factors; NuRD, nucleosome remodeling and deacetylase; NURF, nucleosome remodeling factor; N-WASp, neuronal Wiskott–Aldrich syndrome protein; ORC, origin recognition complex; PCAF, P300/CBP-associated factor; PCNA, proliferating cell nuclear antigen; PID, primary immunodeficiency; PI3K, phosphoinositide 3-kinase; Pol, polymerase; pre-RC, pre-replication complexes; PSGL-1, P-selectin glycoprotein ligand-1; Rho, Ras homolog gene family; RhoA, Ras homolog gene family, member A; ROCK; Rho-associated protein kinase; RPA, replication protein A; TCR, T cell receptor; SRF, serum response factor; SUN domain, Sad1p, UNC-84 domain; TAN, transmembrane actin-associated nuclear; Th, T helper (cell); Treg, regulatory T cell; VCA, verprolin cofilin acidic; VCAM-1, vascular cell adhesion molecule 1; VLA-4, very late antigen 4; WASp, Wiskott–Aldrich syndrome protein; WAVE/SCAR, WASp-family verprolin-homologous protein/suppressor of the cyclic AMP receptor; WASH, WASp and SCAR homolog; WHAMM, WASp homolog associated with actin, membranes, and microtubules; WWTR1/TAZ, WW domain-containing transcription regulator protein 1; YAP, yes-associated protein.

INTRODUCTION

The immune system is tasked with detecting and responding to harmful non-self and self- molecules through the cooperative action of different cells. Immune cells are among the most motile cells in the body which enables the rapid communication between leukocytes specialized in gathering information about pathogens and altered self with other leukocytes specialized in mounting effector responses in lymphoid organs as well as the delivery of these cells to the sites of inflammation. Thus, leukocytes continually change shape to adapt to their environment but also to communicate with other cells. For instance, at sites of infection chemokine and selectin receptors on the surface of circulating immune cells are engaged by factors released from the endothelial cells lining the capillaries. This causes leukocytes such as neutrophils and lymphocytes to roll on the activated endothelium and trigger outside-in activation of integrin molecules which stimulates the immune cells to slow down and stop (Vestweber, 2015). The immune cell will then polarize to acquire a motile shape, characterized in the direction of movement by the dynamic branched actin network of the lamellipodia and an acto-myosin rich trailing uropod that generates force to propel the cell body forward. This will allow migration on and through the endothelium to reach the inflamed tissue. Endothelial transmigration is often limited by the deformability of the cells' largest organelle – the nucleus (Vargas et al., 2017). Motility within the inflamed tissue is essential to reach and clear the infection but also in improving the odds of antigen specific immune responses. Immune cells need to directly communicate with other immune cells and diseased cells, and they do so by establishing an immune synapse characterized by a drastic remodeling of their cytoskeleton. While stable in relation to the communicating cells, immune synapses are extremely dynamic, and sites of multiple cellular processes (Dustin, 2014). Studies of primary immunodeficiencies where patients have a mutation in specific actin regulators have provided remarkable insights into the unique and redundant functions of these regulators in immune cells (Saeed et al., 2020).

Defense against non-self pathogens is intuitively seek and destroy. Paradoxically, however, this same detection machinery is used to distinguish harmless non-self pathogens such as commensal bacteria leading to tolerance. Recent studies of have established the importance of immune cells' ability to sense the mechanical properties of their environment and a role for such mechanosenstion in fine-tuning the strength and outcome of immune cells' interactions with the environment and between cells (Zhu et al., 2019). Moreover, a growing body of work on nuclear actin dynamics and regulators, mostly in non-immune cells, highlights their role in cell signaling, differentiation, proliferation, and gene transcription. Therefore, these aspects of regulation could play critical roles in shaping the overall outcome of immune responses.

Immune cells uniquely face the challenge of requiring a single cell or its lineage to have plastic differentiation potential, migrate and adapt to diverse environments (**Figure 1**). Here, we describe how the actin cytoskeleton enables sensing of mechanical stimuli at the plasma membrane and its' transmission to the nucleus. We will also discuss, largely based on studies of non-immune cells, the emerging role of nuclear actin in genomic organization and nuclear functions and discuss the implications such regulation may have on immune cells.

SETTING THE STAGE: IMMUNE DYSREGULATION CAUSED BY MUTATIONS IN ACTIN REGULATORS

The first described so called "actinopathy" is Wiskott–Aldrich syndrome (WAS) in which patients suffer from severe immunodeficiency caused by loss-of-function mutations in the hematopoietic specific WAS protein (WASp). WASp gave the name to the WASp family of actin promoting factors also containing the ubiquitously expressed neural WASp (N-WASp), the WASp-family verprolin-homologous protein/suppressor of the cyclic AMP receptor (WAVE/SCAR), WASp and SCAR homolog (WASH), and WASp homolog associated with actin, membranes, and microtubules (WHAMM) (Campellone and Welch, 2010; Moulding et al., 2013; Alekhina et al., 2017). The activity of WASp family members is regulated by the small Rho GTPases Cdc42 and Rac1/2. WASp family members have a carboxy terminal verprolin cofilin acidic (VCA) domain that mediates binding to the actin related protein (Arp2/3) complex that polymerize actin branching from existing actin filaments (Campellone and Welch, 2010; Moulding et al., 2013; Alekhina et al., 2017). With increased accessibility to whole genome sequencing approaches for immunodeficient patients, patients have been described with mutations in hematopoietic protein-1 (Hem1, a component of the WAVE regulatory complex), Arp2/3 subunit Arp complex 1B (ARPC1B), Cdc42, Rac2, RhoA, and dedicator of cytokinesis 8 [Dock8, a guanine exchange factor (GEF) for Cdc42 and Rac1/2] (Saeed et al., 2020). Moreover, mutations in β-actin and the actin sensor Myocardin Related Transcription Factor A (MRTF-A)/Megakaryoblastic leukemia 1 protein (MKL1) lead to severe immunodeficiencies with poorly functional immune cells (Saeed et al., 2020). As a testimony to the enormous need for rapid cell cytoskeletal adaptation, cells of the hematopoietic lineage often express multiple copies of seemingly redundant regulators of the actin cytoskeleton. This is exemplified by co-expression of hematopoietic-specific WASp and the highly homologous and ubiquitously expressed N-WASp (Cotta-de-Almeida et al., 2007; Recher et al., 2012; Westerberg et al., 2012). Moreover, naturally occurring gain-of-function mutations, such as the $WASp^{L270P}$ and $WASp^{I294T}$ and increased activity of MRTF-A/MKL1 have further increased the understanding of actin regulators in the hematopoietic lineage cells (Devriendt et al., 2001; Ancliff et al., 2006; Keszei et al., 2018; Record et al., 2020). Studies of immune cells from patients and animal models with mutations in actin regulators has revealed the critical role of actin remodeling and dynamics in immune cell functions opening up the question — what are the unique and redundant roles of these regulators in mechanical and

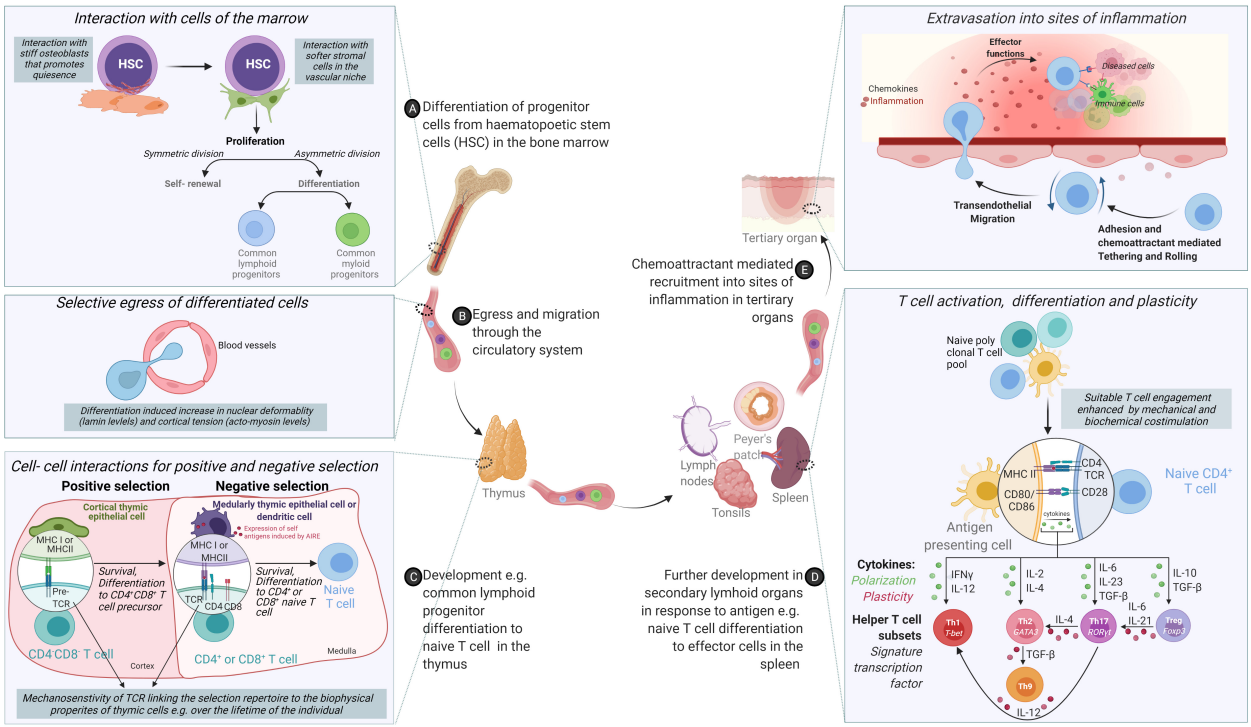

FIGURE 1 | *From origin to function – an odyssey to the battlefront guided through cooperation and tested by competition*. **(A)** Cells of the immune system originate from hematopoietic stem cells (HSCs) in the bone marrow via differentiation cues received from the mechanical and chemical composition of the bone marrow. **(B)** Following differentiation, acquisition of migratory behavior enables cells to egress the bone marrow and circulate through the body via lymphatic and circulatory systems. **(C)** While some cells of the innate immune system compartment complete their differentiation in the bone marrow, adaptive cells such as T cells need comprehensive training in self- non-self-discrimination before acquisition of effector molecules through positive and negative selection in secondary lymphoid organs. **(D)** Differentiated immune cells colonize different organs in the body or continue circulating. **(E)** Functional immune cells are called upon to sites of inflammation to control infection or determine the magnitude and nature of immune responses.

biochemical signal transduction from the cell surface to the nucleus?

MECHANOSENSING TRANSMITTED TO IMMUNE CELL ACTIVATION

Cells are exposed to normative and shear mechanical forces from their microenvironment. The complex interplay between such mechanical stresses and cellular behavior were brought to the forefront by pioneering observations that compliance or rigidity of a substrate that presents collagen affects the adherence and motility of differentiated epithelial and fibroblastic cells (Pelham and Wang, 1997) and mesenchymal stem cell differentiation (Engler et al., 2006). In general, structures at the cellular level (microscale) and at the molecular level (nanoscale) that are sensitive to mechanical stimuli enable cellular responses such as activation, differentiation, and migration through their coupling to the cell's cytoskeleton (Orr et al., 2006). A useful framework for understanding cellular mechanosensing breaks down the process to four distinctive components [reviewed in Chen et al. (2017)]: (1) *mechanopresentation*- the mechanical stimuli is presented to the cells, (2) *mechanoreception*- the ligand is engaged by the mechanoreceptor at the cell surface, (3) *mechanotransmission*- the signal propagates away from the ligand/receptor binding site and, (4) *mechanotransduction*- the mechanical stimuli is converted into a biochemical signal.

MECHANOPRESENTATION

Stiffness in the Immunological Synapse Sets the Activation Threshold

Tissue composition and architecture are increasingly implicated in driving inflammation and pathophysiology (Winkler et al., 2020). How the mechanical property, particularly its stiffness or deformability, affects immune cell activation and differentiation have been studied using 2 dimensional hydrogels of varying stiffness in different immune cells [reviewed in Rossy et al. (2018)]. For T cells, the presentation of similar amounts of ligands for the T cell receptor (TCR) and the integrin lymphocyte function-associated antigen 1(LFA-1) on hydrogels with varying stiffness (0.5–100 kPa) showed hydrogel stiffness dependent modulation of cell migration and morphological changes. Interestingly, metabolic properties and cell cycle progression were affected only at the highest stiffness tested (100 kPa)

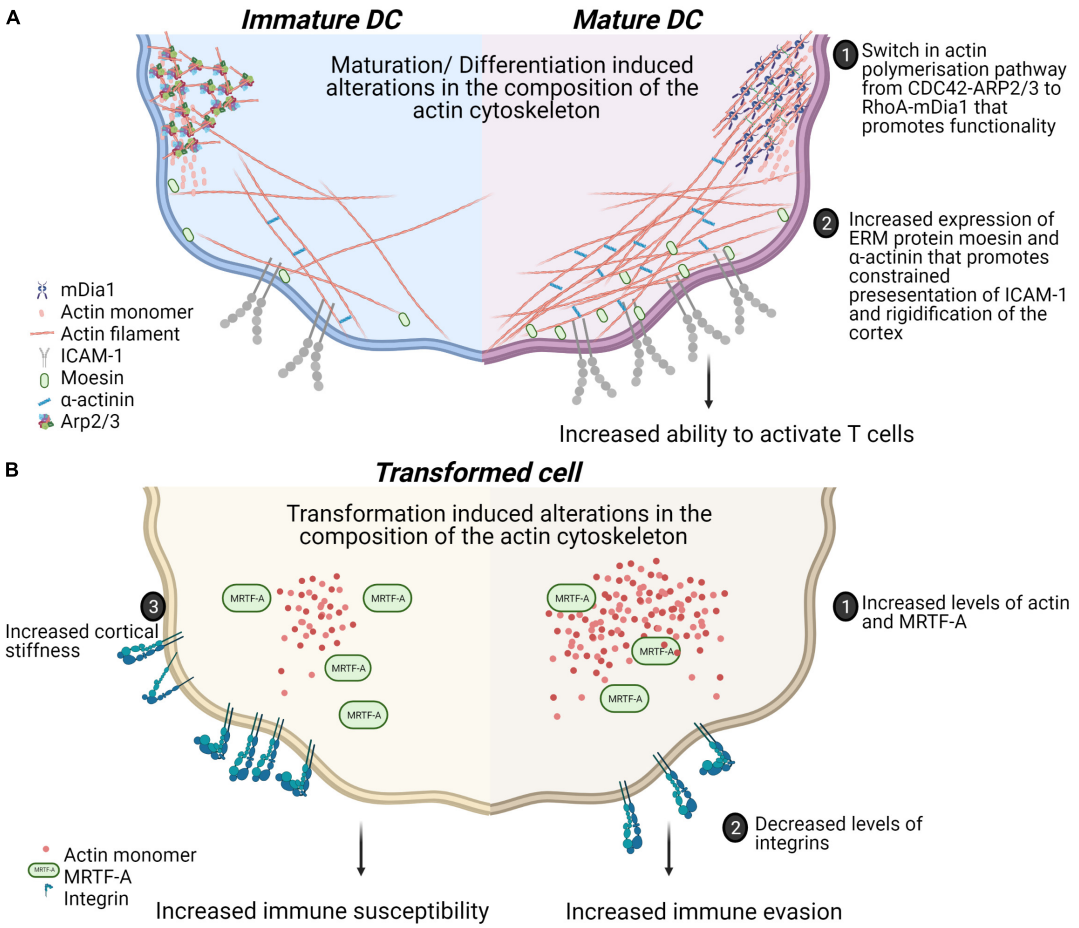

FIGURE 2 | *Physiological and pathophysiological alterations in mechanical properties of immune cells alter functionality of cell-cell contacts*. **(A)** Maturation of dendritic cells in response to Th1 polarizing antigens is associated with alterations in actin polymerization pathways. This is associated with a switch from more adherent, micropinocytosis favoring phenotype to a more migratory phenotype. These changes also include increased confinement of membrane proteins and rigidifying of the cotext that collectively enhance the activation of T cells. **(B)** Transformation induces changes in biophysical properties of cells through alterations in the actin cytoskeleton. Increased levels of MRTF contribute to prometastatic changes such as decreased expression of integrins and increased actin content enhancing migration. However, these adaptations could also lead to increased cortical rigidity and increased susceptibility to cytotoxic cells.

(Saitakis et al., 2017). This is consistent with other reports of maximal cytokine production and proliferation through TCR engagement on stiff substrates (100 kPa) (Judokusumo et al., 2012; O'Connor et al., 2012). Dissecting the specific contributions of the TCR and LFA-1 to spreading on varying stiffnesses revealed a biphasic response when only TCR is ligated and a monotonous response upon LFA-1 co-ligation (Wahl et al., 2019). These results suggest that T cells discriminate between the wide range of substratum stiffnesses found in the body and adapt their responses accordingly. In human dendritic cells (DCs) the culture substrate stiffness during *in vitro* differentiation has been shown to negatively regulate the expression of C-type lectins, β2 integrins as well as podosome formation leading to decreased antigen uptake (Mennens et al., 2017). In addition to the relevance of such studies for *ex vivo* culture and expansion of immune cells, these studies reveal cellular rigidity as an additional layer for regulating cell-cell interactions. In this regard, the rigidity of antigen presenting DCs has been studied in physiological and pathophysiological contexts (**Figure 2**). Firstly, DCs are particularly potent primers of T cell responses. The DC-T cell immunological synapse is characterized by actin rearrangements in both cells. At the DC side, actin rearrangements through WASp and Hem1 containing WAVE complexes promote the appearance of podosomes, which is thought to restrict the mobility of proteins and increased rigidity that promotes stability of contacts and CD4 T cell activation (Malinova et al., 2016; Leithner et al., 2021). Secondly, during T helper (Th) 1 immune response driving maturation, DCs upregulate levels of the actin cytoskeletal regulators moesin and α-actinin 1 which serves to restrict the mobility of Intercellular Adhesion Molecule 1 (ICAM-1) and promote T cell activation (Comrie et al., 2015). Atomic force microscopy experiments established similar twofold stiffening during *in vivo* LPS mediated DC maturation and *in vitro* differentiation of bone marrow derived DCs (BMDCs). Using BMDCs from murine models of WASp, Fascin or HS1 deficiency, a role for WASp expression

in this maturation response was also shown. Surprisingly, this study revealed that DC stiffness lowers the activation threshold for CD4 but not CD8 T cells (Blumenthal et al., 2020). The rigidity of follicular DCs, found in germinal centers, was found to be twofold higher than BMDCs (Spillane and Tolar, 2016). As B cells are thought to preferentially use mechanical extraction of antigens as opposed to enzymatic liberation, tethering of antigens to stiff surfaces in germinal centers could be a critical mechanism for stringent B cell affinity discrimination further expanding the role played by such cell mechanics in immunity.

Moving Against the Flow

Immune cells circulating in the periphery are exposed to mechanical stress from the blood flow. The recruitment of immune cells during inflammation is regulated by a multi-step cascade of cell rolling, activation, adhesion, and transmigration through the endothelial cell barrier. After selectin-mediated adhesion, immune cells migrate along the activated vascular endothelium on which ligands, including ICAM-1 and vascular cell adhesion molecule-1 (VCAM-1) are expressed. Hematopoietic stem cells use this route to home and migrate into the bone marrow. *In vitro* experiments where cells are introduced to controlled unidirectional shear flow reveal that interaction with VCAM-1 leads to migration downstream of the flow direction whereas LFA-1 – ICAM-1 interactions mediated upstream migration, in reverse direction of the flow (Buffone et al., 2018). Effector T cells oriented their migration on ICAM-1, but not on ICAM-2 and VCAM-1, on endothelial monolayers (Valignat et al., 2013; Dominguez et al., 2015). Neutrophils express LFA-1 and they also express macrophage-1 antigen (Mac-1) that binds to ICAM-1. Neutrophils use Mac-1 to migrate downstream on ICAM-1 coated surfaces or activated endothelium during shear flow. However, blocking of Mac-1 lead to upstream migration through LFA-1 - ICAM-1 interactions (Buffone et al., 2019). Marginal zone B cells that depend on strong adhesion forces to localize to the marginal sinus of the spleen where they are exposed to shear stress from the blood flow show similar differential migration in response to VLA-1 and LFA-1 (Tedford et al., 2017). This shows that adhesion molecules steer migration under shear flow stress and that LFA-1 is a key receptor responsible for upstream migration on the endothelium for transmigration of various immune cells into tissues.

MECHANORECEPTION AND MECHANOTRANSMISSION

Immune Receptors Act as Mechanosensors

Mechanoreception by the cell is mediated by cell surface receptors and ion channels and transmitted from these receptors by force induced conformational changes or alteration of receptor-ligand bond properties [reviewed in Zhu et al. (2019)]. While the responsiveness of integrins and ion channels to mechanical force have been appreciated for some time, the ability of immunoreceptors such as the T cell receptor (TCR), B cell receptor (BCR), FcγRIIA (the receptor for the Fc fragment of immunoglobulin G, IgG) and glycoprotein Ib (GPIb) to directly sense force was surprising. Direct mechanoreception was initially demonstrated for the TCR where controlled presentation of mechanical stimulus led to T cell activation regardless if the force is tangential or normal to the receptor (Kim et al., 2009; Li et al., 2010; Pryshchep et al., 2014; Feng et al., 2017). Further characterization of the mechanosensing capacity of the TCR showed that the TCR can generate forces in the 12–19 pN range during binding with peptide-MHC molecules. While weak compared to forces generated by integrin-ligand bonds, these forces contribute to the remarkable sensitivity of TCR triggering and affinity discrimination (Das et al., 2015; Liu et al., 2016). Recently, it was shown that selection of CD8 T cell in the thymus relies on a mechanotransduction signaling loop which via TCR–pMHC–CD8 heterotrimer enables cells to differentiate signals for positive or negative selection (Hong et al., 2018). The TCR acts as a mechanosensory receptor in the early steps of T cell activation and is dependent on the actin cytoskeleton and can also be modulated by co-engagement of the integrin LFA-1 (Husson et al., 2011). Mechanical activation of the TCR leads to the generation of cytoskeletal forces from actin polymerization and myosin mediated retrograde actin flow enabling the cell to counteract mechanical forces exerted on the TCR (Bashour et al., 2014; Hui et al., 2014; Colin-York et al., 2019). Thus, actin cytoskeletal dynamics enable crosstalk between the cell and its environment (Gupta et al., 2015) and critically modulate T cell activation thresholds (Kaizuka et al., 2007; Babich et al., 2012; Murugesan et al., 2016; Jankowska et al., 2018). Intriguingly, while abrogation of actin cytoskeletal dynamics prevents T cell activation through mechanical stimulation, applying oscillatory forces on T cells with an inhibited actin cytoskeleton still leads to cellular activation. This suggests the formation of short-lived signal intermediates that accumulate to successfully activate the T cell if the force that trigger the TCR is applied with a high frequency (Hu and Butte, 2016). The development of sensitive probes such as double strand DNA tension sensors, revealed differential sensitivity of the IgM or isotype switched IgG/IgE B cell receptors (BCRs) (Wan et al., 2015).

MECHANOTRANSDUCTION

Rho GTPases as Messengers in Immune Cells

Mechanotransduction is the translation of mechanical stimuli sensed by the mechanoreceptor into biochemical signals which activates signaling pathways inside the cell via cytoskeletal remodeling. In a wide range of cells, the Ras homology gene family, member A (RhoA) pathway is activated in response to forces particularly downstream of integrin signalling and has been extensively studied in this context as it regulates both actin cytoskeletal changes and myosin contractility. When tension is applied, for instance, on α5β1 integrins, it promotes the binding of the fibronectin synergy motif leading to the activation of focal adhesion kinase (FAK) (Friedland et al., 2009) and the Src family of kinases (SFKs) (Na et al., 2008). Activation of

SFK and FAK leads to the activation of the RhoA GEFs LARG and GEF-H1, respectively (Guilluy et al., 2011). Rho GTPases act as molecular switches alternating between their activated GTP-bound form and their inactivated GDP-bound form. GTP-bound active RhoA regulates both actin polymerization by direct activation of the formin mDia1 (Watanabe et al., 1999) as well as cell contractility via Rho-associated protein kinase (ROCK) mediated phosphorylation of the regulatory light chain of myosin (MLC). ROCK can directly phosphorylate MLC on Serin-19 (Amano et al., 1996) and inhibit the MLC phosphatase MYPT (Kimura et al., 1996). RhoA further promotes buildup and reorganization of actin filaments by phosphorylating and activating LIM kinase which in turn phosphorylates cofilin and prevents its filament severing activities (Maekawa et al., 1999).

Deficiency in Rho GTPases Cause Immune Cell Alterations

Dysregulation of Rho GTPases is associated with cell transformation and immunodeficiency (Hall, 2012). RhoA is important for immune cell functions. In B cells, RhoA regulates BCR signaling with the loss of RhoA activity abolishing calcium influx and proliferation upon BCR activation (Saci and Carpenter, 2005). RhoA is also activated through p190RhoGEF upon CD40 stimulation and drives plasma cell differentiation (Lee et al., 2003; Ha et al., 2012). RhoA regulates T cell development and function with T cells devoid of RhoA showing a block at the pre-TCR stage during thymic development (Zhang et al., 2014). Cytokinesis and chromosome segregation is impaired when the RhoA GTPase activating protein (GAP) ARHGAP19 is overexpressed in T cells (David et al., 2014). Activation of integrins is regulated by RhoA in T cells (Smith et al., 2003; Vielkind et al., 2005) controlling T cell polarization with the formation of the leading edge and the uropod necessary for transendothelial migration (Heasman et al., 2010). Furthermore, T cell migration in non-lymphoid tissues is dependent on RhoA and the absence of RhoA in these cells results in impaired control of skin infections (Moalli et al., 2018). Finally, RhoA regulates immune synapse formation by adjusting cofilin activity. The increased expression of RhoA in naïve T cells leads to the formation of smaller and stiffer immunological synapses when compared to synapses formed by effector T cells which have a relatively lower levels of RhoA (Thauland et al., 2017). Another well know role of RhoA, is the activation of the MKL1/MRTF-A/serum response factor (SRF) pathway which downstream of actin changes regulates numerous genes including cytoskeletal genes. This highlights the importance of RhoA in the coordination of mechanical cues and cellular response to these stimuli via the actin cytoskeleton.

CYTOPLASMIC COMMUNICATION TO THE NUCLEUS

The nucleus can sense mechanical stimuli from the environment through biochemical signal transduction from mechanoresponsive cell surface receptors resulting in nucleo-cytoplasmic shuttling of mechanoresponsive biochemical cues (**Figure 3**) or more directly, through coupling of cytoskeletal proteins and motors with mechanoresponsive elements in the nuclear envelop and nucleoplasm (Cho et al., 2017; Pennacchio et al., 2021).

NUCLEO-CYTOPLASMIC SHUTTLING PROTEINS

Myocardin Related Transcription Factor A (MRTF-A)/Megakaryoblastic Leukemia 1 Protein (MKL1)

The Myocardin Related Transcription Factor A (MRTF-A), also known as Megakaryoblastic leukemia 1 protein (MKL1) (Ma et al., 2001), is probably the best described mediator between cytoskeletal dynamics and nuclear responses. MRTF-A is a transcription cofactor that binds to SRF to regulate expression of numerous genes and is involved in several processes such as development, cell migration, and immunity (Arsenian et al., 1998; Cen et al., 2004; Esnault et al., 2014; Record et al., 2015). MRTF-A binds to G-actin via its RPEL domain which can form tri- and pentameric complexes with G-actin, serving as a sensor for the levels of G-actin monomers inside the cytosol (Miralles et al., 2003; Vartiainen et al., 2007; Mouilleron et al., 2008; Mouilleron et al., 2011). A second RPEL domain contains an extended bipartite nuclear localization signal (NLS) that is hidden when MRTF-A is bound to G-actin. In the absence of interaction with G-actin, the MRTF-A NLS can interact with importin αβ and promote nuclear translocation of MRTF-A (Mouilleron et al., 2008; Pawłowski et al., 2010; Hirano and Matsuura, 2011; Panayiotou et al., 2016). Activation of RhoA dependent actin polymerization by mechanical or mitogenic stimuli leads to a decrease in actin monomer concentration releasing MRTF-A and promoting its nuclear import via its exposed NLS (Cen et al., 2004; Zhao et al., 2007; Muehlich et al., 2008; Esnault et al., 2014). Therefore, MRTF-A constantly shuttles between the cytoplasm and the nucleus depending on its interaction with actin monomers. MRTF-A/G-actin interactions in the nucleus on the other hand leads to MRTF-A nuclear export via interaction with the nuclear export chaperone Crm1 (Miralles et al., 2003; Vartiainen et al., 2007). In the nucleus MRTF-A binds to SRF and acts as a co-transcription factor when its actin binding is disrupted. Nuclear formin mediated actin polymerization via and depolymerization by MICAL2 (Molecules Interacting with CasL 2) have been shown to be an important regulator of MRTF-A/SRF (Baarlink et al., 2013; Lundquist et al., 2014; McNeill et al., 2020). Phosphorylation of MRTF-A also regulates its localization in cells with phosphorylation of residue Serin-549 by ERK resulting in MRTF-A export from the nucleus (Miralles et al., 2003; Muehlich et al., 2008). Other phosphorylation sites also regulate MRTF-A localization such as residue Serin-98 that when phosphorylated prevent the interaction between MRTF-A and G-actin leading to MRTF-A nuclear accumulation. Phosphorylation of Serin-33 increases the activity of a Crm1-dependent nuclear export

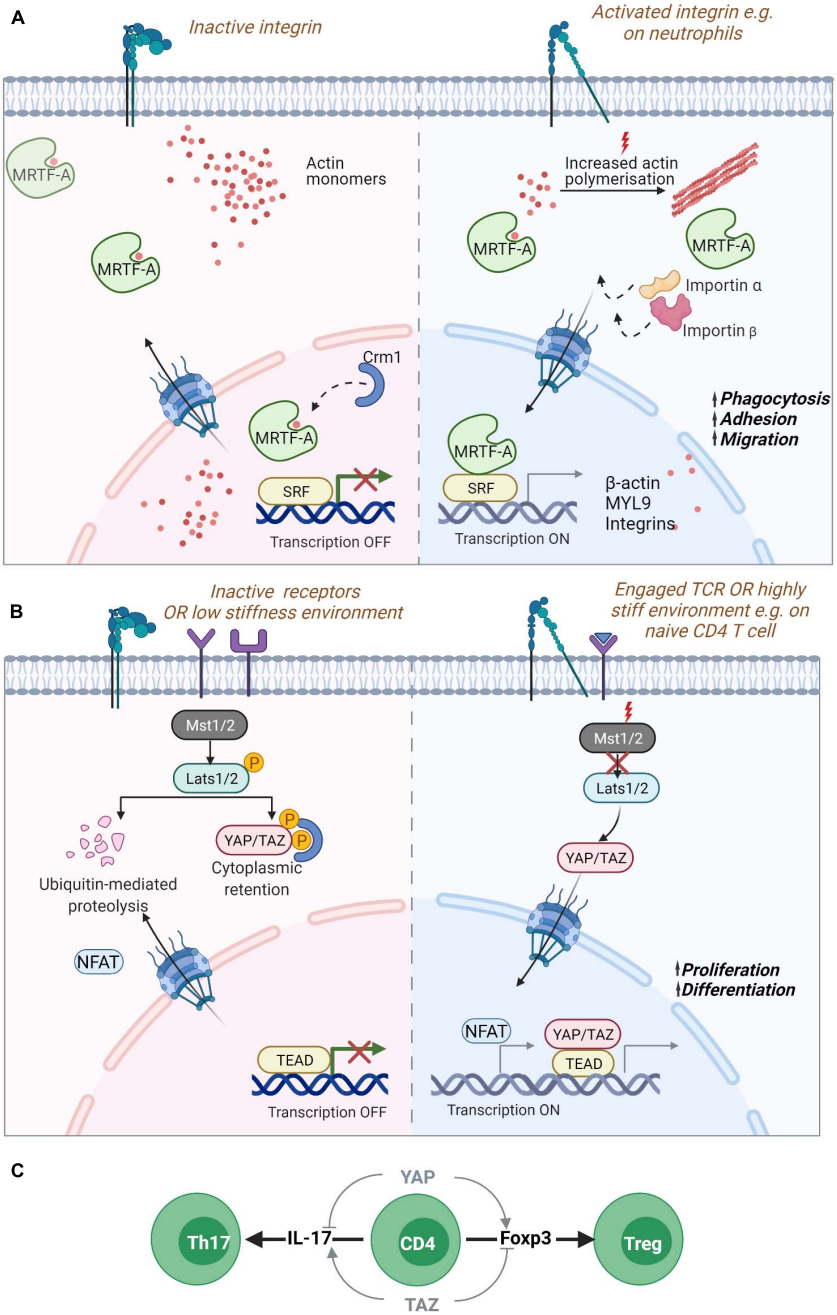

FIGURE 3 | *Nucleo-cytoplasmic shuttling proteins*. Mechanical information from the cell surface can be transduced to the nucleus through the shuttling of gene regulators such as **(A)** MRTF-A/MKL1 or **(B)** YAP or TAZ. **(A)** MRTF-A contains two RPEL domains that can bind to monomeric actin sequestering them in the cytoplasm. Reduction of actin monomers due to filament build up in the cytoplasm leads to the exposure of NLS sequences in MRTF-A, promoting its transport via the chaperones importin α/β into the nucleus. Inside the nucleus, reduced levels of monomeric actin enable its binding to SRF transcription factors for the expression of cytoskeletal genes. Increased levels of monomeric actin in the nucleus in turn promote its association with Crm1 chaperone and export from the nucleus. MRTF-A nuclear translocation is also regulated by phosphorylation (not shown). In neutrophils, MRTF-A is known to drive the expression of β-actin, myosin light chain (MLC) and integrins promoting phagocytosis, adhesion and migration. **(B)** The YAP/TAZ proteins are retained in the cytoplasm via phosphorylation through activated Lats1/2 kinase targeting the proteins for degradation or retention. Mechanosensitive signaling leading to reduced phosphorylation of Lats1/2 by Mst1/2 leads to hypo-phosphorylation of the protein and its translocation to the nucleus for association with TEAD containing transcriptional regulators. YAP regulates the enhanced proliferation of T cells on stiff environments. **(C)** During naïve T cell differentiation, YAP and TAZ have opposing effects. The expression of the YAP paralog promotes Foxp3 expression and thus, regulatory T cell formation while also inhibiting IL-17 expression Th17 differentiation. While TAZ promotes Th17 differentiation and blocks Treg differentiation. Myocardin Related Transcription Factor A (MRTF-A)/Megakaryoblastic leukemia 1 protein (MKL1); Yes-associated protein (YAP) and its paralog WW Domain-Containing Transcription Regulator Protein1 (WWTR1/TAZ); Nuclear localization signal (NLS); Serum response factor (SRF); TEA domain family (TEAD).

signal (NES) (Panayiotou et al., 2016). However, the mechanisms regulating these phosphorylation events are unknown.

A homozygous nonsense mutation p.K723X in MRTF-A leading to a strongly reduced expression of the protein has been described in a patient presenting with severe immunodeficiency (Record et al., 2015). The patient suffered from recurrent and severe bacterial infections, such as Pseudomonas septic shock associated with meningitis, malignant otitis externa and abundant cutaneous and subcutaneous abscesses suggesting impaired innate immune cell functionality. This was confirmed by reduced levels of monomeric and filamentous actin in neutrophils which showed severe defects in phagocytosis and migration. MRTF-A deficient cells displayed a decrease in the expression of MYL9 but increased expression of the integrin CD11b which could explain the uropod retraction defect and the failed migration (Record et al., 2015) (**Figure 3A**). More recently, two siblings were reported with a frameshift mutation p.V453Rfs*16 resulting in the absence of MRTF-A in patient cells and severe migratory defects in patient's neutrophils (Sprenkeler et al., 2020).

Yes-Associated Protein (YAP) and Its Paralog WW Domain-Containing Transcription Regulator Protein1 (WWTR1/TAZ)

Another important pathway for mechanotransduction into the nucleus is the Hippo pathway that activates transcription by Yes-associated protein (YAP) and its paralog WW Domain-Containing Transcription Regulator Protein1 (WWTR1/TAZ) proteins (Oka and Sudol, 2009). YAP and TAZ are both considered as mechanotransducers that relay signals about substrate stiffness during cell spreading and cell-cell interactions (Dupont et al., 2011; Kim et al., 2011; Nardone et al., 2017). When the Hippo pathway is "On," it leads to the phosphorylation of YAP (on Serin-127) and/or TAZ (Serin-89) via the kinase linker of activation (LAT)-Serin-172 (LATS1/2) resulting in the cytoplasmic sequestration or degradation of these proteins (Meng et al., 2016). The activation of Rho GTPases or of FAK - Phosphoinositide 3-kinase (PI3K) signaling during attachment to the extracellular matrix leads to inhibitory phosphorylation of LATS1/2 resulting in the translocation of YAP/TAZ into the nucleus (Mo et al., 2012; Zhao et al., 2012; Kim and Gumbiner, 2015). The stability of the actin cytoskeleton is essential for YAP shuttling into the nucleus. Disruption of F-actin promotes the phosphorylation of YAP and blocks its nuclear localization (Mo et al., 2012; Zhao et al., 2012). YAP/TAZ shuttling is also regulated by mechanical cues from the extracellular matrix and when cells are exposed to stiff matrices, forces are transmitted from the focal adhesions to the nucleus via the cytoskeleton leading to the stretching of the nuclear pores and increased import of YAP into the nucleus (Elosegui-Artola et al., 2017) (**Figure 3B**). In the nucleus, YAP/TAZ bind to TEA domain transcription factors (Zhao et al., 2008). YAP/TAZ interactions with TEA activates the transcription of many genes involved in cell growth cell-matrix interactions, extracellular matrix composition and cytoskeleton integrity (Aragona et al., 2013; Morikawa et al., 2015; Zanconato et al., 2015; Nardone et al., 2017).

While there is increasing evidence for the role of the Hippo pathway in immune cells (Yamauchi and Moroishi, 2019), the specific contributions of YAP and TAZ have only recently been unveiled. YAP and TAZ have distinctive roles in T cells displaying reciprocal regulation in the differentiation and function of specific T cell subsets. TAZ regulates T regulatory (Treg) and Th17 differentiation while YAP supports Treg cell functions. In Th17 cells, TAZ co-activates the transcription factor RORγt which is critical for the expression of the cytokine IL-17 and Th17 differentiation. Thus, TAZ enhances Th17 differentiation and potentiates Th17 mediated autoimmune diseases. On the other hand, TAZ attenuates Treg cell differentiation by promoting degradation of the Treg master transcription factor Foxp3 (Geng et al., 2017). YAP seems to have a distinctive role from TAZ and promotes Treg cell differentiation when overexpressed, possibly via TGFβ receptor 2 (Fan et al., 2017). Such a role for YAP in Treg cells has been confirmed in another study showing that YAP sustains Foxp3 and repress IL-17 and IFNγ expression (**Figure 3C**). YAP promotes expression of genes involved in TGFβ/Smad signaling and suppresses anti-tumor activity leading to increased tumor growth (Ni et al., 2018). Moreover, recent data show that the absence of YAP increases the activity of cytotoxic T cells and leads to higher production of pro inflammatory cytokines, increased expression of Granzyme B and Perforin, and decreased expression of exhaustion receptors, indicating higher tumor killing capacity by YAP deficient T cells (Lebid et al., 2020). Interestingly, it has been shown that T cells proliferate less in soft microenvironments compared to stiff microenvironments. Strikingly, T cells lacking YAP in soft microenvironment proliferate as fast as T cells in stiff microenvironment indicating that stiffness dependent T cell proliferation depends on YAP activity. On soft matrix, YAP is hyperphosphorylated on the Serine 397 and impairs NFAT1 nuclear localization affecting T cell activation and metabolism. As the stiffness of lymph nodes decreases when infection is resolved, YAP activity via mechanosensing of the tissue mechanical properties is speculated to dampen post-infection T cell responses (Meng et al., 2020) (**Figure 3B**).

NUCLEAR MECHANOSENSING THROUGH CYTOSKELETAL COUPLING

LINCing the Nuclear and Cytoplasmic Cytoskeletons

Approaches for quantitatively studying the mechanical properties of the nucleus and for determining the relevance of various biomolecules in mechanotransduction have included nuclear deformation in response to controlled presentation of force at the plasma membrane and nuclear positioning during migration (Obino et al., 2016). During migration, the progressive positioning of the nucleus toward the leading edge allows leukocytes to use their largest organelle to sense

the path of least resistance for fast migration through tissues (Renkawitz et al., 2019) (**Figure 4B**). When the migrating cell is subjected to compression that exceeds the deformability of the nucleus, the nuclear envelop disassembles, triggering the generation of resistant pushing forces enabling the cell evade (Lomakin et al., 2020) (**Figure 4C**). Neutrophils, which have multi-lobed deformable nuclei, or cells with induced nuclear flexibility do not display perinuclear actin accumulation when encountering restrictive spaces, while cells with rigid nuclei do (Thiam et al., 2016). The eukaryotic nuclear envelop is a double membrane bilayer where the with an inner nuclear membrane attached to nucleoskeleton and chromatin and an outer membrane that forms a continuum with the endoplasmic reticulum (ER). Cell nuclei are physically integrated with the cytoskeleton through the mechanosensitive components of the nuclear envelop such as the Linker of Nucleoskeleton and Cytoskeleton (LINC) complexes and the intermediate filaments of the nucleoskeleton that in response to mechanical stresses can undergo physical unfolding revealing cryptic sites and changes in biochemical property (Wong et al., 2021) (**Figure 4A**). Interestingly, during DC migration, perinuclear actin drives passage through constrictive structures independently of the LINC complex (Thiam et al., 2016).

The LINC complex is composed of outer nuclear envelop membrane protein Nesprin containing the KASH (Klarsicht, ANC-1, Syne Homology) domain. The KASH domain interacts directly with inner nuclear envelop membrane SUN (Sad1p, UNC-84 domain) proteins, that are anchored to the nucleoskeleton by interactions with the carboxyl terminus of Lamin A (Haque et al., 2006; Chang et al., 2015). Various isoforms of Nesprins exist and are coupled to different types of

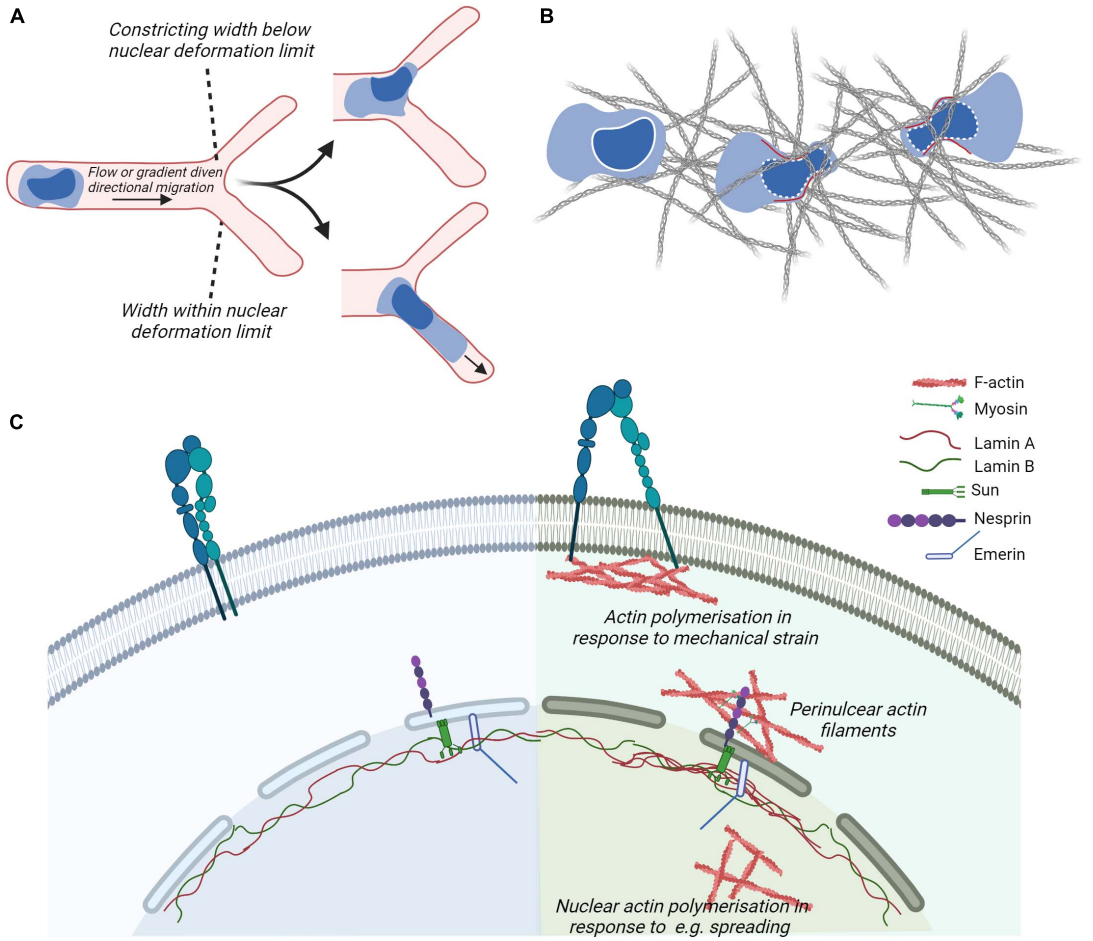

FIGURE 4 | *Cytoskeletal coupling of the nucleus and cytoplasm*. **(A,B)** In leukocytes navigating confined environment such as vessel entrances or dense matrices, the mechanical properties and responses of their nuclei play important regulatory roles such that constraints induce nuclear envelope disassembly and generation of forces (in red) to promote leukocyte escape from the compressive environment and identify paths of least resistance. **(C)** Actin cytoskeletal adaptations to plasma membrane proximal signaling or mechanical strain, e.g., through the generation of focal adhesions and perinuclear actin filaments couple to the nuclear cytoskeleton through the nuclear envelop. The outer nuclear envelop proteins such as Nesprin confer recognition of cytoplasmic cytoskeletal proteins such as actin or microtubules (not shown). Inner envelop proteins such as Sun and Emerin enable the connection of Nesprin family of proteins to the intermediate filaments making up the nuclear lamina. The nuclear lamina contribute to the mechanical properties of cell and adapt to mechanical stimulation, e.g., by displaying localized accumulation in response to strain.

the cytoskeleton as well as motor proteins. These include the largest isoforms of Nesprin-1 and -2 containing an N-terminal actin-binding domain that enables interaction with cytoplasmic actin filaments and signal transduction from actin caps or form transmembrane actin-associated nuclear (TAN) lines. Moreover, these isoforms contain spectrin-repeats that can interact with kinesin and/or dynein subunits and thus microtubules. Nesprin-3 can bind to intermediate filaments via plectin. Nesprin-4, which is only expressed in secretory epithelial cells, is a kinesin-binding protein that connects the nucleus to microtubules. SUN proteins of the inner nuclear envelop are highly evolutionarily conserved. Studies in non-immune cells demonstrate that depletion or expression of dominant-negative Nesprin or SUN proteins severely impairs nucleo–cytoskeletal force transmission (Lombardi et al., 2011). The nuclear lamina is composed of alpha helical rods of type V intermediate filaments that assemble hierarchically to produce a thin meshwork associated with the nuclear side of the inner nuclear membrane. The nuclear lamina is thought to be associated with chromatin through nuclear envelope transmembrane proteins (Wilkie et al., 2011; Solovei et al., 2013; Zuleger et al., 2013). Lamin A/C contribute to nuclear mechanics such that local pressure induces local accumulation of Lamin A (Lammerding et al., 2006). Moreover, in adherent cells, Lamin A/C and transcriptionally active chromatin were shown to be vertically polarized. Perinuclear actin fibers enriched in contractile myosin fibers were linked to the LINC complex and disorganized by inhibition of myosin activity or in laminopathies (Khatau et al., 2009; Kim and Wirtz, 2015). The absence of Lamin A results in a decrease in RhoA activity, reduced adhesion, softened the cytoplasm, and decreased cell migration. This suggests a cross-talk between the nuclear skeleton and the cytoskeleton via RhoA (Hale et al., 2008). Moreover, the proteins of the nuclear envelope Lamin A/C and Emerin regulate MRTF-A translocation into the nucleus. In cells lacking Lamin A/C, actin polymerization is altered resulting in a sequestration of MRTF-A in the cytoplasm. Ectopic expression of Emerin reverted the phenotype (Ho et al., 2013). Emerin stimulation of MRTF-A/SRF activity is dependent on the substrate stiffness (Willer and Carroll, 2017), reinforcing the importance of MRTF-A in mechanotransduction.

Nuclear Viscosity, Cell Polarization and Migration

Somatic cells express Lamin A/C and Lamin B1 and B2. Genetic disorders that result in altered Lamin A expression or duplication of Lamin B result in human diseases and are collectively termed laminopathies (Rankin and Ellard, 2006). These diseases as well as Lamin A/C and Lamin B deficient mice indicate a tight coupling of Lamin A expression to muscle, nerve and cardiac cell functionality and viability. Mouse embryonic fibroblasts that lacked Lamin A/C or had the truncated form of the gene lacking the CAAX motif had increased numbers of misshapen nuclei, severely reduced nuclear stiffness, and decreased cell viability under strain (Lammerding et al., 2006; Swift et al., 2013). The nucleus is often the largest and stiffest (i.e., most resistant to deformation) organelle in the cell with the nucleoplasm having higher viscoelastic modulus compared to the cytoplasm in various cell types (Noel et al., 2008). Leukocyte nuclei are 50- to 100-fold softer than the nuclei of most non-hematopoietic cells (Shin et al., 2013) due to their low expression of Lamin A/C, a key regulator of nuclear lamina stiffness (Shin et al., 2013). This is thought to facilitate transendothelial migration and during migration in tissues. Although easily deformed, the leukocyte nuclei are nonetheless stiff enough to compress the endothelial cortical cytoskeleton such that it can get displaced and possibly disassembled independently of endothelial myosin IIA contractility (Shin et al., 2013). Transmigration of T cells leads to nuclear lobulation that is independent of the contractility of the underlying endothelium but dependent on myosin IIA to complete the movement of their relatively rigid nucleus through the endothelial junctions (Jacobelli et al., 2013). Moreover, during the activation of naïve T cells with ligand coated beads actin filament accumulation at the interface resulted in nuclear elongation (Gupta et al., 2012; Fabrikant et al., 2013).

Lamin A/C are not expressed in non-activated T cells but transiently upregulated following TCR activation. In adoptive transfer experiments, Lamin A null T cells failed to respond to recall stimulation. Strikingly, Lamin A deficiency led to aberrant immunological synapse formation and altered TCR dynamics and reduced activation (González-Granado et al., 2014). Quantitative proteomic analysis of naïve T cells from wildtype or Lamin A knockout mice stimulated by TCR activation, showed a direct role for Lamin A in regulating expression of epigenetic modifying enzymes. Functional consequence of these changes was reduced ability for T cell polarization to the Th1 T cell subset and enhanced Treg cell differentiation and functionality *in vitro*. The preferred Treg cell differentiation of Lamin A deficient T cells was further confirmed using an *in vivo* model for inflammatory bowel disease in which Lamin A deficient T cells were protected from disease development (Toribio-Fernández et al., 2019). This shows a direct role for Lamin A in controlling differentiation of T cell subsets, critical for T cell mediated immunity.

The centrosome plays an important role for cell polarity and at steady state in B cells, the centrosome is tethered to the nucleus via the LINC complex by centrosome-associated Arp2/3 that locally nucleates F-actin (Obino et al., 2016). Upon B cell activation, Arp2/3 is partially depleted from the centrosome leading to a reduction in F-actin at the centrosome, detachment from the nucleus, and polarization to the immunological synapse. Actin filament density at the centrosome is negatively affected by the degree of cell spreading following BCR and LFA-1 activation (Inoue et al., 2019), suggesting that actin filaments constitute a physical barrier blocking elongation of nascent microtubules. Moreover, during differentiation of hematopoietic stem cells to myeloid lineage cells, large invaginations on the swelling nucleus are generated by microtubule constraints. These invaginations are associated with a local reduction of Lamin B density, local loss of heterochromatin H3K9me3 and H3K27me3 marks, and changes in expression of specific hematopoietic genes.

This highlights the role of microtubules in defining the unique lobulated nuclear shape observed in myeloid progenitor cells and suggests that this nuclear shape is important to establish hematopoietic lineage genes (Fabrikant et al., 2013; Biedzinski et al., 2020).

NUCLEAR ACTIN IN TRANSCRIPTION, CHROMATIN REMODELING, AND NUCLEAR REPROGRAMMING

Cytoskeletal proteins such as actin, myosin, Arp2/3, and WASp family of proteins have recently emerged as key regulators of nuclear functions [reviewed in Ulferts et al. (2021)]. In eukaryotic cells, they have been implicated in chromatin and transcription regulation and more recently there is evidence for their involvement in chromosomal movements, and functional architecture of the genome (Visa and Percipalle, 2010; Miyamoto and Gurdon, 2013; Percipalle, 2013; Kelpsch and Tootle, 2018). These nuclear actin-based mechanisms appear to impact on key cellular processes such as DNA repair and nuclear reprograming during differentiation (Venit et al., 2020b; Xie et al., 2020) by leveraging on regulated actin dynamics (Plessner and Grosse, 2019) (**Figure 5**). In hematopoietic cells, WASp family members are in the nucleus and can have activity both dependent and independent on their capacity to induce Arp2/3 mediated actin polymerization.

Nuclear Actin in Transcription and Chromatin Remodeling

Soon after initial discoveries of actin in the nucleus, its association with RNA Pol II and direct involvement in transcription was revealed (Egly et al., 1984; Scheer et al., 1984; Percipalle et al., 2001, 2003). Actin is associated with all the RNA polymerases facilitating recruitment of histone modifying enzymes (Kukalev et al., 2005; Obrdlik et al., 2008) and forms a complex with Nuclear myosin 1 (NM1), an isoform of the Myo1C gene (Pestic-Dragovich et al., 2000; Fomproix and Percipalle, 2004; Hofmann et al., 2004; Hu et al., 2004; Philimonenko et al., 2004; Grummt, 2006; Dzijak et al., 2012). NM1 can switch between polymerase-bound actin and the ATPase SNF2H, which is a part of chromatin remodeling complex B-WICH. Repositioning of the nucleosomes by B-WICH remodeler leads to the binding of histone acetyltransferase P300/CBP-associated factor (PCAF) and histone methyltransferase Set1 to DNA. This leads to acetylation and methylation of histone H3, generating a more favorable conformation for RNA polymerase to access the chromatin and transcribe genes (Percipalle and Farrants, 2006; Sarshad et al., 2013; Almuzzaini et al., 2015; Almuzzaini et al., 2016; Venit et al., 2020a).

Actin itself is part of several remodeling complexes, with BAF (Brg1- or BRM-associated factors) complex being the most studied (Peterson et al., 1998; Olave et al., 2002; Rando et al., 2002). Out of more than 15 subunits of the BAF complex, the ATPase Brg1 forms a backbone for the whole remodeler and is associated with β-actin (He et al., 2020). This interaction is critical for BAF association with the chromatin as deletion of β-actin leads to dissociation of Brg1 from DNA, an increase of repressive histone marks, and defective localization of heterochromatin (Xie et al., 2018). Reorganization of heterochromatin can be explained by a dual role of the BAF complex on transcriptional regulation and organization of chromatin. Depending on its interactions, BAF can either activate a set of genes by eviction of Polycomb repressive complexes from DNA, or it can repress other genes in complex with transcription repressor REST and repressive remodeling complex NuRD (nucleosome remodeling and deacetylase) (Shimono et al., 2003; Ooi et al., 2006; Yildirim et al., 2011; Kadoch et al., 2017). Therefore, deletion of actin leads to increased association of polycomb repressive complex 2 subunit EZH2 with the chromatin and decreased association of the REST complex which is accompanied by higher-order chromatin switching between heterochromatin and euchromatin (Mahmood et al., 2020). This can have far-reaching consequences for transcriptional reprogramming, differentiation, and cell fate, as Brg1 is required for maintaining pluripotency of stem cells by regulating expression and binding of pluripotency marker Oct4 together with other pluripotency factors Sox2 and Nanog (Ho et al., 2009; Singhal et al., 2014; King and Klose, 2017). Similarly, during direct reprogramming, β-actin knockout cells failed to be properly differentiated to neurons, adipocytes or osteogenic cells due to Brg1 deposition from respective early differentiation genes (Xie et al., 2018; Al-Sayegh et al., 2020; Gjorgjieva et al., 2020). For hematopoietic lineage cells, deletion of Srg3/mBaf155, a scaffold subunit of the BAF complex, causes defects at both the common lymphoid progenitor stage and the transition from pre-pro-B to early pro-B cells due to failures in the expression of B lineage-specific genes, such as Ebf1 (Early B cell factor 1) and IL7ra (IL-7 receptor alpha chain), and their downstream target genes (Choi et al., 2012). Moreover, mice that are deficient in the expression of Brg1 show defects in early B cell development (Choi et al., 2012) (**Figure 5**).

Actin and the WASp Family Proteins in the Nucleus

In most of the remodeling complexes, actin serves in its monomeric state, often bound to different actin-related proteins (Shen et al., 2000; Wu et al., 2005; Kapoor et al., 2013; He et al., 2020). Studying the regulation and functions of polymeric actin proved to be technically challenging as actin does not form typical long fibers visible in the cytoplasm but rather short-lived rods and oligomers present under certain conditions such as serum stimulation (Baarlink et al., 2013; Wang et al., 2020), cellular spreading (Plessner et al., 2015), and cellular stress (Munsie et al., 2012; Figard et al., 2019). A breakthrough in the nuclear actin field came from the development of methods and tools to visualize nuclear actin polymerization using NLS tagged actin-specific chromobodies (Plessner et al., 2015) and the 17-amino-acid peptide LifeActGFP for staining of polymeric actin (Riedl et al., 2008). These tools were critical in visualizing nuclear

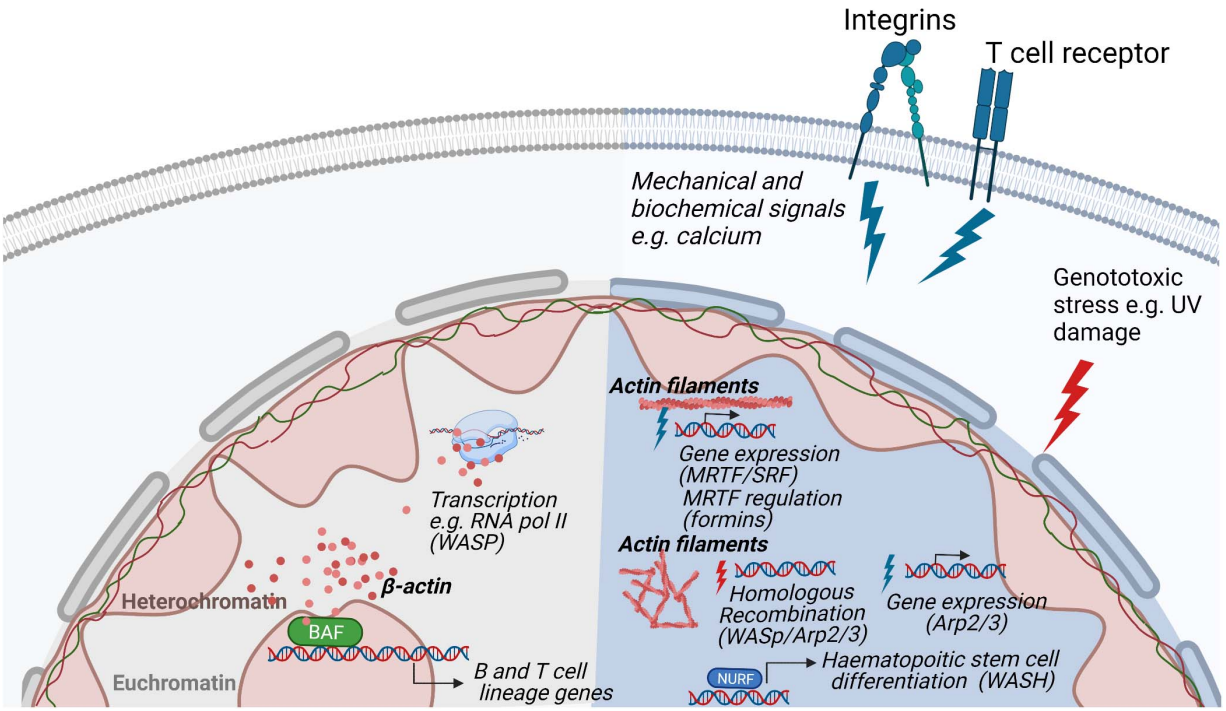

FIGURE 5 | *Regulation of nuclear functions by the actin cytoskeleton*. Nuclear actin plays a role in genome organization and associates and with the transcription machinery. In hematopoietic cells, the actin based chromatin remodeller BAF is involved in the development of B- and T lymphocytes lineages. In response to stimulation, polymerization of actin filaments through various biochemical pathways regulate gene expression and nuclear damage responses. During homologous recombination, WASp, Arp2/3 and actin polymerization promote the movement of DNA damaged foci to the nuclear lamina for repair. In T cells, WASp is involved in RNA Pol II dependent transcription of T cell development genes and it absence results in a decreased of RNA pol II transcription.

actin dynamics in living cells and to manipulate its levels to distinguish the function of nuclear and cytoplasmic actin. Actin dynamics has been suggested to be important for transcription and transcriptional reprogramming, as actin polymerization-defective mutants inhibit RNA Polymerase (Pol) I transcription (Ye et al., 2008) and several regulators of actin polymerization have been found to be essential for proper assembly and processing of the transcription machinery (Venit et al., 2020b). For example, transcriptional reactivation of the pluripotency gene Oct4 is dependent on the WASp family member WAVE1 and polymeric actin (Miyamoto et al., 2011; Miyamoto and Gurdon, 2013). Similarly, upon serum stimulation, Arp2/3 and N-WASp, known to be responsible for branching and polymerization of actin filaments in the cytoplasm, induce formation of nuclear actin fibers which serves as a scaffold for RNA Pol II clustering around serum-response genes (Yoo et al., 2007; Sadhukhan et al., 2014; Wei et al., 2020). Similar movement along the actin filaments in the nucleus seems to be present in the relocation of chromosome territories upon gene activation (Chuang et al., 2006; Dundr et al., 2007; Wang et al., 2020), DNA damage (Kulashreshtha et al., 2016), and serum starvation (Mehta et al., 2010). During repair of double strand DNA breaks by homologous recombination, movement of single DNA damage foci toward the nuclear lamina favors DNA repair and this movement is dependent on WASp, Arp2/3, and actin polymerization (Chiolo et al., 2011; Tsouroula et al., 2016; Aymard et al., 2017; Caridi et al., 2018; Schrank et al., 2018) (**Figure 5**).

In haematopoietic stem cells, WASH associates with the nucleosome remodeling factor (NURF) complex in the nucleus where the NURF complex binds to the promoter of the c-Myc gene, necessary for haematopoietic stem cell differentiation (Xia et al., 2014). The nuclear activity of WASH is dependent on nuclear actin polymerization induced by WASH (Xia et al., 2014). In T cells, WASp associates with RNA Pol II for transcription of specific genes for T cell development and T cell lineage commitment (Taylor et al., 2010; Kuznetsov et al., 2017). Deficiency of WASp expression lead to reduced overall RNA Pol II transcription in T cells (Kuznetsov et al., 2017). The absence of WASp results in increased R-loops related double strand breaks causing genomic instability and an imbalance between Th1 and Th2 cells among WAS patient T cells (Sarkar et al., 2018). Both T cells and B cells devoid of WASp show accumulation of R loops, a three-stranded DNA:RNA hybrid structure that can lead to DNA damage by stalling transcription and replication (Wen et al., 2020). In support of a role for the WASp VCA domain for nuclear function, T cells that express constitutively active WASp-I296T, a mutation found in X-linked neutropenia patients, show interaction with a larger number of genes and accumulate target gene products in the nucleus (Kuznetsov et al., 2017). This suggests that constant exposure of the WASp VCA domain leads to increased nuclear WASp

activity. A recent study suggests that actin polymerization in the nucleus may be one of the earliest steps in TCR signaling such that nuclear actin polymerization may even precede actin polymerization at the plasma membrane which organizes the immunological synapse (Tsopoulidis et al., 2019). Intriguingly, nuclear actin polymerization was demonstrated to be required to produce specific cytokines upon TCR stimulation (Tsopoulidis et al., 2019). In the nuclear compartment, actin is therefore likely to regulate several nuclear processes by interacting with a plethora of nuclear factors and this might be tightly regulated by actin dynamics.

THE IMPORTANCE OF NUCLEAR ACTIN TO AVOID CELL TRANSFORMATION

Clearance of Actin for Cell Division

The final stage of cell division, cytokinesis, is tightly coordinated during chromosome segregation and dependent on actin polymerization and depolymerization. At the terminal stage of cytokinesis, the daughter cells are connected by a thin cytoplasmic canal, the cytokinetic intercellular bridge, that is eventually cut in a complex process called abscission (Green et al., 2012; Nähse et al., 2017; Pollard, 2017). In response to the abnormal presence of lagging chromatin between dividing cells, an evolutionarily conserved abscission/NoCut checkpoint delays abscission to prevent the formation of binucleated cells (Mendoza et al., 2009). The abscission/NoCut checkpoint induces arrest in cytokinetic cells with chromatin bridges, high intercellular bridge membrane tension, defective assembly of nuclear pore complexes, and DNA replication stress. The abscission checkpoint relies on prolonged activity of the mechanosensor Aurora B activity (Nähse et al., 2017). Successful abscission depends on clearance of microtubules and actin filaments from the intercellular bridge (Addi et al., 2018). Interestingly, the redox state of actin is important and the oxidase MICAL1 directly oxidizes Met44 and Met47 of F-actin into methionine-R-sulfoxides and triggers depolymerization of the actin filaments (Frémont et al., 2017). Oxidation-mediated clearance of F-actin by MICAL1 is counteracted by actin reduction by methionine sulfoxide reductases (MsrBs). When lagging chromatin is present, actin polymerization is essential to stabilize the cytokinetic intercellular bridge. Actin reduction by the MsrBs reductases is a key component of the abscission checkpoint that favors F-actin polymerization and limits tetraploid cells (Bai et al., 2020). Importantly, depletion of MsrBs reductases in Drosophila cells leads to a specific reduction of F-actin in the cytokinetic intercellular bridge without a global effect on the cellular actin cytoskeleton as evident from the occurrence of normal cell spreading (Bai et al., 2020).

Dysregulated Actin Polymerization and Cell Transformation

The importance of the abscission/NoCut checkpoint becomes apparent during cell transformation. Cancer cell genomes can contain multiple chromosomal rearrangements. During cell transformation to cancer cells, faulty metaphase progression can lead to presence of chromosomes in the cytokinetic intercellular bridge (Tanaka and Watanabe, 2020). Chromosomal bridges arise in late metaphase from end-to-end chromosome fusions after DNA breakage or telomere instability, incomplete DNA replication, or failed resolution of chromosome catenation (two chromatids structurally linked together during replication). Chromosome bridges can persist post miosis in interphase cells, linking the two daughter cells together (Umbreit et al., 2020). Breakage of chromosome bridges requires acto-myosin generated forces and is partly dependent on activation of the LINC complex as shown using inhibitors for the acto-myosin forces and shRNA for LINC complex proteins (Umbreit et al., 2020). Broken bridge chromosomes undergo mitotic DNA damage and frequent missegregation to form micronuclei. These data indicate that a single cell division error can rapidly generate extreme genomic complexity and genetic instability in daughter cells (Umbreit et al., 2020).

Elevated actin polymerization during mitosis is associated with genomic instability and cell transformation. Gain-of-function mutations of WASp in X-linked neutropenia patients lead to increased F-actin that abnormally localize around the mitotic spindle and chromosomes during their alignment and separation, and during anaphase accumulates within the cleavage furrow around the spindle midzone (Moulding et al., 2007). This results in genomic instability as evident in polyploid cells, cells with micronuclei and structural chromosomal aberrations (Moulding et al., 2007, 2012; Westerberg et al., 2010). The mitotic error of cells expressing constitutively active WASp can be prevented by lowering total F-actin using the Arp2/3 inhibitor CK666. Nuclear actin polymerization is linked to functional integrin signaling and components of the LINC complex, suggesting that cellular adhesion and mechanosensing between the cytoplasm and nucleus contribute to nuclear actin dynamics (Chang et al., 2015). However, mitotic nuclear actin filaments can form upon silencing of the nucleoskeletal proteins Emerin or Lamin A/C or upon disruption of the LINC complex, suggesting that these filaments also can form independently of cell spreading and integrin-dependent signaling (Baarlink et al., 2017).

Elevated F-actin in the cytoplasm is associated with increased cell viscosity leading to activation of mechanosensors such as Aurora A and B during mitosis. Aurora A and Aurora B jointly coordinate chromosome segregation and anaphase microtubule dynamics (Hégarat et al., 2011). Aurora A regulates the actin cytoskeleton reorganization during early mitotic stages by phosphorylation of cofilin, thereby preventing the actin depolymerizing function of cofilin (Ritchey and Chakrabarti, 2014). Aurora B regulates chromosome alignment at metaphase and delays abscission in cells with structural defects or chromatin bridges (Liu et al., 2009). Aurora B activity is crucial in sensing mechanical changes to the centromere during chromosome alignment (Liu et al., 2009). Aurora B is interesting since it is a target for hematopoietic malignancies. A selective Aurora B inhibitor induces growth arrest and apoptosis by the accumulation of 4N and 8N DNA content of human acute leukemia cells *in vitro* and *in vivo* (Yang et al., 2007). On the other hand, overexpression of Aurora B can prevent polyploidy

in cells that have chemically and genetically induced mitosis defects (Nair et al., 2009) and rescues mitosis defect in cells expressing constitutively active WASp (Moulding et al., 2012). Cells expressing gain-of-function of WASp activity leads to increased cell viscosity as determined by atomic force microscopy and activation of the Aurora B mechanical sensor during mitosis (Moulding et al., 2012). Increased MRTA-A/MKL1 expression is associated with elevated G- and F-actin in patient B cells leading to tetraploidity, increased proliferation, tumor formation, and development of Hodgkin lymphoma (Record et al., 2020). Together, this suggests that increased F-actin content is associated with genetic instability and malignant transformation.

Actin Polymerization at the Mitotic Exit

During mitotic exit, the nuclear volume of the two daughter cells is expanding in a process dependent on dynamic assembly of nuclear actin filaments enabling chromatin decondensation. Interfering with the polymerization-competent nuclear actin pool by overexpression of the non-polymerizable actin^{R62D}-NLS mutant or the actin exporter exportin-6 results in a decreased volume of the daughter cell nuclei as well as an increase in chromatin compaction at mitotic exit (Baarlink et al., 2017). The post mitotic nuclear actin filaments are tightly controlled by the actin-depolymerizing factor cofilin-1 (Baarlink et al., 2017). The nuclear activity of cofilin-1 is regulated by phosphorylation in a cell cycle dependent process with an increase in phosphorylated and thus inactive cofilin-1 during mitotic exit. For adherent cells, adhesion to the extracellular matrix persists during mitosis. The so called 'reticular adhesions' are a class of adhesion complexes mediated by the integrin αvβ5 which are formed during interphase, and preserved at cell–extracellular matrix attachment sites throughout cell division (Lock et al., 2018). Depletion of β5 integrins perturbs mitosis by disruption of reticular adhesions. Formation of reticular adhesions maintains cell–extracellular matrix attachment during mitotic rounding and division as a spatial memory transmission between cell generations. Together, these studies reveal that in addition to mechanosensing by the Aurora B kinase, the oxidative state of F-actin in the abscission checkpoint prevents the formation of genetically unstable, tetraploid cancer cells. Rapidly proliferating hematopoietic linage cells, especially B and T cells activated during an immune response, may therefore be particularly vulnerable to increased or decreased F-actin during mitotic exit. Targeted actin reduction and clearance during cytokinesis may be beneficial in general for cancer patients and specifically in cancer therapy for primary immunodeficiency patients with mutations in actin regulators.

PERSPECTIVE

The rapid development of biophysical and bioimaging tools to probe cell mechanics has enabled the study of mechanical properties in immune cells [reviewed in Schneider et al. (2021)], greatly expanding our understanding of how mechanical forces can crosstalk with biochemical signals to regulate cell functions. This shift from an exclusively biochemical understanding of signaling reveals the necessity to incorporate the physical status of tissues and cells in our experimental designs to better elucidate physiology and treat pathologies. The role of mechanosensing in immune cells is emerging as a critical signal transduction pathway and strengthens the evidence for the pivotal role of rapid cytoskeletal dynamics in immune cell functions. Moreover, the development of new tools for visualizing actin in the nucleus together with high throughput genomics data reveal that monomeric and filamentous actin exist in the nucleus and have distinct functions (Venit et al., 2020b) reviving the discussion on the form and function of nuclear actin. Many of the actin regulators described in the cytoplasm have been identified in the nucleus and like actin and nuclear myosin, a major function is through interactions with the RNA polymerase machinery. Recent studies uncovered new roles in chromatin remodeling, DNA repair, establishment of chromosomal territories and, in T cells, alteration of chromosome territories following activation (Ioannou et al., 2015). During an immune response, activation of B and T cells leads to changes in transcription, receptor maturation and hyper proliferation of the selected clone as fast as every 6 h. We can easily imagine that defects in nuclear actin would greatly impact such processes as they rely on DNA repair machinery and chromosomal territories.

Understanding immune cell mechanosensing and nuclear actin function is likely to have direct clinical implications. Efforts using whole genome sequencing have revealed an increasing number of diseases caused by mutations in actin regulators. This subgroup of primary immunodeficiency diseases called actinopathies provide a unique opportunity to understand how deficiency in a specific actin regulator affects immune cells (Saeed et al., 2020). The study of hematopoietic specific actin regulators has focused on their cytoplasmic role. As nuclear actin begins to be understood better, the hopes of targeting actin dynamics to influence immune cell activation and differentiation to enhance or dampen the immune response becomes even more tantalizing. Similarly, the cell mechanical response could be used as an output for drug screening to target early immune cell activity. Finally, as forces regulates T cell activation, it is possible that cancer cell stiffness influences their susceptibility to cytotoxic T cells and may be a therapeutic target. In fact, cancer cells need to carefully tune the rigidity of their actin cytoskeleton via MRTF activity to optimize their resistance to cytotoxic attacks when they metastasize (Tello-Lafoz et al., 2021). Alteration of cancer cells physical properties could be used as a clinical means to improve cytotoxic T cell response and might be of use in combinatory treatments with standard chemotherapies, as well as immunotherapies such as checkpoint blockade antibodies (anti-PD1 and anti-CTLA4 antibodies) and treatment with engineered T cells expressing Chimeric Antigen Receptors [reviewed in Li et al. (2020)].

AUTHOR CONTRIBUTIONS

JR, MS, and TV wrote the manuscript. JR, MS, TV, PP, and LW edited the manuscript. All authors contributed to the article and approved the submitted version.

FUNDING

This work was supported by postdoctoral fellowships from the Childhood Cancer Fund and the Swedish Society for Medical Research to JR, the Swedish Research Council, Cancer Society, Childhood Cancer Fund, a StratCan Blue Sky award, the European Commission 7th Framework Program Marie Curie Reintegration Grant (#249177), Åke Olsson Foundation, Åke Wiberg Foundation, Bergvall Foundation, King Gustaf V's 80-year Foundation, and Karolinska Institutet to LW. LW is a Ragnar Söderberg Fellow in Medicine and holds a Senior Researcher Position supported by the Childhood Cancer Fund.

ACKNOWLEDGMENTS

Illustrations were generated using Biorender.com.

REFERENCES

Addi, C., Bai, J., and Echard, A. (2018). Actin, microtubule, septin and ESCRT filament remodeling during late steps of cytokinesis. *Curr. Opin. Cell Biol.* 50, 27–34. doi: 10.1016/j.ceb.2018.01.007

Alekhina, O., Burstein, E., and Billadeau, D. D. (2017). Cellular functions of WASP family proteins at a glance. *J. Cell Sci.* 130, 2235–2241. doi: 10.1242/jcs.199570

Almuzzaini, B., Sarshad, A. A., Farrants, A. K., and Percipalle, P. (2015). Nuclear myosin 1 contributes to a chromatin landscape compatible with RNA polymerase II transcription activation. *BMC Biol.* 13:35. doi: 10.1186/s12915-015-0147-z

Almuzzaini, B., Sarshad, A. A., Rahmanto, A. S., Hansson, M. L., Euler, A. V., Sangfelt, O., et al. (2016). In β-actin knockouts, epigenetic reprogramming and rDNA transcription inactivation lead to growth and proliferation defects. *FASEB J.* 30, 2860–2873. doi: 10.1096/fj.201600280R

Al-Sayegh, M. A., Mahmood, S. R., Khair, S. B. A., Xie, X., El Gindi, M., Kim, T., et al. (2020). β-actin contributes to open chromatin for activation of the adipogenic pioneer factor CEBPA during transcriptional reprograming. *Mol. Biol. Cell* 31, 2511–2521. doi: 10.1091/mbc.E19-11-0628

Amano, M., Ito, M., Kimura, K., Fukata, Y., Chihara, K., Nakano, T., et al. (1996). Phosphorylation and activation of myosin by rho-associated kinase (Rho-kinase) *. *J. Biol. Chem.* 271, 20246–20249. doi: 10.1074/jbc.271.34.20246

Ancliff, P. J., Blundell, M. P., Cory, G. O., Calle, Y., Worth, A., Kempski, H., et al. (2006). Two novel activating mutations in the Wiskott-Aldrich syndrome protein result in congenital neutropenia. *Blood* 108, 2182–2189. doi: 10.1182/blood-2006-01-010249

Aragona, M., Panciera, T., Manfrin, A., Giulitti, S., Michielin, F., Elvassore, N., et al. (2013). A mechanical checkpoint controls multicellular growth through YAP/TAZ regulation by actin-processing factors. *Cell* 154, 1047–1059. doi: 10.1016/j.cell.2013.07.042

Arsenian, S., Weinhold, B., Oelgeschläger, M., Rüther, U., and Nordheim, A. (1998). Serum response factor is essential for mesoderm formation during mouse embryogenesis. *EMBO J.* 17, 6289–6299. doi: 10.1093/emboj/17.21.6289

Aymard, F., Aguirrebengoa, M., Guillou, E., Javierre, B. M., Bugler, B., Arnould, C., et al. (2017). Genome-wide mapping of long-range contacts unveils clustering of DNA double-strand breaks at damaged active genes. *Nat. Struct. Mol. Biol.* 24, 353–361. doi: 10.1038/nsmb.3387

Baarlink, C., Plessner, M., Sherrard, A., Morita, K., Misu, S., Virant, D., et al. (2017). A transient pool of nuclear F-actin at mitotic exit controls chromatin organization. *Nat. Cell Biol.* 19, 1389–1399. doi: 10.1038/ncb3641

Baarlink, C., Wang, H., and Grosse, R. (2013). Nuclear actin network assembly by formins regulates the SRF coactivator MAL. *Science* 340, 864–867. doi: 10.1126/science.1235038

Babich, A., Li, S., O'Connor, R. S., Milone, M. C., Freedman, B. D., and Burkhardt, J. K. (2012). F-actin polymerization and retrograde flow drive sustained PLCγ1 signaling during T cell activation. *J. Cell Biol.* 197, 775–787. doi: 10.1083/jcb.201201018

Bai, J., Wioland, H., Advedissian, T., Cuvelier, F., Romet-Lemonne, G., and Echard, A. (2020). Actin reduction by MsrB2 is a key component of the cytokinetic abscission checkpoint and prevents tetraploidy. *Proc. Natl. Acad. Sci. U.S.A.* 117, 4169–4179. doi: 10.1073/pnas.1911629117

Bashour, K. T., Gondarenko, A., Chen, H., Shen, K., Liu, X., Huse, M., et al. (2014). CD28 and CD3 have complementary roles in T-cell traction forces. *Proc. Natl. Acad. Sci. U.S.A.* 111, 2241–2246. doi: 10.1073/pnas.1315606111

Biedzinski, S., Agsu, G., Vianay, B., Delord, M., Blanchoin, L., Larghero, J., et al. (2020). Microtubules control nuclear shape and gene expression during early stages of hematopoietic differentiation. *EMBO J.* 39:e103957. doi: 10.15252/embj.2019103957

Blumenthal, D., Chandra, V., Avery, L., and Burkhardt, J. K. (2020). Mouse T cell priming is enhanced by maturation-dependent stiffening of the dendritic cell cortex. *eLife* 9:e55995. doi: 10.7554/eLife.55995

Buffone, A., Anderson, N. R., and Hammer, D. A. (2018). Migration against the direction of flow is LFA-1-dependent in human hematopoietic stem and progenitor cells. *J. Cell Sci.* 131:jcs205575. doi: 10.1242/jcs.205575

Buffone, A., Anderson, N. R., and Hammer, D. A. (2019). Human neutrophils will crawl upstream on ICAM-1 if Mac-1 is blocked. *Biophys. J.* 117, 1393–1404. doi: 10.1016/j.bpj.2019.08.044

Campellone, K. G., and Welch, M. D. (2010). A nucleator arms race: cellular control of actin assembly. *Nat. Rev. Mol. Cell Biol.* 11, 237–251. doi: 10.1038/nrm2867

Caridi, C. P., D'Agostino, C., Ryu, T., Zapotoczny, G., Delabaere, L., Li, X., et al. (2018). Nuclear F-actin and myosins drive relocalization of heterochromatic breaks. *Nature* 559, 54–60. doi: 10.1038/s41586-018-0242-8

Cen, B., Selvaraj, A., and Prywes, R. (2004). Myocardin/MKL family of SRF coactivators: key regulators of immediate early and muscle specific gene expression. *J. Cell. Biochem.* 93, 74–82. doi: 10.1002/jcb.20199

Chang, W., Worman, H. J., and Gundersen, G. G. (2015). Accessorizing and anchoring the LINC complex for multifunctionality. *J. Cell Biol.* 208, 11–22. doi: 10.1083/jcb.201409047

Chen, Y., Ju, L., Rushdi, M., Ge, C., and Zhu, C. (2017). Receptor-mediated cell mechanosensing. *Mol. Biol. Cell* 28, 3134–3155. doi: 10.1091/mbc.e17-04-0228

Chiolo, I., Minoda, A., Colmenares, S. U., Polyzos, A., Costes, S. V., and Karpen, G. H. (2011). Double-strand breaks in heterochromatin move outside of a dynamic HP1a domain to complete recombinational repair. *Cell* 144, 732–744. doi: 10.1016/j.cell.2011.02.012

Cho, S., Irianto, J., and Discher, D. E. (2017). Mechanosensing by the nucleus: from pathways to scaling relationships. *J. Cell Biol.* 216, 305–315. doi: 10.1083/jcb.201610042

Choi, J., Ko, M., Jeon, S., Jeon, Y., Park, K., Lee, C., et al. (2012). The SWI/SNF-like BAF complex is essential for early B cell development. *J. Immunol.* 188, 3791–3803. doi: 10.4049/jimmunol.1103390

Chuang, C.-H., Carpenter, A. E., Fuchsova, B., Johnson, T., de Lanerolle, P., and Belmont, A. S. (2006). Long-range directional movement of an interphase chromosome site. *Curr. Biol.* 16, 825–831. doi: 10.1016/j.cub.2006.03.059

Colin-York, H., Javanmardi, Y., Skamrahl, M., Kumari, S., Chang, V. T., Khuon, S., et al. (2019). Cytoskeletal control of antigen-dependent T cell activation. *Cell Rep.* 26, 3369–3379.e5. doi: 10.1016/j.celrep.2019.02.074

Comrie, W. A., Li, S., Boyle, S., and Burkhardt, J. K. (2015). The dendritic cell cytoskeleton promotes T cell adhesion and activation by constraining ICAM-1 mobility. *J. Cell Biol.* 208, 457–473. doi: 10.1083/jcb.201406120

Cotta-de-Almeida, V., Westerberg, L., Maillard, M. H., Onaldi, D., Wachtel, H., Meelu, P., et al. (2007). Wiskott Aldrich syndrome protein (WASP) and N-WASP are critical for T cell development. *Proc. Natl. Acad. Sci. U.S.A.* 104, 15424–15429. doi: 10.1073/pnas.0706881104

Das, D. K., Feng, Y., Mallis, R. J., Li, X., Keskin, D. B., Hussey, R. E., et al. (2015). Force-dependent transition in the T-cell receptor β-subunit allosterically

regulates peptide discrimination and pMHC bond lifetime. *Proc. Natl. Acad. Sci. U.S.A.* 112, 1517–1522. doi: 10.1073/pnas.1424829112

David, M. D., Petit, D., and Bertoglio, J. (2014). The RhoGAP ARHGAP19 controls cytokinesis and chromosome segregation in T lymphocytes. *J. Cell Sci.* 127, 400–410. doi: 10.1242/jcs.135079

Devriendt, K., Kim, A. S., Mathijs, G., Frints, S. G., Schwartz, M., Van Den Oord, J. J., et al. (2001). Constitutively activating mutation in WASP causes X-linked severe congenital neutropenia. *Nat. Genet.* 27, 313–317. doi: 10.1038/85886

Dominguez, G. A., Anderson, N. R., and Hammer, D. A. (2015). The direction of migration of T-lymphocytes under flow depends upon which adhesion receptors are engaged. *Integr. Biol.* 7, 345–355. doi: 10.1039/c4ib00201f

Dundr, M., Ospina, J. K., Sung, M.-H., John, S., Upender, M., Ried, T., et al. (2007). Actin-dependent intranuclear repositioning of an active gene locus in vivo. *J. Cell Biol.* 179, 1095–1103. doi: 10.1083/jcb.200710058

Dupont, S., Morsut, L., Aragona, M., Enzo, E., Giulitti, S., Cordenonsi, M., et al. (2011). Role of YAP/TAZ in mechanotransduction. *Nature* 474, 179–183. doi: 10.1038/nature10137

Dustin, M. L. (2014). What counts in the immunological synapse? *Mol. Cell* 54, 255–262. doi: 10.1016/j.molcel.2014.04.001

Dzijak, R., Yildirim, S., Kahle, M., Novak, P., Hnilicova, J., Venit, T., et al. (2012). Specific nuclear localizing sequence directs two myosin isoforms to the cell nucleus in calmodulin-sensitive manner. *PLoS One* 7:e30529. doi: 10.1371/journal.pone.0030529

Egly, J. M., Miyamoto, N. G., Moncollin, V., and Chambon, P. (1984). Is actin a transcription initiation factor for RNA polymerase B? *EMBO J.* 3, 2363–2371. doi: 10.1002/j.1460-2075.1984.tb02141.x

Elosegui-Artola, A., Andreu, I., Beedle, A. E. M., Lezamiz, A., Uroz, M., Kosmalska, A. J., et al. (2017). Force triggers YAP nuclear entry by regulating transport across nuclear pores. *Cell* 171, 1397–1410.e14. doi: 10.1016/j.cell.2017.10.008

Engler, A. J., Sen, S., Sweeney, H. L., and Discher, D. E. (2006). Matrix elasticity directs stem cell lineage specification. *Cell* 126, 677–689. doi: 10.1016/j.cell.2006.06.044

Esnault, C., Stewart, A., Gualdrini, F., East, P., Horswell, S., Matthews, N., et al. (2014). Rho-actin signaling to the MRTF coactivators dominates the immediate transcriptional response to serum in fibroblasts. *Genes Dev.* 28, 943–958. doi: 10.1101/gad.239327.114

Fabrikant, G., Gupta, S., Shivashankar, G. V., and Kozlov, M. M. (2013). Model of T-cell nuclear deformation by the cortical actin layer. *Biophys. J.* 105, 1316–1323. doi: 10.1016/j.bpj.2013.07.024

Fan, Y., Gao, Y., Rao, J., Zhang, F., Wang, K., and Zhang, C. (2017). YAP-1 promotes tregs differentiation in hepatocellular carcinoma by enhancing TGFBR2 transcription. *Cell. Physiol. Biochem.* 41, 1189–1198. doi: 10.1159/000464380

Feng, Y., Brazin, K. N., Kobayashi, E., Mallis, R. J., Reinherz, E. L., and Lang, M. J. (2017). Mechanosensing drives acuity of alphabeta T-cell recognition. *Proc. Natl. Acad. Sci. U.S.A.* 114, E8204–E8213. doi: 10.1073/pnas.1703559114

Figard, L., Zheng, L., Biel, N., Xue, Z., Seede, H., Coleman, S., et al. (2019). Cofilin-mediated actin stress response is maladaptive in heat-stressed embryos. *Cell Rep.* 26, 3493–3501.e4. doi: 10.1016/j.celrep.2019.02.092

Fomproix, N., and Percipalle, P. (2004). An actin–myosin complex on actively transcribing genes. *Exp. Cell Res.* 294, 140–148. doi: 10.1016/j.yexcr.2003.10.028

Frémont, S., Hammich, H., Bai, J., Wioland, H., Klinkert, K., Rocancourt, M., et al. (2017). Oxidation of F-actin controls the terminal steps of cytokinesis. *Nat. Commun.* 8:14528. doi: 10.1038/ncomms14528

Friedland, J. C., Lee, M. H., and Boettiger, D. (2009). Mechanically activated integrin switch controls α5β1 function. *Science* 323, 642–644. doi: 10.1126/science.1168441

Geng, J., Yu, S., Zhao, H., Sun, X., Li, X., Wang, P., et al. (2017). The transcriptional coactivator TAZ regulates reciprocal differentiation of TH17 cells and Treg cells. *Nat. Immunol.* 18, 800–812. doi: 10.1038/ni.3748

Gjorgjieva, T., Xie, X., Commins, P., Pasricha, R., Mahmood, S. R., Gunsalus, K. C., et al. (2020). Loss of β-actin leads to accelerated mineralization and dysregulation of osteoblast-differentiation genes during osteogenic reprogramming. *Adv. Sci.* 7:2002261. doi: 10.1002/advs.202002261

González-Granado, J. M., Silvestre-Roig, C., Rocha-Perugini, V., Trigueros-Motos, L., Cibrián, D., Morlino, G., et al. (2014). Nuclear envelope lamin-A couples actin dynamics with immunological synapse architecture and T cell activation. *Sci. Signal.* 7:ra37. doi: 10.1126/scisignal.2004872

Green, R. A., Paluch, E., and Oegema, K. (2012). Cytokinesis in animal cells. *Annu. Rev. Cell Dev. Biol.* 28, 29–58. doi: 10.1146/annurev-cellbio-101011-155718

Grummt, I. (2006). Actin and myosin as transcription factors. *Curr. Opin. Genet. Dev.* 16, 191–196. doi: 10.1016/j.gde.2006.02.001

Guilluy, C., Swaminathan, V., Garcia-Mata, R., O'Brien, E. T., Superfine, R., and Burridge, K. (2011). The Rho GEFs LARG and GEF-H1 regulate the mechanical response to force on integrins. *Nat. Cell Biol.* 13, 722–727. doi: 10.1038/ncb2254

Gupta, M., Sarangi, B. R., Deschamps, J., Nematbakhsh, Y., Callan-Jones, A., Margadant, F., et al. (2015). Adaptive rheology and ordering of cell cytoskeleton govern matrix rigidity sensing. *Nat. Commun.* 6:7525. doi: 10.1038/ncomms8525

Gupta, S., Marcel, N., Sarin, A., and Shivashankar, G. V. (2012). Role of actin dependent nuclear deformation in regulating early gene expression. *PLoS One* 7:e53031. doi: 10.1371/journal.pone.0053031

Ha, Y. J., Jeong, J. H., Park, Y., and Lee, J. R. (2012). Increased p190RhoGEF expression in activated B cells correlates with the induction of the plasma cell differentiation. *Exp. Mol. Med.* 44, 138–148. doi: 10.3858/emm.2012.44.2.009

Hale, C. M., Shrestha, A. L., Khatau, S. B., Stewart-Hutchinson, P. J., Hernandez, L., Stewart, C. L., et al. (2008). Dysfunctional connections between the nucleus and the actin and microtubule networks in laminopathic models. *Biophys. J.* 95, 5462–5475. doi: 10.1529/biophysj.108.139428

Hall, A. (2012). Rho family GTPases. *Biochem. Soc. Trans.* 40, 1378–1382. doi: 10.1042/BST20120103

Haque, F., Lloyd, D. J., Smallwood, D. T., Dent, C. L., Shanahan, C. M., Fry, A. M., et al. (2006). SUN1 interacts with nuclear lamin A and cytoplasmic nesprins to provide a physical connection between the nuclear lamina and the cytoskeleton. *Mol. Cell. Biol.* 26, 3738–3751. doi: 10.1128/MCB.26.10.3738-3751.2006

He, S., Wu, Z., Tian, Y., Yu, Z., Yu, J., Wang, X., et al. (2020). Structure of nucleosome-bound human BAF complex. *Science* 367, 875–881. doi: 10.1126/science.aaz9761

Heasman, S. J., Carlin, L. M., Cox, S., Ng, T., and Ridley, A. J. (2010). Coordinated RhoA signaling at the leading edge and uropod is required for T cell transendothelial migration. *J. Cell Biol.* 190, 553–563. doi: 10.1083/jcb.201002067

Hégarat, N., Smith, E., Nayak, G., Takeda, S., Eyers, P. A., and Hochegger, H. (2011). Aurora A and Aurora B jointly coordinate chromosome segregation and anaphase microtubule dynamics. *J. Cell Biol.* 195, 1103–1113. doi: 10.1083/jcb.201105058

Hirano, H., and Matsuura, Y. (2011). Sensing actin dynamics: structural basis for G-actin-sensitive nuclear import of MAL. *Biochem. Biophys. Res. Commun.* 414, 373–378. doi: 10.1016/j.bbrc.2011.09.079

Ho, C. Y., Jaalouk, D. E., Vartiainen, M. K., and Lammerding, J. (2013). Lamin A/C and emerin regulate MKL1–SRF activity by modulating actin dynamics. *Nature* 497, 507–511. doi: 10.1038/nature12105

Ho, L., Ronan, J. L., Wu, J., Staahl, B. T., Chen, L., Kuo, A., et al. (2009). An embryonic stem cell chromatin remodeling complex, esBAF, is essential for embryonic stem cell self-renewal and pluripotency. *Proc. Natl. Acad. Sci. U.S.A.* 106, 5181–5186. doi: 10.1073/pnas.0812889106

Hofmann, W. A., Stojiljkovic, L., Fuchsova, B., Vargas, G. M., Mavrommatis, E., Philimonenko, V., et al. (2004). Actin is part of pre-initiation complexes and is necessary for transcription by RNA polymerase II. *Nat. Cell Biol.* 6, 1094–1101. doi: 10.1038/ncb1182

Hong, J., Ge, C., Jothikumar, P., Yuan, Z., Liu, B., Bai, K., et al. (2018). A TCR mechanotransduction signaling loop induces negative selection in the thymus. *Nat. Immunol.* 19, 1379–1390. doi: 10.1038/s41590-018-0259-z

Hu, K. H., and Butte, M. J. (2016). T cell activation requires force generation. *J. Cell Biol.* 213, 535–542. doi: 10.1083/jcb.201511053

Hu, P., Wu, S., and Hernandez, N. (2004). A role for β-actin in RNA polymerase III transcription. *Genes Dev.* 18, 3010–3015. doi: 10.1101/gad.1250804

Hui, K. L., Balagopalan, L., Samelson, L. E., and Upadhyaya, A. (2014). Cytoskeletal forces during signaling activation in Jurkat T-cells. *Mol. Biol. Cell* 26, 685–695. doi: 10.1091/mbc.E14-03-0830

Husson, J., Chemin, K., Bohineust, A., Hivroz, C., and Henry, N. (2011). Force generation upon T cell receptor engagement. *PLoS One* 6:e19680. doi: 10.1371/journal.pone.0019680

Inoue, D., Obino, D., Pineau, J., Farina, F., Gaillard, J., Guerin, C., et al. (2019). Actin filaments regulate microtubule growth at the centrosome. *EMBO J.* 38:e99630. doi: 10.15252/embj.201899630

Ioannou, D., Kandukuri, L., Simpson, J. L., and Tempest, H. G. (2015). Chromosome territory repositioning induced by PHA-activation of lymphocytes: A 2D and 3D appraisal. *Mol. Cytogenet.* 8:47. doi: 10.1186/s13039-015-0146-3

Jacobelli, J., Matthews, M. E., Chen, S., and Krummel, M. F. (2013). Activated T cell trans-endothelial migration relies on myosin-IIA contractility for squeezing the cell nucleus through endothelial cell barriers. *PLoS One* 8:e75151. doi: 10.1371/journal.pone.0075151

Jankowska, K. I., Williamson, E. K., Roy, N. H., Blumenthal, D., Chandra, V., Baumgart, T., et al. (2018). Integrins modulate T cell receptor signaling by constraining actin flow at the immunological synapse. *Front. Immunol.* 9:25. doi: 10.3389/fimmu.2018.00025

Judokusumo, E., Tabdanov, E., Kumari, S., Dustin, M. L., and Kam, L. C. (2012). Mechanosensing in T lymphocyte activation. *Biophys. J.* 102, L5–L7. doi: 10.1016/j.bpj.2011.12.011

Kadoch, C., Williams, R. T., Calarco, J. P., Miller, E. L., Weber, C. M., Braun, S. M., et al. (2017). Dynamics of BAF-Polycomb complex opposition on heterochromatin in normal and oncogenic states. *Nat. Genet.* 49, 213–222. doi: 10.1038/ng.3734

Kaizuka, Y., Douglass, A. D., Varma, R., Dustin, M. L., and Vale, R. D. (2007). Mechanisms for segregating T cell receptor and adhesion molecules during immunological synapse formation in Jurkat T cells. *Proc. Natl. Acad. Sci. U.S.A.* 104, 20296–20301. doi: 10.1073/pnas.0710258105

Kapoor, P., Chen, M., Winkler, D. D., Luger, K., and Shen, X. (2013). Evidence for monomeric actin function in INO80 chromatin remodeling. *Nat. Struct. Mol. Biol.* 20, 426–432. doi: 10.1038/nsmb.2529

Kelpsch, D. J., and Tootle, T. L. (2018). Nuclear actin: from discovery to function. *Anat. Rec.* 301, 1999–2013. doi: 10.1002/ar.23959

Keszei, M., Record, J., Kritikou, J. S., Wurzer, H., Geyer, C., Thiemann, M., et al. (2018). Constitutive activation of WASp in X-linked neutropenia renders neutrophils hyperactive. *J. Clin. Invest.* 128, 4115–4131. doi: 10.1172/JCI64772

Khatau, S. B., Hale, C. M., Stewart-Hutchinson, P. J., Patel, M. S., Stewart, C. L., Searson, P. C., et al. (2009). A perinuclear actin cap regulates nuclear shape. *Proc. Natl. Acad. Sci. U.S.A.* 106, 19017–19022. doi: 10.1073/pnas.0908686106

Kim, D.-H., and Wirtz, D. (2015). Cytoskeletal tension induces the polarized architecture of the nucleus. *Biomaterials* 48, 161–172. doi: 10.1016/j.biomaterials.2015.01.023

Kim, N.-G., and Gumbiner, B. M. (2015). Adhesion to fibronectin regulates Hippo signaling via the FAK–Src–PI3K pathway. *J. Cell Biol.* 210, 503–515. doi: 10.1083/jcb.201501025

Kim, N.-G., Koh, E., Chen, X., and Gumbiner, B. M. (2011). E-cadherin mediates contact inhibition of proliferation through Hippo signaling-pathway components. *Proc. Natl. Acad. Sci. U.S.A.* 108, 11930–11935. doi: 10.1073/pnas.1103345108

Kim, S. T., Takeuchi, K., Sun, Z.-Y. J., Touma, M., Castro, C. E., Fahmy, A., et al. (2009). The αβ T cell receptor is an anisotropic mechanosensor. *J. Biol. Chem.* 284, 31028–31037. doi: 10.1074/jbc.M109.052712

Kimura, K., Ito, M., Amano, M., Chihara, K., Fukata, Y., Nakafuku, M., et al. (1996). Regulation of myosin phosphatase by rho and rho-associated kinase (Rho-Kinase). *Science* 273, 245–248. doi: 10.1126/science.273.5272.245

King, H. W., and Klose, R. J. (2017). The pioneer factor OCT4 requires the chromatin remodeller BRG1 to support gene regulatory element function in mouse embryonic stem cells. *eLife* 6:e22631. doi: 10.7554/eLife.22631

Kukalev, A., Nord, Y., Palmberg, C., Bergman, T., and Percipalle, P. (2005). Actin and hnRNP U cooperate for productive transcription by RNA polymerase II. *Nat. Struct. Mol. Biol.* 12, 238–244. doi: 10.1038/nsmb904

Kulashreshtha, M., Mehta, I. S., Kumar, P., and Rao, B. J. (2016). Chromosome territory relocation during DNA repair requires nuclear myosin 1 recruitment to chromatin mediated by γ-H2AX signaling. *Nucleic Acids Res.* 44, 8272–8291. doi: 10.1093/nar/gkw573

Kuznetsov, N. V., Almuzzaini, B., Kritikou, J. S., Baptista, M. A. P., Oliveira, M. M. S., Keszei, M., et al. (2017). Nuclear Wiskott-Aldrich syndrome protein co-regulates T cell factor 1-mediated transcription in T cells. *Genome Med.* 9:91. doi: 10.1186/s13073-017-0481-6

Lammerding, J., Fong, L. G., Ji, J. Y., Reue, K., Stewart, C. L., Young, S. G., et al. (2006). Lamins A and C but not lamin B1 regulate nuclear mechanics *. *J. Biol. Chem.* 281, 25768–25780. doi: 10.1074/jbc.M513511200

Lebid, A., Chung, L., Pardoll, D. M., and Pan, F. (2020). YAP attenuates CD8 T cell-mediated anti-tumor response. *Front. Immunol.* 11:580. doi: 10.3389/fimmu.2020.00580

Lee, J. R., Ha, Y. J., and Kim, H. J. (2003). Cutting edge: induced expression of a rhoa-specific guanine nucleotide exchange factor, p190RhoGEF, following CD40 stimulation and WEHI 231 B cell activation. *J. Immunol.* 170, 19–23. doi: 10.4049/jimmunol.170.1.19

Leithner, A., Altenburger, L. M., Hauschild, R., Assen, F. P., Rottner, K., Stradal, T. E. B., et al. (2021). Dendritic cell actin dynamics control contact duration and priming efficiency at the immunological synapse. *J. Cell Biol.* 220:e202006081. doi: 10.1083/jcb.202006081

Li, R., Ma, C., Cai, H., and Chen, W. (2020). The car T-cell mechanoimmunology at a glance. *Adv. Sci.* 7:2002628. doi: 10.1002/advs.202002628

Li, Y.-C., Chen, B.-M., Wu, P.-C., Cheng, T.-L., Kao, L.-S., Tao, M.-H., et al. (2010). Cutting edge: mechanical forces acting on T cells immobilized via the TCR complex can trigger TCR signaling. *J. Immunol.* 184, 5959–5963. doi: 10.4049/jimmunol.0900775

Liu, D., Vader, G., Vromans, M. J. M., Lampson, M. A., and Lens, S. M. A. (2009). Sensing chromosome bi-orientation by spatial separation of aurora B kinase from kinetochore substrates. *Science* 323, 1350–1353. doi: 10.1126/science.1167000

Liu, Y., Blanchfield, L., Ma, V. P.-Y., Andargachew, R., Galior, K., Liu, Z., et al. (2016). DNA-based nanoparticle tension sensors reveal that T-cell receptors transmit defined pN forces to their antigens for enhanced fidelity. *Proc. Natl. Acad. Sci. U.S.A.* 113, 5610–5615. doi: 10.1073/pnas.1600163113

Lock, J. G., Jones, M. C., Askari, J. A., Gong, X., Oddone, A., Olofsson, H., et al. (2018). Reticular adhesions are a distinct class of cell-matrix adhesions that mediate attachment during mitosis. *Nat. Cell Biol.* 20, 1290–1302. doi: 10.1038/s41556-018-0220-2

Lomakin, A. J., Cattin, C. J., Cuvelier, D., Alraies, Z., Molina, M., Nader, G. P. F., et al. (2020). The nucleus acts as a ruler tailoring cell responses to spatial constraints. *Science* 370:eaba2894. doi: 10.1126/science.aba2894

Lombardi, M. L., Jaalouk, D. E., Shanahan, C. M., Burke, B., Roux, K. J., and Lammerding, J. (2011). The interaction between nesprins and sun proteins at the nuclear envelope is critical for force transmission between the nucleus and cytoskeleton*. *J. Biol. Chem.* 286, 26743–26753. doi: 10.1074/jbc.M111.233700

Lundquist, M. R., Storaska, A. J., Liu, T.-C., Larsen, S. D., Evans, T., Neubig, R. R., et al. (2014). Redox modification of nuclear actin by MICAL-2 regulates SRF signaling. *Cell* 156, 563–576. doi: 10.1016/j.cell.2013.12.035

Ma, Z., Morris, S. W., Valentine, V., Li, M., Herbrick, J.-A., Cui, X., et al. (2001). Fusion of two novel genes, RBM15 and MKL1, in the t(1;22)(p13;q13) of acute megakaryoblastic leukemia. *Nat. Genet.* 28, 220–221. doi: 10.1038/90054

Maekawa, M., Ishizaki, T., Boku, S., Watanabe, N., Fujita, A., Iwamatsu, A., et al. (1999). Signaling from Rho to the actin cytoskeleton through protein kinases ROCK and LIM-kinase. *Science* 285, 895–898. doi: 10.1126/science.285.5429.895

Mahmood, S. R., Xie, X., Said, N. H. E., Gunsalus, K. C., and Percipalle, P. (2020). β-actin dependent chromatin remodeling mediates compartment level changes in 3D genome architecture. *bioRxiv* [Preprint]. doi: 10.1101/2020.06.14.150425

Malinova, D., Fritzsche, M., Nowosad, C. R., Armer, H., Munro, P. M. G., Blundell, M. P., et al. (2016). WASp-dependent actin cytoskeleton stability at the dendritic cell immunological synapse is required for extensive, functional T cell contacts. *J. Leukoc. Biol.* 99, 699–710. doi: 10.1189/jlb.2A0215-050RR

McNeill, M. C., Wray, J., Sala-Newby, G. B., Hindmarch, C. C. T., Smith, S. A., Ebrahimighaei, R., et al. (2020). Nuclear actin regulates cell proliferation and migration via inhibition of SRF and TEAD. *Biochim. Biophys. Acta* 1867:118691. doi: 10.1016/j.bbamcr.2020.118691

Mehta, I. S., Amira, M., Harvey, A. J., and Bridger, J. M. (2010). Rapid chromosome territory relocation by nuclear motor activity in response to serum removal in primary human fibroblasts. *Genome Biol.* 11:R5. doi: 10.1186/gb-2010-11-1-r5

Mendoza, M., Norden, C., Durrer, K., Rauter, H., Uhlmann, F., and Barral, Y. (2009). A mechanism for chromosome segregation sensing by the NoCut checkpoint. *Nat. Cell Biol.* 11, 477–483. doi: 10.1038/ncb1855

Meng, K. P., Majedi, F. S., Thauland, T. J., and Butte, M. J. (2020). Mechanosensing through YAP controls T cell activation and metabolism. *J. Exp. Med.* 217:e20200053. doi: 10.1084/jem.20200053

Meng, Z., Moroishi, T., and Guan, K.-L. (2016). Mechanisms of Hippo pathway regulation. *Genes Dev.* 30, 1–17. doi: 10.1101/gad.274027.115

Mennens, S. F. B., Bolomini-Vittori, M., Weiden, J., Joosten, B., Cambi, A., and Dries, K. V. D. (2017). Substrate stiffness influences phenotype and function of human antigen-presenting dendritic cells. *Sci. Rep.* 7:17511. doi: 10.1038/s41598-017-17787-z

Miralles, F., Posern, G., Zaromytidou, A.-I., and Treisman, R. (2003). Actin dynamics control SRF activity by regulation of its coactivator MAL. *Cell* 113, 329–342. doi: 10.1016/S0092-8674(03)00278-2

Miyamoto, K., and Gurdon, J. B. (2013). Transcriptional regulation and nuclear reprogramming: roles of nuclear actin and actin-binding proteins. *Cell. Mol. Life Sci.* 70, 3289–3302. doi: 10.1007/s00018-012-1235-7

Miyamoto, K., Pasque, V., Jullien, J., and Gurdon, J. B. (2011). Nuclear actin polymerization is required for transcriptional reprogramming of Oct4 by oocytes. *Genes Dev.* 25, 946–958. doi: 10.1101/gad.615211

Mo, J.-S., Yu, F.-X., Gong, R., Brown, J. H., and Guan, K.-L. (2012). Regulation of the Hippo–YAP pathway by protease-activated receptors (PARs). *Genes Dev.* 26, 2138–2143. doi: 10.1101/gad.197582.112

Moalli, F., Ficht, X., Germann, P., Vladymyrov, M., Stolp, B., de Vries, I., et al. (2018). The Rho regulator myosin IXb enables nonlymphoid tissue seeding of protective CD8+ T cells. *J. Exp. Med.* 215, 1869–1890. doi: 10.1084/jem.20170896

Morikawa, Y., Zhang, M., Heallen, T., Leach, J., Tao, G., Xiao, Y., et al. (2015). Actin cytoskeletal remodeling with protrusion formation is essential for heart regeneration in Hippo-deficient mice. *Sci. Signal.* 8:ra41. doi: 10.1126/scisignal.2005781

Mouilleron, S., Guettler, S., Langer, C. A., Treisman, R., and McDonald, N. Q. (2008). Molecular basis for G−actin binding to RPEL motifs from the serum response factor coactivator MAL. *EMBO J.* 27, 3198–3208. doi: 10.1038/emboj.2008.235

Mouilleron, S., Langer, C. A., Guettler, S., McDonald, N. Q., and Treisman, R. (2011). Structure of a pentavalent G-actinMRTF-A complex reveals how G-actin controls nucleocytoplasmic shuttling of a transcriptional coactivator. *Sci. Signal.* 4:ra40. doi: 10.1126/scisignal.2001750

Moulding, D. A., Blundell, M. P., Spiller, D. G., White, M. R. H., Cory, G. O., Calle, Y., et al. (2007). Unregulated actin polymerization by WASp causes defects of mitosis and cytokinesis in X-linked neutropenia. *J. Exp. Med.* 204, 2213–2224. doi: 10.1084/jem.20062324

Moulding, D. A., Moeendarbary, E., Valon, L., Record, J., Charras, G. T., and Thrasher, A. J. (2012). Excess F-actin mechanically impedes mitosis leading to cytokinesis failure in X-linked neutropenia by exceeding Aurora B kinase error correction capacity. *Blood* 120, 3803–3811. doi: 10.1182/blood-2012-03-419663

Moulding, D. A., Record, J., Malinova, D., and Thrasher, A. J. (2013). Actin cytoskeletal defects in immunodeficiency. *Immunol. Rev.* 256, 282–299. doi: 10.1111/imr.12114

Muehlich, S., Wang, R., Lee, S.-M., Lewis, T. C., Dai, C., and Prywes, R. (2008). Serum-induced phosphorylation of the serum response factor coactivator MKL1 by the extracellular signal-regulated kinase 1/2 pathway inhibits its nuclear localization. *Mol. Cell. Biol.* 28, 6302–6313. doi: 10.1128/MCB.00427-08

Munsie, L. N., Desmond, C. R., and Truant, R. (2012). Cofilin nuclear-cytoplasmic shuttling affects cofilin-actin rod formation during stress. *J. Cell Sci.* 105(Pt 17), 3977–3988. doi: 10.1242/jcs.097667

Murugesan, S., Hong, J., Yi, J., Li, D., Beach, J. R., Shao, L., et al. (2016). Formin-generated actomyosin arcs propel T cell receptor microcluster movement at the immune synapse. *J. Cell Biol.* 215, 383–399. doi: 10.1083/jcb.201603080

Na, S., Collin, O., Chowdhury, F., Tay, B., Ouyang, M., Wang, Y., et al. (2008). Rapid signal transduction in living cells is a unique feature of mechanotransduction. *Proc. Natl. Acad. Sci. U.S.A.* 105, 6626–6631. doi: 10.1073/pnas.0711704105

Nähse, V., Christ, L., Stenmark, H., and Campsteijn, C. (2017). The abscission checkpoint: making it to the final cut. *Trends Cell Biol.* 27, 1–11. doi: 10.1016/j.tcb.2016.10.001

Nair, J. S., Ho, A. L., Tse, A. N., Coward, J., Cheema, H., Ambrosini, G., et al. (2009). Aurora B kinase regulates the postmitotic endoreduplication checkpoint via phosphorylation of the retinoblastoma protein at serine 780. *Mol. Biol. Cell* 20, 2218–2228. doi: 10.1091/mbc.e08-08-0885

Nardone, G., Cruz, J. O.-D. L., Vrbsky, J., Martini, C., Pribyl, J., Skládal, P., et al. (2017). YAP regulates cell mechanics by controlling focal adhesion assembly. *Nat. Commun.* 8:15321. doi: 10.1038/ncomms15321

Ni, X., Tao, J., Barbi, J., Chen, Q., Park, B. V., Li, Z., et al. (2018). YAP is essential for treg-mediated suppression of antitumor immunity. *Cancer Discov.* 8, 1026–1043. doi: 10.1158/2159-8290.CD-17-1124

Noel, D. K., Ribeiro, A. J. S., and Jan, L. (2008). Nuclear shape, mechanics, and mechanotransduction. *Circ. Res.* 102, 1307–1318. doi: 10.1161/CIRCRESAHA.108.173989

O'Connor, R. S., Hao, X., Shen, K., Bashour, K., Akimova, T., Hancock, W. W., et al. (2012). Substrate rigidity regulates human T cell activation and proliferation. *J. Immunol.* 189, 1330–1339. doi: 10.4049/jimmunol.1102757

Obino, D., Farina, F., Malbec, O., Sáez, P. J., Maurin, M., Gaillard, J., et al. (2016). Actin nucleation at the centrosome controls lymphocyte polarity. *Nat. Commun.* 7:10969. doi: 10.1038/ncomms10969

Obrdlik, A., Kukalev, A., Louvet, E., Farrants, A.-K. Ö, Caputo, L., and Percipalle, P. (2008). The histone acetyltransferase PCAF associates with actin and hnRNP U for RNA polymerase II transcription. *Mol. Cell. Biol.* 28, 6342–6357. doi: 10.1128/MCB.00766-08

Oka, T., and Sudol, M. (2009). Nuclear localization and pro-apoptotic signaling of YAP2 require intact PDZ-binding motif. *Genes Cells* 14, 607–615. doi: 10.1111/j.1365-2443.2009.01292.x

Olave, I. A., Reck-Peterson, S. L., and Crabtree, G. R. (2002). Nuclear actin and actin-related proteins in chromatin remodeling. *Annu. Rev. Biochem.* 71, 755–781. doi: 10.1146/annurev.biochem.71.110601.135507

Ooi, L., Belyaev, N. D., Miyake, K., Wood, I. C., and Buckley, N. J. (2006). BRG1 chromatin remodeling activity is required for efficient chromatin binding by repressor element 1-silencing transcription factor (REST) and facilitates REST-mediated repression. *J. Biol. Chem.* 281, 38974–38980. doi: 10.1074/jbc.M605370200

Orr, A. W., Helmke, B. P., Blackman, B. R., and Schwartz, M. A. (2006). Mechanisms of mechanotransduction. *Dev. Cell* 10, 11–20. doi: 10.1016/j.devcel.2005.12.006

Panayiotou, R., Miralles, F., Pawlowski, R., Diring, J., Flynn, H. R., Skehel, M., et al. (2016). Phosphorylation acts positively and negatively to regulate MRTF-A subcellular localisation and activity. *eLife* 5:e15460. doi: 10.7554/eLife.15460

Pawłowski, R., Rajakylä, E. K., Vartiainen, M. K., and Treisman, R. (2010). An actin-regulated importin α/β-dependent extended bipartite NLS directs nuclear import of MRTF-A. *EMBO J.* 29, 3448–3458. doi: 10.1038/emboj.2010.216

Pelham, R. J., and Wang, Y.-L. (1997). Cell locomotion and focal adhesions are regulated by substrate flexibility. *Proc. Natl. Acad. Sci. U.S.A.* 94, 13661–13665. doi: 10.1073/pnas.94.25.13661

Pennacchio, F. A., Nastały, P., Poli, A., and Maiuri, P. (2021). Tailoring cellular function: the contribution of the nucleus in mechanotransduction. *Front. Bioeng. Biotechnol.* 8:596746. doi: 10.3389/fbioe.2020.596746

Percipalle, P. (2013). Co-transcriptional nuclear actin dynamics. *Nucleus* 4, 43–52. doi: 10.4161/nucl.22798

Percipalle, P., and Farrants, A. K. (2006). Chromatin remodelling and transcription: be-WICHed by nuclear myosin 1. *Curr. Opin. Cell Biol.* 18, 267–274. doi: 10.1016/j.ceb.2006.03.001

Percipalle, P., Fomproix, N., Kylberg, K., Miralles, F., Bjorkroth, B., Daneholt, B., et al. (2003). An actin-ribonucleoprotein interaction is involved in transcription by RNA polymerase II. *Proc. Natl. Acad. Sci. U.S.A.* 100, 6475–6480. doi: 10.1073/pnas.1131933100

Percipalle, P., Zhao, J., Pope, B., Weeds, A., Lindberg, U., and Daneholt, B. (2001). Actin bound to the heterogeneous nuclear ribonucleoprotein hrp36 is associated with Balbiani ring mRNA from the gene to polysomes. *J. Cell Biol.* 153, 229–236. doi: 10.1083/jcb.153.1.229

Pestic-Dragovich, L., Stojiljkovic, L., Philimonenko, A. A., Nowak, G., Ke, Y., Settlage, R. E., et al. (2000). A myosin I isoform in the nucleus. *Science* 290, 337–341. doi: 10.1126/science.290.5490.337

Peterson, C. L., Zhao, Y., and Chait, B. T. (1998). Subunits of the yeast SWI/SNF complex are members of the actin-related protein (ARP) family. *J. Biol. Chem.* 273, 23641–23644. doi: 10.1074/jbc.273.37.23641

Philimonenko, V. V., Zhao, J., Iben, S., Dingova, H., Kysela, K., Kahle, M., et al. (2004). Nuclear actin and myosin I are required for RNA polymerase I transcription. *Nat. Cell Biol.* 6, 1165–1172. doi: 10.1038/ncb1190

Plessner, M., and Grosse, R. (2019). Dynamizing nuclear actin filaments. *Curr. Opin. Cell Biol.* 56, 1–6. doi: 10.1016/j.ceb.2018.08.005

Plessner, M., Melak, M., Chinchilla, P., Baarlink, C., and Grosse, R. (2015). Nuclear F-actin formation and reorganization upon cell spreading* ♦. *J. Biol. Chem.* 290, 11209–11216. doi: 10.1074/jbc.M114.627166

Pollard, T. D. (2017). Nine unanswered questions about cytokinesis. *J. Cell Biol.* 216, 3007–3016. doi: 10.1083/jcb.201612068

Pryshchep, S., Zarnitsyna, V. I., Hong, J., Evavold, B. D., and Zhu, C. (2014). Accumulation of serial forces on TCR and CD8 frequently applied by agonist antigenic peptides embedded in MHC molecules triggers calcium in T cells. *J. Immunol.* 193, 68–76. doi: 10.4049/jimmunol.1303436

Rando, O. J., Zhao, K., Janmey, P., and Crabtree, G. R. (2002). Phosphatidylinositol-dependent actin filament binding by the SWI/SNF-like BAF chromatin remodeling complex. *Proc. Natl. Acad. Sci. U.S.A.* 99, 2824–2829. doi: 10.1073/pnas.032662899

Rankin, J., and Ellard, S. (2006). The laminopathies: a clinical review. *Clin. Genet.* 70, 261–274. doi: 10.1111/j.1399-0004.2006.00677.x

Recher, M., Burns, S. O., de la Fuente, M. A., Volpi, S., Dahlberg, C., Walter, J. E., et al. (2012). B cell-intrinsic deficiency of the Wiskott-Aldrich syndrome protein (WASp) causes severe abnormalities of the peripheral B-cell compartment in mice. *Blood* 119, 2819–2828. doi: 10.1182/blood-2011-09-379412

Record, J., Malinova, D., Zenner, H. L., Plagnol, V., Nowak, K., Syed, F., et al. (2015). Immunodeficiency and severe susceptibility to bacterial infection associated with a loss-of-function homozygous mutation of MKL1. *Blood* 126, 1527–1535. doi: 10.1182/blood-2014-12-611012

Record, J., Sendel, A., Kritikou, J. S., Kuznetsov, N. V., Brauner, H., He, M., et al. (2020). An intronic deletion in megakaryoblastic leukemia 1 is associated with hyperproliferation of B cells in triplets with Hodgkin lymphoma. *Haematologica* 105, 1339–1350. doi: 10.3324/haematol.2019.216317

Renkawitz, J., Kopf, A., Stopp, J., Vries, I. D., Driscoll, M. K., Merrin, J., et al. (2019). Nuclear positioning facilitates amoeboid migration along the path of least resistance. *Nature* 568, 546–550. doi: 10.1038/s41586-019-1087-5

Riedl, J., Crevenna, A. H., Kessenbrock, K., Yu, J. H., Neukirchen, D., Bista, M., et al. (2008). Lifeact: a versatile marker to visualize F-actin. *Nat. Methods* 5:605. doi: 10.1038/nmeth.1220

Ritchey, L., and Chakrabarti, R. (2014). Aurora A kinase modulates actin cytoskeleton through phosphorylation of cofilin: implication in the mitotic process. *Biochim. Biophys. Acta* 1843, 2719–2729. doi: 10.1016/j.bbamcr.2014.07.014

Rossy, J., Laufer, J. M., and Legler, D. F. (2018). Role of mechanotransduction and tension in T cell function. *Front. Immunol.* 9:2638. doi: 10.3389/fimmu.2018.02638

Saci, A., and Carpenter, C. L. (2005). RhoA GTPase regulates B cell receptor signaling. *Mol. Cell* 17, 205–214. doi: 10.1016/j.molcel.2004.12.012

Sadhukhan, S., Sarkar, K., Taylor, M., Candotti, F., and Vyas, Y. M. (2014). Nuclear role of WASp in gene transcription is uncoupled from its ARP2/3-dependent cytoplasmic role in actin polymerization. *J. Immunol.* 193, 150–160. doi: 10.4049/jimmunol.1302923

Saeed, M. B., Record, J., and Westerberg, L. S. (2020). "Chapter 1 – two sides of the coin: cytoskeletal regulation of immune synapses in cancer and primary immune deficiencies," in *International Review of Cell and Molecular Biology*, eds C. Thomas and L. Galluzzi (Cambridge, MA: Academic Press), 1–97. doi: 10.1016/bs.ircmb.2020.06.001

Saitakis, M., Dogniaux, S., Goudot, C., Bufi, N., Asnacios, S., Maurin, M., et al. (2017). Different TCR-induced T lymphocyte responses are potentiated by stiffness with variable sensitivity. *eLife* 6:e23190. doi: 10.7554/eLife.23190

Sarkar, K., Han, S.-S., Wen, K.-K., Ochs, H. D., Dupré, L., Seidman, M. M., et al. (2018). R-loops cause genomic instability in T helper lymphocytes from patients with Wiskott-Aldrich syndrome. *J. Allergy Clin. Immunol.* 142, 219–234. doi: 10.1016/j.jaci.2017.11.023

Sarshad, A., Sadeghifar, F., Louvet, E., Mori, R., Bohm, S., Al-Muzzaini, B., et al. (2013). Nuclear myosin 1c facilitates the chromatin modifications required to activate rRNA gene transcription and cell cycle progression. *PLoS Genet.* 9:e1003397. doi: 10.1371/journal.pgen.1003397

Scheer, U., Hinssen, H., Franke, W. W., and Jockusch, B. M. (1984). Microinjection of actin-binding proteins and actin antibodies demonstrates involvement of nuclear actin in transcription of lampbrush chromosomes. *Cell* 39, 111–122. doi: 10.1016/0092-8674(84)90196-x

Schneider, F., Colin-York, H., and Fritzsche, M. (2021). Quantitative bio-imaging tools to dissect the interplay of membrane and cytoskeletal actin dynamics in immune cells. *Front. Immunol.* 11:612542. doi: 10.3389/fimmu.2020.612542

Schrank, B. R., Aparicio, T., Li, Y., Chang, W., Chait, B. T., Gundersen, G. G., et al. (2018). Nuclear ARP2/3 drives DNA break clustering for homology-directed repair. *Nature* 559, 61–66. doi: 10.1038/s41586-018-0237-5

Shen, X., Mizuguchi, G., Hamiche, A., and Wu, C. (2000). A chromatin remodelling complex involved in transcription and DNA processing. *Nature* 406, 541–544. doi: 10.1038/35020123

Shimono, Y., Murakami, H., Kawai, K., Wade, P. A., Shimokata, K., and Takahashi, M. (2003). Mi-2 beta associates with BRG1 and RET finger protein at the distinct regions with transcriptional activating and repressing abilities. *J. Biol. Chem.* 278, 51638–51645. doi: 10.1074/jbc.M309198200

Shin, J. W., Swift, J., Ivanovska, I., Spinler, K. R., Buxboim, A., and Discher, D. E. (2013). Mechanobiology of bone marrow stem cells: from myosin-II forces to compliance of matrix and nucleus in cell forms and fates. *Differentiation* 86, 77–86. doi: 10.1016/j.diff.2013.05.001

Singhal, N., Esch, D., Stehling, M., and Scholer, H. R. (2014). BRG1 is required to maintain pluripotency of murine embryonic stem cells. *Biores. Open Access* 3, 1–8. doi: 10.1089/biores.2013.0047

Smith, A., Bracke, M., Leitinger, B., Porter, J. C., and Hogg, N. (2003). LFA-1-induced T cell migration on ICAM-1 involves regulation of MLCK-mediated attachment and ROCK-dependent detachment. *J. Cell Sci.* 116, 3123–3133. doi: 10.1242/jcs.00606

Solovei, I., Wang, A. S., Thanisch, K., Schmidt, C. S., Krebs, S., Zwerger, M., et al. (2013). LBR and lamin A/C sequentially tether peripheral heterochromatin and inversely regulate differentiation. *Cell* 152, 584–598. doi: 10.1016/j.cell.2013.01.009

Spillane, K. M., and Tolar, P. (2016). B cell antigen extraction is regulated by physical properties of antigen-presenting cells. *J. Cell Biol.* 216, 217–230. doi: 10.1083/jcb.201607064

Sprenkeler, E. G. G., Henriet, S. S. V., Tool, A. T. J., Kreft, I. C., van der Bijl, I., Aarts, C. E. M., et al. (2020). MKL1 deficiency results in a severe neutrophil motility defect due to impaired actin polymerization. *Blood* 135, 2171–2181. doi: 10.1182/blood.2019002633

Swift, J., Ivanovska, I. L., Buxboim, A., Harada, T., Dingal, P. C. D. P., Pinter, J., et al. (2013). Nuclear lamin-A scales with tissue stiffness and enhances matrix-directed differentiation. *Science* 341:1240104. doi: 10.1126/science.1240104

Tanaka, H., and Watanabe, T. (2020). Mechanisms underlying recurrent genomic amplification in human cancers. *Trends Cancer* 6, 462–477. doi: 10.1016/j.trecan.2020.02.019

Taylor, M. D., Sadhukhan, S., Kottangada, P., Ramgopal, A., Sarkar, K., D'Silva, S., et al. (2010). Nuclear role of WASp in the pathogenesis of dysregulated TH1 immunity in human Wiskott-Aldrich syndrome. *Sci. Transl. Med.* 2:37ra44. doi: 10.1126/scitranslmed.3000813

Tedford, K., Steiner, M., Koshutin, S., Richter, K., Tech, L., Eggers, Y., et al. (2017). The opposing forces of shear flow and sphingosine-1-phosphate control marginal zone B cell shuttling. *Nat. Commun.* 8:2261. doi: 10.1038/s41467-017-02482-4

Tello-Lafoz, M., Srpan, K., Sanchez, E. E., Hu, J., Remsik, J., Romin, Y., et al. (2021). Cytotoxic lymphocytes target characteristic biophysical vulnerabilities in cancer. *Immunity* 54, 1037–1054.e7. doi: 10.1016/j.immuni.2021.02.020

Thauland, T. J., Hu, K. H., Bruce, M. A., and Butte, M. J. (2017). Cytoskeletal adaptivity regulates T cell receptor signaling. *Sci. Signal.* 10:eaah3737. doi: 10.1126/scisignal.aah3737

Thiam, H.-R., Vargas, P., Carpi, N., Crespo, C. L., Raab, M., Terriac, E., et al. (2016). Perinuclear Arp2/3-driven actin polymerization enables nuclear deformation to facilitate cell migration through complex environments. *Nat. Commun.* 7:10997. doi: 10.1038/ncomms10997

Toribio-Fernández, R., Herrero−Fernandez, B., Zorita, V., López, J. A., Vázquez, J., Criado, G., et al. (2019). Lamin A/C deficiency in CD4+ T-cells enhances regulatory T-cells and prevents inflammatory bowel disease. *J. Pathol.* 249, 509–522. doi: 10.1002/path.5332

Tsopoulidis, N., Kaw, S., Laketa, V., Kutscheidt, S., Baarlink, C., Stolp, B., et al. (2019). T cell receptor-triggered nuclear actin network formation drives CD4(+) T cell effector functions. *Sci. Immunol.* 4:eaav1987. doi: 10.1126/sciimmunol.aav1987

Tsouroula, K., Furst, A., Rogier, M., Heyer, V., Maglott-Roth, A., Ferrand, A., et al. (2016). Temporal and spatial uncoupling of DNA double strand break repair pathways within mammalian heterochromatin. *Mol. Cell* 63, 293–305. doi: 10.1016/j.molcel.2016.06.002

Ulferts, S., Prajapati, B., Grosse, R., and Vartiainen, M. K. (2021). Emerging properties and functions of actin and actin filaments inside the nucleus. *Cold Spring Harb. Perspect. Biol.* 13:a040121. doi: 10.1101/cshperspect.a040121

Umbreit, N. T., Zhang, C.-Z., Lynch, L. D., Blaine, L. J., Cheng, A. M., Tourdot, R., et al. (2020). Mechanisms generating cancer genome complexity from a single cell division error. *Science* 368:eaba0712. doi: 10.1126/science.aba0712

Valignat, M.-P., Theodoly, O., Gucciardi, A., Hogg, N., and Lellouch, A. C. (2013). T lymphocytes orient against the direction of fluid flow during LFA-1-mediated migration. *Biophys. J.* 104, 322–331. doi: 10.1016/j.bpj.2012.12.007

Vargas, P., Barbier, L., Sáez, P. J., and Piel, M. (2017). Mechanisms for fast cell migration in complex environments. *Curr. Opin. Cell Biol.* 48, 72–78. doi: 10.1016/j.ceb.2017.04.007

Vartiainen, M. K., Guettler, S., Larijani, B., and Treisman, R. (2007). Nuclear actin regulates dynamic subcellular localization and activity of the SRF cofactor MAL. *Science* 316, 1749–1752. doi: 10.1126/science.1141084

Venit, T., El Said, N. H., Mahmood, S. R., and Percipalle, P. (2020a). A dynamic actin-dependent nucleoskeleton and cell identity. *J. Biochem.* 169, 243–257. doi: 10.1093/jb/mvaa133

Venit, T., Mahmood, S. R., Endara-Coll, M., and Percipalle, P. (2020b). "Chapter 3 – nuclear actin and myosin in chromatin regulation and maintenance of genome integrity," in *International Review of Cell and Molecular Biology*, eds C. Thomas and L. Galluzzi (Cambridge, MA: Academic Press), 67–108. doi: 10.1016/bs.ircmb.2020.05.001

Vestweber, D. (2015). How leukocytes cross the vascular endothelium. *Nat. Rev. Immunol.* 15, 692–704. doi: 10.1038/nri3908

Vielkind, S., Gallagher-Gambarelli, M., Gomez, M., Hinton, H. J., and Cantrell, D. A. (2005). Integrin regulation by RhoA in thymocytes. *J. Immunol.* 175, 350–357. doi: 10.4049/jimmunol.175.1.350

Visa, N., and Percipalle, P. (2010). Nuclear functions of actin. *Cold Spring Harb. Perspect. Biol.* 2:a000620. doi: 10.1101/cshperspect.a000620

Wahl, A., Dinet, C., Dillard, P., Nassereddine, A., Puech, P.-H., Limozin, L., et al. (2019). Biphasic mechanosensitivity of T cell receptor-mediated spreading of lymphocytes. *Proc. Natl. Acad. Sci. U.S.A.* 116, 5908–5913. doi: 10.1073/pnas.1811516116

Wan, Z., Chen, X., Chen, H., Ji, Q., Chen, Y., Wang, J., et al. (2015). The activation of IgM- or isotype-switched IgG- and IgE-BCR exhibits distinct mechanical force sensitivity and threshold. *eLife* 4:e06925. doi: 10.7554/eLife.06925

Wang, A., Kolhe, J. A., Gioacchini, N., Baade, I., Brieher, W. M., Peterson, C. L., et al. (2020). Mechanism of long-range chromosome motion triggered by gene activation. *Dev. Cell* 52, 309–320.e5. doi: 10.1016/j.devcel.2019.12.007

Watanabe, N., Kato, T., Fujita, A., Ishizaki, T., and Narumiya, S. (1999). Cooperation between mDia1 and ROCK in Rho-induced actin reorganization. *Nat. Cell Biol.* 1, 136–143. doi: 10.1038/11056

Wei, M., Fan, X., Ding, M., Li, R., Shao, S., Hou, Y., et al. (2020). Nuclear actin regulates inducible transcription by enhancing RNA polymerase II clustering. *Sci. Adv.* 6:eaay6515. doi: 10.1126/sciadv.aay6515

Wen, K. K., Han, S. S., and Vyas, Y. M. (2020). Wiskott-Aldrich syndrome protein senses irradiation-induced DNA damage to coordinate the cell-protective Golgi dispersal response in human T and B lymphocytes. *J. Allergy Clin. Immunol.* 145, 324–334. doi: 10.1016/j.jaci.2019.09.026

Westerberg, L. S., Dahlberg, C., Baptista, M., Moran, C. J., Detre, C., Keszei, M., et al. (2012). Wiskott-Aldrich syndrome protein (WASP) and N-WASP are critical for peripheral B-cell development and function. *Blood* 119, 3966–3974. doi: 10.1182/blood-2010-09-308197

Westerberg, L. S., Meelu, P., Baptista, M., Eston, M. A., Adamovich, D. A., Cotta-de-Almeida, V., et al. (2010). Activating WASP mutations associated with X-linked neutropenia result in enhanced actin polymerization, altered cytoskeletal responses, and genomic instability in lymphocytes. *J. Exp. Med.* 207, 1145–1152. doi: 10.1084/jem.20091245

Wilkie, G. S., Korfali, N., Swanson, S. K., Malik, P., Srsen, V., Batrakou, D. G., et al. (2011). Several novel nuclear envelope transmembrane proteins identified in skeletal muscle have cytoskeletal associations. *Mol. Cell. Proteomics* 10:M110.003129. doi: 10.1074/mcp.M110.003129

Willer, M. K., and Carroll, C. W. (2017). Substrate stiffness-dependent regulation of the SRF-Mkl1 co-activator complex requires the inner nuclear membrane protein Emerin. *J. Cell Sci.* 130, 2111–2118. doi: 10.1242/jcs.197517

Winkler, J., Abisoye-Ogunniyan, A., Metcalf, K. J., and Werb, Z. (2020). Concepts of extracellular matrix remodelling in tumour progression and metastasis. *Nat. Commun.* 11:5120. doi: 10.1038/s41467-020-18794-x

Wong, X., Loo, T.-H., and Stewart, C. L. (2021). LINC complex regulation of genome organization and function. *Curr. Opin. Genet. Dev.* 67, 130–141. doi: 10.1016/j.gde.2020.12.007

Wu, W. H., Alami, S., Luk, E., Wu, C. H., Sen, S., Mizuguchi, G., et al. (2005). Swc2 is a widely conserved H2AZ-binding module essential for ATP-dependent histone exchange. *Nat. Struct. Mol. Biol.* 12, 1064–1071. doi: 10.1038/nsmb1023

Xia, P., Wang, S., Huang, G., Zhu, P., Li, M., Ye, B., et al. (2014). WASH is required for the differentiation commitment of hematopoietic stem cells in a c-Myc-dependent manner. *J. Exp. Med.* 211, 2119–2134. doi: 10.1084/jem.20140169

Xie, X., Jankauskas, R., Mazari, A. M. A., Drou, N., and Percipalle, P. (2018). beta-actin regulates a heterochromatin landscape essential for optimal induction of neuronal programs during direct reprograming. *PLoS Genet.* 14:e1007846. doi: 10.1371/journal.pgen.1007846

Xie, X., Mahmood, S. R., Gjorgjieva, T., and Percipalle, P. (2020). Emerging roles of cytoskeletal proteins in regulating gene expression and genome organization during differentiation. *Nucleus* 11, 53–65. doi: 10.1080/19491034.2020.1742066

Yamauchi, T., and Moroishi, T. (2019). Hippo pathway in mammalian adaptive immune system. *Cells* 8:398. doi: 10.3390/cells8050398

Yang, J., Ikezoe, T., Nishioka, C., Tasaka, T., Taniguchi, A., Kuwayama, Y., et al. (2007). AZD1152, a novel and selective aurora B kinase inhibitor, induces growth arrest, apoptosis, and sensitization for tubulin depolymerizing agent or topoisomerase II inhibitor in human acute leukemia cells in vitro and in vivo. *Blood* 110, 2034–2040. doi: 10.1182/blood-2007-02-073700

Ye, J., Zhao, J., Hoffmann-Rohrer, U., and Grummt, I. (2008). Nuclear myosin I acts in concert with polymeric actin to drive RNA polymerase I transcription. *Genes Dev.* 22, 322–330. doi: 10.1101/gad.455908

Yildirim, O., Li, R., Hung, J. H., Chen, P. B., Dong, X., Ee, L. S., et al. (2011). Mbd3/NURD complex regulates expression of 5-hydroxymethylcytosine marked genes in embryonic stem cells. *Cell* 147, 1498–1510. doi: 10.1016/j.cell.2011.11.054

Yoo, Y., Wu, X., and Guan, J. L. (2007). A novel role of the actin-nucleating Arp2/3 complex in the regulation of RNA polymerase II-dependent transcription. *J. Biol. Chem.* 282, 7616–7623. doi: 10.1074/jbc.M607596200

Zanconato, F., Forcato, M., Battilana, G., Azzolin, L., Quaranta, E., Bodega, B., et al. (2015). Genome-wide association between YAP/TAZ/TEAD and AP-1 at enhancers drives oncogenic growth. *Nat. Cell Biol.* 17, 1218–1227. doi: 10.1038/ncb3216

Zhang, S., Konstantinidis, D. G., Yang, J.-Q., Mizukawa, B., Kalim, K., Lang, R. A., et al. (2014). Gene targeting RhoA reveals its essential role in coordinating mitochondrial function and thymocyte development. *J. Immunol.* 193, 5973–5982. doi: 10.4049/jimmunol.1400839

Zhao, B., Li, L., Wang, L., Wang, C.-Y., Yu, J., and Guan, K.-L. (2012). Cell detachment activates the Hippo pathway via cytoskeleton reorganization to induce anoikis. *Genes Dev.* 26, 54–68. doi: 10.1101/gad.173435.111

Zhao, B., Ye, X., Yu, J., Li, L., Li, W., Li, S., et al. (2008). TEAD mediates YAP-dependent gene induction and growth control. *Genes Dev.* 22, 1962–1971. doi: 10.1101/gad.1664408

Zhao, X.-H., Laschinger, C., Arora, P., Szászi, K., Kapus, A., and McCulloch, C. A. (2007). Force activates smooth muscle α-actin promoter activity through

the Rho signaling pathway. *J. Cell Sci.* 120, 1801–1809. doi: 10.1242/jcs.001586

Zhu, C., Chen, W., Lou, J., Rittase, W., and Li, K. (2019). Mechanosensing through immunoreceptors. *Nat. Immunol.* 20, 1269–1278. doi: 10.1038/s41590-019-0491-1

Zuleger, N., Boyle, S., Kelly, D. A., de las Heras, J. I., Lazou, V., Korfali, N., et al. (2013). Specific nuclear envelope transmembrane proteins can promote the location of chromosomes to and from the nuclear periphery. *Genome Biol.* 14:R14. doi: 10.1186/gb-2013-14-2-r14

Conflict of Interest: The authors declare that the research was conducted in the absence of any commercial or financial relationships that could be construed as a potential conflict of interest.

Publisher's Note: All claims expressed in this article are solely those of the authors and do not necessarily represent those of their affiliated organizations, or those of the publisher, the editors and the reviewers. Any product that may be evaluated in this article, or claim that may be made by its manufacturer, is not guaranteed or endorsed by the publisher.

frontiers in Cell and Developmental Biology

MINI REVIEW
published: 19 August 2021
doi: 10.3389/fcell.2021.676066

Super-Resolution Imaging Approaches for Quantifying F-Actin in Immune Cells

Evelyn Garlick[1,2†], *Steven G. Thomas*[1,2†] *and Dylan M. Owen*[2,3*†]

[1] *Institute of Cardiovascular Sciences, College of Medical and Dental Science, University of Birmingham, Birmingham, United Kingdom,* [2] *Centre of Membrane Proteins and Receptors, University of Birmingham and University of Nottingham, Midlands, United Kingdom,* [3] *Institute for Immunology and Immunotherapy, College of Medical and Dental Science and School of Mathematics, College of Engineering and Physical Science, University of Birmingham, Birmingham, United Kingdom*

OPEN ACCESS

Edited by:
Sudha Kumari, Massachusetts Institute of Technology, United States

Reviewed by:
Maté Biro, University of New South Wales, Australia
Pieta Mattila, University of Turku, Finland

***Correspondence:**
Dylan M. Owen
d.owen@bham.ac.uk

†ORCID:
Evelyn Garlick
orcid.org/0000-0002-9292-1354
Steven G. Thomas
orcid.org/0000-0001-8733-7842
Dylan M. Owen
orcid.org/0000-0002-5284-2782

Specialty section:
This article was submitted to Cell Growth and Division, a section of the journal Frontiers in Cell and Developmental Biology

Received: *04 March 2021*
Accepted: *20 May 2021*
Published: *19 August 2021*

Citation:
Garlick E, Thomas SG and Owen DM (2021) Super-Resolution Imaging Approaches for Quantifying F-Actin in Immune Cells. Front. Cell Dev. Biol. 9:676066. doi: 10.3389/fcell.2021.676066

Immune cells comprise a diverse set of cells that undergo a complex array of biological processes that must be tightly regulated. A key component of cellular machinery that achieves this is the cytoskeleton. Therefore, imaging and quantitatively describing the architecture and dynamics of the cytoskeleton is an important research goal. Optical microscopy is well suited to this task. Here, we review the latest in the state-of-the-art methodology for labeling the cytoskeleton, fluorescence microscopy hardware suitable for such imaging and quantitative statistical analysis software applicable to describing cytoskeletal structures. We also highlight ongoing challenges and areas for future development.

Keywords: actin, microscopy, super-resolution, fiber analysis, cytoskeleton

INTRODUCTION

The actin cytoskeleton is a key cellular component in many biological processes and is particularly implicated in a range of functions associated with immune cells. For example, actin polymerization is responsible for the spreading of lymphocytes over target antigen-presenting cells (APC), creating a large contact area (Dustin and Cooper, 2000), whereas cortical actin retrograde flow drives T cell signaling microclusters toward the synapse center through frictional coupling (Billadeau et al., 2007; DeMond et al., 2008; Hartman et al., 2009; Yu et al., 2013; Kumari et al., 2014; Ashdown et al., 2017). In cytotoxic lymphocytes, cortical actin at the immunological synapse must be remodeled to an actin mesh, which allows the release of cytotoxic granules (Carisey et al., 2018). Actin is also responsible for driving cell migration in response to cytokines (Samstag et al., 2003; Shannon et al., 2020) and processes such as phagocytosis (Castellano et al., 2001; May and Machesky, 2001).

For these reasons, there has been a long-standing goal to understand the architecture of the cytoskeleton in immune cells and numerous techniques have been deployed for this purpose. For example, transmission electron microscopy has been used to image the ultrastructure of cytoskeletal components (Svitkina, 2009). However, in recent years, optical microscopy has come to the forefront of these endeavors for several reasons. Firstly, optical microscopy is relatively non-invasive, allowing cytoskeletal architecture to be imaged in live cells and cytoskeletal dynamics to

be captured and analyzed. Fluorescence microscopy is also specific, allowing particular proteins of interest to be labeled and observed (Lichtman and Conchello, 2005).

For many years, fluorescence microscopy has been held back by its intrinsic resolution limit of around 200 nm. The development of super-resolution (Hell and Wichmann, 1994; Betzig et al., 2006) approaches has broken this barrier and now allows cytoskeletal architecture to be imaged and quantified on the nanoscale. Combined with developments in probes, labeling technology, and in quantitative analysis, advances in microscope design are proving transformative to our understanding of the many diverse functions of the cytoskeleton in immune cell function.

Here, we will review the latest developments in cytoskeletal labeling, applicable microscope hardware, and the latest quantitative analysis methodology.

LABELING

For fixed samples, the gold standard label for filamentous (F-) actin is phalloidin. A bicyclic heptapeptide initially isolated from the death cap mushroom (*Amanita phalloides*), phalloidin is an F-actin stabilizing toxin first used to visualize F-actin in 1979 (Wulf et al., 1979). Fluorescent phalloidins are widely used to visualize F-actin in many applications. Interestingly, the specific fluorophore conjugated to phalloidin can affect imaging outcomes. For example, phalloidin-AlexaFluor 488 has been shown to provide superior detail and longevity of stain over other derivatives like AlexaFluor 405 (DesMarais et al., 2019). However, the choice of label will, to some degree, be application dependent.

Since phalloidin cannot permeate live cells, fixation is important. Paraformaldehyde (PFA) can lead to disruption of the actin cytoskeleton (Leyton-Puig et al., 2016; Pereira et al., 2019) so use of a cytoskeletal stabilizing buffer is recommended. This results in more faithful preservation of actin architecture. Methanol fixation, while often favored for microtubule preservation, results in significant actin disruption and should be avoided (Whelan and Bell, 2015; DesMarais et al., 2019).

There are also numerous staining options for live imaging of actin. For a thorough review of actin labeling, see Melak et al. (2017). Direct tagging of actin subunits with recombinant fluorescent proteins (FP) is possible and has been used extensively. These constructs must be expressed exogenously, and although capable of co-polymerizing with the untagged endogenous actin (Westphal et al., 1997), FP-actin kinetics and behavior can be impeded (Aizawa et al., 1997; Deibler et al., 2011; Nagasaki et al., 2017) and non-integrated monomers can generate background. Tagging actin binding proteins (ABPs) is therefore a more attractive option. Their capacity to bind more efficiently to actin filaments than monomers results in better identification of the filamentous cytoskeleton. Examples of ABPs include derivatives of the calponin homology domain of utrophin (Burkel et al., 2007), a short peptide from the rat inositol 1,4,5-trisphosphate 3-kinase (ITPK) called F-Tractin (Schell et al., 2001) and a 17-amino acid peptide derived from Abp140 called Lifeact (Riedl et al., 2010). The generation of a GFP-Lifeact transgenic mouse line (Riedl et al., 2010) has allowed live actin imaging *in vivo*, along with tissue-specific expression using a cre inducible mouse line (Schachtner et al., 2012). Additionally, Lifeact can be adapted for use with single-molecule imaging strategies such as IRIS (Kiuchi et al., 2015). While widely used, actin binding protein derivatives should still be approached with caution. For example, Utrophin derivatives can induce actin aggregates in both the nucleus and cytoplasm, and recent findings suggest that Lifeact-TagGFP2 can disrupt actin architecture in a dose-dependent manner (Flores et al., 2019).

SiR actin is an F-actin probe based on jasplakinolide, an actin binder and potent promoter of nucleation. The silicon rhodamine (SiR) probe is fluorogenic (Lukinavičius et al., 2014), cell permeable, and can be added to live cells in culture without washing. As SiR actin is a derivative of jasplakinolide, however, higher concentrations can impact dynamics significantly (Lukinavičius et al., 2014).

Newer labeling strategies like nanobodies and affimers have generated interest in recent years. For example, fluorophore fused nanobodies ("chromobodies") can retain labeling functionality when expressed intracellularly, allowing for specific live-cell imaging (Rothbauer et al., 2006; Schiavon et al., 2020). In general, nanobodies offer significant antigen specificity and reduced size over standard antibodies. Affimers are synthetic reagents generated from non-antibody scaffold proteins such as Adhirons (Tiede et al., 2014). Lopata et al. (2018) demonstrated the identification and validation of four affimers that specifically recognize F-actin. Their versatility and potential for live-cell application make them important reagents for the future (Lopata et al., 2018). Some of the more widely used labeling strategies are summarized in **Table 1**.

MICROSCOPY TECHNIQUES

Simple assessment of gross actin structures is easily achieved using diffraction-limited imaging systems. Abbe's law, often referred to as the diffraction limit, describes how the minimum resolution achievable in a system is dependent on the numerical aperture of the lens and the wavelength of the incident light. Due to these limitations, the maximum resolving power of diffraction-limited systems is ∼200 nm laterally and ∼600 nm axially. One of the simplest fluorescence techniques, wide-field epifluorescence imaging, involves illumination of the full sample. This results in the camera or detector receiving all emitted light, both in and out of focus, which can reduce the images' signal-to-noise ratio (SNR) significantly as well as limit optical sectioning capacity. Epifluorescence microscopes are, however, simple systems capable of high-speed acquisition, and combination with image post-processing like deconvolution can provide powerful insight into dynamic actin processes.

Total internal reflection fluorescence microscopy (TIRF) is achieved by angling the incident light such that it is entirely reflected, rather than refracted. At this so-called critical angle, an evanescent wave is generated that decays exponentially

TABLE 1 | Summary of the advantages and disadvantages of different actin labeling strategies.

	Label	Uses	Pros	Cons
Phalloidin	F-actin binding peptide (Wulf et al., 1979)	Fixed F-actin labeling	Gold standard for fixed actin imaging	Unsuitable for studying actin dynamics in live cells
Tagged β-actin	Exogenously expressed fluorescently tagged actin subunits (Westphal et al., 1997)	Live imaging	Can incorporate into endogenous filaments	Can affect dynamics G-actin also visible
Utrophin and F-tractin	FP-tagged region of actin binding proteins (Schell et al., 2001; Burkel et al., 2007)	Live imaging	Does not require direct tagging of actin Does not require over-expression of actin monomers Does not label G actin	Can affect dynamics
LifeAct	17 amino acid peptide derived from Abp140 (Riedl et al., 2008)	Live imaging	Does not require direct tagging of actin Does not require overexpression of actin monomers Small probe adaptable for many techniques	Can affect dynamics G-actin can be labeled
SiR Actin	Silicon Rhodamine probe conjugated to a jasplakinolide derivative (Lukinavičius et al., 2014)	Live imaging	Fluorogenic Cell permeable Concentration is titratable	High concentrations can affect dynamics
Chromabodies	Fluorophore fused anti-actin nanobodies (Rothbauer et al., 2006)	Live imaging	Significantly improved specificity over antibodies Reduced size over antibodies	G-actin can be labeled
Affimers	Synthetic reagents generated from non-antibody scaffold proteins (Lopata et al., 2018)	Live and fixed imaging	Small probe size Potential for structural sub- selectivity	Not yet used routinely Further screening required

with depth, restricting fluorophore excitation to approximately 200 nm from the coverslip and reducing the out-of-focus background. TIRF is therefore often the technique of choice when imaging dynamic actin in adherent cells.

The dynamics of actin in T cell synapses are well imaged with TIRF. For example, Ritter et al. (2017) used TIRF imaging to follow cortical actin recovery in cytotoxic T cell synapses following lytic granule secretion (Ritter et al., 2017). Time lapse imaging allowed assessment of the cortical actin structure pre- and post-secretion, providing insight into the tightly regulated process. The relatively lengthy time courses (<10 min) with high temporal resolution (2.4-s intervals for two color experiments) were possible due to TIRF microscopy. Variation in the actin structure of stable and unstable immune synapses has also been investigated using TIRF, including on supported lipid bilayers (Kumari et al., 2020). Wagh et al. (2020) used TIRF to quantify actin reorganization in the immune synapse of CD8 effector T cells relative to Bcl10 expression. Analysis resulted in the identification of two phases of dynamics—a faster initial stage and slower latter, both of which were significantly faster in $Bcl10^{-/-}$ cells. In this case, the high temporal resolution possible with TIRF was essential.

Confocal microscopy is another workhorse of diffraction-limited imaging. By applying a pinhole in front of the detector, out-of-focus light is discarded. Point scanning microscopes must raster scan across the sample, meaning the method is less suited to fast imaging. Laser intensity is often increased too. Spinning disk confocal microscopes can overcome some of the limitations on speed and phototoxicity by inclusion of an array of microlenses, allowing multiple focused beams of light to be swept across the sample to reduce intense laser exposure. Resonant scanning confocal microscopy also improves acquisition speed in single point scanning systems, using a resonant mirror scanner that oscillates at a fixed frequency to improve framerate to video rate (30 fps) and beyond. Confocal microscopes are a solid choice for actin imaging given their advantages over widefield microscopy and common presence in core facilities.

Lightsheet microscopy is regarded as one of the gentlest techniques for live-cell imaging. A sheet of light, hundreds of nanometers thick, is generated perpendicular to the imaging objective and moved through the sample. This planar illumination significantly reduces out-of-focus light, improving signal to noise and reducing phototoxicity. This technique also permits rapid capture of 3D data. A variant of this concept, lattice light sheet (Chen et al., 2014) microscopy, replaces the conventional sheet with an optical lattice, further reducing phototoxicity and improving imaging speed. Examples of light-sheet imaging of the cytoskeleton in immune cells include imaging the retrograde flow of cortical actin in cell–cell synapses (Ritter et al., 2015) and actin protrusions in cytotoxic T cells (Tamzalit et al., 2019) and neutrophils (Fritz-Laylin et al., 2017).

While the diffraction-limited techniques are widely used to study immune cells, in many cases, cytoskeletal structures need to be studied on the nanoscale. There are now multiple techniques capable of breaking the diffraction limit (Illustrated in **Figure 1**). Fluorescence microscopy can obtain resolutions only previously possible with electron microscopy, with single-molecule localization microscopy (SMLM) techniques routinely reporting resolving power of up to 10 nm.

Structured illumination microscopy (SIM) allows extraction of higher-resolution information by illuminating the sample in a known pattern—usually stripes, but variations like lattice SIM use differing illumination patterns. The pattern is translated and rotated across several frames, and the interference of this light pattern with the sample generates so-called Moiré fringes. High-frequency information is then extracted during

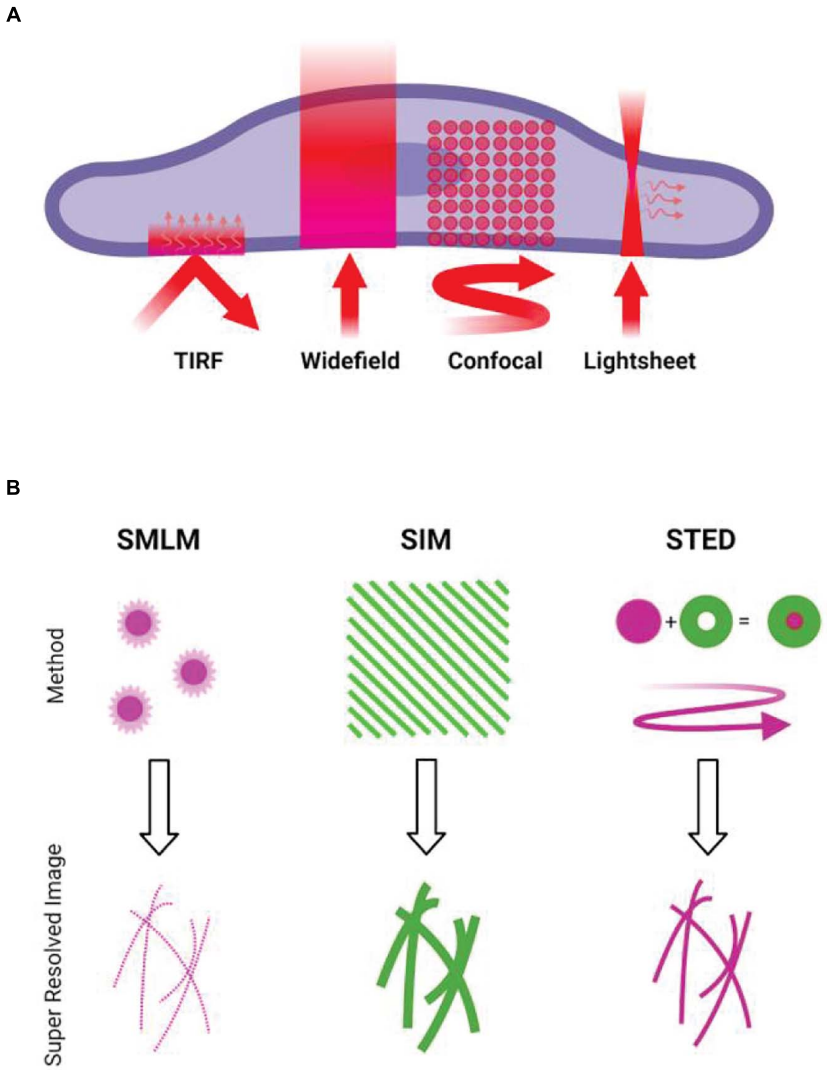

FIGURE 1 | Overview of microscopy techniques commonly used for imaging actin. **(A)** Diffraction-limited techniques. TIRF, showing the incident light and resulting evanescent wave. Widefield epifluorescence, showing illumination of the full volume of the specimen. Confocal, showing the rastering of the scanning focal point. Lightsheet, showing the sheet illumination and resulting detection at an angle to illumination. **(B)** Illustrations of the concepts behind common super-resolution techniques. SMLM requires the stochastic activation and localization of single fluorophores, building up a pointillist image of the structure. SIM involves projection of patterned illumination at multiple angles, using the resulting Moiré fringes to reconstruct a higher frequency information. STED uses a depletion laser that surrounds the point of illumination, reducing the size of the point spread function of the illumination beam.

computational reconstruction, generating images with roughly a 2× increase in resolution. Reconstruction artifacts can be an issue, especially in thicker or more densely labeled samples [see Demmerle et al. (2017), for images and explanations of common issues]. Critical inspection of reconstruction results, as well as using packages such as SIMCheck (Ball et al., 2015), is best practice. Structured Illumination can also be applied to lattice light sheet microscopy, allowing rapid and gentle acquisition of live-cell super-resolved data (Wagh et al., 2020). In immune cells, SIM has been used with TIRF illumination to image cortical actin labeled with phalloidin (Ritter et al., 2017) and in live cells using LifeAct (Ashdown et al., 2017), both at the T-cell immunological synapse. Colin-York used TIRF SIM to show differences between cytoskeletal behavior in primary and immortalized T cells (Colin-York et al., 2020) and Brown used SIM to analyze cortical actin at the sites of lytic granule release at NK cell synapses (Brown et al., 2011).

Another point scanning technique, stimulated emission depletion (STED) microscopy (Hell and Wichmann, 1994), achieves super-resolution by selectively depleting fluorophores around a central focal point. As the size of the excitation point is reduced by a doughnut-shaped depletion laser, resolutions of 30–80 nm can be achieved. Optical sectioning is also a particular strength, as the technique is point scanning, and diffractive optical elements can be introduced to generate an additional depletion doughnut in z (Klar et al., 2000). Intense laser power in the depletion beam is required, making phototoxicity a key consideration. Recent developments in this technique

(MINFLUX) (Balzarotti et al., 2017) reduces the phototoxicity caused by the high laser intensities of STED. Fritzche used STED to image the actin cytoskeleton in immune cells (Fritzsche et al., 2017) and Clausen used the method to analyze the relationship between the actin cortex and the membrane (Clausen et al., 2017). Carisey showed the applicability of STED (as well as TIRF SIM) to image the dynamics of actin in NK cells (Carisey et al., 2018) and Rak used similar methodology to analyze the architecture of the actin cortex during lytic granule release (Rak et al., 2011).

Single-molecule localization microscopy techniques boast impressive resolutions. All techniques under this umbrella rely on detection and mathematical localization of individual fluorophores, but achieve this stochastic imaging in different ways. Key examples include stochastic optical reconstruction microscopy (STORM) (Rust et al., 2006), which utilizes the photophysical properties of certain fluorophores (most often Alexa-Fluor 647) in order to push them in and out of a transient dark state. Photoactivated localization microscopy (PALM) (Betzig et al., 2006) relies on photoswitchable proteins to illuminate limited subsets of the sample. Points accumulation for imaging in nanoscale topography (PAINT) (Sharonov and Hochstrasser, 2006) makes use of repeated association and dissociation of the labeled probe, be that through transient interaction between complementary DNA oligonucleotides (DNA-PAINT) (Schnitzbauer et al., 2017), the most commonly implemented option, and IRIS uses the repeated binding of the LifeAct peptide (Kiuchi et al., 2015). IRIS was later used with quantitative analysis to dissect the architecture of cortical actin at the T-cell immune synapse (Peters et al., 2018). Actin has been successfully imaged using all of these techniques. Given the small size of individual actin filaments (∼7 nm), the approximate resolution of 100 nm of techniques like SIM can still obscure significant detail in the actin architecture, which can be revealed with SMLM. As yet, however, this high resolution comes at the expense of live-cell imaging. Most examples are of fixed cells, as toxic blinking buffers (mostly for dSTORM), high laser intensities, and long acquisition times needed limit live applicability.

Many live super-resolution techniques require specialized optical setups and can have limitations in terms of labels and imaging speed. Development of algorithmic approaches to live super-resolution microscopy allows circumvention of some of these issues. Examples include SOFI (super-resolution optical fluctuation imaging, which analyzes temporal fluctuations of the emitters) (Dertinger et al., 2009) and super-resolution radial fluctuations (SRRF) (Gustafsson et al., 2016). SRRF, which uses fluorescence fluctuations over time to calculate radiality on a subpixel basis, is a widely applicable technique, being capable of taking raw widefield, TIRF, confocal, and even SMLM data. The technique has been demonstrated as a way to image LifeAct-GFP labeled actin in T-cell immunological synapses (Gustafsson et al., 2016), with significant improvement in resolution.

Correlative approaches, where multiple imaging techniques are applied to the same cell, are becoming more prevalent in the field. Correlative light and electron microscopy (CLEM) provides the as-yet unparalleled resolving power of electron microscopy techniques while also overcoming some of the labeling limitations inherent in using EM alone. Much of this work has been done outside of immune cells, for example, in neurons, elucidating new nanoscale cytoskeletal structures (Vassilopoulos et al., 2019); however, super-resolution CLEM has been used to image multiple proteins relative to the actin structure around clusters of podosomes in dendritic cells (Joosten et al., 2018), providing insight into differential association of particular proteins with different structures in the podosome. Correlative approaches do extend beyond EM, however. For example, a recent study used SMLM in conjunction with AFM to image podosomes in THP-1 cells (Hirvonen et al., 2020), opening possibilities for dual structural and mechanobiological mapping. The main recent imaging strategies used to image F-actin are summarized in **Table 2**.

TABLE 2 | Summary of key microscope techniques applied to cytoskeletal imaging.

Imaging method	Advantages	Disadvantages	Immune cell use examples
TIRF	Improved SNR Rapid imaging	Diffraction limited Focal plane limited to ∼200 nm proximal to coverslip	Ritter et al., 2017; Wagh et al., 2020
Light Sheet	Good optical sectioning Improved SNR Rapid and gentle imaging	Diffraction limited if not SIM-lattice) Specialized system required	Ritter et al., 2015; Fritz-Laylin et al., 2017; Tamzalit et al., 2019
SIM	2× improvement in resolution vs. diffraction limited, axially and laterally (3D SIM)	Potential for reconstruction artifacts Acquisition speed can be limiting for live imaging Specialized system required	Brown et al., 2011; Ashdown et al., 2017; Colin-York et al., 2020
STED	30–80 nm resolution No computationally intensive post-processing	High laser powers necessary for depletion beam Specialized system required	Rak et al., 2011; Clausen et al., 2017; Fritzsche et al., 2017; Carisey et al., 2018
SMLM	20 nm + resolutions, up to ∼10 nm localization precision Data obtained as a point cloud	Lengthy image acquisitions can be necessary Sample preparation can be complex Potential for reconstruction artifacts	Kiuchi et al., 2015; Hirvonen et al., 2020
Computational techniques (e.g., SRRF, SOFI)	Simple image acquisitions No specialized hardware necessary	Potential for reconstruction artifacts	Gustafsson et al., 2016

QUANTIFICATION

Once sample preparation, labeling, and imaging have been performed, images must be analyzed to extract biologically meaningful, quantitative data. The type of analysis performed depends largely on the biological question being asked. For example, a key differentiator is whether dynamic, live-cell data are being analyzed. Dynamic imaging analysis may involve quantifying flow or the stability of a particular architecture (Ashdown and Owen, 2018; Shannon et al., 2020), for example. In static structures, far richer descriptions of the actin architecture are generally possible.

For components of the cytoskeleton that are typically fibrous structures, the first step is usually to attempt to trace the fibers themselves to generate a mathematical representation of the architecture. This can then be interrogated to extract specific descriptive features. Examples of descriptors that might be desirable when quantifying a fibrous pattern include the number or density of fibers in a given area or volume, the lengths of fibers, or measures of co-orientation and co-linearity between fibers. They may also include the sizes and shapes of enclosed areas between fibers and analysis of branching angles and cross-points as well as curvature measures. These different parameters are illustrated in **Figure 2**.

There are many competing algorithms capable of analyzing fibrous architecture and providing these descriptions, but they can generally be divided into two groups—those that work on pixelated images such as those derived from widefield, TIRF, confocal, STED, or reconstructed SIM images, and those that work with pointillist data—the *x*,*y* coordinates derived from SMLM imaging.

For methods that produce pixelated images, methods for analyzing actin distributions have existed for some time. Many of the algorithms are related to those that can be used to trace other fibrous structures—dendrites or axons from neuronal images are another common example (Kayasandik et al., 2018). Many are available in image analysis packages such as ImageJ (Schneider et al., 2012) and more exist in various proprietary packages (Schindelin et al., 2012). They often take the form of a ridge estimating algorithm. Many of these, however, begin with some form of cleanup of the raw image—for example, noise filtering. Recently, machine-learning approaches have proven to be well suited for this task and user-friendly packages capable of using machine learning to clean and enhance cytoskeletal images have become available (von Chamier et al., 2021).

One particularly widely applied method of analyzing actin fibrous architecture from pixelated images in immune cells is to quantify the size distributions of clearances between fibers. For

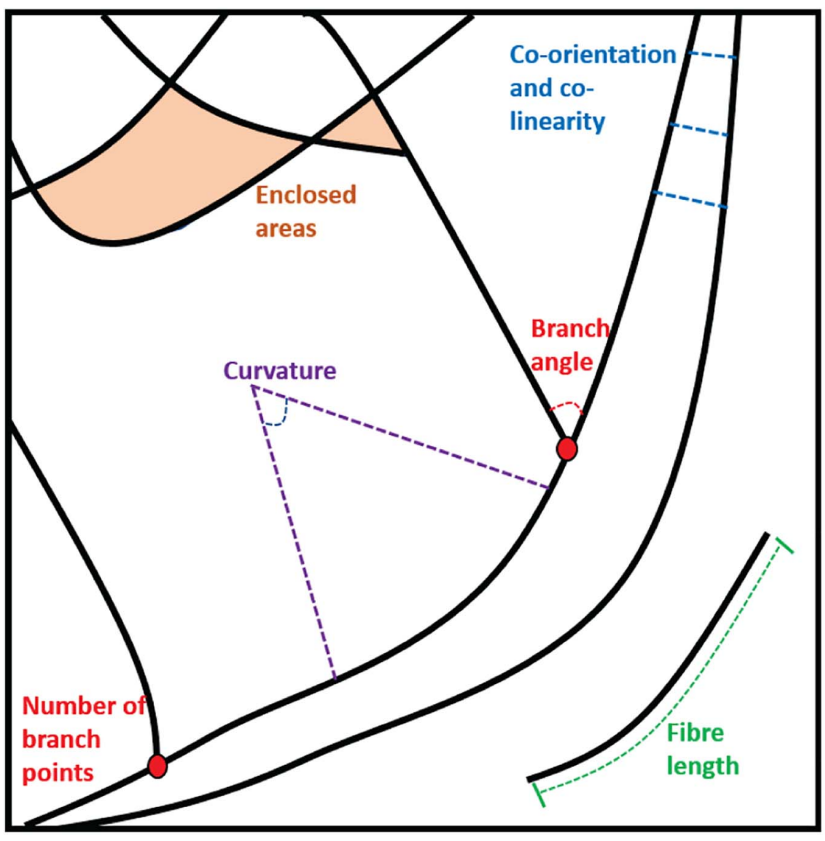

FIGURE 2 | Examples of the parameters that can be extracted from static fiber analysis: Enclosed areas, branch points and angles, fiber lengths and measures of curvature, co-orientation, and co-linearity.

cortical actin, this parameter represents a measure of what size of object could traverse the meshwork when traveling from an intracellular pool to the plasma membrane. Such a method has been used to analyze clearances in NK cells (Rak et al., 2011), showing that cortical actin must be cleared for lytic granule release, and the application of such methodology to live-cell imaging of the cytoskeleton allowed the analysis of the dynamics of this clearance process (Carisey et al., 2018).

Zhang et al. (2017) described a method for extracting quantitative descriptions of microtubule architecture from super-resolution SMLM data, provided those data are first converted into pixelated images. Here, filamentous features are enhanced using filters and biologically derived constraints are used to join filament sections together. This allowed the extraction of many of the desirable descriptors: filament length, number of filaments, and so on (Zhang et al., 2017). Somewhat similarly, Kittisopikul also use filters to detect fibrous structures; however, the use of a tunable filter allows particularly detailed analysis of fiber junctions (Kittisopikul et al., 2020). Very recently, one of the most complete algorithms for analyzing fibrous patterns from pixelated images has been developed. FiNTA (Flormann et al., 2021) is based on the vector tracing of grayscale images. It provides rich descriptors of fibrous patterns such as connectivity between fibers, hold sizes and shapes, filament density, and length and measures of curvature.

One way of describing fibrous architecture directly from SMLM-derived point coordinates is to re-purpose statistical methodology designed to analyze other types of structure such as molecular clusters. One such method is Ripley's K-function, which is based on counting the number of points within ever-increasing circles, centered on each data point. Peters et al. (2018) showed that when a fibrous cytoskeletal network is regular and periodic, this periodicity becomes evident in the Ripley's K-function curves (Peters et al., 2017). The K-function can therefore be used to measure how regular or chaotic a fibrous pattern is (Peters et al., 2017). Moreover, for immune cell synapses, which are generally radially symmetric, especially in artificial cases such as on a hard surface or a planar-supported lipid bilayer, the method could describe the proportion of tangential and radial fiber orientations.

To extract richer descriptors, algorithms have been developed that trace fiber positions through point clouds (Peters et al., 2018). Such algorithms start at a particular point on a fiber and then attempt to "walk" along the structure, analogous to attempting to navigate along a mountain ridge. This allowed the extraction of fiber lengths, branch points, and so on. Other methods, for example, cluster analysis by Voronoi Tessellation, are applicable to fibers (Levet et al., 2015) as are machine-learning approaches (Williamson et al., 2020).

CONCLUSION

The actin cytoskeleton is a diverse structure. Its organization and dynamics have a profound effect on the regulation of immune cells. Here, we have reviewed optical imaging approaches for this purpose, examining labeling strategies, imaging hardware, and the associated statistical analysis. Taken together, these allow the structure and dynamics of the cytoskeleton to be quantitatively described, even on scales far below the resolution of conventional optical imaging.

Despite the recent progress, several aspects of the role of the cytoskeleton in immune cells remain to be uncovered and further developments in imaging techniques might shed light on these questions. One interesting aspect concerns the role of cortical actin in regulating the distributions and dynamics of membrane proteins. For example, it is known that many proximal signaling proteins on the surface of NK cells, B cells, and T cells are clustered on the nanoscale and show various kinds of constrained diffusion, especially at immunological synapses (Fooksman et al., 2010; Yokosuka and Saito, 2010; Pageon et al., 2013). Frameworks such as the picket fence model (Fujiwara et al., 2016) seek to explain the role of cortical actin in these processes. However, even for super-resolution techniques, the density of fibers in the cortex can be a challenge to accurately describe, especially given their dynamic nature. Correlative methods, ultra-high-resolution imaging, and live-cell SMLM could be applicable to this problem (Henriques et al., 2011; Balzarotti et al., 2017; Griffié et al., 2018; Cnossen et al., 2020).

Another aspect frequently left understudied is the 3D organization of the cytoskeleton. In immune cell processes such as phagocytosis, actin is necessarily remodeled in 3D. 3D SMLM and fiber analysis have been attempted (Peters et al., 2019), but advancements in other 3D modalities, including light sheet, would also be advantageous (Sapoznik et al., 2020).

Finally, a perhaps undervalued area is the mathematical modeling of the resulting data. A common goal is often not to image or understand the actin organization in any particular cell, but to be able to model and predict the organization in an average cell or a population of cells. To do this, statistical modeling approaches and machine learning require large amounts of data, and so high-throughput and high-content imaging systems, centered on automation, will be key.

AUTHOR CONTRIBUTIONS

All authors listed have made a substantial, direct and intellectual contribution to the work, and approved it for publication.

FUNDING

This work was supported by the British Heart Foundation (BHF) (NH/18/3/33913) and BBSRC grant BB/R007365/1. EG was funded on a COMPARE Studentship.

ACKNOWLEDGMENTS

The authors would like to thank the Centre of Membrane Proteins and Receptors, University of Birmingham.

REFERENCES

Aizawa, H., Sameshima, M., and Yahara, I. (1997). A green fluorescent protein-actin fusion protein dominantly inhibits cytokinesis, cell spreading, and locomotion in dictyostelium. *Cell Struct. Funct.* 22, 335–345. doi: 10.1247/csf.22.335

Ashdown, G. W., Burn, G. L., Williamson, D. J., Pandžiæ, E., Peters, R., Holden, M., et al. (2017). Live-Cell super-resolution reveals F-Actin and plasma membrane dynamics at the T cell synapse. *Biophys. J.* 112, 1703–1713. doi: 10.1016/j.bpj.2017.01.038

Ashdown, G. W., and Owen, D. M. (2018). Spatio-temporal image correlation spectroscopy and super-resolution microscopy to quantify molecular dynamics in T cells. *Methods* 140-141, 112–118. doi: 10.1016/j.ymeth.2018.01.017

Ball, G., Demmerle, J., Kaufmann, R., Davis, I., Dobbie, I. M., and Schermelleh, L. (2015). SIMcheck: a toolbox for successful super-resolution structured illumination microscopy. *Sci. Rep.* 5:15915. doi: 10.1038/srep15915

Balzarotti, F., Eilers, Y., Gwosch, K. C., Gynnå, A. H., Westphal, V., Stefani, F. D., et al. (2017). Nanometer resolution imaging and tracking of fluorescent molecules with minimal photon fluxes. *Science* 355, 606–612. doi: 10.1126/science.aak9913

Betzig, E., Patterson, G. H., Sougrat, R., Lindwasser, O. W., Olenych, S., Bonifacino, J. S., et al. (2006). Imaging intracellular fluorescent proteins at nanometer resolution. *Science* 313:1642. doi: 10.1126/science.1127344

Billadeau, D. D., Nolz, J. C., and Gomez, T. S. (2007). Regulation of T-cell activation by the cytoskeleton. *Nat. Rev. Immunol.* 7, 131–143. doi: 10.1038/nri2021

Brown, A. C. N., Oddos, S., Dobbie, I. M., Alakoskela, J.-M., Parton, R. M., Eissmann, P., et al. (2011). Remodelling of cortical actin where lytic granules dock at natural killer cell immune synapses revealed by super-resolution microscopy. *PLoS Biol.* 9:e1001152. doi: 10.1371/journal.pbio.1001152

Burkel, B. M., von Dassow, G., and Bement, W. M. (2007). Versatile fluorescent probes for actin filaments based on the actin-binding domain of utrophin. *Cell Motil. Cytoskeleton* 64, 822–832. doi: 10.1002/cm.20226

Carisey, A. F., Mace, E. M., Saeed, M. B., Davis, D. M., and Orange, J. S. (2018). Nanoscale dynamism of actin enables secretory function in cytolytic cells. *Curr. Biol. CB* 28, 489–502.e9. doi: 10.1016/j.cub.2017.12.044

Castellano, F., Chavrier, P., and Caron, E. (2001). Actin dynamics during phagocytosis. *Semin. Immunol.* 13, 347–355. doi: 10.1006/smim.2001.0331

Chen, B.-C., Legant, W. R., Wang, K., Shao, L., Milkie, D. E., Davidson, M. W., et al. (2014). Lattice light-sheet microscopy: imaging molecules to embryos at high spatiotemporal resolution. *Science* 346:1257998. doi: 10.1126/science.1257998

Clausen, M. P., Colin-York, H., Schneider, F., Eggeling, C., and Fritzsche, M. (2017). Dissecting the actin cortex density and membrane-cortex distance in living cells by super-resolution microscopy. *J. Phys. D: Appl. Phys.* 50, 064002–064002. doi: 10.1088/1361-6463/aa52a1

Cnossen, J., Hinsdale, T., Thorsen, R. Ø, Siemons, M., Schueder, F., Jungmann, R., et al. (2020). Localization microscopy at doubled precision with patterned illumination. *Nat. Methods* 17, 59–63. doi: 10.1038/s41592-019-0657-7

Colin-York, H., Kumari, S., Barbieri, L., Cords, L., and Fritzsche, M. (2020). Distinct actin cytoskeleton behaviour in primary and immortalised T-cells. *J. Cell Sci.* 133:jcs232322. doi: 10.1242/jcs.232322

Deibler, M., Spatz, J. P., and Kemkemer, R. (2011). Actin fusion proteins alter the dynamics of mechanically induced cytoskeleton rearrangement. *PLoS One* 6:e22941. doi: 10.1371/journal.pone.0022941

Demmerle, J., Innocent, C., North, A. J., Ball, G., Müller, M., Miron, E., et al. (2017). Strategic and practical guidelines for successful structured illumination microscopy. *Nat. Protocols* 12, 988–1010. doi: 10.1038/nprot.2017.019

DeMond, A. L., Mossman, K. D., Starr, T., Dustin, M. L., and Groves, J. T. (2008). T cell receptor microcluster transport through molecular mazes reveals mechanism of translocation. *Biophys. J.* 94, 3286–3292. doi: 10.1529/biophysj.107.119099

Dertinger, T., Colyer, R., Iyer, G., Weiss, S., and Enderlein, J. (2009). Fast, background-free, 3D super-resolution optical fluctuation imaging (SOFI). *Proc. Natl. Acad. Sci. U S A.* 106:22287. doi: 10.1073/pnas.0907866106

DesMarais, V., Eddy, R. J., Sharma, V. P., Stone, O., and Condeelis, J. S. (2019). Optimizing leading edge F-actin labeling using multiple actin probes, fixation methods and imaging modalities. *BioTechniques* 66, 113–119. doi: 10.2144/btn-2018-0112

Dustin, M. L., and Cooper, J. A. (2000). The immunological synapse and the actin cytoskeleton: molecular hardware for T cell signaling. *Nat. Immunol.* 1, 23–29. doi: 10.1038/76877

Flores, L. R., Keeling, M. C., Zhang, X., Sliogeryte, K., and Gavara, N. (2019). Lifeact-TagGFP2 alters F-actin organization, cellular morphology and biophysical behaviour. *Sci. Rep.* 9:3241. doi: 10.1038/s41598-019-40092-w

Flormann, D. A. D., Schu, M., Terriac, E., Thalla, D., Kainka, L., Koch, M., et al. (2021). A novel universal algorithm for filament network tracing and cytoskeleton analysis. *FASEB J.* 35:e21582. doi: 10.1096/fj.202100048R

Fooksman, D. R., Vardhana, S., Vasiliver-Shamis, G., Liese, J., Blair, D. A., Waite, J., et al. (2010). Functional anatomy of T cell activation and synapse formation. *Annu. Rev. Immunol.* 28, 79–105. doi: 10.1146/annurev-immunol-030409-101308

Fritz-Laylin, L. K., Riel-Mehan, M., Chen, B. C., Lord, S. J., Goddard, T. D., Ferrin, T. E., et al. (2017). Actin-based protrusions of migrating neutrophils are intrinsically lamellar and facilitate direction changes. *eLife* 6:e26990. doi: 10.7554/eLife.26990

Fritzsche, M., Fernandes, R. A., Chang, V. T., Colin-York, H., Clausen, M. P., Felce, J. H., et al. (2017). Cytoskeletal actin dynamics shape a ramifying actin network underpinning immunological synapse formation. *Sci. Adv.* 3:e1603032. doi: 10.1126/sciadv.1603032

Fujiwara, T. K., Iwasawa, K., Kalay, Z., Tsunoyama, T. A., Watanabe, Y., Umemura, Y. M., et al. (2016). Confined diffusion of transmembrane proteins and lipids induced by the same actin meshwork lining the plasma membrane. *Mol. Biol. Cell* 27, 1101–1119. doi: 10.1091/mbc.E15-04-0186

Griffié, J., Burn, G. L., Williamson, D. J., Peters, R., Rubin-Delanchy, P., and Owen, D. M. (2018). Dynamic bayesian cluster analysis of live-cell single molecule localization microscopy datasets. *Small Methods* 2:1800008. doi: 10.1002/smtd.201800008

Gustafsson, N., Culley, S., Ashdown, G., Owen, D. M., Pereira, P. M., and Henriques, R. (2016). Fast live-cell conventional fluorophore nanoscopy with ImageJ through super-resolution radial fluctuations. *Nat. Commun.* 7:12471. doi: 10.1038/ncomms12471

Hartman, N. C., Nye, J. A., and Groves, J. T. (2009). Cluster size regulates protein sorting in the immunological synapse. *Proc. Natl. Acad. Sci. U S A.* 106, 12729–12734. doi: 10.1073/pnas.0902621106

Hell, S. W., and Wichmann, J. (1994). Breaking the diffraction resolution limit by stimulated emission: stimulated-emission-depletion fluorescence microscopy. *Opt. Lett.* 19, 780–782. doi: 10.1364/OL.19.000780

Henriques, R., Griffiths, C., Hesper Rego, E., and Mhlanga, M. M. (2011). PALM and STORM: unlocking live-cell super-resolution. *Biopolymers* 95, 322–331. doi: 10.1002/bip.21586

Hirvonen, L. M., Marsh, R. J., Jones, G. E., and Cox, S. (2020). Combined AFM and super-resolution localisation microscopy: investigating the structure and dynamics of podosomes. *Eur. J. Cell Biol.* 99:151106. doi: 10.1016/j.ejcb.2020.151106

Joosten, B., Willemse, M., Fransen, J., Cambi, A., and van den Dries, K. (2018). Super-Resolution Correlative Light and Electron Microscopy (SR-CLEM) reveals novel ultrastructural insights into dendritic cell podosomes. *Front. Immunol.* 9:1908. doi: 10.3389/fimmu.2018.01908

Kayasandik, C., Negi, P., Laezza, F., Papadakis, M., and Labate, D. (2018). Automated sorting of neuronal trees in fluorescent images of neuronal networks using NeuroTreeTracer. *Sci. Rep.* 8:6450. doi: 10.1038/s41598-018-24753-w

Kittisopikul, M., Vahabikashi, A., Shimi, T., Goldman, R. D., and Jaqaman, K. (2020). Adaptive multiorientation resolution analysis of complex filamentous network images. *Bioinformatics* 36, 5093–5103. doi: 10.1093/bioinformatics/btaa627

Kiuchi, T., Higuchi, M., Takamura, A., Maruoka, M., and Watanabe, N. (2015). Multitarget super-resolution microscopy with high-density labeling by exchangeable probes. *Nat. Methods* 12, 743–746. doi: 10.1038/nmeth.3466

Klar, T. A., Jakobs, S., Dyba, M., Egner, A., and Hell, S. W. (2000). Fluorescence microscopy with diffraction resolution barrier broken by stimulated emission. *Proc. Natl. Acad. Sci. U S A.* 97:8206. doi: 10.1073/pnas.97.15.8206

Kumari, S., Curado, S., Mayya, V., and Dustin, M. L. (2014). T cell antigen receptor activation and actin cytoskeleton remodeling. *Biochimica et Biophysica Acta (BBA) - Biomembranes* 1838, 546–556. doi: 10.1016/j.bbamem.2013.05.004

Kumari, S., Mak, M., Poh, Y.-C., Tohme, M., Watson, N., Melo, M., et al. (2020). Cytoskeletal tension actively sustains the migratory T-cell synaptic contact. *EMBO J.* 39:e102783. doi: 10.15252/embj.2019102783

Levet, F., Hosy, E., Kechkar, A., Butler, C., Beghin, A., Choquet, D., et al. (2015). SR-Tesseler: a method to segment and quantify localization-based super-resolution microscopy data. *Nat. Methods* 12, 1065–1071. doi: 10.1038/nmeth.3579

Leyton-Puig, D., Kedziora, K. M., Isogai, T., Broek, B. V. D., Jalink, K., and Innocenti, M. (2016). PFA fixation enables artifact-free super-resolution imaging of the actin cytoskeleton and associated proteins. *Biol. Open* 5, 1001–1009. doi: 10.1242/bio.019570

Lichtman, J. W., and Conchello, J. A. (2005). Fluorescence microscopy. *Nat. Methods* 2, 910–919. doi: 10.1038/nmeth817

Lopata, A., Hughes, R., Tiede, C., Heissler, S. M., Sellers, J. R., Knight, P. J., et al. (2018). Affimer proteins for F-actin: novel affinity reagents that label F-actin in live and fixed cells. *Sci. Rep.* 8:6572. doi: 10.1038/s41598-018-24953-4

Lukinavičius, G., Reymond, L., D'Este, E., Masharina, A., Göttfert, F., Ta, H., et al. (2014). Fluorogenic probes for live-cell imaging of the cytoskeleton. *Nat. Methods* 11, 731–733. doi: 10.1038/nmeth.2972

May, R. C., and Machesky, L. M. (2001). Phagocytosis and the actin cytoskeleton. *J. Cell Sci.* 114, 1061. doi: 10.1242/jcs.114.6.1061

Melak, M., Plessner, M., and Grosse, R. (2017). Actin visualization at a glance. *J. Cell Sci.* 130, 525–530. doi: 10.1242/jcs.204487

Nagasaki, A., Kijima, T. S., Yumoto, T., Imaizumi, M., Yamagishi, A., Kim, H., et al. (2017). The position of the GFP tag on actin affects the filament formation in mammalian cells. *Cell Struct. Funct.* 42, 131–140. doi: 10.1247/csf.17016

Pageon, S. V., Cordoba, S. P., Owen, D. M., Rothery, S. M., Oszmiana, A., and Davis, D. M. (2013). Superresolution microscopy reveals nanometer-scale reorganization of inhibitory natural killer cell receptors upon activation of NKG2D. *Sci. Signal.* 6:ra62. doi: 10.1126/scisignal.2003947

Pereira, P. M., Albrecht, D., Culley, S., Jacobs, C., Marsh, M., Mercer, J., et al. (2019). Fix your membrane receptor imaging: actin cytoskeleton and CD4 membrane organization disruption by chemical fixation. *Front. Immunol.* 10:675. doi: 10.3389/fimmu.2019.00675

Peters, R., Benthem Muñiz, M., Griffié, J., Williamson, D. J., Ashdown, G. W., Lorenz, C. D., et al. (2017). Quantification of fibrous spatial point patterns from single-molecule localization microscopy (SMLM) data. *Bioinformatics* 33, 1703–1711. doi: 10.1093/bioinformatics/btx026

Peters, R., Griffié, J., Burn, G. L., Williamson, D. J., and Owen, D. M. (2018). Quantitative fibre analysis of single-molecule localization microscopy data. *Sci. Rep.* 8:10418. doi: 10.1038/s41598-018-28691-5

Peters, R., Griffié, J., Williamson, D., Aaron, J., Khuon, S., and Owen, D. (2019). Development of 2-colour and 3D SMLM data analysis methods for fibrous spatial point patterns. *J. Phys. D* 52:014005. doi: 10.1088/1361-6463/aae7ac

Rak, G. D., Mace, E. M., Banerjee, P. P., Svitkina, T., and Orange, J. S. (2011). Natural killer cell lytic granule secretion occurs through a pervasive actin network at the immune synapse. *PLoS Biol.* 9:e1001151. doi: 10.1371/journal.pbio.1001151

Riedl, J., Crevenna, A. H., Kessenbrock, K., Yu, J. H., Neukirchen, D., Bista, M., et al. (2008). Lifeact: a versatile marker to visualize F-actin. *Nat. Methods* 5, 605–607. doi: 10.1038/nmeth.1220

Riedl, J., Flynn, K. C., Raducanu, A., Gärtner, F., Beck, G., Bösl, M., et al. (2010). Lifeact mice for studying F-actin dynamics. *Nat. Methods* 7, 168–169. doi: 10.1038/nmeth0310-168

Ritter, A. T., Asano, Y., Stinchcombe, J. C., Dieckmann, N. M. G., Chen, B.-C., et al. (2015). Actin depletion initiates events leading to granule secretion at the immunological synapse. *Immunity* 42, 864–876. doi: 10.1016/j.immuni.2015.04.013

Ritter, A. T., Kapnick, S. M., Murugesan, S., Schwartzberg, P. L., Griffiths, G. M., and Lippincott-Schwartz, J. (2017). Cortical actin recovery at the immunological synapse leads to termination of lytic granule secretion in cytotoxic T lymphocytes. *Proc. Natl. Acad. Sci. U S A.* 114, E6585–E6594. doi: 10.1073/pnas.1710751114

Rothbauer, U., Zolghadr, K., Tillib, S., Nowak, D., Schermelleh, L., Gahl, A., et al. (2006). Targeting and tracing antigens in live cells with fluorescent nanobodies. *Nat. Methods* 3, 887–889. doi: 10.1038/nmeth953

Rust, M. J., Bates, M., and Zhuang, X. (2006). Sub-diffraction-limit imaging by stochastic optical reconstruction microscopy (STORM). *Nat. Methods* 3, 793–795. doi: 10.1038/nmeth929

Samstag, Y., Eibert, S. M., Klemke, M., and Wabnitz, G. H. (2003). Actin cytoskeletal dynamics in T lymphocyte activation and migration. *J. Leukoc. Biol.* 73, 30–48. doi: 10.1189/jlb.0602272

Sapoznik, E., Chang, B.-J., Huh, J., Ju, R. J., Azarova, E. V., Pohlkamp, T., et al. (2020). A versatile oblique plane microscope for large-scale and high-resolution imaging of subcellular dynamics. *eLife* 9:e57681. doi: 10.1101/2020.04.07.030569

Schachtner, H., Li, A., Stevenson, D., Calaminus, S. D. J., Thomas, S., et al. (2012). Tissue inducible Lifeact expression allows visualization of actin dynamics in vivo and ex vivo. *Eur. J. Cell Biol.* 91, 923–929. doi: 10.1016/j.ejcb.2012.04.002

Schell, M. J., Erneux, C., and Irvine, R. F. (2001). Inositol 1,4,5-Trisphosphate 3-Kinase a associates with f-actin and dendritic spines via its N terminus *. *J. Biol. Chem.* 276, 37537–37546. doi: 10.1074/jbc.M104101200

Schiavon, C. R., Zhang, T., Zhao, B., Moore, A. S., Wales, P., Andrade, L. R., et al. (2020). Actin chromobody imaging reveals sub-organellar actin dynamics. *Nat. Methods* 17, 917–921. doi: 10.1038/s41592-020-0926-5

Schindelin, J., Arganda-Carreras, I., Frise, E., Kaynig, V., Longair, M., Pietzsch, T., et al. (2012). Fiji: an open-source platform for biological-image analysis. *Nat. Methods* 9, 676–682. doi: 10.1038/nmeth.2019

Schneider, C. A., Rasband, W. S., and Eliceiri, K. W. (2012). NIH Image to ImageJ: 25 years of image analysis. *Nat. Methods* 9, 671–675. doi: 10.1038/nmeth.2089

Schnitzbauer, J., Strauss, M. T., Schlichthaerle, T., Schueder, F., and Jungmann, R. (2017). Super-resolution microscopy with DNA-PAINT. *Nat. Protocols* 12, 1198–1228. doi: 10.1038/nprot.2017.024

Shannon, M. J., Pineau, J., Griffié, J., Aaron, J., Peel, T., Williamson, D. J., et al. (2020). Differential nanoscale organisation of LFA-1 modulates T-cell migration. *J. Cell Sci.* 133:jcs232991. doi: 10.1242/jcs.232991

Sharonov, A., and Hochstrasser, R. M. (2006). Wide-field subdiffraction imaging by accumulated binding of diffusing probes. *Proc. Natl. Acad. Sci. U S A.* 103:18911. doi: 10.1073/pnas.0609643104

Svitkina, T. (2009). Imaging cytoskeleton components by electron microscopy. *Methods Mol. Biol. (Clifton, N.J.)* 586, 187–206. doi: 10.1007/978-1-60761-376-3_10

Tamzalit, F., Wang, M. S., Jin, W., Tello-Lafoz, M., Boyko, V., Heddleston, J. M., et al. (2019). Interfacial actin protrusions mechanically enhance killing by cytotoxic T cells. *Sci. Immunol.* 4:eaav5445. doi: 10.1126/sciimmunol.aav5445

Tiede, C., Tang, A. A. S., Deacon, S. E., Mandal, U., Nettleship, J. E., et al. (2014). Adhiron: a stable and versatile peptide display scaffold for molecular recognition applications. *Protein Eng. Des. Select. PEDS* 27, 145–155. doi: 10.1093/protein/gzu007

Vassilopoulos, S., Gibaud, S., Jimenez, A., Caillol, G., and Leterrier, C. (2019). Ultrastructure of the axonal periodic scaffold reveals a braid-like organization of actin rings. *Nat. Commun.* 10:5803. doi: 10.1038/s41467-019-13835-6

von Chamier, L., Laine, R. F., Jukkala, J., Spahn, C., Krentzel, D., Nehme, E., et al. (2021). Democratising deep learning for microscopy with ZeroCostDL4Mic. *Nat. Commun.* 12:2276. doi: 10.1038/s41467-021-22518-0

Wagh, K., Wheatley, B. A., Traver, M. K., Hussain, I., Schaefer, B. C., and Upadhyaya, A. (2020). Bcl10 is associated with actin dynamics at the T cell immune synapse. *Cell Immunol.* 356:104161. doi: 10.1016/j.cellimm.2020.104161

Westphal, M., Jungbluth, A., Heidecker, M., Mühlbauer, B., Heizer, C., Schwartz, J.-M., et al. (1997). Microfilament dynamics during cell movement and chemotaxis monitored using a GFP–actin fusion protein. *Curr. Biol.* 7, 176–183. doi: 10.1016/S0960-9822(97)70088-5

Whelan, D. R., and Bell, T. D. M. (2015). Image artifacts in Single Molecule Localization microscopy: why optimization of sample preparation protocols matters. *Sci. Rep.* 5:7924. doi: 10.1038/srep07924

Williamson, D. J., Burn, G. L., Simoncelli, S., Griffié, J., Peters, R., Davis, D. M., et al. (2020). Machine learning for cluster analysis of localization microscopy data. *Nat. Commun.* 11:1493. doi: 10.1038/s41467-020-15293-x

Wulf, E., Deboben, A., Bautz, F. A., Faulstich, H., and Wieland, T. (1979). Fluorescent phallotoxin, a tool for the visualization of cellular actin. *Proc. Natl. Acad. Sci. U S A.* 76, 4498–4502. doi: 10.1073/pnas.76.9.4498

Yokosuka, T., and Saito, T. (2010). The immunological synapse, TCR microclusters, and T cell activation. *Curr. Top. Microbiol. Immunol.* 340, 81–107. doi: 10.1007/978-3-642-03858-7_5

Yu, Y., Smoligovets, A. A., and Groves, J. T. (2013). Modulation of T cell signaling by the actin cytoskeleton. *J. Cell Sci.* 126:1049. doi: 10.1242/jcs.098210

Zhang, Z., Nishimura, Y., and Kanchanawong, P. (2017). Extracting microtubule networks from superresolution single-molecule localization microscopy data. *Mol. Biol. Cell* 28, 333–345. doi: 10.1091/mbc.e16-06-0421

Conflict of Interest: The authors declare that the research was conducted in the absence of any commercial or financial relationships that could be construed as a potential conflict of interest.

Advantages of publishing in Frontiers

OPEN ACCESS
Articles are free to read for greatest visibility and readership

FAST PUBLICATION
Around 90 days from submission to decision

HIGH QUALITY PEER-REVIEW
Rigorous, collaborative, and constructive peer-review

TRANSPARENT PEER-REVIEW
Editors and reviewers acknowledged by name on published articles

Frontiers
Avenue du Tribunal-Fédéral 34
1005 Lausanne | Switzerland

Visit us: www.frontiersin.org
Contact us: frontiersin.org/about/contact

REPRODUCIBILITY OF RESEARCH
Support open data and methods to enhance research reproducibility

DIGITAL PUBLISHING
Articles designed for optimal readership across devices

FOLLOW US
@frontiersin

IMPACT METRICS
Advanced article metrics track visibility across digital media

EXTENSIVE PROMOTION
Marketing and promotion of impactful research

LOOP RESEARCH NETWORK
Our network increases your article's readership